Calendar of forthcoming meetings

26–27 April 2007
Belgrade, Serbia
2nd EMCO Workshop on Emerging Contaminants in Wastewaters: Monitoring Tools and Treatment Technologies.
Contact: Dr M. Petrovic, Department of Environmental Chemistry, IIQAB-CSIC, c/Jordi Girona 18-26, 08034 Barcelona, Spain.
Fax: (+34-93) 204-5904;
E-mail: mpeqam@cid.csic.es;
URL: http://www.cid.csic.es/belgrade2007/home.htm

3–5 May 2007
St. Petersburg, Russia
ISOEN 2007: International Symposium on Olfaction and Electric Noses.
Contact:
E-mail: info@isoen2007.spb.ru;
URL: http://www.isoen2007.spb.ru

5–7 June 2007
Dalian, China
30th International Symposium on Capillary Chromatography and 4th GCxGC Symposium.
Contact: Professor Guowang Xu, National Chromatographic R&A Center, Dalian Institute of Chemical Physics, Chinese Academy of Sciences, Dalian 116023, China.
Tel.: (+86-411) 8437-9530;
Fax: (+86-411) 8437-9559;
E-mail: iscc@dicp.ac.cn or xugw@dicp.ac.cn;
URL: http://www.iscc.dicp.ac.cn

5–7 June 2007
Manila, Philippines
AsiaSense 2007: 3rd Asian Conference on Sensors.
Contact: Professor Fortunato Sevilla III or Professor Christina Binag, Research Center for the Natural Sciences, University of Santo Tomas, Espana Blvd., Manila 1008, Philippines.
Tel./Fax: (+63-2) 731-4031;
E-mail: fbsevilla@mnl.ust.edu.ph or cabinag@mnl.ust.edu.ph

6–9 June 2007
Gargnano, Lake Garda, Italy
Future Trends in Phytochemistry – A Young Scientists Symposium.
Contact: Professor F. Tome, Dipartimento di Biologia, via Celoria 26, 20133 Milano, Italy.
Tel.: (+39-02) 5031-4773;
Fax: (+39-02) 5031-2764;
E-mail: franca.tome@unimi.it;
URL: http://users.unimi.it/ftpsymp

10–15 June 2007
Corfu, Greece
ICAVS-4: 4th International Conference on Advanced Vibrational Spectroscopy.
Contact: Dr V. Gregoriou, ICAVS-4, PO Box 1414, Patras, Greece.
Tel.: (+30-2610) 911-580;
Fax: (+30-2610) 911-585;
E-mail: icavs4@adventech.gr;
URL: http://www.icavs.info/corfu2007

18–22 June 2007
Trento, Italy
TXRF 2007: 12th Conference on Total Reflection X-Ray Fluorescence Analysis and Related Methods.
URL: http://fcs.its.it/events/TXRF07.html

16–19 August 2007
Changchun, China
11th ISEC and 1st SIBSEC: 11th International and First Sino-Japan Bilateral Symposium on Electroanalytical Chemistry.
Contact: Professor Bailin Zhang, Changchun Institute of Applied Chemistry, Chinese Academy of Sciences, 5625 Renmin Street, Changchun, Jilin, 130022, China.
Tel./Fax: (+86-431) 8526-2430;
E-mail: blzhang@ciac.jl.cn;
URL: http://isec.skleac.org

9–12 September 2007
Torun, Poland
11th EuCheMS International Conference on Chemistry and the Environment; chemistry, environment and human activity in civilization development.
Contact: Professor B. Buszewski or Dr Katarzyna Krupczynska, Department of Environmental Chemistry and Ecoanalytics, Faculty of Chemistry, Nicolas Copernicus University, 7 Gagarin St,m 87-100 Torun, Poland.
Tel.: (+48-56) 611-4308 or 611- 4753;
Fax: (+48-56) 611-4837;
E-mail: analityk@chem.uni.torun.pl;
URL: http://www.chem.uni.torun.pl

9–14 September 2007
Antwerp, Belgium
Euroanalysis XIV.
Contact: L. Van't Dack, Department of Chemistry, Unviersity of Antwerp, Universiteitsplein 1, B-2610 Antwerp, Belgium.
Tel.: (+32-3) 820-2343;
Fax: (+32-3) 820-2376;
E-mail: luc.vantdack@ua.ac.be;
URL: http://www.euroanalysisxiv.ua.ac.be

10–13 September 2007
Paris, France
Euro-Mediterranean Symposium on Laser-Induced Breakdown Spectroscopy: EMSLIBS 2007.
URL: http://www.emslibs2007.com

12–14 September 2007
Sevilla, Spain
3rd World Congress on Synthetic Receptors.
URL: www.syntheticreceptors.elsevier.com

N2

7–9 November 2007
Prague, Czech Republic
3rd International Symposium on Recent Advances in Food Analysis.
Contact: Mrs Marianne Frei-Häusler, Postfach 46, CH-4123 Allschwil 2, Switzerland.
Tel.: (+41-61) 481-2789;

Fax: (+41-61) 482-0805;
E-mail: iaeac@dplanet.ch;
URL: www.iaeac.ch

6–12 January 2008
Temecula, CA, USA
2008 Winter Conference on Plasma Spectrochemistry.

Contact: Ramon Barnes, ICP Information Newsletter, Inc., PO Box 666, Hadley, MA 01003-0666, USA.
Tel.: (+1-413) 256-8942;
Fax: (+1-413) 256-3747;
E-mail: wc2006@chem.umass.edu;
URL: http://www-unix.oit.umass.edu/~wc2006

Development of a long-term stable organic membrane-based thin-film microsensor using new-type substrate surface treatment

Hassan A. Arida *

Hot Laboratory Center, Atomic Energy Authority, 13759 Cairo, Egypt

Abstract

A novel long lifetime organic membrane-based thin-film Cu(II) microsensor has been elaborated. The advantages of the suggested microsensor include: excellent stability, long lifetime, and reasonable good selectivity. The significant improvements of the lifetime (>4 months) of the organic membrane-based thin-film microsensors have been realized for the first time using new-type electrodeposition treatment of the solid-state substrate surface in combination with a new nebulization method for applying the organic membrane coating mixture on the thin-film gold substrate. The electrochemical behavior of the thin-film microsensor in terms of ionic sensitivity, limit of detection, the effect of the pH, dynamic response time, Nernstian response interval, selectivity coefficients and lifetime has been evaluated. The results are compared to those obtained with the conventional ion-selective and coated graphite rod macroelectrodes prepared with the same ionophore. The reliability of the suggested thin-film microsensor with the low cost of its microfabrication makes it promising for the miniaturized application.
© 2006 Elsevier B.V. All rights reserved.

Keywords: Thin-film sensor; Cu(II) determination; Potentiometry; Microfabrication; Substrate surface treatment; Organic membrane nebulization

1. Introduction

Microfabricated chemical sensor devices are playing a critically important role for sensing ions in solutions due to the possibility of sensor miniaturization as well as multi-sensor configuration. Among various types of chemical sensors, thin-film microsensors will be most befitted from the rapidly advancing technology [1,2]. The advantages brought by these new microsensors are: reduced size, small sample volume, low fabrication cost and miniaturization feasibility. Furthermore, the integration of microsensors can be realized easily for multianalyte detection [3–5]. The variety of applications of the thin-film sensors is extremely diverse, including their uses in detection of glucose [6] and NO_x gases [7] as well as in microfabrication of thin-film sensor array for gas sensing [8], for simultaneous detection of some transition metal cations [9], and microelectrode array devices to biological applications [10,11]. Recently, microfabrication, application and miniaturization of chalcogenide glasses-based thin-film sensors have been reported, since minia-

turization can be regards as critically important aspect [12–16]. With regards to chalcogenide glasses and based on their long-term stability, these materials have been used for the first time in microfabrication of thin-film sensor array for potentiometric detection of some heavy metal cations using pulsed laser deposition techniques [12]. Nevertheless, the chalcogenide glasses-based thin-film sensors and related multisensor array, electronic tongue and electronic nose are suffer from a lack of selectivity due to the well-known cross-sensitivity of the chalcogenide glasses materials [17]. Moreover, the potentiometric response of these sensors may become very complicated in complex media of the environmental and the technological process control samples [18]. The attempts to solve the selectivity problem of these microsensors have also been demonstrated [17,19,20]. For example, methods of statistical pattern recognition, artificial neural network, chemometrics and machine learning have been reviewed [21]. However, the topology of such network continuously changes over time due to a variety of reasons [22].

Our previous paper, demonstrates the realization of thin-film sensor with enhanced selectivity using organic PVC-based membrane for the first time as a sensitive layer in a novel concept to solve the selectivity problem of such microsensors [23]. Although, the response characteristics of the sug-

---

* Tel.: +20 27570276; fax: +20 24620806.
  E-mail address: aridaha@hotmail.com.

gested organic membrane-based thin-film microsensors agree with those obtained by the conventional selective membranes and coated graphite rod-based macroelectrodes, the lifetime of the thin-film microsensors is relatively short (one working day). This is due to the low adhesion of PVC-based organic membrane to the solid substrate surface, which leads to a short lifetime of the fabricated microsensor due to the peeling off of the organic membrane sensitive layer from the substrate surface [24]. On the other hand, different organic membrane-based macroelectrodes with enhanced response characteristics have been recently, reported [25–27].

In this work, the stability and consequently the lifetime of the organic membrane-based thin-film microsensor are dramatically enhanced (from 1 day to more than 4 months). In addition to the miniaturization feasibility and selectivity features of the suggested microsensor, this advantage has been realized by significant improvements of the adhesive properties of the organic membrane sensitive layer on to the thin-film solid-state surface. This was achieved using to new approaches, including precipitating a thin-film of Ag deposits electrochemically on gold solid-state substrate surface in combination with nebulizing the organic membrane coating mixture on the treated substrate surface in a novel concept.

2. Experimental

2.1. Reagents and materials

All salts and the membrane components (analytical-reagent grade), namely, high molecular weight poly (vinyl chloride) (PVC), dioctylphthalate plasticizer, tetrahydrofurane (THF) were purchased from Fluka (Buch, Switzerland). *m*-Phenylenediamine (*m*-phen), sodium tetraphenyl borate and cupric nitrate were obtained from Merk Chemical Co., and salicylaldehyde was from BDH. Standard solutions were prepared with bi-distilled deionized water.

2.2. Procedure for the thin-film substrate surface treatment

As metal contact solid-state substrates, gold and platinum thin-films prepared as described in our previous work [23] have been used. The surfaces of these substrates were treated electrochemically to enhance their adhesion to the organic membrane sensitive layer. This treatment was realized by deposits thin-films of Ag precipitate on the substrates surfaces from 10^{-3} mol l^{-1} AgNO$_3$ solution for 1 h using laboratory made small electrodeposition cell. In this cell, the solid-state thin-film substrates were parallel connecting as a cathode in conjunction with a metal anode. Prior to the ion-sensitive organic membrane layer deposition, the treated thin-film substrates were allowed to cure at room temperature for 24 h.

2.3. Fabrication of organic membrane thin-film Cu(II) microsensor

N-N′-Bis(salicylidene)-*m*-phenylenediamine Schiff base ligand was synthesized by condensing 50 ml of *m*-phenylene-

diamine (purified by crystallization from benzene in presence of activated charcoal) with 50 ml salicylaldehyde in ethanol (ratio 1:2). The mixture was refluxed for 2 h over a water-bath and then allowed to cool at room temperature. The product filtered off and crystallized from pure ethanol as shining orange plates were obtained.

The ion-sensitive ionophore copper complex was prepared by reacting 0.315 g of Cu(CH$_3$COO)$_2$·6H$_2$O in 50 ml CHCl$_3$ with 0.5 g of *N-N′*-bis(salicylidene)-*m*-phenylenediamine Schiff base ligand in 50 ml CHCl$_3$. The mixture was refluxed with constant stirring for 3 h on a water-bath and then concentrated to a small volume and allowed to cool where an olive green precipitate was separated. The solid filtered off, washed several times with CHCl$_3$ and dried in vacuo at room temperature.

The sensor cocktail mixture of the following components (weight, mg): ionophore (10), DOP (350), NaTPB (20), PVC (190) was mixed and dissolved homogeneously in THF. A small aliquot of the cocktail coating mixture was evenly nebulized over the treated thin-film substrate surface using small manual nebulizing system. After evaporation of the solvent the nebulization step was repeated until a uniform film membrane has been obtained. The sensor was allowed drying for 24 h and was soaked in 10^{-3} mol l^{-1} solution of cupric nitrate for 1 h before calibration.

The cocktail coating mixture was also used in preparation of conventional membrane and coated graphite rod-based electrodes as described in our previous work [23].

2.4. Evaluating potentiometric response and lifetime

The potentiometric behavior of the new thin-film-based Cu(II) microsensor as well as of the conventional membrane and the coated graphite rod-based Cu(II) macroelectrodes were – individually – electrochemically evaluated for comparison. The potential changes of the sensors were measured against an Ag/AgCl reference electrode using Hanna (model 8417) pH/mV meter. At least two sensors of each type have been used and not less than four repeated calibration have been done. All measurements were taken at ambient room temperature (25 ± 5) °C. During the measurements, the sample was stirred using a magnetic stirrer. The lifetimes of the investigated Cu(II) microsensors were measured from the response potential to the varying cupric nitrate concentration 3 days a week for more than 4 months.

3. Results and discussion

Typical sensor characteristics like sensitivity, response time, detection limit, selectivity and long-term stability of the thin-film Cu(II) microsensors and bulk macroelectrodes presented here were investigated with *N-N′*-bis(salicylidene)-*m*-phenylenediamine copper complex. This Schiff base complex was used as a new electroactive material sensitive and selective to copper cations based on its high stability constant compared with those of other metal Schiff base complexes prepared by the same ligand as described elsewhere [28].

As already discussed in our previous work [23], the selectivity of the thin-film microelectrodes was enhanced by
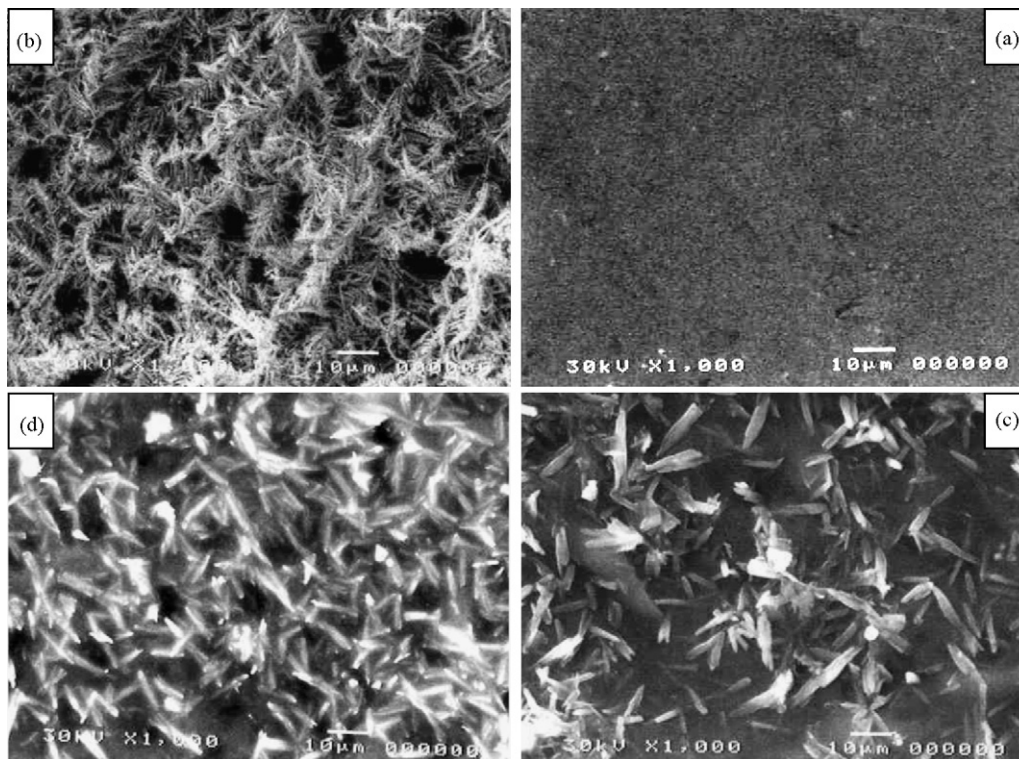
Fig. 1. Typical SEM micrograph of the surface of the thin-film Cu(II) microsensor: (a) gold substrate before treatment; (b) electrochemically treated gold substrate; (c) nebulized organic membrane on platinum substrate; (d) nebulized organic membrane on gold substrate.

realizing organic membrane-based thin-film microsensors. Nevertheless, the lifetime of such sensor is relatively short. New substrate surface treatment in combination with new nebulization method for applying the organic membrane sensitive layer have been tested here for the first time to solve this problem.

Fig. 1, presents a typical scanning electron microscope (SEM) micrograph of the solid-state substrate surface (Au and Pt) before treatment, after electrochemical treatment and after nebulizing the organic membrane sensitive layer. For the two thin-film substrates investigated (Au and Pt), SEM micrograph before and after treatment are quite different. In addition, the surface of the Ag deposits as well as the surface of the organic membrane are textured and have nearly homogeneous distribution on the two tested substrates.

3.1. Microsensors characteristics

Fig. 2 demonstrates a typical calibration curve of the suggested thin-film Cu(II) microsensors using gold and platinum substrates. For comparison, the potentiometric calibration response of both conventional and coated graphite rod-based macroelectrodes have also, been presented. It can be seen that, the potentiometric responses of the two thin-film microsensors and the tested macroelectrodes are nearly comparable. The properties of the sensors may be characterized by the following parameter: sensitivity 27–31.5 mV per concentration decade, lifetime 3–4 months, response time <30 s and detection limit of 7×10^{-7} to 5×10^{-6} mol l^{-1} (Table 1). For simplicity, the gold

thin-film-based microsensor of the best sensitivity (31.5 ± 0.5) has been selected for the rest of measurements.

3.2. Response time and stability

In this study, the dynamic response time was recorded by changing the primary ion concentration in the test solution over
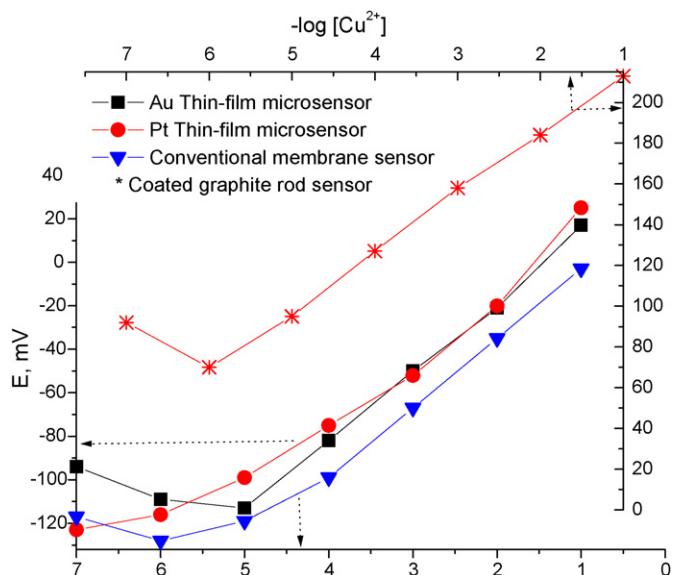
Fig. 2. Potentiometric calibration response of organic membrane-based Cu(II) microsensors.

Table 1
Potentiometric response characteristics of the organic membrane-based Cu(II) thin-film microsensors

Sensor parameter	Conventional membrane	Coated graphite rod	Pt thin-film microsensor	Au thin-film microsensor
Slope (mV/decade)	29.0 ± 0.5	28.5 ± 0.5	27.0 ± 0.5	31.5 ± 0.5
Linear range ($mol\,l^{-1}$)	1×10^{-5} to 1×10^{-1}	1×10^{-6} to 1×10^{-1}	1×10^{-6} to 1×10^{-2}	1×10^{-5} to 1×10^{-1}
Lower limit of linear range ($mol\,l^{-1}$)	1×10^{-5}	1×10^{-6}	1×10^{-6}	1×10^{-5}
Lower limit of detection ($mol\,l^{-1}$)	6×10^{-6}	8×10^{-7}	7×10^{-7}	5×10^{-6}
Response time (s)	<30	<30	<30	<30
Lifetime (months)	3	3	>4	>4

a concentration range 1×10^{-5} to 1×10^{-1} $mol\,l^{-1}$. The actual potential versus time tracer is presented in Fig. 3. As can be seen, the microsensor provides fast response time (30 s) to reach 95% of its final steady state potential in whole concentration range.

The second important factor is the long-term stability has investigated for more than 4 months. The organic membrane-based thin-film microsensors offer long lifetime (>4 months). The dramatic enhancement in the stability and consequently in the lifetime is attributed to the excellent adhesion properties of the organic membrane sensitive layer on the electrochemically treated substrate surface. Moreover, the nebulization of the organic membrane coating mixture reduced the leachibility of the electroactive material and hence improved the lifetime of the nebulizing microsensors rather than those of the conventional membrane and the coated graphite rod-based macroelectrodes.

3.3. Effect of pH

The influence of pH of the test solutions (1×10^{-3} and 1×10^{-4} $mol\,l^{-1}$ Cu^{2+}) on the thin-film microsensor response was tested in the pH range 1–6. The pH of the test solution was changed by adding very small aliquots of HNO_3 0.1 $mol\,l^{-1}$. The results presented in Fig. 4 showed that, the suggested thin-film microsensor showed a negligible response to hydrogen ion over a pH range 1.5–3.5. The subsequent measurements, therefore, were performed in this range using the same acid solution.
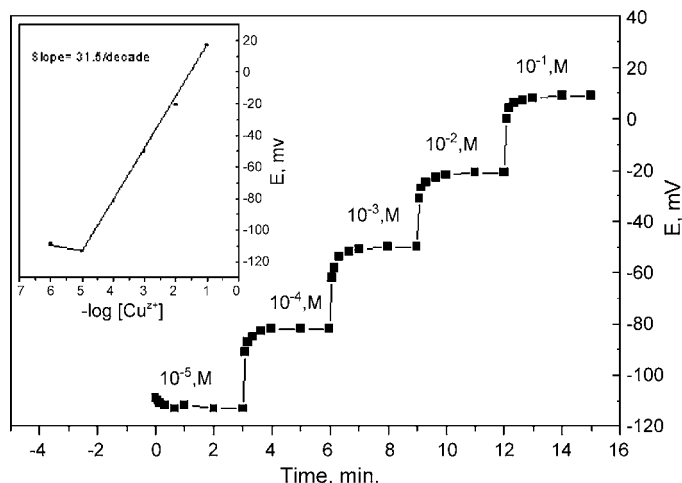
Fig. 3. Potentiometric dynamic response of Au thin-film-based Cu(II) microsensor.
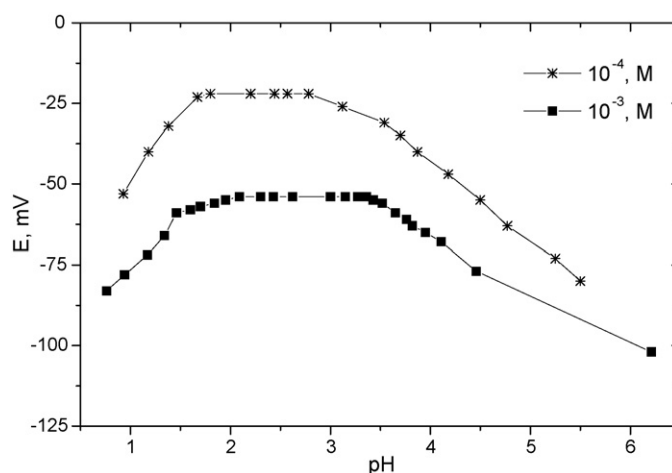
Fig. 4. Influence of the pH of the test solution on the response of the thin-film Cu(II) microsensor at different concentration.

3.4. Potentiometric selectivity

Our goal in the preparation of the new-type organic membrane-based microsensors is the enhancement of the selectivity characteristics of the solid-state thin-film microsensors. Therefore, in order to evaluate the influence of interfering ions on the response of the suggested new microsensor, the selectivity coefficient was investigated by the separate solution method with a fixed concentration (1×10^{-3} $mol\,l^{-1}$) of the primary and the interfering ions. The resulting values of the selectivity coefficients are summarized in Table 2. As can be seen, the suggested thin-film microsensor showed a reasonable good selectivity towards the tested divalent cations which attributed

Table 2
Selectivity coefficients values ($K_{Cu^+,B}^{pot.}$) of the of organic membrane-based Cu(II) thin-film microsensors towards some tested cations

Interferent species, B	$K_{Cu^+,B}^{pot.}$
Cu^{2+}	1
Co^{2+}	1.36×10^{-3}
Ni^{2+}	2.15×10^{-3}
Mn^{2+}	1.71×10^{-3}
Cd^{2+}	2.59×10^{-2}
Ca^{2+}	2.77×10^{-3}
Zn^{2+}	1.32×10^{-2}
Mg^{2+}	3.60×10^{-3}
K^+	8.64×10^{-1}
NH_4^+	7.35×10^{-1}

Table 3
Potentiometric recovery studies on the thin-film microsensor

Sample	AAS	Thin-film microelectrode	Recovery (%)
S_1	4.0×10^{-1}	3.5×10^{-1}	87.5
S_2	3.0×10^{-1}	2.8×10^{-1}	93.3
S_3	4.8×10^{-1}	4.4×10^{-1}	91.6
S_4	4.7×10^{-1}	4.0×10^{-1}	85.1

Average recovery: 89.3 (S_1, S_2; soft layer pool and S_3, S_4; hard layer pool).

to the high stability constant of the *N-N′*-bis(salicylidene)-*m*-phenylenediamine Schiff base copper complex ionophore compared with those obtained with the *N-N′*-bis(salicylidene)-*m*-phenylenediamine Schiff base complexes of other divalent cations [28].

3.5. Microsensor application

The thin-film microsensor prepared by the new approaches has been successfully used in the direct potentiometric determination of Cu(II) in real samples. Different real samples from different electroplating pools of the "Technical Company of the Rotogravure Cylinders, 10th of Ramadan City" was diluted and used for this purpose. For comparison, these samples were also determined by atomic absorption spectroscopy. The results obtained (Table 3) show a good agreement with those obtained by the independent standard technique.

4. Conclusions

A new selective and sensitive organic membrane-based thin-film Cu(II) microsensor has been successfully realized. For its fabrication, electrochemically substrate surface treatment has been developed in combination with a new nebulization method for applying organic membrane sensitive layer. The microsensor based on these new approaches reveals a linear response with a Nernstian slope of 31.5 mV per decade within the concentration range of 1×10^{-5} to 1×10^{-1} mol l^{-1} Cu^{2+} ions. The microsensor showed excellent stability and long-term lifetime (>4 months), fast response time (<30 s) and good reasonable selectivity over some tested cations. Realization of the promising long-term stable and selective organic membrane-based thin-film microsensor should facilitate the miniaturization and integration of multisensor configuration.

References

[1] H. Suzuki, Electroanalysis 12 (2000) 703.
[2] X. Cai, A. Glidle, J.M. Cooper, Electroanalysis 12 (2000) 631.
[3] R. Feeny, S.P. Kounaves, Electroanalysis 12 (2000) 677.
[4] A. Economou, R.P. Fielden, Analyst 128 (2003) 205.
[5] A.J. Miller, S.J. Cookson, S.J. Smith, D.M. Wells, Exp. Botany 52 (2001) 541.
[6] S.K. Kang, R.A. Jeong, S. Parks, T.D. Chung, S. Park, H.C. Kim, Anal. Sci. 19 (2003) 1481.
[7] Z. Jiao, M. Wu, Z. Qin, M. Lu, J. Gu, Sensors 3 (2003) 285.
[8] K. Toda, Y. Komatsu, S. Oguni, S. Hashiguchi, I.A. Sanemasa, Anal. Sci. 15 (1999) 87.
[9] Y.G. Mourzina, J. Schubert, W. Zander, A. Legin, Y.G. Vlasov, H. Lüth, M.J. Schöning, Electrochim. Acta 47 (2001) 251.
[10] M. Kudera, H.A.O. Hill, P.J. Dobson, P.A. Leigh, W.S. McIntire, Sensors 1 (2001) 18.
[11] F.L. Cheng, M.L. Zhang, H. Wang, Sensors 5 (2005) 245.
[12] J.P. Kloock, Y.G. Mourzina, J. Schubert, M.J. Schöning, Sensors 2 (2002) 356.
[13] Y.G. Mourzina, M.J. Schöning, J. Schubert, W. Zander, A. Legin, Y.G. Vlasov, H. Lüth, Anal. Chim. Acta 433 (2001) 103.
[14] M.J. Schöning, Y.G. Mourzina, J. Schubert, W. Zander, A. Legin, Y.G. Vlasov, H. Lüth, Electroanalysis 13 (2001) 727.
[15] Y.G. Mourzina, M.J. Schöning, J. Schubert, W. Zander, A. Legin, Y.G. Vlasov, P. Kordos, H. Lüth, Sens. Actuators B 71 (2000) 13.
[16] A. Simonis, T. Krings, H. Lüth, J. Wang, M.J. Schöning, Sensors 1 (2001) 183.
[17] Y.G. Vlasov, A. Legin, A. Rudnitskaya, Sens. Actuators B 44 (1997) 532.
[18] C.K. Ho, A. Robinson, D.R. Miller, M.J. Davis, Sensors 5 (2005) 4.
[19] H. Zhou, M.L. Homer, A.V. Shevade, M.A. Ryan, Sensors 6 (2006) 1.
[20] A.V. Kalch, Sensors 5 (2005) 97.
[21] R.G. Osuna, IEEE Sensors 2 (2002) 189.
[22] M. Segal, Sensors 4 (2004) 181.
[23] H.A. Arida, J.P. Kloock, M.J. Schöning, Sensors 6 (2006) 435.
[24] N. Abramova, Y. Borisov, A. Bratov, P. Gavrilenko, C. Dominguez, V. Spiridonov, E. Suglobova, Talanta 52 (2000) 533.
[25] V.K. Gupta, R.N. Goyal, N. Bachheti, L.P. Singh, S. Agarwal, Talanta 68 (2) (2005) 193.
[26] A.K. Jain, V.K. Gupta, L.P. Singh, J.R. Raisoni, Talanta 66 (5) (2005) 1353.
[27] V.K. Gupta, R. Prasad, Azad Kumar, J. Appl. Electrochem. 33 (2003) 381.
[28] R.H. Molina, A. Mederos, P. Gili, S. Domínguez, F. Lloret, J. Cano, M. Julve, C.R. Pérez, X. Solans, Chem. Soc. Dalton Trans. (1997) 4327.

Design and application of a flow cell for carbon-film based electrochemical enzyme biosensors

Madalina M. Barsan [a], Janja Klinčar [b,c], Martin Batič [b], Christopher M.A. Brett [a,*]

[a] *Departamento de Química, Universidade de Coimbra, 3004-535 Coimbra, Portugal*
[b] *Food Science and Technology Department, Biotechnical Faculty, University of Ljubljana, Jamnikarjeva 101, 1000 Ljubljana, Slovenia*
[c] *Research Institute for Viticulture and Enology of the Ministry of Agriculture and Rural Development, Urihegy 5/A, 6001 Kecskemét, Hungary*

Abstract

A flow cell has been designed for use with an electrochemical enzyme biosensor, based on low-cost carbon-film electrodes. Three types of mediators were used: cobalt and copper hexacyanoferrates and poly(neutral red) (PNR), covered with glucose oxidase (GOx) immobilised by cross-linking with glutaraldehyde in the presence of bovine serum albumin or inside a oxysilane sol–gel network. Mixtures of sol–gel precursors were made from 3-aminopropyl-triethoxysilane (APTOS) together with methyltrimethoxysilane (MTMOS), methyltriethoxysilane (MTEOS), tetraethyloxysilane (TEOS) or 3-glycidoxypropyl-trimethoxysilane (GOPMOS), and the best chosen for encapsulation. Optimisation in batch mode, using amperometric detection at fixed potential, showed the PNR-GOx modified carbon-film electrodes to be best for flow analysis for both glutaraldehyde and sol–gel enzyme immobilisation. Both types of enzyme electrode were tested under flow conditions and the reproducibility and stability of the biosensors were evaluated. The biosensors were used for fermentation monitoring of glucose in grape must and interference studies were also performed.
© 2006 Elsevier B.V. All rights reserved.

Keywords: Flow cell; Electrochemical enzyme biosensor; Enzyme immobilisation; Sol–gel; Glucose determination; Grape must

1. Introduction

Biosensors have found extensive application in different fields such as medicine, food quality and safety control and environment pollution monitoring. The selectivity of the biosensor for the target analyte is mainly determined by the biorecognition element, while the selectivity of the biosensor is greatly influenced by the transducer [1]. Very often the biorecognition elements are enzymes [2] and a good functioning of an electrochemical enzyme biosensor requires a redox mediator, which shuttles electrons between the recognition element and the transducer and reduces interferences since lower applied potentials can be employed.

More than 90% of commercially available enzyme based biosensors and analytical kits contain oxidase enzymes, and the hydrogen peroxide produced is monitored. When metal hexacyanoferrates, such as copper hexacyanoferrate (CuHCF) or cobalt hexacyanoferrate (CoHCF), are deposited onto the electrode, they can react electrocatalytically with hydrogen peroxide [3]. Since the electrocatalytic process proceeds at a low applied potential (∼0 V versus SCE), it is possible to eliminate many of the reactions of interfering species. Such redox mediator-modified electrodes are, therefore, currently being investigated to develop sensors with a suitable catalytic surface for the amperometric detection of hydrogen peroxide, at low potentials, produced by an oxidase [4], such as on carbon-film electrode substrates [5].

The phenazine neutral red (NR) was found to be a convenient artificial enzyme substrate and as a redox mediator for electrochemical investigations of biological redox systems [6]. It has a much lower redox potential than analogous phenothiazine and phenoxazines, due to the second heteroatom which is nitrogen instead of a divalent oxygen or sulphur [6] and has a formal potential at pH 7 of −0.325 V versus SHE. The chemical structure of NR, with an amino functionality located on the heteroaromatic phenazine ring, makes it amenable to electropolymerisation. The monomer can be polymerised from neutral aqueous solutions producing stable redox-active layers [7].

Immobilisation of enzyme may lead to changes in enzyme structure, stability and specificity, differing from that of the enzyme in homogeneous solution. Therefore, great interest is devoted to find an immobilisation matrix, which can retain its specific biological function. Glutaraldehyde has usually been used as a protein cross-linking agent in biosensor fabrication using carbon-film electrodes [8–13]. Biosensors for glucose determination have been reported using ferrocene [9], CoHCF [10], methyl viologen [11] and PNR [12] as redox mediators, and multienzyme sensors have been used for analysis of various foodstuffs [13]. It is a bifunctional cross-linking agent which reacts with lysine residues on the exterior of the proteins. Addition of bovine serum albumin accelerates the cross-linking process, because of the 35–40 lysine groups present in its structure.

An alternative immobilisation strategy is provided by sol–gel networks. In recent years sol–gel chemistry has paved a versatile path for the immobilisation of biomolecules with a good stability and good activity retention. Enzymes such as horseradish peroxidase (HRP), glucose oxidase (GOx) and acetylcholinesterase (AChE) have been successfully immobilised into oxysilane sol–gel matrices and employed in sensing applications, e.g. [14–17]. The sol–gel reactions proceed by hydrolysis of an alkoxide precursor under acid or basic conditions and condensation of the hydroxylated monomers to form a porous siloxane polymer gel [18,19]. Enzyme encapsulation in sol–gel rather than in other matrices can improve some properties such as operational stability and activity compared to cross-linking with glutaraldehyde, and a longer linear range [14,20–22]. Sol–gel biosensors using PNR and CuHCF as mediators were characterized by cyclic voltammetry, electrochemical impedance spectroscopy and atomic force microscopy [15].

The objective of this work was to develop an electrochemical enzyme biosensor, based on low-cost carbon-film resistor electrodes [23–25], for use in flow analysis. The redox mediators cobalt and copper hexacyanoferrates and poly(neutral red) were tested together with enzyme immobilisation by cross-linking with glutaraldehyde in the presence of bovine serum albumin or by a novel sol–gel GOx encapsulated biosensor with PNR mediator using a combination of oxysilane sol–gel precursors. After optimisation in batch experiments, the best electrodes with PNR mediator were tested in a specially designed flow cell and used to analyse samples of wines. Reproducibility, stability and storage were also evaluated.

2. Experimental

2.1. Reagents

Glucose oxidase (GOx, EC 1.1.3.4, from *Aspergillus niger*, 24 units/mg) and phenol were obtained from Fluka, Switzerland, α-D(+)-glucose, glutaraldehyde (GA) 25% (v/v), bovine serum albumin (BSA), were from Sigma, Germany, D(+) fructose, L(−) ascorbic acid from Sigma Chemical Co., St. Louis, USA, citric acid, potassium hexacyanoferrate(III) and copper(II) chloride dihydrate were purchased from Merck, Germany. Nafion 5% (v/v) in ethanol and neutral red (65% dye content) were from

Sigma–Aldrich, Germany and tartaric acid from PAHI, Lisbon, Portugal.

For sol–gel enzyme encapsulation, five different oxysilanes were tested in mixtures: 3-aminopropyl-triethoxysilane (APTOS) and tetraethyloxysilane (TEOS) from Fluka, Switzerland, and 3-glycidoxypropyl-trimethoxysilane (GOPMOS), methyltriethyloxysilane (MTEOS) and methyltrimethyloxysilane (MTMOS), all from Aldrich, Germany.

For electrochemical experiments, the supporting electrolyte was sodium phosphate buffer saline (NaPBS) (0.1 M phosphate buffer + 0.05 M NaCl, pH 7.0), prepared from sodium dihydrogenphosphate, di-sodium hydrogenphosphate and sodium chloride (Riedel-de Haën). Polymerisation of neutral red was carried out in an electrolyte composed of 0.025 M potassium phosphate buffer solution and 0.1 M KNO_3 (pH 6).

A stock solution of 1.0 M glucose was prepared in supporting electrolyte at least 1 day before use, to permit equilibration of α and β anomers of D-glucose; it was kept in the refrigerator and used within 1 week.

Millipore Milli-Q nanopure water (resistivity > 18 MΩ cm) was used for preparation of all solutions. Experiments were performed at room temperature ($25 \pm 1\,^{\circ}$C).

2.2. Apparatus

For batch experiments, a three-electrode electrochemical cell of volume 10 cm^3 was used, containing the enzyme modified carbon-film resistor as working electrode, a platinum foil counter electrode and a saturated calomel electrode (SCE) as reference.

A flow cell was specially designed to accommodate the cylindrical carbon-film resistor electrode-based biosensor as working electrode, with a miniature Ag/AgCl (3 M KCl) electrode as reference upstream and a stainless steel tube downstream in the cell exit as counter electrode. After flow rate optimisation in order to achieve the best compromise between sensitivity and consumption of carrier electrolyte, under the optimised conditions a constant flow rate of 13.9 μl s^{-1} was employed, using a peristaltic pump (Pharmacia, Fine Chemicals, Model P-3) connected to a 1-m length of 1 mm internal diameter Teflon tubing to damp flow oscillations.

All electrochemical measurements were performed using a computer-controlled μ-Autolab Type II potentiostat-galvanostat running with GPES (General Purpose Electrochemical System) for Windows Version 4.9, software (EcoChemie, Utrecht, The Netherlands).

The pH-measurements were carried out with a CRISON 2001 micro pH-meter at room temperature.

HPLC measurements for glucose in grape must were performed using a K-120 pump with an Aminex HPX-87H (369 mm × 7.8 mm) column containing a sulphonated divinyl benzene-styrene copolymer as support, with detection by differential refractometer (Knauer, Germany). The column was operated at 36 °C and eluted with 5 mM sulphuric acid (Carlo Erba, Italy) at flow rate 0.6 ml min^{-1}. Peak areas were integrated with Knauer Eurochrome 2000 software and interface box. For sample analysis the external standard method was used. Before analysis, samples were filtered through Chromafil®

membrane filters (Macherey-Nagel, Germany) with 0.2 µm pore size. A constant volume of 20 µl sample or standard solution was injected via a 20 µl sample loop using an injection valve from NiBest, CA, USA.

2.3. Electrode and mediator film preparation

Electrodes were made from carbon-film electrical resistors (2 Ω resistance) of length 6 mm and diameter 1.5 mm, as described elsewhere [23]. The exposed geometric area was ~0.20 cm^2. Before use, the electrodes were electrochemically pre-treated by cycling the potential between 0.0 and +1.0 V versus Ag/AgCl in order to decrease the background currents and to increase the potential window. In the case of hexacyanoferrate deposition, the electrolyte was 0.05 M KCl and in the case of PNR deposition, 0.025 M potassium phosphate buffer solution, pH 5.5 was used.

Films of cobalt(II)-hexacyanoferrate (CoHCF) were electrochemically deposited. This was accomplished by cycling the potential 15 times between 0.0 and 0.9 V versus SCE at a scan rate of 50 mV s^{-1}, in a freshly prepared solution containing: 0.5 mM CoCl$_2$·6H$_2$O, 0.25 mM K$_3$Fe(CN)$_6$, 0.05 M NaCl at pH 3.0 (pH adjusted with HCl). Subsequently, the CoHCF film electrodes were stabilised for 1 h in 0.05 M NaCl, pH 3.0. They were then left to dry at room temperature [5,10].

Copper(II)-hexacyanoferrate (CuHCF) was deposited in three different ways: by potential cycling between 0.25 and +0.9 V versus SCE for 25 cycles at scan rate 50 mV s^{-1}, by galvanostatic deposition applying a constant current (100 µA cm^{-2}) for 300 s and by direct adsorption, immersing the carbon-film electrode substrate in the deposition solution. Solutions contained 10 mM CuCl$_2$·2H$_2$O, 10 mM K$_3$Fe(CN)$_6$ and 100 mM KCl for all three types of deposition. The solutions were freshly prepared before used and adjusted to pH 3.0 with HCl [5]. After film formation, the electrodes were dried in a hot-air stream (3–4 min) and left for 24 h in air, at room temperature, to stabilise.

Unfortunately, the structure of the CuHCF mediator film did not lead to good adhesion between the mediator and the enzyme layer. It is also believed that copper ions interact with enzyme molecules leading to a decrease of its biological activity. To avoid this problem, a different strategy was adopted in which mediator powder was added to the enzyme solution and placed on the top of the carbon-film electrode substrate (see below).

The preparation of poly(neutral red) films was carried out by cyclic voltammetry from a solution containing 1 mM neutral red in 0.025 M KPB + 0.1 M KNO$_3$, pH 6.0. The potential was cycled from −1.0 to 1.0 V versus Ag/AgCl at a scan rate 50 mV s^{-1} for 15 cycles [12].

Glucose oxidase was immobilised using two methods. In the first, glutaraldehyde (GA) cross-linking, a volume of 35 µl of an enzyme mixture contain 25 µl enzyme solution (100 mg glucose + 40 mg BSA per ml 0.1 M NaPBS, pH 7) and 10 µl GA (2.5%, v/v diluted in water) was prepared. Of this mixture, 10 µl was dropped onto the electrode surface and left to dry at room temperature during 1 h [10]. To prepare the CuHCF/GOx modified biosensors the enzyme mixture contained: 10% (w) CuHCF
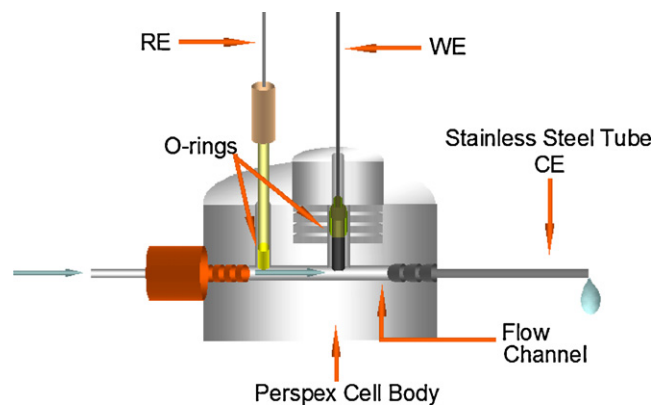
Fig. 1. Cross-section of flow-through cell, diameter 5 cm, height 2.5 cm; flow channel 1.5 mm diameter. RE, Ag/AgCl reference electrode; WE, carbon-film working electrode; CE, counter electrode.

powder, 25 µl enzyme solution and 9 µl GA 2.5%; the enzyme solution was the same as for the preparation of PNR/GOx and CoHCF/GOx biosensors.

For the second method, sol–gel enzyme encapsulation, sol–gel solutions were prepared using mixtures of APTOS and one other sol–gel precursor in NaPBS solution, pH 7.0. Two sol–gel mixture were found to be most appropriate for enzyme encapsulation, which contained APTOS:GOPMOS and APTOS:MTMOS, both in the ratio 1:3. About 15 µl of sol–gel solution was mixed with 15 µl of enzyme solution (100 mg glucose + 40 mg BSA per ml of 0.1 M NaPBS, pH 7) and 5 µl of glycerol to improve homogeneity.

The enzyme layer of all biosensors prepared was coated with 5 µl of Nafion (5% solution) to improve the physical robustness of the sensor and to act as a barrier against interferences.

3. Results and discussion

The principal objective of this work is to develop an efficient and reproducible analytical flow cell method for continuous monitoring, so that it is particularly important that the biosensor assembly be robust and the enzyme activity remain unchanged over time. For this reason, a comparison between the three mediators and the two enzyme immobilisation techniques was carried out in batch mode before application in the flow cell and testing with natural samples.

3.1. Flow cell

The specially designed cylindrical flow cell was constructed from Perspex and is shown in Fig. 1 in cross-section. Samples are introduced 10 cm before the cell inlet. The working electrode is centred in the cell and located between the upstream reference electrode and the downstream counter electrode; the inlet tubing is of 1 mm internal diameter and the flow channel is 1.5 mm in diameter. Various flow rates were tested by amperometry using the assembled biosensors (see below). The results of these studies were that the best compromise between biosensor sensitivity and carrier solution consumption was the pump setting corresponding to 13.9 µl s^{-1}. At a lower flow rate of 6.9 µl s^{-1} the

sensitivity decreased by 37%. A higher flow rate increases the mass transfer of analyte to the electrode surface so an increase in response current should be obtained, but above $13.9\,\mu l\,s^{-1}$, no significant increase in sensitivity was observed, presumably due to kinetic limitations.

3.2. Mediator deposition

The modification of carbon-film electrodes with hexacyanoferrates has previously been described in detail [5]. Optimised deposition of CoHCF by potential cycling between 0.0 and 0.9 V versus SCE, as in Ref. [10], is shown in Fig. 2a. The modified electrodes were kept in 0.05 M NaCl supporting electrolyte, in this way yielding a stable CV response. As described in Section 2, electrodes modified by CuHCF films were found not to be as stable as CoHCF when covered with the sol–gel enzyme layer.

(a)

(b)
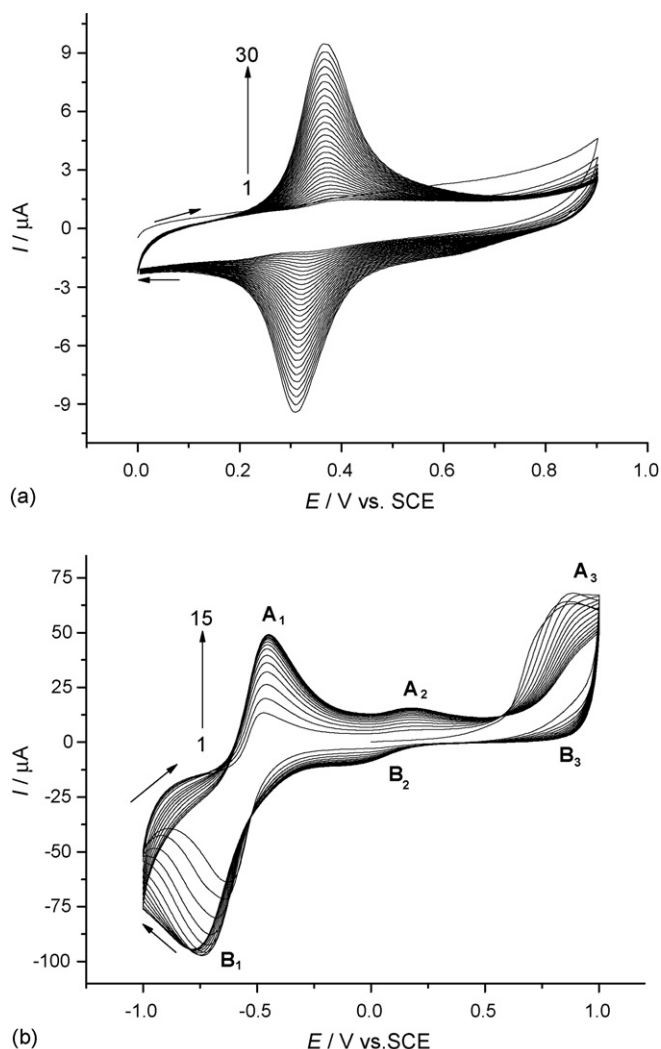
Fig. 2. Cyclic voltammograms showing growth of mediator films on carbon-film electrodes by potential cycling. (a) CoHCF from a solution containing 0.5 mM $CoCl_2 \cdot 6H_2O$, 0.25 mM $K_3Fe(CN)_6$, 0.05 M NaCl at pH 3; scan rate $= 50\,mV\,s^{-1}$; 30 cycles; (b) poly(neutral red) from a solution containing 1 mM neutral red, 0.025 M potassium phosphate buffer pH 6.0, 0.1 KNO_3; initial scan in positive direction from 0 V; scan rate $50\,mV\,s^{-1}$; 15 cycles.

Preparation of PNR films was done as in Ref. [12] by potential cycling from −1.0 to 1.0 V versus SCE for 15 cycles, see Fig. 2b. The 0.1 M KNO_3 electrolyte was chosen because of the observed catalytic effect of NO_3^- anions on neutral red polymerisation. After initial formation of a radical cation, the electropolymerisation is fast in the first 10 cycles after which the current increased less. The peak system B_1, A_1 corresponds to the reduction and reoxidation of the polymer, in the presence of aqueous medium or hydrogen ions, respectively [26–30], in the same potential range as for reduction and oxidation of the neutral red monomer.

3.3. Evaluation of glucose biosensors in batch mode

3.3.1. Immobilisation of GOx by cross-linking with GA

The biosensors with a film of one of the three different mediators covered by GOx immobilised by cross-linking with GA were tested in a batch cell in order to compare their properties. The applied potential was 0.0 V for the CoHCF-GOx biosensor, +0.05 V for the CuHCF-GOx biosensor and −0.35 V versus SCE for the PNR-GOx biosensor, optimum values found in previous work [5,10,15]. After stabilisation of the current baseline, amperometric measurements were performed, by injection of glucose into 0.1 M NaPBS solution containing the biosensor, under continuous stirring. The results obtained are shown in Table 1.

The PNR-GOx biosensor had the best sensitivity of $820\,nA\,mM^{-1}$ compared with 38.5 for CuHCF-GOx and $9.6\,nA\,mM^{-1}$ for CuHCF-GOx sensors, as well as the lowest detection limit (46 μM) and a linear range up to 1.2 mM. PNR-GOx was therefore chosen for use in the flow cell and PNR was also chosen as the redox mediator for testing the biosensors with enzyme encapsulated in a sol–gel matrix.

3.3.2. Sol–gel immobilisation of GOx

3.3.2.1. Optimisation of sol–gel composition and preparation.
Different sol–gel mixtures were tested and analysed, see Table 2, all containing APTOS as one of the sol–gel components. Solutions were prepared by first mixing APTOS with 0.1 M NaPBS pH 7.0 and then adding the second sol–gel precursor in different volume ratios. Initially, the second monomer was added after mixing APTOS with NaPBS solution, but in all cases precipitation occurred. In order to avoid this problem, prior to adding the second monomer, the APTOS-NaPBS solution was neutralized with 1:1 HCl. The solutions were then intensively stirred and sonicated during 10–15 min and heated in a hot-air stream at ~70 °C for different times as necessary.

Table 1
Analytical data obtained from glucose calibration curves registered at CoHCF-, CuHCF- and PNR-GOx (GA) biosensors in batch analysis

Mediator	Sensitivity (nA mM^{-1})	Detection limit (μM)	K_M (mM)
CoHCF	9.6	140	4.2
CuHCF	38.5	130	5.0
PNR	820	54	6.0

Table 2
Sol–gel mixture preparation from different precursors

Sol–gel composition (µl)	Heating time (min)	Gelation time (h)	Other observations
APTOS:MTMOS:PBS:HCl 146.6:74.4:580:15	–	Prompt	Immediately after precursor mixing, a white precipitate is formed
APTOS:MTMOS:PBS:HCl 55:165:580:3	5	3	APTOS neutralized prior to MTMOS addition; enzyme goes into solution
APTOS:MTMOS:PBS:HCl 146.6:74.4:580:15	8	15	APTOS neutralized prior to MTMOS addition
APTOS:TEOS:PBS:HCl 146.6:74.4:580:15	–	24	Sol–gel dissolves from the electrode into solution
APTOS:TEOS:PBS:HCl 55:165:580:3		22	APTOS neutralized prior to TEOS addition; mixture not homogeneous
APTOS:MTEOS:PBS:HCl 74.4:146.6:580:10	5	Prompt	Gelation during heating
APTOS:MTEOS:PBS:HCl 110:110:580:20	15	Prompt	Gelation during heating
APTOS:GOPMOS:PBS:HCl 74.4:146.6:580:10	40	24	APTOS neutralized prior to GOPMOS addition
APTOS:GOPMOS:PBS:HCl 110:110:580:20	15	Prompt	Gelation during heating
APTOS:GOPMOS:PBS:HCl 55:165:580:20	–	8	APTOS neutralized prior to GOPMOS addition

Table 3
Analytical data obtained from glucose calibration curves at PNR-GOx (sol–gel) biosensors in batch analysis

Sol–gel mixture	Sensitivity ($\mu A\,mM^{-1}$)	Correlation coefficient (R^2)	Limit of detection (µM)
APTOS:GOPMOS:PBS:HCl 55:165:580:20	0.70	0.999	20
APTOS:MTMOS:PBS:HCl 55:165:580:3	0.39	0.998	73

It was not possible to find a good method to mix TEOS or MTEOS with APTOS. In the first case, the mixture was not homogeneous and in the second, prompt gelation occurred after a few minutes of heating, which was necessary to remove as much alcohol as possible, since it is prejudicial to the enzyme.

Two mixtures were found to be appropriate for enzyme encapsulation, using APTOS:GOPMOS 1:3 and APTOS:MTMOS 1:3, as mentioned in Section 2 and following the protocol described in Table 2.

3.3.2.2. Comparison of sol–gel precursor mixtures with the PNR-GOx biosensor. Using optimised mixtures of sol–gel precursors, PNR-GOx (sol–gel) biosensors were constructed and applied in batch analysis for glucose determination, performing amperometric measurements at fixed potential. Analytical data calculated from the calibration curves are shown in Table 3. A higher sensitivity was achieved with biosensors using the mixture APTOS:GOPMOS 1:3, also having a lower detection limit and a longer linear range, up to 1.1 mM. The relative standard deviation was found to be ∼3.6% ($n = 3$) in the case of APTOS:GOPMOS 1:3 and 7.6% ($n = 3$) for APTOS:MTMOS 1:3.

3.4. Flow analysis

3.4.1. Voltammetric behaviour of PNR-GOx biosensors

Since PNR-GOx biosensors had been identified as the ones with the most favourable response characteristics in batch analysis, they were evaluated for analysis in the flow cell using enzyme immobilisation by cross-linking with glutaraldehyde (BSA) or by sol–gel entrapment.

Cyclic voltammograms were recorded in the flow cell at these biosensors in 0.1 M NaPBS pH 7.0 electrolyte using a constant

flow rate of $13.9\,\mu l\,s^{-1}$, without and with the enzyme layer, Fig. 3. As can be seen, deposition of enzyme using the cross-linking method led to a decrease of the oxidation peak current by 44%, while in the case of sol–gel enzyme entrapment the oxidation peak current decreased by 74%. Nevertheless, PNR exhibits the same reversible behaviour after immobilisation of enzyme using either of the two techniques, with the same peak separation of 0.27 V.

3.4.2. Glucose determination at PNR-GOx biosensors

The two types of biosensor were applied to glucose determination in the flow cell at the optimised flow rate of $13.9\,\mu l\,s^{-1}$ (see Section 3.1). The carrier electrolyte solution was 0.1 M
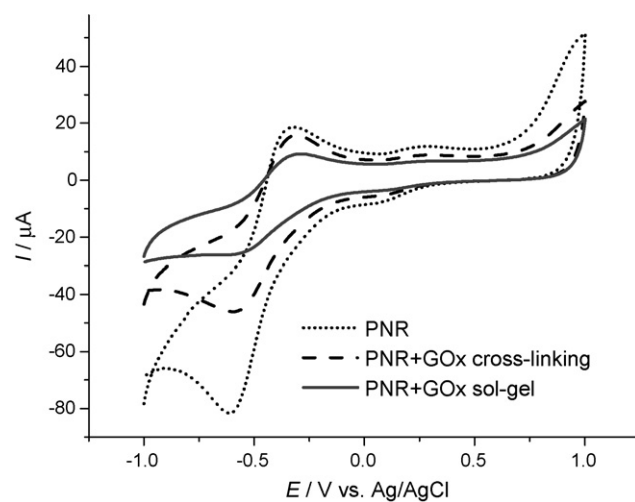

Fig. 3. Cyclic voltammograms in flow cell at PNR modified carbon-film electrodes and at PNR-GOx biosensors (GA, sol–gel) in 0.1 NaPBS, pH 7.0; scan rate = $50\,mV\,s^{-1}$.
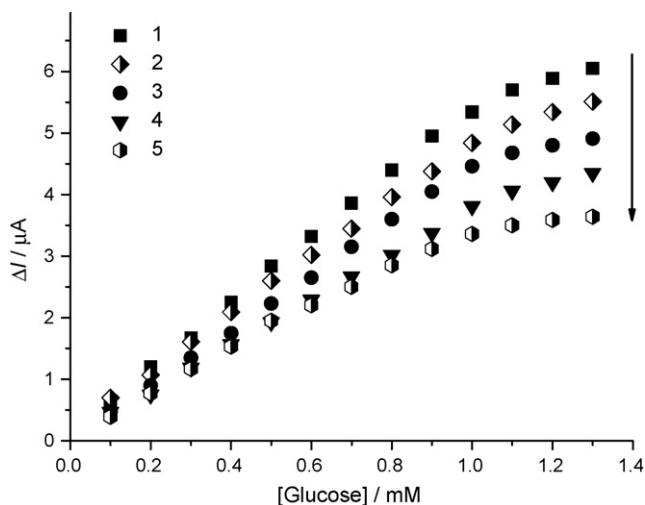
Fig. 4. Calibration curves for glucose at PNR-GOx (GA) biosensor, at −0.35 V vs. Ag/AgCl: 1, initially; 2, after 7 days; 3, after 14 days; 4, after 21 days; 5, after 30 days.

Fig. 5. Calibration curves for glucose at PNR-GOx (sol–gel) biosensor, at −0.35 V vs. Ag/AgCl: 1, initially; 2, after 4 days; 3, after 14 days; 4, after 35 days; 5, after 46 days.

NaPBS and glucose-containing solution was injected directly into the carrier stream.

3.4.2.1. PNR-GOx biosensor (GA). Fig. 4 shows calibration curves registered at the PNR-GOx (GA) biosensor. The biosensor response was found to be higher under flow conditions than in stationary solution, as expected, with a sensitivity of $5.34 \, \mu A \, mM^{-1}$, an increase of a factor of 5, and a detection limit of 35 μM.

In order to examine the reproducibility of the biosensor, the amperometric response to glucose at three PNR-GOx (GA) modified electrodes was recorded in the same experimental conditions. The biosensors showed a linear range up to 0.9 mM and the corresponding detection limit (signal-to-noise ratio = 3) was $36.0 \pm 3.2 \, \mu M$ ($n = 3$). The biosensor sensitivity was $5.28 \pm 0.10 \, \mu A \, mM^{-1}$. Thus, the sensors showed a sufficiently good, reproducible behaviour to be used for on-line measurements. Kinetic studies of the immobilised enzyme were also carried out. The Michaelis–Menten constant was calculated from Lineweaver–Burk plots and the value obtained was $5.1 \pm 0.4 \, mM$ ($n = 3$).

A good biosensor for flow analysis has to be robust and to show a good long-term stability. In order to check these characteristics, the biosensors were tested during 1 month, see Fig. 5. After 1 week the sensitivity decreases by only 13.1%, continuing to decrease linearly until the end of the month, 30 days, when it reached a value of $3.32 \, \mu A \, mM^{-1}$, corresponding to 62% of the initial value. At this point in time, the enzyme layer also showed evidence of beginning to crack.

3.4.2.2. PNR-GOx biosensor (sol–gel). The PNR-GOx biosensor with enzyme trapped in sol–gel made from the optimised precursor ratio of APTOS:GOPMOS 1:3 was used for the determination of glucose in the flow cell, at −0.35 V versus Ag/AgCl. As seen in Fig. 5, a lower sensitivity but a longer linear range than in the PNR-GOx (GA) biosensor was obtained. The sensitivity was $0.81 \pm 0.02 \, \mu A \, mM^{-1}$ and the detection limit 62.0 μM. The
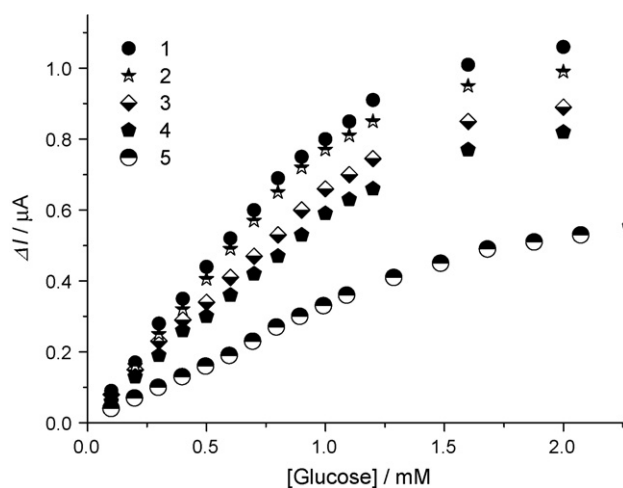
calculated Michaelis–Menten constant from Lineweaver–Burk plots was $3.2 \pm 0.8 \, mM$.

The biosensor was tested during 46 days, 2–3 times per week. Some of these calibration curves are plotted in Fig. 5: the sensitivity decreases with time, reaching 63% of the initial value after 46 days. This decrease is less than at the GA-immobilised enzyme, demonstrating that sol–gel encapsulation of the enzyme leads to a biosensor that is stable over a longer period. Other work cited in the literature regarding the application of a GOx biosensor in flow analysis is not focused on long-term stability evaluation of the electrochemical biosensor. A comparison regarding the sensitivity and the detection limit of the biosensor showed a very good performance of the developed system [31–35]. The $4000 \, nA \, mM^{-1} \, cm^{-2}$ sensitivity of the sol–gel biosensor developed here is much higher when compared with other sol–gel biosensors developed for flow analysis with a sensitivity of $96 \, nA \, mM^{-1}$ or $81 \, nA \, mM^{-1} \, cm^{-2}$ [31,34] or with other biosensor assemblies such as an epoxy-graphite-TTF·TCNQ-GOD biocomposite developed for flow analysis with a sensitivity of $23.5 \, nA \, mM^{-1} \, cm^{-2}$ [35].

3.5. Interference study in the flow cell

The final aim of this work is to use the flow cell biosensors for monitoring of glucose during fermentation of grape must or in wine. A study of interferences from compounds usually present in wine was therefore performed and the results obtained for the two types of enzyme immobilisation, are presented in Table 4. Fructose, the main sugar present in wine besides glucose, decreases the biosensor response by only 4% for the PNR-GOx biosensor (GA) and 7% for the PNR-GOx biosensor (sol–gel). From the acids mainly found in wine, only ascorbic acid interferes with glucose, but only slightly decreases the response to glucose with 20 for the first type of biosensor or 12% for the second one. The interference from phenol does not need to be taken into account in glucose measurements, since its concentration is small in wine.

Table 4
Interference of some compounds on the response to glucose at PNR-GOx biosensors

Compound	Relative response (%) 2:1 (molar ratio) interferent compound:glucose	
	PNR-GOx (GA)	PNR-GOx (sol–gel)
Fructose	96	93
Acetic acid	100	92
Tartaric acid	93	96
Phenol	86	89
Ascorbic acid	80	88

4. Conclusions

A new flow cell, using electrochemical glucose redox-mediated enzyme biosensors, based on low-cost carbon-film resistors, has been designed and evaluated. Of the three types of mediator film tested – Co(II) hexacyanoferrate, Cu(II) hexacyanoferrate and poly(neutral red) – PNR was found to lead to the best results. Glucose oxidase enzyme was immobilised by cross-linking with glutaraldehyde or by encapsulation in a sol–gel matrix. Various mixtures of sol–gel precursor were tested, the best being GOPMOS and APTOS in a proportion of 3:1. The biosensors were tested in batch analysis and the stability and reproducibility evaluated. Both biosensors were tested in flow analysis leading to the conclusion that sol–gel encapsulation led to superior sensor characteristics. Biosensors with cross-linked enzyme were used for fermentation monitoring of glucose in three different musts and the obtained glucose values compared with HPLC values. The results show that the developed biosensors can be successfully applied to glucose monitoring in wines and during grape fermentation processes.

3.6. Flow analysis of glucose in natural samples

The biosensors based on the PNR polymer-film were applied to the amperometric determination of glucose at -0.35 V versus Ag/AgCl (3 M KCl). The results obtained in grape must samples, collected at different fermentation times in a winery are represented in Fig. 6. The concentrations for glucose were compared with those obtained using HPLC.

Wine samples were analysed using the standard addition method and also from calibration curves. The samples were diluted 250, 500 and 1000 times in 0.1 M NaPBS.

The recovery of the analytical signal for each of the must samples is 105, 106, 92, 101, 98 and 102%, respectively [36], and the maximum loss in biosensor activity after the sample assay was 4%.

As can be seen in Fig. 6, the glucose concentration in the grape must decreases during the fermentation process, as expected. The fermentation profile for glucose is very similar using the two determination methods. The differences can be explained taking into account that the preservation conditions of the samples were different, and it was not possible to filter the samples immediately after they were removed from the fermentation vat, so that the yeasts could cause further fermentation after sample collection.

Fig. 6. Glucose determination in grape must during fermentation with PNR-GOx (GA) biosensor; comparison with HPLC results.

References

[1] J. Castillo, S. Gáspár, S. Leth, M. Niculescu, A. Mortari, I. Bontidean, V. Soukharev, S.A. Dorneanu, A.D. Ryabov, E. Csöregi, Sens. Actuators B: Chem. 102 (2004) 179.
[2] J.-C. Vidal, E. Garcia-Ruiz, J.-R. Castillo, Microchim. Acta 143 (2003) 93.
[3] F.W. Scheller, D. Pfeiffer, F. Schubert, R. Reneberg, D. Kirstein, in: A.P.F. Turner, I. Karube, G.S. Wilson (Eds.), Biosensors: Fundamental and Applications, Oxford University Press, Oxford, 1987.
[4] L. de Mattos, L. Gorton, T. Laurell, A. Malinauskas, A.A. Karyakin, Talanta 52 (2000) 792.
[5] R. Pauliukaite, M. Florescu, C.M.A. Brett, J. Solid State Electrochem. 9 (2005) 354.
[6] A.A. Karyakin, E.E. Karyakina, H.L. Schmidt, Electroanalysis 11 (1999) 149.
[7] A.A. Karyakin, O.A. Bobrova, E.E. Karyakina, J. Electroanal. Chem. 399 (1995) 181.
[8] M. Florescu, C.M.A. Brett, Talanta 65 (2005) 306.
[9] M.E. Ghica, C.M.A. Brett, Anal. Lett. 38 (2005) 907.
[10] M. Florescu, C.M.A. Brett, Anal. Lett. 37 (2004) 871.
[11] M.E. Ghica, C.M.A. Brett, Anal. Chim. Acta 532 (2005) 145.
[12] M.E. Ghica, C.M.A. Brett, Electroanalysis 18 (2006) 748.
[13] S. De Luca, M. Florescu, M.E. Ghica, A. Lupu, G. Palleschi, C.M.A. Brett, D. Compagnone, Talanta 68 (2005) 171.
[14] R. Pauliukaite, C.M.A. Brett, Electrochim. Acta 50 (2005) 4973.
[15] R. Pauliukaite, A.-M. Chiorcea-Paquim, A.M. Oliveira Brett, C.M.A. Brett, Electrochim. Acta 52 (2006) 1.
[16] P.C. Pandey, S. Upadhyay, I. Tiwari, V.S. Tripathi, Electroanalysis 11 (1999) 1251.
[17] P.C. Pandey, S. Upadhyay, I. Tiwari, V.S. Tripathi, Sens. Actuators B: Chem. 72 (2001) 224.
[18] T. Noguer, D. Szydlowska, J.-L. Marty, M. Trojanowicz, Polish J. Chem. 78 (2004) 1679.
[19] A.C. Pierre, Biocatal. Biotransfor. 22 (2004) 145.

[20] O. Lev, Z. Wu, S. Bharathi, V. Glezer, A. Modestov, J. Gun, L. Rabinovich, S. Sampath, Chem. Mater. 9 (1997) 2354.
[21] L. Rabinovich, O. Lev, Electroanalysis 13 (2001) 265.
[22] G. Shustak, S. Marx, I. Turyan, D. Mandler, Electroanalysis 15 (2003) 398.
[23] C.M.A. Brett, L. Angnes, H.-D. Liess, Electroanalysis 13 (2001) 765.
[24] O.M.S. Filipe, C.M.A. Brett, Electroanalysis 16 (2004) 994.
[25] C. Gouveia-Caridade, C.M.A. Brett, Electroanalysis 17 (2005) 549.
[26] C. Kuhnhardt, J. Electroanal. Chem. 369 (1994) 71.
[27] P.J. Kulesza, M.A. Malik, S. Zamponi, M. Berretoni, R. Marassi, J. Electroanal. Chem. 397 (1995) 288.
[28] J.M. Bauldreay, M.D. Archer, Anal. Chim. Acta 28 (1983) 1515.
[29] T. Selvaraju, R. Ramaraj, Electrochem. Commun. 5 (2003) 667.
[30] D. Benito, J.J. Garcia-Jareño, J. Navarro-Laboulais, F. Vincente, J. Electroanal. Chem. 446 (1998) 47.
[31] V.B. Kandimalla, V.S. Tripathi, H. Ju, Biomaterials 27 (2006) 1167.
[32] E. Maestre, I. Katakis, A. Narváez, E. Domínguez, Biosens. Bioelectron. 21 (2005) 774.
[33] C.G. Tsiafoulis, A.B. Flourou, P.N. Trikalitis, T. Bakas, M.I. Prodromidis, Electrochem. Commun. 7 (2005) 781.
[34] C.M.C.M. Couto, A.N. Araújo, M.C.B.S.M. Montenegro, J. Rohwedder, I. Raimundo, C. Pasquini, Talanta 56 (2002) 997.
[35] X. Llopis, A. Merkoçi, M. del Valle, S. Alegret, Sens. Actuators B 107 (2005) 42.
[36] D.T. Burns, K. Danzer, A. Townshend, Pure Appl. Chem. 74 (2002) 2201.

Soluble manganese(IV) as a chemiluminescence reagent for the determination of opiate alkaloids, indoles and analytes of forensic interest

Allyson J. Brown [a], Claire E. Lenehan [b], Paul S. Francis [a],
David E. Dunstan [c], Neil W. Barnett [a],*

[a] *School of Life and Environmental Sciences, Deakin University, Geelong, Victoria 3217, Australia*
[b] *School of Chemistry, Physics and Earth Sciences, Flinders University, South Australia 5001, Australia*
[c] *Department of Chemical and Biomolecular Engineering, The University of Melbourne, Victoria 3010, Australia*

Abstract

We present the results of our investigations into the use of soluble manganese(IV) as a chemiluminescence reagent, which include a significantly faster method of preparation and a study on the effect of formaldehyde and orthophosphoric acid concentration on signal intensity. Chemiluminescence detection was applied to the determination of 16 analytes, including opiate alkaloids, indoles and analytes of forensic interest, using flow injection analysis methodology. The soluble manganese(IV) reagent was less selective than either acidic potassium permanganate or tris(2,2′-bipyridyl)ruthenium(III) and therefore provided a more universal chemiluminescence detection system for HPLC. A broad spectral distribution with a maximum at 730 ± 5 nm was observed for the reaction between the soluble manganese(IV) and a range of analytes, as well as the background emission from the reaction with the formaldehyde enhancer. This spectral distribution matches that reported for chemiluminescence reactions with acidic potassium permanganate, where a manganese(II) emitting species was elucidated. This provides further evidence that the emission evoked in reactions with soluble manganese(IV) also emanates from a manganese(II) species, and not bimolecular singlet oxygen as suggested by previous authors.
© 2006 Elsevier B.V. All rights reserved.

Keywords: Soluble manganese(IV); Chemiluminescence spectra; Flow injection analysis; Formaldehyde enhancement; Monolithic column HPLC

1. Introduction

Since our initial evaluation of soluble manganese(IV) as a chemiluminescence reagent [1], this chemistry has been applied to the determination of various inorganic and organic analytes (Table 1) [2–11]. In each of these previous studies, the manganese(IV) reagent was prepared by the method of Jáky and Zrinyi [12], where solid manganese dioxide was formed from the reduction of potassium permanganate by sodium formate and dissolved in 3 mol L^{-1} orthophosphoric acid overnight, following ultrasonication. The chemiluminescence evoked in reactions

with the manganese(IV) reagent can be improved by the addition of formaldehyde [1–11], but investigations into this enhancement, including conditions to provide the greatest signal-to-noise ratio, have been limited. Lu and co-workers [3,4,6,9,11] have suggested that the chemiluminescence from the reaction between manganese(IV) and formaldehyde in the presence of various analytes emanates from singlet molecular oxygen. However, this conflicts with our previous evidence for emission from an excited manganese(II) species [1,13]. In this paper, we present a series of investigations into the use of soluble manganese(IV) as a chemiluminescence reagent, including the preparation method, the effect of formaldehyde on chemiluminescence intensity, the nature of the emitting species, and the application of this chemistry to the determination of analytes of interest in process analysis, clinical diagnostics and forensic science.

* Corresponding author. Tel.: +61 3 52271409; fax: +61 3 52271040.
E-mail address: barnie@deakin.edu.au (N.W. Barnett).

Table 1
Detection limits reported for the chemiluminescence reactions of various analytes with the soluble manganese(IV) reagent

Analyte	Detection limit (mol L^{-1})	Reference
Analgin	4.0×10^{-8}	[7]
Ascorbic acid	5.0×10^{-8}	[2]
Ascorbic acid	2.0×10^{-8}	[3]
Cefazolin sodium	4.2×10^{-7}	[9]
Cefoperazone sodium	3.0×10^{-7}	[9]
Cefradine	2.8×10^{-8}	[9]
Ceftriaxone sodium	3.0×10^{-9}	[9]
Ciprofloxacin	3.0×10^{-8}	[8]
Codeine	5.0×10^{-8}	[1]
Indomethacin	1.0×10^{-7}	[6]
Iron(II)	5.0×10^{-7}	[1]
Manganese(II)	2.5×10^{-7}	[1]
Metamizol sodium	2.0×10^{-7}	[5]
Morphine	7.5×10^{-8}	[1]
Norfloxacin	3.0×10^{-8}	[8]
Ofloxacin	5.0×10^{-8}	[8]
Sulfadiazine	1.2×10^{-7}	[11]
Sulfaguanidine	9.3×10^{-8}	[11]
Sulfamethoxazole	7.8×10^{-8}	[11]
Tamoxifen	1.0×10^{-7}	[10]
L-Tyrosine	1.0×10^{-6}	[4]

2. Experimental

2.1. Instrumentation

2.1.1. Flow injection analysis

A flow injection analysis manifold (Fig. 1a) was used, where both the soluble manganese(IV) (5×10^{-4} mol L^{-1}) and formaldehyde carrier streams were propelled (2.7 mL min^{-1}) through PVC tubing (1.02 mm i.d., ProTech. Group, Queensland, Australia) using a peristaltic pump (Gilson Minipuls 3, John Morris Scientific, Melbourne, Australia). All other manifold tubing was PTFE (0.8 mm i.d., Chromalytic Technology, Melbourne, Australia). Standard solutions (50 μL) were injected into the carrier stream using a six-port injection valve (Valco

(a)

(b)
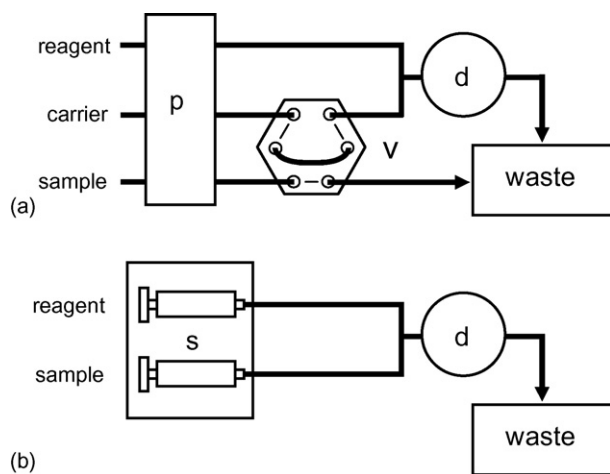
Fig. 1. (a) Flow injection analysis and (b) stopped-flow analysis manifolds. p, peristaltic pump; s, syringe pump; v, 6-port injection valve; d, chemiluminescence detector.

Instruments, Houston, TX, USA). The two streams were merged at a T-piece and reacted in a coiled Teflon flow-cell (200 μL, 0.8 mm i.d.) mounted flush between a piece of mirrored glass and the window of an extended range photomultiplier tube (Thorn EMI Model 9828SB, ETP Ltd., Middlesex, UK) operated at 1000 V, provided by a stable power supply (Thorn EMI Electron Tubes Power Supply, PM28BN). The detection system was encased in a light-tight housing. The chemiluminescence output signal from the photomultiplier tube was monitored using a chart recorder (Type 3066, Yokogawa Hokushin Electric, Tokyo, Japan) and peak heights were measured manually.

2.1.2. Chemiluminescence spectra

Chemiluminescence spectra were collected with a Cary Eclipse fluorescence spectrophotometer (Varian, Mulgrave, Victoria, Australia) operating in chemiluminescence mode with the photomultiplier tube (R928, Hamamatsu, Shizuokaken, Japan) set to 800 V. The emission slit width, gate time and data interval were 20 nm, 1000 ms and 5 nm, respectively. Ten consecutive scans were averaged to reduce random noise. A two-line continuous flow manifold delivered the manganese(IV) reagent (5×10^{-4} mol L^{-1}) and analyte solutions (5×10^{-5} mol L^{-1} in 3 mol L^{-1} formaldehyde) to an integrated glass Y-piece and coiled glass flow-cell (1 mm i.d.) positioned against the emission window within the light-tight sample compartment of the instrument. The chemiluminescence spectra were corrected using the method described previously [1].

2.1.3. UV–vis spectrophotometry

UV–vis spectra for manganese(IV) solutions were recorded using a Varian Cary 300 Bio UV–vis spectrophotometer (1 cm path length) over a range of 190–800 nm, with 3 mol L^{-1} orthophosphoric acid in the reference cuvette.

2.1.4. Stopped-flow kinetics

Kinetics experiments were performed using a custom-made stopped-flow instrument (Fig. 1b). The manganese(IV) reagent (5×10^{-4} mol L^{-1}) and analyte streams (5×10^{-5} mol L^{-1}, 250 μL) were delivered by a syringe pump (10 mL Terumo syringes, World Precision Instruments WPI210iw, Australia) through PTFE tubing (0.8 mm i.d., Chromalytic Technology, Australia) to a flow-through luminometer with integral T-piece and a Teflon flow-cell (100 μL) mounted flush against the window of the photomultiplier tube (Thorn EMI, Model 9828SB, ETP Ltd., Australia) in a light-tight housing. The syringe pump was controlled and data was acquired with a desktop computer (Pentium Colorsonic, 120 MHz), data acquisition board (LabPC 1200, National Instruments) and software written in LabVIEW® (version 6.0, National Instruments). Intensity *versus* time profiles from five replicate injections were averaged after the data was smoothed with an FFT filter using *Origin* software.

2.1.5. High performance liquid chromatography

Chromatographic runs were performed using a Hewlett Packard 1100 LC system that consisted of a quaternary pump, solvent degasser system and auto sampler (Agilent Technologies). Sample components were separated with a monolithic

column (Chromolith^{TM} SpeedROD RP-18e, 50 mm × 4.6 mm i.d.). A solvent composition of 10% methanol in an aqueous solution of trifluoroacetic acid (0.1%, v/v, pH 2) was increased to 50% methanol over 3 min and held at that concentration for a further minute. Aqueous analyte stock solutions were prepared in $0.1 \, mol \, L^{-1}$ hydrochloric acid and diluted to the required concentration ($1 \times 10^{-4} \, mol \, L^{-1}$). The analyte solutions and mobile phases were filtered through a 0.45 μm membrane prior to analysis. A flow rate of $2 \, mL \, min^{-1}$ and an injection volume of 2 μL were used for all experiments. The UV–vis absorbance detector was operated at 280 nm. For chemiluminescence measurements, the column eluate and formaldehyde carrier were merged at a T-piece. This stream was then combined with the manganese(IV) reagent in the flow-through detector constructed for the flow-injection analysis manifold described above. A peristaltic pump was used to deliver the formaldehyde solution ($1 \, mol \, L^{-1}$) and manganese(IV) reagent ($5 \times 10^{-4} \, mol \, L^{-1}$). Data was acquired with Hewlett Packard Chemstation software.

2.1.6. Dynamic light scattering

A Malvern 4700 apparatus with a 10 mW AR^{+} ion laser at 488 nm was used to measure dynamic light scattering of the manganese(IV) solutions at an angle of 90° and a temperature of 25 °C. Solutions were diluted in the background electrolyte to ensure that multiple scattering and particle–particle interactions were negligible. The time autocorrelation functions were analysed by an inverse Laplace transform algorithm, CONTIN, to obtain a distribution of relaxation times related to the diffusion coefficient, D. The particle hydrodynamic radii were interpreted using the Stokes–Einstein equation for the given temperature and solvent viscosity (0.89 Pa s).

2.2. Reagent and samples

All solutions were prepared using analytical grade reagents and diluted with deionised water (Millipore, MilliQ Water System, USA) unless otherwise stated. Atropine sulfate, fenoterol, 5-hydroxyindole-3-acetic acid (5-HIAA), 5-hydroxytryptophan (5-HTP), serotonin, 2-thiobarbituric acid, tryptamine and DL-tryptophan were purchased from Sigma–Aldrich (Castle Hill, NSW, Australia). Codeine, heroin, morphine, oripavine, papaverine, pseudomorphine and thebaine were obtained from GlaxoSmithKline (Port Fairy, Victoria, Australia). Formaldehyde, potassium iodide, potassium permanganate, pyrogallol, soluble starch and sodium thiosulfate were from Ajax (Melbourne, Australia). Orthophosphoric acid (85%, w/v) and sodium formate were obtained from BDH (Poole, UK).

The preparation of the soluble manganese(IV) reagent was based on the method of Jáky and Zrinyi [12]. This process involved the reduction of potassium permanganate using excess sodium formate to yield manganese dioxide, which was collected on glass microfibre filter paper (GF/A, Whatman, England) by vacuum filtration and rinsed with water. Freshly precipitated, wet manganese dioxide (~2.4 g) was subsequently placed in 2 L of orthophosphoric acid ($3 \, mol \, L^{-1}$) and ultrasonicated for 30 min. The resultant colloid was then heated for approx-

imately 1 h (80 °C) or until the mixture became transparent. The solubility of commercially available manganese dioxides of varying particle sizes and activities were also examined, but these compounds did not dissolve under the above conditions. In accordance with the method described in [14], an iodometric titration was performed to determine the concentration of manganese(IV) in solution, where excess sodium thiosulfate was used to titrate the iodine released upon reaction with manganese. Stock solutions of manganese(IV) were diluted to the required concentration using orthophosphoric acid ($3 \, mol \, L^{-1}$). The analyte standards were made up in the same formaldehyde concentration as the carrier solution, unless otherwise stated.

3. Results and discussion

3.1. Manganese(IV) solubility and stability

For the preparation of soluble manganese(IV), Jáky and Zrinyi [12] noted that 24 h were required to completely dissolve the manganese dioxide in $3 \, mol \, L^{-1}$ orthophosphoric acid. In our experience, manganese(IV) solutions ($0.1–5.0 \, g \, L^{-1}$) can take up to 72 h at room temperature to change from colloidal to a transparent auburn colour, even with ultrasonication. However, we found that ultrasonication of the solution for 30 min, followed by heating for 1 h at 80 °C, was sufficient for rapid and complete dissolution. Within 24 h, precipitation was visible for all solutions above $0.01 \, mol \, L^{-1}$, presumably owing to the proliferation of aggregated macromolecular particles. Solutions at $0.01 \, mol \, L^{-1}$ or less were observed to be temporally stable for several weeks. The most enduring concentration was $0.001 \, mol \, L^{-1}$.

Although the manganese(IV) solutions were visibly transparent, light scattering experiments revealed the presence of particles. The size of the particles was dependent on the temperature and the time of both dissolution and storage. Twenty-four hours after preparation, visibly transparent and colloidal manganese(IV) solutions (prepared with and without heating, respectively), both contained two particle size groups; one with an average size between 150 and 200 nm, and the other at approximately 350 nm. Over the period of 1 week at room temperature, the proportion of the larger particles changed from 60% to 9% and from 98% to 5% for the visibly transparent and colloidal manganese(IV) solutions, respectively. The average particle size of the two groups also decreased to approximately 93 nm, and between 280 and 330 nm during this time. Consequently, the manganese(IV) reagent behaved as a colloidal solution throughout our investigations.

To ascertain the optimal orthophosphoric acid concentration in which to dissolve the manganese dioxide, a series of concentrations ($0.1–6.0 \, mol \, L^{-1}$) were investigated. Solutions containing orthophosphoric acid concentrations below $2 \, mol \, L^{-1}$ appeared colloidal, even after heating, and this was therefore considered the approximate minimum concentration required to achieve dissolution. After several months, a brown precipitate appeared in solutions containing between 2 and $3 \, mol \, L^{-1}$ orthophosphoric acid. Solutions containing higher orthophos-
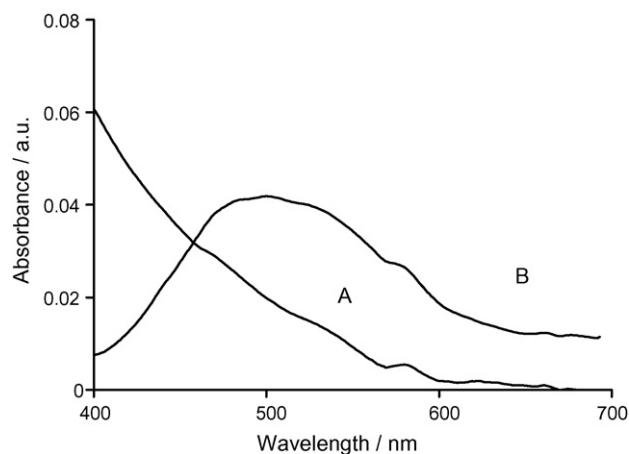
Fig. 2. Visible absorption spectrum of solutions of (A) manganese(IV) and (B) manganese(III) pyrophosphate.

Fig. 3. Chemiluminescence responses for the manganese(IV) reagent $(5 \times 10^{-4}\,\mathrm{mol\,L^{-1}})$ using flow injection analysis with formaldehyde in the carrier and injected sample solutions: (A) height of the constant baseline signal due to the continuous reaction with formaldehyde; (B) response for 5-HIAA $(5 \times 10^{-5}\,\mathrm{mol\,L^{-1}})$ above the baseline.

phoric acid concentrations gradually changed colour from transparent auburn to pale pink and precipitation was markedly less apparent. The visible absorption spectrum for the pale pink solution had a maximum at 505 nm (Fig. 2) and was attributed to manganese(III) pyrophosphate [12]. Although the composition of the original manganese(IV) solution is unknown, its spectrum appears consistent with reports of a soluble colloidal manganese(IV) species [12,15,16]. Over the period of a week, the absorbance peak at 196 nm increased, and the shoulder at approximately 270 nm decreased, with an isosbestic point at 230 nm. The changes were most apparent during the first day, and by the final day the scans were reasonably consistent, reiterating the requirement of time for the system to equilibrate.

3.2. Reaction conditions

Given the changes observed for manganese(IV) solutions within several months of preparation, the chemiluminescence response over time was investigated using a flow injection analysis manifold to combine the manganese(IV) reagent with various analytes. The analyte solutions and carrier stream each contained $1\,\mathrm{mol\,L^{-1}}$ formaldehyde. Only minor variations were observed for chemiluminescence responses over the first 14 days, which were mainly attributed to fluctuations in room temperature. However, after 2 months, the signal was around 80 times less than that achieved using freshly prepared reagent.

Our investigations suggest that the use of $\sim 5 \times 10^{-4}\,\mathrm{mol\,L^{-1}}$ manganese(IV) reagent provides optimum chemiluminescence responses when reacted with various analytes in the presence of a formaldehyde carrier under the specified conditions. Formaldehyde has been shown to significantly enhance the chemiluminescence emission from manganese(IV) and manganese(VII) reactions [1–12,17,18] and therefore a study was undertaken to determine the optimum formaldehyde conditions. Initial experiments involved injecting analyte solutions containing different concentrations of formaldehyde into a water carrier stream and comparing the results with those obtained with 'blank' solutions that contained the same concentration of formaldehyde but no analyte. Both analyte and blank signals became more

intense as the formaldehyde concentration was increased, but the signal-to-blank ratio remained relatively constant for formaldehyde concentrations between 0.1 and $3\,\mathrm{mol\,L^{-1}}$. For example, when using $5 \times 10^{-5}\,\mathrm{mol\,L^{-1}}$ 5-HIAA, a signal-to-blank ratio of approximately 3 was observed. For all subsequent experiments, formaldehyde was added to both analyte and carrier solutions, where the constant merging of the formaldehyde carrier with the reagent produced a measurable background signal. The use of $3\,\mathrm{mol\,L^{-1}}$ formaldehyde produced the greatest chemiluminescence response above the background: a 500-fold increase in signal intensity (Fig. 3) compared to responses obtained when analyte and carrier solutions contained no formaldehyde. Yet, despite this notable enhancement in manganese(IV) chemiluminescence intensity, the reactions were still not visible to the naked eye in a darkened room.

An increase in both signal and background intensity was also observed using higher orthophosphoric acid concentrations to dilute the stock manganese(IV) solution (Fig. 4). For example, the use of $6\,\mathrm{mol\,L^{-1}}$ orthophosphoric acid gave approximately a 12-fold increase in signal (compared to the $3\,\mathrm{mol\,L^{-1}}$ dilution used in previous chemiluminescence studies [1–11]), and the reagent remained stable for over 4 months without precipitating. These improvements in chemiluminescence response and reagent stability are possibly due to the stabilising effect of orthophosphoric acid on the manganese dioxide particles in solution *via* adsorption to the particle's surface [15,19]. However, concentrations above $3\,\mathrm{mol\,L^{-1}}$ orthophosphoric acid were generally avoided due to the viscosity of the solutions and the large increases in background signal, which compromised low level detection.

3.3. Emitting species

Lu and co-workers [3,4,6,9,11] have suggested that the reaction between manganese(IV) and formaldehyde in the presence of various analytes leads to chemiluminescence from singlet molecular oxygen, but in our previous studies we
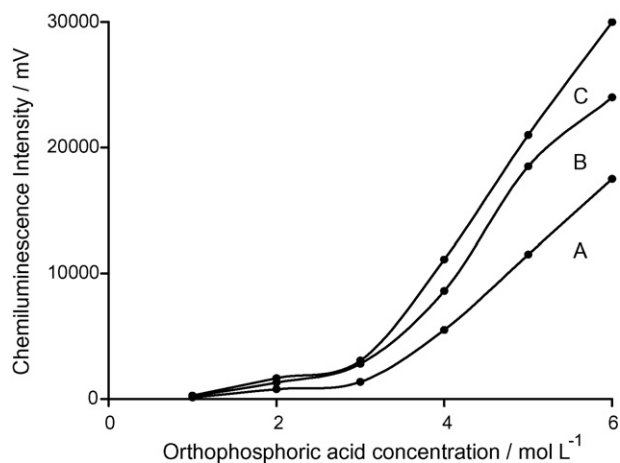
Fig. 4. Chemiluminescence response from the reaction of manganese(IV) $(5 \times 10^{-4} \, mol \, L^{-1})$ with 5-HIAA $(5 \times 10^{-5} \, mol \, L^{-1})$ using (A) $1.0 \, mol \, L^{-1}$, (B) $2.0 \, mol \, L^{-1}$ or (C) $3.0 \, mol \, L^{-1}$ formaldehyde carrier and varying the orthophosphoric acid concentration in the manganese(IV) reagent solution.

have presented evidence for a manganese(II) emitting species [1,13]. To further investigate the emission from these reactions, chemiluminescence spectra were obtained using a Cary Eclipse spectrofluorometer for eight different analytes by merging the manganese(IV) reagent with the analyte solutions. Reactions of manganese(IV) with aqueous analyte solutions without formaldehyde produced insufficient chemiluminescence intensities for the collection of spectra. The corrected chemiluminescence spectra for eight analyte solutions containing $3 \, mol \, L^{-1}$ formaldehyde all exhibited a maximum emission around 730 ± 5 nm (Fig. 5). Furthermore, the background emission from the reaction of $3 \, mol \, L^{-1}$ formaldehyde with the manganese(IV) reagent displayed a similar spectral distribution to the oxidation of each analyte, which suggests a common emitting species. The chemiluminescence from these reactions is unlike that of singlet oxygen, which contains two intense bands at 634 and 703 nm [13,20], but is similar to our previous reports for reactions with manganese(III), manganese(IV)

and manganese(VII), in which a manganese(II) emitting species was postulated [1,13].

3.4. Reaction kinetics

The kinetics of chemiluminescence reactions between manganese(IV) and various analytes was examined using a stopped-flow instrument, where the manganese(IV) reagent and analyte (dissolved in $0.2 \, mol \, L^{-1}$ formaldehyde) were delivered by syringe pump to the detector (Fig. 1b). In each case, the chemiluminescence intensity reached a maximum between 2 and 6 s after the reaction was initiated and returned to baseline within 25 s. Steady decay rates were observed, but a reproducible shoulder was present on the rise portion of the intensity-time profile for most phenolic analytes. In some cases, as shown in Fig. 6a, a separate initial peak was present. However, this was not observed for non-phenolic analytes (Fig. 6b), with the exception of papaverine. We tentatively postulate that the differences in the intensity-time profiles arise from an initial dimerization of the phenolic analytes via oxidative coupling at the *ortho*-position. For example, the C-2 position on morphine is activated by the presence of the C-3 phenolic group through quinone-type tautomerisation, but the methoxy group at the C-3 position of codeine would block this process.

(a)

Fig. 5. Corrected chemiluminescence spectra for the reaction of manganese(IV) $(5 \times 10^{-4} \, mol \, L^{-1})$ with (A) pseudomorphine $(5 \times 10^{-5} \, mol \, L^{-1})$; (B) serotonin $(5 \times 10^{-5} \, mol \, L^{-1})$; (C) formaldehyde $(3.0 \, mol \, L^{-1})$.

(b)

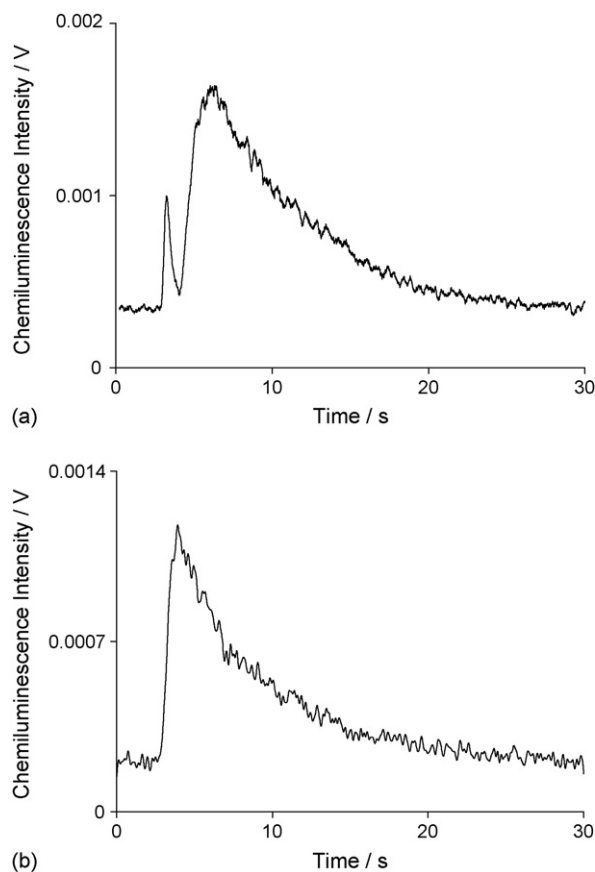Fig. 6. Examples of stopped-flow chemiluminescence intensity *vs*. time profiles for the reactions of manganese(IV) $(5 \times 10^{-4} \, mol \, L^{-1})$ with analytes $(5 \times 10^{-5} \, mol \, L^{-1})$ in $0.2 \, mol \, L^{-1}$ formaldehyde, containing (a) phenolic moieties and (b) non-phenolic moieties.

Table 2
Analytical figures of merit for various analytes using flow injection analysis with soluble manganese(IV) chemiluminescence detection in the presence of formaldehyde

Analyte	Detection limit[a] (mol L^{-1})	log–log calibration function[b]	Correlation coefficient, r^2
Atropine	5.0×10^{-6}	$y = 0.50x + 4.34$	0.9496
Codeine	1.0×10^{-8}	$y = 0.96x + 8.95$	0.9973
Fenoterol	1.0×10^{-8}	$y = 0.96x + 9.14$	0.9997
Heroin	1.0×10^{-6}	$y = 0.72x + 6.06$	1.0000
5-Hydroxyindole-3-acetic acid	1.0×10^{-8}	$y = 1.01x + 9.52$	0.9987
5-Hydroxytryptophan	1.0×10^{-8}	$y = 0.99x + 9.28$	0.9999
Morphine	5.0×10^{-8}	$y = 1.01x + 8.89$	0.9998
Oripavine	5.0×10^{-9}	$y = 0.76x + 7.81$	0.9684
Papaverine	1.0×10^{-9}	$y = 0.67x + 7.38$	0.9715
Pseudomorphine	1.0×10^{-9}	$y = 0.70x + 7.38$	0.9617
Pyrogallol	5.0×10^{-9}	$y = 0.86x + 8.59$	0.9887
Serotonin	1.0×10^{-8}	$y = 0.99x + 9.32$	0.9995
Thebaine	5.0×10^{-9}	$y = 0.74x + 7.76$	0.9905
2-Thiobarbituric acid	5.0×10^{-9}	$y = 0.62x + 6.49$	0.9553
Tryptamine	5.0×10^{-9}	$y = 0.86x + 8.76$	0.9977
Tryptophan	1.0×10^{-8}	$y = 0.94x + 9.20$	0.9990

[a] Calculated as $3 \times S/N$.
[b] From detection limit to 1×10^{-5} mol L^{-1}, $y =$ log peak height (mV), $x =$ log concentration (mol L^{-1}).

3.5. Analytical figures of merit

Using a flow injection analysis manifold, analytical figures of merit were obtained for the chemiluminescence reactions of manganese(IV) with 16 analytes. Formaldehyde (3 mol L^{-1}) was used in both analyte solutions and carrier stream. The manganese(IV) reagent was diluted to 5×10^{-4} mol L^{-1} from the original stock solution using 3 mol L^{-1} orthophosphoric acid. Similar detection limits (between 1×10^{-9} and 5×10^{-8} mol L^{-1}) were observed for most opiate alkaloids and indoles under investigation (Table 2). Many of these compounds have previously been determined with manganese(VII) chemiluminescence, but the sensitivity towards certain analytes, such as codeine and thebaine, is relatively poor [21]. The wider detection capability of the manganese(IV) reagent compared to manganese(VII), may be a consequence of the favourable two-electron transfer required to reduce the manganese(IV) reagent to the manganese(II) emitting species. However, poorer responses with the manganese(IV) reagent were observed for atropine and heroin and no significant response was obtained from barbitone, cocaine, glyphosate, iodate and sulfite.

3.6. High performance liquid chromatography

To demonstrate the use of the manganese(IV) reagent in post-column chemiluminescence detection, it was applied to the rapid determination of six opiate alkaloids separated with HPLC. The use of a monolithic column allowed flow rates that were comparable to those in the flow injection analysis experiments, and separation of all analytes in less than 4 min (Fig. 7). The column eluate and formaldehyde carrier were merged at a T-piece prior to reacting with the manganese(IV) reagent in the flow-through detector. Retention times for morphine, pseudomorphine, codeine, oripavine, thebaine and papaverine were 1.00, 1.26, 1.75, 2.02, 2.82 and 3.23 min, respectively

(a)

(b)
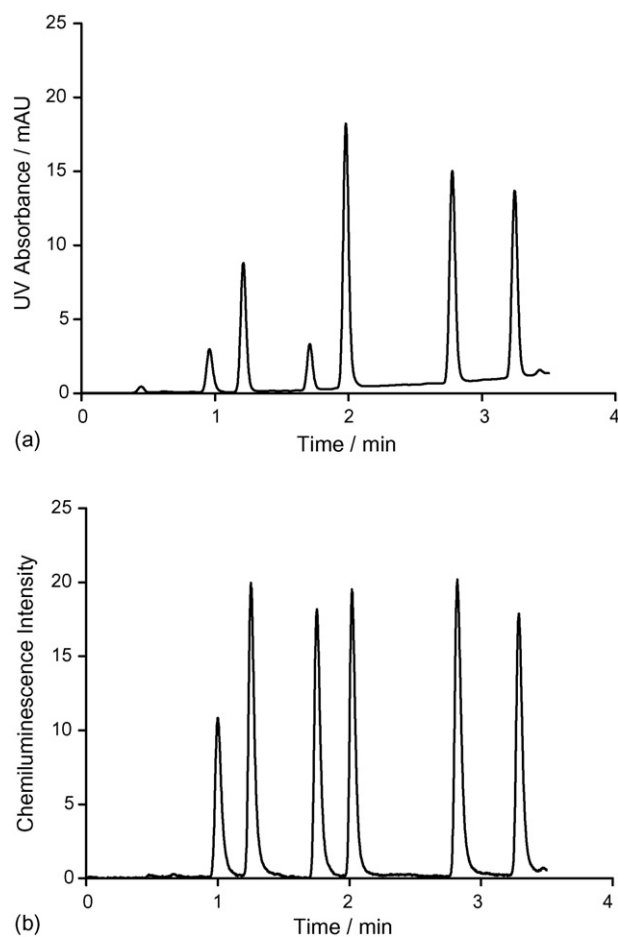
Fig. 7. A HPLC separation of six opiate alkaloids (1×10^{-4} mol L^{-1}) with (a) UV–vis detection at 280 nm and (b) manganese(IV) (5×10^{-4} mol L^{-1}) chemiluminescence detection with formaldehyde enhancement (1 mol L^{-1}).

(<0.3% R.S.D.). Unlike chemiluminescence detection with manganese(VII) [21] and tris(2,2′-bipyridyl)ruthenium(III) [22], similar emission intensities were observed for phenolic and non-phenolic alkaloids at equal analyte concentrations. Using an injection volume of 2 μL, the limit of detection for all six analytes was approximately 5×10^{-7} mol L^{-1} and the %R.S.D. for peak area using analyte concentrations of 1×10^{-4} mol L^{-1} was less than 4%.

4. Conclusion

Freshly precipitated manganese(IV) dioxide can be dissolved in orthophosphoric acid within 90 min using ultrasonication and heating, to produce a soluble colloidal manganese(IV) species containing two distinct particle sizes. The chemiluminescence evoked by the reaction of this colloidal manganese(IV) reagent with a range of analytes is enhanced by the presence of formaldehyde and results from a manganese(II) species. The comparable responses from the opiate alkaloids with manganese(IV) offers a distinct advantage over other chemiluminescence reagents such as manganese(VII) and tris(2,2′-bipyridyl)ruthenium(III), as their selectivity towards certain structural features limits their use as detection systems for HPLC and CE. The manganese(IV) reagent offers the advantages of highly sensitive chemiluminescence detection, while providing a more universal response to the presence of organic species that is less dependant on analyte structure.

References

[1] N.W. Barnett, B.J. Hindson, S.W. Lewis, P. Jones, P.J. Worsfold, Analyst 126 (2001) 1636.
[2] N. Anastos, N.W. Barnett, B.J. Hindson, C.E. Lenehan, S.W. Lewis, Talanta 64 (2004) 130.
[3] X. Zhu, Y. He, M. Liu, J. Du, J. Lu, Fenxi Huaxue 32 (2004) 752.
[4] F. Nie, X. Zhu, Y. He, J. Lu, Ziran Kexueban 32 (2004) 75.
[5] H. Zhang, X. Zhu, Y. He, Fenxi Shiyanshi 24 (2005) 5.
[6] F. Nie, J. Lu, Y. He, J. Du, Talanta 66 (2005) 728.
[7] Y. He, J. Lu, H. Zhang, J. Du, Chem. J. Chin. Univ. 26 (2005) 642.
[8] J. Du, Y. Li, J. Lu, Luminescence 20 (2005) 30.
[9] Y. He, J. Lu, X. Zhu, J. Du, Acta Chim. Sinica 63 (2005) 729.
[10] F. Nie, J. Lu, Y. He, J. Du, Luminescence 20 (2005) 315.
[11] Y. He, X. Zhu, J. Lu, Chin. J. Anal. Lab. 25 (2006) 69.
[12] M. Jáky, M. Zrinyi, Polyhedron 12 (1993) 1271.
[13] N.W. Barnett, B.J. Hindson, P. Jones, T.A. Smith, Anal. Chim. Acta 451 (2002) 181.
[14] A.I. Vogel, A Text Book of Quantitative Inorganic Including Elementary Instrumental Analysis, Longmans, Green and Co., London, 1957, p. 343.
[15] J.F. Perez-Benito, C. Arias, J. Colloidal Interf. Sci. 152 (1992) 70.
[16] F. Freeman, L.Y. Chang, J.C. Kappos, L. Sumarta, J. Org. Chem. 52 (1987) 1460.
[17] B.J. Hindson, N.W. Barnett, Anal. Chim. Acta 445 (2001) 1.
[18] J. Zhao, H. Xu, G. Wan, Talanta 64 (2004) 467.
[19] F. Mata-Perez, J. Perez-Benito, Z. Phys. Chem. (Leipzig) 267 (1986) 120.
[20] P.S. Francis, N.W. Barnett, S.W. Lewis, K.F. Lim, Luminescence 19 (2004) 94.
[21] N.W. Barnett, D.G. Rolfe, T.A. Bowser, W.T. Paton, Anal. Chim. Acta 282 (1993) 551.
[22] R.D. Gerardi, N.W. Barnett, S.W. Lewis, Anal. Chim. Acta 378 (1999) 1.

ELSEVIER

Determination of cadmium in leaves by ultrasound-assisted extraction prior to hydride generation, pervaporation and atomic absorption detection

A. Caballo-López, M.D. Luque de Castro *

Department of Analytical Chemistry, Annex C-3, Campus of Rabanales, University of Córdoba, E-14071 Córdoba, Spain

Abstract

A flow injection-pervaporation approach, where the samples – beech or olive leaves – were introduced as slurry, has been used for continuous derivatization hydride generation and separation of cadmium prior to determination by atomic absorption spectrometry. The removal of the analyte is achieved with an 1 mol/l HCl + 16% H_2O_2 aqueous solution with the help of an ultrasound probe acting for 17 min. Thiourea and cobalt were also added to the slurry for kinetic catalysis of hydride generation. A CRM – beech leaves – where the analyte had not been certified but estimated was used for optimisation of the leaching step. The results obtained using direct calibration against aqueous standards demonstrated the reliability of the method. The linear concentration range of the calibration curve was from pg/ml to ng/ml, with a correlation coefficient, r^2, better than 0.99. The detection and quantification limits were 0.3 and 0.9 ng/ml, respectively. The relative standard deviation for within-laboratory reproducibility was 5.7%. Olive leaves CRM was used for validation.
© 2006 Elsevier B.V. All rights reserved.

Keywords: Ultrasound; Pervaporation; Hydride generation; Cadmium; Leaves

1. Introduction

Cadmium is widely dispersed in the environment and exposure to this element gives rise to accumulation in several organs in the body, with consequent adverse health effects. Even at low exposure levels (mg/kg), the risk of renal tubular damage due to industrial exposure to cadmium can be considerable [1]. The increasing global emission, of Cd compounds into the atmosphere, together with aqueous and solid emissions lead to local contamination problems [2]. An additional problem of Cd toxicity is its cumulative character (about 30 mg can be accumulated during a person lifetime). The results are elevated Cd levels in the terrestrial, aquatic and marine food chains. Adverse effects in plants and mammalians have been observed for mg/kg levels in agriculture soils and food [3].

The classical pretreatment of solid samples to dissolve the Cd present is acid digestion. An alternative to solid sample pretreatment is slurry formation helped by ultrasound and direct analysis on the suspension.

Slurry sampling coupled to atomic absorption spectrometry combined both with hydride generation (HG-AAS) [4–6] and electrothermal atomization (ETA-AAS) [7–9], has been extensively used in the last years, as it allows direct analysis of solids with little sample preparation and has practical advantages over time-consuming and more prone to interferences conventional methods based on total dissolution of the samples. The concentration range covers from ng/ml to µg/ml. However, the slurry approach is not free from problems by blockage of the manifold when the solid particles are introduced into the dynamic system. Hence, slurry particles should be filtered out (providing the analyte has been transferred to the liquid phase by appropriate treatment with the required reagents and/or auxiliary energies [10]) for avoiding nebuliser clogging, insufficient nebulisation, damage of the graphite furnace and/or light dispersion; thus, protecting the spectrometer.

Analytical pervaporation emerged in the late 1980s as a nonchromatographic continuous separation technique competing with other membrane-based separation techniques thanks to the

---

* Corresponding author. Tel.: +34 957218615; fax: +34 957218615.
E-mail address: QA1LUCAM@uco.es (M.D. Luque de Castro).

absence of sample-membrane contact, which makes it useful for dirty and/or aggressive samples [11–13]. A key characteristic of analytical pervaporation is the presence of a constant-volume air gap between the sample in the donor chamber and the membrane. Since there is no direct contact between the sample and the membrane, clogging or deterioration of the membrane permeability due to pore blockage or corrosion by the sample-reagents mixture, respectively, is avoided. The pervaporator constitutes a multitask device for solid samples where leaching and derivatization of the analytes take place simultaneously. The only requirement of the experimental setup is for adequating sized diameters of the units in the dynamic manifold assisting the donor chamber in order to avoid clogging by the suspended particles.

2. Experimental section

2.1. Instruments and apparatus

Ultrasonic irradiation was applied by means of a Brason 450 sonifier (20 kHz, 400 W) equipped with a cylindrical titanium alloy probe (12.70 mm diameter), which was immersed in a water bath in which the sample was placed.

The flow injection-pervaporation manifold was constructed by a Gilson Minipuls-3 low-pressure peristaltic pump (Gilson, Worthington, OH, USA), a 5054 Rheodyne low-pressure injection valve (Rheodyne, Cotati, CA, USA), three-way standard connectors, PTFE tubing of 1.5 mm i.d. (Scharlau, Barcelona, Spain) and a pervaporation unit, which consists of a lower donor chamber (12.0 mm deep) and upper acceptor chamber (0.3 mm deep), both hexagonal in shape, and a single layer of glass beads (3.6 mm diameter) used to partially fill the donor chamber. The two chambers were fitted with inlet and outlet orifices. Firm contact between parts was achieved by screwing the pervaporation unit between aluminum supports with four screws. PTFE membranes (47 mm diameter and 1.5 mm thickness) from Trace, Braunschweig, Germany, were used.

A Spectra 110 atomic absorption spectrometer (Varian, Madrid) furnished with a hydride absorption cell of quartz (VGA-76/77, Varian) was used for Cd determination. The atomization cell was positioned over the burner capable of supporting an air–acetylene flame, which was kept off for all the experiments. The hollow-cathode lamp current was 4 mA. The monochromator was set at 228.8 and 0.7 nm spectral bandpass.

2.2. Reagents and samples

All reagents were of analytical reagent grade. 0.8% (w/v) NaBH$_4$ (Sigma–Aldrich, Deisenhufen, Germany) in 1% (w/v) NaOH (Merck, Darmstadt, Germany) and 0.4 mol/l HCl (Merck) solutions were used for hydride generation. An 1.0 mol/l HCl aqueous solution was employed as a dispersing medium. H$_2$O$_2$ was added to the slurry for helping to leach the analyte.

A 0.5% (m/v) solution of thiourea (Merck), in the presence of 1 μg ml^{-1} Co (prepared from an 1000 mg/l stock standard solution), kinetically catalysed the formation of volatile species of Cd by hydride generation.

The 0.16% (m/v) KCN (Panreac) solution used as masking agent was dissolved in the NaBH$_4$ solution. Some cautions were taken in order to prevent an accident by formation of HCN: neutralisation of the waste with sodium hydroxide and location of the detector in a hood-fume, as well as the use of gloves and mask.

All working solutions were prepared daily using distilled water of high purity obtained from a Millipore (Bedford, MA, USA) Milli-Q plus system.

Argon (Carburos Metálicos, Barcelona, Spain) was used to carry the hydride formed to the detector.

Two materials (CRM 062 and CRM 100) were used for optimisation and validation of the developed method. The materials consisted of cleaned, dried, ground and homogenised leaves of Olea europaea and Beech, having a particle size of less than 125 μm. In the beech leaves (CRM 100) cadmium concentration had not been certified and this material was used for optimisation; meanwhile a Cd-CRM (CRM 062) was used for validation.

2.3. Proposed method

The overall arrangement for the slurry sampling-ultrasound assisted leaching prior to hydride generation–pervaporation–AAS is illustrated in Fig. 1. The dynamic system consists of an upper manifold (including the acceptor chamber of the pervaporator) through which a gas phase circulates, and a lower flow injection manifold, including the donor chamber of the pervaporator. The samples were weighed directly (200 mg of sample) into plastic bottles to which 1 mol/l HCl + 16% (m/v) H$_2$O$_2$ aqueous solution was added for a final volume of 10 ml. Batches of eight of those suspensions were located in the sampler and sonicated for 17 min (duty cycle 0.9 s and output amplitude 100%) at the maximum power of the ultrasound probe. After aspirating each sample to the dynamic system, stirring was applied for 1 min in order to ensure homogeneous distribution of the solid particles. While stirring, the pump aspirated an aliquot and filled the loop (250 μl) of the injection valve, which unloaded its content into a 0.4 mol/l HCl carrier stream that merged with a 0.8% (w/v) NaBH$_4$ + 0.16% (w/v) KCN stream. The volatile hydride formed in the reaction coil reached the pervaporator and evaporated into the headspace of the donor chamber and diffused through the PTFE membrane into the acceptor chamber where an argon stream, at 200 ml/min, led the hydride into the atomization cell. There is convincing evidence that the species responsible for the absorption of radiation at 228.8 nm is "cold" atomic cadmium vapor, possibly produced by the decomposition of unstable CdH$_2$ [14].

The addition of 0.16% KCN to the NaBH$_4$ solution as masking agent led to a total elimination of the matrix effect.

The size of the in suspension particles was small as compared with the inner diameter of the tubing system; so not clogging problems took place. It was observed that the peak areas were approximately three times larger by keeping the flame off than those obtained with the flame on. This observation is in agreement with the results obtained by Sanz-Medel and co-workers [14,15]. All experiments were performed at a working room of 25 °C.
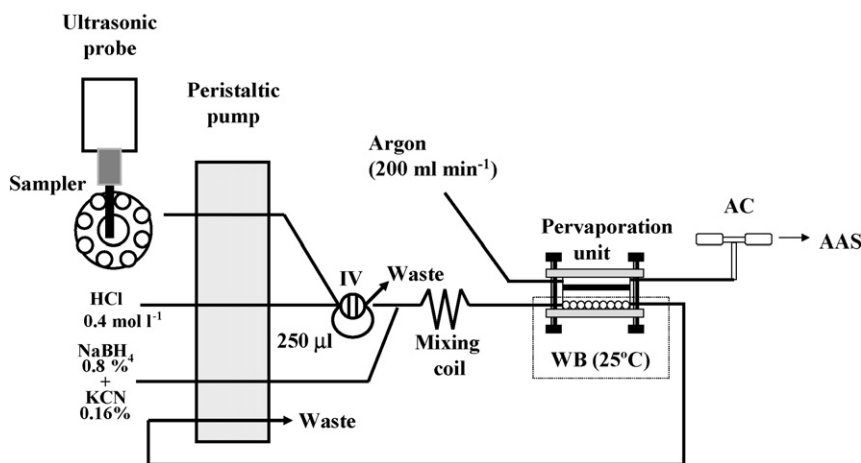
Fig. 1. Overall approach for the determination of cadmium in solid samples by slurry formation ultrasound-assisted leaching, hydride generation, pervaporation and atomic absorption detection. IV, injection valve; WB, water bath; AC, atomization cell; AAS, atomic absorption spectrometer.

The use of a carrousel allowed to sonicate eight samples simultaneously.

3. Results and discussion

3.1. Optimisation of the method

The variables which affect the method for the determination of cadmium were studied by either a multivariate or univariate approach depending on the existence or not of interrelation. The ranges studied and the optimal values found are shown in Table 1.

The central composite design (CCD) used here is one of the multivariate methods for optimisation more frequently used at present. Multivariate methods provide advantages over traditional univariate methods such as the possibility of finding interactions between variables and the use of a shorter number of experiments. Statistical software [16] was used to analyse the data from the experimental values.

3.2. Optimisation of chemical variables

The influence of HCl both in the sample and carrier and NaBH$_4$ on hydride generation in the experimental system was

Table 1
Ranges assessed and optimal values of the variables

Variables	Studied range	Optimum value
HCl carrier (mol/l)	0.2–0.6	0.4
HCl sample (mol/l)	0.2–1.6	1.0
NaBH$_4$ (%, m/v)	0.5–1.5	0.8
H$_2$O$_2$ (%, m/v)	5–20	16
KCN (%, m/v)	0.1–0.3	0.16
Thiourea (%, m/v)	0.1–1.0	0.5
Co (µg/g)	0.25–1.9	1
Spacers (mm)	2–8[a]	8
Temperature (°C)	25–95	25
Slurry concentration (%, m/v)	1–4	2
Sonication time (min)	1–30	17

[a] Values assayed: 2, 4, 6, and 8 mm thickness.

investigated. The concentration of H$_2$O$_2$ used to help to leaching Cd was also studied. The variables were studied using a 50 ng/ml Co standard solution. A full factorial 2^4 design allowing 8 degrees of freedom involved 19 randomized runs plus three centered points was built for the optimisation study of these variables. The upper and lower values given to each factor were selected from the available data and experience gathered in the preliminary experiments.

The conclusions of this study were that the HCl concentration both in the carrier and NaBH$_4$ were factors not statistically influential at 95% confidence level in the ranges under study. However, the results showed better signal and precision with 0.4 mol/l HCl and 0.8% (m/v) NaBH$_4$. Analysing the design for HCl and H$_2$O$_2$ in the sample a second-order polynomial equation was obtained. The optimal values were obtained by equalising to zero the first derivate of the polynomial. Optimum values of 1.1 mol/l HCl and 16% H$_2$O$_2$ were obtained and used for subsequent experiments.

The addition of 0.16% KCN to the NaBH$_4$ solution as masking agent revealed a total elimination of the matrix effect, without causing decrease of the cadmium signal [17]. For concentrations above 0.2% the masking effect levelled off and was decreased for concentrations below 0.15%.

3.3. Optimisation of the kinetic conditions

It has been reported that the generation of cadmium volatile species must be free from organic media in order to achieve better sensitivity [14,15,18–21]. In addition, the use of some transition metals has been reported to produce an increase in sensitivity by means of a catalytic effect [18–21]. Thiourea and Co^{II+}, at different concentrations, were added to the sample solution (50 ng/ml Cd) and studied by a multivariate approach.

A CCD was also used for optimisation of the two variables. The CCD used consisted of a two-level full factorial design and the star points. This design allowed 5 degrees of freedom involved 8 randomised runs plus 3 centered points. The results showed that 0.5% (w/v) thiourea in the presence of 1 µg/ml Co,

kinetically catalyse to some extent the formation of volatile Cd species by hydride generation. An increase of 20% in the analyte signal was obtained in the presence of the catalyst mixture as compared with the value in its absence.

3.4. Optimisation of the flow injection variables

The development of hydride generation was studied for different flow-rates of both HCl/NaBH$_4$ and Ar. To simplify the optimisation of the flow-rates, it was decided that those of HCl and NaBH$_4$ streams should be equal. The same CCD used before was used for optimisation of the two variables. The Cd signal increased with two opposite effects: an increase of the HCl/NaBH$_4$ flow-rate up to about 8 ml/min and decrease of the Ar flow rate to about 200 ml/min.

The effect of the coil length where the acidified sample and NaBH$_4$ were mixed was evaluated by employing lengths from 20 to 300 cm of the PTFE tube of 0.8 mm i.d. and from 20 to 100 cm of the PTFE tube of 1.5 mm i.d. Changes in the length of the reaction coil produced insignificant effects on the signal from Cd for both internal diameters; however, the tube of 0.8 mm i.d. produced an increased on the signal. A reaction coil of 100 cm was used for subsequent experiments.

Sample volumes ranging from 100 to 500 μl were studied. As expected, small sample volumes increased the sample throughput; however, they led to a decrease of sensitivity. A sample volume of 250 μl was selected as optimum as the peak area levelled off at higher volumes.

3.5. Optimisation of the pervaporation variables

The maintenance of a constant liquid level in the donor chamber is crucial for the reproducibility of flow injection-pervaporation methods. A satisfactory control of the liquid level in the donor chamber was achieved by introduction of glass beads (3.6 mm diameter), by aspiration of the waste from the donor chamber and by appropriate selection of the length of the tubing upstream and downstream the donor chamber.

The influence of the volume of the donor chamber on the sensitivity was studied by placing in it spacers of 2, 4, 6 and 8 mm thickness. The presence of spacers lowered the sensitivity, since they increased the volume of the headspace, but also increased both life-time of the PTFE membranes and reproducibility of the analyses; so, a 8 mm spacer was used. In this case, a metal membrane support was unnecessary.

In the present study, the temperature of the water bath was varied between 25 and 95 °C. The change of temperature has a slight effect on the analytical signal (less than 4% of the total signal); thus, 25 °C was used as working temperature.

3.6. Optimisation of the ultrasound-assisted leaching step

The influence of the sonication time was studied in a univariate way fixing the other variables at their optimal values. The sample in this case was the beech leaves CRM. The ultrasound radiation amplitude and the percentage of duty cycle of ultra-
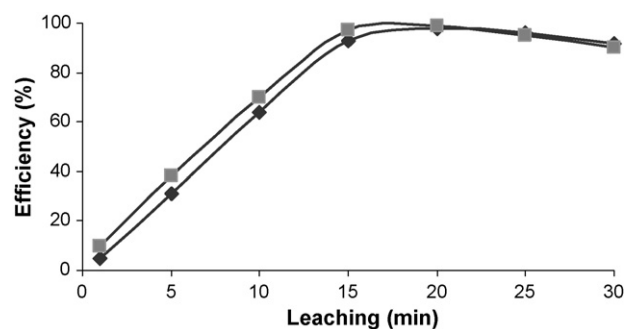
Fig. 2. Kinetics of the analyte leaching from the two CRMs. (♦) CRM 100; (■) CRM 062.

sonic exposure were fixed at their maximum values. In all cases, the probe position was the same. The optimisation was carried out using a slurry of 2% (m/v) in 1 mol/l HCl.

Different sonication times were tested in order to determine the time necessary for total removal the Cd from the CRM. As can be seen in Fig. 2, quantitative removal of Cd was obtained after 17 min sonication.

3.7. Optimisation of the slurry concentration

A key factor in preparing slurries is concentration. Samples with high analyte content are easier to handle by slurry sampling than by direct solid sampling. Precision degrades with high dilution slurry as a result of the small number of particles. On the other hand, when the analyte content in the original sample is very low, the concentration of the slurry can be increased accordingly. One factor to be taken into account is that increased slurry concentration also increases matrix effects.

Slurry concentrations from 1 to 4% (w/v) with 10 min of sonication were used, which resulted in deteriorated accuracy above 3% as a consequence of both matrix effects and inefficient homogenisation of the slurry; while for concentrations below 2% the precision degraded. Slurry concentration at 2% (m/v) was selected as a compromise between the conflicting requirements for absence of matrix effects and precision.

3.8. Calibration of the proposed method

The detection and quantification limits, established as $3s_b + x_b$/slope and $10s_b + x_b$/slope (where s_b is the standard deviation and x_b is the mean of 11 blank measurements), are 0.3 and 0.9 ng/ml, respectively. The linear concentration range of the calibration curve covers from 0.9 to 100 ng/ml, with a correlation coefficient, r^2, better than 0.998.

3.9. Validation of the method

The optimised method was applied to two certified reference materials: beech-leaves (CRM 100) – with non-certified but estimated Cd – and olive-leaves (CRM 062) with certified Cd. The results, summarised in Table 2, show that this method is a good alternative for the extraction and determination of Cd

Table 2
Validation of the method

Samples	Certified	Estimated	Found[a]
CRM 100		0.34	0.337 ± 0.012
CRM 062	0.1 ± 0.02		0.097 ± 0.003

[a] Relative standard deviation ($n = 3$).

Table 3
Experiments for the determination of within-laboratory reproducibility and repeatability from an experimental set-up

Day	Cd measured	
	Replicate 1	Replicate 2
1	0.3477	0.3298
2	0.3451	0.3643
3	0.3562	0.3774
4	0.3657	0.3494
5	0.3232	0.3247
6	0.359	0.3298
7	0.374	0.3799

Table 4
ANOVA (cadmium)

Source	SS[a]	d.f.[b]	MS[c]
Between days	0.0038	6	0.00063
Within days	0.0011	7	0.00016
Total	0.0049	13	

[a] Sum of squares.
[b] Degrees of freedom.
[c] Mean square.

from leaves as the efficiency achieved from the different samples tested was higher than 97% in all instances.

To evaluate the precision of the proposed method, within-laboratory reproducibility and repeatability were estimated in a single experimental setup with duplicates [22]. The experiments were carried out using the CRM 100 at 2% (w/v) in 1 mol/l HCl. The optimal values obtained for the variables were used in all the experiments. Two measurements of Cd per day were carried out on 7 days. The results obtained are listed in Tables 3 and 4. The repeatability and within-laboratory reproducibility, both expressed as relative standard deviation, were 3.6 and 5.7%, respectively.

4. Conclusions

A flow injection-pervaporation method, where the sample was introduced as slurry, has been developed for the continuous derivatization and determination of cadmium in leaves by hydride generation atomic absorption spectrometry. The removal of cadmium was achieved with the help of both an ultrasound probe and 16% of H_2O_2 in the leaching solution.

This approach offers several advantages:

(1) Thanks to use of slurry:
   - reduced preparation time by avoiding a filtration step;
   - reduced sample contamination as well as analyte losses because less manipulation of the sample is required.
(2) Thanks to use of the pervaporation unit:
   - reduced sample and reagents amount needed;
   - no filter requirement in the manifold before the atomization cell to avoid solid particles that can cause drawbacks (scattering).
   - avoidance of small amounts of water vapour transferred to the atom cell and condensed to droplets which partially obscure the light path.
(3) A decrease on the cadmium signal by the presence of other heavy metals is avoided thanks to the use of KCN. The use of Ba^{II+} and SO_4^{II-} for avoiding the interference from Pb by $PbSO_4$ coprecipitation [16] did not overcome interferences from other heavy metals.

References

[1] S. Binder, T. Matte, J. Am Med. Assoc. 269 (1993) 1679.
[2] B. Griepink, H. Muntau, C. Colinet, Fresenius Anal. Chem. 318 (1984) 490.
[3] M. Stoeppler, Metals and their compounds in the environment occurrence, in: G. Merian (Ed.), Analysis and Biological Relevance, VCH, Weinheim, 1991, p. 803.
[4] H. Gürleyük, J.F. Tyson, P.C. Uden, Spectrochim. Acta Part B 55 (2000) 935.
[5] J. Mierzwa, R. Dobrowolski, Spectrochim. Acta Part B 53 (1998) 117.
[6] J. Mierzwa, S.B. Adeloju, H.S. Dhindsa, Analyst 122 (1997) 539.
[7] E. Vassileva, H. Baeten, M. Hoening, Fresenius' J. Anal. Chem. 369 (2001) 159.
[8] P. Viñas, M. Pardo-Martínez, M. Hernández-Córdoba, J. Anal. Atom. Spectrom. 14 (1999) 1215.
[9] I. Lopez-García, M. Sánchez-Merlos, M. Hernández-Córdoba, Spectrochim. Acta Part B 52 (1997) 437.
[10] M.D. Luque de Castro, F. Priego-Capote, Analytical Applications of Ultrasound, Elsevier, Amsterdam, 2006.
[11] M.D. Luque de Castro, I. Papaesftathiou, Trends Anal. Chem. 17 (1997) 41.
[12] M.D. Luque de Castro, I. Papaefstathiou, Encyclopedia of Environmental. Analysis and Remediation, John Wiley & Sons, Inc., Chichester, 1998, p. 3462.
[13] M.D. Luque de Castro, L. Gámiz-Gracia, Analytical pervaporation, in: R.A. Meyers (Ed.), Enciclopedia of Analytical Chemistry, Wiley, New York, 2000, p. 3084.
[14] A. Sanz-Mendel, M.R. Fernández de la Campa, M.C. Valdez-Hevia, N. Bordel, Anal. Chem. 67 (1995) 2216.
[15] A. Sanz-Mendel, M.R. Fernández de la Campa, M.C. Valdez-Hevia, N. Bordel, Anal. Proc. 32 (1995) 49.
[16] Statgraphics Plus for Windows v 2.1, Rockville, MD, 1992.

[17] M.L. Garrido, R. Muñoz-Olivas, C. Cámara, J. Anal. Atom. Spectrom. 13 (1998) 295.

[18] M.C. Valdez-Hevia, M.R. Fernández de la Campa, A. Sanz-Mendel, J. Anal. Atom. Spectrom. 8 (1995) 847.

[19] X.W. Guo, X.M. Guo, J. Anal. Atom. Spectrom. 10 (1995) 987.

[20] M. Liu, S. Xu, Atom. Spectrosc. 18 (1997) 195.

[21] X.W. Guo, X.M. Guo, Anal. Chim. Acta 310 (1995) 377.

[22] D.L. Massart, B.G.M. Vanderginste, L.M.C. Buydens, S. De Jong, P. Lewi, J. Semeyers-Verbeke, Handbook of Chemometrics and Qualimetrics, Part A, Elsevier, Amsterdam, 1997.

Analysis for chloroanisoles and chlorophenols in cork by stir bar sorptive extraction and gas chromatography–mass spectrometry

R.M. Callejon, A.M. Troncoso, M.L. Morales *

Área de Nutrición y Bromatología, Facultad de Farmacia, Universidad de Sevilla, C/P García González no. 2, E-41012 Seville, Spain

Abstract

A complete methodology for the determination of chloroanisoles and chlorophenols in cork material is proposed. The determination is accomplished by means of a previous liquid–solid extraction followed by stir bar sorptive extraction (SBSE) coupled to gas chromatography–mass spectrometry (GC–MS). Two different liquid–solid extraction experiments were conducted and eight compounds considered (2,6-dichloroanisole, 2,4-dichloroanisole, 2,4,6-trichloroanisole, 2,4,6-trichlorophenol, 2,3,4,6-tetrachloroanisole, 2,3,4,6-tetrachlorophenol, pentachloroanisole and pentachlorophenol). From the results obtained we can conclude that high volume extraction extending extraction time up to 24 h is the best choice if we have to release compounds from the inner surfaces of cork stoppers. Recovery percentages ranged from 51% for pentachloroanisole to 81% for 2,4-dichloroanisole. This method allows the determination of an array of compounds involved in cork taint at very low levels from 1.2 ng g^{-1} for 2,4,6-tricholoroanisole to 23.03 ng g^{-1} for 2,3,4,6-tetrachlorophenol.
© 2006 Elsevier B.V. All rights reserved.

Keywords: Chloroanisole; Chlorophenol; Cork; Stir bar sorptive extraction; Gas chromatography–mass spectrometry

1. Introduction

Musty odours are one of the most unpleasant organoleptic defects in wine. Several molecules have been identified as responsible of this unpleasant smell. Chloroanisoles, especially 2,4,6-trichloroanisole (TCA) due to its particularly low sensory threshold and, in a lesser extent, 2,3,4,6-tetrachloroanisole (TrCA) and pentachloroanisole (PCA) are responsible of a high percentage of cork taint cases reported. Besides, other compounds such as 2,4-dichloroanisole (2,4-DCA) and 2,6-dichloroanisole (2,6-DCA), degradation products of 2,4,6-trichloroanisole, may also contribute to wine off-flavour [1]. Its origin in wine can be traced back to contaminated cork stoppers and it is either already present in the corkwood or produced during corkwood processing. The migration of these compounds from cork stoppers to wine depends on the temperature and the time of contact between them [2]. Chloroanisoles can be formed by methylation of the corresponding chlorophenols by certain fungi. These chlorophenols, in many cases, are used as pesti-

cides. Chlorophenolic compounds can be considered the main precursors of chloroanisoles, so their joint determination is of great interest for cork industries [3,4].

Although chlorophenols are polar compounds and can form hydrogen bounds with the GC columns [5] several authors have proposed the simultaneous determination of TCAs and TCPs in cork [3,6–8] and wines [3,4,9] by means of GC–MS.

These compounds are present in very low concentrations, especially in wine, hence it is necessary to apply a preconcentration technique before their analytical determination. Different extraction methodologies have been applied: solvent extraction employing dichloromethane [3], *n*-hexane [6] or *n*-pentane [10]; solid phase extraction (SPE) [10–12], pervaporation (PV) [13], headspace solid-phase microextraction (HS-SPME) [2,5,7,14,15] and more recently, stir bar sorptive extraction (SBSE) [4,8,16]. The obtained extracts, when a solvent is used, need to be concentrated by means of a rotary evaporator or solid-phase extraction.

SBSE methods are based on a non-polar polydimethylsiloxane (PDMS) immobilized liquid phase coated onto a magnetic stir bar to selectively concentrate compounds. The SBSE has two steps: partitioning of analytes between the coating (PDMS) and the sample matrix, followed by desorption into the GC

---

* Corresponding author. Tel.: +34 954556760; fax: +34 954233765.
 E-mail address: mlmorales@us.es (M.L. Morales).

Table 1
Calibration plots data for the chloroanisoles and chlorophenols under study and the IS of extraction (lindane)

Analytes	Selected ion (*m/z*)	Intercept	Slope	*r*	LOD (ng L^{-1})	LOQ (ng L^{-1})
2,6-Dichloroanisole	176	−0.0013	0.0039	0.9999	1.56	5.2
2,4-Dichloroanisole	176	0.0090	0.0037	0.9996	2.56	8.5
2,4,6-Trichloroanisole	195	−0.0021	0.0036	1.0000	0.81	2.7
2,4,6-Trichlorophenol	196	0.0249	0.0007	0.9997	3.28	10.9
2,3,4,6-Tetrachloroanisole	231	−0.0014	0.0043	0.9999	1.29	4.3
2,3,4,6-Tetrachlorophenol	232	−0.0126	0.0027	0.9832	17.7	59.1
Pentachloroanisole	265	−0.0057	0.0037	0.9990	6.8	22.7
Pentachlorophenol	266	−0.1481	0.0002	0.9926	956	3188
Lindane	181	−0.0663	0.0016	0.9998	30.6	102

LOD: limit of detection; LOQ: limit of quantification.

inject port. SBSE had been shown a much higher sensitivity than SPME by a factor within 50 and 250 due to the higher content of PDMS in which the amount of analyte extracted is proportional to the coating thickness increasing the limit of detection of ultra trace compounds [17]. The theory of SBSE is quite similar to that of SPME, which the efficiency of analytes partitioning into PDMS phase on the stir bar at the equilibrium, can rugged be predicted by the octanol–water partition coefficients [18]. Zalacain et al. [4] employed SBSE to determine chloroanisoles and chlorophenols in wine obtaining low limits of quantification (LOQ), between 1 and 20 pg L^{-1}, except for pentachlorophenol (PCP) for which LOQ was 6 µg L^{-1}.

Regarding cork material, the main problem arises in the extraction from a so complex matrix. The recovery assays performed by most authors are based on spiking cork by impregnation with standard solutions [1,3,15]. Hence, only those compounds present in the surface area of cork are effectively extracted. These methods led to the evaluation of a short-term wine tainting [2]. On the other hand, if we attempt to study a short-term as well as a long-term taining, cork material has to be spiked by injecting standard solution inside cork.

The aim of this work is the determination of a total of eight compounds, chloroanisoles and their precursors chlorophenols, present in cork stoppers by gas chromatography–mass spectrometry (GC–MS) applying liquid–solid and stir bar sorptive extractions. Cork stoppers are spiked with chloroanisoles and chlorophenols in the inner layers. The following three steps have been performed: firstly, optimisation of an extraction procedure for chloroanisoles and chlorophenols from cork; secondly, application of a SBSE technique to the obtained extract and finally, determination of the compounds absorbed to stir bar by thermal desorption and GC–MS.

The proposed method can be used in quality control in cork industries since it accomplishes the joint determination of an array of compounds and the release of these compounds from the inner layers in cork stoppers. Hence it offers a prediction of potential contamination along time.

2. Experimental

2.1. Chemicals and reagents

Analytical grade ethanol, methanol and glacial acetic acid from Merck (Darmstadt, Germany) were used. Ultrapure water was obtained from Milli-Q water purification system (Millipore, Bedford, MA, USA).

2,6-Dichloroanisole (2,6-DCA; 97%), 2,4,6-trichloroanisole (TCA; 99%), 2,4,6-trichloroplenol (TCP; 98%), 2,3,4,6-tetrachloroplenol (TrCP; 99.9%), pentachloroanisole (PCA; 97%), pentachlorophenol (PCP; 98%), lindane (LIND as internal standard for extraction; 97% [13]) and 3,4-dimethylphenol (as internal standard for quantification; 99%) were supplied by Sigma–Aldrich (Madrid, Spain). 2,4-dichloroanisole (2,4-DCA; 95%) and 2,3,4,6-tetrachloroanisole (TrCA; 95%) were obtained from LGC Promochem S.L. (Barcelona, Spain).

Stock solutions were prepared in ethanol in amber glass vials and kept at −20 °C.

Calibration plots were built with five concentration levels for each compound as follows: from 15 to 120 ng L^{-1} for 2,6-DCA, 2,4-DCA, TCA, TrCA and TrCP; from 25 to 165 ng L^{-1} for TCP; from 25 to 200 ng L^{-1} for PCA; from 1.17 to 9.38 µg L^{-1} for PCP and from 0.243 to 1.94 µg L^{-1} for lindane (Table 1).

2.2. Cork material

Natural cork stoppers were cleaned by continuous extraction with methanol in a Soxhlet for 24 h [3] and then dried in a oven at 105 ± 2 °C. Cork stoppers (ca. 2 g) were spiked by injecting, in different points (surface and inner), 100 µL of a stock solution containing 2,6-DCA, 2,4-DCA, TCA, TCP, TrCA, TrCP, PCA, PCP and lindane. They were stored in a freezer (−20 °C) during approximately 2 h. Then, spiked cork samples were milled with a granulating mill with stainless steel bowl. Extraction experiments were conducted immediately. The mill was decontaminated between samples by soaking it in a detergent solution with added ethanol and dried overnight in an oven at 80 °C.

2.3. Extraction studies

Two different liquid–solid extraction methods were tested:

(i) High volume extraction (HVE): milled cork was placed into a tea infuser and then it was submerged in a total volume of 60 mL of different extraction media: 100% ethanol; 50% ethanol:50% Milli-Q water; 75% ethanol:25% Milli-Q water and 50% ethanol:50% Milli-Q water at pH 3.6 (pH was adjusted with glacial acetic acid [3]). The extraction

procedure was carried out using ultrasonic bath and shaking bath. The resulting extract was filtered through paper.

(ii) Low volume extraction (LVE): milled cork was distributed into two 12 mL vials and 6 mL of ethanol added in each one. Vials were immersed in an ultrasonic bath during 15 min and then submitted to a strong shaking during 15 min. Solvent was separated and another 4 mL of ethanol added for a second extraction, and similar steps were followed. Total extract (ca. 18 mL) was filtered through paper and concentrated up to ca. 2 mL in a rotary evaporator at 35 °C. Several assays were previously conducted to test if significant losses of these compounds takes place at this temperature in a rotary evaporator (35 °C). No significant losses were achieved in these experimental conditions.

To optimise time and number of extractions for the HVE method several experiments were conducted. The samples (2 g cork stopper spiked with 100 μL of standard solution) were submitted to successive extraction steps. Then the solvent was separated, filtered through paper and recorded its volume. A subsequent SBSE and GC-analysis was performed. Thus for every extraction we have a recovery value. Experiments were conducted by triplicate.

(i) HVE procedure was followed using 75:25 ethanol–water, extraction took place during 30 min in an ultrasonic bath followed by 6 h in shaking bath. A second extraction was performed in the same conditions and the third consisted of 30 min in ultrasonic bath and 12 h in shaking bath (short-term extraction).

(ii) HVE procedure was applied using 75:25 ethanol–water, extraction was performed in different and successive steps involving ultrasonic bath 30 min, shaking bath 6 h, ultrasonic bath 30 min, shaking bath 18 h. A second extraction was performed in the same conditions (long-term extraction).

2.4. Precision recovery studies

Cleaned cork stoppers were spiked by injecting three different volumes (75, 100 and 125 μL) of a standard solution of chloroanisoles and chlorophenols (Table 2). Spiked cork stoppers were stored at −20 °C during one night before processing.

2.5. SBSE procedure

A 10 mm long stir bar coated with 0.5 mm PDMS layer (Twister, Gerstel, Müllheim an der Ruhr, Germany) was placed into a 11 mL glass vial containing: 1 mL of extract or standard solution (calibration plots), 0.5 mL of ethanol, 8.5 mL of Milli-Q water at pH 3.6 (adjusted with acetic acid) and 2 μL of IS for quantification (3,4-dimethylphenol at 30 μg L^{-1}). Ethanol is preferred as solvent since less damage is produced to PDMS Twister. Final ethanol concentration must be under 15% (v/v) according to manufacturer instructions.

pH is adjusted to 3.6 in order to facilitate the migration of phenols into the non-polar PDMS [3,4,19].The mixture was

Table 2
Results for recovery assays

Compounds	Added (ng g^{-1})	Recovery (%)	Mean recovery ± S.D.
2,6-Dichloroanisole	18.9	68.8	65 ± 4
	27.1	65.2	
	33.6	61.1	
2,4-Dichloroanisole	18.4	80.3	80 ± 3
	25.5	83.6	
	31.3	77.6	
2,4,6-Trichloroanisole	22.5	70.3	67 ± 3
	33.9	67.0	
	41.3	64.6	
2,4,6-Trichlorophenol	32.2	148.9	152 ± 4
	40.1	156.4	
	52.5	151.4	
2,3,4,6-Tetrachloroanisole	18.7	63.3	64.5 ± 0.3
	27.8	67.2	
	35.0	63.1	
2,3,4,6-Tetrachlorophenol	26.6	67.4	77 ± 9
	31.6	84.6	
	38.8	79.5	
Pentachloroanisole	44.5	43.4	51 ± 7
	64.8	58.0	
	81.0	51.0	
Pentachlorophenol[a]	2.80	57.9	75 ± 22
	3.21	100.0	
	4.77	67.3	
Lindane	289	82.4	87 ± 6
	400	93.7	
	482	86.5	

[a] Amount added in μg g^{-1} of cork

stirred for 60 min at 700 rpm [4]. After sampling, the stir bar was removed with tweezers, rinsed in Milli-Q water and dried with a lintfree tissue paper. Finally, for thermal desorption (TD), the stir bar was put into a glass tube of 60 mm in length, 6 mm o.d. and 4 mm i.d., which was placed in the autosampler tray of the thermodesorption unit for GC–MS analysis.

2.6. GC–MS equipment and chromatographic conditions

Gas chromatography analyses were performed with a 6890 Agilent GC system coupled to a quadrupole mass spectrometer Agilent 5975inert and equipped with a Gerstel Thermo Desorption System (TDS2) and a cryo-focusing CIS-4 PTV injector (Gerstel).

The thermal desorption was carried out in splitless mode and with a flow rate of 75 mL min^{-1}. Desorption temperature program: 40 °C held 1 min, ramped at 60 °C min^{-1} to 250 °C held for 5 min. The CIS-4 PTV injector, with a Tenax TA inlet liner, was held at −20 °C with liquid nitrogen for total desorption time and then ramped at 10 °C s^{-1} to 290 °C and held for 3 min. Solvent vent mode was employed for transfer of sample to analytical column.

Table 3
Comparison of extraction medium in high volume extraction experiments

Extraction media	TA (%)[a]	CA (%)[a]	CP (%)[a]
100% ethanol	93 ± 14	100 ± 3	89 ± 16
75% ethanol:25% Milli-Q water	100 ± 5	91.6 ± 0.1	100 ± 6
50% ethanol:50% Milli-Q water	72 ± 27	77 ± 7[b]	68 ± 32
50% ethanol:50% Milli-Q water at pH 3.6	69 ± 12	66.9 ± 1.2[b,c]	68 ± 14

TA: total chromatographic area; CA: sum of chromatographic areas of chloroanisole compounds; CP: sum of chromatographic areas of chlorophenol compounds.

[a] Results are expressed as percentage with reference to the highest value ± confidence interval.

[b] Significant differences compared with 100% ethanol extraction medium.

[c] Significant differences compared with 75% ethanol:25% Milli-Q water extraction medium.

An HP-5MS capillary column (30 m × 0.25 mm i.d. × 0.25 μm film thickness, Agilent Technologies) was used. The carrier gas was He at a flow rate of 1.0 mL min^{-1}.

Oven temperature program: 50 °C for 2 min, then raised to 110 °C at 25 °C min^{-1} (held 0.5 min), at a rate of 2.5 °C min^{-1} to 170 °C and to 310 °C at 25 °C min^{-1} (held for 3 min). The quadrupole, source and transfer line temperatures were maintained at 150, 230 and 280 °C, respectively. Electron ionisation mass spectra in the full-scan mode were recorded at 70 eV electron energy in the range 35 to 500 amu. All data were recorded using a MS ChemStation. Blank runs of empty glass tube were done before and after each analysis. The identity of each compound was assigned using the NIST library and quantification by means of calibration plots of respective standards using their characteristic *m/z* values (Table 1).

3. Results and discussion

Calibration plots were built with different standard solutions, which were submitted to SBSE. Concentration ranges for all compounds under study are shown in Section 2.1. Each level of concentration was analysed by triplicate. The correlation coefficients obtained ranged from 0.992 to 1.00, except for TrCP whose value was 0.983 (Table 1).

Quantification (LOQ) and detection (LOD) limits were calculated with data generated in the calibration plots according to Miller and Miller [20] as indicated below (Table 1):

$$LOD = \frac{3 \times S_a}{b}, \qquad LOQ = \frac{10 \times S_a}{b}$$

where S_a is the standard deviation of the interception and b is the slope of calibration straightline.

Two different extraction experiments named HVE and LVE were conducted. Their efficacy is evaluated by means of the following: total chromatographic area (TA), total chromatographic areas of chloroanisole compounds (CA) and total chromatographic areas of chlorophenol compounds (CP).

In Table 3 there is a display of the results obtained with different extraction media using the HVE procedure. Considering area values, ANOVA results and less consuming solvents, we hence selected as extraction medium a mixture of 75% ethanol–25% Milli-Q water. Conversely, if we employ this medium (75% ethanol–25% Milli-Q water) and the resulting extract is concentrated by mean of a rotary evaporator, poorer results are obtained (Fig. 1).
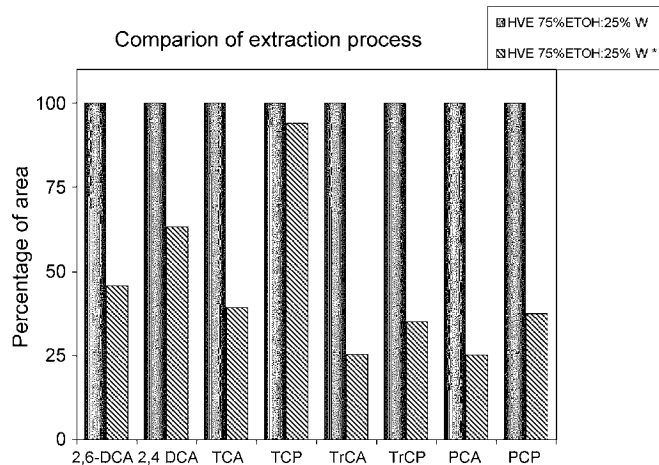
Fig. 1. Effect of the extract concentration in HVE extraction procedure (*The extract was concentrated in a rotary evaporator).

Fig. 2 shows results for both extraction methods (HVE and LVE). As can be seen, the highest figures for chromatographic areas were obtained for HVE extraction. Therefore, the extraction method selected was HVE employing 75% ethanol–25% Milli-Q water.

To optimise time and number of extractions two experiments were conducted (short and long-term extractions). Results were evaluated by means of recovery percentages (Table 4).
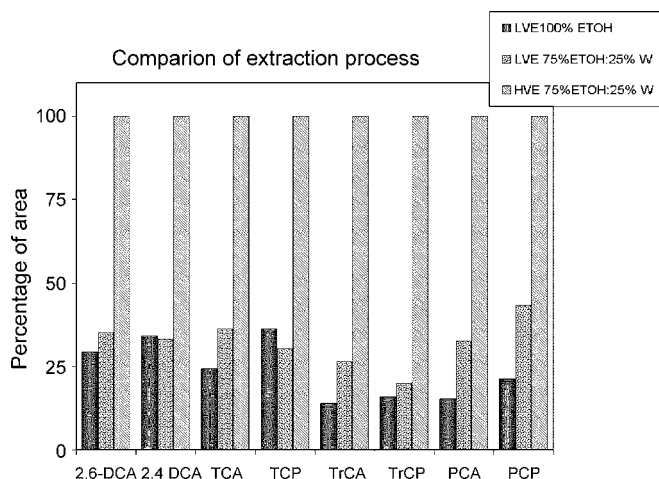
Fig. 2. Comparison of extraction method: LVE (low volume extraction) and HVE (high volume extraction).

Table 4
Recovery values obtained when different time of extraction is applied

Compounds	Mean recovery (%)						
	Short-term extraction				Long-term extraction		
	First extraction	Second extraction	Third extraction	Total	First extraction	Second extraction	Total
2,6-Dichloroanisole (2,6-DCA)	51.8 ± 1.7	8.7 ± 1.1	–	60.4 ± 0.6	53.4 ± 0.9	11.9 ± 0.7	65 ± 2
2,4-Dichloroanisole (2,4-DCA)	57 ± 5	9.4 ± 1.0	–	66 ± 4	67.8 ± 1.7	15.8 ± 0.9	83.6 ± 1.6
2,4,6-Trichloroanisole (2,4,6-TCA)	54 ± 4	9.7 ± 1.3	2.9 ± 0.4	66.5 ± 2.2	53.3 ± 1.4	13.7 ± 1.3	67.0 ± 2.4
2,4,6-Trichlorophenol (2,4,6-TCP)	58 ± 5	–	–	58 ± 5	121.3 ± 2.0	35.2 ± 2.1	156.4 ±
2,3,4,6-Tetrachloroanisole (2,3,4,6-TrCA)	57 ± 3	10.9 ± 1.3	–	68.3 ± 1.7	52.0 ± 2.8	15.2 ± 0.5	67 ± 3
2,3,4,6-Tetrachlorophenol (2,3,4,6-TrCP)	65 ± 3	10.5 ± 1.2	–	76 ± 4	66.9 ± 6.4	17.7 ± 2.1	84.6 ± 1.1
Pentachloroanisole (PCA)	46.2 ± 1.2	11.2 ± 0.5	–	57.4 ± 0.7	42.3 ± 3.4	15.6 ± 0.6	58.0 ± 0.5
Pentachlorophenol (PCP)	58 ± 5	8.6 ± 0.1	–	67 ± 2	87.4 ± 8.2	12.6 ± 1.4	100.0 ± 0.8
Lindane (LIND)	64 ± 3	11.6 ± 1.9	6.0 ± 0.4	81.2 ± 1.4	70.2 ± 1.9	23.6 ± 0.3	93.7 ± 1.6

–: Value below limit of quantification.

Regarding the short procedure, the recovery coefficients obtained by the first extraction were similar to those found for the long procedure for 2,6-DCA, TCA and PCA; higher for TrCA and lower for the remaining compounds. The amount recovered in the second extraction step ranged between 8.6 and 11.6% lower than that obtained for the long extraction method (11.9–35.2%). The last extraction step yields amounts below quantification limits for most of the studied compounds.

As can be seen in the results for the second extractions the remaining quantity of cloroanisoles and chlorophenols present in cork stoppers is very low (most of the situations) and the time required to release them is higher (approximately 24 h).

Hence for an efficient extraction the second method (long term extraction) is preferred, as pointed out by several authors [6,7,11].

Regarding the shaking method, Juanola et al. [10] found that prolonged shaking leads to better results than the ultrasonic bath. Our results suggest that a combination of both techniques could be the best choice.

Repeatability is calculated as the relative standard deviation of five extraction at one level spiked cork stoppers (100 μL), values obtained range between 3% (PCA, TCA and TrCA) and 17% for PCP. These values are considered as suitable for the corresponding analyte concentration under AOAC requirements [21].

Finally, in these extraction conditions, recovery percentages (mean of values obtained for three spiking levels) were calculated (Table 2). Results show values ranging between 64.5% (TrCA) and 152% (TCP). Best recoveries were obtained for PCP (75%) and 2,4-DCA (80%). Lindane seems to be a suitable IS of extraction, its recovery value meets the requirements of the AOAC for the concentration levels between 1 ppm and 100 ppb [20].

To our knowledge it is the first time that previous extraction and direct immersion SBSE technique is used to determine these compounds in cork stoppers. It is difficult to compare these results with other obtained by authors, since our method supposes the spiking of cork material in the inner surfaces and has the utility of evaluating potential migration to wine. In fact certain authors have reported that spiking the surface of cork may not reflect true recoveries from cork [22]. Sensibly higher recoveries are obtained in these cases [23].

If we take into account threshold values for these compounds and consider the minimum cork stopper contamination to provoke a taint wine, we can estimate the validity of our method for potential contamination diagnosis. When we compare (Table 5) expected values in contaminated stopper with our LOQ corrected values, we can see that all the compounds studied, except TCA, yield concentration levels lower then those resulting in cork taint. Only occasionally no more than 10% of these compounds are

Table 5

Compound	Threshold[a] (ng L^{-1})	Corresponding amount in a bottle of wine[b] (ng)	Concentration in cork stopper[c] (ng g^{-1})	Concentration in cork stopper[d] (ng g^{-1})	LOQ[e] (ng g^{-1})
TCA	4	3	1	0.67	1.21
PCA	4000	3000	1000	500	13.6
2,3,4,6-TrCA	14	10.5	3.5	2.24	2.02
2,4-DCA	400	300	100	80	3.19
2,6-DCA	40	30	10	6.5	2.40
TCP	350	262.5	87.5	133	2.15

[a] Thresholds references [4,11].
[b] Seven hundred and fifty millilitres of wine.
[c] Three grams cork stopper and a transference rate from cork stopper: 100%.
[d] Expected concentration quantified by the proposed method.
[e] LOQ corrected values calculated taking into account recovery percentage (Table 2).
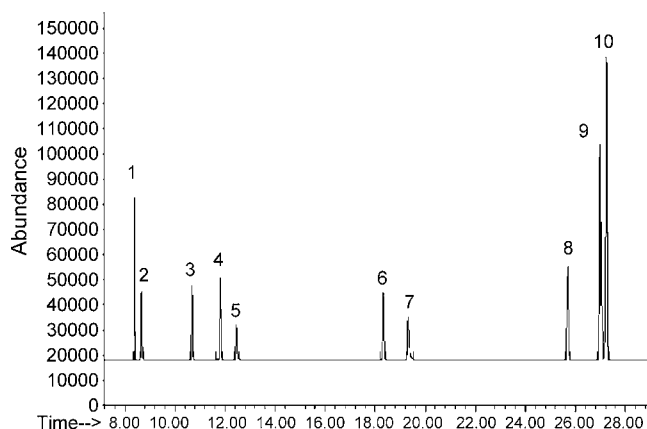
Fig. 3. Chromatogram of merged characteristic ion (*m/z*) of each molecule of the extract from a spiked cork stopper sample with 75 μL of stock solution: (1) IS; (2) 2,6-DCA; (3) 2,4-DCA; (4) TCA; (5) TCP; (6) TrCA; (7) TrCP; (8) PCA; (9) PCP; (10) lindane. *Time unit: min.

released from cork to wine [24], the proposed is suitable since allows their detection despite some low recoveries.

We can conclude that GC–MS coupled to SBSE with a previous extraction (HVE, 24 h) in the conditions above described, allow to estimate the total content of chloroanisoles and chlorophenols in cork stoppers. Taking into account LOQ and recovery values obtained, it is possible to determine the presence of these compounds in cork at very low levels (from $1.2 \, \text{ng g}^{-1}$ for TCA to $23.03 \, \text{ng g}^{-1}$ for TrCP), except for PCP due to different polarities between PCP and polymethylsiloxane phase [4]. The advantage of the proposed methodology is the possibility of determination of eight different compounds (chloroanisoles and chlorophenols) in a single run (Fig. 3). This fact points out that this method could be a useful tool for quality control in cork stopper industries.

References

[1] F. Bianchi, M. Careri, A. Mangia, M. Musci, J. Sep. Sci. 26 (2003) 369.
[2] R. Juanola, D. Subirà, V. Salvadó, J.A. Garcia Reguero, E. Anticó, Eur. Food Res. Technol. 220 (2005) 347.
[3] P. Chatonnet, S. Bonnet, S. Boutou, M.D. Labadie, J. Agric. Food Chem. 52 (2004) 1255.
[4] A. Zalacain, G.L. Alonso, C. Lorenzo, M. Iñiguez, M.R. Salinas, J. Chromatogr. A 1033 (2004) 173.
[5] A. Martínez-Uruñuela, J.M. González-Sáiz, C. Pizarro, J. Chromatogr. A 1048 (2004) 141.
[6] A. Peña-Neira, B. Fernández de Simón, M.C. garcía-Vallejo, T. Hernández, E. Cadahía, J.A. Suárez, Eur. Food Res. Technol. 211 (2000) 257.
[7] S. Insa, E. Besalú, C. Iglesias, V. Salvadó, E. Anticó, J. Agric. Food Chem. 54 (2006) 627.
[8] C. Lorenzo, A. Zalacain, G.L. Alonso, M.R. Salinas, J. Chromatogr. A. 1114 (2006) 250.
[9] A. Martínez-Uruñuela, I. Rodriguez, R. Cela, J.M. González-Sáiz, C. Pizarro, Anal. Chim. Acta 549 (2005) 117.
[10] R. Juanola, D. Subirà, V. Salvadó, J.A. Garcia Reguero, E. Anticó, J. Chromatogr. A 953 (2002) 207.
[11] G.J. Soleas, J. Yan, T. Seaver, D.M. Goldberg, J. Agric. Food Chem. 50 (2002) 1032.
[12] S. Insa, E. Anticó, V. Ferreira, J. Chromatogr. A 1089 (2005) 235.
[13] J.L. Gómez-Ariza, T. García-Barrrera, F. Lorenzo, A.G. González, Anal. Chim. Acta 540 (2005) 17.
[14] M. Riu, M. Mestre, O. Busto, J. Guasch, J. Chromatogr. A 977 (2002) 1.
[15] O. Ezquerro, M.T. Tena, J. Chromatogr. A 1068 (2005) 201.
[16] Y. Hayasaka, K. MacNamara, G.A. Baldock, R.L. Taylor, A.P. Pollnitz, Anal. Bioanal. Chem. 375 (2003) 948.
[17] R.F. Alves, A.M.D. Nascimento, J.M.F. Nogueira, Anal. Chim. Acta 546 (2005) 11.
[18] E. Baltussen, P. Sandra, F. David, C. Cramers, J. Microcol. Sep. 11 (1999) 737.
[19] E. Pfannkoch, J. Whitecavage, A. Hoffmann, Gerstel Appl. Note 2 (2001) 1.
[20] J.C. Miller, J.N. Miller, Statistics for Analytical Chemistry, 3rd ed., Ellis Horwood Limited, Chichester, 1993, p. 155.
[21] AOAC, Peer Verified methods Program. Manual on Policies and Procedures, AOAC, VA, 1993.
[22] M.K. Taylor, T.M. Young, C.E. Butzke, S.E. Ebeler, J. Agric. Food Chem. 48 (2000) 2208.
[23] M. Riu, M. Mestre, O. Busto, J. Guash, J. Chromatogr. A 1107 (2006) 240.
[24] D.L. Capote, G.K. Shouroumounis, D.A. Barker, H.J. Mclean, A.P. Pollnitz, M.A. Sefton, Aust. J. Grape Wine Res. 5 (1999) 91.

An electrochemical amplification immunoassay using bi-electrode signal transduction system

Zhao-Peng Chen, Jian-Hui Jiang, Xiao-Bing Zhang, Guo-Li Shen, Ru-Qin Yu *

State Key Laboratory for Chemo/Biosensing and Chemometrics, College of Chemistry and Chemical Engineering, Hunan University, Changsha 410082, China

Abstract

An electrochemical immunoassay technique has been developed based on the sensitive detection of the enzyme-generated product with a bi-electrode signal transduction system. The system uses two separate electrodes, an immunoelectrode and a detection electrode to form a galvanic cell to implement the redox reactions on two different electrodes, that is the enzyme-generated reductant in the anode region is electrochemically oxidized by an oxidant (silver ions) in the cathode apartment. Based on a sandwich procedure, after immunoelectrode with antibody immobilized on its surface bound with the corresponding antigen and alkaline phosphatase conjugated antibody successively, the immunoelectrode was placed in enzyme reaction solution and wired to the detection electrode which was immerged into a silver deposition solution. These two solutions are connected with a salt bridge. Thus a bi-electrode signal transduction system device is constructed in which the immunoelectrode acts as anode and the detection electrode serves as cathode. The enzyme bound on the anode surface initiates the hydrolysis of ascorbic acid 2-phosphate to produce ascorbic acid in the anode region. The ascorbic acid produced in the anodic apartment is electrochemically oxidized by silver ions coupled with the deposition of silver metal on the cathode. Via a period of 30 min deposition, silver will deposited on the detection electrode in an amount corresponding to the quantity of ascorbic acid produced, leading to a great enhancement in the electrochemical stripping signal due to the accumulation of metallic silver by enzyme-generated product. Compared with the method using chemical deposition of silver, the electrochemical deposition of silver on a separate detection electrode apartment avoids the possible influence of silver deposition on the enzyme activity.
© 2006 Elsevier B.V. All rights reserved.

Keywords: Immunoassay; Bi-electrode signal transduction system; Immunoelectrode

1. Introduction

The development of sensitive immunoassay and DNA assay techniques has been a long-sought goal in biomedical studies. Many strategies have been proposed to enhance the sensitivity of immuno or DNA sensing. Typical examples include the use of gold nanoparticles as signal amplifier [1–7], the incorporation of silver staining into gold nanoparticle labeling [8,9] the utilization of ferrocene capped gold nanoparticle tags [10], the application of carbon nanotubes to load more enzyme labels and to accumulate enzyme-generated product [11] as well as the implementation of enzyme conjugate-catalyzed precipitation of insoluble products [12–15].

Enzyme conjugated biochemistry is routinely used as the amplifier in electrochemical immunoassay. A common method for electrochemical detection of enzymes is based on the voltammetric behavior of the enzyme-generated product. This method, however, is not sensitive enough for clinical diagnosis applications in some cases. Recently a novel method for electrochemical detection of DNA hybridization was proposed based on chemical accumulation of silver metal by an enzyme-catalyzed product of *p*-aminophenol. The subsequent anodic stripping voltammetry provided a DNA detection method with high sensitivity [16]. The coupling of enzyme catalysis and metal deposition seems to be a promising strategy for sensitive immunoassay. However, the chemical deposition of metal on the transducer on which the enzyme is present would block the catalytic centers of enzyme molecules, hindering a continual accumulation of the metal. The heavy metal ions coexisting in the substrate solution might also inhibit the activity of the enzyme [17–19]. These factors may all lead to a loss of detection sensitivity. On the other hand, the deposition of metal on the transducer with immobilized biomolecules makes it impossible to construct a renewable biosensor in which the biointerface should be regenerated without loss of activity.

---

* Corresponding author. Fax: +86 731 8822577.
 E-mail address: rqyu@hnu.cn (R.-Q. Yu).

To circumvent the aforementioned drawbacks associated with chemical deposition of silver metal, we have developed herein a sensitive electrochemical immunoassay technique that utilizes two separate electrodes, an immunoelectrode with immobilized antibody for antigen and antibody-enzyme conjugate recognition at the anode and a detection electrode for electrochemical deposition of silver as the cathode to form a galvanic cell. The immunochemical recognition event between human IgG and goat anti-human IgG antibody is chosen as the model system to illustrate the proposed immunoassay approach. After the human IgG was sandwiched between the immobilized antibodies and the ALP conjugated antibodies, the ALP conjugated antibodies bound to the immunoelectrode surface catalyzed the generation of ascorbic acid, which in turn was oxidized at the anode to dehydroascorbic acid while the silver ions was reduced at the cathode. This resulted in silver deposition on the detection electrode, enabling a sensitive detection of the immunorecognition event by stripping analysis.

2. Experimental

2.1. Reagents

Goat-anti-human IgG antibody (affinity purification), human IgG and anti-human IgG-alkaline phosphatase conjugate were obtained from Sino-Americal Biotechnology Company (Shanghai). Ascorbic acid 2-phosphate AA-p was purchased from Express Technology Co., Ltd. (Japan). Other reagents were of analytical purity, and doubly distilled water was used throughout all experiments.

2.2. Apparatus

Electrochemical measurements were performed with a three-electrode system comprising a platinum foil as auxiliary electrode, a saturated calomel electrode as reference electrode, and the glass carbon electrode or the carbon paste electrode as working electrode. All electrochemical experiments were performed on CH660 electrochemical workstation (Shanghai Chenhua Instruments, Shanghai) connecting with a personal computer.

2.3. Immunoassay procedure

Carbon paste electrode was fabricated by pressing a mixture of graphite powder and melting paraffin into a Teflon tube (6 mm inner diameter). Before antibody adsorption, the carbon paste electrode was pretreated in 0.1 mol/l sodium hydroxide solution with a potential of 2.0 V versus SCE reference electrode for 10 min [20]. Then the electrochemically pretreated carbon paste electrode was exposed to $0.2\,\text{mg}\,\text{ml}^{-1}$ anti-human IgG in tris buffer (pH 7.4). Through 1 h incubation at room temperature, the anti-human IgG were immobilized through passive adsorption, and an immunoelectrode was fabricated. After the immunoelectrode was immersed in 1% BSA for 30 min to block the non-occupied adsorption sites, the anti-human IgG modified carbon paste electrode was exposed to human IgG solutions of different
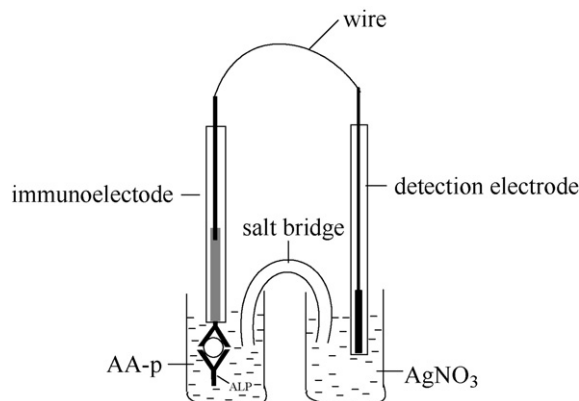
Scheme 1. The bi-electrode signal transduction system.

concentrations for 40 min at 37 °C, and subsequently contacted with $0.02\,\text{mg}\,\text{ml}^{-1}$ anti-human IgG-alkaline phosphatase (ALP) conjugate for 40 min at 37 °C. The human IgG was sandwiched between the immobilized antibodies and the ALP conjugated antibodies. To detect ALP bound on the immunoelectrode with high sensitivity, a novel bi-electrode signal transduction device was designed. As shown in Scheme 1, after the immunoreactions were completed, the immunoelectrode was immersed into 1 ml enzyme reaction solution (pH 9.0) composed of 80 mM glycin and 1 mM ascorbic acid 2-phosphate. The immunoelectrode was wired to the detection electrode, which was a clean glassy carbon electrode (4 mm in diameter) immerged in 1 ml silver deposition solution (pH 9.0) composed of 80 mM glycin and 1 mM $AgNO_3$. These two solutions were connected with a salt bridge. Thus a bi-electrode signal transduction device was constructed with the immunoelectrode as the anode and the detection electrode as the cathode. The signal transduction device was maintained to work at 37 °C for a fixed time. Then, the detection electrode was taken out of the cell and rinsed with water. Anodic stripping voltammetry (ASV) measurement was applied to the electrode in a solution of 0.6 M KNO_3 and 0.1 M HNO_3 with a scan rate of 100 mV/s to detect silver deposited on cathode.

3. Results and discussion

It is well known, if a shiny piece of copper is placed into a solution of silver nitrate, a spontaneous reaction occurs. Grayish white silver will deposit on the copper and the solution will turn blue because of the oxidation of copper to ions(II). The redox reaction can be described as follow:

$$2Ag^+ + Cu \Rightarrow Cu^{2+} + 2Ag$$
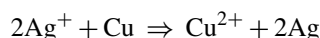
The same chemical reaction can occur and produce electricity in a galvanic cell. A galvanic cell consists of two containers with a salt bridge between them. The two containers each encase the half-reactions of the equation above.

$$Ag^+ + e^- \rightarrow Ag$$

$$Cu \rightarrow Cu^{2+} + 2e^-$$
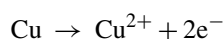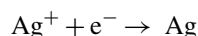
The electron flow from the anode to the cathode is what creates electricity, resulting in the deposition of Ag on anode. In a galvanic cell, the cathode is potential positive with respect to that of the anode.

In the present study, the interaction between antibody and antigen was measured indirectly via detection of enzyme labeled antibody after sandwich immunoreactions using a bi-electrode transduction system. In the system, the ALP bound on the immunoelectrode catalyzed the generation of ascorbic acid which 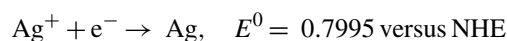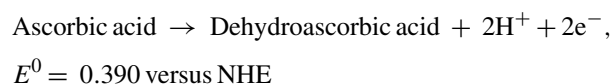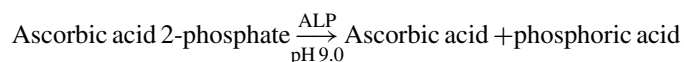was oxidized at the anode to dehydroascorbic acid while the silver ions was reduced at the cathode, resulting in silver deposition on the detection electrode. The ALP catalysis [21] and the electrochemical reactions can be expressed as follows:

$$\text{Ascorbic acid 2-phosphate} \xrightarrow[\text{pH 9.0}]{\text{ALP}} \text{Ascorbic acid} + \text{phosphoric acid}$$

$$\text{Ascorbic acid} \rightarrow \text{Dehydroascorbic acid} + 2H^+ + 2e^-,$$

$$E^0 = 0.390 \text{ versus NHE}$$

$$Ag^+ + e^- \rightarrow Ag, \quad E^0 = 0.7995 \text{ versus NHE}$$

The deposited silver metal was measured by anodic stripping voltammetry. Curves a–d in Fig. 1 depict the anodic stripping voltammograms for determination of 0, 10, 100 and 1000 ng/ml human IgG obtained using the developed immunoassay technique with a deposition time of 30 min. The concentration of AA-p in enzyme reaction solution and the silver ions in silver deposition solution were both 1 mM. Obviously, the presence of human IgG results in the binding of ALP conjugated anti-human IgG on the immunoelectrode, producing relatively large stripping currents (curves b–d). In contrast, with the immunoelectrode exposed to ALP conjugated anti-human IgG in the absence of analyte human IgG, only a small stripping current is obtained due to non-specific adsorption of ALP conjugate (curve a).
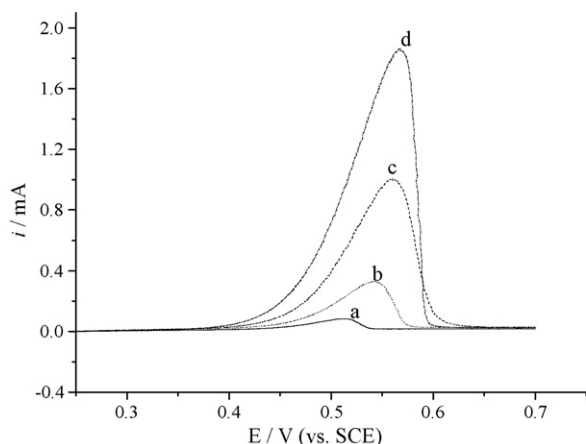
Fig. 1. The anodic stripping voltammograms obtained using the developed immunoassay technique with a deposition time for determination of different concentration of human IgG. (a) 0 ng/ml; (b) 10 ng/ml; (c) 100 ng/ml and (d) 1000 ng/ml. The anode solution contained 1 mM of AA-p and the cathode solution had 1 mM AgNO$_3$.
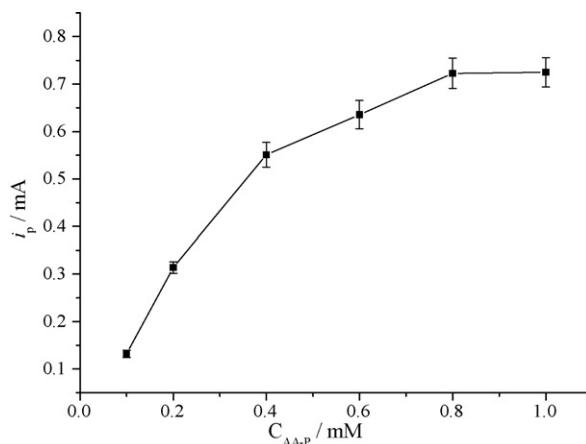
Fig. 2. Effect of AA-p concentration on i_p. The deposition time is 15 min and the concentration of Ag$^+$ is 1 mM.

3.1. Effect of the AA-p concentration

Since the amount of deposited silver metal on the detection electrode is depended on the amount of enzyme-generated ascorbic acid which is controlled by the concentration of AA-p, the dependence of the amount of deposited silver metal on the concentration of AA-p should be investigated. As shown in Fig. 2, with a fixed deposition time of 15 min, the silver metal stripping current for detection of 100 ng/ml human IgG increased with the increase of the concentration of AA-p in enzyme reaction solution up to 0.8 mM, and became stable for AA-p concentration over 0.8 mM (Fig. 2). As a result, an AA-p concentration of 1.0 mM was selected in the subsequent work. No appreciable stripping current was obtained in the absence of AA-p. This confirmed that sliver deposition is attributed to the enzyme-mediated generation of ascorbic acid.

3.2. Effect of the deposition time

Obviously, the amount of silver metal deposited on the detection electrode is related to the deposition time. One can predict that more deposition time should result in more silver deposition. This would affect the sensitivity of the immunoassay and should be optimized. As shown in Fig. 3, the stripping current for determination of 100 ng/ml human IgG increases as the deposition time increases up to 20 min. With a deposition time more than 30 min, the stripping current tends to level off, indicating that the enzyme activity becomes low and enzyme catalytic reaction becomes very slow over 20 min. A deposition period of 30 min was adopted in this work to obtain a better reproducibility because the effect of time under this condition is insignificant.

3.3. Effect of the Ag$^+$ concentration

To determination quantitatively the amount of the enzyme bound on the immunoelectrode, the enzyme-generated ascorbic acid was measured by the amount of the deposited silver on the detection electrode. Sufficient Ag$^+$ should be added in the cathodic solution to ensure ascorbic acid generated at the
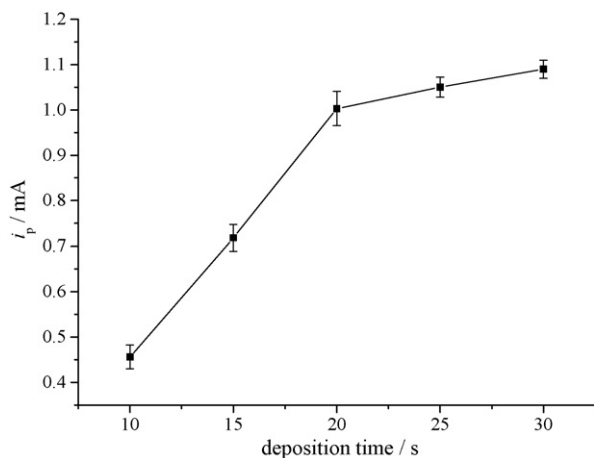
Fig. 3. Effect of the deposition time on i_p. The concentration of AA-p is 1 mM and the concentration of Ag$^+$ is 1 mM.

immunoelectrode to be electrochemically oxidized as quickly as possible. Two different concentrations of Ag$^+$, 1 mM and 10 mM, were investigated. The results showed that the stripping currents had no obvious difference in these two conditions. Then, Ag$^+$ concentration of 1 mM was used for complete oxidation of ascorbic acid. No ascorbic acid remained in the enzyme reaction solution was detectable with differential pulse voltammetry or the bi-electrodes system in which the immunoelectrode was replaced by a glassy carbon electrode, evidencing that ascorbic acid generated at the immunoelectrode was practically completely oxidized by silver ions. This also indicates 1 mM silver ions is sufficient to oxidize enzyme-generated product.

3.4. Detection of human IgG

Under the optimized conditions, the stripping current was dynamically correlated to the concentration of human IgG. The current showed a linear correlation to human IgG concentration in the range of 10–1000 ng/ml with a regression equation i (mA) $= -0.338 + 0.66 \log C_{IgG}$ (ng/ml) ($r = 0.9963$). The detection limit was 3.6 ng/ml. The sensitivity of this immunoassay technique was comparable to those for the immunosensors based on iridium oxide matrices [22] and the immunoassay using of nanoparticles as amplifier [4].

4. Conclusion

We have developed a new immunoassay technique that using a bi-electrode signal transduction device where the reductant catalytically generated by enzyme bound on the anode electrochemically initiates the deposition of silver metal on the cathode. The developed immunoassay technique embodies several attractive features. First, the accumulation of the enzyme conjugate-catalyzed product in a relatively long period via the silver deposition enables a highly sensitive stripping analysis of the metal in a relative short time, thereby offering a substantial signal amplification of the immunorecognition events. Second,

compared with the procedure based on chemical deposition of silver, the silver deposition on a separate detection electrode instead of the immunoelectrode itself circumvents possible influence of silver deposition and heavy metal ion inhibitors on the enzyme activity. Finally, the deposition of silver on the separate detection electrode instead of the immunoelectrode makes it possible to fabricate renewable immunosensors by regenerating the immunoelectrode under mild conditions [23–25].

To our knowledge, this is the first report demonstrating the implementation of a bi-electrode signal transduction system for sensitive immunoassay. The device can also be applied for sensitive detection of ascorbic acid, hydroquinone, aminophenol or other reductants, which, in some sense, can be regarded as the stripping voltammetry for detecting organic substance. Some preliminary experiments showed that ascorbic acid as low as 10^{-7} M could be detected using this device, which is more sensitive than some other electrochemical methods for ascorbic acid detection [26,27]. It was expected that this device would hold great promise in detecting enzyme-catalyzed products for immunoassay.

Acknowledgment

References

[1] L. He, M.D. Musick, S.R. Nicewarner, F.G. Salinas, S.J. Benkovic, M.J. Natan, C.D. Keating, J. Am. Chem. Soc. 122 (2000) 9071.
[2] L.A. Lyon, M.D. Musick, M.J. Natan, Anal. Chem. 70 (1998) 5177.
[3] X.C. Zhou, S.J. O'Shea, S.F.Y. Li, Chem. Commun. 11 (2000) 953.
[4] C. Zhang, Z. Zhang, B. Yu, J. Shi, X. Zhang, Anal. Chem. 74 (2002) 96.
[5] M. Dequaire, C. Degrand, B. Limoges, Anal. Chem. 72 (2000) 5521.
[6] T.A. Taton, R.C. Mucic, C.A. Mirkin, R.L. letsinger, J. Am. Chem. Soc. 122 (2000) 6305.
[7] F. Patolsky, K.T. Ranjit, A. Lichtentein, I. Willner, Chem. Commun. 12 (2000) 1025.
[8] X.D. Su, S.F.Y. Li, S.J. O'Shea, Chem. Commun. 8 (2001) 755.
[9] X. Chu, X. Fu, K. Chen, G.L. Shen, R.Q. Yu, Biosens. Bioelectron. 20 (2005) 1805.
[10] J. Wang, J. Li, A.J. Baca, J. Hu, F. Zhou, W. Yan, D.W. Pang, Anal. Chem. 75 (2003) 3941.
[11] J. Wang, G. Liu, M.R. Jan, J. Am. Chem. Soc. 126 (2004) 3010.
[12] L. Alfonta, I. Willer, D.J. Throchmorton, A.K. Singh, Anal. Chem. 73 (2001) 5287.
[13] C. Ruan, K. Zeng, O.K. Varghese, C.A. Grimes, Anal. Chem. 75 (2003) 6494.
[14] E. Katz, L. Alfonta, I. Willner, Sens. Actuators B 76 (2001) 134.
[15] L. Alfonta, A.K. Singh, I. Willner, Anal. Chem. 73 (2001) 91.
[16] S. Hwang, E. Kim, J. Kwak, Anal. Chem. 77 (2005) 579.
[17] C. Durrieu, C. Tran-Minhw, Ecotoxicol. Environ. Saf. 51 (2002) 206.
[18] S.D. Kamtekar, R. Pande, M.S. Ayyagari, K.A. Marx, D.L. Kaplan, J. Kumar, S. Tripathy, Anal. Chem. 68 (1996) 216.
[19] Q.X. Chen, W.Z. Zheng, J.Y. Lin, Y. Shi, W.Z. Xie, H.M. Zhou, Int. J. Biochem. Cell Biol. 32 (2000) 879.
[20] Y.M. Zhou, S.Q. Hu, G.L. Shen, R.Q. Yu, Biosens. Bioelectron. 18 (2003) 473.
[21] Kokado, H. Arakawa, M. Maeda, Anal. Chim. Acta 407 (2000) 119.
[22] M.S. Wilson, R.D. Rauh, Biosens. Bioelectron. 19 (2004) 693.

[23] V.B. Kandimalla, N.S. Neeta, N.G. Karanth, M.S. Thakur, K.R. Roshini, B.E.A. Rani, A. Pasha, N.G.K. Karanth, Biosens. Bioelectron. 20 (2004) 903.

[24] Z. Gao, F. Chao, Z. Chao, G. Li, Sens. Actuators B 66 (2000) 193.

[25] R.D. Vaughan, C.K. O'Sullivan, G.G. Guilbault, Enzyme Microb. Technol. 29 (2001) 635.

[26] J.B. Raoof, R. Ojani, S. Rashid-Nadimi, Electrochem. Acta 49 (2004) 271.

[27] S. Wang, D. Du, Sens. Actuators 97 (2004) 371.

A thin cover glass chip for contactless conductivity detection in microchip capillary electrophoresis

Zuanguang Chen [a,*], Quanwen Li [a], Oulian Li [a], Xie Zhou [a],
You Lan [a], Yuanfang Wei [b], Jinyuan Mo [b]

[a] School of Pharmaceutical Sciences, Sun Yat-sen University, Guangzhou 510089, China
[b] School of Chemistry and Chemical Engineer, Sun Yat-sen University, Guangzhou 510275, China

Abstract

A microfabricated thin glass chip for contactless conductivity detection in chip capillary electrophoresis is presented in this contribution. Injection and separation channels were photolithographed and chemically etched on the surface of substrate glass, which was bonded with a thin cover glass (100 μm) to construct a new microchip. The chip was placed over an independent contactless electrode plate. Owing to the thinness between channel and electrodes, comparatively low excitation voltage (20–110 V in V_{p-p}) and frequency (40–65 kHz) were suitable, and favorable signal could be obtained. This microchip capillary electrophoresis device was used in separation and detection of inorganic ions, amino acids and alkaloids in amoorcorn tree bark and golden thread in different buffer solutions. The detection limit of potassium ion was down to 10 μmol/L. The advantages of this microchip system exist in the relative independence between the microchip and the detection electrodes. It is convenient to the replacement of chip and other operations. Detection in different position of the channel would also be available.
© 2006 Elsevier B.V. All rights reserved.

Keywords: Micro-total analysis systems (μ-TAS); Microchip; Contactless conductivity detection; Capacitively coupled contactless conductivity detection; High frequency conductivity detection

1. Introduction

In recent years, the multidisciplinary field micro-total analysis systems (μ-TAS) or lab-on-chip (LOC) has received much attention. Many research efforts were poured in due to its advantages, such as high degree of integration, remarkable sensitivity, low reagent consumption and short separation time, so an intense activity has taken place in this field. It is a challenge to find sensitive, selective and universal detection methods for μ-TAS adapting to the development of the recent microchip capillary electrophoresis study except the expensive and complicated laser-induced fluorescence (LIF) detection [1] and mass spectrum (MS) detection. Electrochemistry detection (ECD) offers great promise for such microsystems, as well as its low cost and ease of miniaturization due to the inherent characters. ECD

includes amperometry, conductimetry, potentiometry detection [2–4]. On one hand, the electrochemical reactions of amperometry and potentiometry take place at the electrodes surface, which lead to higher selectivity than conductimetry. On the other hand, the origin of selectivity makes them hard to fit the measured system. However, although both amperometry and potentiometry detections have remarkable sensitivity, the former only detects the electrochemically active compounds while the latter is restricted by the electrodes. Conductimetry is comparatively simple and sensitive, which theoretically can be applied to all charged analytes, especially for small inorganic ions and organic ions which have low electrochemical activity for amperometry detection or weak optical absorbance for optical measurements. It also has the potential application in environmental analysis, food analysis, and in various samples, like urine, serum, saliva, herb extracts. Hence, it has become one of the most attractive assay methods in analytical chemistry. Conductimetry detection can be classified into contact [3,5] and contactless (oscillometric) modes [6–9]. In contact mode the galvanic electricity comes into contact with the electrodes and electrolyte,

* Corresponding author. Tel.: +86 20 8836 4586; fax: +86 20 8733 0558.
E-mail address: chenzg@mail.sysu.edu.cn (Z. Chen).

whereas contactless mode the electrodes are insulated from the electrolyte.

Although contact conductimetry is comparatively sensitive, the contact between the electrolyte solution and the electrodes induces a lot of potential problems, such as bubble generation, electrode degradation and undesirable crosstalk. Therefore, contactless conductimetry has been paid close attention because it offers distinct advantages, the effective isolation between the electrodes and the electrolyte, simple construction, convenient manipulation and so on. The contactless conductivity detection includes jegger coupling [6] and capacitive coupling [10,11], but only the latter has been applied in microchip up to now.

Wang and his co-workers [12] reported an integrated contactless conductivity detection microchip system in which two opposite aluminum film electrodes were pasted outside a polymethylmethacrylate (PMMA) chip with the distance from the electrodes to the channel exceeded to 125 μm. The separation of four cations as well as five anions was performed. With an operating frequency of 200 kHz and excitation voltage of 5 V (in V_{p-p}), detection limit was down to 2.8 μmol/L for potassium. They also used their contactless conductivity detection of microfluidic device to separate four kinds of organophosphonate nerve agent degradation products [13] and for fast measurement of low-explosive ionic components [14]. Afterward, they used polished 150 μm thick cover plate on glass microfluidic chip in contactless conductivity detection microchip device to monitor aliphatic aminies in UV-absorbing solvents (dimethylformamide, dimethylacetamide, dimethyl sulfoxide, or propylene carbonate media) [15]. The same glass chip was used to in the simultaneous contactless conductivity detection and ampperometric measurement detection device [16]. They [17] have actualized a movable contactless conductivity detection system for microchip capillary electrophoresis, which could detect the signal at different points along the separation channel. The 1 mmol//L ammonium, methylammonium and sodium were detected with sine waveform at 200 kHz and 5 V (V_{p-p}).

Relatively recently, the development of microfabrication techniques made it comparatively easy to integrate the electrodes into the channels, or deposit the electrodes nearby the channel. Several research groups have used this technology in the contactless conductivity detection. Laugere et al. [18] put a thin aluminous layer directly into the channel. In their papers a 30 μm thick silicon carbide was used to meet the insulation between the electrodes and the analytes. The detection was carried out with the operating frequency lower than 10 kHz. They [19] also designed an integrated four-electrode contactless conductivity detection microchip system: the silver electrodes covered by 30 nm silicon carbide were mounted inside the glass microchannel. The detection was made of two or four electrodes, and detection limit for potassium reached 5 μmol/L at the optimal measurement frequency of 100 kHz and excitation voltage of 5 V (in V_{p-p}). Lichtenberg et al. [20] placed the platinum in the separation channel, with the distance between the electrodes and buffer electrolyte of 10–15 μm. They used a frequency of 58 kHz and maximum output voltage 15 V (in V_{p-p}) and the limit of detection for potassium was 18 μmol/L. Tanyanyiwa and Hauser [21] placed 0.5 mm width and 5 mm

length sliver electrodes into troughs with the distance to the channel of 200 μm. Better sensitivity was obtained by using an alternating current excitation voltage of 500 V (in V_{p-p}) and a frequency of 100 kHz. The detection of small inorganic ions, heavy metal, citric, lactic acids, three antiinflammatory nonsteroid drugs, 4-acetamidophenol, ibuprofen and salicylic were demonstrated.

Subsequently, Tanyanyiwa and Hauser [22] used a polymeric planar microchip device and placed the electrodes on the chip holder to construct external electrodes for contactless conductivity detection measurement. A thin PMMA foil of 100 μm allowed the channel close coupling to the electrodes. Sine wave of 100 kHz and high excitation voltage of 500 V (in V_{p-p}) were used to detect alkali, heavy metal ions, as well as inorganic anions and carboxylates. The detection limits were found to be 1–5 μmol/L for inorganic ions and 5–50 μmol/L for the organic species. Some further applications were demonstrated in their subsequent work, such as the analysis of basic drugs (physiologically active amines and b-adrenergic blocking agents) [23], the detection of human immunoglobulin M (IgM) [24], the analysis of beverages [25] and the determination of vitamine and preaevatives [26].

Generally, the thinner the insulating layer, the greater capacitance between solution and electrodes, and the stronger alternating current passed the solution. For the glass-based microchip, it means that the thin cover glass plate in the chip would make it possible to monitor the signal accurately and easily in contactless conductivity detection. Hence, this paper presents a new contactless conductivity detection device with thin microfabricated chip, in which the chip and electrodes are independent and replaceable. The usage of this device, to some extent, would enhance the power and scope of microfluidic analytical devices.

2. Experimental

2.1. Reagents and solutions

All the amino acids were purchased from Shanghai Bio Life Science & Technology Co. Ltd. (Shanghai, China) and used without further purification. 2-(*N*-Morpholino)ethanesulfonic acid (MES) was obtained from AMRES Co., Hong Kong. Other reagents in the grade of analytical reagent were purchased from Guangzhou Chemical Reagent Co. (China). All stock solutions and buffer solutions were prepared with redistilled water, degassed by ultrasonication and filtered through 0.2 μm nylon filters prior to use. Stock sample solutions of amino acids, potassium and magnesium, were prepared in a concentration of 10 mmol/L by redistilled water. Their operation solutions were diluted to suitable concentrations with redistilled water.

2.2. Apparatus

2.2.1. Device fabrication

The homemade microchip capillary electrophoresis system consisted of a high voltage supplier, a contactless conductivity detector and a thin microchip. The high voltage supplier was made of piezoelectric ceramics which provided a potential of
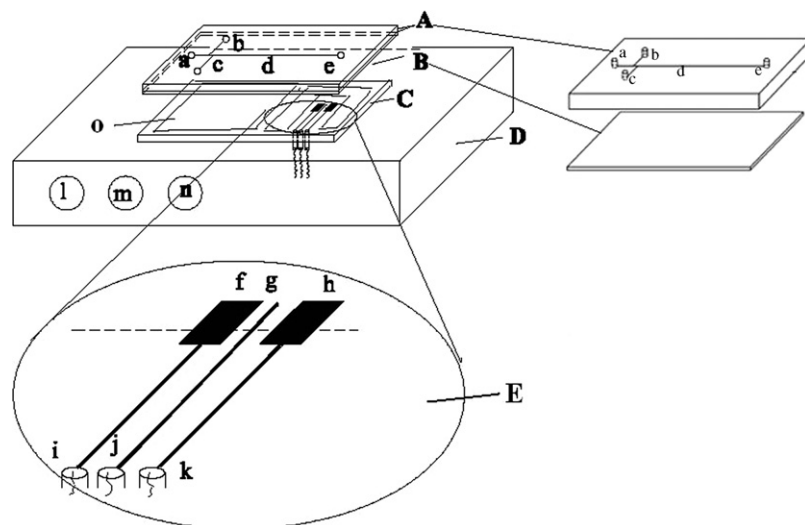
Fig. 1. Schematic illustration for glass microchip system. (A) Etched substrate glass; (B) thin cover glass; (C) contactless electrode plate; (D) contactless conductivity detector; (E) enlarges of electrodes ((a) buffer reservoir; (b) sample reservoir; (c) sample waste reservoir; (d) separation channel; (e) buffer waste reservoir; (f) input electrode; (g) shielding (earth) electrode; (h) output electrode; (i) input electrode terminal; (j) shielding electrode terminal; (k) output electrode terminal; (l) frequency adjustor; (m) excitation amplitude adjustor; (n) baseline adjustor; (o) rectangle of copper).

constant direct current of 100–500 V for injection and a potential of constant direct current or pulse of 500–5000 V for separation, described in detail in our previous literature [27]. The contactless conductivity detector provided three waveforms (sine, square, and triangle) with oscillation frequency of 0–300 kHz and oscillation voltage of 0–300 V (in $V_{p–p}$) [28]. The detector was connected to a personal computer with an A/D converter (model PCL-711B, EVOC, Taiwan). The construction of this system was showed in Fig. 1. Parts A and B were combined into the thin glass chip. Part C was the contactless electrode plate and part D was the detector shielding in iron box which consisted of excitation signal source, converter, amplifier and rectifier.

2.2.2. Thin glass microchip

In the procedure, two microfluidic channels were photolithographed and chemically etched onto a 1.6-mm thick × 20-mm wide × 60-mm long substrate glass (Fig. 1A, type SG2506 glass substrate with chromium and AZ1805 photoresist coating was obtained from Shaoguang Microeletronics Corp. (Changsha, China)), of which one was separation channel (a-d-e) with 70 μm in width, 30 μm in depth, 40 or 90 mm in effective length, the other was injection channel (b–c) with the same width and depth as the separation channel. Then the etched substrate glass was bonded with a thin cover glass in 100 μm of thickness (Fig. 1B). Two glass plates (A and B in Fig. 1) were combined into a glass-based chip in the process described previously by Yin et al. [29]. Briefly, a net work of microfluidic channels was designed with a CAD program. This design was transferred onto a sheet of film by a high-result ion laser setter. The film was used as a mask for ultraviolet exposure in the photolithographic procedure, a suitable Cr was used as a sacrificial mask, and the microchannels were etched into the plate in a well-stirred bath containing dilute HF/NH$_4$F. Four 1.2-mm-diameter access holes were drilled on the etched plate at channel terminals using an emery drill-bit, forming four reservoirs, and then the sub-

strate glass and the cover glass were rigorously cleaned and brought into close contact with each other in the redistilled water, and after that the glass were put into the vacuum drying oven. The temperature increased by 10 °C/min to 580 °C, after 3 h decreased temperature to the room temperature with the same speed.

2.2.3. Contactless electrodes manufacture

The contactless electrodes were designed as showed as in Fig. 1E. Both electrodes (f) and (h) were 2.0 mm of width in separation channel direction. The distance between the two electrodes was 0.6 mm. In the middle of two electrodes was a 0.2 mm wide copper line which was connected to earth to decrease noise level. The shape of electrodes was printed on the surface of copperplate with ink to protect the copper of electrodes parts, and then the copperplate was dripped into a solution of 20% ferric chloride and 10% hydrogen peroxide. After 1 h the copperplate was taken out to be rinsed. There were two copper areas (the area around the electrodes and a rectangle area part (o) in Fig. 1 were designed to make sure of the consanguineous contact between the microchip and electrodes. Three wires ((i)–(k) in Fig. 1) were connected to contactless conductivity detector. In this way the length of the wires was minimized, which could diminish the sources of noises.

2.2.4. Electronic circuit

The fundamental principle of contactless conductivity detection is that the excitation signal coupled with the solution in channel through the insulating layers, the monitored current has a linear relation to the electric conductance of the solution. The electric equivalent circuit of the contactless conductivity detection system was shown in Fig. 2. When the alternating current signal generated by excitation signal source (ES) acted on the input electrode, the signal overcame the capacitance between electrode and solution, and the resistance of solution in
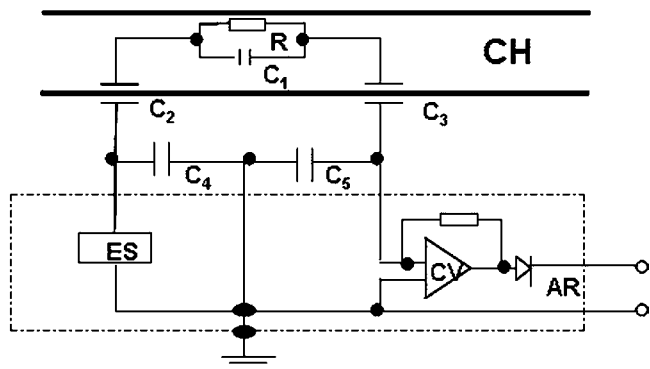
Fig. 2. Electric equivalent circuit of the contactless conductivity system. CH: channel in the chip; R and C_1: resistance and capacitance of the electrolyte solution in the zone between two electrodes; C_2 or C_3: capacitance between electrode and solution; C_4 or C_5: capacitance between electrode and earth; ES: excitation signal source; CV: current-to-voltage converter; AR: absolute rectifier.

the zone between two electrodes. The weak current signal that reached the output electrode was converted into voltage to be amplified.

2.3. Electrophoresis procedures

Prior to use, the channels were flushed with 0.1 mol/L sodium hydroxide aqueous solution, redistilled water, and running buffer for 10, 10, and 15 min, respectively. Reservoirs (a), (c), and (e) (Fig. 1) were filled with electrophoretic running buffer solution, while reservoir (b) (Fig. 1) was filled with sample solution. The injection was performed by applying 0.2 kV between the sample reservoir (b) and sample waste reservoir (c) for 20 s for the first time to facilitate the filling of the injection channel (between (b) and (c) in Fig. 1), but subsequent injection at 0.2 kV for 10 s. These operations could transport the sample into the separation channel through the intersection. Separations were done by switching the high voltage and applying a potential of 1.5 kV. Before the second cycle, the microchannels were treated sequentially with 0.1 mol/L sodium hydroxide for 5 min, redistilled water for 10 min and then flushed with running buffer. At the end of the day the chip channels were filled with redistilled water so as to prevent clogging of the microchip.

3. Results and discussion

3.1. The optimization of the operating parameters

3.1.1. Waveform

Compared the electrophoregrams (Fig. 3) obtained by using of sine wave (a), square wave (b) and triangular wave (c) at frequency of 60 kHz and excitation voltage of 30 V (in V_{p-p}), respectively. The sine wave offered the most favorable signal-to-noise ratio. The square wave led to distortion and broadening of the sample peaks and also resulted in larger noise level. The sensitivity of triangular wave for glycine and glutamic descended, although the baseline was comparatively stable. Wang's group [13] has done the same experiment: the effect of sine, square and triangle waveforms were studied and the results showed that the
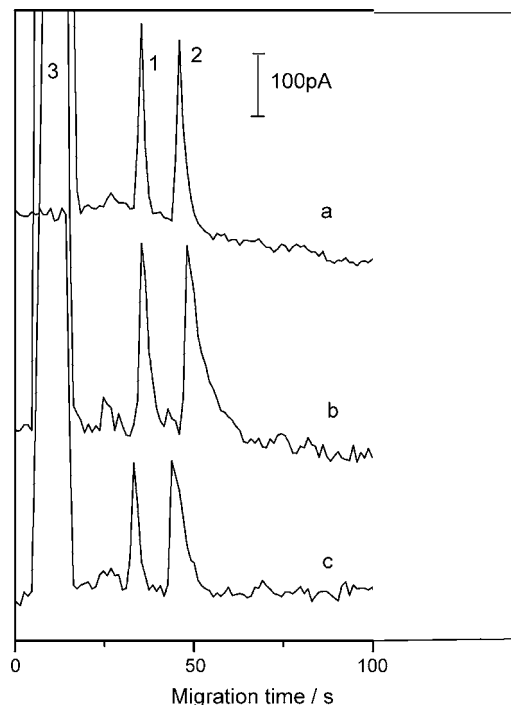
Fig. 3. Effects of the applied waveforms on the detected signal of 2 mmol/L glycine and 2 mmol/L glutamic acid. (a) Sine wave; (b) square wave; (c) triangular wave. Operation conditions: detect at 60 kHz; injection for 0.2 kV at 10 s; separation voltage: 1.5 kV; excitation voltage amplitude: 30 V; running buffer: 10 mmol/L MES–10 mmol/L His; effective separation channel length: 40 mm. Peak assignments: (1) glycine, (2) glutamic acid and (3) switch mark.

sine wave offered the most favorable signal-to-noise characteristics.

As far as high sensitivity and stable response were concerned, all subsequent experiments employed sine wave.

3.1.2. The distance between electrodes

The glycine (1) and glutamic (2) were separated with different dimension electroses plate using a 10 mmol/L MES–10 mmol/L Hisat (pH 6.1). An electropherogram of the two ions at 2 mmol/L with 1.5 kV was shown in Fig. 4. As expected, increasing the distance from 0.6 to 1.8 mm increased the peak width at half height ($W_{1/2}$) of glycine (1) and glutamic (2) from 1.7 to 1.9 s and from 3.2 to 3.6 s, respectively (Fig. 4, inset). Obviously the resolution decreased from 1.71 to 1.06. Therefore, the subsequent experiment chose the electrodes (f) and (h) were 2.0 mm of width in separation channel direction, the distance between the two electrodes of 0.6 mm. In the middle of two electrodes was a 0.2 mm wide copper line which was connected to earth.

3.1.3. Frequency

As expected, the response of the contactless conductivity detection highly depended on the frequencies applied. The influence of the applied frequency to the peak area was shown in Fig. 5(a). When the frequency adjusted from 10 to 180 kHz, the experiment results shown that at the frequencies lower than 20 kHz, detection was no longer possible; there was no response for any running buffer or samples. While the frequencies were enhanced from 20 to 40 kHz, the response was increased sharply,
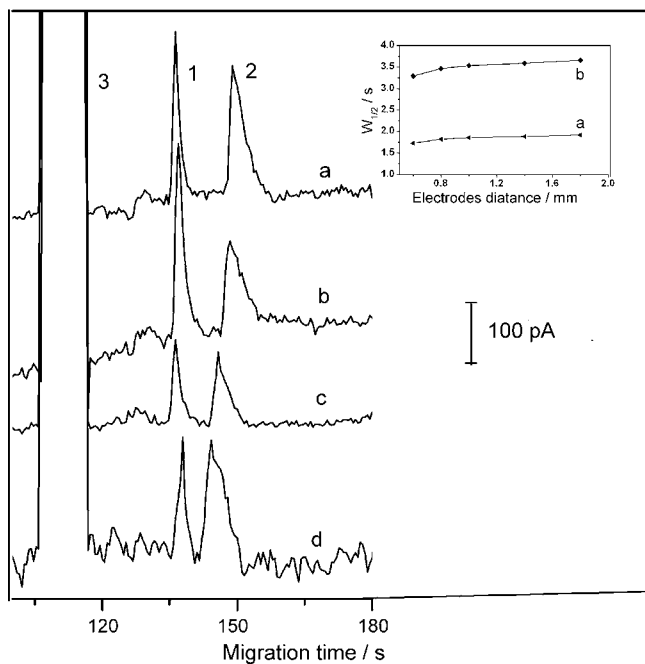
Fig. 4. Influence of the distance between electrodes. Other operation conditions were the same as in Fig. 3. Peak assignments: (1) glycine, (2) glutamic acid and (3) switch mark.

and the tendency got close to straight line, but from 40 to 65 kHz the peak area retained stably. The signal-to-noise ratio (Fig. 5(b)) had the same tendency as the frequencies before 65 kHz, and then both of them descended slowly. If the frequencies were higher than 160 kHz, it was too hard to distinguish the noise and signal. Hence, the optimal frequencies could be from 40 to 65 kHz.

3.1.4. Excitation voltage amplitude

The effect of applied excitation voltage on the peak area and signal-to-noise ratio were illustrated in Fig. 6(a) and (b), respectively. The peak area versus the excitation voltage in the range from 15 to 230 V (in V_{p-p}) was plotted. The response for potassium ion increased nearly linearly with the excitation voltage amplitude from 20 to 170 V (in V_{p-p}). When voltages were lower
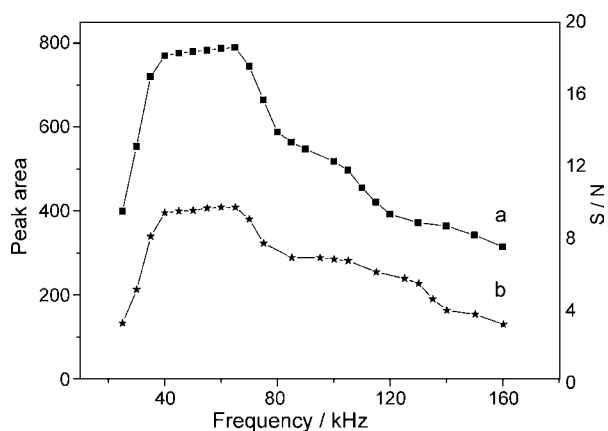
Fig. 5. Influence of frequency to peak area (a) and signal-to-noise ratio (b) upon the response for 500 μmol/L potassium. Operation conditions—running buffer: 20 mmol/L borax–10 mmol/L SDS, other conditions were the same as in Fig. 3.
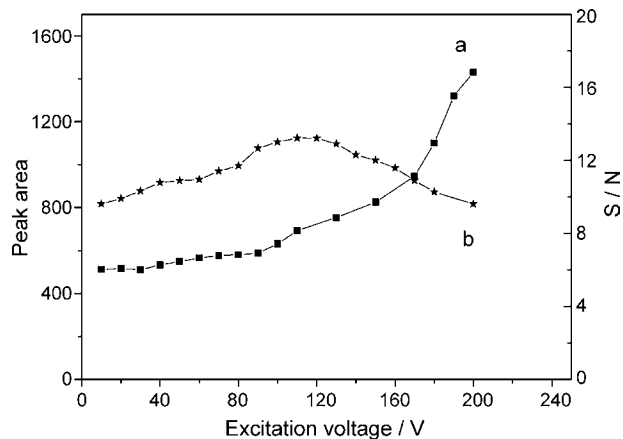

Fig. 6. Influence of excitation voltage amplitude to peak area (a) and signal-to-noise ratio (b) upon the response for 500 μmol/L potassium ion. Operation conditions: frequency 45 kHz, other conditions were the same as in Fig. 4.

than 20 V, there was no response for potassium ion. Fig. 6(b) shows that: when the excitation voltage amplitude was 20–110 V (in V_{p-p}), the signal-to-noise ratio steadily increased, and when the excitation voltages were higher than 110 V (in V_{p-p}), the peak areas continued to increase. However, the high voltages induced peak distortion and baseline drift. These data demonstrated that comparatively lower excitation voltages (from 20 to 110 V in V_{p-p}) could offer favorable response characteristics.

As far as well-defined and stable response were concerned, all subsequent experiments employed excitation voltage of 30 V (in V_{p-p}), as mentioned above, which could offer the favorable response characteristics in safe voltage.

3.1.5. Separation voltage

From Fig. 7(A), it could be seen that when the applied separation voltages were less than 1.0 kV, there were comparatively small current responses. The peak height increased steadily from 0.66 to 3.5 kV. While the separation voltages were higher than 3.5 kV, the curtailment of retention time resulted in the amalgamation of two peaks. Although the detection sensitivity was increased throughout the whole voltage range, the background noise level rose slowly with the increase of separation voltage. When we took into account the signal-to-noise ratio and reproducibility, experimental data showed that detection at 1.5 kV was much better than at other voltages. To obtain a reproducible detection with high sensitivity, 1.5 kV was selected as the optimal separation voltage in the following experiments.

Influence of separation voltage to current and retention time upon the response for 500 μmol/L potassium was shown in Fig. 7(B)(c) and (d), respectively. The tendency of current (c) followed Ohm law. The equation was $i = -4.02 + 16.7E$, with correlation coefficient of 0.9990. As increased the separation voltage from 1.1 to 3.5 kV, the current increase from 15.0 to 55.0 μA. The linear equation for separation voltage versus retention time was $t = 34.6 - 16.0E + 2.06E^2$. With the increase of separation voltage, the retention time curtailed from 18 to 4 s.
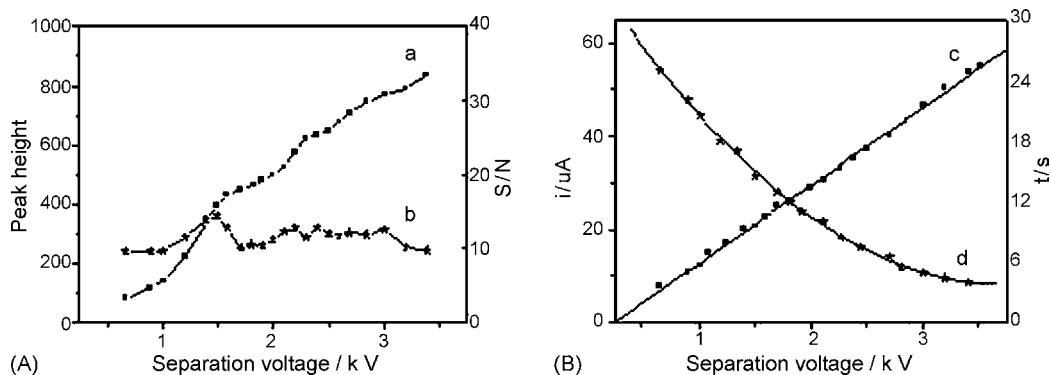
Fig. 7. (A) Influence of separation voltage to peak height (a) and signal-to-noise ratio (b) upon the response for 500 μmol/L potassium ion. (B) Influence of separation voltage to current (c) and retention time (d) upon the response for 500 μmol/L potassium ion. Operation conditions were the same as in Fig. 5.

3.2. Reproducibility

The reproducibility of the detector was tested by 10 consecutive runs. For each run, a sample containing 500 μmol/L potassium and magnesium was injected. Buffer solution of 20 mmol/L borax–10 mmol/L SDS was used as background electrolyte. The injection voltage was 0.2 kV for 10 s and the separation voltage was 1.5 kV. The measurements were carried out at the optimal frequency of 60 kHz and excitation voltage of 30 V (in V_{p-p}). The relative standard deviations of peak area were 1.98% and 2.02% for potassium and magnesium, respectively. Detection limit of 10 μmol/L for potassium was obtained (detection limit defined as three times of the baseline noise-level). The stability of the response was partly attributed to the usage of comparatively lower excitation voltages and frequencies, and partly profited from the contactless conductivity itself.

3.3. Linearity

The linearity of the detector was demonstrated by injecting potassium and magnesium at concentrations ranging from 0.02 to 1.2 mmol/L. The sample solution was injected at 0.2 kV for 10 s, separated in the channel of 40 mm (effective length)

with the buffer solution of 20 mmol/L borax–10 mmol/L SDS at the separation voltage of 1.5 kV, and detected at the excitation voltage of 30 V (in V_{p-p}) and the frequency of 45 kHz. The correlation coefficient was 0.9997 and 0.9989 for the potassium and magnesium, respectively.

3.4. Separation of amino acids and alkaloids

The eletrophoretic separations of glycine, histidine, lysine and glutamic acid were performed in the buffer solution of 15 mmol/L MES and 15 mmol/L His. The injection was done at 0.2 kV for 10 s and the separation at 1.5 kV. The effective separation channel was 90 mm long. The measurements were recorded at the optimal frequency 60 kHz and an excitation voltage of 30V (in V_{p-p}). The four amino acids were completely separated within 90 s (shown in Fig. 8(A)). It can be seen that the 90 mm length of separation channel prolonged the retention time, so the band-broadening of glutamic acid was evident. The separation of berberine and jateorrhizine reference substance (Fig. 8(B)(a)) and extracts from traditional Chinese drug in amoorcorn tree bark (b) and golden thread (c) were determined. A 20 mmol/L MES–20 mmol/L His buffer was used. The other operating conditions were the same as those in the amino acids separation.
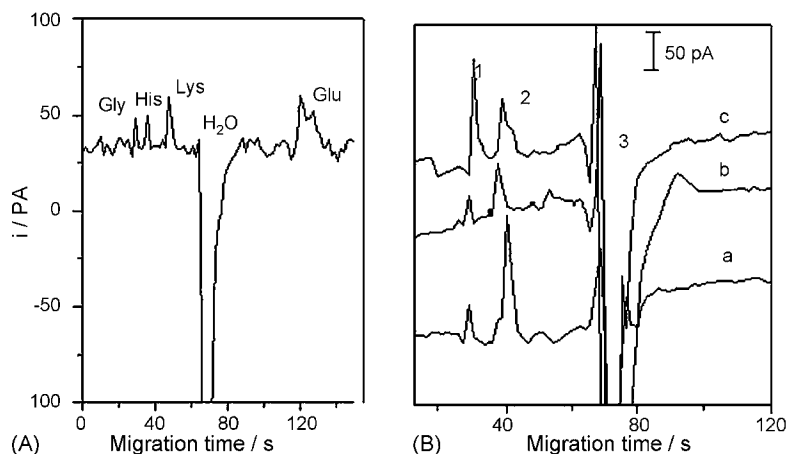
Fig. 8. (A) Separation of glycine, histidine, lysine and glutamic acid (2.5 mmol/L each), running buffer 15 mmol/L MES–15 mmol/L His, effective separation channel 90 mm in length. Other conditions were the same as in Fig. 5. (B) Separation of berberine and jateorrhizine (contains 600 μmol/L reference substance each (a)), the determination of alkaloids was shown in amoorcorn tree bark (b) and golden thread (c) running buffer 20 mmol/L MES-20 mmol/L. Peak assignments: (1) berberine, (2) jateorrhizine and (3) H_2O.

4. Conclusions

The new microfabricated thin glass-based chip, electrodes plate and contactless conductivity detection device have been demonstrated, which can offer three waveforms with oscillation frequency of 0–300 kHz and oscillation voltage of 0–300 V (in V_{p-p}). The advantages of this system exist in the following: it can work in lower optimal frequencies of 40–65 kHz and lower excitation voltages of 20–110 V (in V_{p-p}). In contrast with the devices whose electrodes were embedded or attached to the microchip [12,21], this system was of a significant simplification. The application of comparatively lower frequencies and excitation voltages not only yields better sensitivity but also ensures the stabilization of baseline. Because of the independence between the microchip and electrodes, it is very convenient for the replacement of chip and other operations. Detection in different positions of the channel would be also available. As expected, the glass microchip and electrodes assured a long device lifetime. They can be used for 3 months without noticeable degradation of the detected response, which could promise the lasting and reproducibility of the results.

Acknowledgements

References

[1] R.S. Ramsey, J.M. Ramsey, Anal. Chem. 71 (1999) 3258.
[2] A.J. Zemann, Electrophoresis 24 (2003) 2125.
[3] G. Chen, Y.H. Lin, J. Wang, Talanta 68 (2006) 497.
[4] Y. Zeng, H. Chen, D.W. Pang, Z.L. Wang, J.K. Cheng, Chem. J. Chin. Univ. 23 (2002) 567.
[5] A.J. Zemann, Trends Anal. Chem. 20 (2001) 346.
[6] J. Vacik, J. Zuska, I. Muselasova, J. Chromatogr. A 320 (1985) 233.
[7] P. Kuban, P.C. Hauser, Electrophoresis 25 (2004) 3387.
[8] D. Kaniansky, V. Zelenska, M. Masar, F. Ivanyi, S. Gazdikava, J. Chromatogr. A 884 (1999) 349.
[9] M. Masar, R. Bodor, D. Kaniansky, J. Chromatogr. A 834 (1999) 179.
[10] A.J. Zemann, E. Schnell, D. Volgger, G.K. Bonn, Anal. Chem. 70 (1998) 563–567.
[11] K. Magrhofer, A.J. Zemann, E. Schnell, G.K. Bonn, Anal. Chem. 71 (1999) 3828.
[12] M. Pumera, J. Wang, F. Opekar, I. Jelinek, J. Feldman, H. Lowe, S. Hardt, Anal. Chem. 74 (2002) 1968.
[13] J. Wang, M. Pumera, G. Collins, A. Mulchandani, Anal. Chem. 74 (2002) 6121.
[14] J. Wang, M. Pumera, G. Collins, F. Opekar, I. Jelinek, Analyst 127 (2002) 719.
[15] J. Wang, M. Pumera, Anal. Chem. 74 (2002) 5919.
[16] J. Wang, M. Pumera, Anal. Chem. 75 (2003) 341.
[17] J. Wang, G. Chen, A. MuckJr, Anal. Chem. 75 (2003) 4475.
[18] F. Laugere, G.W. Lubking, J. Bastemeijer, M.J. Vellekoop, Sens. Actuators B 83 (2002) 104.
[19] F. Laugere, R.M. Guijt, J. Bastemeijer, Anal. Chem. 75 (2003) 306.
[20] J. Lichtenberg, N.F. Roij, E. Verpoorte, Electrophoresis 23 (2002) 3769.
[21] J. Tanyanyiwa, P. Hauser, Anal. Chem. 74 (2002) 6378.
[22] J. Tanyanyiwa, E.M. Abad-Villa, M.T. Ferandez-Abedul, A. Costa-Garcia, W. Hoffmann, A.E. Guber, D. Herrmann, A. Gerlach, N. Gottschlich, P.C. Hauser, Analyst 128 (2003) 1019.
[23] J. Tanyanyiwa, P.C. Hauser, Electrophoresis 25 (2004) 3010.
[24] E.M. Abad-Villa, J. Tanyanyiwa, M.T. Ferandez-Abedul, A. Costa-Garcia, P.C. Hauser, Anal. Chem. 76 (2004) 1282.
[25] P. Kubán, P.C. Hauser, Electrophoresis 26 (2005) 3169.
[26] W.S. Law, P. Kubáň, J.H. Zhao, S.F.Y. Li, P.C. Hauser, Electrophoresis 26 (2005) 4648.
[27] Z.G. Chen, L.S. Wang, J.Y. Mo, Chem. J. Chin. Univ. 25 (Suppl.) (2004) 26.
[28] Z.G. Chen, J.Y. Mo, Chem. J. Chin. Univ. 23 (2002) 801.
[29] X.F. Yin, H. Shen, Z.L. Fang, Chin. J. Anal. Chem. 31 (2003) 116.

ELSEVIER

CSE–MECC two-dimensional capillary electrophoresis analysis of proteins in the mouse tumor cell (AtT-20) homogenate

Xingguo Chen [a,1], Md. Abul Fazal [a], Norman J. Dovichi [a,*]

[a] *Department of Chemistry, University of Washington, Seattle, WA 98195, USA*

Abstract

Two-dimensional capillary electrophoresis was used for the separation of proteins and biogenic amines from the mouse AtT-20 cell line. The first-dimension capillary contained a TRIS–CHES–SDS–dextran buffer to perform capillary sieving electrophoresis, which is based on molecular weight of proteins. The second-dimension capillary contained a TRIS–CHES–SDS buffer for micellar electrokinetic capillary chromatography. After a 61-s preliminary separation, fractions from the first-dimension capillary were successively transferred to the second-dimension capillary, where they further separated by MECC. The two-dimensional separation required 60 min.

© 2006 Elsevier B.V. All rights reserved.

Keywords: Capillary electrophoresis; Two-dimensional electrophoresis; AtT-20 cell line

1. Introduction

Capillary electrophoresis is an interesting separation technique for the characterization of proteins. However, the small sample volume and small optical path length used in capillary electrophoresis results in poor concentration detection limits, which prohibits the use of CE for separation and determination of trace-level proteins in many biological samples. Recently, a few techniques have been developed to improve concentration detection limits for CE, such as isotachophoresis [1], field amplification [2], and on-capillary concentration using a small pore plug [3].

Alternatively, improved detection limits are produced by use of laser induced fluorescence detection of native and derivatized proteins [4–10]. Native fluorescence is usually based on tryptophan, which is a rare amino acid in most organisms, has modest molar absorptivity and fluorescence quantum yield, and requires excitation in the ultraviolet with expensive and temperamental lasers. In contrast, derivatization can target the relatively abundant lysine residues to produce strongly fluorescent prod-

uct. However, derivatization is not straightforward for analysis of trace proteins because excess derivatizing reagent and the presence of fluorescent impurities can interfere with the separation. Also, incomplete labeling of reaction sites results in complex electropherograms generated by multiple reaction products [11,12]. Fluorogenic reagents have proven useful for protein analysis [13]. These reagents are not fluorescent until they react with a primary amine; they generate low background signals compared to traditional fluorescent derivatizing reagents. We have exploited 3-(2-furoyl)quinoline-2-carboxaldehyde (FQ) to generate highly fluorescent proteins that are separated efficiently when used a buffer system that contains an anionic surfactant, without noticeable band-broadening due to multiple labeling [9].

While providing rapid analysis of the protein in biological samples, one-dimensional separations are inherently limited in their resolution of complex mixtures. Fortunately, that resolution can be increased by combining two or more separation methods. As Giddings pointed out, the spot capacity of a multidimensional separation is given by the product of the peak capacity for the one-dimensional separations, assuming that the separations are not correlated [14]. A number of two-dimensional capillary electrophoresis methods have been developed for separation of complex protein mixtures [15–17].

AtT-20 is a mouse tumor cell line. These cells secrete β-endorphin and ACTH and have served as a useful model for studying neuropeptide synthesis, transport, and release [18–20].

* Corresponding author. Tel.: +1 206 543 7835; fax: +1 206 685 8665.
 E-mail address: dovichi@chem.washington.edu (N.J. Dovichi).
 URL: http://faculty.washington.edu/dovichi.
[1] Permanent address: Department of Chemistry, Lanzhou University, Lanzhou 730000, PR China.

Strong evidence has been presented that these cells have many enzymatic and structural features common to neuropeptide secreting neurons [21]. Mackie et al. reported the transfection of the AtT-20 cell line with the rat cannabinoid (CB1) receptor [22]. This transfected cell line (AtT-20, CB1) was used as a model for studying Δ^9-tetrahydrocannabinol (THC) induced changes in protein profile in neurons.

We have employed capillary electrophoresis to investigate the sub-cellular localization of components in this cell line [23]. Our first generation separation of components from the AtT-20 cell line employed relatively low electric fields, and the separation required over 3 h. In this paper, we now report an improved separation for this cell line that requires 60 min for completion.

2. Materials and methods

2.1. Reagents

Unless otherwise stated, all chemicals were obtained from Sigma (St Louis, MO). 3-(2-furoyl)-quinoline-2-carboxaldehyde (FQ) and potassium cyanide (KCN) were purchased from Molecular Probes (Eugene, OR, USA). UltraTrol dynamic pre-coatings were purchased from Target Discovery Inc. (Pal Aito, CA, USA). FQ solution was prepared with HPLC grade methanol (Fischer Sci., Houston, TX, USA). Stock solutions of 2-(N-cyclohexylamino)ethanesulphonic acid (CHES), Tris[hydroxymethyl]aminomethane (TRIS), sodium dodecyl sulfate (SDS) were made by dissolving appropriate amounts of reagents in nanopure (Barnstead, Dubuque, WI) distilled water. All chemicals were of analytical reagent grade and were used as received. All solution and buffer were prepared in nanopure distilled water.

Separation buffers were made by mixing aliquots of stock solutions (0.2–0.5 M) and nanopure distilled water. pH was adjusted by adding 0.5 M NaOH or 0.5 M HCl. The buffer solutions were then filtered through a 0.22-μm membrane filter (Millipore Corporation, MA) to remove particulates. Finally the buffer solution was degassed before use by sonication for 30 min. Sieving matrices for capillary sieving electrophoresis experiments were prepared by dissolving dextran (513 kDa or 100–200 kDa) in the CSE buffer. Any insoluble particles were removed by spinning the CSE buffer using a centrifuge (15,000 rpm, 20 min).

2.2. Two-dimensional CE-LIF instrument and data processing

Our two-dimensional capillary electrophoresis instrument employs a post-column sheath flow laser induced fluorescence detector as described elsewhere [15,17,23–26]. A 29.8 mW, 473 nm solid-state laser (Lasermate Corporation, Pomona, CA, USA) was used for excitation of FQ labeled proteins. Fluorescence signal was collected at a right angle with a 60×, 0.7 NA microscope objective, filtered by a 580 nm long-pass filter from Omega Optical (Brattleboro, VA, USA), and single photons were counted using an avalanche photodiode unit (Perkin-Elmer, Fremont, CA, USA). Electrophoresis was performed by applying

voltage using two high-voltage (0–30 kV) power supplies (CZE 1000R, Spellman, Hauppauge, NY, USA). Both first-dimension and second-dimension capillaries were uncoated fused-silica capillary. A laboratory-built multipurpose injection assembly was used to clean and condition the capillary and to inject sample [25].

The injection end of the first dimension capillary was placed in the injection reservoir and the other end was carefully aligned with the second dimension capillary using an interface. The interface was made of a square piece of Plexiglas with four channels in the shape of a cross. Two capillary sleeves (large outer diameter fused silica capillary) were used to guide the separation capillaries. The interface was connected to the interface reservoir containing the second capillary buffer. The detection end of the second dimension capillary was inserted into a sheath flow cuvette.

Data were collected with a PC using software written in Lab-View. The two-dimensional capillary electrophoresis data were treated using software written in MATLAB 7.0.

2.3. Dynamic pre-coating and conditioning of capillaries

Before each experiment, the capillaries were cleaned, conditioned, and coated with UltraTrol, a commercial dynamic coating. First, the capillaries were purged with 1.0 M NaOH for 5 min followed by water for another 5 min. Next, the capillaries were coated with UltraTrol for 5 min. Then the capillaries were flushed with MECC buffer for 5 min to eliminate excess coating. Finally, the first-dimension capillary was flushed with CSE buffer to replace MECC buffer in it for another 5 min. High voltage was applied and let run for 20 min to achieve a stable baseline.

2.4. Two-dimensional CE experiments

In the two-dimensional capillary electrophoresis system, two 20-cm long, 31-μm inner diameter capillaries were used as the first dimension capillary for CSE and second dimension for MECC, respectively. The CSE running buffer contained 50 mM TRIS, 50 mM CHES, 5 mM SDS (pH 8.4) and 5% dextran; dextran acts as a sieving matrix. The MECC running buffer contained 50 mM TRIS, 50 mM CHES, 15 mM SDS (pH 8.4).

The voltage program for the two dimensional capillary electrophoresis is shown in Fig. 1. Samples were injected into the first capillary by applying −5 kV for 2 s on the first capillary electrode. The injection reservoir was filled with the sieving matrix and a preliminary separation was achieved by applying 1100 V/cm for 61 s. The pre-run time was determined experimentally so that at the end of the pre-run, the fastest migrating proteins approached close to the interface. A series of transfer and MECC separation cycles then began. A fraction of partially separated sample from the first capillary was transferred into the second capillary by applying −15 kV on the second capillary and −25 kV on the first capillary for 1 s. Once the fraction was transferred the second dimension separation was performed by applying −18 kV at both electrodes, which drove separation in the second capillary while holding analyte stationary
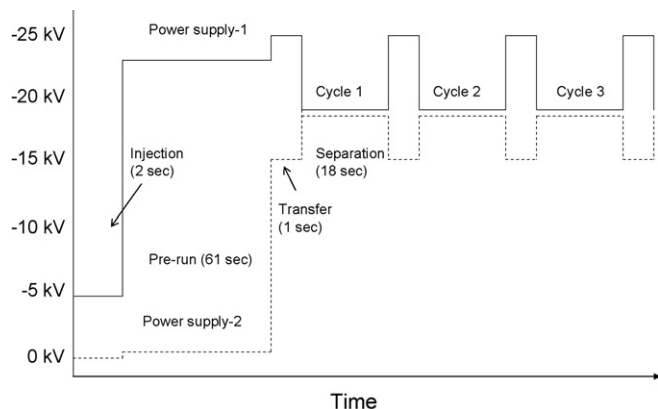
Fig. 1. The voltage program for the two-dimensional capillary electrophoresis.

in the first. These cycles of fraction transfer and second capillary separation were repeated under computer control until the entire sample was transferred and separated in the second capillary.

2.5. AtT-20 cell culture and pre-column labeling of cell homogenate

AtT-20 (CB1) cells were maintained in Dulbecco's modified Eagle's medium supplemented with 10% heat inactivated horse serum, 100 UI/mL streptomycin, 100 UI/mL penicillin at 37 °C in a 5% CO_2 atmosphere. Culture medium was changed after every 3 days. At ∼70% confluence level, cells were harvested by treating with 1× trypsin-EDTA and were washed three times with PBS to remove traces of culture medium. Cells were lysed with 1% SDS on ice for 20 min and then stored at −80 °C.

To denature proteins, 5 μL of 2% SDS was added to 5 μL of protein sample and heated for 4 min at 90 °C. The sample was transferred into a 500 μL microcentrifuge tube which contained 100 nmol of previously dried FQ. 2.5 μL of 10 mM KCN and 2.5 μL water were added to the microcentrifuge tube and then heated for another 5 min at 65 °C. After completion of the derivatization reaction the sample was diluted to 100 μL with 50 mM TRES–50 mM CHES–5 mM SDS (pH 8.4).

3. Results and discussions

3.1. The effect of molecular weight and concentration of dextran in CSE buffer on analysis of proteins in AtT-20 cell homogenate

Polymer concentration and molecular weight are two important characteristics in sieving electrophoresis. In order to obtain high separation efficiency, the concentration of dextran (100–200 kDa) was investigated from 5% to 7% in 100 mM TRIS–100 mM CHES–3.5 mM SDS buffer (pH 8.4). The results indicated that the separation efficiency improved slightly at 7% compared with 5%. However, separation time and viscosity also increased with polymer concentration. A higher molecular weight dextran (513 kDa) was also investigated. Higher separation efficiency was obtained with the higher molecu-

lar weight polymer at the same concentration. However, CSE buffers with higher than 5% dextran (513 kDa) were very viscous and required unacceptably high pressure to fill the capillary. We therefore chose to employ 5% dextran (513 kDa) for further studies.

3.2. The effect of CHES–TRIS–SDS concentration in CSE buffer on analysis of proteins in AtT-20 cell homogenate

The concentrations of CHES, TRIS and SDS in CSE buffer have a significant effect on the separation of proteins through their influence on ionic strength and Joule heating, viscosity of electrolyte, and adsorption on the capillary wall. The effect of the concentrations of CHES, TRIS and SDS on separation of proteins in AtT-20 cell homogenate was investigated. The results indicated that the separation of proteins was better in the 50 mM CHES–50 mM TRIS–5 mM SDS buffer than that in 100 mM CHES–100 mM TRIS–3.5 mM SDS buffer, presumably because of excessive Joule heating at higher ionic strength, and the 50 mM CHES–TRIS–3.5 mM SDS buffer was used in subsequent studies.

3.3. The effect of CHES–TRIS concentration in MECC buffer on analysis of proteins in AtT-20 cell homogenate

SDS concentration was held constant at 15 mM for MECC separations, and the concentrations of CHES and TRIS were varied over the range 50–100 mM. The results showed that varying the concentrations did not result in changes in the migration order of proteins but had a significant effect on the resolutions. As expected, the current roughly doubled from 0.28 μA to 0.42 μA with the increased CHES and TRES concentrations, and the separation degraded. This phenomenon can be attributed to the excessive Joule heating. In order to obtain a higher efficiency, while avoiding the generation of excessive Joule heating, 50 mM CHES–TRIS–15 mM SDS was selected as for the MECC buffer.

3.4. Analysis of proteins in AtT-20 cell homogenate

3.4.1. The relationship of logarithm of molecular weight standard proteins (log MW) and migration time in CSE
A calibration curve was constructed between migration time and molecular weight by analysis of a set of standard proteins, Fig. 2A. Migration time increased with the logarithm of molecular weight, Fig. 2B. The least-squares regression equation for this line was $y = 0.5034x − 0.7762$ with a correlation coefficient $r = 0.993$. Detection limit was 300 zmol for carbonic anhydrase injected onto the capillary, which is rather high for this protein.

3.4.2. Analysis of proteins in AtT-20 cell homogenate by two-dimensional CE
The proteins in AtT-20 cell homogenate were analyzed by two-dimensional capillary electrophoresis. After the 61-s preliminary separation, fractions from the first-dimension capillary were successively transferred to the second-dimension
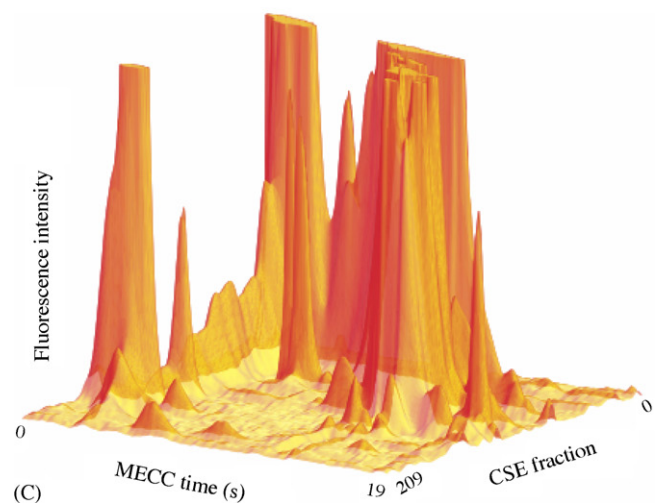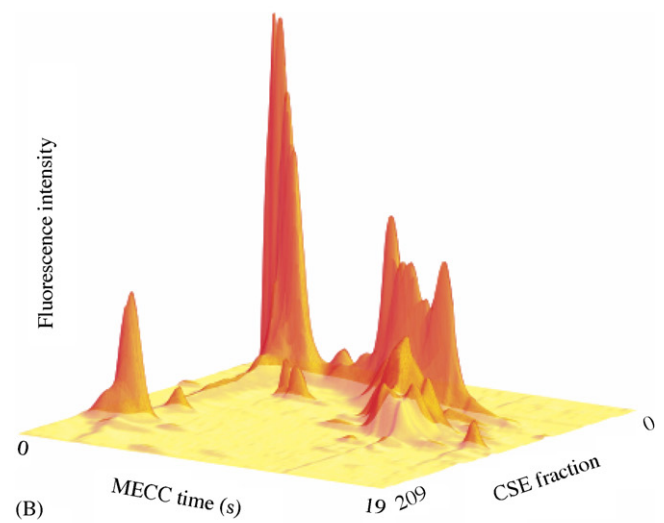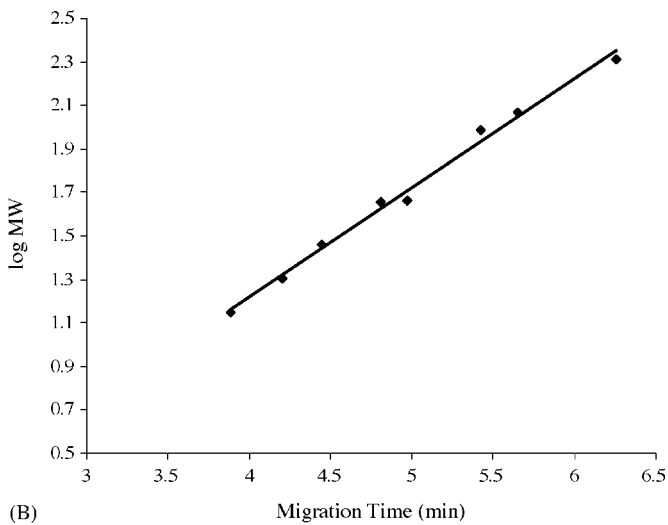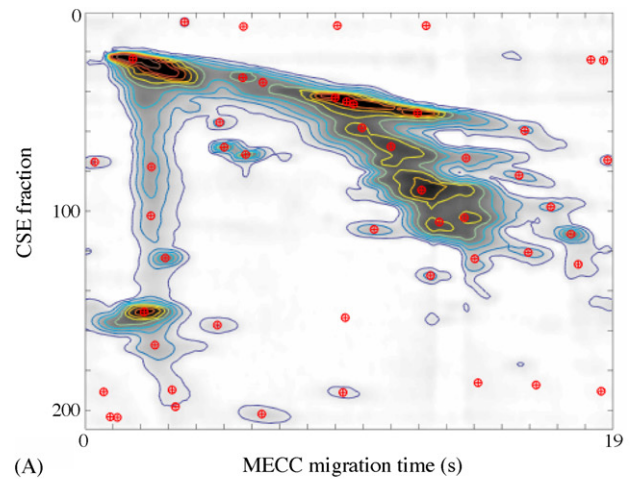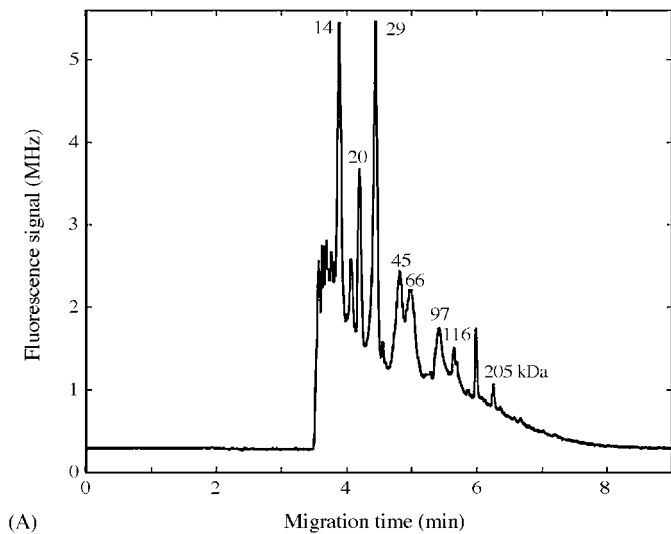
Fig. 2 (A). Electropherograms of 1 μM solution of standard proteins. Capillary: 25 cm × 147 μm O.D. × 31 μm I.D., coated by UltraTrol; buffer: 100 mM CHES–100 mM TRIS–3.5 mM SDS–5% dextran (513 kDa), pH 8.4; injection: −4 kV, 5 s; separation: −20 kV and (B) the relationship of log MW (kDa) and migration time of standard proteins.

capillary, where they further separated by MECC. The second-dimension separation was completed in 60 min. The typical two-dimensional gel stained image and landscape image from AtT-20 cell homogenate are shown in Fig. 3.

A non-linear least-squares regression method was used to fit a Gaussian surface to the 50 most intense components in this separation. The median spot width, expressed as the standard deviation of the Gaussian surface, was 3.6 transfers in the CSE dimension and 0.68 s in the MECC dimension. A plot of the spot position in the CSE versus the MECC dimension was uncorrelated ($r = 0.22$). We can estimate the spot capacity as the product of the peak capacity in the two dimensions. In this case, there were 209 fractions transferred from the CSE capillary, which gives a peak capacity in that dimension of 14.5. The MECC dimension was 19 s in duration, which gives a peak capacity in that dimension of 7. The total spot capacity of the separation was 100.

Fig. 3. Protein gel stained image (A), landscape image (B), and landscape image magnified by 10× (C) from AtT-20 cell homogenate. The 50 components used to estimate run-to-run variation in migration time are marked with a ⊕.

4. Conclusions

Based on peak capacities of one-dimensional CSE and one-dimensional MECC separations (data not shown) the spot capacity of CSE × MECC was estimated to be over a thousand. In reality, about 60 spots were resolved. Band broadening due to molecular diffusion was the main reason for such a huge loss. One-dimensional separations were completed within a few minutes whereas two-dimensional CE took about 1 h. Proteins remain in the first dimension capillary for a relative long time before separation in the second capillary. Molecular diffusion during the long separation results in loss of resolution. Shorter experimental time by using smaller capillaries and higher field strengths would be a potentially effective approach to improve the overall the two-dimensional CE spot resolution.

Acknowledgement

References

[1] F. Foret, E. Szoko, B. Karger, Electrophoresis 14 (1993) 417.
[2] F. Chen, J. Sternberg, Electrophoresis 15 (1994) 13.
[3] A. Tomlinson, S. Naytor, J. High Resolut. Chromatogr. 18 (1995) 384.
[4] I.H. Lee, D. Pinto, E.A. Arriaga, Z. Zhang, N.J. Dovichi, Anal. Chem. 70 (1998) 4546.
[5] T.T. Lee, E.S. Yeung, J. Chromatogr. 595 (1992) 319.
[6] D.B. Craig, J.C.Y. Wong, N.J. Dovichi, Biomed. Chromatogr. 11 (1997) 205.
[7] N.M. Schultz, L. Huang, R.T. Kennedy, Anal. Chem. 67 (1995) 924.
[8] H.B. Lim, J.J. Lee, K.J. Lee, Electrophoresis 16 (1995) 674.
[9] D.M. Pinto, E.A. Arriaga, D. Craig, J. Angelova, N. Sharma, H. Ahmadzadeh, N.J. Dovichi, C.A. Boulet, Anal. Chem. 69 (1997) 3015.
[10] D.Y. Chen, N.J. Dovichi, Anal. Chem. 68 (1996) 690.
[11] J.Y. Zhao, K.C. Waldron, J. Miller, J.Z. Zhang, H.R. Harke, N.J. Dovichi, J. Chromatogr. 608 (1992) 239.
[12] D.B. Craig, N.J. Dovichi, Anal. Chem. 70 (1998) 2493.
[13] S.C. Beale, J.C. Savage, D. Wiesler, S.M. Wiestock, M. Novotny, Anal. Chem. 60 (1988) 1765.
[14] J.C. Giddings, Unified Separation Science, John Wiley & Sons, New York, 1991.
[15] D. Michels, S. Hu, R. Schoenherr, N.J. Dovichi, Mol. Cell Proteom. 1 (2002) 69.
[16] S. Hu, D. Michels, M.A. Fazal, C. Ratisoontorn, M.L. Cunningham, N.J. Dovichi, Anal. Chem. 76 (2004) 4044.
[17] D.A. Michels, S. Hu, K.A. Dambrowitz, M.J. Eggertson, K. Lauterbach, N.J. Dovichi, Electrophoresis 25 (2004) 3098.
[18] L. Matsuuchi, R.B. Kelly, J. Cell Biol. 112 (1991) 843.
[19] P.J. Peters, H.W. Gohlmann, I.V. Wyngert, S.M. Swagemakers, L. Bijnens, S.U. Kass, T. Steckler, Mol. Pharmacol. 66 (2004) 1083.
[20] B. Budziszewska, F.L. Jaworska, M. Tetich, K.A. Basto, M. Kubera, M. Leskiewicz, W. Lason, Neuropychopharmacology 29 (2004) 785.
[21] J. Tooze, M. Holinshead, S.D. Fuller, S.A. Tooze, W.C. Hunter, Eur. J. Cell Biol. 49 (1998) 259.
[22] K. Mackie, Y. Lai, R. Westenbrock, R. Mitchell, J. Neurosci. 15 (1995) 6552.
[23] M.A. Fazal, V.R. Palmer, N.J. Dovichi, J. Chromatogr. A 1130 (2006) 182.
[24] J.R. Kraly, M.R. Jones, D.G. Gomez, J.A. Dickerson, M.M. Harwood, M. Eggertson, T.G. Paulson, C.A. Sanchez, R. Odze, Z. Feng, B.J. Reid, N.J. Dovichi, Anal. Chem. 78 (2006) 5977.
[25] S. Wu, N.J. Dovichi, J. Chromatogr. 480 (1989) 141.
[26] S.N. Krylov, D.A. Starke, E.A. Arriaga, Z. Zhang, N.W. Chan, M.M. Palcic, N.J. Dovichi, Anal. Chem. 72 (2000) 872.

Prediction of protein secondary structure content using support vector machine

Chao Chen, Yuanxin Tian, Xiaoyong Zou *, Peixiang Cai, Jinyuan Mo

School of Chemistry and Chemical Engineering, Sun Yat-Sen University, Guangzhou 510275, People's Republic of China

Abstract

In this paper, the support vector machine was trained to grasp the relationship between the pair-coupled amino acid composition and the content of protein secondary structural elements, including α-helix, 3_{10}-helix, π-helix, β-strand, β-bridge, turn, bend and the rest random coil. Self-consistency and cross validation tests were made to assess the performance of our method. Results superior to or competitive with the popular theoretical and experimental methods have been obtained.
© 2006 Elsevier B.V. All rights reserved.

Keywords: Support vector machine; Protein secondary structure content; Pair-coupled amino acid composition

1. Introduction

A *priori* knowledge of secondary structure content can be greatly helpful for theoretical and experimental determination of protein structure. Experimental techniques, such as circular dichroism spectroscopy, infrared spectroscopy and nuclear magnetic resonance spectrometry, have been routinely used to probe the secondary structure content of a protein. However, as a result of genome and other sequencing projects, the gap between the number of known protein sequences and the number of known protein structures is widening rapidly. In order to narrow this gap, computational prediction methods are badly needed. In the history of predicting protein secondary structure content, Krigbaum and Knutton [1] introduced the multiple linear regression (MLR), and only used the amino acid composition (AA) as the input. About 20 years later, Muskal and Kim [2] addressed a tandem neural network method, where they considered the molecular weight of a protein and its heme presence in addition to the AA. Recently, much convincing evidence has proven that the coupling effect among the residues of a protein sequence plays an important role in predicting the protein secondary structure content. One of the successful methods is the introduction of the pair-coupled AA by Chou et al. [3–8], where

they took into account the coupling effect among the residues of a protein sequence and obtained the results superior to the ones by the single-wise AA approach.

Based on Chou's pair-coupled AA, we developed a support vector machine (SVM) regressing system for the prediction of protein secondary structure content. The SVM, first proposed by Cortes and Vapnik [9], is based on statistical learning theory. Comparing with other machine learning systems, the SVM has many attractive features, including the absence of local minima, its speed and scalability and its ability to condense information contained in the training set. In the past decade, SVMs have performed well in diverse applications of bioinformatics, such as prediction of secondary structure [10–12], classification and validation of cancer tissue samples [13], prediction of protein subcellular localization [14–16], prediction of peptide mobility [17], gene selection and tumor classification [18]. In this article, the present SVM system together with the pair-coupled AA exhibited improved performance compared with several published results.

2. Methods

2.1. Dataset

The first one is the dataset of 513 protein chains proposed by Cuff and Barton [19], referred to as the CB513 set. It is a non-homologous dataset, i.e. an S.D. score of ≥5 is regarded as

---

* Corresponding author. Fax: +86 20 84112245.
  E-mail address: ceszxy@zsu.edu.cn (X. Zou).

homology. The S.D. score is a more stringent measure than the percentage identity.

The other two datasets are constructed by Chou [5], which are used here in order to compare our approach with theirs. One dataset contains 244 protein chains and serves as the training dataset, none of which has more than 35% of homology with the others. The other dataset contains 201 protein chains (note that Table 3 in Ref. [5] at p. 479 does not contain 202 chains) and serves as the testing dataset, none of which has more than 35% of homology with the others, either. They are referred to as the Chou244 set and the Chou201 set in this article, respectively.

2.2. Design

The publicly available LIBSVM software was used to process the SVM regression [20]. First, based on Chou's method [5], a pair-coupled AA is formulated as follows:

$$\Re_{210} = \left\{ \begin{array}{l} P(AA), P(AC), P(AD), P(AE), \ldots, P(AY) \\ P(CC), P(CD), P(CE), \ldots, P(CY) \\ P(DD), P(DE), \ldots, P(DY) \\ \cdots \\ P(YY) \end{array} \right\} \quad (1)$$

where $P(AC)$ is the sum of AC pair occurrence frequency and CA pair occurrence frequency found in the entire sequence, and so forth. The pair-coupled AA thus consists of 210 components. Suppose the 210 components are denoted by x_i $(i = 1, 2, \ldots, 210)$, i.e., $x_1 = P(AA)$, $x_2 = P(AC)$, $x_3 = P(AD)$, $\ldots$, $x_{210} = P(YY)$. Subsequently, normalize them to meet the following conditions:

$$\sum_{i=1}^{210} x_i = 1 \quad (2)$$

Then x_i $(i = 1, 2, \ldots, 210)$ is used as the input of the SVM. The observed secondary structural elements derived from the DSSP file [21] of the proteins have eight classes: H (α-helix), G (3_{10}-helix), I (π-helix), E (β-strand), B (β-bridge), T (turn), S (bend) and – (rest). Thus, the secondary structure content of a protein, e.g. α-helix, can be formulated as

$$y_i = \frac{n_i}{N}, \quad i = 1, 2, 3, \ldots, 8 \quad (3)$$

where N is the chain length of a given protein and n_1 represents the number of residues occurring in its α-helices, n_2 represents the number of residues occurring in its 3_{10}-helices, and so forth. Then, y_i is used as the expected output values of the SVM. In this study, the radial basis function (RBF) was found to have the best performance:

$$K(\vec{u}, \vec{v}) = \exp(-\gamma \|\vec{u} - \vec{v}\|^2) \quad (4)$$

The parameter γ is selected as that which minimized an estimate of the VC-dimension, and it is set at 10. The regularization parameter C, controlling the trade-off between low training error and large margin, is set at 1.5.

2.3. Training and testing

Generally speaking, a prediction method is usually evaluated by the self-consistency test, independent dataset test, and jackknife test. Of these three, the jackknife test is accepted as the most rigorous and objective one [22]. In the jackknife test each protein in the dataset is in turn singled out as an independent test sample and all the rule-parameters are calculated without using this protein. Thus, it is also named as "leave-one-out" test. However, a full jackknife test is not feasible especially on the CB513 set due to the limited computational power. Therefore, we employed seven-fold cross validation to evaluate the performance of the present method. The 513 protein chains in the CB513 set were divided into seven subsets. In fact, several different random partitions were processed. For each partition, we calculated the number of residues and the content of eight secondary structural elements of each subset. The partition which had the minimal bias was finally selected. This procedure would avoid obtaining an inauthentic prediction accuracy caused by the extremely biased partition. Then at each step of the validation process, six subsets were used for training while the remaining one subset was used for testing. This procedure was repeated seven times by changing the test dataset, so that each subset was used for training as well as testing. The final performance was calculated by averaging over all seven subsets.

2.4. Performance measures

The output computed from the SVM was compared with the expected output by using three criteria defined by Chou [5] to evaluate the performance of prediction.

The first criterion is the average absolute error, δ^Θ, of each secondary structural element, calculated for each protein:

$$\delta^\Theta = \frac{\sum_{k=1}^N |\Theta_k - y_k^\Theta|}{N} \quad (5)$$

where Θ_k is the predicted content of the secondary structural element Θ for the kth protein, and y_k^Θ is the content actually observed.

The second criterion is the standard deviation of the average absolute error formulated as follows

$$\sigma^\Theta = \text{sqrt}\left(\frac{\sum_{k=1}^N (\delta^\Theta - |\Theta_k - y_k^\Theta|)^2}{N-1} \right) \quad (6)$$

The third criterion is the overall average error given by

$$\langle \delta \rangle = \frac{1}{8} \sum_\Theta \delta^\Theta. \quad (7)$$

3. Results and discussion

3.1. Performance on the CB513 set

The results of the self-consistency test on the CB513 set are listed in Table 1, where we can see that the prediction of π-helix is the most accurate. Nevertheless, as seen in Table 1 the element

Table 1
Prediction errors by the self-consistency test on the CB513 set

Secondary structure element	Occurrence frequency (%)[a]	Average absolute error δ^{Θ}	Standard deviation σ^{Θ}
H: α-helix	30.9	0.061	0.084
G: 3_{10}-helix	3.68	0.005	0.012
I: π-helix	0.04	0.000	0.001
E: β-strand	21.4	0.049	0.068
B: β-bridge	1.33	0.001	0.002
T: turn	11.8	0.007	0.014
S: bend	9.37	0.007	0.017
–: rest	20.6	0.014	0.028
Overall average error $\langle \delta \rangle$	–	0.018	

[a] The values equal to the proportions of the secondary structure elements to the whole residues in the dataset.

of π-helix has the smallest percentage in the dataset. In view of this, the assessment should be focused on the success rates of the prediction for the most abundant elements, including α-helix, β-strand and random coil (denoted as "–, rest" in tables). The average absolute errors for the prediction of them are 0.061, 0.049 and 0.014 with standard deviations of 0.084, 0.068 and 0.028, respectively. Note that the average absolute error of 0.014 is comparatively small, indicating that the prediction for the element of random coil is very successful. The overall average error is 0.018. Such a small error demonstrates that there is definitely a relationship between the pair-coupled AA and the secondary structure content, and that the SVM can be trained to grasp this relationship and then to predict the secondary structure content of the unknown proteins, provided that the information of their sequences are supplied.

As the self-consistency test is based on a limited number of proteins, and more importantly, the rule parameters derived from the training dataset bear the prior information of proteins later plugged back into the testing dataset, this procedure will certainly give a somewhat optimistic error estimate. Hence, it is very necessary to employ cross validation or jackknife tests to evaluate the capability of generalization of our method. In this work we employed a seven-fold cross validation and the detailed results are listed in Table 2. As expected, the prediction errors become greater when compared with those by the self-

Table 2
Prediction errors by the seven-fold cross validation on the CB513 set

Secondary structure element	Average absolute error δ^{Θ}	Standard deviation σ^{Θ}
H: α-helix	0.132	0.100
G: 3_{10}-helix	0.027	0.022
I: π-helix	0.001	0.003
E: β-strand	0.110	0.078
B: β-bridge	0.012	0.010
T: turn	0.034	0.029
S: bend	0.033	0.030
–: rest	0.049	0.048
Overall average error $\langle \delta \rangle$	0.050	

Table 3
Prediction errors by the self-consistency test on the Chou244 set

Secondary structure element	Occurrence frequency (%)	Average absolute error δ^{Θ}	Standard deviation σ^{Θ}
H: α-helix	31.4	0.049	0.075
G: 3_{10}-helix	3.88	0.002	0.009
I: π-helix	0.02	0.000	0.000
E: β-strand	21.1	0.037	0.061
B: β-bridge	1.34	0.000	0.002
T: turn	11.6	0.004	0.010
S: bend	9.56	0.005	0.017
–: rest	21.1	0.008	0.018
Overall average error $\langle \delta \rangle$	–	0.013	

consistency test in Table 1. Considering that the CB513 set is a more critical test set for the evaluation of the secondary structure prediction methods, the overall average error for all the eight DSSP states, as low as 0.050, is also an acceptable result.

3.2. Performance on the Chou's datasets

Furthermore, in order to roundly assess our method we also performed it on the datasets used in the past by Chou's group [5]. The Chou244 set was used for the self-consistency test and the other Chou201 set was used for the independent test. Both results are listed in Tables 3 and 4 in detail.

As the tables show, the constituents of both the Chou's datasets are similar to those of the CB513 set, where the elements of α-helix, β-strand and random coil have the biggest percentages. As mentioned above, that is why the prediction qualities for them should be emphasized. From Table 3, we can observe that the average absolute errors for the elements of α-helix, β-strand and random coil are 0.049, 0.037 and 0.008, respectively. Compared with the corresponding results in Table 1, improvement was achieved as reducing the errors by 0.012, 0.012 and 0.006. Similar improvement is also seen when comparing the average absolute errors in Tables 2 and 4. In the CB513 set, much more structural variants are included. In contrast, there is always theoretical possibility that the smaller Chou's datasets have missed

Table 4
Prediction errors by the independent test on the Chou201 set

Secondary structure element	Occurrence frequency (%)	Average absolute error δ^{Θ}	Standard deviation σ^{Θ}
H: α-helix	31.8	0.104	0.085
G: 3_{10}-helix	3.78	0.026	0.021
I: π-helix	0.04	0.002	0.002
E: β-strand	21.1	0.097	0.081
B: β-bridge	1.32	0.012	0.009
T: turn	12.0	0.031	0.025
S: bend	9.42	0.032	0.027
–: rest	20.6	0.048	0.042
Overall average error $\langle \delta \rangle$	–	0.044	

Table 5
Comparison with other theoretical and experimental methods[a]

Statistical significance	Algorithm	Input information	Dataset size	Average absolute error δ^{Θ}			Overall average error $\langle \delta \rangle$
				H: α-helix	E: β-strand	–: rest	
	MLR [5]	Pair-coupled AA	244	0.036	0.031	0.012	0.018
	MLR [6]	First-order-coupled AA	244	0.056	0.046	0.020	0.028
Self-consistency	ANN [8]	Pair-coupled AA	244	0.060	0.057	0.031	0.028
	CD [24]	Spectroscopy	29	0.054	0.087	0.101	n/a
	This paper	Pair-coupled AA	244	0.049	0.037	0.008	0.013
	MLR [5]	Pair-coupled AA	202	0.077	0.076	0.088	0.061
	ANN [8]	Pair-coupled AA	202	0.071	0.069	0.037	0.034
Independent test	SVM [25]	AA, evolutionary information	202	0.078	0.072	0.039	0.033
	FT-IR [26]	Spectroscopy	23	0.017	0.023	n/a	n/a
	This paper	Pair-coupled AA	201	0.104	0.097	0.048	0.044

[a] *Abbreviations*: MLR, multiple linear regression; ANN, artificial neural network; SVM, support vector machine; FT-IR, Fourier transform infrared spectroscopy; CD, circular dichroism spectroscopy; AA, amino acid composition; n/a, not available.

some unfavorable proteins. Such improvements may be caused by the various test sets. Accordingly, we surmise that there exists a tendency that smaller test sets will generally result in better prediction accuracies, consistent with the findings by Eisenhaber's research group [23].

3.3. Comparison with other theoretical and experimental methods

Circular dichroism spectroscopy and Fourier transform infrared spectroscopy are two of the routine experimental methods for determining the protein secondary structure. They perform well in predicting the elements of α-helix and β-strand, but perform relatively bad in predicting the element of random coil [24]. From Table 5, we can observe that the estimation error for random coils is roughly 0.1. Nevertheless, as demonstrated in Table 5 the theoretical methods achieved better accuracies for predicting them. Among the four theoretical methods, our method obtained a lowest average absolute error for random coils as well as a lowest overall average error performing on the same Chou244 set by the self-consistency test. In contrast to the 210D pair-coupled AA [5], Liu adopted 400D first-order-coupled AA to represent protein samples [6]. However, the results are rather worse than the former according to their reports. By the self-consistency test Chou's method [5] performed best in predicting the contents of α-helices and β-strands, whereas Cai's method [8] performed worst, where an artificial neural network was trained to learn 210 pair-coupled AA parameters. On the other hand, it is worth noting that Cai's method performed best by the independent test, not only for the prediction of α-helices and β-strands but for the prediction of random coils. Accordingly, it is not appropriate to simply rank them. We believe that the current approach may play an important complementary role to the existing predictors in this area.

Meanwhile, according to the reports by Rost and Eyrich [27] (note that here an 8–3-state reduction scheme is adopted: DSSP [HGI] → helix (H), DSSP [EB] → strand (E), all other DSSP states [TSC] → other (L), and that such a conversion increases accuracy), the average absolute errors for helices and strands by PROFsec [28] on a set of 218 identical proteins, none of which was similar to any protein used to develop the method, were 0.056 and 0.040. The respective errors by PSIPRED [29] and PHD [30,31] were 0.054, 0.044 and 0.077, 0.059. As is well known, all the above three are of the most successful methods for predicting protein secondary structure. Their improvements are resulted not only from using larger databases, but from using evolutionary information that can be obtained from the multiple sequence alignments. Motivated by this, Lee et al. [25] adopted evolutionary information in addition to AA as the input of support vector regression models to predict the content of protein secondary structure. This protein sample representation can incorporate much homologous information. As shown in Table 5, their results are similar to those of Cai's. Recently, the pseudo-amino acid composition (PseAA) has been successfully applied to improving prediction quality in diverse applications of bioinformatics [32–38]. Stimulated by its success, our group introduced a different formulation of the PseAA, which contains more information than the pair-coupled AA relating to the sequence order of a protein and the distribution of the hydrophobic amino acids along its chain. Then, we applied the PseAA to the prediction of protein structural class and achieved more satisfactory results [39,40]. Thus, it is anticipated that the current prediction quality can be further improved if the PseAA and the evolutionary information can be combined with.

Acknowledgements

References

[1] W.R. Krigbaum, S.P. Knutton, Proc. Natl. Acad. Sci. USA 70 (1973) 2809.
[2] S.M. Muskal, S.H. Kim, J. Mol. Biol. 225 (1992) 713.
[3] K.C. Chou, Biopolymers 42 (1997) 837.
[4] K.C. Chou, J. Pept. Res. 49 (1997) 120.

[5] K.C. Chou, J. Protein Chem. 18 (1999) 473.

[6] W.M. Liu, K.C. Chou, Protein Eng. 12 (1999) 1041.

[7] K.C. Chou, Anal. Biochem. 286 (2000) 1.

[8] Y.D. Cai, X.J. Liu, K.C. Chou, J. Comput. Chem. 24 (2003) 727.

[9] C. Cortes, V. Vapnik, Mach. Learn. 20 (1995) 273.

[10] J.J. Ward, L.J. McGuffin, B.F. Buxton, D.T. Jones, Bioinformatics 19 (2003) 1650.

[11] J. Guo, H. Chen, Z.R. Sun, Y.L. Lin, Proteins: Struct. Funct. Bioinform. 54 (2004) 738.

[12] M. Kumar, M. Bhasin, N.K. Natt, G.P.S. Raghava, Nucleic Acids Res. 33 (2005) W154.

[13] T.S. Furey, N. Cristianini, N. Duffy, D.W. Bednarski, M. Schummer, D. Haussler, Bioinformatics 16 (2000) 906.

[14] K.C. Chou, Y.D. Cai, J. Biol. Chem. 277 (2002) 45765.

[15] A. Garg, M. Bhasin, G.P.S. Raghava, J. Biol. Chem. 280 (2005) 14427.

[16] D. Xie, A. Li, M.H. Wang, Z.W. Fan, H.Q. Feng, Nucleic Acids Res. 33 (2005) W105.

[17] K. Yu, Y.Y. Cheng, Talanta 71 (2007) 676–682.

[18] Q. Shen, W.M. Shi, W. Kong, B.X. Ye, Talanta 71 (2007) 1679–1683.

[19] J.A. Cuff, G.J. Barton, Proteins: Struct. Funct. Genet. 34 (1999) 508.

[20] C.C. Chang, C.J. Lin, LIBSVM: A Library for Support Vector Machines, 2001, software available at http://www.csie.ntu.edu.tw/~cjlin/libsvm.

[21] W. Kabsch, C. Sander, Biopolymers 22 (1983) 2577.

[22] K.C. Chou, C.T. Zhang, Crit. Rev. Biochem. Mol. Biol. 30 (1995) 275.

[23] F. Eisenhaber, F. Imperiale, P. Argos, C. Frommel, Proteins: Struct. Funct. Genet. 25 (1996) 157.

[24] N. Sreerama, R.W. Woody, Anal. Biochem. 287 (2000) 252.

[25] S. Lee, B. Lee, D. Kim, Proteins: Struct. Funct. Bioinform. 62 (2006) 1107.

[26] B.M. Smith, L. Oswald, S. Franzen, Anal. Chem. 74 (2002) 3386.

[27] B. Rost, V.A. Eyrich, Proteins: Struct. Funct. Genet. Suppl. 5 (2001) 192.

[28] B. Rost, J. Struct. Biol. 134 (2001) 204.

[29] D.T. Jones, J. Mol. Biol. 292 (1999) 195.

[30] B. Rost, Methods Enzymol. 266 (1996) 525.

[31] D. Przybylski, B. Rost, Proteins: Struct. Funct. Genet. 46 (2002) 197.

[32] K.C. Chou, Proteins: Struct. Funct. Genet. 43 (2001) 246.

[33] K.C. Chou, Y.D. Cai, Proteins: Struct. Funct. Genet. 53 (2003) 282.

[34] K.C. Chou, Y.D. Cai, J. Cell. Biochem. 91 (2004) 1197.

[35] H.B. Shen, K.C. Chou, Biochem. Biophys. Res. Commun. 334 (2005) 288.

[36] H.B. Shen, K.C. Chou, Biochem. Biophys. Res. Commun. 337 (2005) 752.

[37] K.C. Chou, Bioinformatics 21 (2005) 10.

[38] X. Xiao, S.H. Shao, Z.D. Huang, K.C. Chou, J. Comput. Chem. 27 (2006) 478.

[39] C. Chen, Y.X. Tian, X.Y. Zou, P.X. Cai, J.Y. Mo, J. Theor. Biol. 243 (3) (2006) 444–448.

[40] C. Chen, X.B. Zhou, Y.X. Tian, X.Y. Zou, P.X. Cai, Anal. Biochem. 357 (2006) 116.

Amperometric glucose biosensor based on electrodeposition of platinum nanoparticles onto covalently immobilized carbon nanotube electrode

Xia Chu [*], Daxue Duan, Guoli Shen, Ruqin Yu

*State Key Laboratory for Chemo/Biosensing and Chemometrics, College of Chemistry and Chemical Engineering,
Hunan University, Changsha 410082, PR China*

Abstract

A new amperometric biosensor for glucose was developed based on adsorption of glucose oxidase (GOx) at the gold and platinum nanoparticles-modified carbon nanotube (CNT) electrode. CNTs were covalently immobilized on gold electrode via carbodiimide chemistry by forming amide linkages between carboxylic acid groups on the CNTs and amine residues of cysteamine self-assembled monolayer (SAM). The fabricated $GOx/Au_{nano}/Pt_{nano}/CNT$ electrode was covered with a thin layer of Nafion to avoid the loss of GOx in determination and to improve the anti-interferent ability. The immobilization of CNTs on the gold electrode was characterized by quartz crystal microbalance technique. The morphologies of the CNT/gold and Pt_{nano}/CNT/gold electrodes have been investigated by scanning electron microscopy (SEM), and the electrochemical performance of the gold, CNT/gold, Pt_{nano}/gold and Pt_{nano}/CNT/gold electrodes has also been studied by amperometric method. In addition, effects of electrodeposition time of Pt nanoparticles, pH value, applied potential and electroactive interferents on the amperometric response of the sensor were discussed.

The enzyme electrode exhibited excellent electrocatalytic activity and rapid response for glucose in the absence of a mediator. The linear range was from 0.5 to 17.5 mM with correction coefficient of 0.996. The biosensor had good reproducibility and stability for the determination of glucose.
© 2006 Elsevier B.V. All rights reserved.

Keywords: CNTs; Pt nanoparticles; Glucose oxidase; Au nanoparticles

1. Introduction

The carbon nanotube (CNT) represents a new kind of carbon-based material and is superior to other carbon materials mainly in special structural feature and unique electronic and mechanical properties. Since its discovery in 1991 by high-resolution transmission electron microscopy (TEM) [1], extensive interest has been shown in physical, chemical, environmental and material science fields [2–6]. Due to its good electronic properties and electric conductivity, carbon nanotube has also been applied in electrochemical research [7–12]. The direct electron transfer of enzymes such as cytochrome C [13], glucose oxidase (GOx) [14], catalase [15], horseradish peroxidase, myoglobin [16] and hemoglobin [17,18] can be observed in the presence of carbon nanotube. In addition, due to its ability of fast electron transfer, carbon nanotube also shows electrocatalytic activities towards many substances such as H_2O_2, NADH, ascorbic acid, dopamine, catechol, homocysteine and thiocytosine [19–24]. The good catalytic activities towards these molecules together with its good biocompatibility open its application in fabricating excellent amperometric biosensor.

A key barrier for developing CNT-based biosensing devices is the insolubility of CNT in most solvents. CNT-modified electrodes reported previously were relied on dissolving CNT in biopolymers with excellent film-forming ability and biocompatibility such as Nafion [19], chitosan [25,26], etc. The excellent solubility of CNT in these solvents facilitates the construction of electrochemical biosensing platforms. Wang et al. [19] reported that multi-wall carbon nanotubes (MWNTs) dissolved in Nafion could be applied to construct amperometric sensor for hydrogen peroxide. Gorski and co-workers [27] reported that the colloidal solution of CNT-chitosan placed on the surface of glassy carbon electrodes can form robust CNT-chitosan film, which facilitated the electrooxidation of NADH. In this work, we report a new avenue for preparing effective CNT-based electrochemical sensors and biosensors by covalent linkage technique, in

---

[*] Corresponding author. Tel.: +86 731 8821916; fax: +86 731 8821916.
E-mail address: xiachu@hnu.cn (X. Chu).

which CNTs are immobilized onto cysteamine-modified gold substrate by standard water-soluble coupling agents 1-ethyl-3-(3-dimethylaminopropyl) carbodiimide (EDC) and *N*-hydroxy-succinimide (NHS) through forming amide linkages between amine residues and carboxylic acid groups on CNTs. So far very few literatures have been reported concerning this covalent linkage-based approach for fabricating CNT-based amperometric glucose biosensor.

On the other hand, electrochemical behavior and applications of nanoparticles have attracted much attention in the past few years [28–34]. The modification of electrode surfaces with transition metal nanoparticles, especially noble metal nanoparticles, has led to the development of various electrochemical sensors because of their high catalytic activities for many chemical reactions. In particular, Pt nanoparticles have been demonstrated to lower the H_2O_2 oxidation/reduction overvoltage efficiently [35–39]. As a result, nano-structured Pt films modified on electrode surfaces have been frequently used to design amperometric biosensors based on oxidoreductase because H_2O_2 is released during the oxidation of the substrate by a pertinent oxidoreductase in the presence of oxygen. Luong and co-workers [40] reported that electrochemical sensors fabricated with Pt nanoparticles and single-wall carbon nanotubes can improve remarkably the sensitivity towards H_2O_2. With glucose oxidase as an enzyme model, they constructed a glassy carbon or carbon fiber microelectrode-based glucose biosensor. Lin et al. [41] reported a glucose biosensor based on electrodeposition of palladium nanoparticles and GOx onto Nafion-solubilized carbon nanotube electrode.

In this paper, we report the fabrication, characterization and analytical performance of a glucose biosensor based on electrodeposition of Pt nanoparticle onto a carbon nanotube film. The electrodeposition method was selected to produce Pt nanoparticles on electrode surfaces because this method is easy to carry out and the layer thickness can be controlled. The immobilization of glucose oxidase onto electrode surfaces was carried out by adsorption of GOx on gold nanoparticles because nanometer-sized colloidal gold can not only adsorb redox enzymes without loss of biological activity but also facilitate the transfer of electron. The electrochemical behavior of the gold, CNT/gold, Pt_{nano}/gold and Pt_{nano}/CNT/gold electrodes has been investigated by amperometric method. The influence of pH value and applied potential on the sensor performance is also evaluated. The fabricated enzyme electrode results in excellent sensitivity, large linear range and short response time.

2. Experimental

2.1. Chemical and reagents

Multi-wall carbon nanotubes (MWNTs) acquired from college of Material Science and Engineering (Hunan University) were purified according to the reported literature with slight modification [42]. MWNTs were firstly purified by refluxing in a 3:1 (v/v) solution of concentrated sulfuric acid (98%) and concentrated nitric acid (70%) (3:1, H_2SO_4:HNO_3) for 48 h, and

the obtained MWNTs were then shortened by sonicating in the above mixed concentrated acids for 4 h. The shortened tubes were finally filtered and washed with double distilled water to bring the pH to >5. Glucose oxidase (lyophilized powder, $215\,U\,mg^{-1}$, from *Aspergillus niger*) was purchased from Fluka (USA) and used as received. β-D-(+)Glucose was obtained from Sigma and the glucose stock solution was allowed to mutarotate for 24 h at room temperature prior to use and subsequently store at $4\,^{\circ}C$. Nafion 117 solutions (0.5 wt%) were prepared by dilution with alcohols of 5 wt% Nafion 117 solutions (Aldrich). Choroplatinic acid ($H_2PtCl_6·6H_2O$) was obtained from Beijing Chemical Reagent Co. (Beijing, China) and a 7.7 mM H_2PtCl_6 stock solution was prepared for electrodeposition of Pt nanoparticles. 1-Ethyl-3-(3-dimethylaminopropyl) carbodiimide (EDC) and *N*-hydroxy-succinimide (NHS) were purchased from Sigma. Chlorauric acid ($HAuCl_4$) and trisodium citrate were purchased from Shanghai Chemical Reagent Co. (Shanghai, China). Unless otherwise stated all chemicals and reagents used were of analytical grade. All solutions were prepared using double distilled water. The 0.05 M phosphate buffer solutions were used as supporting electrolytes by mixing solution Na_2HPO_4 and NaH_2PO_4.

2.2. Apparatus

The electrodeposition of Pt nanoparticles and amperometric experiments were carried out with a CHI 760B electrochemical workstation (Shanghai, China). A three-electrode system was employed with a gold electrode (1 mm in diameter) as working electrode, a saturated calomel electrode (SCE) as reference electrode, a platinum foil as counter electrode. All potentials are referred to the SCE reference electrode. A magnetic stirrer (Model JB-2, Shanghai Analytical Instruments) provided the convective transport at 300 rpm during the amperometric measurements and the background current was allowed to decay to a steady-state value before spiking the equilibrated β-D-(+)glucose.

The piezoelectric quartz crystals (AT-cut, 9 MHz, gold electrode) were purchased from Shanghai Chenhua Equipment (Shanghai, China). The crystal was powered through an oscillator circuit constructed from a transistor–transistor logic integrated circuit (TTL-IC). The oscillation frequency was monitored with a high frequency counter (Model Fc 1250, Wellstor).

The morphologies of CNT/gold and Pt_{nano}/CNT/gold electrodes were investigated with scanning electron microscopy (SEM, JSM 5600 LV).

2.3. Preparation of colloidal gold

Glassware used in this preparation was thoroughly cleaned in a bath of freshly prepared HNO_3:HCl (3:1) solution and rinsed in double distilled water prior to use. Au nanoparticles were prepared according to the literature with a little modification. Briefly, in a 500 ml round-bottom flask, 250 ml of $HAuCl_4$ (0.01%) solution was brought to a boil with vigorous stirring and 3.75 ml of 1% trisodium citrate was rapidly added into this solution. The solution turned deep blue within 20 s and the final
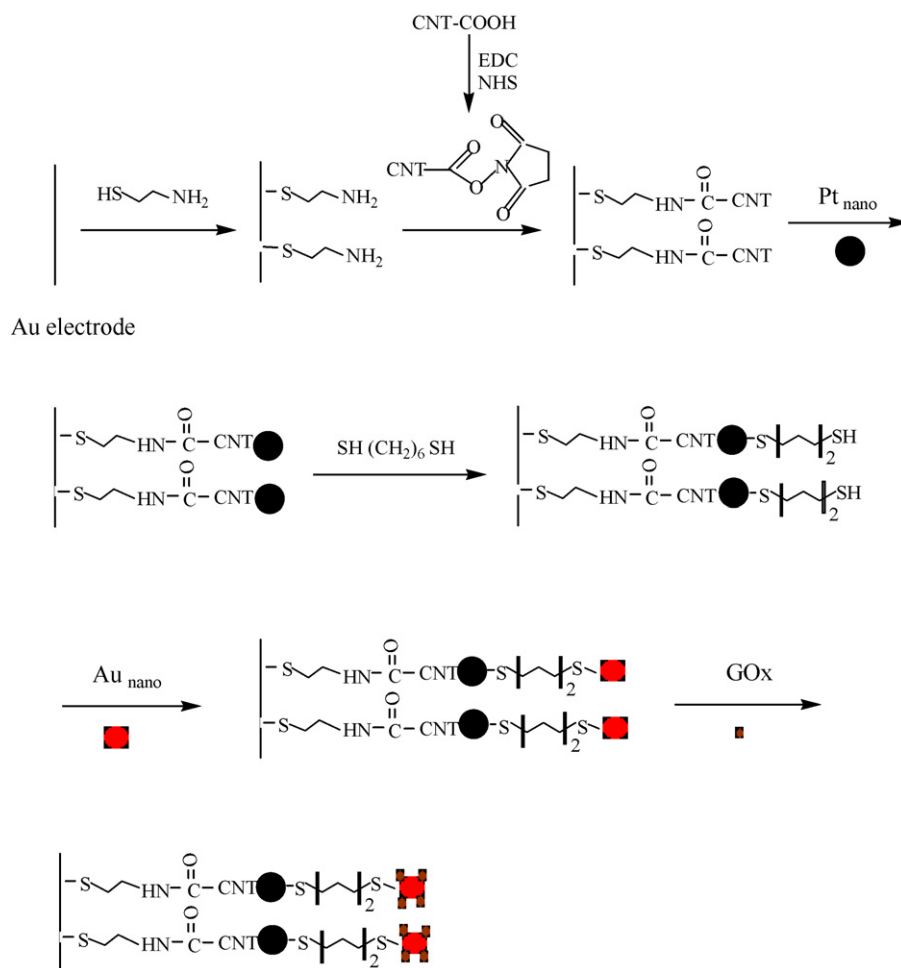
Scheme 1. A schematic showing the steps involved in the fabrication of glucose biosensor based on electrodeposition of Pt nanoparticles onto carbon nanotube electrode.

color changed to wine-red. Boiling was lasted for an additional 10 min. The obtained colloidal gold solution was then stored in dark bottles at 4 °C after cooling.

2.4. Procedures

2.4.1. Preparation of the Pt_{nano}/CNT/gold electrode

The fabrication of the glucose biosensor based on electrodeposition of Pt nanoparticles onto carbon nanotube electrode was summarized in Scheme 1. A polycrystalline gold electrode (99.99%, diameter 1 mm) was first polished with alumina slurry (followed by 0.3 and 0.05 μm) and ultrasonically cleaned with ethanol and double distilled water. After further electrochemical cleaning in 0.5 M sulfuric acid by repeating the potential scan in the potential range of −0.3–1.5 V versus SCE at 100 mV s^{-1} for 10 min, the electrode was then immersed in an ethanol solution containing 1 mM cysteamine for 10 h to give a cysteamine self-assembled monolayer (SAM). The oxidatively shortened MWNTs (0.2 mg) prepared as mentioned in (Section 2.1) were activated as described previously [43] by 100 mM EDC and 100 mM NHS (adjusting pH at 6.0) for 1 h at room temperature to convert the carboxyl groups of the shortened MWNTs into active carbodiimide esters. The cysteamine-modified gold

electrode was placed in above nanotube solution (adjusting pH at 8.5 with NaOH) for 10 h, during which the amines at the terminus of the SAM formed amide bonds with the active carbodiimide esters of the tubes. Electrodeposition of platinum on CNT/gold electrode was carried out in an electroplating bath. The composition of the electroplating bath consisted of 1.3 mM H_2PtCl_6 and 0.5 M H_2SO_4, making a total volume of 10 ml. The CNT-modified gold electrode was immersed in the plating bath and a constant potential of −0.25 V was applied for 5 min under gentle stirring condition [44].

2.4.2. Preparation of the enzyme electrode

The Pt_{nano}/CNT/gold electrode was dipped in an ethanol solution containing 50 mM SH(CH$_2$)$_6$SH for 1 h at 10–20 °C to give a SH(CH$_2$)$_6$SH self-assembled monolayer on Pt nanoparticles. After that, the electrode was washed with water thoroughly and then immersed in a colloidal gold solution for 12 h at 4 °C. The enzyme electrode was prepared by dropping a 10 μl of GOx solution (2 mg ml^{-1}) on the Au_{nano}/Pt_{nano}/CNT/gold electrode at 4 °C for 24 h. After rinsed clearly and dried, the electrode was coated with an extra 2.0 μl layer of 0.5% Nafion. Finally, the enzyme electrode was stored in the buffer solution at 4 °C before use.

3. Results and discussion

3.1. Characteristics of CNT/gold electrode by QCM

The spontaneous adsorption of organosulfur compounds on metal surfaces such as gold, silver and platinum offers a simple method for achieving a variety of modifications of the metal surfaces, resulting in the formation of organic self-assembled monolayers. It has been demonstrated that the resulting SAMs can be used as molecular templates for various technical applications such as chemical sensors. In this work, an amine-functionalized SAM was formed by modified the electrode surface with cysteamine. Sidewalls and end of carbon nanotubes were functionalized with carboxyl groups after reflux and sonication in concentrated sulfuric acid and nitric acid. After activated by coupling agents EDC and NHS, these carboxyl groups converted into carbodiimide esters. The carbon nanotubes were then immobilized onto the electrode surface by forming amide bonds with amines at the terminus of the SAM.

The modification of CNT on electrode surfaces was characterized by quartz crystal microbalance (QCM) technique. QCM is based on the principle that the shift in resonance frequency of QCM is usually correlated with the mass change loading on the quartz crystal surface. The frequency change is described by the Sauerbrey equation as follows [45]:

$$\Delta F = -2.26 \times 10^{-6} F_0^2 \Delta m / A$$

where ΔF is the frequency change of quartz crystal, F_0 the resonance frequency of the unloaded quartz crystal, A the surface area of the crystal and Δm is the mass change on the crystal surface.

Fig. 1 shows the frequency changes of the cysteamine monolayer-functionalized quartz crystal after interaction with activated CNT at different reaction time. It is observed from Fig. 1 that the amount of the CNT immobilized onto the quartz crystal increased with increasing the reaction time. The coupling progress has virtually reached saturation after 10 h and the frequency change becomes a constant value ($\Delta F = 352$ Hz).
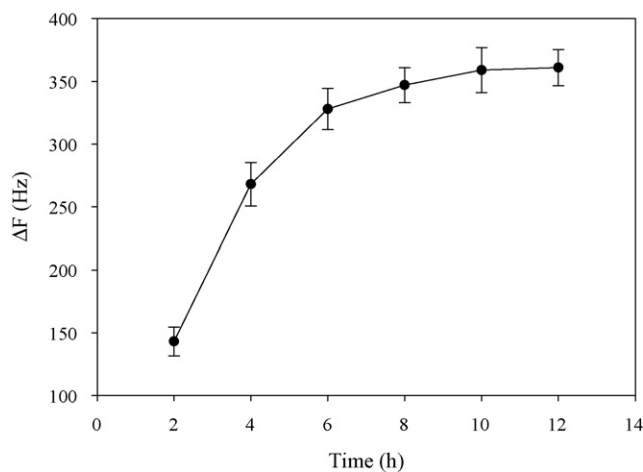
Fig. 1. Frequency changes of the cysteamine monolayer-functionalized quartz crystal after interaction with activated CNT at different reaction time. The frequency changes were measured in air.
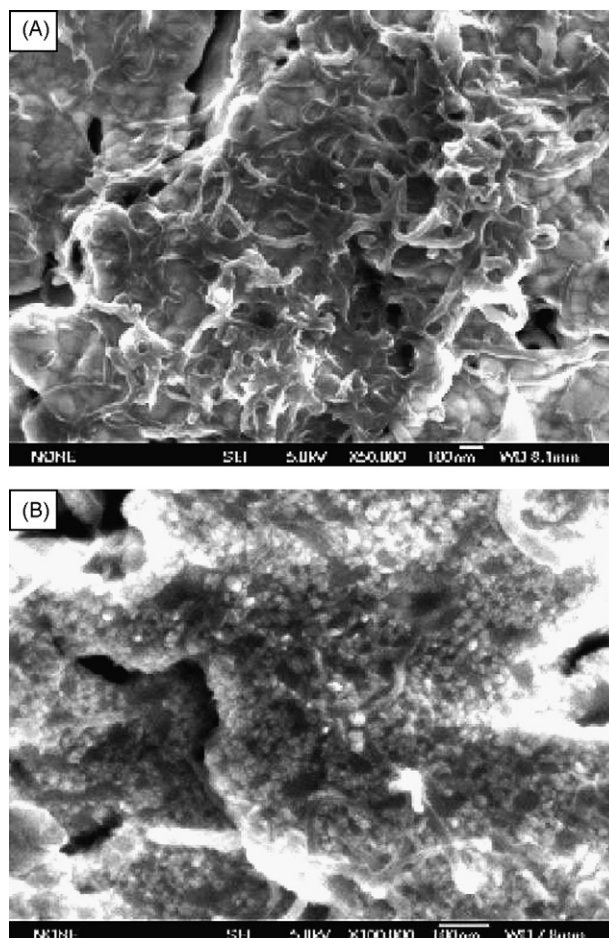
Fig. 2. SEM images of (A) CNT/gold electrode and (B) Pt$_{nano}$/CNT/gold electrode.

According to the mass sensitivity of 0.66 Hz ng^{-1} for a 9 MHz, 5 mm diameter, AT-cut quartz crystal [45], it can be calculated that about 27.2 ng mm^{-2} CNT was immobilized onto the gold surface of quartz crystal through the covalent linkage method.

3.2. SEM images of Pt$_{nano}$/CNT/gold electrode

The surface morphologies of CNT/gold electrode and Pt$_{nano}$/CNT/gold electrode were studies by SEM as shown in Fig. 2(A and B). A network-like structure of CNTs without aggregation was observed on the CNT/gold electrode surface (Fig. 2A), which indicated that the CNTs were immobilized indeed onto the gold electrode surface through covalent linkage method. The diameter of CNTs was about 10–50 nm. Considering that most metals including Pt would not adhere to carbon nanotubes directly because the CNTs were very hydrophobic, surface modification and activation have been attempted to improve metal deposition onto carbon nanotubes [40]. A popular approach is associated with the oxidation of the CNT surface to create functional groups and increase metal nucleation [46]. In this work, the reflux and sonication in mixed concentrated acid introduced relatively large amount of carboxylic acids moieties at defect sites located at the sidewalls of the nanotubes, which converted to carbodiimide esters after activated by EDC
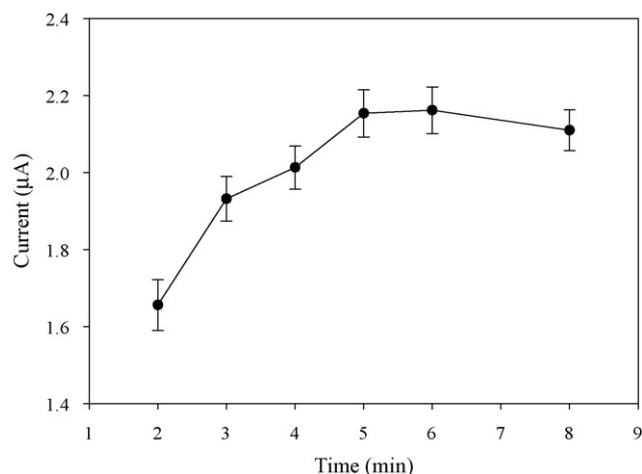
Fig. 3. Effect of Pt deposition time on steady-state response current of Pt$_{nano}$/CNT/gold electrode to addition of 0.1 mM H$_2$O$_2$ to a phosphate buffer solution, pH 7.0. Applied potential, 0.6 V.

and NHS. Choroplatinic ions might be anchored to these ester sites and formed Pt nanoparticles when a −0.25 V potential was applied. As shown from the SEM micrograph in Fig. 2B, roughly spherical Pt nanoparticles were randomly decorated on the CNTs modified on the gold electrode surface. These images revealed that robust and nonuniform thin film of Pt$_{nano}$/CNT could be formed on the gold electrode surface by electrodeposition of Pt nanoparticles on CNTs.

3.3. Effect of Pt deposition time on electrocatalytic property of Pt$_{nano}$/CNT/gold electrode

Platinum electrode has good catalytic activity and is used as a catalyst for H$_2$O$_2$ electrooxidation. The Pt nanoparticles used in this work, dispersed on the surface of CNTs, may provide a large available surface and enhance the electrocatalytic activity for H$_2$O$_2$ electrooxidation. Pt nanoparticles were electrodeposited on the surface of CNTs by the potentiostatic method. The effect of the amount of deposited Pt nanoparticles on the response current was investigated, and the corresponding result was shown in Fig. 3. The response current of the Pt$_{nano}$/CNT/gold electrode to the addition of 0.1 mM H$_2$O$_2$ increased with the increase of the Pt deposition time from 2 to 5 min. However, when the Pt deposition time was more than 5 min, the response current decreased slightly. This may be associated with the decrease of the real surface area of the electrode resulting from the deposition of a large amount of Pt nanoparticles on the electrode surface. Therefore, the deposition time of 5 min was selected in the following investigation.

3.4. Electrochemical characteristics of Pt$_{nano}$/CNT/gold electrode

To discern the role of individual components, four different electrodes of gold, CNT/gold, Pt$_{nano}$/gold and Pt$_{nano}$/CNT/gold were studied in H$_2$O$_2$ solution. Fig. 4 shows current responses of various different electrodes to additions of 0.1 mM H$_2$O$_2$ to a phosphate buffer solution when a 0.6 V potential was applied.
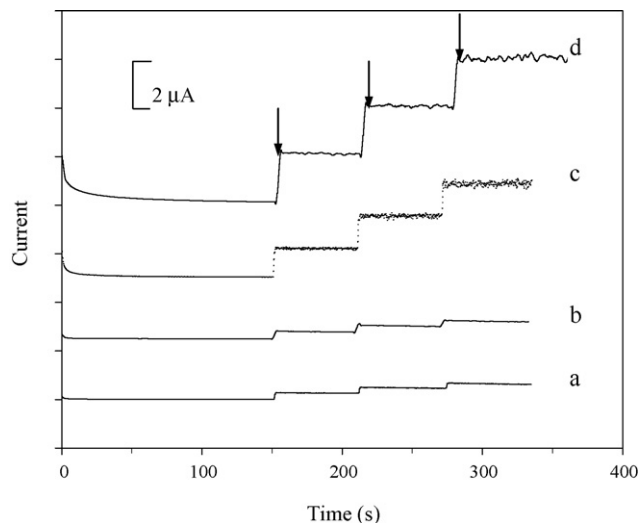
Fig. 4. Current responses of (a) gold electrode, (b) CNT/gold electrode, (c) Pt$_{nano}$/gold electrode and (d) Pt$_{nano}$/CNT/gold electrode. Steps represent the response of the electrode to additions of 0.1 mM H$_2$O$_2$ (indicated by arrows) to a phosphate buffer solution, pH 7.0. Applied potential, 0.6 V.

The gold electrode (trace a) yielded a detectable but very small current response to H$_2$O$_2$, which was due to the H$_2$O$_2$ electrooxidation at the electrode surface when a 0.6 V potential was applied. The small current indicated the direct oxidation of H$_2$O$_2$ at gold electrode was inefficient at 0.6 V. At CNT/gold electrode (trace b), a slight increase in current response to H$_2$O$_2$ was observed compared with the bare gold electrode, which may be ascribed to the fact that relative surface area of the electrode was increased by immobilization of CNTs on Au. The Pt$_{nano}$/gold electrode, prepared by electrodeposition of Pt nanoparticles on the bare gold electrode at a constant potential of −0.25 V for 5 min in an electroplating bath consisting of 1.3 mM H$_2$PtCl$_6$ and 0.5 M H$_2$SO$_4$, yielded a relatively high current response to H$_2$O$_2$ (trace c), which was amplified nearly five times as large as that of bare gold electrode. The significant increase in the current response of Pt$_{nano}$/gold electrode can be ascribed to the good catalytic activity of Pt nanoparticles to the electrooxidation of H$_2$O$_2$. The introduction of Pt nanoparticles into the CNT/gold electrode improved dramatically the current response (trace d). In particular, it amplified the H$_2$O$_2$ current by ∼10 times compared with CNT/gold electrode and ∼2 times compared with Pt$_{nano}$/gold electrode. This phenomenon should be ascribed to the increase in effective electrode surface due to stacking of CNT and Pt nanoparticles on gold electrode.

3.5. Optimization of the glucose determination conditions

A glucose biosensor was fabricated by adsorption of glucose oxidase onto a colloidal gold-film. Nanometer-sized colloidal gold was selected as substrate for immobilizing enzyme because it can not only adsorb redox enzymes without loss of biological activity but also facilitate the transfer of electron. The effect of the determination conditions such as the pH value and the applied potential on the response of the
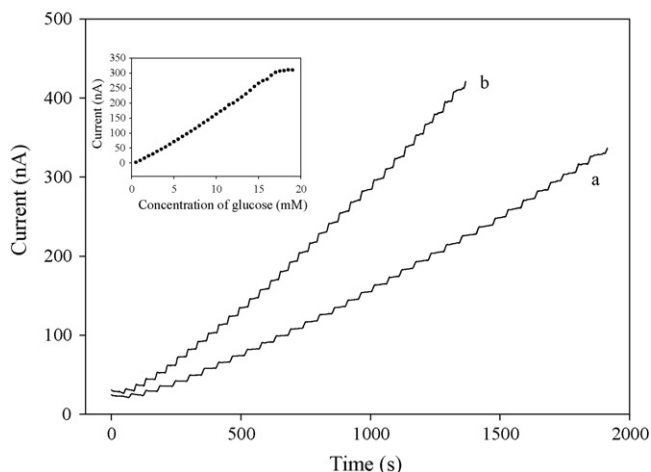
Fig. 5. Chronoamperometric response of the GOx/Au$_{nano}$/Pt$_{nano}$/CNT/gold electrode with (a) and without (b) the Nafion film upon the successive addition of 0.5 mM glucose in the PBS solution (pH 7.0) at an applied potential of 0.6 V. *Inset*: calibration curve of the Nafion-modified enzyme electrode.

GOx/Au$_{nano}$/Pt$_{nano}$/CNT/gold electrode to glucose has been investigated in detail.

The applied potential was changed from 0.2 to 0.9 V, and the corresponding response current to 1 mM glucose was measured (data not shown). For the fabricated enzyme electrode, the oxidation of the enzymatically formed H$_2$O$_2$ started at potential of 0.2 V. The response current increased rapidly with the increase of applied potential when the potential was less than 0.6 V. This indicated that the response of the enzyme electrode was controlled by the electrochemical oxidation of H$_2$O$_2$. When the potential was >0.6 V, a current plateau appeared. The appearance of such a current plateau is attributed to the rate-limiting process of enzymatical kinetics, and the potential at which the current plateau appears is dependent upon the electrode nature. Similar result was also obtained in other work [44]. A potential of 0.6 V was selected as the operational potential of the enzyme electrode.

The effect of the pH value on the response current of the enzyme electrode was also studied between 5.0 and 9.0 in 50 mM phosphate buffer. The response current of the enzyme electrode increased from 5.0 to 7.0 and decreased from 7.0 to 9.0, and the maximum current response can be obtained at pH 7.0. This result is agreement with that previously reported for GOx in solution and shows that the gold nanoparticles matrix has not altered the optimal pH of GOx.

3.6. Amperometric response of glucose at enzyme electrode

Fig. 5 shows the typical chronoamperometric responses of the GOx/Au$_{nano}$/Pt$_{nano}$/CNT/gold electrodes with (a) and without (b) the Nafion film upon the successive addition of 0.5 mM glucose at an applied potential of 0.6 V, along with the resulting calibration curve of the Nafion-modified enzyme electrode (inset). As the glucose was injected into the stirring buffer solution, the enzyme electrode without the Nafion film responded rapidly ($t_{95\%} \approx 5$ s) to changes in the glucose level. In contrast, the responses of the Nafion-modified enzyme electrode to glucose

Table 1
Influence of electroactive interferents on glucose response

Interferent	Physiological content (mM)	Ratio between concentration of glucose and interferent	I_{G+I}/I_G
Ascorbic acid	0.1	56	1.031
Uric acid	0.5	11.2	1.018

I_G, response current to 5.6 mM glucose; I_{G+I}, response current to 5.6 mM glucose in presence of interferent at physiological normal content.

were relatively small, about 20% loss of the response current can be observed and the response time was slightly prolonged ($t_{95\%} \approx 7$ s). The calibration curve of the Nafion-modified enzyme electrode was highly linear with glucose concentration over the entire 0.5–16.5 mM range and then with a slight curvature at a high level (correlation coefficient of 0.992), and the detection limit is 0.4 mM (S/N = 3). This response range for glucose is larger than that reported in other work [44]. According to the Lineweaver–Burk form of the Michaelis–Menten equation, the apparent Michaelis–Menten constant (K_m^{app}) of the enzyme reaction at GOx/Au$_{nano}$/Pt$_{nano}$/CNT/gold electrode can be calculated from the relationship between the reciprocal of current and the reciprocal of glucose concentration and is equal to 10.73 mM. This value is similar to the reported value for the free enzyme. A similar study at GOx/Au$_{nano}$/Pt$_{nano}$/gold electrode is also performed and its apparent Michaelis–Menten constant is equal to 11.89 mM. These results reveal that there is no substantial loss of GOx activity, indicating the immobilization procedures in the present study are biocompatible and can retain the GOx activity. In addition, the CNT can also slightly enhance the enzyme activity. The reproducibility of five Nafion/GOx/Au$_{nano}$/Pt$_{nano}$/CNT/gold electrodes was estimated by the response to 1 mM glucose at the potential of 0.6 V. The results reveal that the sensor has satisfied reproducibility with a mean change of the response current of 21 nA and a relative standard deviation of 4.5%.

3.7. Effect of electroactive interferents

The responses of the enzyme electrode to 0.1 mM ascorbic acid and 0.5 mM uric acid at the operating potential of 0.6 V were investigated with and without the Nafion film. The enzyme electrode without the Nafion film has strong electrocatalytic activity to ascorbic acid and the response was about 5.4 nA. In contrast, the response to ascorbic acid at the Nafion-modified enzyme electrode was small and only 0.8 nA. A similar situation can also be obtained for 0.5 mM uric acid and the responses of the enzyme electrodes without and with the Nafion film were 9.6 and 1.3 nA, respectively. These results indicated that the Nafion film-coated electrode could efficiently avoid the interference of ascorbic acid and uric acid. On the other hand, the magnitude of the interferent current relative to the analytical signal produced by the analyte was also considered in discussing interference of the electroactive compounds [44]. The interference of electroactive compounds to the glucose response was investigated in the presence of their physiological normal level [47] with a glucose concentration of 5.6 mM. The corresponding results were shown

Table 2
Glucose content determination in human blood samples

Sample number	Content determined by Xiangya hospital (mmol l^{-1})	Content determined by current method (mmol l^{-1})	Relative error (percentage)
1	8.23	7.94	−3.5
2	10.88	11.18	+2.8
3	5.94	5.68	−4.4
4	5.24	5.44	+3.8
5	9.65	9.88	+2.4

in Table 1. The influence of ascorbic acid and uric acid on the glucose response was weak under the testing conditions. The ratio of I_{G+I} to I_G was 1.031 for ascorbic acid and 1.018 for uric acid.

3.8. Stability of the enzyme electrode

The stability of the enzyme electrode under storage conditions (PBS, pH 7.0, 4 °C) was investigated using the same PBS containing 1 mM glucose, and the measurement was carried out one time everyday up to 25 days. The enzyme electrode lost ∼3% of the initial response after a storage period of 5 days. With the storage prolonged, the response current decreased. After 25 days, the response current was still retained at 75% value of the initial response. The loss of the current response of the enzyme electrode may result from the decrease of GOx enzyme activity during storage and may not be due to the loss of the enzyme because no significant GOx activity is observed in the storage solution. The relatively good storage stability implies that CNT film immobilized by covalent linkage and Pt nanoparticles electrodeposited on the electrode surface are very stable. Moreover, gold nanoparticle is compatible with the immobilized enzyme and facilitates maintaining the bioactivity of GOx.

3.9. Sample analysis

Human plasma samples were assayed to demonstrate the practical use of the Nafion/GOx/Au$_{nano}$/Pt$_{nano}$/CNT/gold electrode. Fresh plasma samples were first analyzed in the Xiangya hospital with ASCA AG-II Chemistry System (Landmark, USA). The samples were then reassayed with the Nafion/GOx/Au$_{nano}$/Pt$_{nano}$/CNT/gold electrode. A plasma sample was added into 5 ml PBS (pH 7.0), and the response was obtained at 0.6 V. The contents of glucose in blood can then be calculated from the calibration curve. The results were shown in Table 2. As can be seen, the results were satisfactory and agree closely with those measured by the biochemical analyzer in the hospital.

4. Conclusion

A more stable and reproducible deposition of CNTs film onto gold electrode can be achieved using covalent linkage method. The accessible sites of the CNTs facilitate the incorporation of Pt nanoparticles. The optimized enzyme electrode has a good

glucose-biosensing capability. A thin layer of Nafion was necessary to avoid the loss of GOx and suppress the interfering signals from UA and AA. It may be anticipated that other biomaterials can be adsorbed on the colloidal gold matrix for the fabrication of other useful biosensors.

References

[1] S. Iijima, Nature (London) 354 (1991) 56.
[2] Y.-P. Sun, K. Fu, Y. Lin, W. Huang, Acc. Chem. Res. 35 (2002) 1096.
[3] P. Avouris, Acc. Chem. Res. 35 (2002) 1026.
[4] Q.X. Zhou, J.P. Xiao, W.D. Wang, G.G. Liu, Q. Shi, J.H. Wang, Talanta 68 (2006) 1309.
[5] J. Riu, A. Maroto, F.X. Rius, Talanta 69 (2006) 288.
[6] L. Qian, X. Yang, Talanta 69 (2006) 957.
[7] R. Antiochia, I. Lvagnini, F. Magno, F. Valentini, G. Palleschi, Electroanalysis 16 (2004) 1451.
[8] W.C. Poh, K.P. Loh, W.D. Zhang, S. Triparthy, J.S. Ye, F.S. Shen, Langmuir 20 (2004) 5484.
[9] S. Hrapovic, Y.L. Liu, K.B. Mall, J.H.T. Luong, Anal. Chem. 76 (2004) 1083.
[10] H.X. Luo, Z.J. Shi, N.Q. Li, Z.N. Gu, Q.K. Zhuang, Anal. Chem. 73 (2001) 915.
[11] Y.H. Lin, F. Lu, Y. Tu, Z.F. Ren, Nano. Lett. 4 (2004) 191.
[12] Z. Xu, N. Gao, S. Dong, Talanta 68 (2006) 753.
[13] J.X. Wang, M.X. Li, Z.J. Shi, N.Q. Li, Z.N. Gu, Anal. Chem. 74 (2002) 1993.
[14] C.X. Cai, J. Chen, Anal. Biochem. 332 (2004) 75.
[15] L. Wang, J.X. Wang, F.M. Zhou, Electroanalysis 16 (2004) 627.
[16] G.C. Zhao, L. Zhang, X.W. Wei, Z.S. Yang, Electrochem. Commun. 5 (2003) 825.
[17] C.X. Cai, J. Chen, Anal. Biochem. 335 (2004) 285.
[18] Y.D. Zhao, Y.H. Bi, W.D. Zhang, Q.M. Luo, Talanta 65 (2005) 489.
[19] J. Wang, M. Musameh, Y.H. Lin, J. Am. Chem. Soc. 125 (2003) 2408.
[20] M. Musameh, J. Wang, A. Merkoci, Y.H. Lin, Electrochem. Commun. 4 (2002) 743.
[21] Z.A. Xu, X. Chen, X.H. Qu, S.J. Dong, Electroanalysis 16 (2004) 684.
[22] K.P. Gong, Y. Dong, S.X. Xiong, Y. Chen, L.G. Mao, Biosens. Bioelectron. 20 (2004) 253.
[23] Y. Zhao, Y. Gao, D. Zhan, H. Liu, Q. Zhao, Y. Kou, Y. Shao, M. Li, Talanta 66 (2005) 51.
[24] A. Salimi, R. Hallaj, Talanta 66 (2005) 967.
[25] L. Qian, X.R. Yang, Talanta 68 (2006) 721.
[26] Y. Liu, X.H. Qu, H.W. Guo, H.J. Chen, B.F. Liu, S.J. Dong, Biosens. Bioelectron. 21 (2006) 2195.
[27] M.G. Zhang, A. Smith, W. Gorski, Anal. Chem. 76 (2004) 5045.
[28] K.R. Brown, A.P. Fox, M.J. Natan, J. Am. Chem. Soc. 118 (1996) 1154.
[29] C.Y. Wang, X.Y. Hu, Talanta 67 (2005) 625.
[30] M. Siswana, K.I. Ozoemena, T. Nyokong, Talanta 69 (2006) 1136.
[31] A. Wu, W. Cheng, Z. Li, J. Jiang, E. Wang, Talanta 68 (2006) 693.
[32] W. Vastarella, R. Nicastri, Talanta 66 (2005) 627.
[33] C.R. Yonzon, D.A. Stuart, X. Zhang, A.D. McFarland, C. Haynes, Talanta 67 (2005) 438.
[34] S. Liu, Z. Zhang, Y. Wang, F. Wang, M.Y. Han, Talanta 67 (2005) 456.
[35] Q. Chi, S. Dong, Anal. Chim. Acta 278 (1993) 17.
[36] Y. Ikariyama, S. Yamauchi, J. Electrochem. Soc. 136 (1989) 702.
[37] S.A. Miscoria, G.D. Barrera, G.A. Rivas, Electroanalysis 14 (2002) 981.
[38] H. Sakslund, J. Wang, J. Electroanal. Chem. 374 (1994) 71.
[39] D.R. Shankaran, N. Uehara, T. Kato, Biosens. Bioelectron. 18 (2003) 721.

[40] S. Hrapovic, Y. Liu, K.B. Male, J.H.T. Luong, Anal. Chem. 76 (2004) 1083.

[41] S.H. Lim, J. Wei, J. Lin, Q. Li, J.K. You, Biosens. Bioelectron. 20 (2005) 2341.

[42] J.J. Gooding, R. Wibowo, J.Q. Liu, W.R. Yang, D. Losic, S. Orbons, F.J. Mearns, J.G. Shapter, D.B. Hibbert, J. Am. Chem. Soc. 125 (2003) 9006.

[43] J. Wang, G. Liu, M.R. Jan, J. Am. Chem. Soc. 126 (2004) 3010.

[44] H. Tang, J.H. Chen, S.Z. Yao, L.H. Nie, G.H. Deng, Y.F. Kuang, Anal. Biochem. 331 (2004) 89.

[45] J. Hlavay, G.G. Guilbault, Anal. Chem. 49 (1977) 1890.

[46] Y.P. Sun, K. Fu, Y. Lin, W. Huang, Acc. Chem. Res. 35 (2002) 1096.

[47] H. Zheng, H.G. Xue, Y.F. Zhang, Z.Q. Shen, Biosens. Bioelectron. 17 (2002) 541.

ELSEVIER

Study of heterogeneities in steels and determination of soluble and total aluminium and titanium concentration by laser ablation inductively coupled plasma mass spectrometry

Aurora G. Coedo [a,*], Teresa Dorado [a], Isabel Padilla [a], Juan C. Fariñas [b]

[a] *Centro Nacional de Investigaciones Metalúrgicas (CSIC), 28040 Madrid, Spain*
[b] *Instituto de Cerámica y Vidrio (CSIC), Campus de Cantoblanco, 28049 Madrid, Spain*

Abstract

A methodology for bulk analysis of Al and Ti and for determination of soluble and total Al and Ti concentration in steel samples by laser ablation inductively coupled plasma mass spectrometry was developed. The spatial distribution (both at surface and within the sample) of the insoluble fraction of Al and Ti was also qualitatively estimated. Certified reference materials (CRMs) SS-451 to 460 (carbon steel) and 064-1 (Nb/Ti interstitial free steel), from BAS, and JK 2D (carbon steel) and JK 37 (highly alloyed steel), from SIMR, were studied. It was demonstrated that the insoluble fraction of Al and Ti is heterogeneously distributed. A series of nine glass samples (fused beads) with fixed Fe content and different Al and Ti contents was prepared by melting appropriate amounts of Fe_2O_3, Al_2O_3 and TiO_2 with a lithium tetraborate–sodium carbonate mixture. Quantitative determinations were performed by using calibration graphs obtained from the synthetic fused beads, with ^{57}Fe as internal standard; line scan laser sampling mode was used, focusing the laser beam at the sample surface. The optimized laser operating parameters were: laser pulse energy of 1.5 mJ, pulse repetition rate of 5 Hz, scanning speed of 5 $\mu m\,s^{-1}$ and preablation time of 20 s. The concentrations obtained for bulk analysis of CRM samples corresponded with the certified values within the experimental uncertainty. An acceptable concordance between certified and found values was attained for the determination of soluble and total Al and Ti in CRM 064-1 sample.
© 2006 Elsevier B.V. All rights reserved.

Keywords: Laser ablation; Inductively coupled plasma mass spectrometry; Al and Ti inclusions; Steels

1. Introduction

The liquid steel contains a large amount of oxygen in he form of dissolved gases and iron oxides. The amount of oxygen that a steel can contain varies with the temperature and with the content of carbon and other elements. At high temperatures, the steel can dissolve a greater amount of oxygen, which tends to escape as the steel cools. The evolution of the gases and control of them during cooling affects the characteristics of the steel obtained, *i.e.* its internal cleanliness and uniformity, which significantly influences the finished product. All steels contain small amounts of non-metallic inclusions, primarily sulphides,

silicates, and oxidized materials that are chiefly derived from the oxidizing reactions of the refining and casting processes. Deoxiders are added to control the gases given off, combining with the oxygen to form oxides that have a lower density, and float in the liquid steel in the ladle or in the ingot mould. The deoxidation process comprises three stages: dissolving of the deoxidizer, oxide formation and elimination of inclusions. Nevertheless deoxidation products cause the majority of indigenous inclusions, generated by the reaction between the dissolved oxygen and the added deoxidant. Aluminium and titanium provide effective deoxidation and inhibit austenitic grain growth [1]. The technical characteristics of the steel obtained depend on the method, place and deoxidiser used. Inclusions size can vary from sub to hundreds of micrometers where larger particles tend to be agglomerates of small particles rather than single individual precipitates. Steel cleanliness is a key issue that significantly influences the technical characteristics of the final product [2].

* Corresponding author.
  E-mail addresses: coedo@cenim.csic.es (A.G. Coedo),
jcfarinas@icv.csic.es (J.C. Fariñas).

The usual procedure for the quantitative determination of soluble and total Al and Ti content consists in dissolving the sample in acid. The acid soluble fraction is considered as the soluble Al and Ti in the Fe matrix, though a very small part of the aluminium and titanium inclusions (Al_2O_3 and TiO_2, for example) can be partly dissolved in acids. The eventual insoluble residue is melted with alkaline fluxes. This procedure is time-consuming and labour intensive, and in addition increases the range of salts present in the solution and therefore the difficulties connected with subsequent determination by atomic spectrometry. Consequently, a simple and fast method able to identify the Al and Ti heterogeneities and to quantify soluble and total Al and Ti contents is required for product development, process control and quality assurance.

Laser ablation inductively coupled plasma mass spectrometry (LA-ICP-MS) is a rapid and sensitive analytical technique that is used in two major fields of applications: bulk analysis, with a low spatial resolution, and local analysis, with high spatial resolution [3–5]. To obtain information about the distribution of elements in heterogeneous solids, single point, line scan or rastering laser sampling modes can be performed. The depth profile distribution can be measured by focusing the laser beam at a steady position, while movable beam positions with respect to the sample surface allows the lateral distribution across the sample area to be profiled.

LA-ICP-MS was widely adopted in a variety of research areas of materials science [6]. It has been successfully applied to the direct analysis of steel composition and to the depth profile of different coatings on steel substrate. Yasuhara et al. [7] studied the optimum conditions for fixed Q pulse mode and Q-switched pulse mode, demonstrating that the Q-switched pulse mode was better for both non-metallic elements and elements with a high boiling-point. When determining non-metallic elements (Si, P), in order to correct changes in background intensity, normalization with the Fe matrix and with the Ar ion is proposed. Ishibashi [8,9] used a Q-switched Nd-YAG laser system for rapid analysis of steels using ICP-AES and ICP-MS. Calibration curves were prepared with standard steels, using Fe as internal standard. The precision in ICP-MS ranged from 5% to 10%. Also a semi-quantitative method was investigated, using the Fe signal as the base for signal compensation. Coedo et al. [10] used dried aerosol solutions for calibration in LA. Experimentally relative sensitivity factors (RSFs) were calculated and used to compensate for differences in sampling efficiency. Bleiner et al. [11] used ICP-TOFMS in combination with an excimer laser for depth profile analysis of Ti based single layers on different substrates. Plotnikov et al. [12] used a Nd:YAG 266 nm laser with ICP-QMS) to perform depth profile analysis of Ti-based single layers deposited on steel and WC/Co substrates. Kanicky et al. [13] performed qualitative depth profiling of 3 μm ZrTiN coatings using an homogenized beam from an ArF* 193 nm excimer laser. Coedo et al. [14] evaluated the feasibility of a Nd:YAG 266 nm laser for the depth profiling of steel substrate coated with copper single layers (Cu coating thicknesses ranging from 6 to 200 μm). One of the big advantages is the ability of the technique to provide information on spatial distribution in all three dimensions, dealing with inho-mogeneous samples. The changing transient signals produced can provide information about the presence of heterogeneities, although the time delay in the sample transport system (including the sample cell volume) is a limiting factor, causing signal mixing during the transportation of the ablated material, and preventing accurate identification of the exact origin of every signal. Plotnikov et al. [15] used the evolution of the parameters of single-shot response to reveal the true concentration profile of spatially inhomogeneous samples. Bleiner et al. [16] detail the principles and capabilities of the most common spatially resolved analytical techniques (XPS, AES, SIMS, SNMS, GD-OES, GD-MS, SEM-EDX and LA-ICP-MS), comparing their spatial resolution and robust/powerful detection capability. Several of them (XPS, AES, SIMS, SNMS) offer nanometers depth resolution, but no more than qualitative trends. LA-ICP-MS, combining the strong detection power of the ICP-MS with the high spatial resolution of the focused laser beam (10–100 μm lateral, and 0.1–1 μm depth), is presented as an ideal technique for quantitative spatially resolved analysis. Devos et al. [17] compared the advantages and drawbacks of LA-ICP-MS with electron probe microanalysis for spatially resolved trace analysis of early-medieval archaeological iron finds. Kang et al. [18] demonstrated the ability of the technique to provide elemental distribution information in micro spatial areas of dental tissues. Kindness et al. [19] developed a method for two-dimensional mapping of trace elements to identify the influence of metabolic zonation by the liver on trace element distribution. Becker et al. utilized LA-ICP-MS to produce images of element distribution in thin sections (20 μm thickness) of human [20] and rat [21] brain tissues. Karasev et al. [22] applied the technique to the analysis of total and insoluble contents of elements and inclusion composition in Fe–M (M = Al, Ce and Ti) alloys. Izmer et al. [23] compared the use of line scan and single point modes to investigate elemental diffusion at the interface of NiCrAlY-based coatings on high-temperature alloys.

In many of the applications, quantification remains a challenge, and different approaches were proposed to prepare samples for calibration. Preparation of glass samples (fused beads) [24] or pellets [25] was performed to generate solid standards when matrix-matched certified reference materials are not available. Aeschliman et al. [26] used analyte signals from desolvated particles for a two-point calibration method, measuring online the transport of sample particulates from the ablation cell with a piezoelectric microbalance to provide signal normalization. Hoffmann et al. [27] pointed out that the precision and accuracy of the results are influenced by signal standardization, calibration standards and the mass-spectrometric measuring mode. Sanborn and Telmer [28] showed that line scan mode provided some advantages over spot analysis, obviating some complications such as changes in ablation yield and element fractionation that occur with increasing pit depth and Gaussian pit morphology.

The aim of the present work is to study the spatial distribution (both at surface and in depth) of the insoluble fraction of Al and Ti in steel samples by LA-ICP-MS, as well as to develop methodologies for bulk analysis of Al and Ti and for determination of soluble and total Al and Ti.

2. Experimental

2.1. Instrumentation

Experiments were performed with a commercially available quadrupled (266 nm) nanosecond Nd:YAG laser with Q-switch (LSX-100, CETAC Technologies, Omaha, Nebraska, USA) coupled to an ICP quadrupole mass spectrometer (ELAN 6000, Perkin-Elmer, Sciex, Ontario, Canada). The operating conditions of both the laser ablation and the ICP-MS instruments are listed in Table 1. Instrument conditions were optimized for best time-resolved data acquisition. A pure Fe sample was used for optimization. Fe signals were acquired and visually examined as a function of time. The monitoring of the signals in "real-time" allowed to change the operating parameters during the analysis and to select the best parameters setting in terms of sensitivity and stability. Laser pulse energy was measured with a laser power/energy meter (EM 400, Molectron Detector, Inc., USA). The depth and width of the craters and of the tracks were measured by optical microscopy, and their morphology was observed by scanning electron microscopy, SEM (DSM 400, Zeiss, Germany).

2.2. Samples

Certified reference materials (CRMs) SS-451 to 460 (carbon steel, residual series) and 064-1 (Nb/Ti interstitial free steel), from the Bureau of Analysed Samples (BAS), and JK 2D (carbon

steel) and JK 37 (highly alloyed steel), from the Swedish Institute for Metals Research, were analyzed. SS-451 to 460, 064-1 and JK 2D samples have a similar Fe content of about 98–99%, whereas JK 37 sample contains 26.7% of Cr, 30.8% of Ni, 3.5% of Mo and a Fe concentration of about 40%. Certified values for Al and Ti are listed in Table 2. Pure electrolytic iron BAM 098-1, from Bundesanstalt für Materialforschung und- prüfung, with Al and Ti contents lower than 1 ppm, was used as a blank. All of them are spectroscopic standard certified reference materials (38 mm diameter × 19 mm discs).

Table 2
Certified values of Al and Ti in the CRM samples

Sample	Al (%)	Ti (%)
SS-451	–	0.090 ± 0.006
SS-452	–	0.020 ± 0.002
SS-453	–	0.016 ± 0.001
SS-454	–	0.0120 ± 0.0005
SS-455	–	0.028 ± 0.002
SS-456	0.008 ± 0.001	–
SS-457	0.008 ± 0.001	–
SS-458	0.140 ± 0.005	–
SS-459	0.068 ± 0.004	–
SS-460	0.028 ± 0.002	–
JK 37	0.0084 ± 0.0006	0.0039 ± 0.0006
JK 2D	0.0249 ± 0.0006	–
064-1	0.0330 ± 0.0011[a], 0.0302 ± 0.0008[b]	0.0189 ± 0.0007

[a] Total content.
[b] Soluble content.

Table 1
LA-ICP-MS operating conditions

Parameter	Value
LA (CETAC, LSX-100)	
Laser type	Nd:YAG pulsed
Laser mode	Q-switched
Beam profile	>95% fit to Gaussian
Beam diameter	1.0 mm
Wavelength	266 nm (ultraviolet)
Pulse width	8 ns
Transverse mode	TEM_{00} single mode
Pulse energy output	1–20 arbitrary units
Pulse repetition rate	1–20 Hz
Sample movement speed	3–100 μm s^{-1}
Ablation chamber volume	100 cm^3
Transport from ablation cell to MS	Tygon tube (30 cm in length, 5 mm i.d.)
ICP-MS (Perkin-Elmer Sciex, ELAN 6000)	
Rf forward power	1100 W
Ar plasma flow rate	14 l min^{-1}
Ar carrier flow rate	0.65 l min^{-1}
ICP frequency	40.86 MHz (free-running)
Detector	Dual mode
Analytes	^{27}Al, ^{57}Fe, ^{48}Ti
Dwell time	10 ms
Sweeps/reading	3
Estimated reading time	150 ms
Readings/replicate	As many as provide enough replicate time allowing to evaluate the complete signal produced in the laser sampling stage
Replicates	One for transient signal acquisition and three for bulk analysis
Data acquisition	Peak hopping, one point per peak and time resolved mode

Table 3
Preparation and composition of glass samples (fused beads) for calibration

Bead no.	Starting material (g)				Composition (%)		
	Fe$_2$O$_3$	X3913	Al$_2$O$_3$	TiO$_2$	Fe	Al	Ti
0	0.250	–	–	–	2.2	0	0
1	0.230	0.100	–	–	2.2	0.0050	0.0031
2	0.215	0.200	–	–	2.2	0.0098	0.0061
3	0.160	0.500	–	–	2.2	0.0238	0.0149
4	0.120	0.750	–	–	2.2	0.0349	0.0218
5	0.250	–	0.0060	0.0050	2.2	0.0397	0.0374
6	0.250	–	0.0075	0.0075	2.2	0.0496	0.0561
7	0.250	–	0.0100	0.0100	2.2	0.0662	0.0748
8	0.250	–	0.0150	0.0150	2.2	0.0992	0.1122

A series of nine glass samples (fused beads) with fixed Fe content and different Al and Ti contents was prepared for calibration. Mixtures of appropriate amounts of Fe$_2$O$_3$, Al$_2$O$_3$ and TiO$_2$ (99.9%, Aldrich) were melted in a Pt crucible at 1200 °C for 5 min with 6 g of lithium tetraborate and 3 g of sodium carbonate. The molten mass was poured on to a platinum plate, preheated to dull red. To prepare the samples with low Al and Ti contents, and to avoid the addition of very small weights of oxides, appropriate quantities of the certified converted slag X3913 (AG der Dillinger Hüttenwerke, Dillinger, Germany), with certified contents of these elements (Fe = 14.61%; Al$_2$O$_3$ = 0.76%; TiO$_2$ = 0.42%), were added. The amounts of starting materials and final composition of prepared beads are given in Table 3. The weight of the beads was of 8 ± 0.10 g, whereas the total weight of materials used for preparation was 9.25 g. The Fe, Al and Ti contents were calculated considering the real weight of the obtained glasses (8 g), assuming that the weight loss is due to the CO$_2$ detachment from the 3 g of sodium carbonate used in the fusion.

2.3. Procedure

Experiments were done using the following laser sampling modes: single point (laser is fired repetitively over a single position of the sample), line scan (the sample is moving horizontally at a constant speed) and rastering (several discrete single spots are consecutively performed, with a specific number of laser pulses on each spot and a specific distance between spots). The optimization of the laser operating parameters was performed using the pure electrolytic iron BAM 098-1. The laser pulse energy was selected in the range from 6 to 10 (arbitrary units), corresponding to values ranging from 0.6 to 4 mJ pulse^{-1} (energies measured with a laser power/energy meter model EM 400 from Molectron Detector, Inc., USA). As a good spatial resolution requires small spot size, the laser beam was always focused at the sample surface, in order to work with the smallest crater diameter attainable. A pulse repetition rate of 5 Hz was used for all tests, except for the in-depth analysis, where the pulse repetition rate was increased progressively (1 Hz for the first scan, 2 Hz for the two followings, and 4 Hz for the two last). The error bars in the plots represent standard deviation values based on four replicates.

3. Results and discussion

3.1. Influence of laser operating parameters

In LA-ICP-MS analysis, spatial resolution in all three dimensions is theoretically limited by the ablation rate and crater aspect ratio (depth/diameter ratio of the crater) for depth profiling (discrete spots, or single point laser sampling mode) and by the depth and width of the track for lateral profiling (line scan laser sampling mode). By maintaining laser source, focusing conditions and pulse repetition rate constant, all these parameters depend on the laser pulse energy. Crater aspect ratio and depth of the track also depend on the number of laser pulses and scan speed, respectively. On the other hand, the intensity of the measured transient analytical signal is a result of the sum of weighted responses of neighbouring ablation pulses. Hence, the effect of laser pulse energy, number of laser pulses, depth and width of crater and track and scan speed on the analyte signal response has been studied, in order to obtain the best laser operating conditions.

The influence of laser irradiance on analyte signal response was tested for laser pulse energies of 0.6, 1.5, 2.5, 3.3 and 4.0 mJ, resulting in irradiance values of 10, 15, 17, 19 and 21 GW cm^{-2}, respectively. Fig. 1 shows the dependence of the normalized analyte signal response, which corresponds directly to the quantity of mass ablated, with the number of laser pulses for the dif-
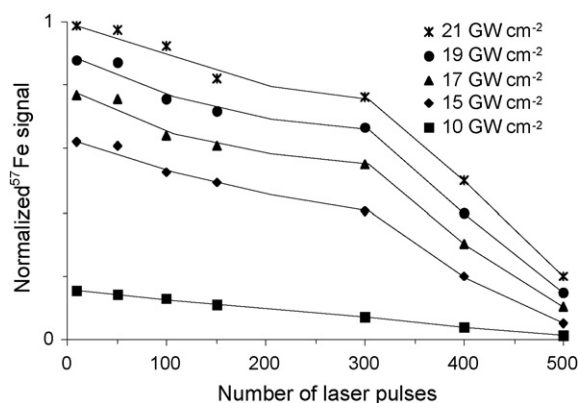

Fig. 1. Influence of number of laser pulses on normalized ^{57}Fe signal for irradiance values ranging from 10 to 21 GW cm^{-2}. Sample: CRM BAM 098-1.

ferent laser pulse energies. As expected, the higher the energy, the higher the analyte signal response. On the other hand, it can be observed that, during progressive ablation, the analyte signal remains nearly constant by the first 50 pulses. Between 50 and 150 pulses, it decreases sharply to about 80% of the initial response, even with the highest irradiance (21 GW cm^{-2}).

Between 150 and 300 pulses, there is a very gradual decay of the signal, falling down later dramatically. This behaviour can be explained, according to Tokarev et al. [29] by the three-dimensional plasma expansion that takes place in the surface and in the shallow craters, which implies a more significant material removal, and by the one-dimensional expansion inside the deep craters, where there is practically no material removal due to dense plasma and strong laser beam attenuation. In addition, both the defocusing and the cone-shaped crater development, can also contribute to a decreasing signal with increasing number of laser pulses, especially for higher laser pulse energies.

As a compromise between ion signal intensity and crater diameter, a laser pulse energy of 1.5 mJ, providing a good sensitivity and a crater diameter of 40 μm ($I = 15$ GW cm^{-2}), was selected for further experiments. Bleiner et al. [30] studied the influence of irradiance in crater morphology for different metals (Al, Cu, Fe, Zn, Mn, Co) showing that at low irradiance the crater morphology did not develop uniformly and the reproducibility of the micro-sampling becomes poor, whereas at high irradiance a more regular pan-shaped morphology was produced and a more efficient material removal mechanism is attained. The dependence of crater aspect ratio (depth/width) on number of laser pulses, for the selected laser pulse energy (1.5 mJ), was also assessed. In agreement with our previous results [14], the diameter at the top of the crater remained nearly constant (≈40 μm), whereas the crater depth increased linearly from about 1 to 140 μm when the number of laser pulses increased from 1 to 150 μm. This corresponds to an ablation rate of approximately 1 μm per pulse. Fig. 2 illustrates the variation of the normalized analyte signal response wit the crater aspect ratio. As can be seen, the signal response clearly decreases for crater aspect ratios higher than 1.0, dropping to about 80% of the initial signal response for values of about 3.5. Consequently, a crater aspect

Fig. 3. Influence of scanning speed on depth of laser track. Sample: CRM BAM 098-1. Laser sampling mode: line scan; laser pulse energy: 1.5 mJ; pulse repletion rate: 5 Hz.

ratio value of *ca.* 1, which is obtained by firing the sample with about 40 laser pulses, was chosen for further tests.

The effect of scanning speed on depth of laser track was studied for 2, 5, 10, 20, and 40 μm s^{-1} by using the line scan laser sampling mode. The applied laser pulse energy was the selected value of 1.5 mJ, so the width of laser track was about 40 μm in all cases. The results are depicted in Fig. 3. As can be seen, for fixed laser conditions the track depth varies inversely with scanning speed. A scanning speed of 5 μm s^{-1} is required to achieve a laser track with a depth/width ratio of *ca.* 1 (*i.e.*, a laser track of about 40 μm both in width and depth), so this scanning speed value was selected for all further lateral profiling analysis. Taking into account an ablation rate of 1 μm pulse^{-1}, the laser track should reach a uniform and unvarying depth of *ca.* 40 μm after about 8 s of line scanning (*i.e.*, 40 laser pulses, at a pulse repetition rate of 5 Hz). Fig. 4 shows the temporal behaviour of the ^{57}Fe signal by using the line scan laser sampling mode and the selected optimal conditions (laser irradiance 1.5 mJ, repetition rate 5 Hz, and scanning speed 5 μm s^{-1}). As can be observed, the ^{57}Fe signal reaches a maximum intensity when ablation starts and, immediately, it drops slowly for about 8 s. This behaviour can be related with the three-dimensional plasma expansion during the firsts pulses, and with the gradual increasing of depth of

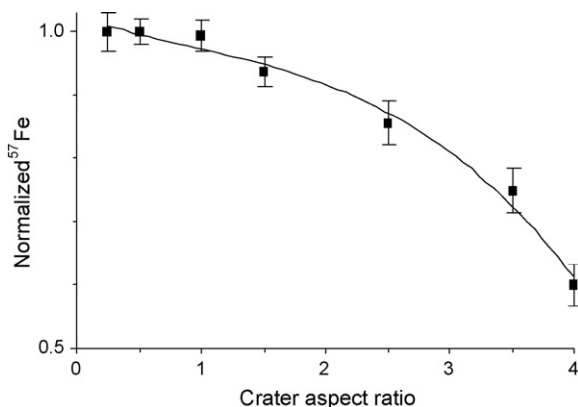Fig. 2. Influence of crater aspect ratio on normalized ^{57}Fe signal. Sample: CRM BAM 098-1. Laser sampling mode: single point; laser pulse energy: 1.5 mJ; pulse repetition rate: 5 Hz; irradiance: 15 GW cm^{-2}.
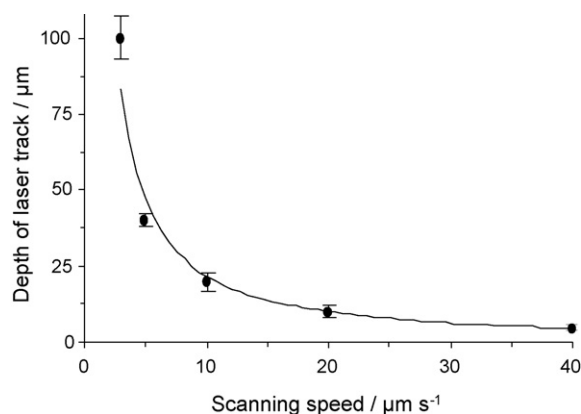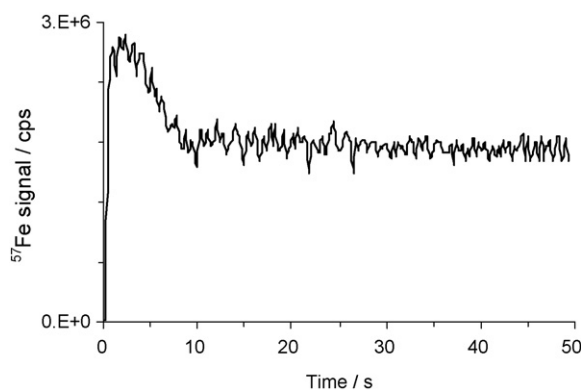

Fig. 4. Temporal behaviour of raw ^{57}Fe signal in CRM BAM 098-1 sample. Laser sampling mode: line scan; laser pulse energy: 1.5 mJ; pulse repetition rate: 5 Hz; scanning speed: 5 μm s^{-1}.
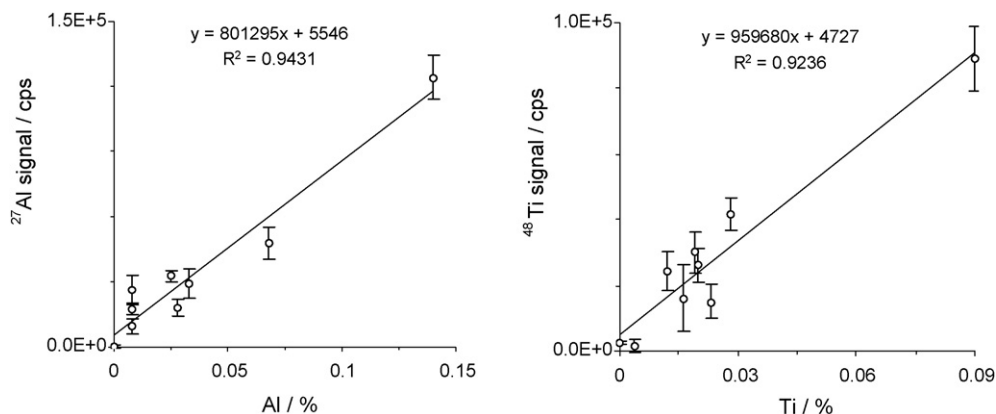
Fig. 5. Correlation between mean ion intensity values and certified content for Al (left) and Ti (right) in CRM steel samples. Laser sampling mode: line scan; laser pulse energy: 1.5 mJ; pulse repetition rate: 5 Hz; number of laser pulses: 400; scanning speed: 5 μm s^{-1}; scanning length: 400 μm; preablation time: 20 s.

the laser track until 40 pulses were fired. From *ca.* 8 to 50 s (*i.e.* 40–250 pulses), the signal reaches a plateau which is associated with the uniform depth of the laser track (*ca.* 40 μm); therefore, the sample must be preablated during at least 8 s, in order to obtain a completely stabilized signal. This behaviour agrees with the dependence of signal intensity on crater aspect ratio, presented in Fig. 2. As crater aspect ratio increased, the ion signal intensity decreased, reaching a stable value when the crater aspect ratio remained constant. This behaviour is in agreement with the effects of crater development on signal intensity presented by Borisov et al. [31].

3.2. Calibration graphs

Before establishing the calibration graphs, the Al and Ti signals behaviour of the CRM steel samples listed in Table 2, as well as the CRM BAM 098-1 (which was used as a blank), was evaluated. The samples were ablated for 80 s (*i.e.*, 400 laser pulses) by using the line scan laser sampling mode and the optimized laser operating parameters (laser pulse energy 1.5 mJ, scanning speed 5 μm s^{-1}, and preablation time 20 s). Fig. 5 shows the correlation between mean ion intensity values and Al and Ti certified content. As can be observed, a poor signal–concentration correlation (see the low regression coefficients in Fig. 5) and large

standard deviation values are attained. Taking into account the high similarity of the matrix in all CRMs (excepting in JK 37 sample), the rather poor linearity could be associated with an inhomogeneous distribution of the Al and Ti in the iron matrix.

In order to create the calibration graphs, the glass samples (fused beads) listed in Table 3 were ablated and analyzed by LA-ICP-MS under the same operating parameters as those used for steel samples. The correlation between mean ion intensity values and Al and Ti contents is illustrated in Fig. 6. As expected for a homogeneous material, a good linearity and low standard deviation values are obtained.

Comparing Figs. 5 and 6, it can be observed that the ion signals are approximately three times higher in the fused bead samples than in the steel samples, with significantly lower standard deviations and better linearity. Differences in the ablation yield resulting from differences in target matrix (differences in the mass of the ablated sample relative to the metal and glass samples, *i.e.* ablation efficiency) can be compensated by the use of internal standardization, which would fit ion signals from metal and glass samples. Hence, as Fe is the matrix element in the CRM steel samples (98–99% for all of them, except for JK 37 sample with a Fe content of about 40%) and it has a constant content in the prepared fused beads (Table 3), this element was chosen as internal standard. Considering the large
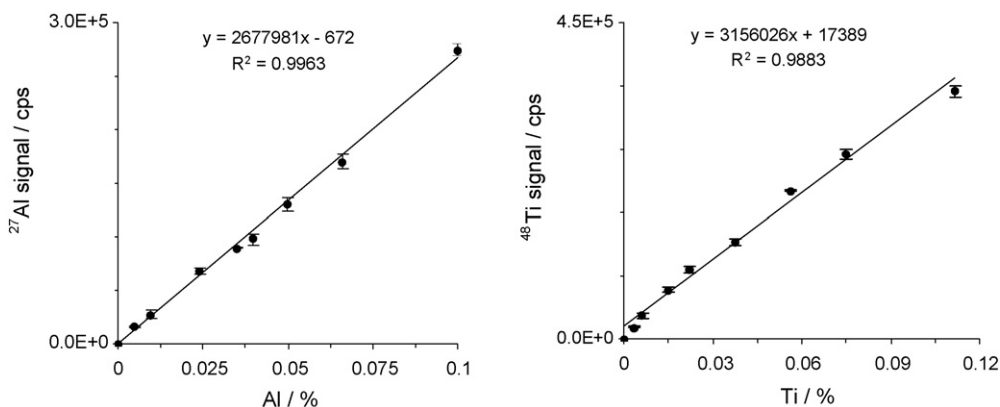
Fig. 6. Calibration graphs for Al (left) and Ti (right) in fused beads. Laser sampling mode: line scan; laser pulse energy: 1.5 mJ; pulse repetition rate: 5 Hz; number of laser pulses: 400; scanning speed: 5 μm s^{-1}; scanning length: 400 μm; preablation time: 20 s.
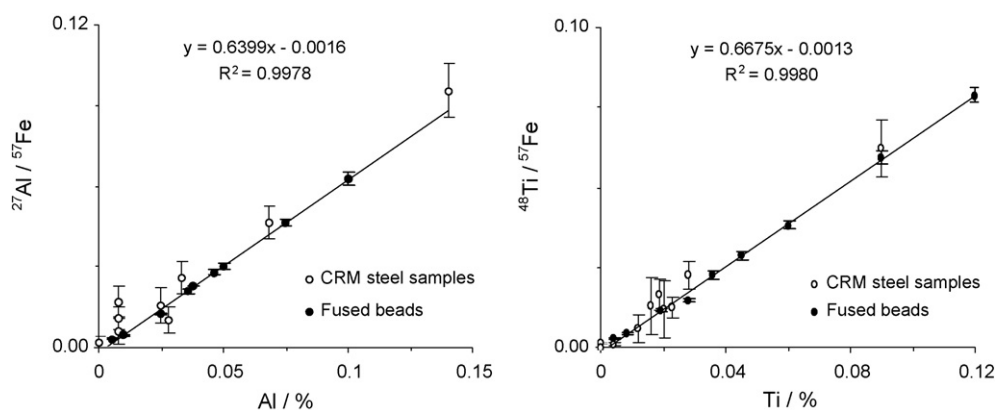
Fig. 7. Calibration graphs for Al (left) and Ti (right) in fused beads, using ^{57}Fe as internal standard. Ratio signals for CRM steel samples are included. Laser sampling mode: line scan; laser pulse energy: 1.5 mJ; pulse repetition rate: 5 Hz; number of laser pulses: 400; scanning speed: 5 μm s^{-1}; scanning length: 400 μm; preablation time: 20 s.

linear dynamic concentration range of the ICP-MS technique, the Fe signal value from the 2.2% of Fe content in the beads (about 8×10^4 cps) was extrapolated to the value that should correspond to a 100% of Fe ($8 \times 10^4 \times 100/2.2 = 36 \times 10^5$). This value ($36 \times 10^5$) is three times higher than the Fe signal for the CRM steel samples (ca. 12×10^5 cps). That is, the signal of both analytes (Al and Ti) and of the internal standard (Fe) is three times higher for the calibration standards (glasses) than for the steel samples (CRMs). The Fe signal of JK 37 high alloy steel sample was also correlated to 100%. Consequently, using Al/Fe and Ti/Fe ratio signals (providing that the Fe signals are those which would correspond to a 100% of this element), the values from beads and from steel samples, with similar Al or Ti

content, should be comparables. Then, the calibration graphs, for Al and Ti determination in steel samples, can be constructed by normalizing the ^{27}Al and ^{48}Ti signals of the glass samples to the signal that would correspond to a 100% of Fe. The obtained plots, from the beads samples listed in Table 3, are depicted in Fig. 7. The ^{27}Al/^{57}Fe and ^{48}Ti/^{57}Fe ratio values for the CRM steel samples are included, only in order to know their coincidence with the linear fit of the calibration graph, but they have not been considered to calculate the regression coefficients. As can be observed, the use of this approach makes possible to compare the ablation yield for both types of samples. However, the use of ratio signals does not improve the standard deviation of the Al and Ti values in the CRM metal samples (they remain simi-
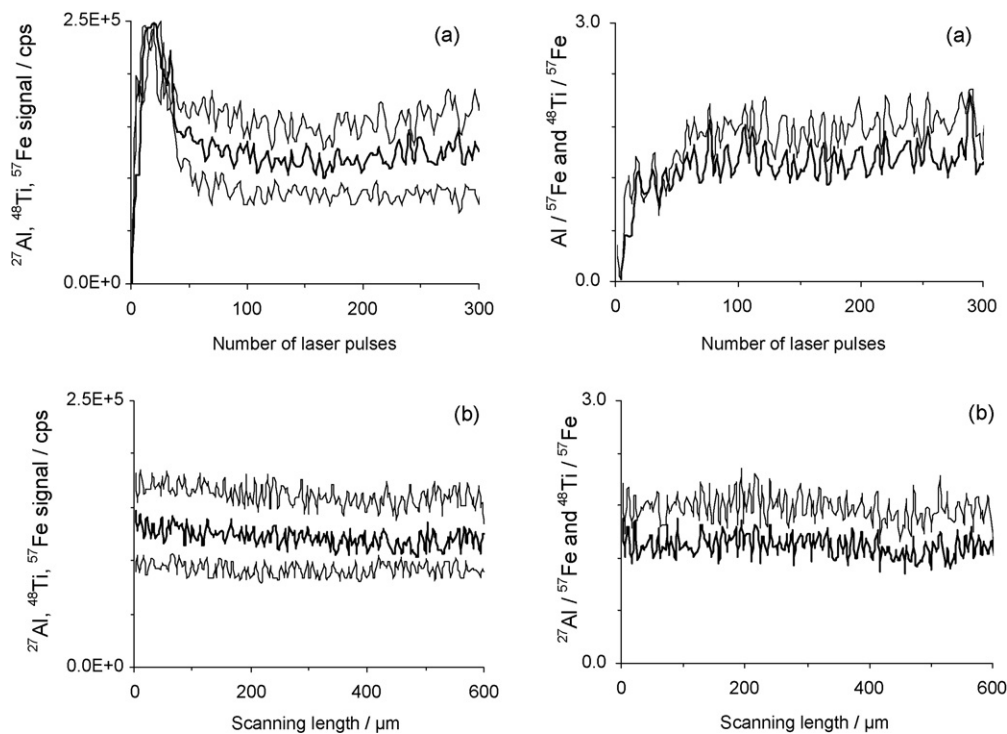
Fig. 8. Temporal behaviour of raw (left) and normalized (right) ^{27}Al (strong line), ^{48}Ti (soft line) and ^{57}Fe (dotted line) signals in a glass sample (fused bead no. 6 in Table 3). (a) Laser sampling mode: single point; number of laser pulses: 300. (b) Laser sampling mode: line scan; scanning speed: 5 μm s^{-1}; scanning length: 600 μm, after a preablation time of 20 s. Laser pulse energy: 1.5 mJ; pulse repetition rate: 5 Hz.
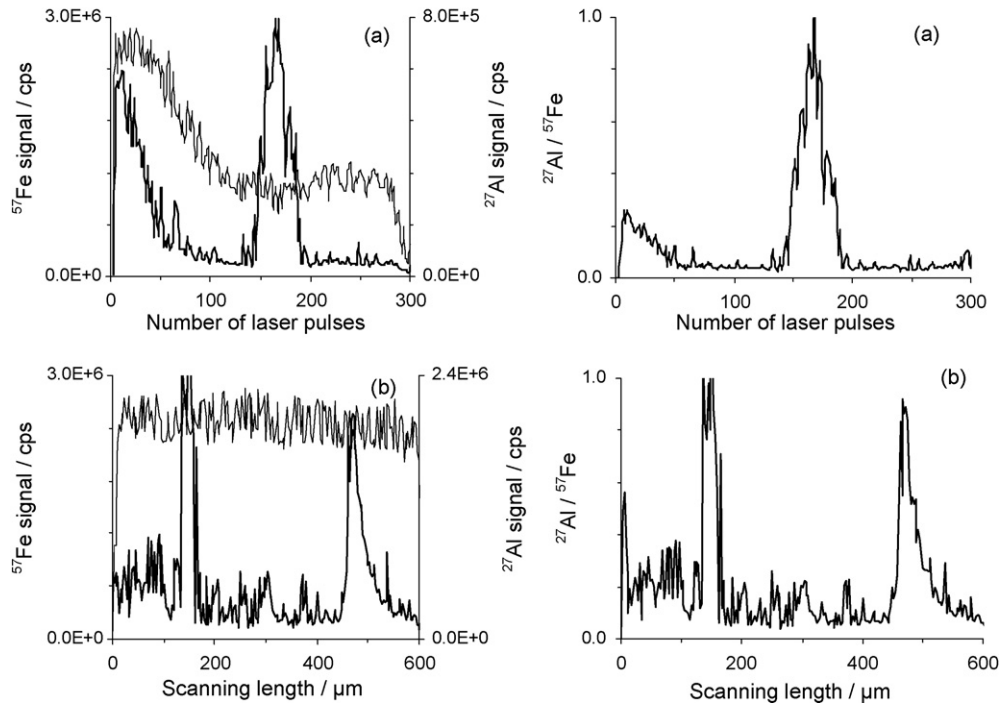
Fig. 9. Temporal behaviour of raw (left) and normalized (right) ^{27}Al (strong line) and ^{57}Fe (soft line) signals in CRM SS-458 carbon steel sample for a spot (a) and a line scan (b). (a) Laser sampling mode: single point; number of laser pulses: 300. (b) Laser sampling mode: line scan; scanning speed: $5 \, \mu m \, s^{-1}$; scanning length: 600 μm, after a preablation time of 20 s. Laser pulse energy: 1.5 mJ; pulse repetition rate: 5 Hz.
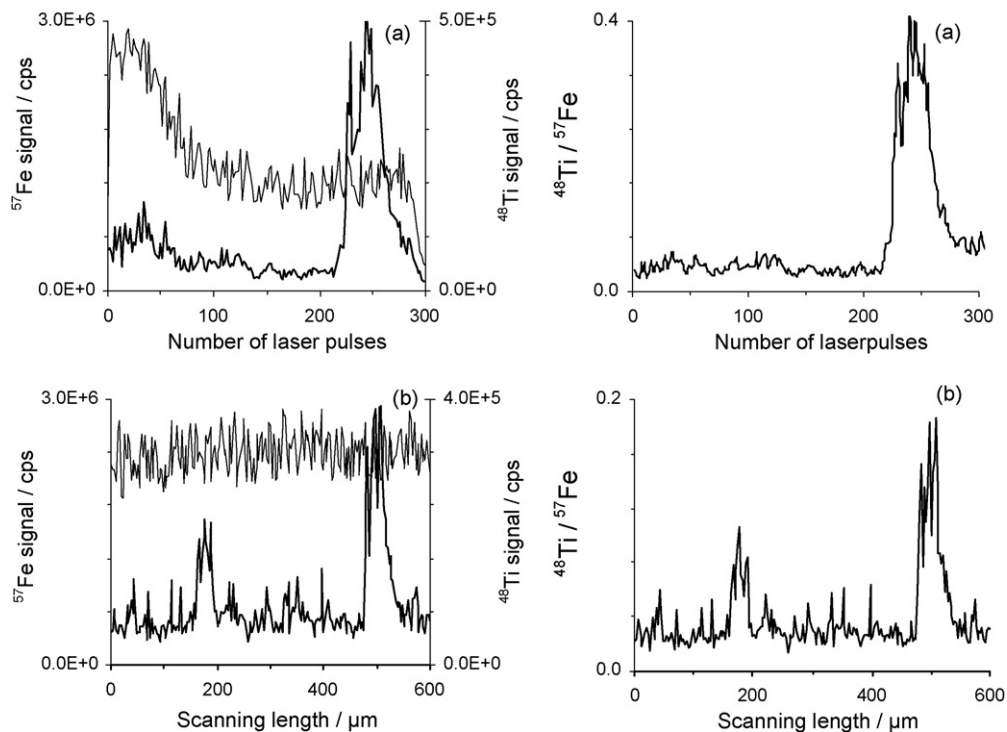
Fig. 10. Temporal behaviour of raw (left) and normalized (right) ^{48}Ti (strong line) and ^{57}Fe (soft line) signals in CRM SS-451 carbon steel sample for a spot (a) and a line scan (b). (a) Laser sampling mode: single point; number of laser pulses: 300. (b) Laser sampling mode: line scan; scanning speed: $5 \, \mu m \, s^{-1}$; scanning length: 600 μm, after a preablation time of 20 s. Laser pulse energy: 1.5 mJ; pulse repetition rate: 5 Hz.

lar and some times higher that when using raw signals, Fig. 5), which proves that the dispersion found in the results is mainly due to the heterogeneous distribution of the insoluble fractions of Al and Ti.

3.3. Spatial distribution of Al and Ti in steel samples

To study the spatial distribution of Al and Ti in the CRM steel samples, several zones were examined for both single point (300 laser pulses) and line scan (600 μm of length, after a preablation time of 20 s) laser sampling modes. Normalization of the raw signals was used to eliminate the variations associated with the crater development in single spot and the fluctuations related with the track growth in line scan. In the graphics, both raw and normalized signals were plotted. Firstly, for comparative purpose, the temporal behaviour of Al, Ti and Fe signals for a homogeneous glass sample (the fused bead no. 6 in Table 3) was studied. The results are shown in Fig. 8. In the plot corresponding to a single spot (Fig. 8a), a different behaviour was found between raw and normalized signals during the firsts pulses. In the temporal behaviour of the raw signals, after a peak associated with the surface three-dimensional plasma expansion, a steady-state appears. In the normalized signals, during the first pulses (associated to the peak) the Al/Fe and Ti/Fe ratios were different

than those of the steady state. This behaviour can be attributed to variations in mass entrainment/transport efficiency, probably due to differences in particle size distribution during ablation at a fresh sample surface and after the crater was developed. After stabilization of the signals, a steady state appears, from 40 to 300 pulses, this proving the homogeneous distribution of Al and Ti along the crater depth. The plot corresponding to the line scan (Fig. 8b) shows stable signals along the whole line, which demonstrates the homogeneous distribution of Al and Ti in the surface. The ^{27}Al and ^{57}Fe ion intensity charts for CRM SS-458 sample corresponding to a single spot and a line scan, in a heterogeneous zone, are shown in Fig. 9; similar charts for ^{48}Ti and ^{57}Fe in CRM SS-451 sample are illustrated in Fig. 10. In both figures, the trend of the ^{57}Fe signal is analogous in all cases to that of the glass sample, as expected for an element homogeneously distributed in the samples, whereas the behaviour of the ^{27}Al and ^{48}Ti signals is quite different. Nevertheless, when ablating zones with a homogeneous Al and Ti distribution, the time resolved signals of these elements do not present differentiated peaks, showing a similar trend to that observed in Fig. 8 for the glass samples".

Al signal in Fig. 9 and Ti signal in Fig. 10, show substantial variations with a very similar shape in both raw and normalized plots, which proves that these variations can be attributed to the
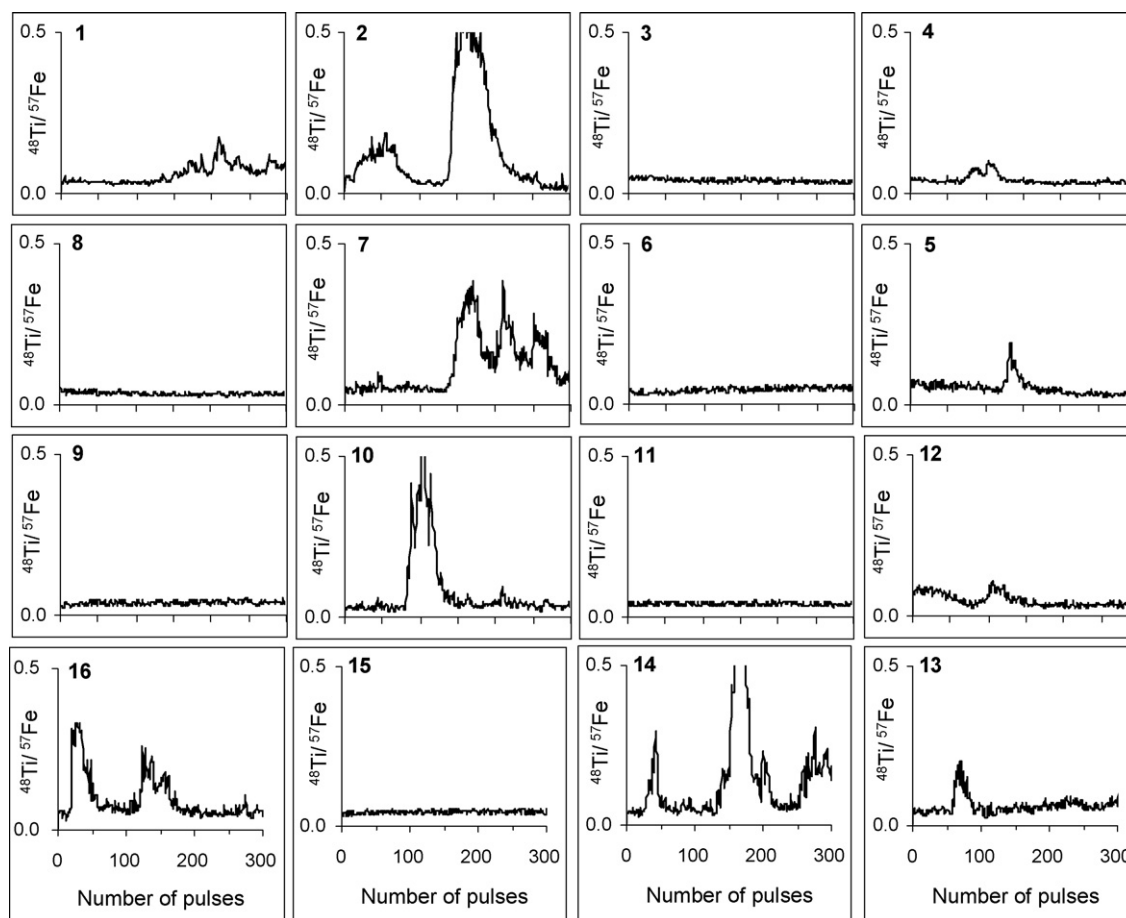
Fig. 11. Temporal behaviour of normalized ^{48}Ti signals for 16 different spots (distributed in four rows, with four spots in each row) in an inclusion zone (175 μm × 175 μm) of CRM SS-451 carbon steel sample. Laser sampling mode: rastering; number of laser pulses: 300 for each spot; distance between spots (both in horizontal and in vertical direction): 45 μm; laser pulse energy: 1.5 mJ; pulse repetition rate: 5 Hz.
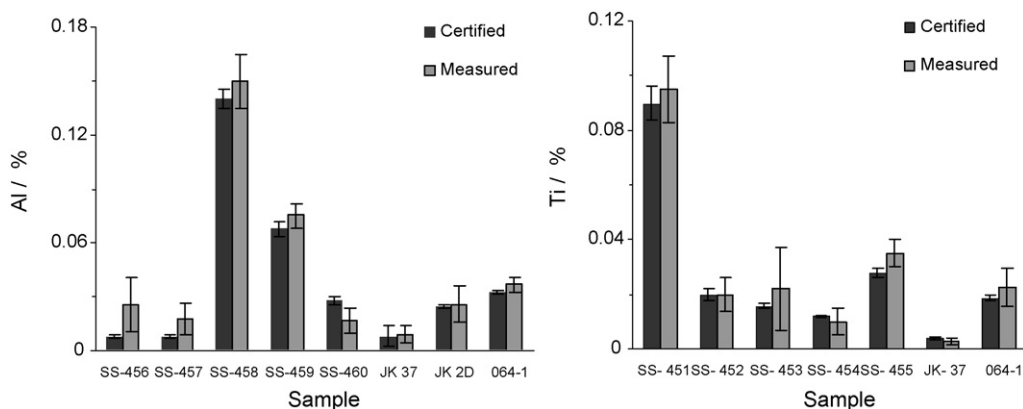
Fig. 12. Analytical results obtained for Al (left) and Ti (right) in CRM steel samples. Quantification was carried out by using the fused bead calibration graphs depicted in Fig. 7 and ^{57}Fe as internal standard. Laser experimental conditions as in Fig. 8.

heterogeneous distribution of the Al and Ti insoluble fractions. Fig. 9a shows a well-differentiated peak of ^{27}Al that appears after firing 150 laser pulses that demonstrates the presence of an inclusion of Al at a position of *ca.* 150 μm below the sample surface (taking into account an ablation rate of 1 μm pulse^{-1}). The line scan reveals the existence at the surface of a zone rich in Al between 0 and 100 μm and two inclusions at about 150 and 450 μm (Fig. 9b). The wide peak of ^{48}Ti shown in Fig. 10a can be attributed to a thick inclusion located at a depth of *ca.* 225 μm. The line scan illustrates the presence at the surface of two inclusions of Ti at about 150 and 475 μm (Fig. 10b).

In addition, a heterogeneous area of 175 μm × 175 μm was examined for Ti in the CRM SS-451 carbon steel sample using rastering mode for laser sampling. In the selected area, 16 single

spots were performed, with 300 laser pulses fired on each spot. The 16 spots were distributed in four rows, with four spots in each row. The distance between spots, both in horizontal and in vertical direction, was 45 μm. Fig. 11 presents the ^{48}Ti transient signals (normalized to ^{57}Fe) corresponding to each spot. As can be seen, there are no peaks (*i.e.*, insoluble inclusions) in spots 3, 6, 8, 9, 11 and 15, whereas the peaks that appear in the other spots reveal the existence of Ti heterogeneities at the surface and inside the sample.

3.4. Bulk analysis

Calibration graphs obtained from fused beads (Fig. 7) were used to determine the concentration of total Al and Ti in the
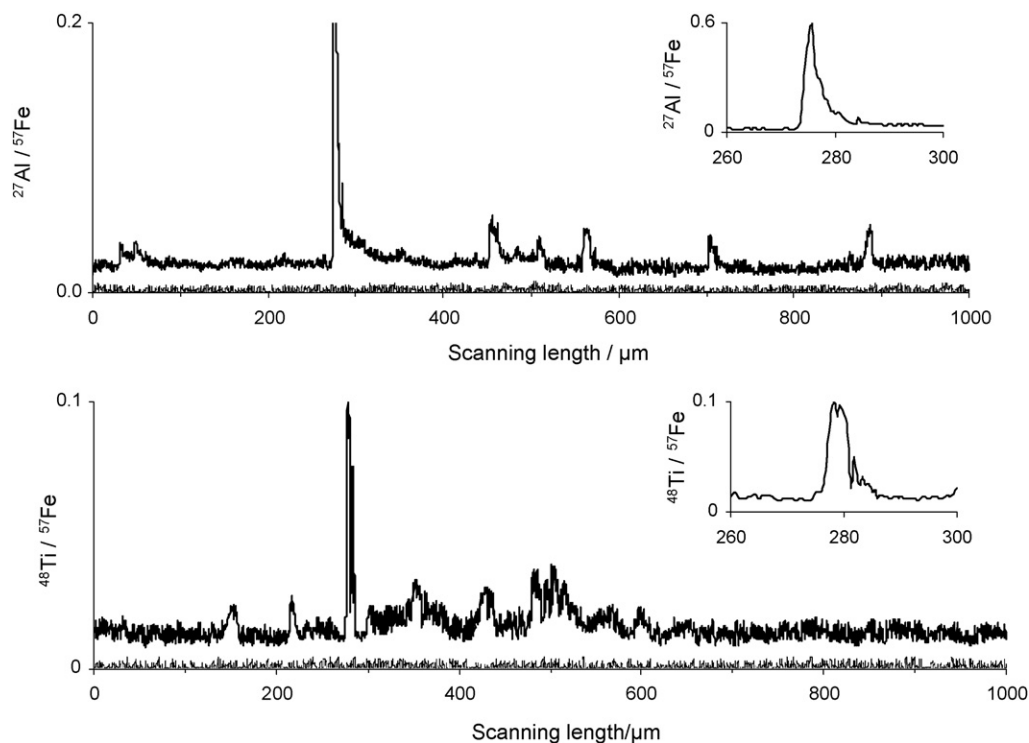
Fig. 13. Temporal behaviour of normalized ^{27}Al and ^{48}Ti signals in CRM 064-1 Nb/Ti interstitial free steel (strong line) and CRM BAM 098-1 pure electrolytic iron (soft line) samples. Insets: detail of the 260–300 μm interval of scanning length. Laser sampling mode: line scan; laser pulse energy: 1.5 mJ; pulse repetition rate: 5 Hz; scanning speed: 5 μm s^{-1}; scanning length: 1000 μm, after a preablation time of 20 s.

CRM steel samples listed in Table 2. The analytical results are included in Fig. 12. As can be seen, the measured concentrations correspond with the certified values within the experimental uncertainty. Only for Al in SS-456 and SS-457 samples the results were not entirely satisfactory, which could be attributed to the low Al concentration (0.008%), together with its heterogeneous distribution. However, the results obtained for Al (and also for Ti) in JK 37 sample are in good agreement in spite of their low content (0.0084% for Al and 0.0039% for Ti). A possible explanation to account for this is that the Al and Ti distribution in JK 37 sample (in fact, a high alloy steel with a Fe content of about 40%) is very probably more homogeneous than in SS samples (carbon steels with a Fe content of 98–99%).

From these results it is clear that, in spite of the heterogeneous distribution of Al and Ti in the CRM steel samples, laser sampling by line scan and calibration with synthetic fused beads can provide, after an optimization of laser operating parameters, an acceptable approach for bulk quantitative analysis by LA-ICP-MS.

3.5. Determination of soluble and total Al and Ti

The determination of soluble and total Al and Ti was performed on the CRM 064-1 (Nb/Ti interstitial free steel) sample with certified values (Table 2) for total and soluble Al and for total Ti. CRM BAM 098-1 (pure electrolytic iron) sample was used as a blank. ^{57}Fe was used as internal standard. The line scan laser sampling mode and the optimized laser operating parameters (laser pulse energy of 1.5 mJ, scanning speed of 5 μm s^{-1} and preablation time of 20 s) were employed. The calibration graphs obtained from fused beads (Fig. 8) were used. The analytical determinations were performed at the sample surface and in-depth.

For the analysis at the sample surface, four line scans of 1000 μm length were carried out at four different positions chosen at random. The normalized ^{27}Al and ^{48}Ti ion intensity charts attained for one of the line scans are illustrated, as an example, in Fig. 13. The ablated zone shows a clear heterogeneity, fundamentally between 250 and 600 μm. For the in-depth analysis, four tests, each one consisting of five successive scans on the same line (300 μm length), at four different positions chosen at random, were carried out. In order to reach a depth of laser track of about 10–12 μm for each scan, the pulse repetition rate was increased progressively: 1 Hz for the first scan, 2 Hz for the two followings, and 4 Hz for the two last. The normalized ^{27}Al and ^{48}Ti ion intensity charts attained for the five scans of one of the tests are plotted, as an example, in Fig. 14, where the cross-section SEM images of the laser track after each scan are also shown. The width of the laser track was ca. 40 μm, as expected, whereas the depth after each one of the five consecutive scans was about 12, 26, 37, 47 and 62 μm (i.e., the depth/width ratio was in all cases lower than 1.5). A noticeable heterogeneous distribution of Al and Ti can be observed at depth.

The quantification was carried out from the normalized ^{27}Al and ^{48}Ti ion intensity values attained for the four line scans (analysis at the sample surface) and for the five successive scans of
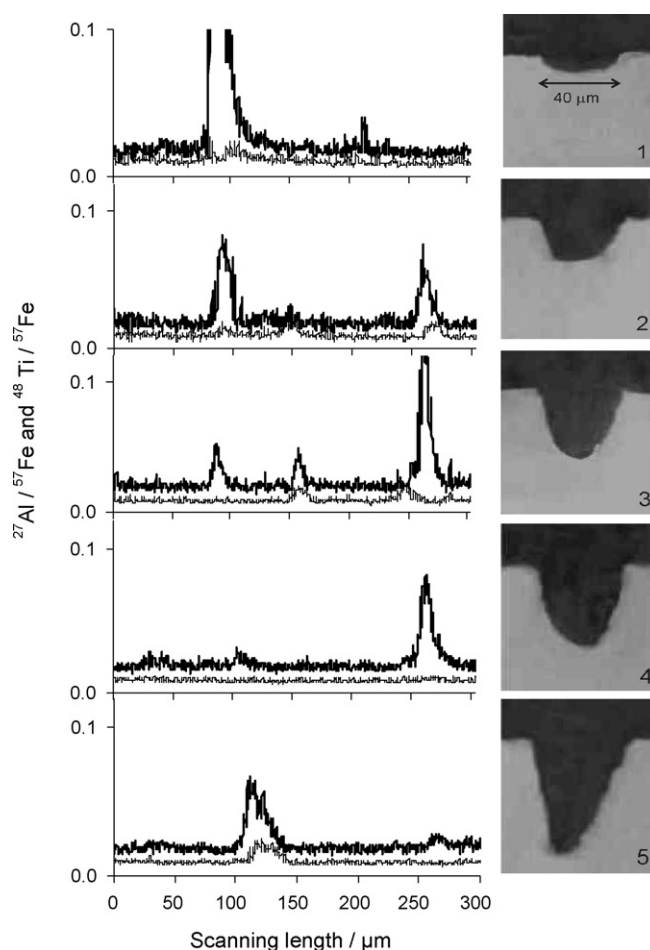
Fig. 14. Temporal behaviour of normalized ^{27}Al (strong line) and ^{48}Ti (soft line) signals in CRM 064-1 Nb/Ti interstitial free steel sample for five successive scans on the same line, and cross-section SEM images of the laser track after each scan. Laser sampling mode: line scan; laser pulse energy: 1.5 mJ; pulse repetition rate: 1 Hz for the scan 1, 2 Hz for the scans 2 and 3, and 4 Hz for the scans 4 and 5; scanning speed: 5 μm s^{-1}; scanning length: 300 μm, after a preablation time of 20 s.

the four tests (in-depth analysis). It was considered that, for each scan, the average of all the net ion intensity values corresponded to the total element content. Similarly, the soluble element content was associated to the average of the net ion intensity values in the zones where no significant peaks appeared (e.g. in the case of Fig. 13, these zones would be the following scanning length intervals: 70–270, 590–690, 730–870, and 900–1000 μm, for Al; 0–130 and 620–1000 μm, for Ti).

Fig. 15 shows the analytical results obtained for total and soluble Al and Ti at the sample surface (average of the results for the four line scans) and in depth (average of the results for the five successive scans of the four tests).

As can be seen, the values obtained by analysis at the sample surface for soluble and total Al concentration in CRM 064-1 differ significantly from each other and both values agree with the certified values. However, analytical results obtained for the in-depth analysis were not completely satisfactory because, although an acceptable concordance between certified and found values is obtained, a distinction cannot be made between soluble and total amount of Al. This can be due to the thermal effects
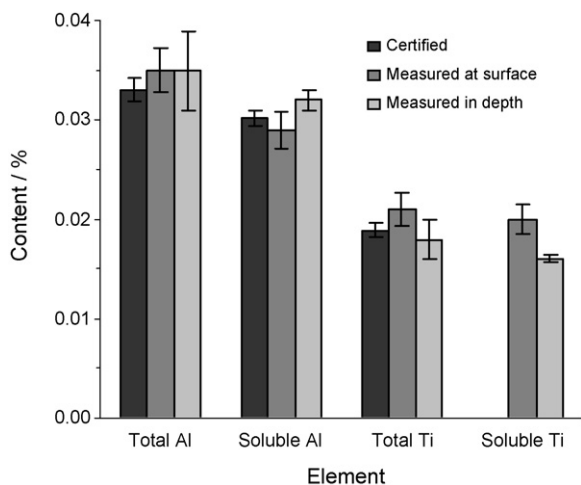
Fig. 15. Analytical results obtained for total and soluble Al and Ti at sample surface and in-depth in CRM 064-1 (Nb/Ti interstitial free steel) sample. Quantification was carried out by using the fused bead calibration graphs depicted in Fig. 7 and ^{57}Fe as internal standard. Laser experimental conditions for the analysis at sample surface as in Fig. 13, and for the in-depth analysis as in Fig. 14.

associated with the nanosecond UV laser ablation of metals, as well as to the Gaussian laser beam profile.

With respect to the Ti, analytical results obtained for total content at sample surface and in-depth agree reasonably well with the certified value. However, there is not significant difference between the total and soluble contents determined by LA-ICP-MS. Probably, the insoluble fraction of Ti is so low (as it can be deduced from the low intensity of the Ti peaks in Figs. 14 and 15) that really cannot quantitatively be distinguished. Unfortunately, only total Ti value is certified in the CRM 064-1 sample and therefore the results cannot be demonstrated. In fact, due to the great difficulty that presents the analytical differentiation between total and soluble Ti in steels by any analytical technique CRM samples with certified values for total and soluble Ti do not exist. Consequently, between the two performed tests (analysis at the sample surface and in-depth), we propose the first one (i.e., analysis at the sample surface) as a suitable alternative to the time-consuming and tedious classical method, taking into account that, in this case, the values obtained for both soluble and total Al concentration in CRM 064-1 differ significantly and agree with the certified values. In addition, this test is easier and faster than the analysis in-depth. In the case of Ti, we think that the proposed method is also acceptable for sufficiently high insoluble Ti contents, although it has not been demonstrated due to the unavailability of CRM samples with certified values for total and soluble Ti.

4. Conclusions

The spatial distribution (both at surface and within the sample) of Al and Ti in steel samples can be qualitatively estimated by LA-ICP-MS using single point, line scan and rastering laser sampling modes. It has been proved that the insoluble fraction of Al and Ti is heterogeneously distributed in the studied CRM steel samples. This heterogeneous distribution of the insoluble fraction may explain the high standard deviation values, as well

as the poor regression coefficients obtained from the correlation of their ion intensities and certified contents. Obviously, with these samples it is not possible to establish calibration graphs for quantification. However, the use of synthetic fused beads for calibration and ^{57}Fe for internal standardization (to compensate the differences in ablation efficiency between steels and glasses) permits the bulk analysis of Al and Ti with acceptable results. Also, it allows the rapid determination of soluble and total Al concentration, by analysis at the sample surface, yielding results that agree reasonably well with the certified values. With regard to the determination of soluble and total Ti concentration, we believe that the proposed method is valid, too, although it could not be demonstrated due to the lack of suitable CRMs. The proposed methodology constitutes a good alternative to the difficult, laborious and time-consuming classical method, and, in addition, avoids the possible errors associated with the partial acid dissolution of the insoluble aluminium and titanium inclusions.

Acknowledgements

References

[1] ASM, in: J.R. Davis, Davis & Associates (Eds.), Specialty Handbook Carbon and Alloy Steels, ASM International, Materials Park, OH 44073-0002, USA, 1996, pp. 1–14.
[2] L. Zhang, B.G. Thomas, ISIJ Int. 43 (2003) 271.
[3] D. Günther, L. Horn, B. Hattendorf, Fresenius J. Anal. Chem. 368 (2000) 4.
[4] D. Günther, B. Hattendorf, Trends Anal. Chem. 24 (2005) 255.
[5] R.E. Russo, X. Mao, H. Liu, J. Gonzalez, S.S. Mao, Talanta 57 (2002) 425.
[6] J.S. Becker, Spectrochim. Acta, Part B 57 (2002) 1805.
[7] H. Yasuhara, T. Okano, Y. Matsumura, Analyst 117 (1992) 395.
[8] Y. Ishibashi, ISIJ Int. 37 (1997) 885.
[9] Y. Ishibashi, ISIJ Int. 42 (2002) S137.
[10] A.G. Coedo, I. Padilla, M.T. Dorado, Appl. Spectrosc. 58 (2004) 1481.
[11] D. Bleiner, A. Plotnikov, C. Vogt, K. Wetzig, D. Günther, Fresenius J. Anal. Chem. 368 (2000) 221.
[12] A. Plotnikov, C. Vogt, V. Hoffmann, C. Täschner, K. Wetzig, J. Anal. Atomic Spectrom. 12 (2001) 1290.
[13] V. Kanicky, H.R. Kuhn, D. Guenther, Anal. Bioanal. Chem. 380 (2004) 218.
[14] A.G. Coedo, T. Dorado, I. Padilla, J.C. Fariñas, J. Anal. Atomic Spectrom. 20 (2005) 612.
[15] A. Plotnikov, C. Vogt, K. Wetzig, J. Anal. Atomic Spectrom. 17 (2002) 1114.
[16] D. Bleiner, P. Lienemann, A. Ulrich, H. Vonmont, A. Wichser, J. Anal. Atomic Spectrom. 18 (2003) 1146.
[17] W. Devos, M. Senn-Luder, C. Moor, C. Salter, Fresenius J. Anal. Chem. 366 (2000) 873.
[18] D. Kang, D. Amarasiriwardena, A.H. Goodman, Anal. Bioanal. Chem. 378 (2004) 1608.
[19] A. Kindness, C.N. Sekaran, J. Feldmann, Clin. Chem. 49 (2003) 1916.
[20] J.S. Becker, M.V. Zoriy, C. Pickhardt, N. Palomero-Gallagher, K. Zilles, Anal. Chem. 77 (2005) 3208.
[21] J.S. Becker, M.V. Zoriy, M. Dehnhardt, C. Pickhardt, K. Zilles, J. Anal. Atomic Spectrom. 20 (2005) 912.
[22] A.V. Karasev, R. Inque, H. Suito, ISIJ Int. 41 (2001) 757.
[23] A.V. Izmer, M.V. Zoriy, C. Pickhardt, W. Quadakkers, V. Shemet, L. Singheiser, J.S. Becker, J. Anal. Atomic Spectrom. 20 (2005) 918.

[24] D. Günther, A. Quadt, R. Wirz, H. Cousin, V.J. Dietrich, Mikrochim. Acta 136 (2001) 101.

[25] A.G. Coedo, I. Padilla, M.T. Dorado, Talanta 67 (2005) 136.

[26] D.B. Aeschliman, S.J. Bajic, D.P. Baldwin, R.S. Houk, J. Anal. Atomic Spectrom. 18 (2003) 872.

[27] E. Hoffmann, C. Lüdke, J. Skole, H. Stephanowitz, J. Wollbrandt, W. Becker, Spectrochim. Acta, Part B 57 (2002) 1535.

[28] M. Sanborn, K. Telmer, J. Anal. Atomic Spectrom. 18 (2003) 1231.

[29] V.N. Tokarev, J. Lopez, S. Lazare, F. Weisbuch, Appl. Phys. A 76 (2003) 385.

[30] D. Bleiner, Z. Chen, D. Auitrique, A. Bogaerts, J. Anal. Atomic Spectrom. 21 (2006) 910.

[31] O.V. Borisov, X. Mao, R.E. Russo, Spectrochim. Acta, Part B 55 (2000) 1693.

Optimisation of ICPMS collision/reaction cell conditions for the simultaneous removal of argon based interferences of arsenic and selenium in water samples

Jérôme Darrouzès, Maïté Bueno *, Gaëtane Lespès, Michel Holeman, Martine Potin-Gautier

Laboratoire de Chimie Analytique Bio-Inorganique et Environnement, Université de Pau et des Pays de l'Adour, UMR 5034, Helioparc Pau Pyrénées, 2 avenue du Président Angot, 64000 Pau, France

Abstract

The optimisation of ICPMS collision/reaction cell conditions for the simultaneous analysis of arsenic and selenium is described. A mixture of $3.8\,mL\,min^{-1}$ of H_2 and $0.5\,mL\,min^{-1}$ of He was found to be suitable for the removal of both $ArAr^+$ and $ArCl^+$ interferences. Detection limits down to $30\,ng$ (element) L^{-1} in total analysis, and between 81 and $230\,ng$ (element) L^{-1} in speciation analysis were achieved in chloride matrix ($1\,g\,L^{-1}$ NaCl). After validation, the method was applied to commercially available mineral waters.
© 2006 Elsevier B.V. All rights reserved.

Keywords: ICPMS; Selenium; Arsenic; Speciation; Collision cell; Reaction cell; Water; Octopole

1. Introduction

The introduction of ICPMS equipped with collision/reaction cell (C/RC) is a promising approach to overcome problems linked with polyatomic interferences [1]. Nevertheless, cell conditions are often optimised considering one element, leading to the loss of ICPMS multielemental capability which is characterized by the use of "multi-mode" analysis (where different settings are successively applied to the C/RC during the measurement of one sample) available for total measurements [2]. For instance, while the addition of a collision gas such as helium [3–5] suppresses the major interferent of arsenic, *i.e.* $ArCl^+$, hydrogen [3,6–8] or methane [9], which are reactive gases, are used for removal of selenium interferences, *i.e.* $ArAr^+$. Few studies deal with the simultaneous elemental analysis of As and Se [10,11]. Chan and Lo have used ammonia to remove As and Se interferences, but two different settings of C/RC bandpass were necessary to eliminate the new interferences created in the C/RC system, which is not suitable for speciation analysis [10]. Niemela et al. have used $7.5\,mL\,min^{-1}$ He premixed with 7%

H_2 in a hexapole C/RC system to remove $ArCl^+$ and $ArAr^+$ interferences [11]. Detection limits were calculated with identical gaseous (C/RC) conditions for both elements but using two separate matrices: $29\,ng\,L^{-1}$ was obtained for ^{80}Se in 2% HNO_3 and $153\,ng\,L^{-1}$ for ^{75}As in 5% HCl. Nevertheless, as far as we know, no paper has presented C/RC conditions suitable for the simultaneous speciation of As and Se.

In this paper, we propose the optimisation of an octopole collision/reaction cell for the simultaneous removal of As and Se interferences. Such working conditions are evaluated for total and speciation (inorganic forms) analysis. Different applications to mineral and certified rain waters are also presented.

2. Experimental

2.1. Reagents

Ultrapure water was obtained from a Milli-Q System (Millipore Co., Bedford, MA, USA). Sodium selenite and selenate (Merck, Darmsdadt, Germany), sodium arsenite (Aldrich, Steinheim, Germany) and arsenate (Prolabo, Fontenay-sous-Bois, France) were used without further purification. Stock standard solutions containing $1000\,mg$ (element) L^{-1} of each compound in ultrapure water were stored in the dark at $4\,°C$. Working stan-

---

* Corresponding author. Tel.: +33 559 407 753; fax: +33 559 407 781.
E-mail address: maite.bueno@univ-pau.fr (M. Bueno).

dard solutions were prepared daily by successive dilutions in ultrapure water and in $1\,\mathrm{g\,L^{-1}}$ NaCl (Suprapur, Merck, Darmsdadt, Germany) for C/RC gas flow rates optimisation.

Ammonium hydrogen phosphate $((NH_4)_2HPO_4)$ (Merck, Darmsdadt, Germany) and methanol (HPLC grade, J.T. Baker, Deventer, Holland) were used for mobile phase preparation. The pH was adjusted by drop wise addition of 30% ammonia solution (Merck, Darmsdadt, Germany). Mobile phase ($12.5\,\mathrm{mmol\,L^{-1}}$ phosphate buffer, pH = 8.5) was continuously degassed while delivered (flow rate $1.5\,\mathrm{mL\,min^{-1}}$).

Glassware was decontaminated by soaking overnight in 10% (v/v) nitric acid solution and rinsed with ultrapure water before use.

A certified reference material, the TM-Rain 95 (National Water Research Institute, Canada), was chosen to validate optimised working conditions, due to its low levels of selenium and arsenic ($1070 \pm 250\,\mathrm{ng}$ (As) $\mathrm{L^{-1}}$, $740 \pm 290\,\mathrm{ng}$ (Se) $\mathrm{L^{-1}}$).

2.2. Instrumentation for ICPMS and HPLC system

The ICPMS instrument used was the 7500c from Agilent technologies (Tokyo, Japan), equipped with an octopole reaction cell. Recommended gases for this instrument are helium and hydrogen (Air Liquide, Paris, France) both having a purity of 99.995%. The sample introduction system consisted of a concentric nebuliser (Meinhard Associates, California, USA) and a Scott double pass spray chamber cooled to $2\,^\circ\mathrm{C}$. The operating conditions were optimised daily using a solution of $10\,\mu\mathrm{g\,L^{-1}}$ of gallium, yttrium, thallium and cerium, with typical settings being: plasma power 1500 W, cooling gas flow $15\,\mathrm{L\,min^{-1}}$, auxiliary gas $0.9\,\mathrm{L\,min^{-1}}$, carrier gas 1–$1.1\,\mathrm{L\,min^{-1}}$, extract lens $-160\,\mathrm{V}$. For total measurements, isotopes from $m/z = 72$ to 83 were monitored (integration time 0.1 s per isotope, 3 points per peak). Sampler and skimmer cones are made of nickel.

The chromatographic system consisted of an Agilent 1100 series HPLC pump, equipped with autosampler and variable volume sample loop, and a Hamilton PRPX-100 column ($10\,\mu\mathrm{m}$ particle size, 25 cm length $\times$ 4.1 mm i.d.). The HPLC–ICPMS interface was made up of a polyetheretherketone (PEEK) tube. In this configuration, plasma power was increased up to 1600 W and isotopes from m/z 75 to 82 were monitored using an integration time of 0.4 s per isotope. Since, As and Se are mainly present as their inorganic forms in waters [12,13], selected chromatography, adapted from Guérin et al. [14], allowed the separation of arsenite AsIII, arsenate AsV, selenite SeIV and selenate SeVI.

2.3. Optimisation strategy for C/RC parameters

Optimisation of gas flow rates added in the C/RC was realized using experimental design methodology according to Goupy [15] and Sado and Sado [16]. This methodology is the only approach allowing a set of discrete experimental results to be converted into continuous information in order to have maximum knowledge in any point of a given experimental field with an optimal precision. It has been successfully applied in previous work devoted to C/RC conditions optimisation for selenium determination [17]. The same approach was used in this work for

the simultaneous determination of As and Se in difficult chloride matrix ($1\,\mathrm{g\,L^{-1}}$ NaCl).

The optimisation was performed in total analysis, in the range 1–$5\,\mathrm{mL\,min^{-1}}$ for H_2 and 0–$2\,\mathrm{mL\,min^{-1}}$ for He, chosen after preliminary experiments. For each combination of levels, a blank solution, *i.e.* $1\,\mathrm{g\,L^{-1}}$ NaCl in ultrapure water, and solutions containing 0.5–$5\,\mu\mathrm{g}$ (element) $\mathrm{L^{-1}}$ in the same matrix were measured. All experiments were performed within one working day in duplicate. Level "0", *i.e.* $3\,\mathrm{mL\,min^{-1}}$ of H_2 and $1.3\,\mathrm{mL\,min^{-1}}$ of He was performed three times: at the beginning, in the middle, and at the end of the experiments. The effects, precision of each factor and interaction between them were determined using an ordinary least squared regression model. For all the experiments, regression and bias factors as well as regression coefficients were checked and shown to be significant.

Ion lens settings were also optimised in a chloride matrix spiked with $10\,\mu\mathrm{g\,L^{-1}}$ of As, Se, Ga and Y. Lens adjustment was conducted, as recommended by the constructor, in the following order: quadrupole bias (QB) and octopole bias (OB) difference (QB $-$ OB), OB (keeping constant the difference between QB and OB), cell entrance (CEn), cell exit (CEx), and plate bias (PB).

2.4. Analytical figures of merit

Analytical performances of the method were described in terms of sensitivity (calibration curves established with standard solutions in $1\,\mathrm{g\,L^{-1}}$ NaCl up to $50\,\mu\mathrm{g}$ (element) $\mathrm{L^{-1}}$), detection limits (LOD, calculated according to IUPAC recommendations [18]) and repeatability (for 10 measurements of $1\,\mu\mathrm{g}$ (element) $\mathrm{L^{-1}}$ solution for total analysis, and for 6 measurements of a solution containing $2\,\mu\mathrm{g}$ (element) $\mathrm{L^{-1}}$ per species for speciation analysis). For total measurements, selenium was used as selenate (SeVI) and arsenic as arsenate As(V).

3. Results and discussion

3.1. Optimisation of C/RC conditions

For each isotope, two responses were chosen to evaluate the C/RC efficiency: the net sensitivity (^{X}S) which is the slope of the calibration curve, and the sensitivity to background ratio (^{X}SBR). For the isotopes ^{75}As and ^{80}Se, the modelling of their respective responses is given in the equations (I) to (IV):

$$^{75}S = 1.0880 - 1.5483(H_2) - 0.5652(He)$$
$$+ 0.4021(H_2 \times He) + 0.5323(H_2)^2 \qquad (I)$$

$$^{80}S = 1.1724 - 0.6825(H_2) - 0.4338(He) \qquad (II)$$

$$^{75}SBR = 0.07395 - 0.03287(H_2)^2 \qquad (III)$$

$$^{80}SBR = 0.01852 + 0.00770(H_2) - 0.00575(H_2)^2 \qquad (IV)$$

For both isotopes, sensitivity decreases with addition of gases (according to equations (I) and (II)). Hence, minimal flow rates were selected. The equations (III) and (IV) show that helium has
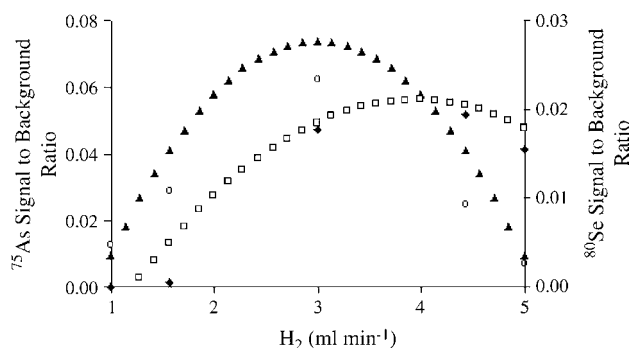
Fig. 1. Modelling of sensitivity to background ratio (SBR) for ^{75}As (▲) and ^{80}Se (□) as a function of H_2 flow rate with 0.5 mL min^{-1} of He – solution of 10 µg (element) L^{-1} of As and Se, in 1 g L^{-1} NaCl. The average of experimental sensitivity to background ratio are represented for ^{75}As (○) and ^{80}Se (♦).

Fig. 2. Comparison of ^{75}As, ^{78}Se, and ^{80}Se signals in three different matrices as a function of plasma power and sample introduction flow rate (10 µg (element) L^{-1} in ultrapure water, ultrapure water + 3% MeOH and phosphate buffer, i.e. 12.5 mmol L^{-1} (NH$_4$)$_2$HPO$_4$ with 3% MeOH).

no influence on signal to background ratio, therefore He flow rate was settled at the minimum, i.e. 0.5 mL min^{-1}. The evolution of ^{75}SBR and ^{80}SBR versus hydrogen flow rate is presented in Fig. 1. For both isotopes, the curves show domains of H_2 flow rates which lead to maximum SBR. For lower flow rates, SBR increases with hydrogen flow due to the removal of interferences. For higher H_2 flows, SBR decreases which is mainly due to the strong decrease of sensitivity as indicated by equations (I) and (II). The domains of H_2 flow rates giving maximum ^{75}SBR and ^{80}SBR do not totally overlap, probably due to the differences both in abundance and bond energy between ArCl$^+$ and ArAr$^+$ dimers. As (i) the value of maximum ^{75}SBR is higher than the one of ^{80}SBR (×3.5) and, (ii) concentrations of arsenic species are generally 10 times higher than those of selenium species in natural waters [12,13], a flow of 3.8 mL min^{-1} of H_2 was selected. Such flow adjustment leads to a ^{75}SBR representing 86% of the maximum.

Appropriate voltages of the five ion lenses around the C/RC allow a better focalisation of the ion beam and kinetic energy discrimination [19]. Their optimisation resulted in the following values: CEn = −20 V, CEx = −20 V, PB = −45 V, OB = −14 V, QB = −13 V.

In order to check if C/RC conditions previously optimised can be applied with HPLC coupling and if no new interferences are created, the influence of mobile phase composition was evaluated using HPLC conditions, i.e. plasma power 1600 W and sample uptake 1 mL min^{-1}. Signals of ^{75}As, ^{78}Se, and ^{80}Se were measured in three different solutions spiked with 10 µg (element) L^{-1}: ultrapure water, ultrapure water + 3% MeOH and phosphate buffer containing 3% MeOH. Net signals are reported in Fig. 2. Whatever the medium and for all measured isotopes, the blank signal remains negligible relative to the signal from a 10 µg (element) L^{-1} solution which suggests no new interferences are created. As expected [20], the addition of a small amount of methanol increases As and Se signals by about a factor 3, and weak matrix effects are observed in phosphate buffer, i.e. 5% lower signal in comparison with ultrapure water containing methanol. A similar pattern was observed with total conditions (i.e. plasma power: 1500 W and sample uptake 0.4 mL min^{-1}) (data not shown). Hence, no new interferences are created and C/RC conditions are suitable for speciation analysis.

3.2. Analytical figures of merit

Analytical performances for ^{75}As, ^{78}Se and ^{80}Se are summarized in Table 1. Linear calibration are precisely adjusted (R^2 > 0.999) in the concentration range tested (up to 50 µg (element) L^{-1}) for total and speciation determinations. For total analysis, detection limits are around 30 ng (element) L^{-1} for both elements which represents a two-fold and five-fold improvement respectively for arsenic and selenium in comparison with standard mode on the same instrument. Detection limits obtained with identical C/RC conditions for As and Se as reported by Niemela et al. are similar to those reported in this work for Se, despite the use of a 2% HNO$_3$ matrix instead of a chloride matrix used in this work [11]. For As, detection limits were calculated in a different matrix than for Se, i.e. 5% HCl, and are five times higher than those calculated here in 1 g L^{-1} NaCl [11].

With HPLC coupling, detection limits are around 100 ng (element) L^{-1} for AsIII, AsV, and SeIV species. The peak of SeVI is broader, leading to a detection limit of around 250 ng (Se) L^{-1}. An example chromatogram is presented in Fig. 3.

Absolute detection limits of different techniques used for simultaneous inorganic arsenic and selenium speciation are

Table 1
Analytical performances for simultaneous analysis of arsenic and selenium in chloride matrix (1 g L^{-1} NaCl)

		LOD (ng (element) L^{-1})	Repeatability (%)
^{75}As	Total	25	2.5
	AsIII	90	5.7
	AsV	95	4.6
^{78}Se	Total	45	1.9
	SeIV	90	2.0
	SeVI	270	5.4
^{80}Se	Total	35	1.4
	SeIV	81	3.0
	SeVI	230	4.6

Data for total and inorganic speciation determinations.
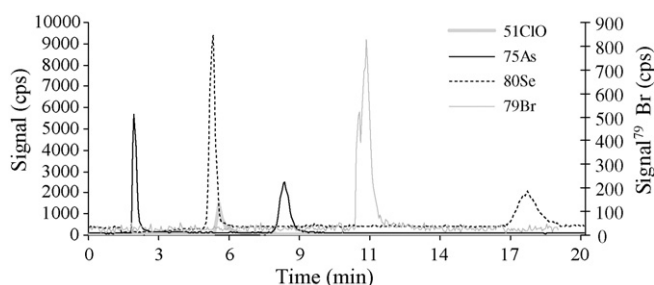
Fig. 3. Example chromatogram for AsIII, AsV, SeIV, and SeVI at 10 μg (element) L^{-1} in 2 g L^{-1} NaCl matrix.

compared in Table 2. The lowest ones are obtained using CZE-ICPMS [26] but due to the small injection volume (0.6 μL), such coupling presents high relative detection limits, not adapted to the analysis of natural waters. In comparison with our results, Ipoly and Fodor [21] have obtained lower detection limits using HPLC connected to two independent atomic fluorescence detectors (one for As detection and the other for Se) via a T-piece. Nevertheless, in this case hydride generation was used for sample introduction and SeVI could not be analyzed simultaneously as no on-line pre-reduction step was included. With HPLC separation, absolute detection limits are in the range of ten picogram for As species and are similar to those found in this work. Considering the higher volume injected, our relative detection limits are lower. For selenium species, the monitoring of ^{80}Se results

in absolute detection limits lower by a factor 2 to 27, depending on the species.

3.3. Application to spiked and natural samples

In order to check accuracy (trueness and precision), our conditions were applied to the certified TM-Rain95 water. Different commercially available mineral waters were also analyzed. Results obtained are presented for ^{75}As, ^{78}Se, ^{80}Se in Table 3. Sample analysis was performed in triplicate using standard additions.

As detailed in a previous paper [17] equations of correction are necessary to correct ^{80}Se signal from Br hydridation when a C/RC system is used. Hydridation of germanium and arsenic were also observed, creating new interferences (^{74}GeH$^+$ and ^{75}AsH$^+$, respectively) but those not corrected here as germanium was not found in analysed samples, and ^{76}Se was not used for quantification.

The samples were also analysed in speciation mode. As shown in Fig. 3, with the chromatographic conditions used, a chlorine-containing species has a retention time of 5.3 min and is separated from As species (retention times of 1.9 and 7.9 min for AsIII and AsV, respectively). However, the use of a C/RC system allows a six-fold reduction of the ArCl$^+$ peak, which prevents possible overlapping. Moreover, a bromine-containing peak (retention time 10.30 min) is separated from selenium species; thus m/z 80 can be monitored without misinterpretation

Table 2
Comparison of absolute detection limits (in pg) of different analytical techniques for simultaneous As and Se speciation

Technique[a]	AsIII	AsV	SeIV	SeVI	Volume (μl)	References
AE-HPLC-ICPMS	17	23	94	177	100	[14]
AE-HPLC-HG-(AFS)₂	0.5	0.7	1	nd	100	[21]
IP-HPLC-ICPMS	1.8	2	16	19	25	[22]
AE-HPLC-ICPMS	4	12	67	227	100	[23]
AE-HPLC-ICPMS	4	6	120	140	100	[24]
AE-HPLC-ICPMS	18	17	185	135	50	[25]
AE-HPLC-ICPMS	10	10	40	40	10	[26]
AE-HPLC-ICPMS	38	29	210	190	50	[27]
EI-CZE-ICPMS	nd	0.048	0.234	0.294	0.6	[28]
PI-CZE-ICPMS	7.8	3.6	21.6	34.8	0.6	[28]
AE-ICP-CRC-MS	9	10	8	23	100	This work

[a] AE, anion exchange; IP, ion pair; PI, pressure injection; EI, electromigrative injection; CZE, capillary zone electrophoresis.

Table 3
As and Se quantification in natural waters, including total and inorganic speciation determinations (values in ng (element) L^{-1})

	^{75}As			^{78}Se			^{80}Se		
	Total	AsIII	AsV	Total	SeIV	SeVI	Total	SeIV	SeVI
TM-R[a]	1340 ± 19	nd[c]	1255 ± 27	611 ± 13	650 ± 26	nd	611 ± 51	649 ± 22	nd
A[b]	300 ± 18	nd	361 ± 22	418 ± 21	nd	398 ± 13	412 ± 8	nd	349 ± 6
B[b]	4372 ± 12	nd	4393 ± 10	133 ± 19	nd	nd	90 ± 8	nd	nd
C[b]	4680 ± 36	nd	4673 ± 22	197 ± 12	nd	nd	149 ± 9	nd	nd
D[b]	3760 ± 39	nd	3573 ± 63	210 ± 18	nd	nd	179 ± 11	nd	nd

Uncertainty represents the standard deviation of three replicate analyses.

[a] TM-Rain 95, certified values: 740 ± 290 ng (Se) L^{-1} and 1070 ± 250 ng (As) L^{-1}.

[b] A, B, C, D are commercially available mineral waters; B, C, and D have the same spring origin with C and D enriched with strawberry and blackcurrant flavours, respectively.

[c] Non-detected.

of selenium quantification, which represents a main advantage of C/RC use [17].

For TM-Rain, total concentrations were in agreement with certified values. AsV and SeIV species were identified in speciation analysis. For selenium, results are in agreement with those previously found in our laboratory for total (674 ± 5 and 655 ± 33 ng (Se) L^{-1} based, respectively on ^{78}Se and ^{80}Se monitoring [17]) and speciation analysis (641 ± 15 and 630 ± 25 ng (Se) L^{-1} as SeIV using HPLC-ICPMS, respectively for ^{78}Se and ^{80}Se monitoring [17]; and 679 ± 13 ng (Se) L^{-1} as SeIV using HPLC-AFS [29]).

In commercial mineral waters, As is generally more concentrated than Se. Total and speciation determinations are in agreement for As, AsV being the only species detected. The low levels of selenium prevent species identification and SeVI was detected only in one sample (water A).

4. Conclusion

Key parameters of ICPMS octopole collision/reaction cell including gas flow rates and ion lenses voltages, were adjusted for the simultaneous removal of As and Se interferences. The use of C/RC has a greater effect on the detection limits for selenium than for arsenic. In total analysis, detection limits are close to 30 ng L^{-1} for both elements in chloride matrix (1 g L^{-1} NaCl), that is to say a two-fold to five-fold improvement respectively for As and Se in comparison with the ones obtained on the same instrument without C/RC use. This is particularly convenient for analysis of natural waters which generally show lower selenium levels compared to arsenic ones. Moreover, interferences removal of both elements with identical C/RC conditions allowed the simultaneous speciation of As and Se inorganic forms. With isocratic HPLC coupling, detection limits are around 100 ng (element) L^{-1} for AsIII, AsV and SeIV, and around 250 ng (Se) L^{-1} for SeVI.

Acknowledgment

References

[1] S.D. Tanner, V.I. Baranov, D.R. Bandura, Spectrochim. Acta, Part B 57 (2002) 1361.
[2] E. McCurdy, G. Woods, J. Anal. At. Spectrom. 19 (2004) 607.
[3] P. Leonhard, R. Pepelnik, A. Prange, N. Yamada, T. Yamada, J. Anal. At. Spectrom. 17 (2002) 189.
[4] T. Nakazato, H. Tao, T. Taniguchi, K. Isshiki, Talanta 58 (2002) 121.
[5] Q. Xie, R. Kerrich, E. Irving, K. Liber, F. Abou-Shakra, J. Anal. At. Spectrom. 17 (2002) 1037.
[6] L. Hinojosa-Reyes, J.M. Garcia-Alonso, J.I. Marchante-Gayon, A. Sanz-Medel, J. Anal. At. Spectrom. 18 (2003) 1210.
[7] S. Mazan, N. Gilon, G. Crétier, J.L. Rocca, J.M. Mermet, J. Anal. At. Spectrom. 17 (2002) 366.
[8] J.M. Marchante-Gayon, C. Thomas, I. Feldmann, N. Jakubowski, J. Anal. At. Spectrom. 15 (2000) 1093.
[9] J.J. Sloth, E.H. Larsen, J. Anal. At. Spectrom. 15 (2000) 669.
[10] Y.-Y. Chan, S.C.-L. Lo, J. Anal. At. Spectrom. 18 (2003) 146.
[11] M. Niemela, P. Peramaki, H. Kola, J. Piispanen, Anal. Chim. Acta 493 (2003) 3.
[12] B.K. Mandal, K.T. Suzuki, Talanta 58 (2002) 201.
[13] H. Robberecht, R.V. Grieken, Talanta 29 (1982) 823.
[14] T. Guerin, M. Astruc, A. Batel, M. Borsier, Talanta 44 (1997) 2201.
[15] J. Goupy, Plans d'expérience pour surface de réponses, ed. Dunod, 1999.
[16] G. Sado, M.C. Sado, Les plans d'expérience: de l'expérimentation à l'assurance qualité, ed. Afnor Technique Editions, 1991.
[17] J. Darrouzès, M. Bueno, G. Lespès, M. Potin-Gautier, J. Anal. At. Spectrom. 20 (2005) 88.
[18] G.L. Long, J.D. Winefordner, Anal. Chem. 55 (1983) 712A.
[19] M.A. Dexter, H.J. Reid, B.L. Sharp, J. Anal. At. Spectrom. 17 (2002) 676.
[20] E.H. Larsen, S. Stürup, J. Anal. At. Spectrom. 9 (1994) 1099.
[21] I. Ipolyi, P. Fodor, Anal. Chim. Acta 413 (2000) 13.
[22] K. Sathrugnan, S. Hirata, Talanta 64 (2004) 237.
[23] C. Casiot, O.F.X. Donard, M. Potin-Gautier, Spectra Analyse 206 (1999) 17.
[24] Y. Martinez-Bravo, A.F. Roig-Navarro, F.J. Lopez, F. Hernandez, J. Chromatogr. A 926 (2001) 265.
[25] T. Lindemann, A. Prange, W. Dannecker, B. Neidhart, J. Fresenius, Anal. Chem. 368 (2000) 214.
[26] A. Woller, H. Garraud, J. Boisson, A.-M. Dorthe, P. Fodor, O.F.X. Donard, J. Anal. At. Spectrom. 13 (1998) 141.
[27] E. Vassileva, A. Becker, J.A.C. Broekaert, Anal. Chim. Acta 441 (2001) 135.
[28] C. Casiot, O.F.X. Donard, M. Potin-Gautier, Spectrochim. Acta, Part B 57 (2002) 173.
[29] S. Simon, A. Barats, F. Pannier, M. Potin-Gautier, Anal. Bioanal. Chem. 383 (2005) 562.

ELSEVIER

Sample preparation for metalloprotein analysis:
A case study using horse chestnuts

Cristiana Schmidt de Magalhães, Marco Aurélio Zezzi Arruda *

Department of Analytical Chemistry, Institute of Chemistry, Universidade Estadual de Campinas, Unicamp, PO Box 6154, 13084-862 Campinas, SP, Brazil

Abstract

In the present work, 11 different procedures for protein and metalloprotein extraction from horse chestnuts (*Aescullus hippocastanum* L.) *in natura* were tested. After each extraction, total protein was determined and, after protein separation through sodium dodecyl sulphate-polyacrylamide gel electrophoresis (SDS-PAGE), those metals belonging to the protein structure were mapped by synchrotron radiation X-ray fluorescence (SRXRF). After mapping the elements (Cr, Fe and Mn) in the protein bands (*ca.* 33 and 23.7 kDa), their concentrations were determined using atomic absorption spectrometry (ET AAS).

Good results were obtained for protein extraction using a combination of grinding and sonication. However, this strategy was not suitable to preserve metal ions in the protein structure. In fact, there was 42% decrease on Mn concentration using this procedure, compared to that performed with sample agitation in water (taken as reference). On the other hand, when grinding and agitation with an extracting buffer was used, there was a 530% increase of Mn concentration, when compared to the reference procedure.

These results indicate agreement between metal identification and determination in proteins as well as the great influence of the extraction procedure (*i.e.*, the sample preparation step) for preserving metals in the protein structures.
© 2006 Elsevier B.V. All rights reserved.

Keywords: Protein; Metalloprotein; Extraction procedures; Horse chestnut

1. Introduction

It is well known that sample preparation is very often the most problematic step in an analytical sequence, because it is generally laborious and time consuming as well as frequently responsible for errors in the final results. Other problems to be considered are related to the instability of the analyte, when specific biomolecules (such as proteins and metalloproteins) are being analyzed [1]. A compromise between effective sample preparation and gentle procedures to maintain the integrity of the analytes is then imperative [2]. Moreover, most protein extraction protocols are utilized without any evaluation of their efficiencies. Additionally, the protocols should be as effective as possible for maintaining the integrity of the metal-protein binding when focused on qualitative and quantitative metallo-proteomics. It is clear that sample preparation for biomolecule analysis is not an easy task, especially if speciation of metalloproteins is taken into account, and even more if proteins belong to vegetal samples [3–5].

An alternative to improve sample preparation for proteins was investigated by Giavalisco et al. [4]. To increase the number of those detectable proteins in plants using two-dimensional (2D) gel electrophoresis, the authors proposed a new procedure for extracting proteins from plant tissue, specifically the leaves and stems of *Arabidopsis thaliana*. The procedure consisted of protein extraction in two fractions. In the first fraction, a supernatant was obtained after centrifugation of ground material containing protease inhibitors, being the portion comprised of cyto-plasmatic proteins. To the remaining pellet, protease inhibitor solution was again added, as well as phosphate buffer. Then, the mixture was ground. The resulting homogenate was mixed with another solution that included dithiotreitol (DTT), urea and thiourea. The supernatant obtained in the second fraction contained predominantly those structures bonded to proteins. Dividing the total amount of proteins into two fractions, sample complexity was decreased. Thus, higher resolutions in 2D

* Corresponding author at: Universidade Federal de Alfenas, Unifal-MG, R. Gabriel Monteiro da Silva, 714, Centro, 37130-000 Alfenas, MG, Brazil. Tel.: +55 19 3788 3089; fax: +55 19 3788 3023.

E-mail address: zezzi@iqm.unicamp.br (M.A.Z. Arruda).

patterns as well as more protein spots were achieved using proposed protocol. According to the number of proteins detected, there was an increase of 3.3-fold in leaf and 2.7-fold in stem tissues compared to the frequently used TCA/acetone precipitation method.

The effects of several variables on sorghum protein extraction were investigated by Park et al. [6]. In that work, factors such as types and concentration of the reducing agent, the detergent and the buffer pH, as well as the sample-to-solvent ratio and extraction time, were tested. Mercaptoethanol, DTT and tris(2-carboxyethyl)phosphine hydrochloride (TCEP-HCl) were evaluated as reducing agents. Among these reagents, the highest amount of proteins was extracted with mercaptoethanol. A 2% (v/v) concentration was chosen for all following experiments. The authors examined, at three levels of concentration, the anionic detergent sodium dodecyl sulphate (SDS), the cationic detergent dodecylammonium bromide (DoTAB) and the zwitterionic detergent *n*-dodecyl-*N,N*-dimethyl-3-ammonio-1-propanesulfonate (SB 3-12). SDS at the higher concentration efficiently extracted the proteins when compared to the other detergents. Then, the effect of buffer concentration was tested, and no significant differences were observed. Furthermore, sorghum proteins were more soluble at pH 10.

To the best of our knowledge, most sample preparation strategies, some of them already exemplified, have been considered only for protein analysis and not for metalloproteins. Due to the importance of sample preparation for attaining accurate results, mainly considering metalloproteomics [1,2], this work aims to evaluate some protein extraction procedures for horse chestnut (*Aescullus hippocastanum* L.) *in natura* samples. They were evaluated in terms of both efficiency and metal-binding preservation after the extraction and separation procedures. The Bradford method [7] to determine total protein concentrations, synchrotron radiation X-ray fluorescence (SRXRF) to identify the metallic ions bonded to the proteins, and atomic absorption spectrometry to quantify those metals present in the protein structures were then used.

Horse chestnuts (*A. hippocastanum* L.) were chosen as the example for this work. In the literature there is a variety of information about the total protein content (from 0.388 up to 10.99%, m/m) [8–10]. Some catalase isoenzymes and superoxide dismutase metalloenzymes have been found in seeds and embryogenic callus, respectively [11]. Additionally, horse chestnut, a traditional phytomedicine, is used to promote circulation through the veins [12], for the treatment of chronic venous insufficiency and to reduce edema following trauma, particularly following sports injuries, surgery, and head injuries [12–14]. The recommended daily dose varies between 500 and 900 mg of standardized extract (16–20%, m/v aescin content) [12–13].

2. Experimental

2.1. Sample preparation

The horse chestnut samples were acquired in a local market (Alfenas, Brazil). Eleven protein extraction procedures were evaluated. For each procedure, the samples were cut, dried at

Table 1
Protein extraction procedures

Procedure number	Remarks
1	Samples manually shaken in water for *ca.* 5 min
2	Samples manually shaken in buffer[a] for *ca.* 5 min
3	Samples beside being shaken in water also dialyzed[b] in water for 42 h
4	Samples manually ground in water, using a mortar and pestle at room temperature for 15 min
5	Samples were manually ground in buffer[a], using a mortar and pestle at room temperature for 15 min
6	Samples, beside being ground in water, were also dialyzed[b] in water for 42 h
7	Samples were shaken in water for 5 min and then submitted to sonication[c] for 10 min
8	Samples were manually ground in water and then submitted to sonication[c] for 10 min
9	Samples were manually ground in buffer[a] and then submitted to sonication[c] for 10 min
10	Samples were prepared as in procedure 8, but at 40 °C
11	Samples were prepared as in procedure 9, but at 40 °C

[a] 1.0 mol L^{-1} Tris–HCl, pH 6.8 buffer.
[b] Membrane MWCO: 6-8000, Spectrum Laboratories Inc., USA.
[c] Unique 1400, Ultrasonik.

40 °C in an oven with forced air circulation, and then 0.5 g was weighted (dry mass). Then, 5 mL of deionized water or 1.0 mol L^{-1} Tris–HCl, pH 6.8 (Merck, Darmstadt, Germany) buffer were added. The different procedures are listed in Table 1, with the respective details.

After finishing each procedure, the samples were centrifuged (Bio-Spin R, BioAgency, São Paulo, Brazil) for 5 min at $16,060 \times g$ and 4 °C. The supernatant solutions were stored in Eppendorf® flasks and frozen at −18 °C. All solutions were prepared with analytical reagent-grade chemicals. High purity water (18.2 MΩ cm) from a Milli-Q water purification system (Millipore, Bedford, USA) was used throughout this work.

2.2. Determination of total protein concentration

The Bradford method [7] to determine the concentration of total proteins was used. The analyses were carried out in a Genesys 5 spectrophotometer and all measurements were made in triplicate. Analytical curves using bovine serum albumin (Merck, Darmstadt, Germany), and the total protein concentration from supernatant solutions, diluted with water or buffer, were obtained.

2.3. Gel electrophoresis

Sodium dodecyl sulphate-polyacrilamide gel electrophoresis (SDS-PAGE) was carried out using a separation gel composed of acrylamide (12.5%, m/v) (Bioangency, São Paulo, Brazil) and *N,N′*-methylene bisacrylamide (0.4%, m/v) (Promega, Madison, USA) at pH 8.8, containing 10% (m/v) SDS (Synth, Diadema, Brazil), *N,N′,N,N′*-tetramethylethylenediamine (TEMED) (J.T. Baker, Phillipsburg, USA) and 10% (m/v) ammonium persulfate (Mallinckrodt, Paris, USA). Tris–HCl buffer solution (1.0 mol L^{-1}) was used for adjusting the pH value in the separa-

tion gel. The gel plate dimensions were 10 cm (height) × 10.5 cm (width). Tris–glycine buffer solution (pH 8.3) was used in the reservoir [15]. The electrophoresis system was composed of a reservoir and an electrophoresis power supply (both from GE Healthcare, USA).

The supernatant solutions obtained from procedures 1 and 2 were not diluted, while the supernatant solution from procedure 8 was diluted with water. That obtained from procedure 9 was diluted with $1.0 \, mol \, L^{-1}$ Tris–HCl buffer, at pH 6.8. All procedures where the supernatant was diluted were performed to obtain the $2.2 \, mg \, g^{-1}$ protein concentration. Therefore, supernatants from procedures 1, 2, 8 and 9 were also separated in non-reducing conditions. However, for comparison purposes, the supernatant solutions from procedures 8 and 9 were diluted with a dissociating buffer, mixing $38 \, \mu L \, 0.5 \, mol \, L^{-1}$ Tris–HCl buffer, pH 6.8, $60 \, \mu L$ 10% (m/v) SDS, $15 \, \mu L$ conc. 2-mercaptoethanol, $30 \, \mu L$ conc. glycerol and $158 \, \mu L \, H_2O$. These supernatants from procedures 8 and 9 were separated in denaturing-reducing conditions. Before each run, the aliquots ($20 \, \mu L$, *i.e.*, $4.4 \, \mu g$ of protein) of diluted (or not) supernatant solutions were immersed in a boiling water bath for 5 min to complete the extraction process. The prepared samples were then cooled at room temperature and each aliquot was loaded onto a single gel slot. One slot was always used for the protein molar mass standard (#SM0431, Fermentas, Hanover, USA). The initial and final currents were 25 and 15 mA, respectively, and the fixed voltage was 100 V. After protein migration, the protein bands were stained with a solution containing 0.15 g Coomassie Brilliant Blue G-250 (J.T. Baker, Xalostoc, Mexico), 90 mL methanol (J.T. Baker, Xalostoc, Mexico), 30 mL glacial acetic acid (J.T. Baker, Xalostoc, Mexico), and 180 mL (v/v) deionized water, for 2 h. Subsequently, the gel was destained for *ca.* 10 h in the same solution, without Coomassie Brilliant Blue G-250.

2.4. Protein molar mass (MM) estimation

The gels were scanned and the protein molar masses were estimated using purified protein marker (#SM0431) including β-galactosidase (116 kDa), bovine serum albumin (66.2 kDa), ovalbumin (45.0 kDa), lactate dehydrogenase (35.0 kDa), restriction endonuclease Bsp98I (25.0 kDa), β-lactoglobulin (18.4 kDa) and lysozyme (14.4 kDa), using the Gel-Pro Analyser® 3.1 software, from MediaCybernetics Inc. (Silver Spring, USA).

2.5. Metal identification by synchrotron radiation X-ray fluorescence (SRXRF)

Elemental analysis on the protein bands was carried out using the DB09 synchrotron radiation (SR) beam line station at the Brazilian Synchrotron Light Laboratory (LNLS). The storage ring was runn at an energy of 1.37 GeV with an intensity of 250 mA. The X-ray microprobe setup of the beamline was used for adjusting the motorized computer-controlled set of slits to limit the white beam to micrometric size. A tantalum collimator of 2 mm diameter was used at the detector entrance. The high purity (HP) Ge detector was placed in the electron orbital plane

perpendicular to the incident beam to collect the XRF signal from the exposed sample.

Since it is considered a non-destructive technique, the protein band was cut out of the gel and mounted onto a 3D sample-moving platform for scanning analysis. After positioning the sample in a $230 \, \mu m \times 220 \, \mu m$ SR beam spot, the beam was turned on. The emitted X-ray spectrum was recorded with a counting time of 300 s. The gel was moved along the horizontal direction (along the band) with 2 mm intervals for each step. Three points were mapped in each band during *ca.* 5 min. In order to correct the effect of SR beam flux variation on the signal intensity, the area of the chemical species peaks were normalized to the peak counts of Ar, which is present in air at constant proportion. The normalized peak areas were used for estimating the relative contents of metal ions. The average intensity data (of all chemical species) were calculated from the three points, as well as the difference between the sample intensity and analytical blank data. The analytical blank considered was a standard protein band gel signal (ovalbumin). It was chosen due to the similarities of the gel organic matrix for both albumin and the proteins being analyzed besides ovalbumin is not considered a metalloprotein, according to the protein data bank [16].

2.6. Microwave assisted gel band decomposition

The gel protein band decomposition used was the same as proposed by Verbi et al. [15]. Each gel protein band was carefully cut off and inserted into Teflon vessels with the oxidant mixture of 5 mL of HNO_3 and 1 mL of H_2O_2. The microwave program was run only after the initial reaction had subsisted (30 min for safety reasons). The decomposition program consisted of three steps: 3 min at 400 W, 6 min at 790 W, and 3 min at 0 W, the program being running twice [15]. After finishing the sample decomposition program, the Teflon vessels were placed on a hot plate ($60–70 \, °C$) for evaporation the excess of HNO_3. The final volumes were adjusted with 0.2% HNO_3 to 5 mL in volumetric flasks. The analytical blanks (also in triplicate), *i.e.*, the ovalbumin protein band in stained/destained polyacrilamide gel, were also decomposed as described.

2.7. Metal quantification using electrothermal atomic absorption spectrometry (ET AAS)

For the metal quantification in the decomposed gel protein bands, a Perkin-Elmer AAnalyst 600 atomic absorption spectrometer (Norwalk, USA) was used for Fe, Cr and Mn determination by ET AAS.

Hollow cathode lamps (Perkin-Elmer, Norwalk, USA) of Cr ($\lambda = 357.9$ nm, slit $= 0.7$ nm), Fe ($\lambda = 248.3$ nm, slit $= 0.2$ nm) and Mn ($\lambda = 279.5$ nm, slit $= 0.2$ nm) were employed as primary radiation sources. Analytical measurements were based on integrated peak area. The ET AAS operating conditions were those recommended by the manufactures [17].

Stock reference solutions ($1000 \, mg \, L^{-1}$) for Fe, Mn and Cr (TecLab, Jundiaí, Brazil) were prepared in 0.2% (v/v) HNO_3. Chemical modifiers such as 0.15% (v/v) $Mg(NO_3)_2$ and 0.05%

Table 2
Total protein concentrations (mg g^{-1}) determined by the Bradford method ($N = 3$) from different protein extraction procedures

Procedures	Total protein concentration (mg g^{-1})
1	1.81 ± 0.06
2	1.51 ± 0.06
3	1.22 ± 0.04
4	3.04 ± 0.08
5	3.59 ± 0.2
6	1.74 ± 0.08
7	2.31 ± 0.04
8	3.38 ± 0.09
9	5.5 ± 0.1
10	4.8 ± 0.2
11	3.8 ± 0.2

(v/v) Pd + 0.03% (v/v) Mg(NO$_3$)$_2$, were used for Fe and Cr, and for Mn determinations, respectively.

3. Results and discussion

3.1. Determination of total protein concentration

The results for total protein concentration of supernatant solutions are shown in Table 2. If a 10-fold dilution (0.5 g of sample diluted in 5 mL of water or 1.0 mol L^{-1} Tris–HCl buffer, at pH 6.8) is considered, then the protein concentrations obtained are in agreement with the range presented in the literature (from 0.388 up to 10.99%, m/m) [8,9,10] of total protein concentration in the seeds. Although the high fat percentage present in the sample (around 5.5%) [9,10], no detergents were used with water or Tris–HCl buffer during the extractions because they could act as interfering in the total protein determination [7]. In such case, the fat was easily separated from protein extracts during the centrifugation and then manually removed.

The analytical curves obtained using the Bradford method always showed linear correlations (R^2 ranged from 0.974 to 0.996). From these results, improvements of 66.9% in the quantities of protein extracted were observed, comparing procedures 1 and 4, of 86.3% between 1 and 8 and of 164% between

1 and 10. All these procedures (1, 4, 8, 10) used only water as the extracting liquid. Increases of 137.4% between procedures 2 and 5 and of 165% between 2 and 9 were detected, where 1.0 mol L^{-1} Tris–HCl buffer, at pH 6.8, was used as the extraction medium. The lowest values of total protein concentrations were found for those procedures using dialysis: decreases of 32.6% between procedures 1 and 3, and 4% between 1 and 6. These results are expected, since dialysis "cleans" the samples.

From determination of total protein concentrations (Table 2) the most efficient extraction procedures were those where shaking, followed by grinding, sonication and centrifugation were utilized, either at room temperature or 40 °C (procedures 7–11, see Table 1), and the worst procedures for protein extraction were those where dialysis was used (procedures 3 and 6, see Table 1). Although these results do not provide information about which kind of proteins were extracted, or if they are intact (or not) after the extraction, they were used for comparing the relative protein extraction efficiency.

3.2. Protein molar mass estimation from gel electrophoresis

From the results of Table 2, the supernatants obtained from procedures 1, 2, 8 and 9 were chosen for protein separation by gel electrophoresis (SDS-PAGE). The gels from horse chestnut separation for these extraction procedures, diluted just with water or Tris–HCl buffer (i.e. under non-reducing conditions), presented only one expressive band around 33 kDa (see Fig. 1 a, b, d and e). As the expected protein to be found was catalase (EC 1.11.1.6 [16]), and it is a soluble water protein these extractors were considered suitable for the objectives. The protein mass in each band was estimated from the differences in the optical density, and a calibration curve using Gel-Pro Analyser® 3.1 software. Protein band masses of 8.4 ± 0.3, 13 ± 4, 9 ± 3, 10 ± 1, 5 ± 1, and 10 ± 1 μg were obtained by procedures 1, 2, 4, 5, 8, and 9, respectively, for the 33 kDa band.

It is interesting to comment that although different total protein concentrations were obtained using different extraction procedures a gel-band with similar migration time was always obtained. Additionally, when the supernatants were diluted with

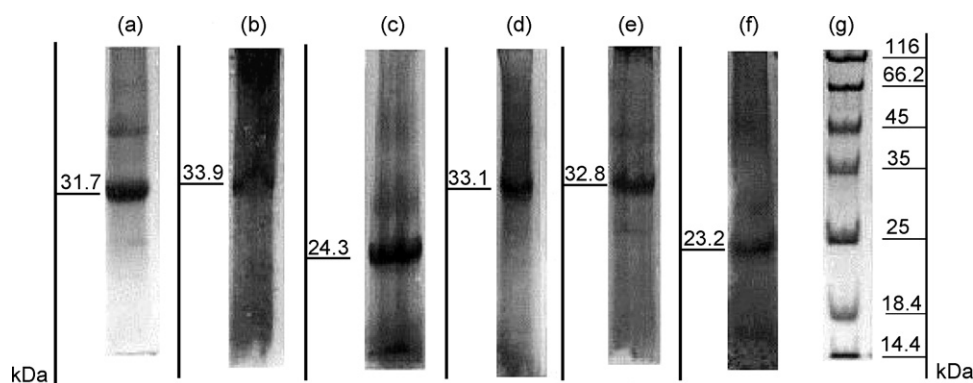Fig. 1. Electrophoretic gels from supernatant solutions of horse chestnut samples, after different extraction procedures: (a) procedure 1; (b) procedure 8, diluted with water; (c) procedure 8, diluted with dissociating buffer; (d) procedure 2; (e) procedure 9, diluted with 1 mol L^{-1} Tris–HCl buffer, pH 6.8; (f) procedure 9, diluted with dissociating buffer. Standard proteins with their respective MM are presented in (g).

a dissociating buffer, a band of around 23.7 kDa became more expressive (Fig. 1 c and f). This is clearly emphasized in Fig. 1, by comparing the gels (b) and (c), as well as (e) and (f). This behavior related to protein mobilities is relatively common when they are extracted from plant materials [6,18,19].

One of the major problems found in plant protein and enzyme extractions is the presence of phenolic compounds released during tissue grinding. These phenols are readily oxidized to quinones by plant enzymes, and the phenolic compounds, as quinones, either react with the proteins, inactivating the enzymes, or change the mobility of protein molecules. Then, substances that avoid both oxidation and complexation to phenols/quinones are strongly recommended to be added to ground samples as well as to the extracting buffer [20,21].

Negishi et al. [21] studied enzymatic reactions in the presence of thiol compounds. These included reactions leading to the formation of 2′-(2-hydroxyethylthio)-(−)-epicatechin, 5′-(2-hydroxyethylthio)-(−)-epicatechin and 2′,5′-bis(2-hydroxyethylthio)-(−)-epicatechin and other conjugates between thiol compounds and several phenolics, using polyphenol oxidase prepared from *Rhododendron mucronatum*. They also discussed the mechanism of inhibition of enzymatic browning and of protection of sulphydryl enzymes by thiol compounds.

In this context, the thiol reducing agent (2-mercaptoethanol) present in the dissociating buffer has two possible functions: to avoid protein mobility modification in the gel (see Fig. 1 c and f), or to extract a new protein with different molar mass. The mobility is a function, among others, of both size and conformation of the migratory ions as well as gel porosity. As no alteration was noted in gel porosity, there is the possibility to change the size or conformation of proteins by adding the reducing agent. In this way, the 23.7 kDa band is then considered as molar mass of the identified protein.

Gumilevskaya et al. [22] also found one group of polypeptides from horse chestnut, of *ca.* 24–25 kDa, a mass that is characteristic of cytosol. These proteins were also classified as heat-stable proteins, comprising about 30% of the total proteins occurring only in cytosol. Therefore, these statements are in agreement with our results (Fig. 1), since the proteins present the same MM range, as well as surviving being heated (5 min at 100 °C) before the electrophoretic separation.

3.3. Qualitative metal evaluation by SRXRF

Through the normalized peak areas from SRXRF spectra of the horse chestnut protein band of 33 kDa obtained from procedures 1 and 2, and of the protein band of 23.7 kDa from procedures 8 and 9, it was possible to identify and to estimate (see Section 2.5) the relative contents of Cr (5.41 keV), Mn (5.89 keV), and Fe (6.40 keV) from their Kα emissions, as presented in Table 3.

3.4. Metal quantification by AAS

After metal species identifications by SRXRF, the protein bands of 33 kDa, obtained from supernatants of procedures 1 and 2, and of 23.7 kDa from procedures 4, 5, 8, 9, as well as the

Table 3
Relative metal contents from Kα metal ion emissions. The average intensity data (ion counts of metals) were calculated from the three points mapped, as well as from data differences between sample intensity and analytical blanks

Procedure	Cr	Mn	Fe
1	6.66E−4	2.22E−4	9.19E−3
2	0	9.9E−4	1.07E−3
8	0	6.78E−4	3.65E−3
9	0	7.5E−4	9.17E−4

analytical blank (ovalbumin protein band) were decomposed (as described in Section 2.6). Chromium, Fe and Mn were determined by ET AAS. The results are presented in Table 4.

From the results of item 3.2 and Table 4, the quantity of each metal present in the proteins (see Table 5) was estimated. From these results, it is observed that procedures using Tris–HCl buffer better preserve Fe in proteins, while procedures using water are better for Cr. Mn presented similar results for both procedures 4 and 5, indicating that grinding is decisive to extract and to preserve this metal in the structure of the studied protein.

As proposed by qualitative metalloproteomics, Cr, Mn, and Fe were identified in band proteins by SRXRF. It is important to mention that the species were identified in procedures where either water or buffer was used. These identifications produced important information to be followed by metal quantification by AAS (quantitative metalloproteomics). The quantification results are in agreement with the metal species identifications. Considering the metal concentrations and comparing procedures 1, 2, 4, 5, 8 and 9, it is observed that Fe concentrations remain constant (taking into account standard deviation), independent of the extraction procedure utilized. This means that iron ions are preserved in the identified proteins, independent of the extraction procedure applied, which can be indicative of the presence of an

Table 4
Metal concentrations in the protein bands. Cr, Fe and Mn were determined by ET AAS ($N = 3$)

Procedure	Cr (μg g^{-1})	Fe (μg g^{-1})	Mn (μg g^{-1})
1	4.98 ± 0.05	35 ± 6	2.7 ± 0.4
2	1.6 ± 0.7	38 ± 2	1.9 ± 0.2
4	4.00 ± 0.02	40 ± 7	15 ± 1
5	1.5 ± 0.4	37 ± 7	12 ± 2
8	<LOD	23 ± 9	<LOD
9	1.3 ± 0.1	38 ± 3	1.1 ± 0.4

LOD: 0.054 μg g^{-1} Cr; 0.99 μg g^{-1} Fe; 0.06 μg g^{-1} Mn.

Table 5
Estimated metal quantities in the separated proteins

Procedure	Cr (pg)	Fe (pg)	Mn (pg)
1	41.8 ± 1.5	294 ± 3	22.68 ± 0.25
2	21 ± 2	494 ± 2	25 ± 2
4	36.0 ± 1.5	360 ± 4	135.0 ± 1.6
5	15.0 ± 0.5	370 ± 4	120.0 ± 1.1
8	_[a]	115 ± 5	_[a]
9	13.0 ± 0.5	380 ± 2	11.0 ± 0.6

[a] <LOD, see Table 5.

iron metalloprotein. Only as a comment, Fe is a key component of heme proteins (catalase) [23], and as a transition metal, it is probably covalently bound to protein. As an example, Bagnoli et al. [11] found catalase isoenzymes of class I and III and the metalloproteins Mn- and Fe-superoxide dismutase in zygotic and somatic embryos of horse chestnut.

When comparing procedures 1 and 8, the metals Cr and Mn were completed lost. When comparing procedures 2 and 9, 19% of Cr and 42% of Mn were also lost. It is interesting that, although procedures 8 and 9 present the best results for extraction of total proteins (see Table 2) they are less effective for preserving the metals in the protein structures. Therefore, although the procedures with sonication provide better results for total protein extraction, they can be considered less favorable for preserving the metals in the proteins. The best results were obtained with procedures 4 and 5, where grinding contributes to extract proteins (compare Tables 2 and 5) without metal loss. Additionally, Gumilevskaya et al. [22] observed that horse chestnut seeds do not accumulate large amounts of storage proteins, and the total content of protein did not exceed 7.5% on a dry weight basis. Therefore, the results obtained from procedures 4 and 5 represent 3.04 and 3.59% of total protein content and are in agreement with the expected value.

4. Conclusions

The present work pointed out the importance of differences in sample preparation for protein and metalloprotein analysis, since both the extraction procedure and the extraction medium are decisive to preserve species in the protein structure. In this way, 11 different extraction procedures were tested and compared in terms of their relative efficiencies for both total protein extraction and metal–protein binding preservation. Although procedure 9 (where Tris–HCl buffer, grinding and sonication were used) could be applied for protein analysis, it was the worst in terms of metal–protein binding preservation and should not be recommended for metalloprotein analysis. Thus, the more gentle procedures (4 and 5) produced appropriate results, because they preserve the metal–protein structure more effectively, assuring more accurate results in terms of quantitative analysis of metalloproteins, as well as also presenting the results that are in agreement with the literature in terms of total protein.

Another interesting point is related to the protein mobility. The presence of phenolic compounds released during sample grinding can change the mobility of the proteins, and produce an incorrect result in terms of protein molar mass. In this way, the use of a reducing agent (such as 2-mercaptoethanol) is imperative for avoiding this problem. This behavior emphasizes matrix complexity and the care need in sample preparation.

It is necessary to points out that a more accurate technique such as LC–MS–MS was not used for characterizing such protein investigated because neither the genome nor the primary structure of the horse chestnut proteins are still know as well as this task was not the objective of this work. However, only through the gel analysis was possible to take some conclusions about the necessity of a well established sample preparation protocol for avoiding changes in the protein mobility.

As a final conclusion, the sample preparation step needs to be carefully evaluated if the objective is to preserve a desired species in the protein structure. It is particularly important when metallomic studies are considered.

Acknowledgements

References

[1] C.S. Magalhães, J.S. Garcia, A.S. Lopes, E.C. Figueiredo, M.A.Z. Arruda, in: M.A.Z. Arruda (Ed.), Trends in Sample Preparation, New York, Nova Science, in press.
[2] J.S. Garcia, C.S. Magalhães, M.A.Z. Arruda, Talanta 69 (2006) 1.
[3] D.I. Jacobs, M.S. van Rijssen, R. van der Heyden, R. Veerpoorte, Proteomics 1 (2001) 1345.
[4] P. Giavalisco, E. Nordhoff, H. Lehrach, J. Gobom, J. Klose, Electrophoresis 24 (2003) 207.
[5] É.A.R. Vasconcelos, F.C.S. Nogueira, E.F.M. Abreu, E.F. Gonçalves, P.A.S. Souza, F.A.P. Campos, Chromatographia 62 (2005) 447.
[6] S.H. Park, S.R. Bean, J. Agric. Food Chem. 51 (2003) 7050.
[7] M.M. Bradford, Anal. Biochem. 72 (1976) 248.
[8] http://www.hort.purdue.edu/newcrop/parmar/02.html (05.04.06).
[9] T. Shimada, Ecol. Res. 16 (2001) 803.
[10] http://botanical.com/botanical/mgmh/c/chehor58.html (16.02.06).
[11] F. Bagnoli, M. Capuana, M.L. Racchi, Aust. J. Plant Physiol. 25 (1998) 909.
[12] http://www.wholehealthmd.com (30.03.06).
[13] http://www.mothernature.com/Library/Ency/Index.cfm/id/210008#3 (15.09.05).
[14] C. Calabrese, P. Preston, Planta Med. 59 (1993) 394.
[15] F.M. Verbi, S.C.C. Arruda, A.P.M. Rodriguez, C.A. Pérez, M.A.Z. Arruda, J. Biochem. Biophys. Meth. 62 (2005) 97.
[16] http://www.expasy.org/uniprot/P01012 (20.02.06).
[17] Perkin-Elmer, Analytical Methods for Atomic Absorption Spectrometry, The Perkin-Elmer Corp, USA, 1994.
[18] T.S. Melo, R.B. Ferreira, A.N. Teixeira, Phytochemistry 37 (1994) 641.
[19] S. El Ouakfaoui, A. Asselin, Phytochemistry 7 (1992) 1513.
[20] J.W. Anderson, Phytochemistry 7 (1968) 1973.
[21] O. Negishi, T. Ozawa, Phytochemistry 54 (2000) 481.
[22] N.A. Gumilevskaya, M.I. Azakovich, M.E. Komarova, N.V. Obroucheva, Russ. J. Plant Physiol. 48 (2001) 1.
[23] J.L. Hall, L.E. Williams, J. Exp. Bot. 54 (2003) 2601.

ELSEVIER

A rapid and simple microwave-assisted digestion procedure for spectrophotometric determination of titanium dioxide photocatalyst on activated carbon

Amjad H. El-Sheikh [*], Jamal A. Sweileh

Department of Chemistry, Faculty of Science, Hashemite University, P.O. Box 150459, Al-zarqa 13115, Jordan

Abstract

Deposition of titanium dioxide (TiO_2) on activated carbon (AC) surface has been widely utilized for the production of TiO_2/AC photocatalyst, which can be used in photo-degradation of pollutants. In this work, a fast and simple digestion procedure has been developed for the spectrophotometric quantitative analysis of TiO_2 in TiO_2/AC photocatalyst. Microwave-assisted digestion was used in the procedure. The microwave-digestion procedure was optimized using the single-variable method. Variables optimized included time of ashing, effective digestion time, volume and concentration of sulfuric acid, effect of adding a digestion catalyst, effect of sample pulverizing and on–off time cycle of the microwave. The analysis was completed spectrophotometrically after addition of hydrogen peroxide to the digested solution. Procedure precision and accuracy was tested by application to photocatalyst samples containing known amounts of TiO_2, and compared with previously published spectrophotometric procedures. The proposed microwave procedure was capable of recovering 98.4–101.1% of TiO_2 in the catalyst in less than 10 min, without the need for sample ashing. Analytical precision is 1.42–2.39% relative standard deviation (R.S.D.). In terms of accuracy and precision, the proposed microwave procedure was comparable with other procedures, but the proposed microwave procedure was superior in terms of shorter procedure duration.
© 2006 Elsevier B.V. All rights reserved.

Keywords: Microwave-assisted digestion; Analytical procedure; Titanium dioxide; Activated carbon; Photocatalyst

1. Introduction

Several published papers and review articles have cited the theory and environmental applications of heterogeneous photo-catalysis by the use of titanium dioxide (TiO_2) [1–3]. Improving the photocatalyst efficiency may be achieved by deposition of the photocatalyst on a high surface area material (support) that will selectively adsorb the pollutant molecules and concentrate them around the photocatalyst [4–7]. The use of activated carbon (AC) as a support for TiO_2 was proposed by many authors [8–14]. Activated carbon appears to give great advantages over other supports, such as its ability to rapidly adsorb pollutants, as well as its high adsorption capacity due to its high surface area and porosity.

The use of titanium dioxide deposited on activated carbon (TiO_2/AC) as photocatalyst necessitates rapid and accurate analytical procedure for quantitative analysis of titanium dioxide. A common method for titanium dioxide analysis is X-ray fluorescence spectrometry [15] which is relatively an expensive technique to use and the instrument is not always available especially in developing countries. Additionally, establishing a calibration graph by XRF suffers from linearity problem (curvature) at high titanium content, which necessitates difficult dilution with solid matrix. The use of X-ray diffraction is possible for comparative purposes but this technique is limited to the crystalline forms of TiO_2 (anatase, rutile and brokite). Some authors [8,14], who conducted studies on TiO_2/AC photocatalyst for pollutants degradation, have used a colorimetric analytical method for TiO_2 deposited on carbon surface by the use of "Tiron" reagent (sodium 1,2-dihydroxybenzene-3,5-disulfate) as a complexing-agent, but they did not give any validation information regarding the suitability of this procedure in carbon matrix. The procedure was originally pro-

---

[*] Corresponding author. Tel.: +962 5 3903333.
E-mail address: amjadelsheikh3@yahoo.com (A.H. El-Sheikh).

posed for analysis of titanium dioxide by Yoe and Armstrong [16].

Titanium dioxide is widely used as a digestibility marker, and thus many authors reported preparation procedures for its analysis in feed and fecal samples from animals [17,18–21]. Procedures were generally based on sample digestion followed by addition of hydrogen peroxide (H_2O_2) to produce an intense orange color [22]. This reaction is extremely sensitive; it is known for a long time and can be used for colorimetric detection of titanium and hydrogen peroxide [23–25]. Njaa [18] analyzed titanium dioxide in rat feces using wet-ash digestion of sample in concentrated sulfuric acid in the presence of copper catalyst followed by addition of hydrogen peroxide. Leone [19] reported a procedure for the determination of TiO_2 in cheese, which involved ashing then addition of anhydrous sodium sulfate and sulfuric acid followed by boiling then addition of H_2O_2. This procedure was modified by Short et al. [20] and used for analyzing TiO_2 in chicken excreta, in which samples were ashed then digested in sulfuric acid. Titgemeyer et al. [21] have then modified Short et al.'s procedure for analysis of TiO_2 in bovine fecal samples. Myers et al. [17] have then reported the use of copper (II) sulfate and potassium sulfate as digestion catalyst. These sequential modifications suggest that the matrix, where TiO_2 present, is of significant effect in determining the validity of the TiO_2 sample preparation procedure. For example, Levine et al. [26] reported the analysis of TiO_2 in lung and lymph node tissues by inductively coupled plasma optical emission spectrometry (ICP-OES) after digestion using nitric and hydrofluoric acids. Levine et al. [26] also reviewed in his paper the major instrumental methods for quantitative and semi-quantitative TiO_2 analysis in biological samples, such as ICP-OES, ICP-MS, AAS, SEM-energy dispersive X-ray analysis. The digestion method also plays a role the process. So that authors, such as Korn et al. [27], have reported and compared the use of different decomposition procedures of TiO_2. None of these simple procedures, or any one analogous to any of them, was applied for the determination of TiO_2 photocatalyst deposited on the surface of activated carbon. It is well known that activated carbon has unique surface area and porosity, which may affect the digestion/analysis process. Additionally no procedure has used microwave-assisted digestion of an activated carbon sample containing TiO_2. Therefore, our objective here is to develop and test a simple-sample preparation microwave-digestion procedure for spectrophotometric analysis of TiO_2 in carbon matrix and compare it with previously published spectrophotometric procedures. The primary application of this method is to determine the concentration of unknown TiO_2 in TiO_2/AC photocatalyst samples.

2. Experimental

2.1. Materials and instruments

Activated carbon "AC" (devoid of TiO_2) was purchased from Sigma (77.5% C, 1.2% H, 0.5% N, 8.3% O and 12.5% ash). Other activated carbons (of different ash contents) were used for studying the effect of changing the carbon source. These carbons were either purchased from Norit (83.5% C, 0.8% H,

0.1% N, 7.3% O and 8.3% ash) or Darco (76.0% C, 1.1% H, 0.2% N, 6.5% O and 16.2% ash); or home-made carbon (84.0% C, 1.3% H, 1.7% N, 6.8%O and 6.2%ash). Titanium (IV) iso-propoxide and all other chemicals were supplied by Aldrich. A microwave oven (Frigidaire RCMV5118W, 900 W, percent microwave power 100%, 2450 MHz) was used in sample digestion. Thermolyne furnace 47900 was used in dry-ashing of the solid samples. Absorbance measurements were recorded using Cary 100Bio UV–vis spectrophotometer.

2.2. Preparation of the photocatalyst samples

Six photocatalyst samples (TiO_2/AC) were prepared by deposition of titanium dioxide on activated carbon surface as follows: 1-g samples of activated carbon were placed in 100 ml beakers. Various accurately weighed (± 0.1 mg) amounts of titanium (IV) iso-propoxide were added to the beakers and sonicated for few minutes. Samples were then subjected to water vapor for 1 h to hydrolyze the titanium salt, and then placed inside an oven maintained at 150 °C overnight and then calcined for 2 h at 500 °C at inert atmosphere to complete the formation of TiO_2 [15]. Photocatalyst samples (TiO_2/AC) were then weighed accurately (± 0.1 mg). Concentration of TiO_2 in the photocatalyst samples was calculated by dividing mass (mg) of TiO_2 (stoichiometrically calculated) by the final mass of the photocatalyst sample obtained. Concentration of TiO_2 in the photocatalyst samples were: 18.0, 33.0, 54.2, 75.9, 97.4 and 112.5 mg TiO_2/g photocatalyst sample. Each sample was then thoroughly homogenized and pulverized. The 18.0 mg/g sample was used in the optimization experiments. Photocatalyst samples are usually prepared to have nominal concentrations in this range. However, if higher concentrations are used, the sample size should be reduced so that TiO_2 mass in the analyzed sample should not exceed 4 mg TiO_2. On the other hand, lower concentrations necessitate the use of larger sample size, and thus possible interferences from activated carbon matrix may occur.

2.3. The microwave-digestion procedure

The general procedure for sample preparation and quantitative analysis of TiO_2 is as follows: photocatalyst sample was accurately weighed (± 0.1 mg) in a Pyrex tube, so that mass of TiO_2 in the analyzed photocatalyst sample should not exceed 4 mg. Three milliliters of 18.0 M sulfuric acid was added to the tube. A digestion catalyst (0.04 g copper (II) sulfate ($CuSO_4$) + 0.35 g potassium sulfate (K_2SO_4)) was added to the tube and the sample was then digested in a microwave oven (percent microwave power 100%) for 4 min (on–off time cycle of the microwave was 30–30 (second–second)). The digested solution was then diluted with 7.00 ml distilled water and centrifuged at 3000 rpm to separate residual carbon. All the supernatant was transferred into another test tube, to which 1.00 ml of 30% hydrogen peroxide was added. The final volume was completed to 10.00 ml and the absorbance of the solution was measured at 410 nm. Blank sample was prepared by repeating the above procedure using an activated carbon sample devoid of TiO_2.

The above procedure is the optimized proposed microwave procedure which was developed by using the single-variable optimization method. Variables studied included time of ashing, effective digestion time, on–off time cycle of the microwave oven, sulfuric acid concentration, volume of sulfuric acid and presence or absence of digestion catalyst and sample particle size. The effect of carbon source was also studied.

2.4. Previously published procedures

Two previously published procedures, which have been previously used by other authors for analysis of TiO_2 in feed and fecal samples, were used in this work for comparison with the proposed microwave procedure.

2.4.1. Short et al.'s procedure

This procedure was described by Short et al. [20] for analysis of TiO_2 in feed or excreta samples. It involved sample dry-ashing then digestion in H_2SO_4 and then spectrophotometric analysis. Summary of the procedure is as follows: sample size, 0.1000 g; time of ashing, 13 h; ashing temperature, 580 °C; H_2SO_4 concentration, 7.4 M; H_2SO_4 volume, 10.0 ml and digestion time, 60 min. Total time of the procedure is approximately 18 h.

2.4.2. Myers et al.'s procedure

This procedure was described by Myers et al. [17] for analysis of TiO_2 in feed and fecal samples. It involved direct sample digestion in H_2SO_4 then spectrophotometric analysis. Summary of the procedure is the following: sample size, 0.5000 g; H_2SO_4 concentration, 18 M; H_2SO_4 volume, 13.00 ml; digestion time, 2 h; catalyst, 3.5 g K_2SO_4 + 0.40 g $CuSO_4$. Total time of the procedure is approximately 4 h.

3. Results and discussion

3.1. Effect of various variables on the microwave-digestion procedure

Sample preparation by the proposed procedure for quantitative analysis of titanium dioxide is generally based on microwave assisted-digestion of the sample with sulfuric acid prior to colorimetric analysis by addition of hydrogen peroxide (H_2O_2). It was thought that sample dry-ashing may be useful to eliminate matrix effects of activated carbon during the digestion step. Other factors that may enhance procedure recovery or reduce the time of the procedure were also considered. Thus, our objective here is to test the effect of various variables on the recovery obtained with the microwave-digestion procedure.

3.1.1. Effect of digestion time and ashing time

Using 0.1000 g sample and 1.00 ml of 18 M H_2SO_4 solution, the effective digestion time was varied between 0.5 and 10 min. The obtained results are plotted in Fig. 1. From Fig. 1, it is clear that the best recovery (68%) was obtained when 4 min of effective digestion time was used. Shorter time gave lower recovery while longer time did not improve the recovery. Varying time of ashing was then studied (Fig. 2), while effective digestion
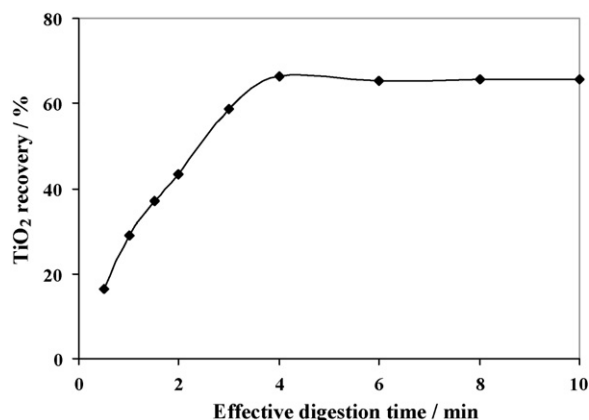
Fig. 1. Effect of effective digestion time on the percentage recovery of TiO_2 (sample not pulverized, no ashing, no digestion catalyst added, 1 ml of 18.0 M H_2SO_4).

time was maintained at 4 min and other procedure conditions were maintained as well. It is seen from Fig. 2 that best recovery of TiO_2 could be obtained (90%) with 240 min of ashing.

3.1.2. Effect of volume and concentration of sulfuric acid and presence of digestion catalyst

It was thought that addition of a digestion catalyst, to this stage of optimized conditions, can improve the recovery, but this did not happen. When the same experiment was repeated by adding a digestion catalyst and without ashing, the TiO_2 recovery decreased probably due to the large amount of solid relative to the amount of liquid. But when 2.00 ml H_2SO_4 was added, instead of 1.00 ml, with the same conditions (no ashing step, digestion catalyst was added, 4 min digestion, 18.0 M H_2SO_4), the recovery increased to 95.5% without the need to an ashing step. Doubling the catalyst amount reduced the recovery due to inappropriate ratio of solid to liquid. Thus, it is important here to use an appropriate volume (of sulfuric acid) to digestion catalyst ratio. Varying the volume of sulfuric acid (with constant amount of digestion catalyst of 0.4 g and without ashing) gave the results shown in Fig. 3, in which best recovery was obtained when 3.00 ml of 18 M H_2SO_4 was used.
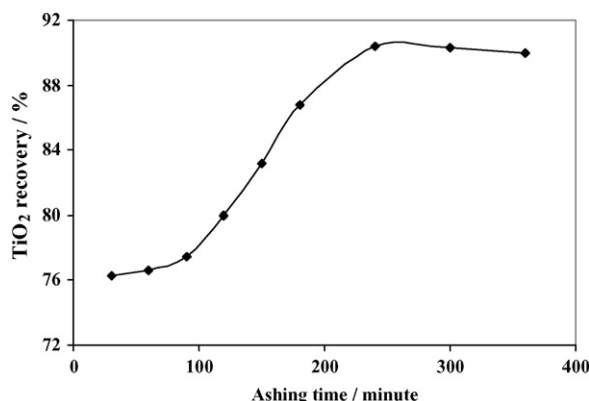
Fig. 2. Effect of ashing time on the percentage recovery of TiO_2 (sample not pulverized, no digestion catalyst added, 4 min digestion, 1 ml of 18.0 M H_2SO_4).
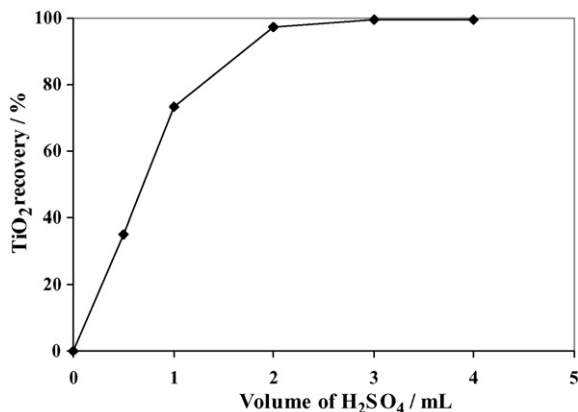
Fig. 3. Effect of sulfuric acid volume (18.0 M) on percentage recovery of TiO$_2$ (sample pulverized, no ashing, 0.4 g digestion catalyst added, 4 min digestion).

Varying sulfuric acid concentration was also studied (Fig. 4), in which it is clear that decreasing the sulfuric acid concentration significantly reduced the recovery. As it is seen, the best recovery was obtained with 18.0 M H$_2$SO$_4$. When the experiment was repeated without the catalyst but under the same other optimized conditions, the recovery decreased to 86.6%, which indicates the positive catalyst role in the digestion process.

3.1.3. Effect of sample pulverization

Further recovery increase was obtained with sample pulverization. With all the optimized conditions (no ashing, 3.00 ml of 18.0 M H$_2$SO$_4$, digestion catalyst added, 4 min digestion, sample pulverized to pass 100 mesh screen), the recovery could be improved up to 99.7%.

3.1.4. Effect of on–off time cycle of the microwave

On–off time cycle of the microwave oven was varied. It was found that when using 60–30, 45–30 and 30–15 (second–second) on–off time cycles, overheating occurred in the early stages of the digestion process and some acid was lost. When 15/15-time cycle was used, digestion was slow and recovery was low probably because energy supplied was not sufficient to cause complete sample digestion within the specified diges-
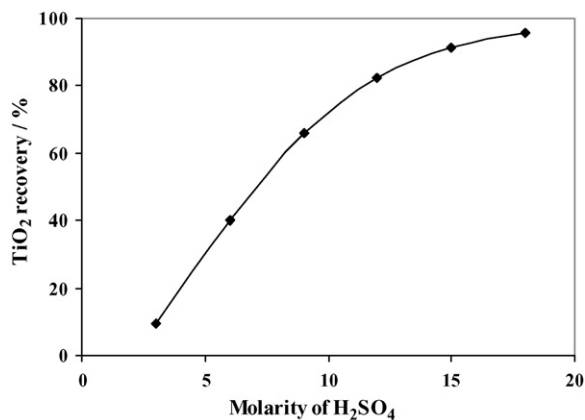
Fig. 4. Effect of sulfuric acid concentration on percentage recovery of TiO$_2$ (sample not pulverized, no ashing, 0.4 g digestion catalyst added, 4 min digestion, 2 ml of 18.0 M H$_2$SO$_4$).
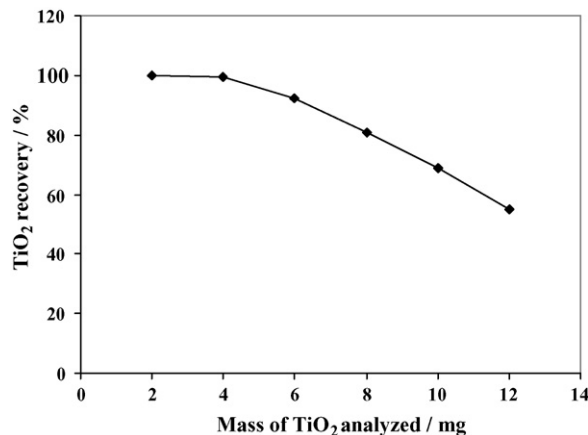
Fig. 5. Effect of mass of TiO$_2$ analyzed (sample mass) on percentage recovery of TiO$_2$ (sample pulverized, no ashing, 0.4 g digestion catalyst added, 3.00 ml of 18 M H$_2$SO$_4$, 4 min digestion).

tion time. When 30–30 on–off time cycle was used, digestion was finished without gas evolution and with almost full recovery (99.7%).

3.1.5. Effect of TiO$_2$ mass contained in the photocatalyst sample (sample mass)

The effect of sample mass was studied by applying the optimized microwave-digestion procedure on various masses of samples containing various amounts of TiO$_2$. Fig. 5 shows recovery change with mass of digested TiO$_2$ in the tube. It is clear that to obtain the full recovery; the mass of TiO$_2$ in the sample should not exceed 4 mg TiO$_2$.

3.1.6. Effect of carbon source

Effect of carbon source was also studied by applying the proposed microwave procedure on various photocatalyst samples prepared using various activated carbons (from Norit, Darco, Sigma and home-made activated carbons) and containing similar amounts of TiO$_2$. The analysis showed a small variation (less than 3% R.S.D.) for different carbon sources.

3.2. Analytical precision

Six photocatalyst (TiO$_2$/AC) samples were analyzed for TiO$_2$ (in four replicates) by the proposed microwave procedure and by

Table 1
Precision of TiO$_2$ determination after digestion with the microwave procedure, Myers et al.'s procedure and Short et al.'s procedure

Sample identification (mg added TiO$_2$/g photocatalyst)	R.S.D. (%) of the found TiO$_2$ ($n = 4$)		
	Microwave procedure	Myers et al.'s procedure	Short et al.'s procedure
18.0	2.39	2.56	4.85
33.0	2.02	2.20	3.70
54.2	1.75	1.86	2.71
75.9	1.70	1.76	2.38
97.4	1.52	1.48	2.06
112.5	1.42	1.46	1.63

Table 2

Comparative determination of TiO_2 in TiO_2/AC photocatalyst samples after digestion with the proposed microwave procedure, Myers et al.'s procedure and Short et al.'s procedure ($n = 4$)

Sample identification (mg added TiO_2/g photocatalyst)	Found TiO_2/g sample ($\pm 95\%$ confidence limits)		
	Microwave procedure	Myers et al.'s procedure	Short et al.'s procedure
18.0	18.2 (± 0.4)	17.9 (± 0.4)	11.5 (± 0.5)
33.0	33.1 (± 0.7)	32.5 (± 0.7)	22.1 (± 0.8)
54.2	54.0 (± 0.8)	53.0 (± 0.8)	35.3 (± 0.9)
75.9	74.7 (± 0.9)	74.7 (± 0.9)	50.2 (± 0.8)
97.4	96.4 (± 0.9)	94.7 (± 0.9)	65.5 (± 0.9)
112.5	111 (± 2)	110 (± 2)	73.9 (± 0.9)
Recovery range (%)	98.4–101.1	97.3–99.2	63.8–67.2
Relative error range (%)	0.384–1.61	0.800–2.74	32.8–36.2

the previously published procedures (Myers et al.'s and Short et al.'s procedure). The results are shown in Table 1, in which it can be concluded that the analytical precision is nearly equal for the proposed microwave procedure and the Myers et al.'s procedure, while the scatter of the results obtained using the Short et al.'s procedure was higher (1.30–4.85% R.S.D.). However the three procedures gave less than 5% R.S.D.

3.3. Analytical accuracy

Photocatalyst (TiO_2/AC) samples were digested by the proposed microwave-digestion procedure and analyzed for the TiO_2 as outlined in Section 2.3. The same samples were also analyzed for TiO_2 by the Myers et al. and Short et al. procedures as outlined in Section 2.4. Four replicates of each sample were analyzed and the average found concentration of TiO_2 ($\pm 95\%$ confidence limits) was recorded in Table 2.

Compared to Myers et al.'s procedure, which has been originally used for TiO_2 analysis in feed and excreta samples; the recovery of TiO_2 by the proposed microwave procedure ranges between 98.4 and 101.1%. This is slightly higher than the quoted recoveries of the Myers et al.'s procedure for the same TiO_2/AC photocatalyst samples, which ranged from 97.3 to 99.2%. However, Myers et al. [17] reported that 4 h and half are required to analyze one sample. But with the proposed microwave-digestion procedure, we could analyze four photocatalyst samples in less than half an hour.

The recoveries of TiO_2 for the same samples treated with the Short et al.'s procedure were much lower than the proposed microwave procedure, and ranged from 63.8 to 67.2%. Fig. 6 shows relationships between the found TiO_2 using the proposed microwave procedure against the found TiO_2 using Myers et al.'s procedure and Short et al.'s procedure.

3.4. Linearity and limit of detection

The calibration curves for TiO_2 are linear ($R^2 > 0.9996$) within the studied concentration range (18.0–112.5 mg TiO_2/g photocatalyst) for all the three procedures. Calibration curves have slopes of 0.0971(± 0.000296), 0.0960(± 0.000301) and 0.0655(± 0.000578) absorbance unites (AU) per (mg
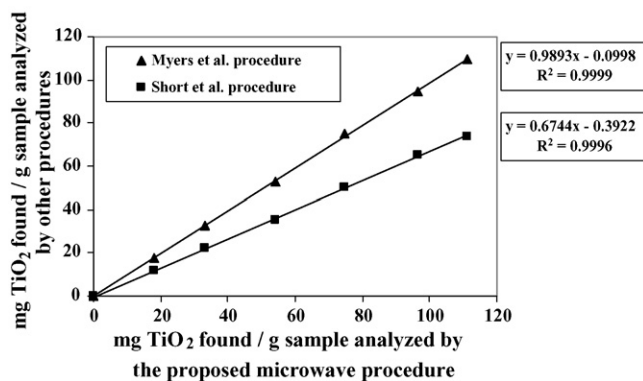
Fig. 6. Relationships between the found TiO_2 using the proposed microwave procedure against the found TiO_2 using Myers et al.'s procedure and Short et al.'s procedure.

TiO_2/g photocatalyst) and y-intercepts of 0.0330(± 0.0201), 0.0250(± 0.0204) and -0.0170(± 0.0192) (mg TiO_2/g photocatalyst) for the microwave procedure, Myers et al.'s procedure and Short et al.'s procedure, respectively.

The limits of detection were calculated (4 replicate blank runs) and found to be 0.0981, 0.124 and 0.281 (mg TiO_2/g photocatalyst) for the microwave procedure, Myers et al.'s procedure and Short et al.'s procedure, respectively.

4. Conclusion

The proposed microwave digestion of TiO_2/AC photocatalyst is a fast and simple method of sample treatment prior to TiO_2 spectrophotometric analysis. This is superior to other procedures because: (1) it is capable of full recovery of TiO_2 in much shorter digestion time, (2) no ashing step is required, (3) less chemicals and sample size are required and (4) many samples can be treated simultaneously. Ashing is not necessary because complete recovery is obtained without ashing. The use of sulfuric acid is an appropriate digesting reagent in this procedure, which is capable of dissolution of TiO_2 while activated carbon will remain undigested. This is appropriate since this will reduce the complexity of the matrix and thus reduce possible interferences. The % recovery of TiO_2 is affected by sample particle size, the presence of a digestion catalyst and the concentration

and volume of sulfuric acid. Complete analysis of four samples is possible in 30 min by the use of the proposed microwave procedure. Precision, accuracy and other figures of merit of the proposed microwave procedure are comparable to or even better than that of Myers et al.'s procedure.

Acknowledgements

References

[1] A. Mills, R. Davis, D. Worsley, Chem. Soc. Rev. 21–22 (1993) 417.
[2] M. Hoffmann, S. Martin, W. Choi, D. Bahnmann, Chem. Rev. 95 (1995) 69.
[3] M. Fox, M. Dulay, Chem. Rev. 93 (1993) 341.
[4] H. Yoneyama, T. Torimoto, Catal. Today 58 (2000) 133.
[5] R. Pelegrini, R. Freire, N. Duran, R. Bertazzoli, Environ. Sci. Technol. 35 (2001) 2849.
[6] A. Prakash, S. Solanki, Sorption Res. Ind. 38 (1993) 35.
[7] R. Suri, J. Liu, D. Hand, J. Crittenden, D. Perram, J. Air Waste Manage. Assoc. 49 (1999) 951.
[8] N. Takeda, T. Torimoto, S. Sampath, S. Kuwabata, H. Yoneyama, J. Phys. Chem. 99 (1995) 9986.
[9] Z. Ding, X. Hu, P. Yue, G. Lu, P. Greenfield, Catal. Today 68 (2001) 173.
[10] M. Nozawa, K. Tanigawa, M. Hosomi, T. Chikusa, E. Kawada, Water Sci. Technol. 44 (2001) 127.
[11] H. Uchida, S. Itoh, H. Yoneyama, Chem. Lett. (1993) 1995.
[12] N. Takeda, M. Ohtani, T. Torimoto, S. Kuwabata, H. Yoneyama, J. Phys. Chem. B 101 (1997) 2644.
[13] T. Torimoto, S. Ito, S. Kuwabata, H. Yoneyama, Environ. Sci. Technol. 30 (1996) 1275.
[14] T. Torimoto, Y. Okawa, N. Takeda, H. Yoneyama, J. Photochem. Photobiol. A: Chem. 103 (1997) 153.
[15] A.H. El-Sheikh, A.P. Newman, H. Al-Daffaee, S. Phull, N. Cresswell, S. York, Surf. Coat. Technol. 187 (2004) 284.
[16] J.H. Yoe, A.R. Armstrong, Anal. Chem. 19 (1947) 100.
[17] W.D. Myers, P.A. Ludden, V. Nayigihugu, B.W. Hess, J. Anim. Sci. 82 (2004) 179.
[18] L.R. Njaa, Acta Agric. Scand. 11 (1961) 227.
[19] L.J. Leone, J. AOAC 56 (1973) 535.
[20] F.J. Short, P. Gorton, J. Wiseman, K.N. Boorman, Anim. Feed Sci. Technol. 59 (1996) 215.
[21] E.C. Titgemeyer, C.K. Armendariz, D.J. Bindel, R.H. Greenwood, C.A. Loest, J. Anim. Sci. 79 (2001) 1059.
[22] J. Muhlebach, K. Muller, G. Schwarzenbach, Inorg. Chem. 11 (1970) 2381.
[23] G.H. Jeffrey, J. Bassett, J. Mendham, R.C. Denney, Vogel's Textbook of Quantitative Chemical Analysis, fifth ed., Longman Scientific and Technical, Essex, England, 1989.
[24] B. Bagshawe, J. Soc. Chem. Ind. 57 (1938) 260.
[25] F.D. Snell, C.T. Snell, Colorimetric Methods of Analysis, D. Van Norstrand Co. Inc., New York, 1949, p. 438.
[26] K.E. Levine, R.A. Fernando, M. Lang, A. Essader, B.A. Wong, Anal. Lett. 36 (2003) 563.
[27] M.G.A. Korn, A.C. Ferreira, A.C.S. Costa, J.A. Nobrega, C.R. Silva, Microchem. J. 71 (2002) 41.

Simultaneous kinetic determination of thiocyanate and sulfide using eigenvalue ranking and correlation ranking in principal component-wavelet neural network

Ali A. Ensafi [*], T. Khayamian, R. Tabaraki

College of Chemistry, Isfahan University of Technology, Isfahan 84156-83111, Iran

Abstract

In this work, two toxic compound, sulfide and thiocyanate were determined simultaneously using kinetic spectrophotometry. These anions have shown the catalytic effects on the reaction between iodine and azide. Since the system was nonlinear, a nonlinear model, principal component-wavelet neural network (PC-WNN) was used as the multivariate calibration method. The principal component analysis was used to decrease the dimension of the original matrix. In other words, the scores of the PCs, 5, instead of the original variables, 301, were used as the input for the model. Two methods were used to select the most relevant principal components: eigenvalue ranking and correlation ranking. In this work, eigenvalue and correlation ranking methods have shown better results for thiocyanate and sulfide, respectively, and it can be concluded that these methods are complementary. The WNN has several advantages relative to other types of neural network such as better convergence ability. The data set was divided to calibration, prediction and validation sets. Each set was selected so that the concentrations of the analytes were approximately covered the entire ranges of the analytes. Mean relative error for thiocyanate and sulfide in validation set were 8.5 and 10.6, respectively. Thiocyanate and sulfide can be determined in the range of 60–700 ng ml^{-1} and 20–400 ng ml^{-1}, respectively. The proposed method was applied for the determination of sulfide and thiocyanate in real samples such as tap, waste and river waters with satisfactory results.
© 2006 Elsevier B.V. All rights reserved.

Keywords: Wavelet neural network; Principal component analysis; Correlation ranking; Eigenvalue ranking; Thiocyanate; Sulfide

1. Introduction

Determination of sulfur anions is important to a variety of studies including groundwater monitoring, food analysis, and assessment of biogeochemical process and in environmental, clinical and industrial samples. It is also playing an important role in the purity assays of chemical and pharmaceutical products [1–6]. From an environmental point of view, the large amount of water containing significant concentration of sulfur-bearing ions is often generically referred to "sour water"[7]. Thus, the simultaneous determination of sulfur species is necessary and some easy and inexpensive methods should be improved. Numerous instrumental methods are available for the determination of sulfide or thiocyanate individually. Some of them are based on the kinetic spectrophotometric methods [8,9], and some use other methods such as ion chromatography [10,11], potentiometry and ion selective electrodes [12,13], capillary electrophoresis [14,15] and gas chromatography [16,17]. In individual determination of sulfide or thiocyanate, kinetic methods [8,9] have better detection limits with respect to ion chromatography [10,11], potentiometry [12,13] and capillary electrophoresis methods [14,15]. However, the gas chromatography methods [16,17] have the lowest detection limits, but the anions must be derivitized with pentafluorobenzyl bromide in order to make them suitable for the measurement. There are few reports for the simultaneous determination of both analytes. These methods are based on ion chromatographic methods [18–23]. These methods have very low detection limits but they need a separation technique before the analysis. Based on our search, however, there are only two papers for simultaneous determination of sulfide and thiocyanate by spectrophotometric methods. Belcher et al. [24] have shown that nanogram amounts of these anions may be determined in samples of a few microliter by molecular emission cavity analysis. In another work, flow-injection

---

* Corresponding author. Tel.: +98 311 3912351; fax: +98 311 3912350.
E-mail address: Ensafi@cc.iut.ac.ir (A.A. Ensafi).

method with flame molecular emission spectrometric detection was used to compare the disulfur emission from sulfite, thiosulfate, sulfide, thiocyanate, diethyldithiocarbamate and colloidal sulfur with that of sulfate. Counter ions were replaced with hydronium through the use of an on-line ion-exchange column [25].

Multicomponent kinetic methods are able to determine and resolve the components based on the differences of their behavior with respect to a common reagent [26]. The kinetic methods have advantages such as selectivity, sensitivity and simple instrumentation. These methods can be associated with different techniques such as chemometrics that could resolve multicomponent kinetic systems without requiring their prior separation. Sensitive photometric determination of sulfide [27–30], thiosulfate [31,32] and thiocyanate [8] have been reported by means of their catalytic effects on the reaction between iodine and azide. This reaction was also employed as a post column reaction for detection of the sulfur anions in ion chromatography [20].

Since the relationship between analytes concentration and absorbance variation with time is essentially nonlinear, artificial neural network (ANN) and wavelet neural network (WNN), which is modeling methods for nonlinear systems, can be dealt with this type of nonlinear kinetic reactions. Wavelet neural network is a novel approach towards the learning function. Wavelet networks, which combine the wavelet theory and feedforward neural networks, utilize wavelets as the basis function to construct a network. Wavelet function is a local function and influences the networks' output only in some local ranges. The wavelet neural network shows surprising effectiveness in solving the conventional problems of poor convergence or even divergence encountered in other kinds of neural networks [33].

Principal component analysis is a useful mathematical technique that has found many applications in multivariate data analysis. One of its applications is reducing the dimension of the data matrix to a several independent and orthogonal principal components. Principal component-artificial neural network (PC-ANN) [34–37] and principal component-wavelet neural network (PC-WNN) [38] are powerful nonlinear modeling systems which have been used for simultaneous spectrophotometric determinations. The dimensional reduction by principal component analysis (PCA) before model construction has advantages such as increasing numerical stability of model, reducing the amount of co-linearity between variables [39]. The scores of the principal component analysis of the response data are used as inputs for the models. Selecting the significant and informative PCs is the main problem in almost all of the PCA-based calibration methods [40–47]. The simplest and the most common method is a top-down variable selection where the PCs are ranked in the order of decreasing eigenvalue. The PC with highest eigenvalue is considered as the most significant one. Another method for selection of the most relevant PCs is called correlation ranking. In this method, the PCs are ranked by their correlation coefficient with the property to be correlated (i.e. the dependent variable) [46,47].

In this work, principal component-wavelet neural network is proposed for simultaneous determination of thiocyanate and sulfide based on their catalytic effects on the indicator reaction between iodine and azide. Two methods are used to select the most relevant principal components: eigenvalue (EV) ranking and correlation (CR) ranking. In this work, eigenvalue and correlation ranking methods have shown better results for thiocyanate and sulfide, respectively.

2. Theory

2.1. Wavelet

Wavelet transform (WT) is a novel signal processing technique developed from the Fourier transform and has been widely used to signal processing. The main characteristic of wavelet transform is its time–frequency localization. Wavelet transformation (WT) has versatile basis functions to be selected based on the type of the signal analyzed. In WT, all basis function $\psi_{a,b}(x)$ can be derived from a mother wavelet $\psi(x)$ through the following dilation and translation processes:

$$\psi_{a,b}(x) = a^{-1/2}\psi\left(\frac{x-b}{a}\right) \quad a, b \in R \text{ and } a > 0 \tag{1}$$

where the parameters of translation are $b \in R$ and of dilation are $a \in R$ and $a > 0$ (R denotes real number). The mother wavelet, $\psi(x)$, is a single fixed function such as Morlet function from which, all basis functions are generated.

Wavelet has been used in processing analytical data such as compression, denoising, variable selection and feature selection [48]. Wavelet functions were also used as basis functions in neural networks [49–53].

2.2. Wavelet neural networks

The topological structure of the WNN employed in this study is shown in Fig. 1. The WNN consists of three layers: input
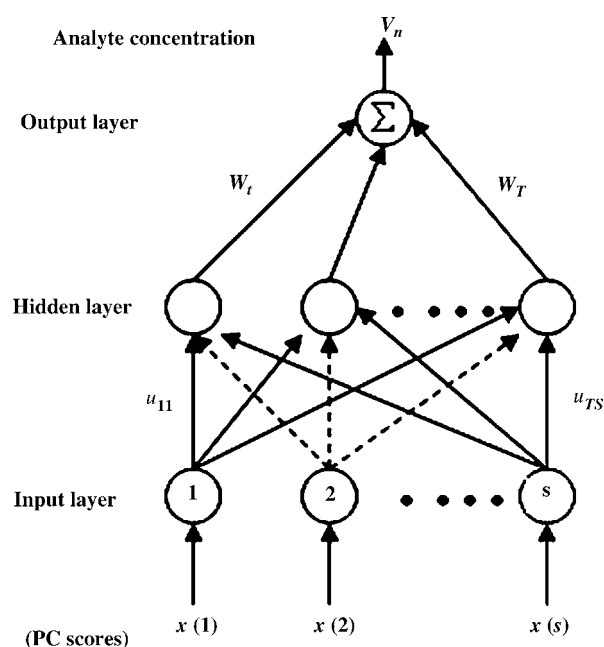

Fig. 1. The WNN topology structure.

layer, hidden layer and output layer. The detailed description of calculation steps of WNN and its applications are described in Refs. [33,52,53]. In brief, the connections between input units and hidden units are called weights u_{ti} and between hidden units and output units are called w_t. A Morlet mother function is used as node activation function for the hidden layer. The dilation and translation parameters, a_t and b_t, of the Morlet function for each node in the hidden layer are different and they need to be optimized. In the WNN, the gradient descend algorithm is employed and the error is minimized by adjusting w_t, u_{ti}, a_t, b_t parameters. In addition to these weights, number of hidden nodes, learning rate, momentum and number of iterations need to be optimized [38].

In the WNN, the following steps are carried out:

(1) Initializing the dilation parameter a_t, translation parameter b_t and node connection weights u_{ti}, w_t to some random values. All those random values are limited in the interval (0, 1).
(2) Inputting data $x_n(i)$ and corresponding output values v_n^T, where the superscript T represents the target output state.
(3) Propagating the initial signal forward through the network using

$$v_n = \sum_{t=1}^{T} w_t h \left(\frac{\sum_{i=1}^{s} u_{ti} x_n(i) - b_t}{a_t} \right) \tag{2}$$

where h is taken as a Morlet wavelet

$$h(t) = \cos(1.75t) \exp\left(-\frac{t^2}{2}\right) \tag{3}$$

(5) Calculation of the WNN parameters:

$$\Delta w_t^{\text{new}} = -\eta \frac{\partial E}{\partial w_t^{\text{old}}} + \alpha \, \Delta w_t^{\text{old}} \tag{4}$$

$$\Delta u_{ti}^{\text{new}} = -\eta \frac{\partial E}{\partial u_{ti}^{\text{old}}} + \alpha \, \Delta u_{ti}^{\text{old}} \tag{5}$$

$$\Delta a_t^{\text{new}} = -\eta \frac{\partial E}{\partial a_t^{\text{old}}} + \alpha \, \Delta a_t^{\text{old}} \tag{6}$$

$$\Delta b_t^{\text{new}} = -\eta \frac{\partial E}{\partial b_t^{\text{old}}} + \alpha \, \Delta b_t^{\text{old}} \tag{7}$$

The error function E is taken as

$$E = \frac{1}{2} \sum_{n=1}^{N} (v_n^T - v_n)^2 \tag{8}$$

where v_n^T and v_n are the experimental and calculated values, respectively. N stands for the data number of training set, and η and α being the learning rate and the momentum term, respectively.

(5) The WNN parameters were changed until the network output satisfies the error criteria.

3. Experimental

3.1. Apparatus and software

A spectrophotometer (Jasco V-570) equipped with 0.50 cm quartz cell was used for the absorbance measurements. A thermostat (Gallenkamp Griffine, BJL-420-V) was used to keep the reaction temperature at 25 °C. Data processing was performed by a Pentium IV computer. The WNN algorithm was written in MATLAB (Math Work, version 6.1) 6.1 by the authors.

3.2. Reagents and chemicals

All solutions were prepared with doubly distilled water. All chemicals were of analytical reagent grade.

A stock solution of sodium azide, 2.5 mol l^{-1}, was prepared by dissolving 16.414 g of sodium azide, Merck, NaN$_3$, in water and diluted in a 100-ml volumetric flask.

A stock solution of iodine, I$_3^-$, 0.010 mol l^{-1}, was prepared by dissolving 0.2540 g of I$_2$, Merck, in potassium iodide solution (4.500 g KI/100 ml) in a 100-ml volumetric flask.

A stock solution of sulfide, 1000 μg ml^{-1}, was prepared by dissolving 1.5000 g of sodium sulfide, Na$_2$S·9H$_2$O Merck, in a basic medium, NaOH, and diluting to 100-ml. The solution was standardized iodometrically. Working solutions were prepared daily from this stock solution by appropriate dilution with water.

A stock solution of thiocyanate, 1000 μg ml^{-1}, was prepared by dissolving 0.1695 g of potassium thiocyanate, Merck, KSCN, in water and diluted in a 100-ml volumetric flask.

3.3. General procedure

All the solutions were kept in a thermostated water bath at 25 °C for 20 min before beginning of the experiment. To a solution containing different amounts of anions in a 10-ml volumetric flask, 1 ml of buffer solution (acetate, pH 4.5) and 0.20 ml of 2.5 mol l^{-1} NaN$_3$ solution were added and the solution was diluted to ca. 8 ml with water. Then 1.0 ml of 0.0018 mol l^{-1} iodine solution was added and the solution was diluted to the mark with water and mixed well. The stopwatch was turned on when the last drop of iodine solution had fallen. Immediately, an appropriate quantity of the reacting solution was transferred into the cell chamber and the change in absorbance at 349 nm (absorption maximum of iodine) was recorded against water after 0.5–5.5 min from beginning of the reaction with 1 s as intervals. The blank solution was treated as the same procedure.

3.4. Binary solutions

Three sets of standard solutions containing the two anions were prepared so that the correlation between concentrations of the two anions was avoided. Each set was selected so that the concentrations of the analytes were approximately covered the entire ranges of the analytes. The calibration and prediction set were used to optimize the network parameters. Prediction set was used to prevent to overfitting of the model. It is necessary to emphasis that the validation set does not participate in

the optimization of the model and only uses for evaluation of the performance of the model. The composition of calibration set solutions is given in Table 2. The calibration and the prediction sets were 25 and 6 standard solutions, respectively. The validation set was six standard solutions. The solutions were prepared by adding different volumes of standard solutions of the anions in 10-ml volumetric flasks. For example, the first solution in Table 2, with the concentrations of $60\,\text{ng}\,\text{ml}^{-1}$ of SCN^- and $20\,\text{ng}\,\text{ml}^{-1}$ of S^{2-} was prepared by adding 0.60 ml of the standard solution of $1000\,\text{ng}\,\text{ml}^{-1}$ of SCN^- and 0.20 ml of the standard solution of $1000\,\text{ng}\,\text{ml}^{-1}$ of S^{2-} to 1 ml buffer solution (acetate, pH 4.5) and 0.20 ml of $2.5\,\text{mol}\,\text{l}^{-1}$ NaN_3 solution in a 10-ml volumetric flask. The solution was diluted to ca. 8 ml with water and then 1.0 ml of $0.0018\,\text{mol}\,\text{l}^{-1}$ iodine solution was added and the solution was diluted to the mark with water and mixed well. The absorption spectra of the solutions were recorded at 349 nm after 0.5–5.5 min from beginning of the reaction in 1 s intervals. The concentration of the anions in the standard solutions was $20–400\,\text{ng}\,\text{ml}^{-1}$ for sulfide and $60–700\,\text{ng}\,\text{ml}^{-1}$ for thiocyanate.

3.5. Data processing

Since 301 data points were recorded for each solution, therefore, the response data of the calibration set was a matrix with 25×301 dimensions. The calibration data matrix ($\mathbf{X}_{cal}$) was subjected to principal component analysis (PCA) using the singular value decomposition (SVD) [54]:

$$\mathbf{X}_{cal} = \mathbf{U}_{cal}\mathbf{S}_{cal}\mathbf{V}_{cal}^{T} \qquad (9)$$

where $\mathbf{U}_{cal}$ and $\mathbf{V}_{cal}$ are the orthonormal matrices which spanned the respective row and column spaces of the data matrix ($\mathbf{X}_{cal}$). $\mathbf{S}_{cal}$ is a diagonal matrix whose elements are the square root of the eigenvalues. The superscript T denote the transpose of the matrix. The eigenvectors included in $\mathbf{U}_{cal}$ are named as principal components (PCs).

The scores of the PCs were selected as input nodes in wavelet neural network. Two methods are used to select the most relevant principal components: eigenvalue (EV) ranking and correlation (CR) ranking. The PC-WNN architectures were different for sulfide and thiocyanate. The number of PCs as an input layer, the number of nodes in hidden layer and other parameters except the number of iterations were optimized simultaneously. In other words, the best value for each variable was not obtained by "one at a time" optimization method.

3.6. Real samples

Water samples were sampled in a Teflon bottle and storage at 4 °C before analysis. The samples were filtered (using filter 0.42 μm) and analyzed before 5 h of sampling. The filtered samples were analyzed with the proposed method. To a 10 ml volumetric flask containing 5.0 ml water sample, 1 ml buffer solution (acetate, pH 4.5) and 0.20 ml of $2.5\,\text{mol}\,\text{l}^{-1}$ NaN_3 solution were added and the solution was diluted to ca. 8 ml with water. Then 1.0 ml of $0.0018\,\text{mol}\,\text{l}^{-1}$ iodine solution was

added and the solution was diluted to the mark with water. The stopwatch was turned on when the last drop of iodine solution had fallen. Immediately, an appropriate quantity of the reacting solution was transferred into the cell chamber and the change in absorbance at 349 nm was recorded against water after 0.5–5.5 min from beginning of the reaction. Then the thiocyanate and sulfide contents were calculated from the model. The relative error was calculated according to the analytes spiked to the samples.

4. Results and discussion

It was found that some oxidants such as iodine could oxidize sodium azide. The reaction proceeds very slowly at pH 5. However, the oxidation of sodium azide by iodine is increased rapidly in the presence of sulfide and thiocyanate. The reaction can be followed spectrophotometrically by monitoring the change in the absorbance at 349 nm (absorption maximum of iodine).

The optimum experimental conditions such as pH, azide concentration, iodine concentration, time and temperature for kinetic determination of sulfide and thiocyanate have been previously reported [14,18]. For their simultaneous determination, the optimization process was repeated and Table 1 shows the optimized experimental conditions. Sulfide and thiocyanate are catalyzed the oxidation of sodium azide by iodine and the decrease of absorbance of iodine at 349 nm was recorded during 300 s in one second intervals. The absorbance–time behavior of the reaction mixture is shown in Fig. 2a. In addition, the variation of iodine spectrum versus the total concentration of sulfide and thiocyanate are shown in Fig. 2b.

Three sets of standard solutions, calibration, prediction and validation sets were prepared, so that the correlation between concentrations was avoided. The composition of calibration set solutions is given in Table 2. Since 301 data points were recorded for each solution, therefore, the response data of the calibration set was a matrix with 25×301 dimensions. The principal component analysis (PCA) was applied to the data set for dimensional reduction and the scores of the PCs were selected as input nodes in wavelet neural network. The PC-WNN architectures were different for sulfide and thiocyanate.

A major question will arise: how many and which PCs constitute a good subset for predictive purpose? Hence, selecting the significant and informative PCs is the main problem in almost all of the PCA-based calibration methods [31–38].

Table 1
The optimized experimental conditions

pH (acetate)	4.5
Azide concentration (mol l^{-1})	0.05
Iodide concentration (mol l^{-1})	1.8×10^{-4}
Time (s)	300
Temperature (°C)	25
λ_{max} (nm)	349
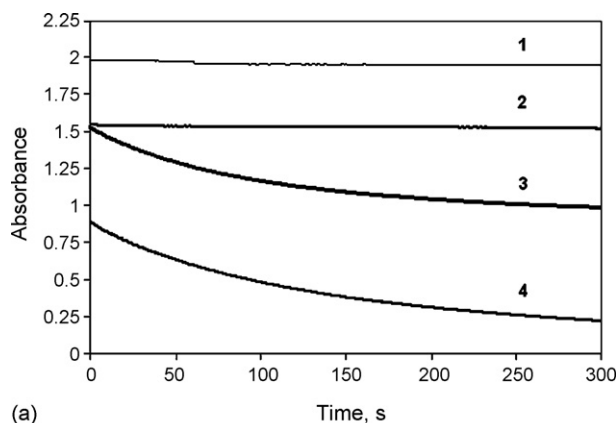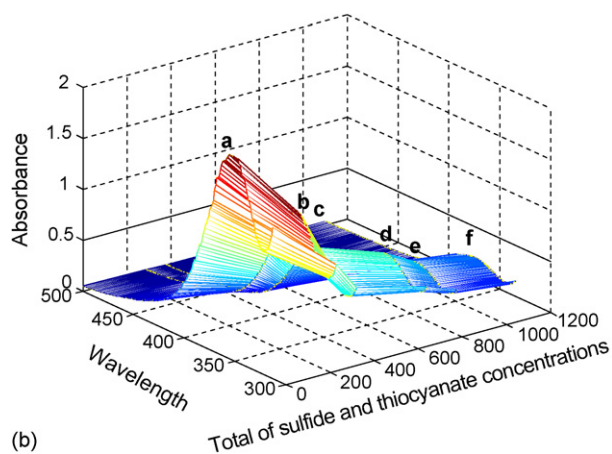
Fig. 2. (a) Absorbance changes vs. time (s) recorded at 349 nm. (1) Blank solution; (2) sulfide, $100.0\,ng\,ml^{-1}$; (3) thiocyanate, $200.0\,ng\,ml^{-1}$; (4) mixture of 2 plus 3. Conditions: pH 4.5; azide, $0.050\,mol\,l^{-1}$; iodine, $1.8\times10^{-4}\,mol\,l^{-1}$; temperature, 25 °C. (b) Landscape for the variation of iodine spectrum vs. the total concentrations of the analytes for mixture of sulfide and thiocyanate; (a) 0.0, $0.0\,ng\,ml^{-1}$; (b) 140.0, $150.0\,ng\,ml^{-1}$; (c) 120.0, $260.0\,ng\,ml^{-1}$; (d) 360.0, $340.0\,ng\,ml^{-1}$; (e) 430.0, $405.0\,ng\,ml^{-1}$; (f) 700.0, $400.0\,ng\,ml^{-1}$, respectively. Conditions: pH 4.5; azide, $0.050\,mol\,l^{-1}$; iodine, $1.8\times10^{-4}\,mol\,l^{-1}$; temperature, 25 °C.

4.1. Eigenvalue ranking

The simplest and the most common method is a top-down variable selection where the PCs are ranked in the order of decreasing eigenvalue. The PC with highest eigenvalue is considered as the most significant one and subsequently, the PCs are introduced into the calibration model one after the other until no further improvement of the calibration model is obtained.

WNN models were developed using different number of the PCs in input layer. The WNN variables consisted of the number of PCs as an input layer, the number of nodes in the hidden layer, the learning rate, the momentum and the number of epochs, which optimized for each anion separately. In this work, the number of PCs as an input layer, the number of nodes in hidden layer and other parameters except the number of iterations were optimized simultaneously. In other words, the best value for each variable was not obtained by "one at a time" optimization method. The number of PCs in input layer can be changed from 1 to 8, while the number of nodes in hidden layer from 2

Table 2
Composition of solutions used for the calibration set

Solution number	SCN^- $(ng\,ml^{-1})$	S^{2-} $(ng\,ml^{-1})$
1	60	20
2	80	220
3	90	350
4	100	40
5	120	260
6	140	150
7	160	320
8	200	80
9	240	280
10	280	370
11	300	200
12	320	30
13	360	120
14	380	330
15	400	50
16	420	140
17	460	240
18	480	360
19	520	130
20	540	70
21	580	380
22	620	60
23	640	170
24	680	210
25	700	400

to 8, the learning rate from 0.001 to 0.1 with a step of 0.001 and momentum from 0.1 to 0.99 with a step of 0.01. Each possible combination was named an index number. The WNN models were constructed with all of the possible combinations of those four variables. The root mean square error (RMSE) for calibration and prediction sets for each WNN model was calculated. The WNN model, which shows minimum RMSE for calibration and prediction sets, was selected as the optimized WNN model and the variables of this model were selected as the optimized variable values. The optimized variable parameters for thiocyanate and sulfide are given in Table 3. Fig. 3 shows the changes of the RMSE values against the index number for thiocyanate in the prediction set. Each number of index number corresponds to a combination of variable values and total number of index number is equal to the all possible combination of the variable values. Fig. 3 shows only the root mean square error for the prediction set for a subset of index number (200

Table 3
The optimized parameters for EV-PC-WNN[a] model

Parameters	SCN^-	S^{2-}
Input nodes	4	3
Hidden nodes	3	2
Output nodes	1	1
Learning rate	0.035	0.089
Momentum	0.91	0.29
Number of iterations	1000	1000
Hidden transfer function	Morlet	Morlet
Output transfer function	Linear	Linear

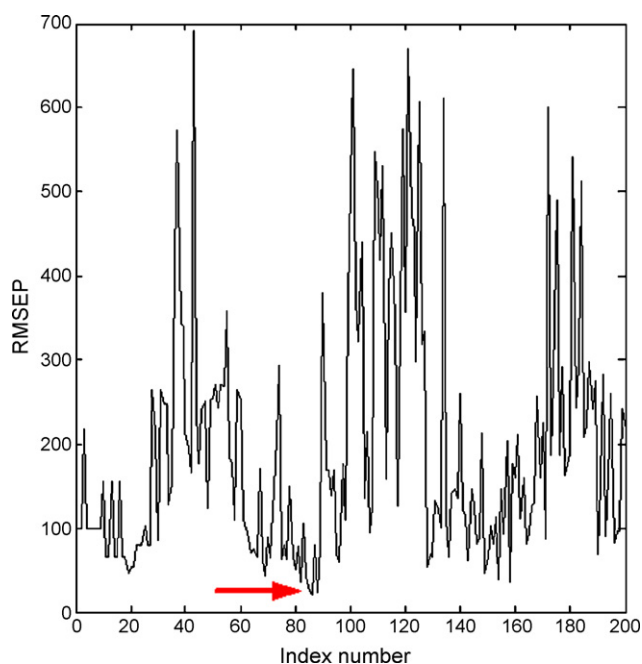[a] EV-PC-WNN: eigenvalue ranking-principal component-wavelet neural network.

Fig. 3. Plot of RMSE values against the index numbers for thiocyanate in the prediction set.

of possible variable combinations). Finally, the number of iterations was optimized with the optimized variable values. It was realized that at 1000 iterations, the RMSE errors for prediction set was minimum. The mean relative errors for thiocyanate and sulfide were 6.8 and 7.7 for the prediction set and 8.5 and 10.6 for the validation set, respectively. The results for prediction and validation sets are given in Tables 4 and 5.

4.2. Correlation ranking

Another method for selection of the most relevant PCs is called correlation ranking. In this method, the PCs are ranked by their correlation coefficient with the property to be correlated (i.e. the dependent variable).

Table 4
Prediction set composition and their predicted values with EV-PC-WNN model

Actual	Found	%RE
SCN^- (ng ml^{-1})		
70	83.1	18.7
220	236.2	7.4
440	404.3	8.1
560	574.3	2.6
600	599.5	0.08
660	634.6	3.8
Mean		6.8
S^{2-} (ng ml^{-1})		
110	100.4	8.7
160	158.0	1.2
100	94.3	5.7
250	213.4	14.6
270	301.4	11.6
310	295.9	4.6
Mean		7.7

Table 5
Validation set composition and their predicted values with EV-PC-WNN model

Actual	Found	%RE
SCN^- (ng ml^{-1})		
510	566.7	11.1
260	273.3	5.1
310	299.8	3.3
390	425.0	9.0
430	373.6	13.1
650	590.6	9.1
Mean		8.5
S^{2-} (ng ml^{-1})		
215	234.8	9.2
340	323.4	4.9
190	165.6	12.9
105	123.4	17.5
405	344.8	14.9
355	339.2	4.4
Mean		10.6

In order to rank the PCs based on their correlation coefficient with their corresponding anion concentration data, the linear correlation coefficient was not used because the relation between the concentration and PCs are not linear. Instead, the correlation coefficients were calculated by a nonlinear model such as WNN. The WNN was first used to calculate the nonlinear relationship between each one of the PCs and concentration separately. Thus, in this case, the WNN model had only one node in its input layer (an individual PC). In the case of each PC, the WNN parameters including of nodes in the hidden layer, momentum and learning rate were optimized simultaneously. Morlet and linear functions were used as hidden and output transfer functions, respectively. The best model in each case was used to calculate the coefficient of determination (R^2) between the calculated and experimental concentration for both calibration and prediction sets. This work was performed for each anion separately. The results are given in Table 6.

The correlative ability or informative contents of the PCs with respect to the concentration data does not show the same trend as their eigenvalues. The order of the PCs based on their decreasing correlation for thiocyanate is PC2 > PC1 > PC19 > PC11 > PC18 > PC7 > PC12 > PC8 > ····. The ranked PCs were then entered into the WNN model successively. When each new PC was introduced into the model, the WNN parameters were optimized simultaneously to reach to minimum of error. The results of this method for thiocyanate and sulfide are given in Tables 7 and 8 and compared with the results of eigenvalue ranking method.

Based on the results in the Table 7, it was found that the correlation ranking selection method has better results for thiocyanate. The mean relative error for prediction and validation sets was 5.6% and 7.1% with correlation ranking method but was 6.8% and 8.5% for eigenvalue ranking, respectively. The number of PCs in input layer of WNN model was three and four for correlation and eigenvalue ranking method, respectively.

The results Table 8 show that the eigenvalue ranking selection method is better than eigenvalue ranking selection method for sulfide. The mean relative error was 7.5% and 10.6% (eigen-

Table 6
The results of WNN for modeling between each one of PCs and anion concentrations

PC no.	SCN−		S²⁻	
	No. of hidden nodes	R^2	No. of hidden nodes	R^2
1	6	0.72	6	0.56
2	6	0.74	6	0.17
3	6	0.22	5	0.33
4	6	0.23	6	0.46
5	5	0.24	6	0.36
6	5	0.29	4	0.27
7	3	0.44	6	0.34
8	5	0.31	6	0.28
9	6	0.29	5	0.47
10	5	0.25	4	0.30
11	5	0.46	5	0.15
12	5	0.43	6	0.51
13	5	0.12	6	0.04
14	6	0.10	5	0.19
15	6	0.12	5	0.07
16	6	0.12	5	0.35
17	5	0.19	3	0.02
18	6	0.44	5	0.08
19	6	0.47	6	0.23
20	5	0.08	6	0.03

value ranking) and 14.7% and 31% (correlation ranking) for prediction and validation sets, respectively. The number of PCs in input layer of WNN model was six and three for correlation and eigenvalue ranking method, respectively.

Based on the above results, it can be concluded that for simultaneous determination of thiocyanate and sulfide, the correlation and eigenvalue ranking methods are complementary.

In this work the WNN architecture and its parameters were also examined for two neurons as the output layer. However the results were not good as the case that WNN architecture and its parameters were optimized for one neuron as the output layer. It is clear that when one neuron is in the output layer, the WNN architecture and its parameters were specifically optimized for one of the analyte and therefore, the results are superior than the WNN with two neurons at the output layer.

4.3. Interference study

Some cations and anions were checked for their possible interference effects on the determination of thiocyanate and sulfide by mixing 200 ng ml⁻¹ standard solution of thiocyanate and sulfide with an appropriate amount of foreign ions by the proposed method. The results are given in Table 9. An error of 5% in concentration was considered to be tolerable.

4.4. Real samples

In order to evaluate the applicability of the proposed method for real sample analysis, three different water samples was chosen for the analysis of sulfide and thiocyanate contents. The standard addition method was used three to four times for quantification of sulfide and thiocyanate concentration in the samples and mean values were considered as real values. The results are

Table 7
Results of CR-PC-WNN and comparison with EV-PC-WNN for SCN−

PC entered	No. of hidden nodes	Mean relative error of prediction set	Mean relative error of validation set
PC2	6	14.1	38.8
PC2 + PC1	5	7.8	27.0
PC2 + PC1 + PC19	4	5.6	7.1
PC2 + PC1 + PC19 + PC11	3	7.6	7.3
PC2 + PC1 + PC19 + PC11 + PC18	2	6.1	32.5
PC2 + PC1 + PC19 + PC11 + PC18 + PC7	2	6.7	12.3
PC2 + PC1 + PC19 + PC11 + PC18 + PC7 + PC12	2	10.9	57.9
PC2 + PC1 + PC19 + PC11 + PC18 + PC7 + PC12 + PC8	2	11.3	24.7
PC1 + PC2 + PC3 + PC4[a]	3	6.8	8.5

[a] EV-PC-WNN model.

Table 8
Results of CR-PC-WNN and comparison with EV-PC-WNN for S²⁻

PC entered	No. of hidden nodes	Mean relative error of prediction set	Mean relative error of validation set
PC1	6	25.5	41.6
PC1 + PC12	5	34.0	41.1
PC1 + PC12 + PC9	4	37.1	27.4
PC1 + PC12 + PC9 + PC4	3	32.0	61.1
PC1 + PC12 + PC9 + PC4 + PC5	2	37.3	34.6
PC1 + PC12 + PC9 + PC4 + PC5 + PC16	2	14.7	31.0
PC1 + PC12 + PC9 + PC4 + PC5 + PC16 + PC7	2	36.5	37.9
PC1 + PC12 + PC9 + PC4 + PC5 + PC16 + PC7 + PC3	2	36.3	32.4
PC1 + PC2 + PC3[a]	2	7.7	10.6

[a] EV-PC-WNN model.

Table 9
Tolerance limits (μg ml^{-1}) of several ions with respect to SCN$^-$ and S^{2-} (200 ng ml^{-1})

Ion added	SCN$^-$	S^{2-}
K$^+$, NO$_3^-$, Na$^+$, Br$^-$, SO$_4^{2-}$, NH$_4^+$, CO$_3^{2-}$, Cl$^-$		
Mg^{2+}, Ca^{2+}, F$^-$, acetate, citrate, BrO$_3^-$, ClO$_4^-$		
PO$_4^{3-}$, C$_2$O$_4^{2-}$, Ba^{2+}, Al^{3+}, B$_4$O$_7^{2-}$	1000	1000
Ni^{2+}, Co^{2+}, Fe^{3+}, Cr^{3+}, Zn^{2+}, Mn^{2+}, Cu^{2+}	50	20
S$_2$O$_3^{2-}$, CN$^-$	5	10
Cr^{6+}, Hg^{2+}	1	1

Table 10
Real sample analysis

Sample	SCN$^-$ (ng ml^{-1})			S^{2-} (ng ml^{-1})		
	Added	Found	%RE	Added	Found	%RE
Tap water	–	ND	–	–	ND	–
Tap water	80.0	86.8 ± 3.8	8.5	35.0	38.7 ± 3.8	10.6
Tap water	100.0	93.7 ± 4.5	6.3	50.0	55.6 ± 4.9	11.2
Tap water	200.0	220.9 ± 10.0	10.5	200.0	204.2 ± 6.1	2.1
Tap water	400.0	406.5 ± 4.0	1.6	100.0	99.7 ± 3.2	0.3
Waste water	–	ND	–	–	28.0 ± 1.1	–
Waste water	80.0	85.4 ± 4.1	6.7	35.0	66.2 ± 2.6	9.1
Waste water	100.0	108.7 ± 5.2	8.7	390.0	393.4 ± 5.7	6.3
Waste water	200.0	210.8 ± 8.1	5.4	100.0	130.5 ± 2.1	2.5
Waste water	400.0	408.2 ± 3.7	2.0	200.0	229.5 ± 3.2	0.8
River water[a]	–	ND	–	–	ND	–
River water[a]	80.0	86.2 ± 3.5	7.7	35.0	37.9 ± 4.6	8.3
River water[a]	200.0	208.9 ± 4.0	4.4	100.0	104.2 ± 3.1	4.2
River water[a]	400.0	405.6 ± 3.6	1.4	200.0	204.3 ± 3.4	2.2

ND – not detected. ± values shows the standard deviation for five replicate measurements.

[a] Zayanderood river (Isfahan city).

given in Table 10, shows good results according to the standard deviations and the relative errors (%RE).

5. Conclusions

The proposed method is suitable for simultaneous determination of thiocyanate and sulfide in water samples using principal component-wavelet neural network. Two methods, eigenvalue ranking and correlation ranking were investigated for selection the most feasible PCs. The results indicate that the methods of PCs selection are complementary in this analysis. The method has good accuracy and precision.

Acknowledgement

References

[1] K. Shimizu, R.A. Osteryoung, Anal. Chem. 53 (1981) 584.
[2] R.D. Rocklin, E.L. Johnson, Anal. Chem. 55 (1983) 4.
[3] G. Schiavon, G. Zotti, R. Toniolo, G. Bontempelli, Anal. Chem. 67 (1995) 318.
[4] N.B.H. Anh, M. Sharp, Anal. Chim. Acta 405 (2000) 145.
[5] H. Parham, B. Zargar, Anal. Chim. Acta 464 (2002) 115.
[6] S. Polesello, S. Valsecchi, S. Cavalli, C. Reschiotto, J. Chromatogr A 920 (2001) 231.
[7] K. Sonne, P.K. Dasgupta, Anal. Chem. 63 (1991) 427.
[8] A.A. Ensafi, J. Tajebakhsh-E-Ardakani, Anal. Lett. 28 (1995) 731.
[9] A.A. Ensafi, M. Samimifar, Anal. Lett. 27 (1994) 153.
[10] D. Connolly, L. Barron, B. Paull, J. Chromatogr. B 767 (2002) 175.
[11] B. Divjak, W. Goessler, J. Chromatogr. A 844 (1999) 161.
[12] Y.H. Tse, P. Janda, H. Lam, A.B.P. Lever, Anal. Chem. 67 (1995) 981.
[13] M. Shamsipur, S. Ershad, N. Samadi, A.R. Rezvani, H. Haddadzadeh, Talanta 65 (2005) 991.
[14] D.R. Saloman, J. Romano, J. Chromatogr. 602 (1992) 219.
[15] Z. Glatz, S. Novakova, H. Sterbova, J. Chromatogr. A 916 (2001) 273.
[16] S. Kage, T. Nagata, K. Kudo, J. Chromatogr. B 675 (1996) 27.
[17] J. Radford-Knoery, G.A. Cutter, Anal. Chem. 65 (1993) 976.
[18] M. Tanaka, H. Takigawa, Y. Yasaka, K. Shono, H. Funazo, J. Wu, J. Chromatogr. A 404 (1987) 175.
[19] M. Tanaka, Y. Yasaka, M. Kamino, T. Shono, K. Funazo, H. Wu, J. Chromatogr. 438 (1988) 253.
[20] Y. Miura, K. Fukasawa, T. Koh, J. Chromatogr. A 804 (1998) 143.
[21] J. Cheng, P. Jandik, N. Avdalovic, Anal. Chim. Acta 536 (2005) 267.
[22] J. Xu, M. Xin, T. Takeuchi, T. Miwa, Anal. Chim. Acta 276 (1993) 261.
[23] F. Hissner, J. Mattusch, K. Heinig, J. Chromatogr. A 848 (1999) 503.
[24] R. Belcher, S.L. Bogdanski, D.J. Knowles, A. Townshend, Anal. Chim. Acta 77 (1975) 53.
[25] S. Hauge, K. Maroy, A. Thorlacius, Anal. Chim. Acta 251 (1991) 197.
[26] H.A. Mottola, Kinetic Aspects of Analytical Chemistry, John Wiley Pubs. Company, New York, 1988.
[27] E. Michalski, A. Wtrokowska, Chem. Anal. (Warsaw) 7 (1962) 691.
[28] N. Kiba, M. Furusawa, Talanta 28 (1981) 601.
[29] O. Kamson, Anal. Chim. Acta 211 (1988) 299.
[30] W. Puacz, W. Szahun, K. Linke, The Analyst 120 (1995) 939.
[31] H. Weisz, W. Meiners, G. Fritz, Anal. Chim. Acta 107 (1979) 301.
[32] A.A. Ensafi, G. Bagherian Dehaghi, Indian J. Chem. 34A (1995) 498.
[33] X. Zhang, J. Qi, R. Zhang, M. Liu, Z. Hu, H. Xue, Comput. Chem. 25 (2001) 125.
[34] C. Hervas, S. Ventura, M. Silva, D.J. Perez-Bendito, J. Chem. Inf. Comput. Sci. 38 (1998) 1119.
[35] M. Kompany-Zareh, A. Massoumi, S.H. Pezeshk-Zadeh, Talanta 48 (1999) 283.
[36] P.J. Gemperline, J.R. Long, V.G. Gergoriou, Anal. Chem. 63 (1991) 2313.
[37] T. Khayamian, A.A. Ensafi, M. Atabati, Anal. Lett. 35 (2002) 2039.
[38] T. Khayamian, A.A. Ansafi, R. Tabaraki, M. Esteki, Anal. Lett. 38 (2005) 1477.
[39] S. Sekulic, M.B. Seasholtz, Z. Wang, B.R. Kowalski, S.E. Lee, B.R. Holt, Anal. Chem. 65 (1993) 835A.
[40] Y.L. Xie, J.H. Kalivas, Anal. Chim. Acta 348 (1997) 19.
[41] U. Depczynski, V.J. Frost, K. Molt, Anal. Chim. Acta 420 (2000) 217.
[42] A.S. Barros, D.N. Rutledge, Chemometr. Intell. Lab. Syst. 40 (1998) 65.
[43] J.M. Sutter, J.H. Kalivas, P.M. Lang, J. Chemometr. 6 (1992) 217.
[44] J. Sun, J. Chemometr. 9 (1995) 21.
[45] J. Verdu-Andres, D.L. Massart, Appl. Spectrosc. 52 (1998) 1425.
[46] B. Hemmateenejad, Chemometr. Intell. Lab. Syst. 75 (2005) 231.
[47] B. Hemmateenejad, J. Chemometr. 19 (2005) 1.
[48] V.J. Barclay, R.F. Bonner, I.P. Hamilton, Anal. Chem. 69 (1997) 78.
[49] A.K. Leung, F. Chau, J. Gao, Chemometr. Intell. Lab. Syst. 43 (1998) 165.
[50] I. Daubechies (Ed.), Ten Lectures on Wavelets, SIAM Press, Philadelphia, 1992.
[51] B. Walczak, Wavelets in Chemistry, Elsevier Science, Amsterdam, 2000.
[52] Q. Guo, L. Liu, W. Cai, Y. Liu, Chem. Phys. Lett. 514 (1998) 518.
[53] L. Liu, Q. Guo, J. Chem. Inf. Comput. Sci. 39 (1999) 133.
[54] I.N. Koprinarov, A.P. Hitchcock, C.T. McCrory, R.F. Childs, J. Phys. Chem., B 106 (2002) 5358.

5(6)-Carboxyfluorescein diacetate as an indicator of *Caenorhabditis elegans* viability for the development of an *in vitro* anthelmintic drug assay

Charlemagne Gnoula [a,b,*], Innocent Guissou [c], Jacques Dubois [a], Pierre Duez [b]

[a] *Université Libre de Bruxelles (ULB), Institute of Pharmacy, Laboratory of Bioanalytical Chemistry, Toxicology and Applied Physical Chemistry, CP 205/1, Bd du Triomphe, Brussels 1050, Belgium*
[b] *Université Libre de Bruxelles (ULB), Institute of Pharmacy, Laboratory of Pharmacognosy, Bromatology and Human Nutrition, CP 205/9, Bd du Triomphe, Brussels 1050, Belgium*
[c] *Université de Ouagadougou, Unité de Formation et de Recherche en Sciences de la Santé, Ouagadougou, Burkina Faso*

Abstract

A new *in vitro* assay for anthelmintic activity using *Caenorhabditis elegans* is based on the ability of 5(6)-carboxyfluorescein diacetate (CFDA) to indicate the worm's viability. It is shown for the first time that the treatment of a suspension of worms with a solution of 5(6)-carboxyfluorescein diacetate (4.2%) for 30 min transiently induces fluorescence in dead worms only, allowing a fast and efficient determination of the proportion of dead worms by fluorescence microscopy.

The proposed test has been validated using mixtures of populations of living and killed *C. elegans* and proved to be selective, linear in the range 0–100%, accurate and precise.

The suitability of the assay to detect anthelmintic activity was then evaluated by studying the toxicity against *C. elegans* of a series of known anthelmintic compounds (mebendazole, levamisole, niclosamide, pyrantel, piperazine, and thiabendazole) with various modes of action.

The worms were exposed to each drug at two concentrations, 50 and 100 μg/ml for piperazine, niclosamide, pyrantel and 5 and 10 μg/ml for the others. We observed that, in the tested range of doses, piperazine and niclosamide were only moderately toxic, yielding 13.1 and 17.5% of dead worms; due to their mode of action and/or specificity, the low toxicity of these compounds was as expected. The marked activities of all the other compound fully agree with those described in the literature and obtained by other more laborious techniques.

These validation data indicate that the proposed *in vitro* anthelmintic assay using 5(6)-carboxyfluorescein diacetate allows for sensitive measurement of worm viability.

© 2006 Elsevier B.V. All rights reserved.

Keywords: *C. elegans*; Anthelmintic assay; Pharmacological validation

1. Introduction

Nowadays the interest in intestinal parasitoses has considerably regressed, probably because of more recent priorities such as AIDS. However more than 2 billions people are affected throughout the world, of which 300 millions suffer from severe morbid associations with more than 155,000 deaths per annum [1]. Paludism put aside, these affections still constitute 40% of the tropical diseases [1].

It is generally considered that the drugs used for the treatment of helminthiasis are relatively effective and inexpensive. Indeed, a standard anthelmintic treatment costs on average only US$ 0.15 (three tablets of mebendazole) [1].

Nevertheless, many cases of resistance to the three principal groups of anthelmintic drugs (benzimidazoles, imidazothiazoles and macrocyclic lactones) are observed in the ovine and caprine breeding of Australia [2], South Africa [3] and certain countries of South America like Paraguay [4]. One of the consequences of this phenomenon was the discontinuance of the breeding of sheep in South Africa [3] and goat in Australia [2], no molecule being effective anymore against digestive strongles. Conversely, the supposed absence of resistance in most countries of Asia or

* Corresponding author. Tel.: +32 2 650 5196; fax: +32 2 650 5187.
E-mail address: cgnoula@ulb.ac.be (C. Gnoula).

Africa can probably be explained by a lack of investigations on the subject. In consequence, identification of new anthelmintic molecules is clearly needed.

The discovery of new anthelmintics relies to a large extent on the use of an effective screening assay to detect anthelmintic activity.

The best test for an anthelmintic drug uses the target species in its normal host. But this requires relatively large quantities of chemicals and animals breeding facilities, which can be quite expensive.

Several nematodes, including a free living soil worm susceptible to all commercially available anthelmintics, *Caenorhabditis elegans*, have been proposed for the development of *in vitro* drug screening assays [5,6].

Usual indicators of anthelmintic activity *in vitro* are based on developmental changes, changes in mobility [7,8] or changes in the secretion of acetylcholinesterase [7]. O'Grady reported that a motility assay was able to detect toxicity of all known anthelmintics [9]. In such an assay, worms motionless after stimulation are considered as dead; thus paralysis and toxic effects of drugs are measured by simple observation of the degree of motility of drug-treated worms compared to controls [10].

However, the need to stimulate the worms under the microscope, together with the fact that the motility assay is not able to distinguish dead worms from paralysed ones, convinced us that a new kind of test was needed, one that would facilitate the counting of dead worms. In this purpose, we began to investigate the use of 5(6)-carboxyfluorescein diacetate (CFDA), a well-known indicator of cell viability. Surprisingly, we found that only the dead worms were fluorescent, which suggests that this fluorophore might be well-adapted to the development of an *in vitro* anthelmintic assay useful for drug screening.

The present study focuses on the development and the validation of this method from both analytical and biological points of view.

2. Material and methods

2.1. Worms culture

C. elegans wild-type strain and *Escherichia coli* OP50 strain were generous gifts from Devgen (Gent, Belgium). The worms were grown on *E. coli* layers in Petri dishes maintained in a thermostated oven at 20 °C; worms for the test were larva L3 obtained after a synchronous culture as previously described [11].

2.2. Chemicals

Tryptone Soy Agar and Tryptone Soy Broth come from Oxoïd (England). Cholesterol, methanol and sodium hydroxyde were obtained from Merck (Darmstadt, Germany), nystatin from Alpha Pharma (Braine-l' Alleud, Belgium), 30% hydrogen peroxide from UCB (Belgium), thiabendazole from Ludeco (Brussels, Belgium), mebendazole from Certa (Braine-l' Alleud, Belgium), levamisole and pyrantel pamoate from Riedel-de Haën (Germany), and 5(6)-carboxyfluorescein diacetate (CFDA)

from Acros (Geel, Belgium). Niclosamide was a gift from Bayer (Germany). The PBS (solution without hydrogenocarbonate and with $CaCl_2$ and $MgCl_2$) was from Invitrogen (Paisley, Scotland), the culture flasks ($25 \, cm^2$ ventilated) from VWR (Leuven, Belgium), the multiwell plates from Greiner Bio-One (Frickenhausen, Germany) and the Petri dishes from Sarstedt (Nuremberg, Germany).

2.3. Fluorescence microscopy

The microscope was an Axiovert S100TV (Zeiss, Germany) equipped in epifluorescence (xenon lamp); a lambda filter wheel 10-2 (Sutter, USA) equipped with a fast obturator allows the selection of the excitation filter ($\lambda_{excitation}$ 480 nm, $\lambda_{emission}$ 560 nm, dichroic 505 nm). The objective is an A-Plan 10x/0.25 Ph1 (Zeiss, Germany) and images are acquired with a Hamamatsu Orca-2, controlled by the AQM software (Kinetic Imaging, United Kingdom).

2.4. Experimental protocol

To prepare a dead worms suspension, worms were collected from 2 to 3 days old Petri dishes in a total volume of 20 ml PBS. 5 ml of this suspension were transferred in a culture flask, treated by 10 ml of 30% hydrogen peroxide and exposed for one hour under a UVA irradiator consisting of 4 tubes Cleo 15 W (Phillips, Holland) assembled in parallel on a support (the four tubes are aligned and distant of 4 cm) and placed at 25 cm over the suspension of worms. The Cleo lamp offers a continuous spectrum from 300 to 450 nm, with a maximum at approximately 354 nm (UVB/UVA ratio, 1.2%). The obtained worm suspension was subsequently transferred into a 15 ml tube and centrifuged (1300 rpm, 2 min), rinsed twice with 5 ml PBS and resuspended in 5 ml PBS.

For the toxicity tests, 5 ml of a worms suspension (approximately 6250–7500 worms) in PBS were added with the tested drug (solutions in DMSO, total volume of DMSO not exceeding 500 μl) and maintained at 20 °C for up to 7 days. At each time point, a 500-μl aliquot of this suspension was labelled by adding 200 μl of a CFDA working solution (dilution 1/25 in PBS of a stock solution of 3.0 mg CFDA in 1 ml acetone) and leaving for 30 min at room temperature in the dark. After centrifugation (1300 rpm, 2 min) and washing with 5 ml PBS, the pellet was resuspended in 1 ml PBS and divided into 200-μl aliquots containing around 250–300 worms. The proportion of dead worms was then measured by visual counting (triplicate counting) in fluorescence microscopy.

Statistics were computed by Excel 2000 equipped with the add-on Analyse-It (Microsoft), the level of significance being classically set at 0.05.

2.4.1. Linearity, accuracy and precision

Mixtures of living and killed worms were prepared in known proportions (eight levels ranging from 10 to 100%), labeled as per our general protocol and visually counted. The response curve "fluorescent worms" versus "dead worms" was investigated on 3 different days. Homoscedasticity was checked by

the Cochran test and, if needed, data were transformed prior to linearity testing (lack of fit test) [12].

For accuracy evaluation, the probability for the *F*-ratio "variance between levels" to "variance within levels" was computed to ascertain that the variation of observations between the levels was due to experimental errors. The mean recovery was then computed along with its confidence interval for a probability level of 0.05.

For precision evaluation, the data were analyzed by a 2-way ANOVA with repetition, considering 2 random effects; "*proportion of dead worms*" and "*analysis day*"; the within-day and total ("between-day") variations for the whole analytical procedure were computed.

3. Results

3.1. Selectivity

It was noticed that only dead worms present an intense fluorescence (Fig. 1). Although a very low fluorescence was emitted by some living worms, the difference was such that straightforward counting could be done without any problem. As there is no reference method to declare a worm as "dead", we resorted to stimulation with a needle.

Stimulation of fluorescent worms systematically leaved them motionless; trials with paralyzing agents (niclosamide and piperazine) yielded equally motionless but CFDA-unlabelled worms. The proposed test was thus considered selective.

3.2. Linearity, accuracy and precision

By using mixtures of living and killed worms in known proportions, a linear relationship fluorescent worms versus dead

Fig. 2. Linear relationship fluorescent worms vs. dead worms (CFDA labelling of known mixtures prepared by mixing dead and living worms suspensions). Tests in triplicate (250–300 worms evaluated per sampling points).

worms could be demonstrated in the investigated range (Fig. 2; Table 1, slope significance and lack of fit tests).

Table 2 comprises the data for the accuracy study; the mean relative recovery was around 100% for all tested proportions of dead and living worms.

Table 1
Linearity study

Investigated range (proportion of dead worms)	10–100%
n	72
Determination coefficient (r^2)	0.9988
p for Cochran C	0.279
Eventual transformation	None[a]
Slope ± standard deviation (R.S.D. %)	0.996 ± 0.004 (0.4%)
p for the slope $\neq 1$	0.376[(NS)]
Intercept ± standard deviation (R.S.D. %)	0.42 ± 0.26 (62%)
p for the intercept $\neq 0$	0.114[(NS)]
p for the slope significance F-test	<0.001[***]
p for the lack of fit F-test	0.622[(NS)]

[a] Homoscedasticity was verified for raw data (Cochran test; $p < 0.05$) and so no transformation was required [12].
[***] Very highly significant, $p < 0.001$.

Table 2
Accuracy study

Prepared proportion of dead worms	Relative recovery (%) (mean ± S.D.)
10	102 ± 7
30	102 ± 4
40	101 ± 3
50	101 ± 2
60	100 ± 3
70	99 ± 1
90	100 ± 1
100	100 ± 1
n[a]	72
p[b] for the Cochran C-test (homoscedasticity)	0.279[(NS)]
p[b] for the F-test ratio "variance between-Prepared Proportion of dead worms" to "variance within-Prepared proportion of dead worms"	0.965[(NS)]
Mean relative recovery (%) ± S.D.	100.7 ± 3.3
Mean recovery confidence interval (%)	99.98–101.52

[a] Eight mixtures counted three times and repeated over 3 days.
[b] NS, non-signifiant, $p > 0.05$.

Fig. 1. Combination of fluorescence image and visible light image, showing dead and living worms.

Table 3
Precision of the whole analytical procedure: 2-way ANOVA with repetition; two random factors ("*prepared proportion of dead worms*" and "*analysis day*")

Source of variation	Degrees of freedom	Sum of squares	Mean square	Variance ratio (F)	p[a]	R.S.D. % (within-analysis day)	R.S.D. % (Total)
Analysis day	2	3.99	2.00	0.82	46.11[(NS)]	1.29	1.29
Prepared proportion of dead worms	7	57071.16	8153.02	3345.21	<0.001[***]		
Analysis day × prepared proportion of dead worms (interaction)	14	34.12	2.44	4.58	0.004[**]		
Residual (error)	48	25.52	0.53				
Total	71	57134.80					

Eight different samples have been analyzed in triplicate on 3 different days

[a] NS, non-significant, $p > 0.05$.

[**] Highly significant, $p < 0.01$.

[***] Very highly significant, $p < 0.001$.

Table 3 details the components of the variance for the precision data. The counting allowed to differentiate the proportions of the different samples without influence of the factor "*analysis day*". However, close examination of data shows that these differences can be considered as negligible (<3%). With the excellent precision of countings, a slight interaction day × sample is revealed ($p = 0.004$). This interaction means that counting of some samples are significantly different according to the "*analysis day*". Considering all the levels, the total precision of the analytical procedure was 1.3%.

3.3. Pharmacological validation

Fig. 3 presents the evolution of toxicity according to time for the 6 tested compounds. All the anthelmintics tested showed activity against *C. elegans* (Table 4), but piperazine and niclosamide were moderately toxic, yielding only 15.5 and 17.5% of dead worms at the higher tested dosage. The examined dose ranges based on the minimum detectable dose according to Simpkin and Coles (thiabendazole, pyrantel) [5] or the doses proposed by Fonseca-Salamanca et al. [13].

Table 4
In vitro effects of various anthelmintics against *Caenorhabditis elegans*

Drug	Dose (μg/ml)	% dead worms after 7 days of incubation (mean of two determinations; R.S.D.: 1.3%)
Control	–	2.4
Mebendazole	1	24.1
	10	89.9
Thiabendazole	5	58.5
	10	82.5
Levamisole	5	74.5
	10	96.4
Piperazine	50	13.1
	100	15.5
Niclosamide	50	15.7
	100	17.5
Pyrantel	50	41.0
	100	53.4

4. Discussion

This study proposes a method for assessing nematode viability to develop an efficient and simple *in vitro* anthelmintic screening test. Suitable screening models are indeed important for both drug discovery and their further pharmacological investigation. *C. elegans* has already been proposed as an *in vitro* test: 7-days incubation with the tested agent followed by light-microscopy visual estimation of effect. This test supposed sensitive enough to detect most of so-called "modern" anthelmintics, was described as particularly suited for the screening of natural products [5].

The present bioassay is an improvement on this test as it considerably eases the visual distinction between dead and living worms and thus the quantitative evaluation of anthelmintic activities. It presents a good selectivity, accuracy and reproducibility and possesses the advantages of being cost-effective and easy to operate for reasonable throughputs.

CFDA, a fluorogenic esterified substrate sometimes used to measure the activity of the cellular esterases [14], is a well-known indicator of cellular viability. The compound crosses the cellular membrane and undergoes hydrolysis to be readily trapped in the cell and label the cytoplasm. As induced fluorescence is transient (36 h) following the death of worms, the monitoring of viability needs to be done repeatedly, which can however be considered as an advantage for kinetic purposes.

The observation of fluorescence in dead worms only supposes hydrolysis of CFDA by cytoplasmic esterases. This suggests on one hand that this enzymatic activity persists in dead worms at least for a certain time and, on the other hand, that there is some mechanism either preventing the penetration of CFDA in living worms or expulsing the fluorophore before enzymatic hydrolysis. Membrane P-glycoproteins which control the passage of toxic substances through the membrane have been described in *C. elegans*, a mechanism similar to the well-known multidrug resistance mechanism in mammalians [15–20].

As worms dead for more than 36 h cannot be labelled anymore, the fluorescence emitted by recently dead worms only could likely be explained by an inactivation of the membrane P-glycoprotein alongside a persistence of the cytoplasmic esterase activity in the hours which follow the death of the worm. Trials to inhibit the P-glycoprotein with verapamil (10, 100 and 1000 μg/ml) to label living worms were however unsuccessful,

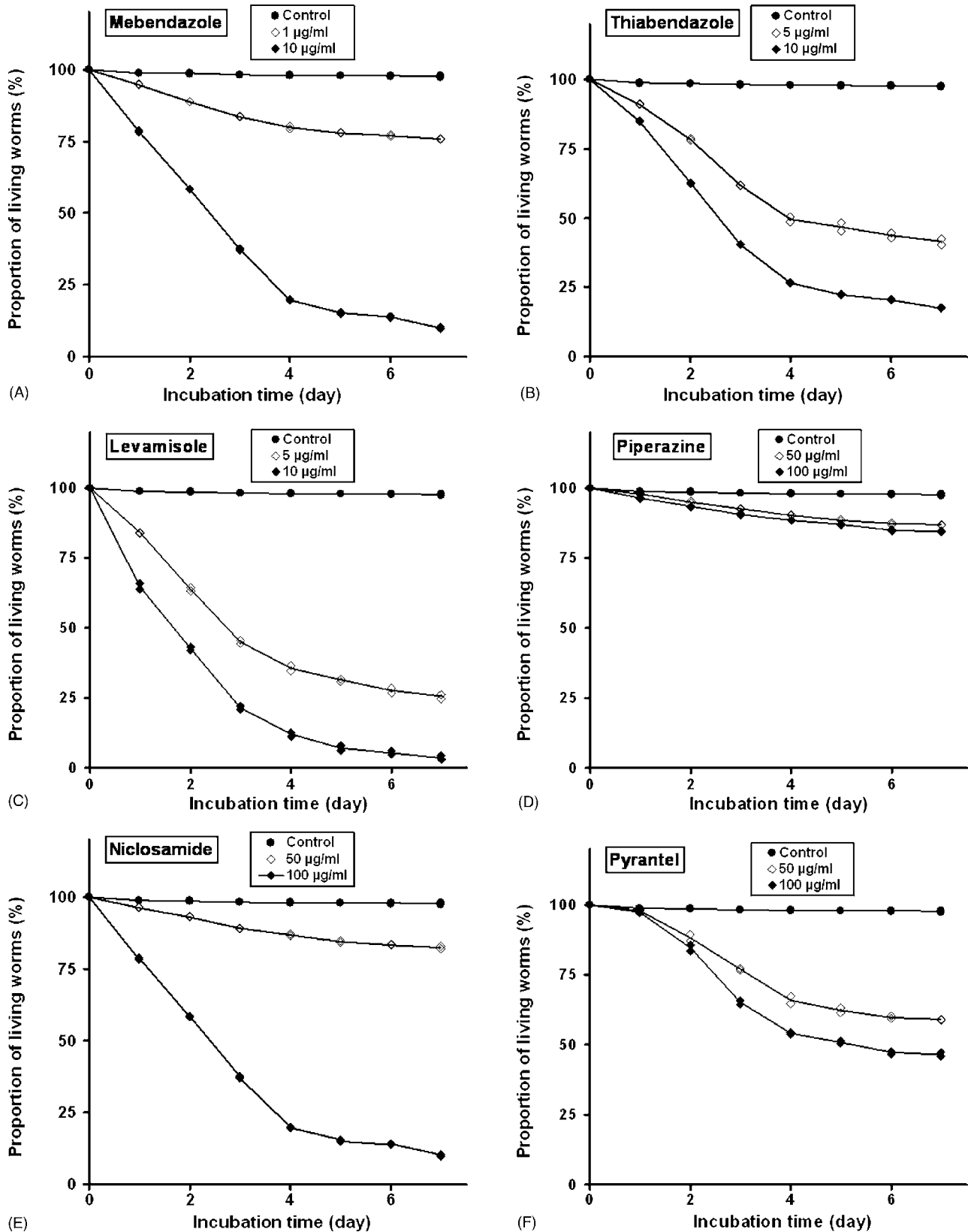Fig. 3. Toxicity vs. *C. elegans* of benzimidazoles and levamisole (two doses tested; CFDA fluorescence labelling and counting every 24 h). Tests in duplicate (250–300 worms evaluated per sampling points). Note: the two points are sometimes superimposed. (A) Toxicity of mebendazole; (B) toxicity of thiabendazole; (C) toxicity of levamisole; (D) toxicity of piperazine; (E) toxicity of niclosamide; (F) toxicity of pyrantel.

due to the high toxicity of this compound to *C. elegans*. Work is in progress with other MDR's inhibitors (SiRNA) to elucidate this mechanism.

The kinetic aspect of the test allows for a daily follow up of long-term toxicity (up to 7 days), which is quite interesting for testing compounds at lower dosages but also for characterizing anthelmintics that require several days to effectively kill worms, depending on the developmental stage target. The effect of the toxic can effectively be observed all along the larval development.

For such tests however, the stability of tested chemicals during the 7-days incubation could be a potential problem.

Most of the literature described anthelmintic assays do not quantify the anthelmintic activity of the tested products, but provide only scoring results such as "not active", "doubtful", "active" [5], which precludes comparisons of data.

Anthelmintics are usually divided into two groups, those acting on metabolic pathways and those acting on the nervous system of nematodes [21].

In our test, the activity of well-known anthelmintic drugs such as benzimidazoles (mebendazole, thiabendazole) and levamisole is evident (Fig. 3). The benzimidazole drugs bind the nematode tubulin, thus inhibiting the formation of microtubules, which are subsequently unable to transport secretory granules or to secrete enzymes within the cell cytoplasm; this eventually results in cell lysis [22]. The mode of action of benzimidazoles is clinically significant in susceptible parasites populations because the duration of exposure of the parasite to drug is a determinant key of efficacy [23]. On *C. elegans*, the activity is marked after 2 days of contact at the higher tested dose (Fig. 3A and B).

Levamisole acts as a cholinergic agonist at nicotinic neuromuscular junctions in nematode parasites, first by opening and then blocking acetylcholine receptor-mediated cations channels [24]. This faster mode of action is apparent on *C. elegans* with significant toxicity already after 1 day of contact (Fig. 3C).

Piperazine acts by blocking the neurotransmitter acetylcholine in the worm, leading to paralysis and faecal excretion of motionless, but still living worms [25]. Placed in a physiological solution, those excreted worms recover in less than 3 h [25], which probably explains the low reduction of worm population growth. Accordingly, the effect of piperazine on *C. elegans* is low, leading to only 20% dead worms at the highest dose tested (Fig. 3D).

Although niclosamide causes paralysis of the taeniasis, facilitating their expulsion, it is not effective against nematodes. This fact, combined with the recovery of paralysed worms, explains the low activity observed on *C. elegans* (Fig. 3E).

Pyrantel is an anthelmintic specifically used against nematodes; it causes their paralysis by blocking the neuro-muscular transmission. On *C. elegans*, about 50% dead worms are observed after 5 days of contact (Fig. 3F), which is in good agreement with the semi-quantitative data of Simpkin and Coles [5].

4.1. Conclusion and perspectives

The proposed model appears suited to detect helminticide activities and is appropriate for *in vitro* screening with rea-

sonable throughputs. Its combination with a test for paralysis (e.g. measurement of the capacity of the worms to cross a filtering membrane) [26] would give a versatile test to detect most of anthelmintic compounds, most precisely nematicide compounds.

Studies have shown that there are many remarkable similarities between *Ascaris* and *C. elegans*, for example in the motoneural system and enzymatic equipment (e.g. isocitrate lyase) [27]. It is thus possible to use *C. elegans* as a model to further investigate the mode of action of anthelmintics.

The resistance of some nematodes to anthelmintics is receiving increasing attention and a model system for predicting resistance would be useful. As mutants of *C. elegans* are easy to develop and maintain [28], the conception and/or selection of drug-resistant mutants for use in such a test system as described here would make it possible to investigate agents effective on resistant parasites or capable of reverting the drug resistance. As *C. elegans* can be easily stored in liquid nitrogen [11] a battery of mutants readily available for testing resistance to any new drug being developed is foreseeable.

References

[1] OMS, Liens entre l'eau, l'assainissement, l'hygiène et la santé: faits et chiffres, OMS, Genève; 2004, 11 pp.
[2] P.J. Waller, Vet. Parasitol. 72 (1997) 391.
[3] J.A. Van Wyk, P.C. Van Schalkwyk, Vet. Parasitol. 35 (1990) 61.
[4] S. Maciel, A.M. Gimenez, C. Gaona, P.J. Waller, J.W. Hansen, Vet. Parasitol. 62 (1996) 207.
[5] K.G Simpkin, G.C. Coles, J. Chem. Technol. Biotechnol. 31 (1981) 66.
[6] T.R. Burglin, E. Lobos, M.L. Blaxter, Int. J. Parasitol. 28 (1998) 395.
[7] E.B. Rapson, D.C. Jenkins, P. Topley, Res. Vet. Sci. 39 (1985) 90.
[8] N.F.H. Ho, S.M. Sims, T.J. Vidmar, J.S. Day, C.L. Barsuhn, E.M. Thomas, T.G. Geary, D.P. Thompson, J. Pharm. Sci. 83 (1994) 1053.
[9] J. O'Grady, A.C. Kotze, Exp. Parasitol. 106 (2004) 164.
[10] J.C. Richards, J.M. Behnke, I.R. Duce, Int. J. Parasitol. 25 (1995) 1185.
[11] I.A. Hope, C. Elegans, A Practical Approach, In: Press OU, editor New York, 1999.
[12] NCCLS, Evaluation Protocols SC1-B, National Committee for Clinical Laboratory Standards, Villanova, PA, 1992.
[13] F. Fonseca-Salamanca, M.M. Martinez-Grueiro, A.R. Martinez-Fernandez, Parasitol. Res. 91 (2003) 321.
[14] D. Hoefel, W.L. Grooby, P.T. Monis, S. Andrews, C.P. Saint, J. Microbiol. Methods 52 (2003) 379.
[15] C.R. Lincke, I. The, M. van Groenigen, P. Borst, J. Mol. Biol. 228 (1992) 701.
[16] T. Usui, M. Yoshida, A. Honda, T. Beppu, S. Horinouchi, Gene 161 (1995) 93.
[17] O. Fardel, V. Lecureur, A. Guillouzo, Gen. Pharmacol. Vasc. Syst. 27 (1996) 1283.
[18] U.A. Germann, Eur. J. Cancer 32 (1996) 927.
[19] M. Dean, Y. Hamon, G. Chimini, J. Lipid Res. 42 (2001) 1007.
[20] D. Kerboeuf, W. Blackhall, R. Kaminsky, G. von Samson-Himmelstjerna, Int. J. Antimicrob. Agents 22 (2003) 332.

[21] G.C. Coles, J.M. East, S.N. Jenkins, Gen. Pharmacol. Vasc. Syst. 6 (1975) 309.
[22] E. Lacey, Int. J. Parasitol. 18 (1988) 885.
[23] Q.A. McKellar, F. Jackson, Trends Parasitol. 20 (2004) 456.
[24] S.J. Robertson, R.J. Martin, Br. J. Pharmacol. 108 (1993) 170.
[25] J. Del Castillo, W.C. De Mello, T. Morales, Experientia 20 (1964) 141.
[26] S.K. Athanasiadou, I. Jackson, K. Brandt, Vet. Rec. 146 (2000) 728.
[27] T.R. Patel, B.A. McFadden, Exp. Parasitol. 44 (1978) 262.
[28] S. Brenner, Genetics 77 (1974) 71.

An iron(III) ion-selective sensor based on a μ-bis(tridentate) ligand

Vinod K. Gupta[*], A.K. Jain, Shiva Agarwal, Gaurav Maheshwari

Department of Chemistry, Indian Institute of Technology Roorkee, Roorkee 247667, India

Abstract

A μ-bis(tridentate) ligand named 2-phenyl-1,3-bis[3′-aza-4′-(2′-hydroxyphenyl)-prop-4-en-1′-yl]-1,3-imidazolidine (**I**) has been synthesized and scrutinized to develop iron(III)-selective sensors. The addition of sodium tetraphenyl borate and various plasticizers, *viz.*, chloronaphthalene, dioctylphthalate, *o*-nitrophenyl octyl ether and dibutylphthalate has been used to substantially improve the performance of the sensors. The membranes of various compositions of the ligand were investigated and it was found that the best performance was obtained for the membrane of composition (**I**) (10 mg):PVC (150 mg):chloronaphthalene (200 mg):sodium tetraphenyl borate (9 mg). The sensor showed a linear potential response to iron(III) over wide concentration range 6.3×10^{-6} to 1.0×10^{-1} M (detection limit 5.0×10^{-6} M) with Nernstian slope (20.0 mV/decade of activity) between pH 3.5 and 5.5 with a quick response time of 15 s. The potentiometric selectivity coefficient values as determined by match potential method (MPM) indicate excellent selectivity for Fe^{3+} ions over interfering cations. The sensor exhibits adequate life of 2 months with good reproducibility. The sensor could be used in direct potentiometry.
© 2006 Elsevier B.V. All rights reserved.

Keywords: μ-Bis(tridentate) ligand; Iron(III)-selective sensors; Chemical sensors; Potentiometry

1. Introduction

It is well known that iron is an essential nutrient which is vital to the processes by which cell generates energy. It provides a fundamental structure of hemoglobin, myoglobin, haemenzymes and many cofactors involved in enzyme activities. The iron can also be damaging when it accumulates in the body causing haemochromatosis. The fact that too little or too much of a nutrient is detrimental seems particularly apropos for iron. Thus, the need for quantification of iron in clinical, medicinal, environmental and industrial samples has led to a number of methods for its measurement [1–3] and one of these methods which offers simple, rapid and reliable tool is ion-selective sensors. However, very few Fe(III)-selective sensors which offer simple, rapid and reliable analytical tool have been reported [4–9]. Out of these electrodes some are based on chalcogenide glass system [4,9] and other are plasticized polymeric electrodes [5–8]. Former once are problematic due to their quirky and poorly understood interfacial chemistry. PVC-based sensors are preferred once as it is possible to optimize the composition to yield high selectivity. Further, they are amenable to miniaturization.

As the reported sensors are not yet highly selective and sensitive, it is still desirable to look for new ionophore for preparing Fe^{3+} sensor. Amongst various materials that can be used for this purpose, Schiff bases are an important group, as they are known to form strong complex with transition metal ions [10,11]. Although a lot of work on the synthesis, characterization and crystalline structures of the metal–salen complexes have been reported, but only limited salen molecules were used as ionophore in ISEs [12–15]. An iron-selective electrode based on a Schiff base was reported by Mashhadizadeh et al. [6] but the electrode showed a super Nernstian response. We have therefore looked at the possibility of using Schiff base as ionophore for preparing Fe^{3+} sensor. For this purpose, we have explored a number of Schiff bases reported in the literature as ionophore for preparing Fe^{3+}-selective sensor. Our results have indicated that PVC-based membrane of μ-bis(tridentate) ligand works as good Fe^{3+} sensor and the results are reported in the present manuscript.

2. Experimental

2.1. Reagents

All reagents were of analytical grade and used without further purification. High molecular weight poly(vinyl chloride) (PVC),

---

[*] Corresponding author. Tel.: +91 1332 285801; fax: +91 1332 285043.
E-mail address: vinodfcy@iitr.ernet.in (V.K. Gupta).

Aldrich, USA; sodium tetraphenylborate (NaTPB) and benzaldehyde, BDH (UK); dibutylphthalate (DBP) and dioctylphthalate (DOP), Reidel (India); chloronaphthalene (CN), Merck (Germany); *o*-nitrophenyl octyl ether (NPOE), Acros Organics (Belgium); triethylenetetramine, G.S. Chemical Lab (India); salicylaldehyde, CDH (India) were used as obtained. Analytical reagent-grade tetrahydrofuran (THF), nitric acid and sodium hydroxide were obtained from Ranbaxy, India. Solutions of metal salts (nitrates) were prepared in double-distilled water. Working solutions of different concentrations were prepared by diluting 0.1 M stock solutions.

2.2. Apparatus and potential measurements

The potential measurements were carried out at $25 \pm 0.1\,^\circ\text{C}$ on digital pH meter/millivoltmeter (Toshniwal Inst. Mfg. Pvt. Ltd., India). pH measurements were made on a digital pH meter (LabIndia pH Conmeter, India; glass electrodes as pH electrode and calomel electrodes as reference electrodes). Elementar Vario EL III CHN analyzer was used for CHN analysis of the synthesized ligand and FT-IR was taken by Thermo Nicolat FT-IR spectrometer.

Metal salt solution ($1.0 \times 10^{-1}\,\text{M}$) was taken as internal solution and all standard or test solutions (1.0×10^{-6} to $1.0 \times 10^{-1}\,\text{M}$) were prepared by successive dilution. The performances of electrodes were accessed by measuring the potentials of the test solutions from low ($1.0 \times 10^{-6}\,\text{M}$) to high ($1.0 \times 10^{-1}\,\text{M}$) concentration or vice versa, stirred with magnetic stirrer.

2.3. Synthesis of the ligand

The ligand was synthesized as per reported procedure [16]. Thus, a methanolic solution of triethylenetetramine (1.46 g; 0.01 mol) (5 mL) was added dropwise to a solution (15 mL) of salicylaldehyde (2.44 g; 0.02 mol) in methanol with continuous stirring at room temperature. After 10 min, a methanolic solution (5 mL) of benzaldehyde (1.05 g; 0.01 mol) was added to the previous yellow solution and continued the stirring for 3 h. The solvent was evaporated in air. The yellow solid was separated by filtration and washed thoroughly with hexane and water. Yield is 60%, m.p. 85–87 $^\circ$C. Anal. Calc. for $C_{27}H_{30}N_4O_2$: C, 73.23: H, 6.83: N,12.65. Found: C, 73.93: H, 6.73: N, 12.62. IR (cm^{-1}, KBr disk): ν(phenolic OH) 3444.27 (w): ν(C=N) 1628.98 (s); ν(phenolic C–O) 1272.86 (s); ν(CH$_2$) 859.81 (m); ν(aromatic CH) 761.31 (s).
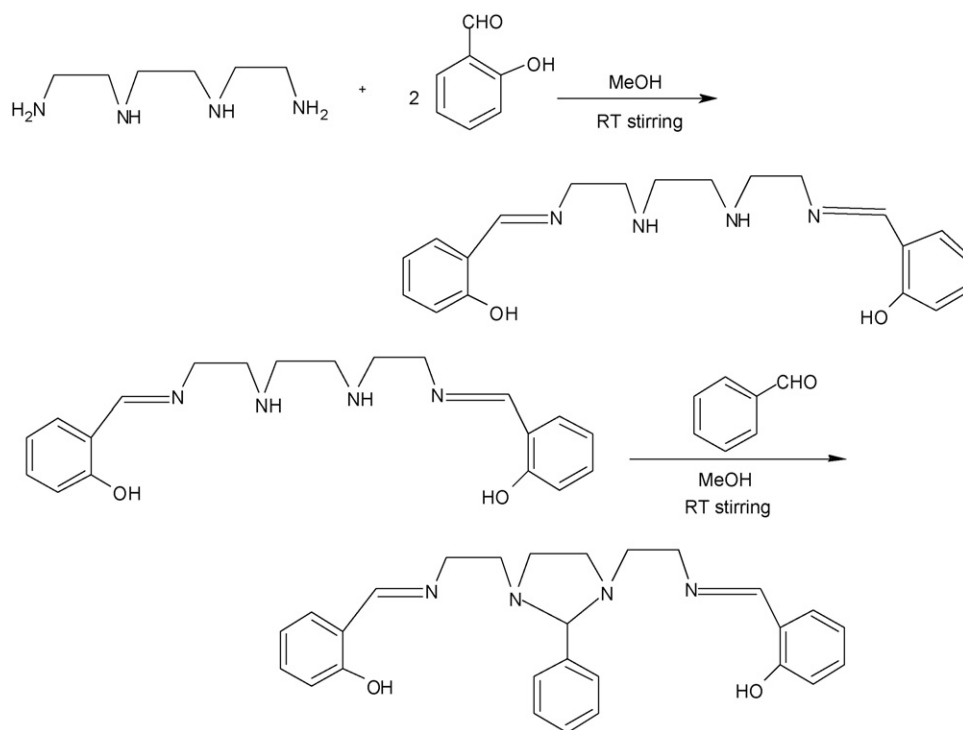
2-phenyl-1,3-bis[3'aza-4'-(2'-hydroxyphenyl)-prop-4-en-1'-yl]-1,3-imidazolidine (**I**)

The electrode potential (EMF) measurements were performed at 25 °C using the following electrochemical cell system.

External saturated calomel electrode (SCE)	Test solution	Membrane	Internal solution	Internal saturated calomel electrode (SCE)

2.4. Membrane preparation

The method reported by Craggs et al. was adopted for the preparation of membranes [17]. A number of membranes incorporating ligand, anion excluder and plasticizer in different compositions in PVC matrix were fabricated. Varying amounts of the ligand and an appropriate amount of PVC were dissolved in

a minimum amount of THF. The solutions thus obtained, after complete dissolution of various components, were poured into acrylic rings placed on a smooth glass and allowed to evaporate at room temperature. After 24 h, transparent membranes of 0.5 mm thickness were obtained which were then cut to size and attached to a Pyrex tube with Araldite. Further, the membranes were equilibrated with corresponding metal salt solution for which the membrane is selective. The ratio of various membrane ingredients, time of contact and the concentration of equilibrating solution were optimized first so that the membranes develop reproducible, stable and noiseless potentials. Besides these, some membranes containing only PVC (blank membranes) were also prepared in order to account for any background potential being generated because of the binder. During non-usage, membranes were stored in 0.1 M salt solution to avoid drying, cracking and poisoning.

2.5. Sample preparation

E-ZIF capsules were dissolved in concentrated nitric acid by gentle warming and filtered off. The resulting solution was diluted to 500 mL in a volumetric flask. Standard solutions were prepared by appropriate dilution with double-distilled water.

3. Results and discussion

3.1. Potentiometric response

The principle of the working of PVC-based membranes is selective recognition by the incorporated carrier via complex formation with the analyte ion. It is reported that the μ-bis(tridentate) ligand form strong complexes with iron(III) [16], thus heterogeneous membranes of 2-phenyl-1,3-bis[3′-aza-4′-(2′-hydroxyphenyl)-prop-4-en-1′-yl]-1,3-imidazolidine (**I**) and PVC matrix in different ratios were fabricated and equilibrated in 0.5 M Fe^{3+} solution for 3 days to obtain stable potentials. The potentiometric response characteristics of the membrane sensors were carried out with a fixed concentration of 1.0×10^{-1} M Fe^{3+} as internal solution and varying the Fe^{3+} concentration in test solutions in the range of 1.0×10^{-6} to 1.0×10^{-1} M. Then potentials determined as a function of Fe^{3+} ions in test solutions were plotted against the logarithm of the activity of Fe^{3+} as shown in Fig. 1. From these plots working concentration range and slope were calculated for each membrane and are summarized in Table 1. It was observed that mem-
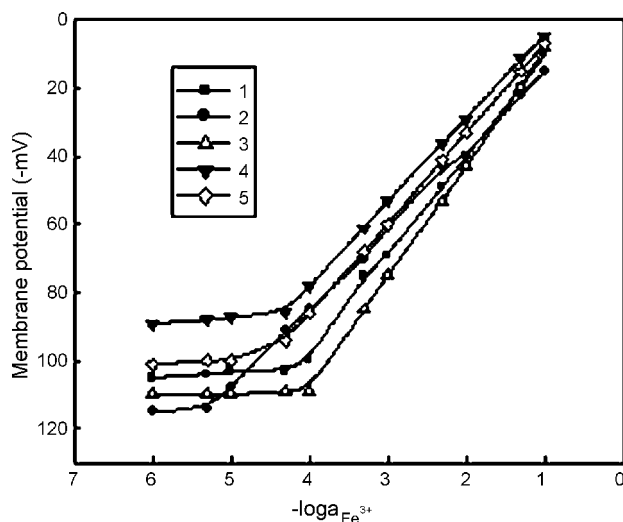

Fig. 1. Variation of membrane potential of PVC-based membranes of (I) with varying concentrations of Fe^{3+} ions (1) without plasticizer; (2) with CN; (3) DOP; (4) NPOE; (5) DBP.

brane which contained only the ligand (**I**) and anion excluder NaTPB in PVC matrix (sensor no. 1) in the ratio 10:150:9 (**I**:PVC:NaTPB) (w/w, mg) exhibited a working concentration range of 1.0×10^{-4} to 1.0×10^{-1} M of Fe^{3+}. The sensor has a super Nernstian slope of 30.0 mV/decade of activity. It is well documented that plasticizers used also influence selectivity and sensitivity of ISEs. Hence, various membranes doped with different plasticizers, *viz.*, DOP, DBP, CN and NPOE have been prepared and studied their response characteristics to see the effect of these plasticizers. The optimum composition with response characteristics of these membranes are listed in Table 1 and showed in Fig. 1. As evident from Fig. 1 and Table 1, the addition of plasticizers showed a marked improvement in the working concentration range of the sensors except DOP. The working concentration range is widened to 6.3×10^{-6} to 1.0×10^{-1}, 8.9×10^{-5} to 1.0×10^{-1}, 5.0×10^{-5} to 1.0×10^{-1} M with the addition of CN, NPOE and DBP, respectively, while there is no change in concentration range by adding DOP. The limit of detection for sensor no. 2 is calculated from the intersection of the two extrapolated segment of the calibration curve (Fig. 1) and is found to be 5.0×10^{-6} M. Since the best response characteristics, i.e. working concentration range and slope were exhibited by the membrane with plasticizer CN (sensor no. 2), the same was chosen for further studies. This

Table 1
Composition and response characteristics of Schiff base ligand (**I**)-based membrane electrodes selective to Fe^{3+}

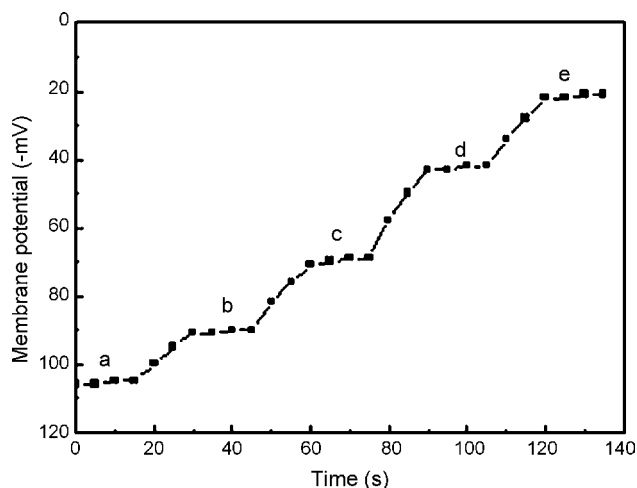| Membrane/sensor no.	Composition of the membrane (w/w, mg)							Working concentration range (M)	Slope (mV/decade of activity)	Response time (s)
	(**I**)	PVC	CN	DOP	NPOE	DBP	NaTPB			
1	10	150	–	–	–	–	9	1.0×10^{-4} to 1.0×10^{-1}	30.0	60
2	10	150	200	–	–	–	9	6.3×10^{-6} to 1.0×10^{-1}	20.0	15
3	10	150	–	200	–	–	9	1.0×10^{-4} to 1.0×10^{-1}	33.0	45
4	10	150	–	–	200	–	9	8.9×10^{-5} to 1.0×10^{-1}	25.0	30
5	10	150	–	–	–	200	9	5.0×10^{-5} to 1.0×10^{-1}	26.0	20

Fig. 2. Dynamic response time of the optimized Fe^{3+}-selective sensor for step changes in concentrations of Fe^{3+}: (a) 1×10^{-5} M; (b) 5×10^{-5} M; (c) 5×10^{-4} M; (d) 5×10^{-3} M; (e) 5×10^{-2} M.

sensor gave a standard deviation of ± 0.1 mV in the observed values of potential in working concentration range from square fit line.

3.2. Response and lifetime

The response speed has a great effect in determining the sensor usability in batch measurements and in flow systems. The dynamic response time is a continuous record of the response, which can easily be made from the initial, conditioning in the supporting solution through stepwise additions encompassing several orders of magnitude of concentration [18]. The dynamic response time for the proposed membrane sensor is depicted in Fig. 2 and mentioned in Table 1. As observed from Fig. 2 the response time for the proposed sensor is 15 s (sensor no. 2).

Performing calibrations periodically with standard solutions and calculating the response and slope over the range 1.0×10^{-6} to 1.0×10^{-1} M Fe^{3+} solution, worked out the lifetime of the sensor. It was found that the sensor worked well over a period of 2 months with good reproducibility and standard deviation of ± 0.1 mV in the observed values of potential in working concentration range from square fit line.

Table 2
Selectivity coefficient $K_{A,B}^{Pot}$ values for Fe(III)-selective sensor as obtained by match potential method (MPM) for various interfering ions

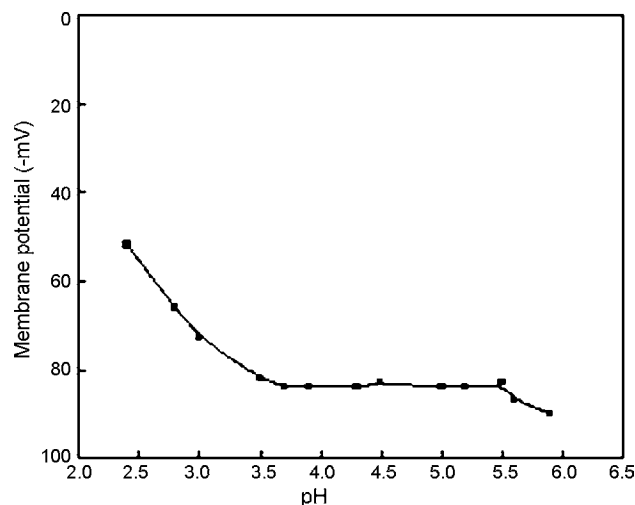| Interfering ion (B)	Selectivity coefficient $-\log K_{A,B}^{Pot}$
Na^+	3.4
K^+	3.7
Li^+	3.5
Cd^{2+}	3.2
Cu^{2+}	2.6
Co^{2+}	2.8
Ni^{2+}	3.0
Pb^{2+}	3.2
Mn^{2+}	3.1
Al^{3+}	3.0
Cr^{3+}	2.5

Fig. 3. Effect of pH on potential; $[Fe^{3+}] = 1.0 \times 10^{-4}$ M for sensor no. 2.

Table 3
Performance of Fe(III)-selective sensor (no. 2) in non-aqueous media

Non-aqueous content (%, v/v)	Slope (± 0.5 mV/decade of activity)	Working concentration range (M)
0	20.0	6.3×10^{-6} to 1.0×10^{-1}
Methanol		
10	20.0	6.3×10^{-6} to 1.0×10^{-1}
15	20.0	6.3×10^{-6} to 1.0×10^{-1}
20	21.0	8.9×10^{-6} to 1.0×10^{-1}
Ethanol		
10	20.0	6.3×10^{-6} to 1.0×10^{-1}
15	20.0	6.3×10^{-6} to 1.0×10^{-1}
20	21.5	1.0×10^{-5} to 1.0×10^{-1}

3.3. Potentiometric selectivity

The response characteristics of the sensors were examined in presence of various foreign ions in order to examine the selectivity. The match potential method (MPM) of Gadzekpo and Christian [19] was used to determine the potentiometric selectivity of the sensor. The selectivity coefficient $K_{A,B}^{Pot}$ is given by the expression:

$$K_{A,B}^{Pot} = \frac{a'_A - a_A}{a_B} = \frac{\Delta a_A}{a_B}$$

and is determined by measuring the change in potential upon increasing by a definite amount the primary ion activity from

Table 4
Quantification of iron(III) in pharmaceutical dosages, Hindon river water, wastewater and standard solution (AAS) by using AAS and Fe^{3+} sensor (no. 2)

Samples	Potentiometry[a]	AAS[a]
E-ZIF (mg per capsule)	48.0 ± 0.50	49.0 ± 0.20
Hindon river water (ppm)	8.45 ± 0.05	8.50 ± 0.05
Wastewater (ppm)	10.21 ± 0.02	10.21 ± 0.04
Standard solution (AAS) (ppm)	8.00 ± 0.05	8.05 ± 0.01

[a] Number of samples = 5.

Table 5
Comparison of proposed Fe(III)-selective sensor with reported sensors

Working concentration range (M)	pH range	Slope (mV/decade)	Selectivity	Response time (s)	Lifetime (months)	Ref.
3.5×10^{-6} to 4.0×10^{-2}	4.5–6.5	28.5	Good	15	2	[6]
1.0×10^{-6} to 1.0×10^{-2}	1.3–3.5	60.0	Very good	25	2	[8]
6.3×10^{-6} to 1.0×10^{-1}	3.5–5.5	20.0	Very good	15	2	Proposed sensor

an initial value of a_A to a'_A and a_B represents the activity of interfering ion added to same reference solution of activity a_A which brings about same potential change. In the present studies a_A and a'_A were kept at 3.0×10^{-5} and 8.0×10^{-5} M Fe^{3+} and a_B was experimentally determined. The selectivity coefficient values determined for various interfering ions are presented in Table 2. It is clear from Table 2 that the proposed sensor is selective for Fe^{3+} over many mono-, di- and trivalent cations.

3.4. Effect of pH and non-aqueous solutions

The pH dependence of the membrane potentials was tested over the pH range 2.5–6.0 for 1.0×10^{-4} M Fe^{3+}. The pH was adjusted with hydrochloric acid and sodium hydroxide. Fig. 3 depicts that the pH dependence of the potentials is insignificant in the pH range 3.5–5.5. The constancy of the potential indicates that Fe^{3+} not getting hydrolyzed in significant amount and remains as main species. The performance of the sensor system was also investigated in partially non-aqueous media using methanol–water and ethanol–water mixtures. The membranes do not show any appreciable change in working concentration range or slope in mixtures up to 15% (v/v) non-aqueous contents (Table 3). Above this, developed potential showed an erratic behavior. This may be due to leaching of the ionophore in organic medium.

4. Analytical applications

In order to test the analytical applicability of the proposed sensor system, it has been applied for the determination of iron in pharmaceutical dosages, Hindon river water, wastewater and standard solution (AAS) by direct potentiometry using the calibration graph. The data obtained by potentiometry are in good agreement with that obtained by AAS (Table 4).

5. Conclusions

It may be concluded that the μ-bis(tridentate) ligand (**I**) has been used successfully to develop a Fe(III)-selective sensor with

a wide concentration range 6.3×10^{-6} to 1.0×10^{-1} M and Nernstian slope. On comparing the proposed sensor (Table 5) with some reported sensors, we find that the present sensor is better than the recently reported sensors in terms of slope [6,7,8], selectivity [7] and pH range [8]. The sensor could be used in direct potentiometry.

Acknowledgements

References

[1] A.F. Oliverra, J.A. Nobrega, O. Fatibello-Filho, Talanta 49 (1995) 505.
[2] A. Safavi, H. Abdollahi, M.R. Hormozi-Nezhad, Talanta 56 (2002) 699.
[3] R.C.C. Costa, A.N. Araújo, Anal. Chim. Acta 438 (2001) 227.
[4] C.E. Koening, E.W. Granber, Electroanalysis 7 (1995) 1090.
[5] S.S.M. Hassan, S.A.M. Marzouk, Talanta 41 (1994) 891.
[6] M.H. Mashhadizadeh, I.S. Shoaei, N. Monadi, Talanta 64 (2004) 1048.
[7] W.H. Mahmoud, Anal. Chim. Acta 436 (2001) 199.
[8] A. Sil, V.S. Ijer, A.K. Srivastava, Sens. Actuators B 106 (2005) 648.
[9] B. Pejcic, R.D. Marco, Electrochim. Acta 49 (2004) 3525.
[10] M. Calligaris, R. Randaccio, In: G., Wilkinson, R.D., Gillard, McCleverty (Eds.), Comprehensive Coordination Chemistry, vol. 2, London, 1987 (Chapter 20).
[11] D.A. Atwood, Coord. Chem. Rev. 176 (1998) 407.
[12] N. Alizadeh, S. Ershad, H. Naeimi, H. Sharghi, M. Shamsipur, Fresen. J. Anal. Chem. 365 (1999) 511.
[13] R.K. Mahajan, M. Kumar, V. Sharma, I. Kaur, Analyst 126 (2001) 505.
[14] M.H. Mashhadizadeh, A. Momeni, R. Razavi, Anal. Chim. Acta 462 (2002) 245.
[15] M. Shamsipur, A. Soleymanpour, M. Akhond, H. Sharghi, M.A. Naseri, Anal. Chim. Acta 450 (2001) 37.
[16] M. Bera, U. Mukhopadhyay, D. Ray, Inorg. Chim. Acta 358 (2005) 437.
[17] A. Craggs, L. Keil, G.J. Moody, J.D.R. Thomas, Talanta 22 (1975) 907.
[18] J. Inczedy, T. Lingyel, A.M. Ure, Compendium of Analytical Nomenclature, Definitive Rules 1997, Blackwell Science, Oxford, UK, 1998.
[19] V.P.Y. Gadzekpo, G.D. Christian, Anal. Chim. Acta 164 (1984) 279.

Short communication

Quantitative characterization of degradation behaviors of antioxidants stabilized in lipid particles

Sang-Hoon Han [a,b], Jong-Suk Lee [a], Yong-Jin Kim [a],
Junoh Kim [a], Ih-Seop Chang [a], Dong June Chung [b],
Kyung-Do Suh [c], Jin-Woong Kim [a,d,∗]

[a] *Amore-Pacific Co. R&D Center, 314-1, Bora-dong, Giheung-gu, Yongin-si, Gyeonggi-do 449-729, South Korea*
[b] *Department of Polymer Science & Engineering, SKKU, Su-Won 440-746, South Korea*
[c] *Department of Chemical Engineering, Hanyang University, Seoul 133-791, South Korea*
[d] *Division of Engineering and Applied Sciences, Harvard University, Cambridge, MA 02138, USA*

Abstract

This study describes a flexible approach that allows us to characterize the long-term stability of antioxidants by using a thermodynamically extended Arrhenius equation. We use retinol, Vitamin A, as a model antioxidant and its degradation behaviors are characterized for both stabilized and non-stabilized systems; in this study, by using a fluid bed technique, we immobilize the retinol in lipid particles, thus increasing its thermal stability in complex formulations, such as aqueous polymer gels and emulsions. Our approach demonstrates that the degradation behaviors of the retinol show a functional relationship with temperature and time, which makes it possible to use the Arrhenius approach. This result allows us to precisely characterize the stability of antioxidants in complex formulations for long time.
© 2006 Elsevier B.V. All rights reserved.

Keywords: Long-term stability; Arrhenius equation; Antioxidant; Degradation behaviors; Fluid bed technique

1. Introduction

It has been known that as aged, drugs are usually loosing their original activity or performance. In many practical applications, this makes product characteristics escape from the required speculations, such as potency, performance, and discoloration [1,2]. Typically, this degradation behavior follows a specific pattern depending on the kinetics of the chemical reaction: zero-, first-, and second-order reactions [3–5]. The relationship between the degradation rate and time determines the order of the reaction [6–9].

By measuring the degradation rate at given conditions and subsequently correlating it with normal conditions, we can estimate the stability of drugs; the degradation rate is influenced by several variables, including humidity, pH, and pressure. Current techniques often use temperature, because temperature is the most common acceleration factor for changing chemical and physical properties of chemicals, pharmaceuticals, and biological products [10–13]. Since reaction kinetics were established by means of differential thermal analysis [10], the relationship between the temperature and degradation rate has been characterized by using the Arrhenius equation: $K = Ae^{-E/RT}$, where K is the observed rate constant, E the activation energy, R the gas constant, T the absolute temperature, and A is the pre-exponential factor.

This Arrhenius equation allows us to characterize the pattern of drug degradation. In fact, related to it, remarkable progresses have been made in the field of pharmaceuticals [14–17]. However, some applications, such as foods and cosmetics, usually consist of heterogeneous complex phases: emulsions, gels, and colloidal suspensions. These complex formulations may have many factors that are critical for the stability of the active materials inside. Therefore, we need to establish a generalized process that can quantitatively characterize the degradation of the active materials in such complex formulations.

∗ Corresponding author. Tel.: +1 617 496 0472; fax: +1 617 496 3088.
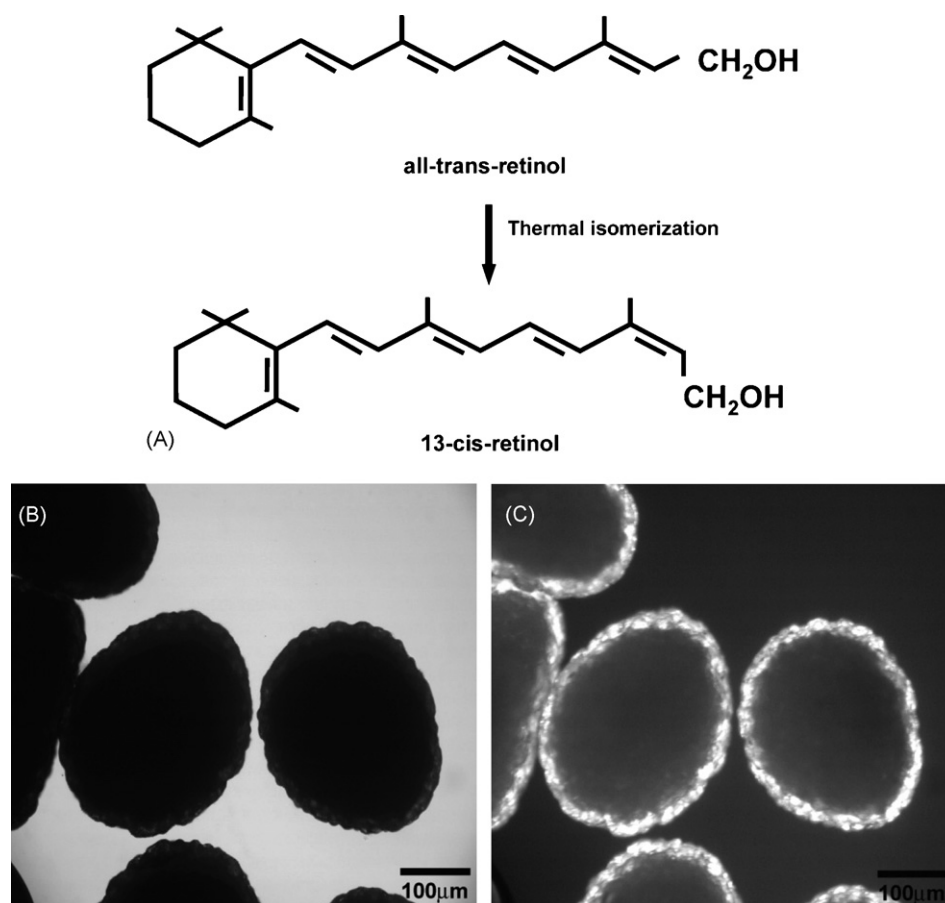*E-mail address:* jwkim@deas.harvard.edu (J.-W. Kim).

Fig. 1. (A) A molecular schematic for the degradation of a retinol molecule. Active all-*trans*-retinol is deformed by thermal isomerization to 13-*cis*-retinol. A bright field (B) and polarized (C) microscope images for the DSPC particles produced using the fluid bed technique. The DSPC particles contain 2 wt% all-*trans*-retinol in the layer of DSPC.

In this paper, we report a flexible and robust approach that allows us to precisely characterize the degradation of active materials, antioxidants, by using a thermodynamically extended Arrhenius equation. We used retinol, Vitamin A, as a model antioxidant. Retinol tends to easily reform by thermal isomerization process (see Fig. 1A) [18–20]. For more systematic characterization, we observe the retinol degradation in non-stabilized and stabilized systems, respectively. In the non-stabilized system, the retinol is just dissolved in a solvent, methanol; by contrast, in the stabilized system, we load the retinol molecules in lipid particles of micrometer size scales, increasing the thermal stability by means of the immobilization effect [21–24]. Then, we demonstrate the applicability of the extended Arrhenius equation for characterizing the long-term stability of the retinol in complex formulations.

2. Experimental methods

To measure the long-term stability of the retinol in the complex formulations, we designed a retinol-stabilized system. In this case, we prepared lipid particles that encapsulate the retinol by using a fluid bed technique (GPCG-1, Glatt, Germany) [25–28]. Sugar seed particles (500 g) (70 mesh, $d_n = 210\,\mu m$, International Product & Service, Italy) were loaded in the chamber. Retinol (20 g, Retinol-50C, BASF, Germany) and DSPC (430 g, 98% purity, 1,2-distearoylphosphatidylcholine, Lipoid GmbH, Germany) were dissolved by 10 wt% in an ethanol/methylene chloride (50/50, w/w) solution. Then, the solution was fed into the chamber of the spray coater with the feed rate of 10 g/min. Continuously, the surface of lipid particles was protected physically by coating with another thin layer of shallac (50 g, Opaglos GS-2-0401, Colorcon). A 10 wt% shallac solution prepared by dissolving in ethanol was fed again into the chamber with the feed rate of 10 g/min. During the coating process, air inlet temperature and air outlet temperature were controlled at 70 and 40 °C, respectively. Microscope observation for the produced lipid particles showed that they have ∼30 μm lipid layers (Fig. 1B and C).

The lipid particles were uniformly dispersed in an aqueous gel or an oil-in-water (O/W) emulsion. The aqueous gel with the lipid particles was prepared by adding them in a neutralized polyacrylic acid (0.01 wt%, Carbopol 941, GoldSchmidt, Germany). We also prepared a simple O/W emulsion containing the lipid particles; the emulsion was prepared by homogenizing a 12.5 wt% oil mixture in water at 7.0×10^3 rpm for 5 min at 70 °C. The oil mixture consisted of cetyl alcohol (4 wt%), stearyl alcohol (4 wt%), polyoxyethylene sorbitan monostearate (Tween-60, 9.6 wt%), sorbitan stearate (Arlacel 60, 2.4 wt%), and liquid

paraffin (80 wt%). Then, the lipid particles were homogeneously dispersed in the emulsion at room temperature. The viscosities of these formulations were adjusted to ~2.5 × 10⁴ cps by tuning the concentration of Carbopol 941. The concentration of retinol in these formulations was controlled with ~0.05 wt%. The formulations were completely sealed in a plastic tube and stored at four different temperatures: 25, 30, 37, and 45 °C.

We also tried to compare the degradation pattern of retinol in a non-stabilized condition. In this case, we simply dissolved 0.1 wt% retinol in methanol and stored at four different temperatures: 25, 30, 37, and 45 °C. Then, the stability of retinol was measured for a given time.

To determine the concentration of retinol in the formulations, we carried out HPLC measurements. First, we dissolved 1 g formulation containing retinol in 100 ml methanol. Ultrasonic was imparted to the diluted mixture for 20 min to completely dissolve retinol in methanol. Then, sample solutions were prepared by filtering the diluted solutions with a sintered-glass filter (pore size ~0.45 µm). The liquid chromatographic system used was a HP 1100 series. The chromatographic separation was achieved by the use of a Nova-Pak® C18 column (3.9 mm × 150 mm, Waters). The flow rate of the carrier solvent composed of acetonitrile/water (97/3, v/v) was 1 ml/min. The detection wavelength was set at 325 nm. The sample injection volume was 10 µl. In this HPLC condition, the retinol was detected at the retention time of 2.7 min. The stability of the retinol, S_0, was defined by the percentage of the remaining concentration compared to the initial concentration, $S_0(\%) = [R]_m/[R]_0 \times 100$, where $[R]_m$ is the measured concentration of retinol in the formulations and $[R]_0$ is the initial concentration of retinol in the formulations.

3. Results and discussion

To characterize the degradation behaviors of the retinol in a complex phase, we immobilize the retinol in the DSPC lipid particles by using a fluidized bed technique and disperse them in complex formulations an aqueous polymer gel and an O/W emulsion. The immobilization improves the thermal stability of the retinol. In our study, it is truly important to confirm whether the degradation of the retinol molecules in the lipid particles follows the Arrhenius equation:

$$\ln S_0 = \ln S_\infty + \frac{E}{RT}, \tag{1}$$

where S_0 is the stability of retinol molecules (%), S_∞ the infinite stability of retinol molecules, E the activation energy of the system, R gas constant, and T is temperature (K). To experimentally confirm this basic requirement, we measure the stability of the retinol in the aqueous gel with the temperature and storage time and rearrange as $\ln S_0$ versus $1/T$, as shown in Fig. 2A. We can observe that for given storage time, all $\ln S_0$ linearly regress. All significance probability values, p-values for these fittings are less than 0.05, which means the linear relationships are confidential for the given data. This shows that the Arrhenius approach can be used for the characterization of retinol stability even in the aqueous gel formulation.
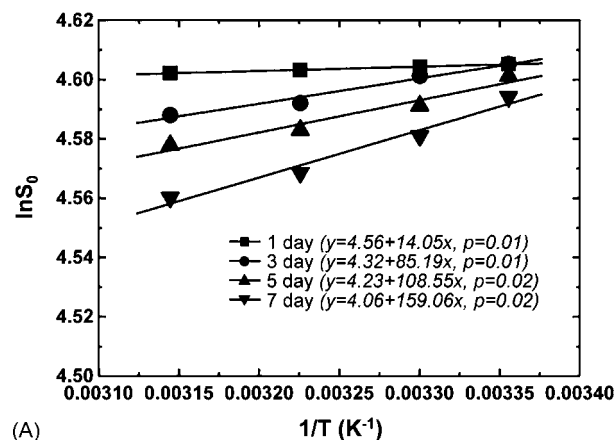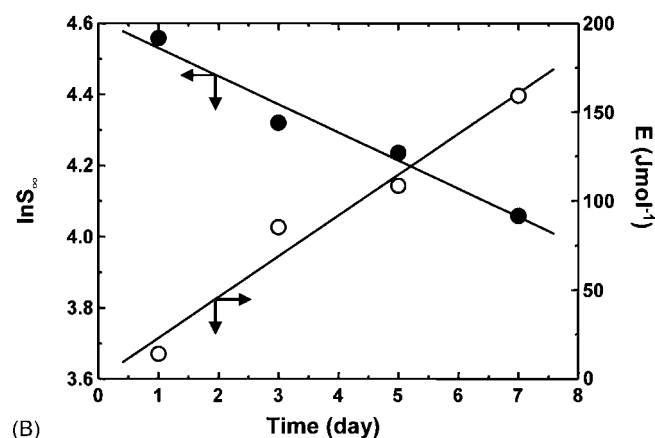
Fig. 2. (A) Linear fitting of retinol stability with reciprocal temperature at four different storage times. (B) Functional relationship of retinol stability (closed circles) and activation energy (open circles) with storage time.

The slopes in Fig. 2A are the activation energies, and the extrapolation points to Y-axis are $\ln S_\infty$. Using the relationships, $\ln S_\infty$ versus time and E versus time, we are able to add a time variable, t. Then, $\ln S_\infty$ and E can be empirically expressed as a linear function of t, respectively:

$$\ln S_\infty = s_1 + s_2 t \tag{2}$$

and

$$E = E_1 + E_2 t, \tag{3}$$

where s_1 is the extrapolated stability corresponding to $\ln S_\infty$ at $t = 0$, s_2 the slope against t, E_2 the extrapolated activation energy corresponding to the activation energy at $t = 0$, and E_2 is the slope against t. The result is shown in Fig. 2B. It can be seen that both $\ln S_\infty$ and E are linearly correlated with t. From this result, we can empirically obtain a thermodynamic equation for the degradation of the retinal:

$$\ln S_\infty = s_1 + \frac{E_1}{RT} + \left(s_2 + \frac{E_2}{RT} \right) t. \tag{4}$$

The applicability of this equation can be demonstrated by determining a thermodynamic criterion. The thermodynamic criterion is determined as follows: the derivative $[\partial \ln S_0/\partial(1/T)]_t$ at a fixed t is $(E_1 + E_2 t)/R$; the derivative $[\partial \ln S_0/\partial t]_{1/T}$

Fig. 4. Characterization of long-term stability of the retinol by using the extended Arrhenius equation, Eq. (4). The retinol stability is calculated at 25 °C (open squares) and 40 °C (open circles) in methanol, and at 25 °C (closed squares) and 40 °C (closed circles) in DSPC particles in aqueous gels. The inset is the comparison of the calculated stability to measured stability.
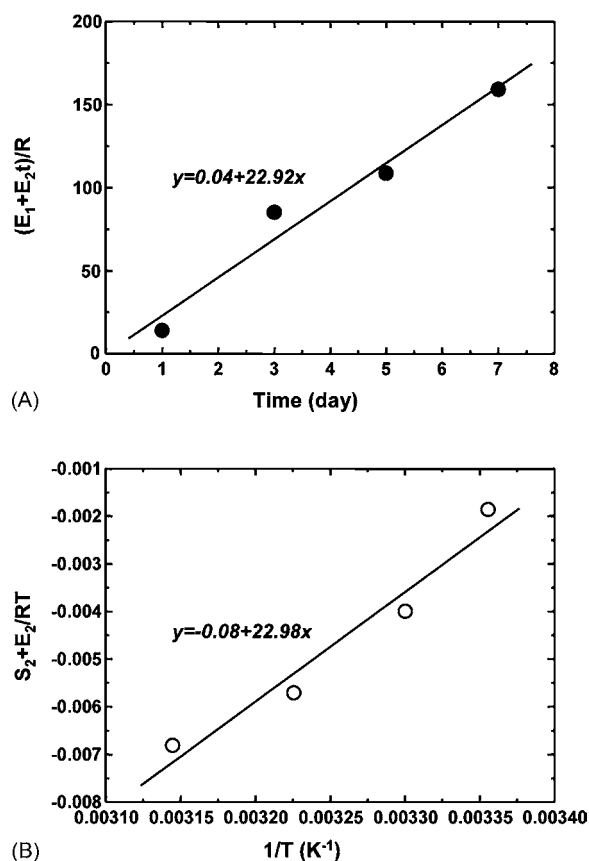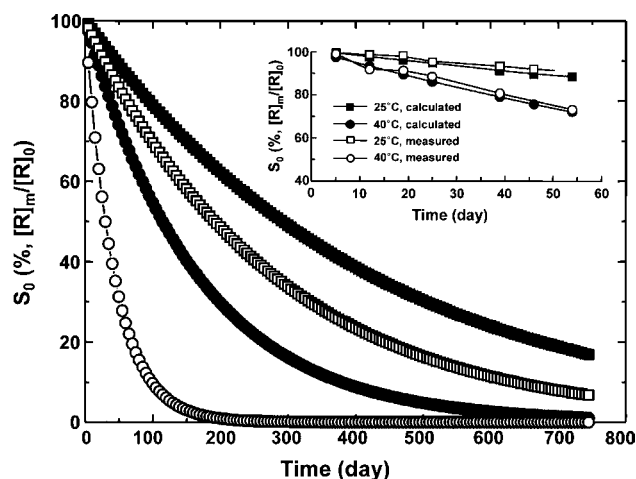
Fig. 3. Determination of thermodynamic criterion from the functional relationships between $(E_1 + E_2 t)/R$ and storage time (A), and $s_2 + E_2/RT$ and $1/T$ (B). For these two fittings, p-values were 0.02, respectively.

$[\partial \ln S_0/\partial t]_{1/T}$ at a fixed temperature is $s_2 + E_2/RT$. Using these two derivatives, we can obtain the thermodynamic criterion:

$$\frac{\partial^2 \ln S_0}{\partial(1/T)\partial t} = \frac{\partial^2 \ln S_0}{\partial t \partial(1/T)} = \frac{E_2}{R}. \tag{5}$$

The values of $(E_1 + E_2 t)/R$ corresponding to the slopes of Fig. 2A are plotted as a function of time, as shown in Fig. 3A. Likewise, $\ln S_0$ is represented against t and the slopes corresponding to $s_2 + E_2/RT$ are plotted again against $1/T$, as shown in Fig. 2B. The slopes in Fig. 3A and B correspond to E_2/R in Eq. (5). As a result, E_2/R values taken from the slopes are 22.92 and 22.98, respectively. These two E_2/R values are almost identical. This result means that Eq. (4) satisfies the thermodynamic criterion and is a state function of time and temperature.

This approach can be generalized by confirming the degradation of retinol in different complex formulations. To do this, we measure the stabilities of retinol in an O/W emulsion and apply them to the extended Arrhenius equation. All the parameters obtained are listed in Table 1. We can observe that the parameters obtained from the OW emulsion are similar to those from the aqueous gel. This means that once the retinol was immobilized between the lipid layers, its degradation pattern is independent on the type of formulations.

Using the thermodynamic equation, we can estimate the long-term stabilities of the retinol. To compare the effect of stabilization method, we carry out the same process for the non-stabilized system in which the retinol is just aged in methanol solution. We observe that in the non-stabilized system, $\ln S_\infty$ also show a linear relationship with t and $1/T$ with $p = 0.01$–0.05. The average value of E_2/R is 123.09. The parameters are summarized in Table 1. By combining these parameters with Eq. (4), we can predict long-term stabilities of retinol, as shown in Fig. 4. The degradation of the retinol is the first-order reaction with t. The shelf life, t_{50}, defined as the time for the retinol to thermally isomerize to 50% from all-*trans*-retinol to 13-*cis*-retinol, is indeed dependent on the temperature; for example, t_{50} of 25 °C is much longer than that of 40 °C, which is ~2.6 times at the stabilized system and ~7.6 times at non-stabilized system. The environment where the retinol molecules are located is also critical for changing their shelf life. In the DSPC particles, they show higher t_{50} than in methanol solution by ~1.5 times at 25 °C and ~4.5 times at 40 °C, respectively, meaning that the immobilization of the retinol between lipid layers changes the activation energy of

Table 1
Parameters for the degradation of the retinol molecules in complex formulations

System	Medium	s_1[a]	s_2	E_1/R	E_2/R[b]
Non-stabilized	Methanol	4.74 (0.3)	−0.42	−41.07	123.09
Stabilized	Polymer gel	4.61 (0.1)	−0.08	0.038	22.95
Stabilized	Oil-in-water emulsion	3.55 (0.5)	0.01	0.020	30.05

[a] These values were empirically determined by using all the experimental data. Values in parenthesis are in percent.

[b] These were taken by average from the two values that satisfy the thermodynamic criterion.

the degradation reaction. The non-stabilized system has a lower value of E_1/R than the stabilized system, causing the retinol to deform more easily in the methanol. This result suggests that the stabilization method is important and plays a role in determining the activation energy which is closely related to the degradation behaviors of the retinol molecules.

In this study, we compare the calculated stability to measured stability to confirm the applicability of this thermodynamic approach. As shown in the inset in Fig. 4, the stability of the retinol calculated by using Eq. (4) shows a good agreement to the measured stability for a long storage time. This demonstrates that a thermodynamic approach correlated with the Arrhenius equation can be used for the quantitative characterization of antioxidant degradation behaviors in the complex formulations.

4. Conclusions

We describe an Arrhenius equation-based thermodynamic approach for quantitatively characterizing the degradation patterns of antioxidants in a complex formulation. We show that the degradation behaviors of antioxidants have a functional relationship with both temperature and time. Based on this result, we thermodynamically extend the Arrhenius equation, which will allow us to estimate the long-term stability for a variety of active materials, such as enzymes and peptides. Furthermore, since we understand the relationship between the thermal stability and activation energy, this approach is expected to provide a useful means that we can characterize the stability of active materials even in a wide variety of complex formulations.

Acknowledgements

References

[1] E.B. Vadas, in: A.R. Gennaro, G.D. Chase, A.D. Marderosian, G.R. Hanson, D.A. Hussar (Eds.), The Science and Practice of Pharmacy, 19th ed., Mack Publishing Co., Easton, Pennsylvania, 1995.
[2] R.T. Darrington, J. Jiao, J. Pharm. Sci. 94 (2004) 838.
[3] W. Nelason, Accelerated Testing: Statistical Models, Test Plans, and Data Analysis, John Wiley & Sons, Inc., New York, 1990.
[4] S.O. King, M. Kung, H. Fung, J. Pharm. Sci. 73 (1984) 2332.
[5] M.S. Tydeman, T.B.L. Kirkwood, J. Biol. Stand. 12 (1984) 195.
[6] A. Oliva, A. Santoveña, J. Farina, M. Llabrés, J. Pharm. Biomed. Anal. 33 (2003) 145.
[7] C.J. Roberts, P.G. Debenedetti, AIChE J. 48 (2002) 1140.
[8] V.G. Dabbene, M.C. Briñón, M.M. Bertorello, Talanta 44 (1997) 159.
[9] D. Stepensky, M. Chorny, Z. Dabour, I. Schumacher, J. Pharm. Sci. 93 (2004) 969.
[10] H.J. Borchardt, F. Daniels, J. Am. Chem. Soc. 79 (1957) 41.
[11] J.T. Carstensen, K.S.E. Su, Bull. Parent Drug Assoc. 25 (1971) 287.
[12] B. Eisen, Y. Ungar, E. Shimoni, J. Agric. Food Chem. 51 (2003) 2212.
[13] J. Lalevee, X. Allonas, J.-P. Fouassier, Macromolecules 38 (2005) 4521.
[14] X.Y. Su, A.L.W. Po, S. Yoshioka, J. Therm. Anal. 41 (1994) 713.
[15] X. Zhan, G. Yin, B. Ma, J. Pharm. Sci. 86 (1997) 1099.
[16] X. Zhan, B. Ma, Acta Pharm. Sin. 29 (1992) 132.
[17] S. Li, C. Schoneich, R.T. Borchardt, Biotechnol. Bioeng. 48 (1995) 490.
[18] M.H. Lee, S.G. Oh, S.K. Moon, S.Y. Bae, J. Colloid Interface Sci. 240 (2001) 83.
[19] V. Jenning, A. Gysler, M. Schäfer-Korting, S.H. Gohla, Eur. J. Pharm. Biopharm. 49 (2000) 211.
[20] L.H. Wang, Anal. Chim. Acta 416 (2000) 193.
[21] G. Gregoriadis, Preparation of Liposomes, CRC, Boca Raton, FL, 1998.
[22] P.F. Devaux, Biochemistry 30 (1991) 1163.
[23] P. Ratanabanangkoon, M. Gropper, R. Merkel, E. Sackmann, A.P. Gast, Langmuir 18 (2002) 4270.
[24] X. Qiu, S. Leporatti, E. Donath, H. Mohwald, Langmuir 17 (2001) 5375.
[25] Y.F. Maa, C.C. Hsu, Biotechnol. Bioeng. 53 (1997) 560.
[26] E. Hamed, A. Sakr, J. Control Rel. 73 (2001) 329.
[27] N. Pearnchob, R. Bodmeier, Int. J. Pharm. 268 (2003) 1.
[28] N. Sinchaipanid, V. Junyaprasert, A. Mitrevej, Powder Technol. 141 (2004) 203.

Short communication

A fluorescence detection scheme for ultra large molecules after gas phase separation

Jian He [a],[1], Wenwan Zhong [a], Aijun Tang [a], Xiaomei Yan [b],[1],
Cris Lewis [a], Vahid Majidi [a], Wei Hang [a],*

[a] *Chemistry Division, MS K484, Los Alamos National Laboratory, Los Alamos, NM 87544, United States*
[b] *Bioscience Division, MS M888, Los Alamos National Laboratory, Los Alamos, NM 87544, United States*

Abstract

A system was proposed to remove the upper mass limitation of mass spectrometry. In present study, ultra large molecules were separated in the gas phase by mass analyzer after electrospray ionization. Instead of conventional detection with electron multiplier, a laser-induced-fluorescence detection scheme was applied. The instrument sensitivity is independent of molecular weight, but related to the spectroscopic properties of the fluorophores presented by the large biomolecules.
© 2007 Published by Elsevier B.V.

Keywords: Ultra large molecules; Fluorescence detection; Ion mobility spectrometry; Mass spectrometry

1. Introduction

With the introduction of matrix assisted laser desorption/ionization (MALDI) and electrospray ionization (ESI) sources, mass spectrometry has emerged as an important bioresearch tool due to its high accuracy, resolution, sensitivity and throughput [1]. Mass spectrometry has been used not only to identify proteins and their sequences, but also to study genotyping, non-covalent interaction and conformational structure. Although over mega-Dalton polymer ions can be generated in the MALDI source, the signal detected was very weak [2]. The popular ESI is a soft ionization technique and non-covalent bonds can be preserved during the ion formation process. Intact ions of large DNA fragments ($>10^8$ Da) have been generated by ESI [3]. However, ions generated in ESI source possess multiple charges; the intricate spectra are hard to resolve if several species are presented. This problem can be solved by exposing the electrospray generated aerosol to a neutralizing gas containing high concentration of bipolar ions, which can

effectively reduce the multiply charged ions to singly charged ions [4].

Despite the viability of generating over-mega-Dalton ions in the ion sources, most of the mass analyzers, such as quadrupole, sector, and ion trap have limited mass detection range (normally several kilo-Dalton). Fourier transform ion cyclotron resonance (FTICR) mass spectrometry has the potential for large ion detection, but instrument cost can easily escalate to multimillion-dollar price tag. Time-of-flight mass spectrometry (TOFMS), like FTICR, has no theoretical upper mass limit. TOFMS exhibits fast response time, high transmission rate and simple design. Its mass precision can be lower than 10 ppm, which is at least 3 orders of magnitude higher than that offered by chromatographic–electrophoretic techniques. However, in practice, the upper mass range of TOF systems is limited by the response (or more precisely, the lack of response) of the detector. Studies conducted by Larson et al. [5] showed that the signals detected for large molecules were very weak because their velocity were too low to initiate electron cascades on the microchannel plate (MCP) detector. Current state-of-the-art mass spectrometry for high molecular weight detection is limited to 100–200 kDa.

Some attempts have been made for mega-Dalton molecule detection in the gas phase. A novel charge detection device has been used to measure ultra large molecules [6], provided the first mass measurement of intact viruses with mega-Dalton

---

mass weight [7]. Gas phase electrophoretic mobility spectrometer has also been applied successfully by several research groups for large molecule detection, including large proteins, protein complexes and viruses [8–10].

In present study, we propose an alternative approach for the detection of ultra large molecules by using laser induced fluorescence (LIF) detection upon their gas phase separation in mass spectrometry. LIF has been widely used for biomolecule detection even down to single molecule level [11]. This technology is mainly used for molecule detection in liquid environment. Here, we adopt LIF detection scheme for the detection of gas phase ions after mass spectrometry separation.

2. Experimental

Proof-of-principle experiment was carried out using electrospray source, ion mobility spectrometer and fluorescence detection cell, as shown in Fig. 1. A commercial electrospray ion source with charge reduction device (Model 3480, TSI, Shoreview, MN) was used in the experiment. The electrospray pushes charged liquid solution through a capillary tube and exerts an electrical field on the liquid at the capillary tip. The electrical field pulls the liquid from the capillary, forming individual droplets. Air and CO_2 mixed with the droplets evaporate the liquid. Multiply charged ions go through charge reduction processes, most of them are neutralized, small amount of them become singly charged [8]. A radioactive source (Po-210) was used for charge reduction. The ion mobility spectrometer (model 3936, TSI), featuring a scanning electrophoretic differential mobility analyzer, was used in the experiment. It provides size separation and analysis of macromolecules (interpretable as a mass spectrum). The size parameter provided is the electrical mobility diameter, related to the collision cross section of the macro-ion in the flow of gas.

Macromolecules separated by the ion mobility spectrometer flow into an in-house built fluorescence detection cell. In this device, macromolecules flow through a stainless steel tubing

of 3 mm o.d.. A laser beam (488 nm, 100 mW, model Innova-90, Coherernt, Santa Clara, CA) passes along the axis of the tubing as the excitation light. An optical fiber (Model P600-2-VIS-NIR, Ocean Optics, Dunedin, FL) and collimate lens collect fluorescence and scattering lights to a simple monochromator. Scattering laser light is filtered out by the monochromator, only the fluorescence near 560 nm is detected by the PMT. The exit of the detection cell links to a standard condensation particle counter (model 3025A, TSI). Signal from the particle counter was used for comparison with the signal from the fluorescence detection cell.

Fluorescent microspheres were used to act as the dyed ultra large molecules. TransFluoSpheres® carboxylate-modified microspheres of 0.04 μm in diameter (about 25 mega-Dalton, T-8864) and 0.1 μm (about 240 mega-Dalton, T-8872, Invitrogen, Carlsbad, CA) were selected. According to the data sheets, both microspheres have excitation and emission wavelengths of 488 and 560 nm in the liquid phase, respectively. Sample solutions were prepared in 20 mM ammonium acetate with a concentration of 1 μg/ml.

3. Results and discussion

The selection of excitation and emission wavelengths of 488 and 560 nm was based on previous investigations by several groups [12–14]. Those studies for characteristic wavelengths were carried out in the gas phase. At the atmospheric pressure, no matter with the MALDI source [12] or electrospray ionization source [13], studies showed that the excitation and emission spectra of the fluorophores are close to those in the solution. Even under high vacuum, fluorescence signals could still be acquired with the emission wavelengths similar to their emission in liquid phase [14]. In our experiment, the excitation wavelength was fixed by argon laser at 488 nm. The maximum fluorescence signal was obtained near 560 nm by scanning the monochromator.

As shown in Fig. 2, experiment result clearly demonstrates the feasibility of laser induced fluorescence detection in the gas phase after mass separation. With particle counting detector, signal of 40- and 100-nm microspheres are observed. Other than these two desired peaks, a small peak representing 65-nm microspheres is also shown in the spectra. This peak was observed only if the 100-nm microspheres run through the system, which indicates that the 100-nm microsphere sample could contain minus amount of 65-nm microspheres. When fluorescence detection was applied, signal obtained from 40-nm microspheres was weaker than that from the 65-nm microspheres. Signal from the 100-nm microspheres was so large that saturated the PMT detector. This phenomenon is within our expectation because larger molecules will have more sites available for fluorophore conjugation and consequently yield stronger fluorescence signal. This characteristic is different from the normal electron-multiplier type detector of the mass spectrometer, in which larger ions yield lower signals due to their slower speeds. Therefore, with fluorescence detection scheme, the sensitivity of the instrument increases with the molecular weight if larger molecules have more binding sites available and more fluorophores are bound. The ion mobility spectrometer used in our experiment
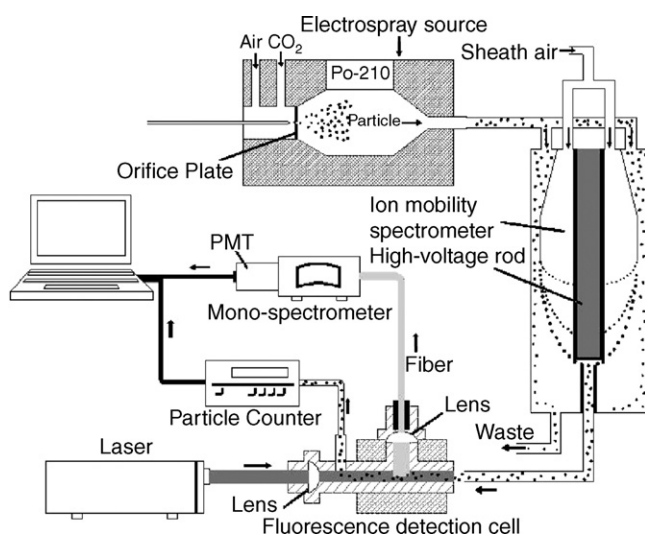

Fig. 1. Schematic diagram of laser induced fluorescence time-of-flight mass spectrometer.
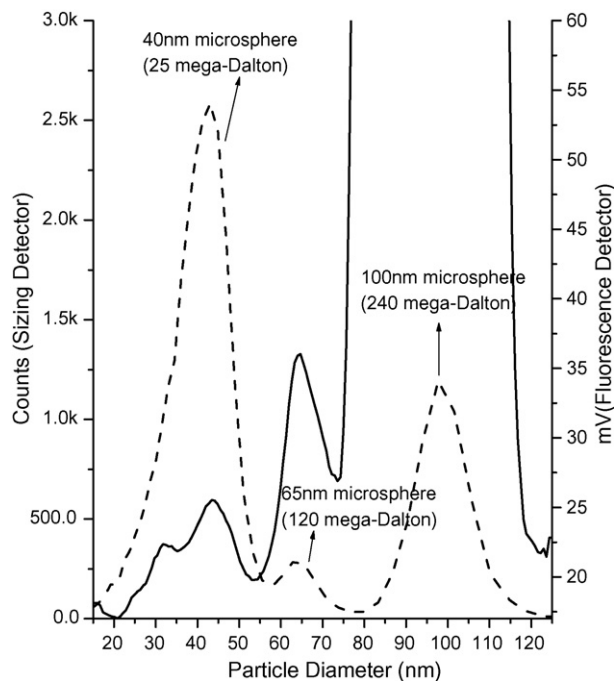
Fig. 2. Spectra of fluorescent microspheres from particle counter (dash line) and fluorescence detector (solid line).

was designed for measuring particles with the size from 2.5 to 1000 nm. Therefore, the transmission efficiency in the range from 40 to 100 nm should be quite even. Its transmission efficiency shall not cause significant mass discrimination to affect the sensitivity of the detection in our experiment.

4. Conclusion and outlook

Although an ion mobility spectrometer offering low resolution spectra was used in this study, LIF detection scheme can be applied to any type of mass spectrometers, as long as intact ions of sample-dye complexes can be generated. With this approach, the upper mass limit barrier in mass spectrometry can be removed while maintaining high-resolution separation inherent in mass spectrometry.

Exact mass of the large molecule can be determined if the binding ratio of the fluorophore to molecule is known. The drawback of the fluorescence detection scheme is that the binding ratio is not known in all cases. For example, for DNA fragments, the binding ratios of commonly used intercalating dyes to DNA fragments are well characterized; but for protein, the ratios are only roughly known. Nevertheless, fluorophores are small molecules; their weight composes only a very small mass fraction of the fluorophore-molecule complex. As a result, the mass spectrometer with fluorescence detection scheme can still offer

molecular weight measurement of ultra large molecules. If high resolution mass analyzer were used, its resolving power should be much better than the resolutions from other techniques, such as size exclusive chromatography [15], light scattering [16] or capillary polyacrylamide gel electrophoresis [17].

Since the molecule excitation and fluorescence emission are carried out in gas phase, background interferences due to Raman scattering and Rayleigh scattering can be substantially reduced compared to the liquid phase. Also, there will be little collisional quenching and background emission associated with fluorescent impurities which are usually encountered in the solvent. Furthermore, the gain of the electron multiplier in MALDI-TOFMS is limited by the saturation of matrix peaks. In our approach, only those molecules bound with fluorophores will have fluorescence. Therefore, signal can be acquired at the full potential of the photon detector, and the spectra will be more explicit than that of conventional mass spectrometer detector.

Acknowledgements

References

[1] G. Siuzdak, The Expanding Role of Mass Spectrometry in Biotechnology, MCC Press, San Diego, 2003.
[2] D.C. Schriemer, L. Li, Anal. Chem. 68 (1996) 2721.
[3] R. Chen, X. Cheng, D.W. Mitchell, S.A. Hofstadler, A.L. Rockwood, R.D. Smith, Anal. Chem. 67 (1995) 1159.
[4] M. Scalf, M.S. Westphall, J. Krause, S.L. Kaufman, L.M. Smith, Science 283 (1999) 194.
[5] B.S. Larsen, W.J. Simonsick Jr., C.N. McEwen, J. Am. Soc. Mass Spectrom. 7 (1996) 287.
[6] W.H. Benner, Rapid Commun. Mass Spectrom. 13 (1999) 15.
[7] S.D. Fuerstenau, W.H. Benner, J.J. Thomas, C. Brugidou, B. Bothner, G. Siuzdak, Angew. Chem. Int. Ed. 40 (2001) 542.
[8] G. Bacher, W.W. Szymanski, S.L. Kaufman, P. Zöllner, D. Blaas, G. Allmaier, J. Mass Spectrom. 36 (2001) 1038.
[9] J.J. Thomas, B. Bothner, J. Traina, W.H. Benner, G. Siuzdak, Spectroscopy 18 (2004) 31.
[10] K. Cottingham, Anal. Chem. 75 (2003) 452A.
[11] N.J. Dovichi, J.C. Martin, J.H. Jett, M. Trkula, R.A. Keller, Anal. Chem. 56 (1984) 348.
[12] T.W. Heise, E.S. Yeung, Anal. Chem. 64 (1992) 2175.
[13] S. Zhou, A.G. Edwards, K.D. Cook, Anal. Chem. 71 (1999) 769.
[14] A.A. Puretzky, D.B. Geohegan, Chem. Phys. Lett. 286 (1998) 425.
[15] C.R. Cantor, P.R. Schimmel, Biophysical Chemistry, Part 2, Freeman WH, New York, 1980.
[16] S.E. Harding, K. Jumel, Curr. Protocols Protein Sci. 7 (1998) 1.
[17] P.D. Grossmann, J.C. Colburn, Capillary Electrophoresis: Theory and Practice, Academic Press, New York, 1996.

Cation selectivity of ionophores based on tripodal thiazole derivatives on benzene scaffold

Hong-Seok Kim [a,*], Dong-Hyun Kim [a], Ki Soo Kim [a], Jun-Hyeak Choi [a],
Heung-Jin Choi [a], Sung-Hoon Kim [b], Jun Ho Shim [c],
Geun Sig Cha [c], Hakhyun Nam [c,**]

[a] *Department of Applied Chemistry, Kyungpook National University, Daegu 702-701, Republic of Korea*
[b] *Department of Textile System Engineering, Kyungpook National University, Daegu 702-701, Republic of Korea*
[c] *Chemical Sensor Research Group, Department of Chemistry, Kwangwoon University, Seoul 139-701, Republic of Korea*

Abstract

The synthesis and potentiometric evaluation of new 1,3,5-tris(thiazolylcarbethoxy)-2,4,6-trimethylbenzene (**3**), 1,3,5-tris(thiazolylhydroxy)-2,4,6-trimethylbenzene (**4**), 1,3,5-tris(thiazolylmethyl)-2,4,6-trimethylbenzene (**5**), and 1,3,5-tris(thiazolylphenyl)-2,4,6-trimethylbenzene (**6**), toward mono and divalent cations under various pH conditions are outlined. The ion-selective properties of the newly synthesized compounds were studied by measuring the potentiometric responses of the **3**-, **4**-, **5**-, and **6**-based membrane electrodes to alkali metal, alkaline earth metal, ammonium, and transition metal ions, under various pH conditions. The **3**-based electrode exhibited a Nernstian response to ammonium and potassium under alkaline pH conditions, while the other three electrodes showed a poor potentiometric performance. All electrodes showed substantial responses to silver ion under acidic condition, but there was almost nil response to other transition metal ions (Fe^{2+}, Co^{2+}, Zn^{2+}, Ni^{2+}, Pb^{2+}, Cd^{2+}, Cu^{2+} and Hg^{2+}). The **3**- and **5**-based electrodes resulted in near Nernstian responses (51.3 mV and 59.5 mV/pAg$^+$, respectively) with low detection limits (~100 ppt), while the **4**- and **6**-based ones showed sub-Nernstian below 40 mV/pAg$^+$. The results were interpreted with semi-empirically modeled structures.
© 2006 Elsevier B.V. All rights reserved.

Keywords: Tripodal thiazole scaffold; Ionophore; Cation selectivity; Silver (I)

1. Introduction

The design and research of artificial receptors for the selective recognition of metal ions has attracted increasing interest because of its significant importance and potential application in physiological, environmental, and supramolecular chemistry [1]. Silver (I) is one of the main transition metals used in industries and drugs. Due to their antibacterial properties, silver compounds have been used to disinfect potable water, and they have been used for dental and pharmaceutical purposes. Therefore, the design of Ag$^+$-selective neutral carriers and the

construction of ion-selective electrodes (ISEs) have attracted much attention regarding environmental and clinical analyses [2,3].

A benzene ring may be used as a small, rigid platform for receptor systems. Since McNicol discovered the preorganization of functional groups in hexasubstituted benzene derivatives [4], benzene-based receptor molecules have been widely used as building blocks for extended, well-defined molecular architecture and as a scaffold of synthetic receptors that show high selectivity toward cations, anions and organic molecules [5–12]. Raymond et al. synthesized tripodal ionophores by attaching three catechol units to benzene and mesitylene and their cation affinity was evaluated [13]. They found that the binding constant of 1,3,5-tris(catechol)mesitylene for Fe (III) is higher than that of the natural compound enderrobactin, which showed uniquely strong binding affinity toward Fe (III). This discovery has led to the exploration of this benzene motif for cation

---

* Corresponding author. Tel.: +82 53 950 5588; fax: +82 53 950 6594.
** Co-corresponding author. Tel.: +82 2 940 5246; fax: +82 2 942 4635.
E-mail addresses: kimhs@knu.ac.kr (H.-S. Kim),
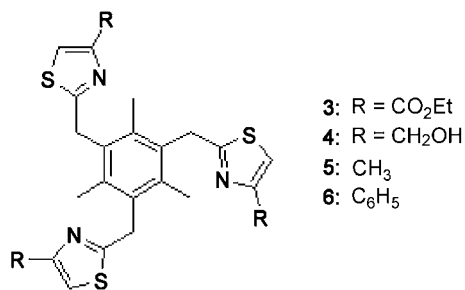namh@daisy.kw.ac.kr (H. Nam).

Fig. 1. Structures of the newly-synthesized ionophores.

recognition purposes. By incorporating heterocyclic units such as pyrazol, indole, and pyridine into a benzene motif, complexation studies with Pd(II) [14], Fe(II) [15,16], and Cu(I) [17] were performed. Kim et al. synthesized tris(pyrazol)benzene for the recognition of NH_4^+ and alkyl ammonium cations [18,19]. They found that ion-selective electrodes using the immobilized tris(pyrazol)benzene showed profound selectivity toward NH_4^+ over Na^+ and K^+. Ahn et al. also studied the complexities of alkylammonium cations by tris(oxazolin)benzene [11].

Various ionophores including calix[4]arenas [20–22], crown ether derivatives [23–25], and steroidal tweezers [26] have been used for the selective detection of Ag^+ ions by introducing soft heteroatoms such as N and S, as an electron donor to metal cations. In order to enhance their complexing cation selectivity, many heterocyclic units such as pyridyl, bipyridyl, bithiazoloyl have been introduced into calixarene on their lower and upper rims [20–22].

Recently, we have designed new neutral carriers that contain thiazole moieties [27–31]. The ISEs based on solvent polymeric membranes (plasticized PVC) doped with these ionophores, exhibited large cation selectivity. To better understand the cation recognition mechanisms of these membranes, we synthesized four different mesitylene-based receptors having tripodal thiazole units (compounds **3**–**6** in Fig. 1 and Scheme 1), and prepared those receptor-based membrane ISEs. In this paper, we report their response characteristics to various mono and divalent cations (alkali metal, alkaline earth metal, transition metal ions and ammonium), as well as our understanding of

their ion-recognition properties by the use of model structures [32].

2. Experimental

2.1. General

Melting points were determined using a Thomas–Hoover capillary melting point apparatus (Thomas Scientific, USA). ^{1}H and ^{13}C NMR spectra were obtained using a Varian UNITY Inova 300WB FT-NMR Spectrometer (Varian Inc., Palo Alto, USA) in $CDCl_3$. Chemical shifts in the ^{1}H NMR spectra were reported using δ units downfield from the internal tetramethylsilane. The IR spectra were measured with a Galaxy FT-IR 7000 spectrophotometer (Mattson Instrument, Madison, USA). Mass spectra were recorded on a Shimadzu QP-1000 spectrometer (Shimadzu Scientific Instrument, Kyoto, Japan). Elemental analyses were performed on a Calro Erba 1106 (CE Instruments, Millan, Italy) at the Center for Scientific Instruments, Kyungpook National University. TLC analyses were carried out on Merck silica gel 60F$_{254}$ plates, visualized with a 254-nm UV lamp. For routine column chromatography, Merck silica gel (70–230 mesh) was used as the adsorbent (Merck, Darmstadt, Germany, Art 7734). All anhydrous reactions were carried out under a nitrogen atmosphere. Solutions were dried over anhydrous sodium sulfate.

Mesitylene, sodium cyanide, lithium aluminum hydride, ethyl bromopyruvate, chloroacetone, and 2-bromoacetophenone were obtained from commercial chemical companies and used without further purification. Solvents were obtained and dried by usual laboratory techniques. Poly(vinyl chloride) (PVC) and bis(2-ethylhexyl) adipate (DOA) were purchased from Fluka Chemie AG (Buch, Switzerland). 1,3-Bis[tris(hydroxymethyl)methylamino]propane (Bis–tris propane) and 2-amino-2-(hydroxymethyl)-1,3-propanediol (Tris) were purchased from Sigma (St. Louis, MO, USA). All other chemicals for analytical experiments were of analytical-reagent grade. Standard solutions and buffers were prepared with freshly deionized water (18 MΩ cm). 1,3,5-Tris(cyanomethyl)-2,4,6-trimethylbenzene (**1**) was prepared by known literature procedure [5].

Reaction Conditions: i) H_2S (g), Et_3N/DMF; ii) $BrCH_2COCO_2Et$/dry EtOH; iii) $ClCH_2COCH_3$/benzene; iv) $BrCH_2COC_6H_5$/benzene; v) $LiAlH_4$/THF.
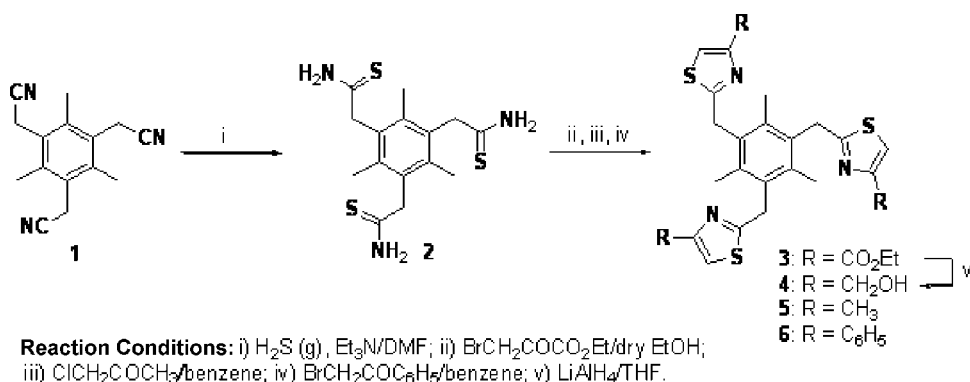
Scheme 1. Synthetic procedure of tripodal thiazole derivatives.

2.2. Synthesis

2.2.1. 1,3,5-Tris(thioamidomethyl)-2,4,6-trimethylbenzene (2)

H_2S gas was introduced to a mixture of **1** (500 mg, 2.11 mmol) and triethylamine (10 mL) in a DMF (30 mL) at room temperature for 5 h with stirring. After the solvent was removed, the residue was crystallized with CH_2Cl_2 and hexane to give **2** (550 mg, 77%). TLC, R_f 0.40 (100% EtOAc); mp 195–196 °C; IR (KBr) 3273, 3133, 1632, 1425, 1215, 951, 789, 721 cm^{-1}; ^{1}H NMR, δ: 8.99 (s, 3H, N*H*), 7.45 (s, 3H, N*H*), 3.61 (s, 6H, ArC*H*$_2$CSNH$_2$), 1.65 (s, 9H, ArC*H*$_3$); ^{13}C NMR, δ: 204.6 (*C*SNH$_2$), 135.8, 130.2, 46.4, 15.7; Anal. Calcd. for $C_{15}H_{21}N_3S_3$: C, 53.06; H, 6.23; N, 12.38; S, 28.33; Found: C, 53.21; H, 6.03; N, 12.16; S, 28.16.

2.2.2. 1,3,5-Tris[2′(4′-carbethoxythiazolyl)methyl]-2,4,6-trimethylbenzene (3)

A mixture of **2** (1.0 g, 2.95 mmol) and ethyl bromopyruvate (1.9 g, 9.74 mmol) in dry EtOH (50 mL) was refluxed for 4 h. After the solvent was removed, the mixture was extracted with CH_2Cl_2. The organic layer was dried and concentrated. The residue was chromatographed (elution with EtOAc:hexane, 2:1) on silica gel to give **3** (1.69 g, 91%). TLC, R_f 0.50 (100% EtOAc); mp 219 °C (CH_2Cl_2–hexane); IR (KBr) 3097, 2982, 1719, 1480, 1335, 1230, 1099, 1022, 777 cm^{-1}; ^{1}H NMR, δ: 8.01 (s, 3H, Thz*H*), 4.54 (s, 6H, ArC*H*$_2$Thz), 4.44 (q, $J = 6.9$ Hz, 6H, ThzCO$_2$C*H*$_2$CH$_3$), 2.29 (s, 9H, ArC*H*$_3$), 1.42 (t, $J = 6.9$ Hz, 9H, ThzCO$_2$CH$_2$C*H*$_3$); ^{13}C NMR, δ: 172.1, 161.3, 147.2, 136.5, 133.9, 127.1, 61.4, 34.8, 17.0, 14.2; MS, m/z: 627 (M^+, 100), 594 (45), 512 (29), 494 (29), 470 (65), 300 (33); Anal. Calcd. for $C_{30}H_{33}N_3O_6S_3$: C, 57.39; H, 5.30; N, 6.69; S, 15.32; Found: C, 57.59; H, 5.34; N, 6.55; S, 15.43.

2.2.3. 1,3,5-Tris[2′(4′-hydroxymethylthiazolyl)methyl]-2,4,6-trimethylbenzene (4)

LiAlH$_4$ (115 mg, 3.01 mmol) was added to a solution of **3** (317 mg, 0.50 mmol) in a dry THF (20 mL) in an ice bath. The mixture was stirred for 6 h at the same temperature and ethyl acetate was added to the resulting mixture to destroy excess LiAlH$_4$. After the solvent was removed, the residue was extracted with ethyl acetate. The organic layer was dried and concentrated. The residue was chromatographed (elution with 100% ethyl acetate) on silica gel to give **4** (190 mg, 75%). TLC, R_f 0.21 (1:9, CH$_3$OH:EtOAc); mp 184 °C (CH$_3$OH–H$_2$O); IR (KBr) 3420, 2920, 1628, 1464, 1385, 1127, 1026 cm^{-1}; ^{1}H NMR, δ: 7.08 (s, 3H, Thz*H*), 5.26 (bs, 3H, ThzCH$_2$O*H*), 4.65 (s, 6H, ThzC*H*$_2$OH), 4.41 (s, 6H, ArC*H*$_2$Thz), 2.29 (s, 9H, ArC*H*$_3$); ^{13}C NMR, δ: 170.5, 157.3, 135.4, 133.6, 113.4, 60.0, 34.2, 16.6; MS, m/z: 501 (M^+, 100), 355 (26), 258 (30); Anal. Calcd. for $C_{24}H_{27}N_3O_3S_3$: C, 57.46; H, 5.42; N, 8.38; S, 19.17; Found: C, 57.39; H, 5.68; N, 7.98; S, 18.96.

2.2.4. 1,3,5-Tris[2′(4′-methylthiazolyl)methyl]-2,4,6-trimethylbenzene (5)

A solution of **2** (214 mg, 0.63 mmol) and chloroacetone (292 mg, 3.16 mmol) in benzene (20 mL) was refluxed for 6 h.

After the solvent was removed, the residue was extracted with CH_2Cl_2. The organic layer was dried and concentrated. The residue was chromatographed (elution with EtOAc:hexane, 2:1) on silica gel to give **5** (135 mg, 47%). TLC, R_f 0.28 (1:1, EtOAc:hexane); mp 138 °C (CH_2Cl_2–hexane); IR (KBr) 2919, 1526, 1459, 1305, 1163, 1120, 719, 611 cm^{-1}; ^{1}H NMR, δ: 6.67 (s, 3H, Thz*H*), 4.43 (s, 6H, ArC*H*$_2$Thz), 2.43 (s, 9H, ThzC*H*$_3$), 2.30 (s, 9H, ArC*H*$_3$); ^{13}C NMR, δ: 170.7, 152.6, 136.0, 134.0, 112.9, 34.7, 17.1, 16.9; MS, m/z: 453 (M^+, 100), 396 (22), 341 (35), 242 (50), 229 (48), 112 (47); Anal. Calcd. for $C_{24}H_{27}N_3S_3$: C, 63.54; H, 6.00; N, 9.26; S, 21.20; Found: C, 63.16; H, 6.16; N, 8.95; S, 21.12.

2.2.5. 1,3,5-Tris[2′(4′-phenylthiazolyl)methyl]-2,4,6-trimethylbenzene (6)

A solution of **2** (204 mg, 0.60 mmol) and 2-bromo-acetophenone (598 mg, 3.00 mmol) in benzene (20 mL) was refluxed for 6 h. After the solvent was removed, the residue was extracted with CH_2Cl_2. The organic layer was dried and concentrated. The residue was chromatographed (elution with EtOAc:hexane, 1:1) on silica gel to give **6** (161 mg, 42%). TLC, R_f 0.56 (1:2, EtOAc:hexane); mp 102 °C (CH_2Cl_2-hexane); IR (KBr) 3064, 2918, 1601, 1489, 1296, 1148, 1071, 733 cm^{-1}; ^{1}H NMR, δ: 7.87–7.90 (m, 6H), 7.32–7.44 (m, 9H), 7.30 (s, 3H, Thz*H*), 4.56 (s, 6H, ArC*H*$_2$Thz), 2.42 (s, 9H, ArC*H*$_3$); ^{13}C NMR, δ: 171.2, 155.5, 136.2, 134.6, 134.1, 128.7, 128.0, 126.3, 112.4, 34.9, 17.1; Anal. Calcd. for $C_{39}H_{33}N_3S_3$: C, 73.20; H, 5.20; N, 6.57; S, 15.03; Found: C, 72.98; H, 5.13; N, 6.51; S, 15.20.

2.3. Preparation of electrodes and their potentiometric evaluation

Ion-selective membrane cocktails [33,34] were prepared by dissolving a newly synthesized ionophore 1 wt%, PVC 33 wt% and DOA 66 wt% in a THF (1 mL). The cocktail solutions were then poured into a glass ring (i.d. 22 mm) placed on a slide glass, and dried at room temperature for a day. Small disks were punched from the cast films and mounted in Phillips electrode bodies (IS-561; Glasblaserei Möller, Zürich, Switzerland). For all electrodes, 0.1 M of KCl was used as the internal reference electrolyte. All electrodes were presoaked in distilled water for 1 h before use. Potential differences between the ISEs and the Orion sleeve-type double junction Ag/AgCl reference electrode (Model 90-02) were measured using a PC equipped with a high-impedance input 16-channel analog-to-digital converter (KOSENTECH Inc., Busan, Korea). The dynamic response curves were obtained at room temperature by adding standard solutions to 200 mL of a magnetically stirred background electrolyte (0.05 M of Tris–HCl, pH 7.4; 0.05 M of Bis–tris propan-H$_2$SO$_4$, pH 9.0; 0.01 M of magnesium acetate–HNO$_3$, pH 4.5; deionized water) every 100 s to vary the concentration of each ionic species stepwise from 10^{-6} to 10^{-1} M. The potentials were measured every second at room temperature. The response of the electrodes to pH changes was tested by adding aliquots of a 1N NaOH solution to a solution of 11.4 mM of boric acid, 6.7 mM of citric acid, and 10.0 mM of NaH$_2$PO$_4$ at room temperature.

Selectivity coefficients were estimated according to the separate solution-matched potential method (IUPAC SSM II method) by comparing the activity of an interfering cation that induced the same potential change as that which was induced by ammonium activity of 1.0×10^{-2} M [35].

3. Results and discussion

Newly synthesized ion-selective neutral carriers **3–6** were evaluated with DOA-plasticized PVC membranes. In measuring their potentiometric responses to various cations, e.g., alkali metal, alkaline earth metal cations, and ammonium ion, the ligating properties of the tripodal binding site (nitrogens and sulfurs in a pendant thiazole ring, or pendant carbonyl, hydroxyl and phenyl groups) was studied. Since the interaction between a cation and the thiazole nitrogen may compete with the proton in a solution, we examined the potentiometric responses of the **3**-, **4**-, **5**-, and **6**-based membrane electrodes to varying pH. The results are summarized in Fig. 2. The compound **5**-based electrode exhibited the most sensitive responses to protons with a pH between 3 and 8. Other electrodes show the pH responses in the same range, but less sensitive than the **5**-based one. The pH response test suggests that the proton affinity of compounds **3–6** varies with the type of substituent used on pendant thiazoles; they are in the order of $-CH_3$, $-COOC_2H_5 \approx -C_6H_6$ and $-CH_2OH$. Since the pH responses of the **3**-, **4**-, **5**-, and **6**-based membrane electrodes begin to level down near pH 8, we examined their responses to other cations under near neutral and alkaline conditions.

At pH of 7.4 (0.05 M of Tris–HCl), **4**-, **5**- and **6**-based electrodes exhibited negligible responses to common physiological cations (Li^+, Na^+, K^+, Ca^{2+} and Mg^{2+}) and a slightly increased to ammonium (ΔE change of 50–80 mV from 10^{-3} to 10^{-1} M). The **3**-based electrode, on the other hand, exhibited substantially increased responses to ammonium and similarly to potassium. Fig. 3 shows the slopes of 47.2 and 45.0 mV per decade and the detection limits of 1.3×10^{-4} and 5.0×10^{-4} M, respec-

Fig. 3. The potentiometric responses of the **3**-based membrane electrode to Li^+ (-■-), Na^+ (-□-), K^+ (-●-), NH_4^+ (-○-), Mg_2^+ (-▲-), and Ca_2^+ (-△-) at pH 7.4 (0.05 M Tris–HCl).

tively. Considering the similar responses of the **3**- and **6**-based membranes to protons, the noticeably increased responses of the **3**-based membrane, compared to those of the **6**-based one to ammonium and potassium, may suggest that the carbonyl group participates in the ligation of those cations. A simple, semi-empirical modeling using MOPAC at the AM1 level confirms that three thiazole nitrogens and carbonyl oxygens form a hexadentate cavity that can hold a cation [32]. The average distances between the cation and thiazole nitrogens and between the cation and carbonyl oxygens are about 3.1 and 2.9 Å, respectively. On the other hand, the small potentiometric responses of the **4**-, **5**- and **6**-based electrodes, to all cations at near neutral pH levels may indicate that thiazole nitrogens are partially screened by protons.

Also, we examined the same potentiometric responses of the four electrodes at pH 9 (0.05 M Bis–tris propan-H_2SO_4); the results are shown in Fig. 4. The elevated pH greatly increased the potentiometric responses to ammonium and potassium of all electrodes. Only the **3**-based membrane electrode, however, exhibited near Nernstian responses (58.9 mV/pNH_4^+ and 57.0 mV/pK^+) to both ammonium and potassium, with a relatively low detection limit (2×10^{-6} and 5×10^{-6} M, respectively). The nearly identical potentiometric response of the **3**-based membrane electrode, to both ammonium and potassium, implicate that the binding site of compound **3** is a size-selective cavity. It seems that the electrostatic interaction between the cavity and a size-fitting cation contributes more to the selectivity of the binding site than does hydrogen-bonding interaction. The **4**- and **5**-based membrane electrodes exhibit less sensitive responses to ammonium and potassium than the **3**-based electrode, while showing similar potentiometric responses to other cations. The results implicate that the cation-binding ability of the tripodal thiazoles is similar to each other otherwise the substituents on thiazoles are capable of capping the binding site. The **6**-based membrane electrode exhibited much inferior potentiometric responses to the other three electrodes; the semi-empirical calculation model suggests that the bulky phenyl substituents hinder the formation of a symmetrical binding site. The poten-
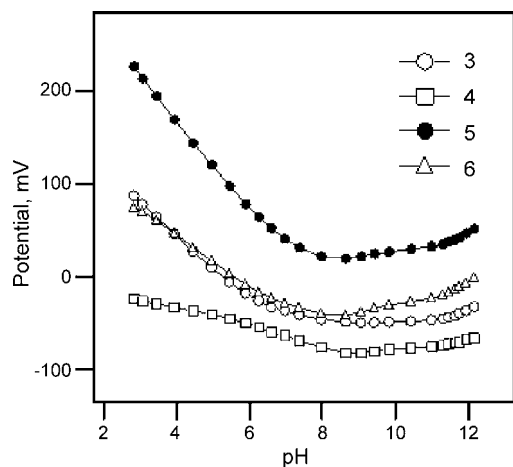

Fig. 2. The pH responses of the **3**-, **4**-, **5**-, and **6**-based membrane (1 wt.% of ionophore in 33 wt.% of PVC plasticized with 66 wt.% of DOA) electrodes to varying pH levels.
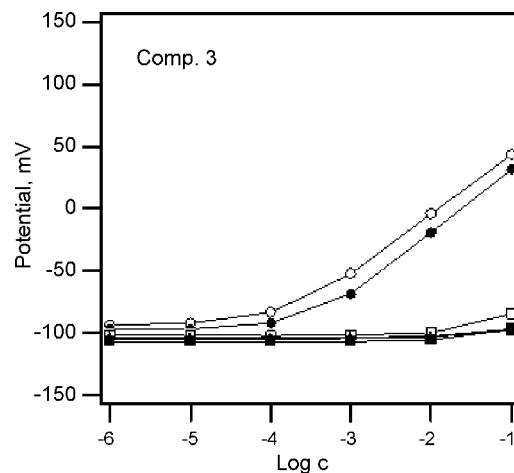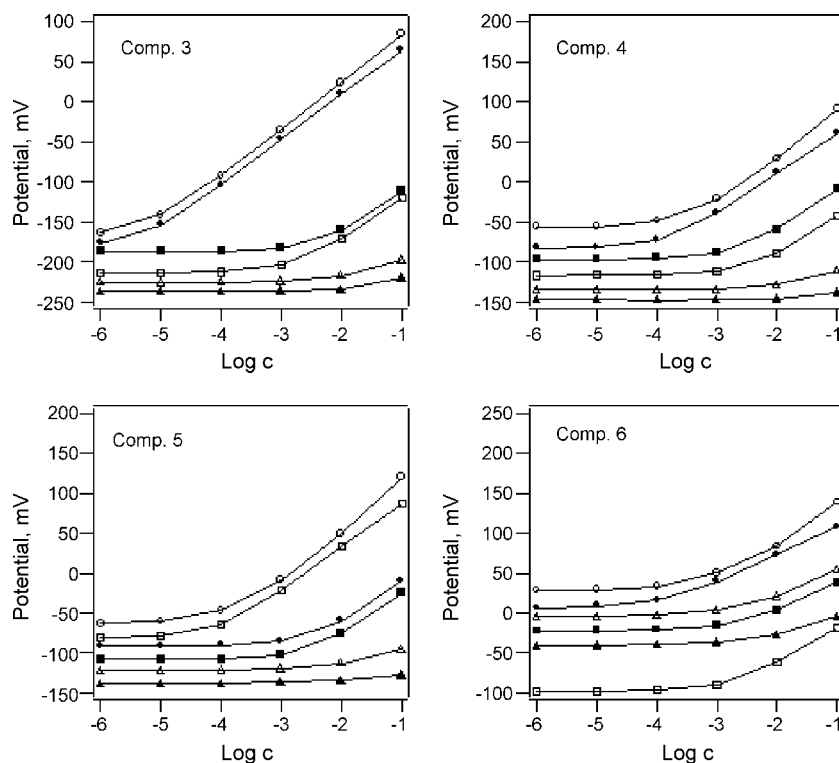
Fig. 4. The potentiometric responses of the DOA-plasticized PVC membranes prepared with the tripodal carbethoxy (**3**), hydroxymethyl (**4**), methyl (**5**), and phenyl (**6**), containing thiazole: Li$^+$ (-■-), Na$^+$ (-□-), K$^+$ (-●-), NH$_4^+$ (-○-), Mg$_2^+$ (-▲-), and Ca$_2^+$ (-△-).

tiometric characteristics of the **3**-, **4**-, **5**-, and **6**-based membrane electrodes are summarized in Table 1.

Sulfur atoms in tripodal thiazole derivatives may provide a binding site for the transition metal ions. To examine the transition metal ion selectivity of the **3**-, **4**-, **5**-, and **6**-based membrane electrodes, the potentiometric responses of the four electrodes to Ag$^+$, Fe^{2+}, Co^{2+}, Zn^{2+}, Ni^{2+}, Pb^{2+}, Cd^{2+}, Cu^{2+} and Hg^{2+} have been measured under acidic conditions (0.01 M of magnesium acetate–HNO$_3$, pH 4.5). Acidic conditions prevent the transition metal ions from forming precipitates with hydroxide, and it provides favorable silver ion binding ability [36]. It was interesting to observe that all four electrodes exhibited nearly negligible potentiometric responses to all transition metal cations with the exception of Ag$^+$: the linear dynamic ranges were between 10^{-5} and 10^{-3} M.

To examine the response characteristics of the four electrodes to Ag$^+$, without the effect of interferents, measurements were taken in deionized water. The results are shown in Fig. 5, and summarized in Table 2. The response characteristics of the four electrodes to silver ion do not show a clear correlation with their responses to ammonium. The compound with methyl group containing thiazole, **5**, showed a Nernstian response to Ag$^+$ in the 1×10^{-8} to 1×10^{-4} M range. On the other hand, the electrode based on **4**, which showed similar response characteristics to those based on **5**, had the poorest response to silver ion (35.9 mV/pAg$^+$ in the 1×10^{-7} to 3×10^{-3} M range). The response of the **6**-based electrode was similar to that of the **4**-based one. The semi-empirical modeling study (PM3) provides little information regarding the role of the thiazole substituents in silver binding, while there are some changes in the electron density levels on sulfur atoms, depending on the substituents, we were not inclined to draw conclusions at this time. The **3**-based electrode exhibited near a Nernstian response to silver in the 3×10^{-8} to 1×10^{-3} M range. The molecular modeling

Table 1

The potentiometric properties of the thiazole derivatives in DOA-plasticized PVC membranes

Compound	Slope[a]	Detection limit[b]	Selectivity coefficient $\left(\log k_{\mathrm{NH_4^+},\,j}^{\mathrm{pot}}\right)$				
			K$^+$	Na$^+$	Li$^+$	Ca^{2+}	Mg^{2+}
3	58.9	−5.3	−0.2	−2.5	−3.1	−4.0	−4.5
4	46.8	−4.0	−0.2	−1.0	−1.2	−2.6	−3.4
5	56.2	−4.1	−0.2	−1.1	−1.3	−2.7	−3.2
6	34.9	−3.9	−0.2	−0.8	−1.0	−1.0	−1.6

[a] Slopes from 10^{-4} to 10^{-1} M (mV/decade).
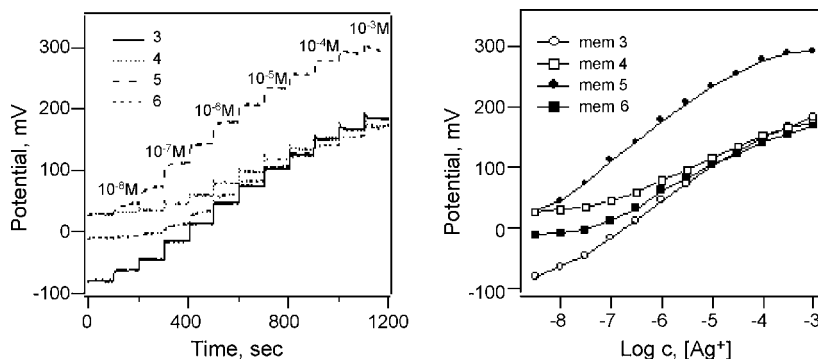
[b] log [NH$_4^+$].

Fig. 5. The potentiometric responses of the electrodes to Ag$^+$ based on neutral carriers **3**, **4**, **5** and **6**: (left) dynamic response curves; (right) calibration curves.

Table 2
The potentiometric response properties of the **3**-, **4**-, **5**-, and **6**-based membrane electrodes

No.	Ionophore	Slope[a] (mV/decade)	Detection limit[b], $-\log [Ag^+/M]$	Linear range (M)
1	Compound **3**	51.3	−8.4	3×10^{-8} to 1×10^{-3}
2	Compound **4**	35.9	−7.9	1×10^{-7} to 3×10^{-3}
3	Compound **5**	59.5	−8.6	1×10^{-8} to 1×10^{-4}
4	Compound **6**	39.3	−8.0	3×10^{-7} to 1×10^{-3}

[a] Slopes from the linear range.
[b] Logarithmic scale.

study suggests that the high potentiometric responses of the **3**-based electrode to silver ion could be attributed to the long-range interaction of the substituents on thiazole.

4. Conclusion

The potentiometric responses of the **3**-, **4**-, **5**-, and **6**-based membrane electrodes to alkali metal, alkaline earth metal, ammonium, and transition metal ions have been examined under various pH conditions. The **3**-based electrode exhibited a Nernstian response to ammonium and potassium under alkaline pH conditions. The other three electrodes showed poor potentiometric performances in both near neutral and high pH conditions, implicating that the binding ability of the cavity, formed by three thiazoles, is not sufficient to hold alkali metal or alkaline earth metal cations including ammonium. It was suggested that the carbethoxy group, which contains thiazole derivative **3**, forms a size-selective binding site, which in turn was formed by three thiazole nitrogens and three carbonyl groups. On the other hand, the potentiometric responses of the four electrodes to transition metal cations were quite different; all electrodes showed substantial responses to silver ion, but there was almost no response to all other transition metal ions examined (Fe^{2+}, Co^{2+}, Zn^{2+}, Ni^{2+}, Pb^{2+}, Cd^{2+}, Cu^{2+} and Hg^{2+}). The **3**- and **5**-based electrodes resulted in near Nernstian responses (51.3 mV and 59.5 mV/pAg$^+$, respectively) with low detection limits (~100 ppt), while the **4**- and **6**-based ones showed sub-Nernstian responses below 40 mV/pAg$^+$. It was assumed that the difference in the potentiometric responses to silver ion arose from the difference in the charge density of sulfur atoms induced by a long range, through the bond interaction of substituents. A detailed theoretical study is in progress in order to examine the nature of such interactions.

References

[1] J.W. Steed, J.L. Atwood, Supramolecular Chemistry, John Wiley & Sons Ltd., 2000.
[2] K. Wygladacz, A. Radu, C. Xu, Y. Qin, E. Bakker, Anal. Chem. 77 (2005) 4706.
[3] X.-B. Zhang, Z.-X. Han, Z.-H. Fang, G.-L. Shen, R.-Q. Yu, Anal. Chim. Acta 562 (2006) 210.
[4] D.D. MacNicol, A.D.U. Hardy, D.R. Wilson, Nature 266 (1976) 611.
[5] G. Hennrich, E.V. Anslyn, Chem. Eur. J. 8 (2002) 2219.
[6] S. Sasaki, D. Citterio, S. Ozawa, K. Suzuki, J. Chem. Soc. Perkin Trans. 2 (2001) 2309.
[7] H.J. Choi, Y.S. Park, S.H. Yun, H.-S. Kim, C.S. Cho, K. Ko, K.H. Ahn, Org. Lett. 4 (2002) 795.
[8] D.R. Turner, M.J. Paterson, J.W. Steed, J. Org. Chem. 71 (2006) 1598.
[9] J. Kim, B. Raman, K.H. Ahn, J. Org. Chem. 71 (2006) 38.
[10] H.R. Seong, D.-S. Kim, S.G. Kim, H.J. Choi, K.H. Ahn, Tetrahedron Lett. 45 (2004) 723.
[11] S.-G. Kim, K.H. Ahn, Chem. Eur. J. 6 (2000) 3399.
[12] A. Vacca, C. Nativi, M. Cacciarini, R. Pergoli, S. Roelens, J. Am. Chem. Soc. 126 (2004) 16456.
[13] T.D.P. Stack, Z. Hou, K.N. Raymond, J. Am. Chem. Soc. 115 (1993) 6466.
[14] C.M. Hartshorn, P.J. Steel, Chem. Commun. (1997) 541.
[15] R.H. Holm, P. Kennepohl, E.I. Solomon, Chem. Rev. 96 (1996) 2239.
[16] T.D.P. Stack, R.H. Holm, J. Am. Chem. Soc. 109 (1987) 2546.
[17] C. Walsdorff, W. Saak, S. Pohl, J. Chem. Soc., Dalton Trans. (1997) 1857.
[18] C. Walsdorff, S. Park, J. Kim, J. Heo, K.-M. Park, J. Oh, K.J. Kim, Chem. Soc., Dalton Trans. 6 (1999) 923.
[19] J. Chin, C. Walsdorff, B. Stanix, J. Oh, H.J. Oh, S.-M. Park, K. Kim, Angew. Chem. Int. Ed. 38 (1999) 2756.

[20] H. Higuchi, T. Matsufuji, T. Oshima, K. Ohto, K. Inoue, T. Tsend-Ayush, K. Gloe, Chem. Lett. 34 (2004) 80.

[21] X. Zeng, L. Weng, L. Chen, F. Xu, Q. Li, X. Leng, X. He, Z.-Z. Zhang, Tetrahedron 58 (2002) 2647.

[22] L. Chen, H. Ju, X. Zeng, X. He, Z. Zhang, Anal. Chim. Acta 437 (2001) 191.

[23] M.J. Goldcamp, K. Ashley, S.E. Edison, J. Pretty, J. Shumaker, Electroanalysis 17 (2005) 1015.

[24] I. Isildak, M. Yolcu, O. Isildak, G. Topal, H. Horsgoren, Microchim. Acta 144 (2004) 177.

[25] C.C. Su, M.C. Chang, L.L.K. Liu, Anal. Chim. Acta 432 (2001) 261.

[26] B.H. Kim, H.P. Hong, K.T. Cho, J.H. On, Y.M. Jun, I.S. Jeong, G.S. Cha, H. Nam, Talanta 66 (2005) 794.

[27] J.H. Choi, Y.K. Koh, I.-C. Kwon, H.-S. Kim, H.J. Park, S.J. Kim, G.S. Cha, H. Nam, Bull. Korean Chem. Soc. 20 (1999) 581.

[28] H.-S. Kim, J.H. Choi, Y.K. Koh, H.J. Choi, G.S. Cha, H. Nam, J. Inclusion Phenom. 40 (2001) 265.

[29] H.-S. Kim, H.J. Park, H.J. Oh, Y.K. Koh, J.H. Choi, D.-H. Lee, G.S. Cha, H. Nam, Anal. Chem. 72 (2000) 4683.

[30] J.H. Shim, I.S. Jeong, M.H. Lee, H.P. Hong, J.H. On, K.S. Kim, H.-S. Kim, B.H. Kim, G.S. Cha, H. Nam, Talanta 63 (2004) 61.

[31] H.-S. Kim, K.S. Do, K.S. Kim, J.H. Shim, G.S. Cha, H. Nam, Bull. Korean Chem. Soc. 25 (2005) 1465.

[32] P. Buhlmann, E. Pretsch, E. Bakker, Chem. Rev. 98 (1998) 1593.

[33] G. Craggs, G.J. Moody, J.D.R. Thomas, J. Chem. Educ. 51 (1974) 541.

[34] G.J. Moody, R.B. Oke, J.D.R. Thomas, Analyst 95 (1970) 910.

[35] Y. Umezawa, K. Umezawa, H. Sato, Pure Appl. Chem. 67 (1995) 507.

[36] J. Lu, X. Tong, X. He, J. Electroanal. Chem. 540 (2003) 111.

1-Naphthol as an excited state proton transfer fluorescent probe for sensing bound-water hydration of polyvinyl alcohol

Anitha C. Kumar, A.K. Mishra *

Department of Chemistry, Indian Institute of Technology Madras, Chennai 600 036, India

Abstract

When 1-naphthol incorporated polyvinyl alcohol (PVA) films are allowed to swell in water, there is a loss of fluorescence intensity of the neutral form with a concomitant increase of the anionic form fluorescence intensity. This fluorescence response due to the excited state prototropism (ESPT) of 1-naphthol is very sensitive to the initial stage of hydration of the PVA. Using an existing model of hydrogel swelling and DSC experiments, it was reasoned that 1-naphthol senses the bound-water component of PVA hydration. Thus, 1-naphthol is proposed as an ESPT fluorescent sensor for the specific sensing of bound-water hydration of PVA hydrogel.
© 2006 Elsevier B.V. All rights reserved.

Keywords: Excited state proton transfer; Polymer hydration; 1-Naphthol; Fluorescence

1. Introduction

Polymeric hydrogels are three-dimensionally cross-linked networks containing water. The swelling behavior of polymer hydrogels has been a topic of intense research because of various potential biomedical applications [1]. Polyvinyl alcohol (PVA) is a particularly interesting polymer system for such applications because of its low toxicity, high biocompatibility and high degree of swelling in water. The process of swelling and nature of water in the gels has been a subject of extensive investigation [2–4]. Depending on the degree of association between water and polymer, the behavior of water can change. Three different states of water have been identified in swollen hydrogels, i.e. non-freezable bound-water, freezable bound-water and free water [3]. From a DSC study of partially swollen PVA hydrogels, Li et al. [3] differentiated the relative content of these water states. Nagura et al. [4] suggested the existence of three different ice forms in a frozen PVA hydrogel by DSC measurements. The total weight of water present in a swollen hydrogel is the sum of two main parts, the weight of freezable water and that of non-freezable water. It was suggested that the non-freezable bound-water molecule has two hydrogen bonds directly fixed to

polymer network chain and could not freeze to ice upon cooling. When more water is introduced to the gel, these two end fixed hydrated water gradually change to one end fixed and merged with freezable hydrated water. The free hydrogen atom of the one end fixed hydrated water may join with another free water molecule; the mobility of the molecule is partially retained and could freeze upon cooling.

A variety of techniques have been used to monitor the polymer swelling. Some of them are DSC, PNMR [3,4], AFM [5], etc. The swelling of PVA films have been characterized using DSC and PNMR by Nagura et al. [4]. Using AFM, Paredes et al. studied the nanometer scale swelling of poly(*p*-phenylene terephthalamide) [5].

Fluorescence molecular probes and sensors based on 'excited state proton transfer' (ESPT) are increasingly found to be very useful in obtaining structural and dynamical information on a verity of organized and aggregate systems like micelles, lipid bilayer membranes, polymeric gels, cyclodextrin cavity, etc. [6,7]. 1-Naphthol (1-ROH) which shows about 10^9 orders of magnitude enhancement in the excited singlet state acidity ($pK_a = 9.4$) ($pK^* = 0.41$), often serves as a prototype ESPT molecular probe. It has the longest wavelength absorption maximum at ∼295 nm. After partitioning into an organized medium, it emits from the excited state neutral form (1-ROH*, $\lambda_{em} \sim 350$ nm) when it is present in a water-inaccessible microenvironment and emits from the exited state anionic form

* Corresponding author. Tel.: +91 44 2257 4207; fax: +91 44 2257 4202.
E-mail address: mishra@iitm.ac.in (A.K. Mishra).

(1-RO^{-*}, $\lambda_{em} \sim 465$ nm) when present in the water-accessible regions of the organized media. It has been shown by Lee that in an aqueous environment the proton accepted is a cluster of 4 ± 1 water molecules [8]. At hydrophilic–hydrophobic interphases, the rate constant of the deprotonation dynamics is significantly retarded, which is manifested by a significant increase in the fluorescence lifetime of the neutral form and an enhancement of neutral form fluorescence intensity [6,9,10].

Thus, 1-ROH as an ESPT molecular sensor could posses the ability to monitor hydration of polymers like PVA. The fluorescence response of the different prototropic forms could reflect the nature of hydrating water in hydrogels. The objective of this work is to examine the applicability of 1-ROH as an ESPT fluorescent sensor for monitoring the hydration of PVA films.

2. Experimental

2.1. Materials

Polyvinyl alcohol (PVA, MW 14,000) was purchased from S.D. fine Chem. Ltd. and used as such. 1-ROH brought from SRL and purified by sublimation. Triply distilled water was used for sample preparation. ^{13}C NMR spectrum of the PVA solution in D$_2$O was taken for finding out the presence of acetate groups. The absence of any peak above 150 ppm [11] showed that no residual acetate groups were present in the PVA.

2.2. Sample preparation and characterization

PVA dry films were prepared by incorporating 10^{-4} M 1-ROH solutions into 4% (w/v) PVA solution. These solutions were poured into flat-bottomed dishes in such a manner that a uniform thin layer of liquid covers the surface. These dishes were kept in a vacuum desiccator and films were allowed to dry. The dry polymer film could be easily detached from the dish. Under this condition of film preparation, the thickness of the films formed was 0.2 ± 0.01 mm. For finding the degree of crystallinity of the dry film, DSC measurements were done with a Netzsch DSC 204 instrument; in the temperature range 30–250 °C at a specific heating rate of 10 K/min. The degree of crystallinity of the PVA sample was calculated by comparing the heat required to melt sample to the heat required to melt a 100% crystalline PVA sample (138.6 J/g) [12]. The degree of crystallinity of the sample prepared under the above-mentioned conditions was found to be $50.3 \pm 2.0\%$.

2.3. Method of analysis

Fluorescence measurements were carried out with a Hitachi F-4500 spectrofluorimeter, with a 150 W Xenon lamp as the light source. The excitation and emission spectra were recorded with slit widths of 5/5 nm. The scan speed was kept at 1200 nm min^{-1}.

The swelling behavior of PVA in water was studied in terms of various parameters like increase in length, breadth and weight with time. A known weight of the dry film was taken and its dimensions were measured. Then, the film was allowed to swell in a small flat-bottomed dish containing water. The length, breadth and weight of the swollen film were measured at regular intervals of time. To remove the excess water it was pat dried with a piece of tissue paper prior to the weight measurements.

DSC measurements for obtaining the ice melting endotherm were done on Netzsch DSC 204 instrument by heating the sample at a specific rate of 2 K/min in closed alumina pans under N$_2$ atmosphere. Small pieces of equally weighted PVA films (2.3×10^{-3} g) were simultaneously put it in to water and were allowed to swell. At regular intervals of time, a piece of swollen film was taken out, quickly pat dried with tissue paper and used as sample for DSC. The dry film was kept as reference. A plot of difference in the heat output of the two heaters against temperature (i.e., the heat absorbed by the polymer) is obtained.

3. Results and discussion

The emission spectra of 1-ROH in PVA dry film and in water are shown in Fig. 1(a). It is known that the emission from the excited state neutral form of 1-ROH is around 340–360 nm and that of anion is around 460–480 nm. In dry film, the emission of 1-ROH is seen around 342 nm corresponding to the neutral form and in water it is at 464 nm due to the anionic form. Only neutral peak is observed from the dry film, indicating the absence of water around the 1-ROH microenvironment.

The variation of fluorescence intensity of 1-ROH with time in PVA film on addition of water is shown in Fig. 1(b). After placing the film in water, fluorescence spectra were recorded
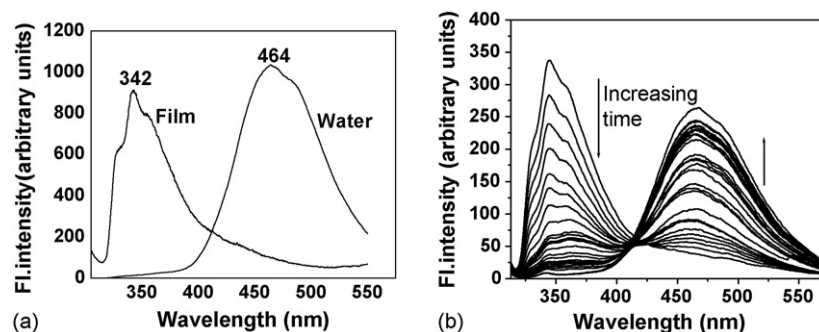

Fig. 1. (a) Emission spectra of 1-naphthol in water and PVA film and (b) emission spectra of PVA/1-naphthol film in water with increasing time, at 15 s intervals (λ_{ex} 297 nm).
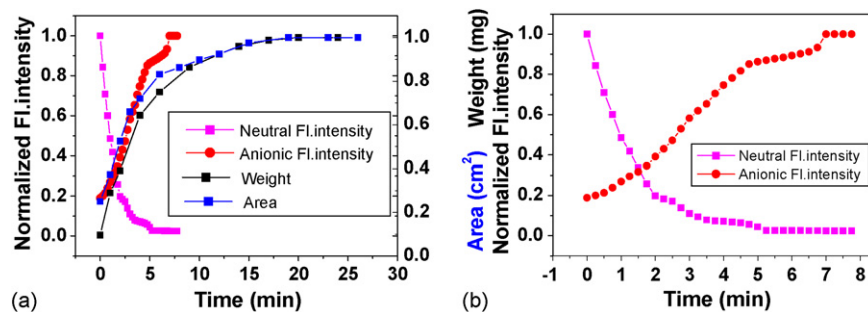
Fig. 2. (a) Plot of variation of the area, weight and normalized fluorescence intensity of 1-ROH in the PVA film in water as a function of time and (b) expanded plot of variation of normalized fluorescence intensity of 1-ROH in the PVA film in water as a function of time.

every 15 s. It is seen in Fig. 1(b) that the intensity of neutral peak at 342 nm decreases with a concomitant increase in the anionic peak at 464 nm. The presence of a good iso-emissive point indicates a two state equilibrium, with the anionic form appearing at the expense of the neutral form.

The variation of area, weight and fluorescence intensity of 1-ROH in PVA film is shown in Fig. 2.

Fluorescence intensities were monitored at 342 nm for the neutral form and at 464 nm for the anion form. The time of each intensity data collection was calculated by taking the rate of scan (20 nm s^{-1}). The films, prepared under the experimental conditions of this study, showed complete saturation of swelling in about 20 min, as monitored by the changes in the weight and area of the films. However, the loss of the neutral form fluorescence intensity (342 nm) was saturated in just 3 min. Such a response of 1-ROH* fluorescence is rather interesting and significant. In addition, it was observed that a small residual fluorescence at 342 nm persists even at complete saturation. Leaching of 1-ROH to the aqueous medium was found to be minimal during the observation time of about 30 min.

PVA belongs to the class of polymers, which have sufficient non-polar interchain interaction to show saturation swelling behavior, i.e. it does not dissolve completely even on prolonged exposure to water. 1-ROH is a small and fairly hydrophobic molecule that is not very soluble in water at room temperature. When used as a probe for liposome membranes, it is known to have a very large partition coefficient (5×10^6 at 30 °C for dimyristoylphosphatidylcholine vesicles) [13]. In 1-ROH incorporated PVA films, 1-ROH is expected to remain associated with the polymer matrix both because of hydrophobic interactions as well as possible hydrogen bonding interaction with the hydroxy groups of the polymer. This could be the reason for the minimal leaching of 1-ROH during polymer swelling. The initial phase of hydration is expected to occur in the form of non-freezable bound-water. This form of water is directly associated with the polymer framework of the gel through hydrogen bonding. 1-ROH molecules associated with the polymer chain are expected to sense the presence of bound-water in their environment. This 'sensing' being manifested as excited state transfer of proton to water and emission from the anionic 1-RO^{-*} form. The saturation of the 1-ROH* fluorescence loss during the initial 3 min of swelling, thus, could correspond to the completion of bound-water hydration. For a verification of this explanation, DSC experiments were carried out.

Fig. 3 shows the DSC thermograms of swollen PVA film with increasing time and the corresponding data are given in Table 1. The energies are calculated from the area under the peaks. The complete absence of endotherm for dry PVA film indicates that the dry film does not have any freezable water. After 2 min of swelling, two peaks are observed in DSC: a major broad peak at lower temperature and a small sharper peak at around 0 °C. According to Hatakeyama et al. the peak at lower temperature side is assigned to the freezing of bound-water and that at higher temperature corresponded to freezing of free water [14]. Going by this explanation, the large enthalpy change observed in DSC between 3 and 4 min of swollen samples indicated that after 3 min, the freezable free water becomes the predominant form in the swollen film. The change of the DSC thermogram features thus corresponds with the 1-ROH* fluorescence intensity saturation in the initial stage of swelling. The amount of film-incorporated water can be easily estimated by taking the net weight of the film at different stages of swelling. The ratio of weights of completely swollen film to the film up to 3 min of swelling was estimated to be 2.14. The ratio of area under the DSC thermogram curves for completely swollen film to 3 min swollen film was reasonably close at 2.20. Thus, it can be generally concluded that by 3 min of swelling, the water associated with the film is predominantly the bound-water.
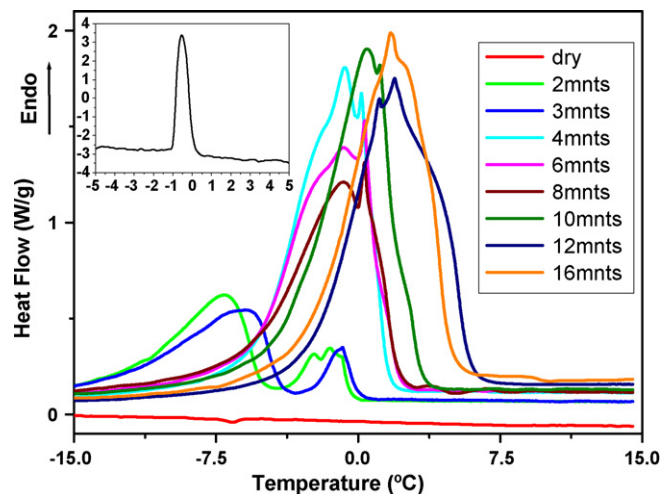

Fig. 3. DSC thermograms of PVA film in water with increasing time. Inset is DSC peak of pure water.

Table 1
Water content, neutral form fluorescence intensity of 1-ROH, position of DSC endotherm and enthalpy change of PVA film at various stages of swelling in water

Time of swelling (min)	Water content (mg)	Relative intensity of 1-ROH* fluorescence at 342 nm (normalized to the maximum for the dry film)	Endotherm peaks from DSC measurements (°C)	Enthalpy changes from DSC measurements (J/g)
0	0	1.00	0	0
1	40	0.49	−8.5, −2.1	98.35, 14.95
2	61	0.20	−7.1, −1.5	101.75, 020.35
3	–	0.11	−6.0, −0.8	106.05, 013.65
4	113.4	0.07	−0.7, 0.2	178.5, 045.7
6	–	0.03	−0.8, 0.4	155.76, 050.24
8	–	0.03	−0.8, 1.3	127.11, 044.09
9	159.8	–	–	–
10	–	–	0.4	235.6
12	171.3	–	2.0	259.0
14	178.8	–	–	–
16	–	–	1.7	263.3
17	184.5	–	–	–
20	187	–	–	–
24	187	–	–	–
26	187	–	–	–
Water	–	0	−0.6	140.8

Dry weight of the film 19.7 mg. Heating rate 2 K/min.

The DSC experiments were repeated for a different heating rate (10 K/min), which gave almost similar results: after 3 min of swelling, the peaks shifted to higher temperatures and after 6 min there was only one peak corresponding to free water. Since the sample preparation conditions were same through out the course of this study, the extent of crystallinity of the dry sample is expected to be same. Although the degree of crystallinity of a PVA membrane is expected to change with aging and annealing [15], we do not expect an ESPT probe to respond directly to any difference in the nature of bound-water structure in the crystalline and non-crystalline regions of the polymer.

Table 1 also shows the comparison of neutral form fluorescence intensity and DSC endotherm peaks of PVA film in water with increasing time. The significant shift of the DSC peak position from −6.0 to −0.7 °C corresponds to the almost leveling of 1-ROH* fluorescence intensity. The results also show that after about 6 min there is a significant increase in amount of free water and the signature for bound-water is progressively lost.

Thus, it is seen that both the DSC results and the response of 1-ROH ESPT fluorescence have a common basis of explanation in the Hatakeyama's model of PVA swelling [14].

4. Conclusion

When 1-naphthol incorporated PVA films are allowed to swell in water, the loss of the neutral form (1-ROH*) fluorescence intensity and the increase of the anionic form (1-RO*) fluorescence intensity is very sensitive to polymer hydration in the initial stage of swelling. Using the Hatakeyama's model of PVA swelling [14] and DSC experiments, it was reasoned that 1-ROH senses the bound-water component of PVA hydration. Thus this work adds one more application of 1-naphthol as an ESPT fluorescence sensor for specific sensing of bound-water hydration.

Acknowledgements

References

[1] H.B. Bohidar, Curr. Sci. 80 (8) (2001) 1008–1017.
[2] F. Urushzaki, H. Yamguchi, K. Nakamura, S. Numajiri, K. Sugibayashi, Y. Morimoto, Int. J. Pharm. 58 (1990) 135–142.
[3] W. Li, F. Xue, R. Cheng, Polymer 46 (2005) 12026–12031.
[4] M. Nagura, N. Takagi, H. Katakami, Y. Gotoh, Y. Ohkoshi, T. Koyano, N. Minoura, Polym. Gels Networks 5 (1997) 455–468.
[5] J.I. Paredes, S. Villar-Rodil, K. Tamargo-Martínez, A. Martínez-Alonso, J.M.D. Tascón, Langmuir 22 (2006) 4728–4733.
[6] A.K. Mishra, Understanding and manipulating excited state processes, in: V. Ramamurthy, K.S. Schanze (Eds.), Molecular and Supramolecular Photochemistry Series 8, Marcel Dekker Inc., New York, 2001, pp. 577–635 (Chapter 10).
[7] K. Kalyanasundaram, in: V. Ramamurthy (Ed.), Photochemistry in Organized and Constrained Media, VCH Publishers Inc., New York, 1991, pp. 39–77 (Chapter 2).
[8] J. Lee, J. Phys. Chem. 94 (1990) 258.
[9] J. Sujatha, A.K. Mishra, Langmuir 14 (1998) 2256–2262.
[10] K. Bhattacharyya, Acc. Chem. Res. 36 (2) (2003) 95–101.
[11] H. Gunther, NMR Spectroscopy—Basic Principles, Concepts, and Applications in Chemistry, John Wiley & Sons Inc., New York, 1995, pp. 515–539 (Chapter 12).
[12] N.A. Peppas, E.W. Merrill, J. Appl. Polym. Sci. 20 (1976) 1457–1465.
[13] J. Sujatha, A.K. Mishra, J. Photochem. Photobiol. A 101 (1996) 215–219.
[14] T. Hatakeyama, A. Yamanouchi, H. Hatakeyama, Eur. Polym. J. 20 (1984) 61.
[15] C.M. Hassan, N.A. Peppas, Macromolecules 33 (2000) 2472–2479.

Short communication

Determination of methimazole in urine by liquid chromatography

Krzysztof Kuśmierek, Edward Bald*

Department of Environmental Chemistry, University of Lodz, 90-236 Lodz, Poland

Abstract

A liquid chromatography methodology is developed and validated for detection and quantification of methimazole in urine. The approach is based on derivatization with 2-chloro-1-methylquinolinium tetrafluoroborate, reversed-phase high-performance liquid chromatography (HPLC) separation of so formed methimazole 2-S-quinolinium derivative from other urine matrix components, followed by detection and quantification with the use of ultraviolet–visible detector. Neither extraction, nor preconcentration of the sample are necessary. The methimazole standards added to normal urine before derivatization step show that the response of the detector, set at 345 nm, is linear within the concentration range studied, that is, from 0.25 to 50 mg/l urine. The relative standard deviation values for precision and recovery within the calibration range were from 1.8 to 5.0% and from 95.7 to 103.3%, respectively. Lower limits of detection and quantitation were 0.15 and 0.25 mg/l urine, respectively.
© 2006 Elsevier B.V. All rights reserved.

Keywords: Methimazole; Urine; Derivatization; LC

1. Introduction

Methimazole (1-methyl-2-mercaptoimidazole, tapazole) and carbimazole (1-methyl-2-mercapto-3-carbethoxyimidazole) are orally active drugs used in the therapy of hyperthyreosis. Carbimazole is considered to be metabolized fully to methimazole, which is absorbed by the gastrointestinal tract and concentrates in the thyroid gland [1]. Methimazole, termed also an antihormone, is widely used in medicine for treatment of hyperthyroidism and even as model substance for endocrine disruption in physiological and genomic studies. Its action is to slow iodide integration into tyrosine and thus inhibits the production of thyroid hormones. In human body methimazole is metabolized to *N*-methylimidazole and sulfite via sulfenic and sulfinic acid intermediates that are associated with the cytotoxic effects [2]. Substantial portion of orally taken drug is excreted with urine [3]. Methimazole may cause side effects such as irritation of skin, impaired taste, olfaction, allergies or pharyngitis with fever, and in rare occasions, nephritis and liver cirrhosis [1,2]. Thyreostatic drugs, among others methimazole, have been applied illegally to animals to obtain a higher live weight gain. The first effect

gives a fraudulent higher weight due to water retention in edible tissue and filling of the gastrointestinal tract, which in turn leads to a reduction of the meat quality. Although methimazole has been used in the treatment of hyperthyroidism, the uncontrolled introduction of this and other thyreostats into the human food chain could have serious health implications [4]. Consequently, the use of thyreostats in animal production has been prohibited in many countries including European Union [5]. Various methods have already been reported to detect and determine methimazole in urine [6–9] and tissues [7,10–13]. Techniques used were gas chromatography–mass spectrometry (GC–MS) [6,9,12], high-performance liquid chromatography–mass spectrometry (HPLC–MS) [7,11], HPLC with ultraviolet detection [10,13], and flow-injection with ultraviolet detection [8]. Since tissues and urine matrices are complex, sample preparation is very important step of the analytical procedure. In order to simplify the matrix, preconcentrate the analyte and enhance sensitivity of the method several operations were carried out. These were mostly single or double extraction [6–13] and single or double derivatization [6,9,11,12]. In this paper, the application of standard LC equipment with ultraviolet detector for determination of methimazole in urine with sensitivity 0.15 mg/l is described. The method requires neither extraction, nor preconcentration and uses simple sample preparation in the form of a single derivatization with 2-chloro-1-methylquinolinium tetrafluoroborate.

---

* Corresponding author.
  E-mail address: ebald@uni.lodz.pl (E. Bald).

2. Experimental

2.1. Instrumentation

HPLC analysis was carried out using a Hewlett-Packard 1100 system (Waldbronn, Germany) equipped with quaternary pump, an autosampler, thermostated column compartment, vacuum degasser and diode-array detector. The system was controlled by HP ChemStation software. The separations were accomplished with a Zorbax SB C-18 (5 μm, 150 mm × 4.6 mm) analytical column (Agilent Technologies, Waldbronn, Germany). Water for solutions was prepared with a Millipore Milli-QRG system (Vien, Austria). For pH measurement, a Hach One (Loveland, USA) pH meter was used.

2.2. Chemicals and reagents

All chemicals were of analytical or HPLC grade and all solutions were prepared from deionized water. Methimazole was purchased from Aldrich (Steinheim, England). 2-Chloro-1-methylquinolinium tetrafluoroborate (CMQT) was synthesized in our laboratory as described earlier [14]. Perchloric acid (PCA), sodium hydroxide (NaOH), sodium hydrogen phosphate heptahydrate ($Na_2HPO_4 \cdot 7H_2O$), sodium dihydrogen phosphate dihydrate ($NaH_2PO_4 \cdot 2H_2O$) and HPLC-grade acetonitrile and methanol were from J.T. Baker (Deventer, The Netherlands). Trichloroacetic acid (TCA) was from Merck (Darmstadt, Germany), cysteine was from Reanal (Budapest, Hungary), Tris(2-carboxyethyl)phosphine (TCEP), lithium hydroxide monohydrate and cysteinylglycine were received from Sigma (St. Luis, MO, USA). Stock standard solution of methimazole (10 g/l) was prepared in methanol. The working solutions were prepared by dilution with water as needed. TCEP (0.25 mol/l) was prepared by dissolving appropriate amount of the compound in 0.2 phosphate buffer and adjusted to pH about 7.5 with 10 mol/l NaOH. For derivatization, a 0.1 mol/l water solution of CMQT was used. To prepare phosphate buffer (0.2 mol/l) appropriate quantities of sodium hydrogen phosphate heptahydrate ($Na_2HPO_4 \cdot 7H_2O$) and sodium dihydrogen phosphate dihydrate ($NaH_2PO_4 \cdot 2H_2O$) solutions were mixed. TCA buffer was prepared using 0.05 mol/l trichloroacetic acid and adjusted to the desired pH (3.2) with lithium hydroxide (0.05 mol/l). The pH of the buffers was adjusted by potentiometric titrations. The titration system was calibrated with standard pH solutions. All reagents were tested and found to be stable for unattended analysis.

2.3. Sample preparation

To 200 μl of freshly collected methimazole-containing urine, 100 μl of 0.2 mol/l phosphate buffer (pH 7.5) and 10 μl of TCEP (0.25 mol/l) were added. The mixture was vortex-mixed and after 5 min 30 μl of CMQT reagent (0.1 mol/l) was added. The mixture was put aside for another 5 min and acidified with 100 μl of PCA (3 mol/l) followed by centrifugation ($10,000 \times g$, 5 min). A 20 μl of the solution was injected into the chromatographic system.

2.4. Chromatography

Final analytical solution (20 μl) was injected using an autosampler into a Zorbax SB C-18 column. For separation of 2-*S*-quinolinium derivative of methimazole gradient elution was used. The elution profile was as follows: 0–3 min 12% B, 3–9 min 12–30% B, 9–12 min 30–12% B, where A is 0.05 mol/l, pH 3.2, TCA buffer, and B is acetonitrile. The flow-rate used was 1.2 ml/min and the column was kept at a temperature of 25 °C. The analytical wavelength was 345 nm. Both retention times and UV spectra were used for peaks identification by comparison of retention times and UV diode-array spectra, taken at real time of analysis, with corresponding set of data obtained for authentic compounds.

2.5. Calibration

A stock standard solution of methimazole calibrator (10 g/l) was prepared by dissolving an appropriate amount of methimazole in methanol. To prepare the urine calibration standards used to determine the drug in urine, portions of 200 μl of normal urine were each placed in a sample tube and spiked with increasing amounts of the working standard solution of methimazole (prepared daily by dissolving of standard solution with water) to give methimazole concentrations of 0.25, 1.0, 5.0, 10.0, 20.0, 30.0 and 50.0 mg/l of urine. Calibration standards were processed according to recommended analytical procedure. Calibration curve was fitted by linear regression using the peak height versus concentration.

2.6. Stability of the 2-S-quinolinium derivative

To test stability of the 2-*S*-quinolinium derivative of methimazole in the final analytical solution, a urine sample was spiked with appropriate amount of methimazole to a final concentration of 1 mg/l urine, processed as described in Section 2.3, and kept at 4 °C or ambient temperature. Aliquot of the sample was injected into HPLC system at time zero and after 1, 6 and 24 h, and 3, 7, 14, 21 and 28 days.

3. Results and discussion

The complexity of the matrix, whether it is urine, plasma or tissue necessitates the use of some form of sample pretreatment. There are several sample preparation techniques that are employed to facilitate final analysis. The most commonly used approaches are protein removal, solid phase extraction, liquid–liquid extraction and chemical modification of the analyte.

3.1. Chemical modification of the analyte

In order to facilitate separation and detection of methimazole in urine matrix, derivatization with a thiol specific UV-tagging reagent, 2-chloro-1-methylquinolinium tetrafluoroborate (CMQT), previously applied for determination of plasma and urinary endogenous thiols [15,16] is recommended.
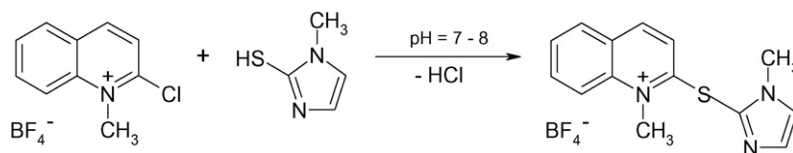
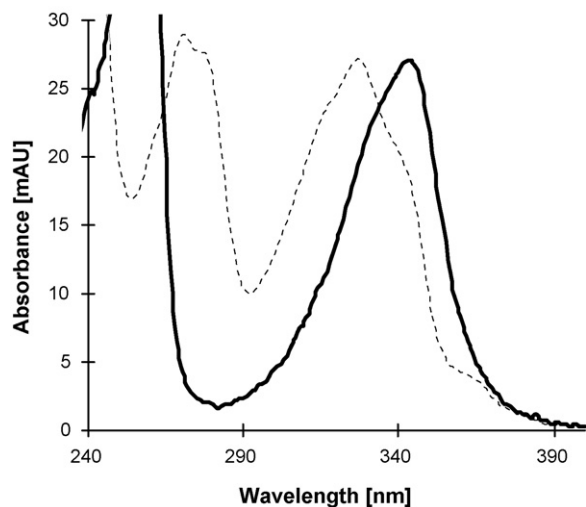Fig. 1. Derivatization reaction equation of methimazole with 2-chloro-1-methylquinolinium tetrafluoroborate.

Fig. 2. Comparison of the absorption spectra of derivatization reagent—CMQT (dotted line) and methimazole derivative—methimazole–CMQT (continuous line).

Methimazole reacts with CMQT in slightly alkaline water solution to form stable thioether, 2-S-quinolinium derivative. The derivatization scheme, shown in Fig. 1, takes advantage of great susceptibility of the quinolinium molecule to nucleophilic displacement at 2 position, and the high nucleophilicity of the −SH group of methimazole. The methimazole–CMQT derivative exhibits a well-defined absorption maximum at 345 nm (Fig. 2). In order to optimize derivatization conditions, reaction yield as a function of the reagent excess, pH of the buffer, and time were studied. Derivative yields versus time and pH are plotted in Fig. 3 and demonstrate that the yields reach a

maximum after 5 min in the pH range 7.5–8.0 with seven-fold reagent excess. Therefore, for subsequent assays, pH 7.5, 0.2 mol/l phosphate buffer and seven-fold reagent excess were used. Since conjugation of methimazole to other thiol components of the sample, via −S−S− bond, cannot be excluded, reductive agent (TCEP) is added before derivatization step.

3.2. Chromatogram

Chromatographic profiles were obtained for urine blank spiked with methimazole (Fig. 4) at optimized HPLC conditions described in Section 2.4. Retention time for methimazole–CMQT derivative was 7.0 min ($k' = 5.47 \pm 0.01$; $n = 21$). Cysteine and cysteinylglycine known to form CMQT derivatives under the same derivatization conditions [17] were eluted after 8.4 and 9.3 min, respectively, and can be measured concurrently if needed.

Fig. 3. Derivatization reaction yield as function of time and buffer pH. Conditions: 0.2 mol/l phosphate buffer, seven-fold molar excess of the derivatization reagent, room temperature.

Fig. 4. LC–UV chromatogram (345 nm) of normal urine sample reduced with TCEP and derivatized with CMQT. Urine blank (black line), and urine spiked with methimazole (3.5 mg/l) (gray line). Peaks: (1) methimazole; (2) cysteine; (3) cysteinylglycine. Chromatographic conditions are described in the text.

Table 1
Precision and recovery study ($n = 3$)

Taken [mg/l]	Found ± S.D. [mg/l]	Precision (R.S.D.) [%]	Recovery [%]	Intermediate precision (R.S.D.)[a] [%]
0.25	0.25 ± 0.01	5.05	98.19	7.58
1	0.98 ± 0.05	4.64	98.19	5.00
5	4.78 ± 0.18	3.67	95.67	3.02
10	10.14 ± 0.39	3.82	101.20	4.10
20	20.67 ± 0.39	1.88	103.33	2.52
30	29.76 ± 0.53	1.79	99.21	2.12
50	49.95 ± 1.02	2.05	99.90	2.64

[a] Results for 4 consecutive days.

3.3. Validation

Method validation protocol encompassed specificity, response function, precision, recovery, limit of quantitation, limit of detection and stability.

3.3.1. Specificity and response function
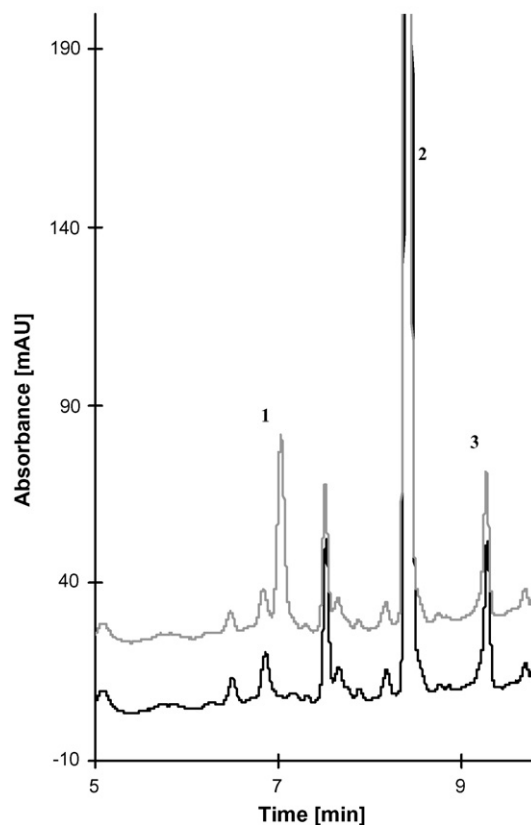
Specificity was demonstrated by the ability to assess unequivocally the analyte in the presence of endogenous compounds of closely related structures. The urine sample was spiked with methimazole, cysteine and cysteinylglycine, and processed according to recommended analytical procedure. Homocysteine eluted shortly after the solvent front and cysteine and cysteinylglycine eluted separately with longer retention times than methimazole (Fig. 4).

To demonstrate the linear response function between the concentration of methimazole and the peak height across the entire range of the analytical procedure the normal urine spiked with the standard solution of analyte was assayed. Seven-point calibration plot was constructed using triplicate injections of the final analytical solution prepared according to the recommended procedure. Analysis of the results demonstrates the good agreement of the detector response with a linear model within the concentration range from 0.25 to 50 mg/l urine studied. The equation of the calibration line was as follow: $y = 11.407x + 0.406$. Standard errors for slope and intercept were 0.085 [mAU] and 0.2023 [mAU/(mg/l)], respectively. The coefficient of determination for the calibration regression line was 0.9997.

3.3.2. Precision and recovery

In order to judge the quality of the elaborated method precision and recovery were determined. They were measured by the addition of the analyte standards to methimazole free urine samples. The samples were analyzed in triplicates according to elaborated procedure. Percentages of recoveries and relative standard deviation values for precision, and intermediate precision were calculated and are inserted in Table 1.

3.3.3. Detection and quantitation limits

Lower limit of detection (LLD) was experimentally estimated by analysis of urine samples spiked with serially diluted methimazole standard until the signal-to-noise ratio reached 3. The lower limit of quantitation (LLQ) serving as the lowest point on the standard curve, was understood to be the lowest measurable concentration for which relative standard deviation values for precision and relative bias were lower then 20% [18]. In our method LLD and LLQ were 0.15 and 0.25 mg/l urine, respectively. At concentration level of 0.25 mg/l, the R.S.D. value for precision was 5.0% and the relative bias was equal to 0.98% ($n = 3$).

3.3.4. Stability of the derivative

2-*S*-Quinolinium derivative of the drug in final analytical solution was stored both at the room temperature, intended for use for HPLC separation during the day of preparation, and at 4 °C. The latter being the reference sample or for unattended analysis after collection of a big number of samples. The derivative was found to be stable at room temperature for at least 24 h, and at 4 °C for at least 28 days. Longer times were not investigated.

4. Conclusion

The technology used for determination of methimazole in human urine by this CMQT derivatization method involves only conventional HPLC-UV equipment without a need of extraction or sample preconcentration. The sensitivity of this method (LLD, 0.15 mg/l urine) is comparable to, or better than those of liquid phase separation methods for urine described by others. Blanchflower et al. (double extraction, preconcentration and HPLC–MS analysis) reported 0.025 mg/l [7] and Sanchez-Pedreno et al. (extraction, preconcentration and flow-injection analysis) 6.70 mg/l urine [10]. Batjoens et al. [12] after liquid–liquid extraction, evaporation with vacuum concentrator, derivatization, and final analysis by GC–MS received about three orders of magnitude better sensitivity. Other analytical figures of merit, including precision and recovery, demonstrated by us during the method validation procedure, are well within the criteria for biological sample analysis [18].

High stability of methimazole–CMQT derivative itself and all the reagents used enable running the analysis in unattended fashion. If necessary, this approach might be complemented for determination of endogenous cysteine and cysteinylglycine.

Acknowledgement

References

[1] A.C. Edward, in: C.M. Smith, A.M. Reynard (Eds.), Textbook of Pharmacology, Saunders, Philadelphia, 1992, pp. 652–656.

[2] M.B. Genter, J. Biochem. Mol. Toxicol. 12 (1998) 305–314.

[3] J. Sun, C. Zheng, X. Xiao, L. Niu, T. You, E. Wang, Electroanalysis 17 (2005) 1675–1680.

[4] M.L. Martinez-Frias, A. Cereijo, E. Rodriguez-Pinilla, M. Urioste, Lancet 339 (1992) 742–743.

[5] European Community Directive 86/649 Off. J. Eur. Commun. 36 (1986) Document Number L275.

[6] Q.H. Zou, Y. Liu, M.X. Xie, J. Han, L. Zhang, Anal. Chim. Acta 551 (2005) 184–191.

[7] W.J. Blanchflower, P.J. Hughes, A. Cannavan, M.A. McCoy, D.G. Kennedy, Analyst 122 (1997) 967–972.

[8] L. Hollosi, A. Kettrup, K.W. Schramm, J. Pharmaceut. Biomed. 36 (2004) 921–924.

[9] L. Zhang, Y. Liu, M.X. Xie, Y.M. Qiu, J. Chromatogr. A 1074 (2005) 1–7.

[10] C. Sanchez-Pedreno, M.I. Albero, M.S. Garcia, V. Rodenas, Anal. Chim. Acta 308 (1995) 457–461.

[11] K. De Wasch, H.F. De Brabander, S. Impens, M. Vandewiele, D. Courtheyn, J. Chromatogr. A 912 (2001) 311–317.

[12] P. Batjoens, H.F. De Wasch Brabander, K. De, J. Chromatogr. A 750 (1996) 127–132.

[13] R.K. Buick, C. Barry, I.M. Traynor, W.J. McCaughey, C.T. Elliott, J. Chromatogr. B 720 (1998) 71–79.

[14] E. Bald, R. Glowacki, J. Liq. Chromatogr. 24 (2001) 1323–1339.

[15] E. Bald, G. Chwatko, R. Glowacki, K. Kuśmierek, J. Chromatogr. A 1032 (2004) 109–115.

[16] E. Bald, R. Glowacki, J. Drzewoski, J. Chromatogr. A 913 (2001) 319–329.

[17] K. Kuśmierek, R. Glowacki, E. Bald, Anal. Bioanal. Chem. 385 (2006) 588–860.

[18] V.P. Shah, K.K. Midha, S. Dighe, I.J. McGilveray, J.P. Skelly, A. Yacobi, T. Layloff, C.T. Viswanathan, C.E. Cook, R.D. McDowall, K.A. Pittman, S. Spector, J. Pharm. Sci. 81 (1992) 309–312.

DNA analysis of a radiotolerant bacterium *Pantoea agglomerans* by FT-IR spectroscopy

Canh Le-Tien [a], Roxanne Lafortune [a], Francois Shareck [b], Monique Lacroix [a,*]

[a] *Research Laboratories in Sciences Applied to Food, Canadian Irradiation Center, INRS-Institut Armand-Frappier,*
531 boul. des Prairies, Laval, Québec, Canada H7V 1B7
[b] *INRS-Institut Armand-Frappier, 531 boul. des Prairies, Laval, Québec, Canada H7V 1B7*

Abstract

A radiation tolerance strain, *Pantoea agglomerans* was isolated from γ-irradiated carrot samples (*Daucus carota*). D_{10} determination showed that the radioresistance of this bacterium is five-fold higher than *Escherichia coli*, both belonging to the family of *Enterobacteriaceae*. DNA isolated from untreated and irradiated bacterial cells was analyzed by FT-IR spectroscopy to investigate the radiotolerance of this bacterium. At doses <5 kGy, an alteration of the interbase hydrogen networks was observed and characterized mainly by an increase of bands assigned to the carbonyl non-pairing and the free amine groups. Moderate breakage of the DNA backbone and damage of the osidic structure were also observed. Similar spectral profiles were noticed at doses ≥5 kGy, but additional increase of the band intensity of C=C and C=N suggests damages of nucleobases. High number of asymmetric PO_2^- and upper shift of symmetric PO_2^- are indicative of DNA strand breaks. Osidic damages were evidenced by decrease of the absorption bands ascribed to deoxyribosyl moieties and by appearance of C–OH band. DNA degradation at high irradiation doses was also noticed by electrophoresis using agarose gel. It appeared that DNA underwent covalent cross-linking, as revealed by agglomeration of DNA in the wells of agarose gel.
© 2006 Elsevier B.V. All rights reserved.

Keywords: Radiotolerance; DNA; γ-Irradiation; *Pantoea agglomerans*; FT-IR; Electrophoresis

1. Introduction

Various mechanisms are involved in radiation toxicity. Since the effects of ionizing radiations are oxygen-enhanced, the reactive oxygen species (ROS) produced plays an important role and thus contribute to cellular damage [1]. Among them, superoxide anion, hydrogen peroxide and hydroxyl radicals (•OH) lead to a series of biological damage including protein alterations, membrane lipid peroxidation and DNA-strand cleavage [2–4]. It is well accepted that DNA is one of the principal macromolecular targets for radiation damage and that double-strand breaks are the most lethal, resulting in loss of essential genetic information. However, some bacteria appear to develop multiple mechanisms to adapt and protect themselves against their environment in extreme conditions. As example, bacteria belonging to the family *Deinococcaceae* are some of the most radiation-resistant organisms yet discovered and particularly, *Deinococcus radiodurans* was first reported by Anderson et al. in 1956 [5]. Culture of bacteria yielded a red-pigmented, non-sporulating, Gram-positive coccus that was extremely resistant to hydrogen peroxide, UV light, ionizing radiation and numerous other agents that damage DNA [6–8]. Several reports have shown its ability to survive extremely high doses of acute ionizing radiation (10 kGy) without cell-killing [4,5,9].

A number of hypothesis have been postulated to explain the resistance of *D. radiodurans*, which shows no loss of viability up to radiation doses of 5 kGy, while *Escherichia coli* cultures are 100 times less resistant [10]. These hypotheses have been proposed: (i) *D. radiodurans* uses conventional repair pathways with greater efficiency than other bacteria [11–13]; (ii) there are repair functions encoded among its hypothetical genes [14]; or (iii) repair is facilitated by its ringlike nucleoids [15]. Recently, Daly et al. [9] reported that accumulation of intracellular manganese (Mn) facilitates γ-radiation resistance. This hypothesis emphasize repair of DNA damage caused by the direct effects of γ-photons and the indirect effects of ROS

---

* Corresponding author. Tel.: +1 450 687 5010x4489; fax: +1 450 687 5792.
E-mail address: monique.lacroix@iaf.inrs.ca (M. Lacroix).

induced during irradiation [16]. When ROS exceed the capacity of endogenous scavengers to neutralize them, cells become vulnerable to damage, a condition referred as oxidative stress [17].

Other radiation-resistance mechanisms are in relationship to protective systems such as antioxidative enzymes, which involve peroxidase, catalase and superoxide dismutase [18]. These bacterial enzymes represent an important defensive system against ROS induced by hydrogen peroxide and/or radiation [19]. Several bacteria possess a substantial amount of non-enzymatic systems (e.g., Vitamins A and E), which contribute to the resistance phenomenon against the deleterious effects of radiation damages [20]. It is also important to mention that certain bacteria able to produce carotenoids pigments or other membrane pigment such as *D. radiodurans* [21] are more resistant to $^{\bullet}OH$ than the colorless ones.

Recently, Lacroix and Lafortune [22] reported the presence of the radiation resistance of *Pantoea agglomerans* (formerly, *Erwinia herbicola*) isolated from carrot irradiated at 7 kGy. This microorganism belonging to the family *Enterobacteriacea* is a Gram-negative, non-sporulated and non-capsulated bacterium, which was often detected in vegetables flora [23]. It is well known that *Enterobacteriaceae* are very sensitive to irradiation (*10*). However, several studies [24–27] were reported that the epiphytic bacteria developed a superior stress tolerance, particularly *P. agglomerans*.

The aim of this paper is to evaluate the radiation tolerance of *P. agglomerans* submitted to various doses of γ-irradiation. As mentioned previously, DNA is one of the principal targets for radiation damage and, the analysis of these biomolecules by Fourier Transform Infrared (FT-IR) spectroscopy is of interest to investigate the bacterial behavior when treated with different doses of γ-irradiation. FT-IR spectroscopy has recently emerged as a novel technique and provides several informations about the vibrational and rotational motions of DNA molecules [28]. FT-IR spectra reflect the total chemical composition of DNA and some of the spectral bands can be assigned to distinct functional groups or chemical substructures [29]. Finally, agarose gel electrophoresis allows correlating results in order to highlight this biomolecular changes occurring after γ-irradiation.

2. Material and methods

2.1. Bacterial cultures preparation

P. agglomerans strain was isolated as described by Lacroix and Lafortune [22]. Practically, carrots (*Daucus carota* from IGA, Laval, CA) were washed and shredded using a food processor (Hamilton Beach/Proctor-Silex Inc., USA). An amount of 30 g of grated carrots was placed in metallized polyester/EVA copolymer sterile bag (305 mm × 210 mm, Winpak, St-Leonard, CA). Packages of carrots were then sealed and stored approximately at $-80\,^{\circ}C$ for 15 h before irradiation treatment at 5 kGy. Irradiation treatment was done at the Canadian Irradiation Center (CIC) in a ^{60}Co underwater calibrator unit (UC-15, MDS Nordion, Kanata, Ont., Canada) with a mean dose

rate of 25.6 kGy/h. Thereafter, all the bags were stored at $4\,^{\circ}C$ and the identification of appearance of *P. agglomerans* (from day 20) was carried out with an API-20E miniaturized diagnostic kit (BioMérieux, Canada). Isolated *P. agglomerans* was maintained in 1 mL cryogenic vials at $-80\,^{\circ}C$ in Tryptic Soy Broth (TSB, Difco Laboratory, Detroit, MI) containing glycerol (10%, v/v). A volume of 1 mL cultures was incubated through two cycles of 24 h at $30\,^{\circ}C$ in 9 mL of TSB to obtain a working culture. The working culture was transferred to 1 L of TSB and incubated during 18 h of incubation at $30\,^{\circ}C$, in order to obtain a bacterial culture containing 1.0×10^8 CFU/mL.

2.2. D_{10} determination

For the D_{10} determination, an amount of 5 mL of *P. agglomerans* culture (18 h) was irradiated at various doses 0, 1, 2, 3, 4 and 5 kGy. After irradiation, various dilutions were prepared and appropriate ones were pour-plated in tryptic soy agar (TSA, Difco Laboratories, Detroit, USA) and incubated at $30\,^{\circ}C$ during 48 h for bacterial count. A similar procedure was applied to *E. coli* for comparative studies, but irradiation doses applied were at 0, 0.15, 0.30, 0.45, 0.60 and 0.90 kGy.

2.2.1. DNA preparations for FT-IR analysis
2.2.1.1. Irradiation treatment. The bacterial cultures of *P. agglomerans* (1 mL) were irradiated as described previously with doses of 0, 2, 4, 5, 8 and 16 kGy.

2.2.1.2. DNA extraction and electrophoresis. The DNA extraction was performed as described by Marmur [30]. Non-irradiated and irradiated bacteria were harvested by centrifugation at $2000 \times g$ for 20 min and cells were washed with Tris buffer 10 mM, pH 8.0. Afterward, the cells were suspended in 0.5 mL the same buffer containing 10 mg/mL of freshly prepared lysozyme and incubated at $37\,^{\circ}C$ for 30 min. Complete lysis was obtained by the addition of 50 μL of 10% SDS followed by several inversions of the microtube. To purify DNA from the RNA contamination, an amount of 2 mL of Tris–HCl (10 mM) EDTA (1 mM) buffer (pH 8.0) containing 20 μL of RNase A (1 mg/mL) was added in the precipitate. The step following consists in precipitation with ethanol 70% in order to remove the ribonucleotides and other residues. Proteins were denatured by successive additions of phenol–chloroform (1:1) and centrifugations until the interface was cleared of any cloudy material. The DNA was precipitated from the aqueous phase with Na-acetate (0.3 M) and 2 volumes of ethanol ($-20\,^{\circ}C$). The final precipitate was dissolved in 450 μL of distilled water for the determination of the DNA purity by determination of the absorption ratio of A260/280 nm using a DMS 200 spectrophotometer (Varian Techtron Pty. Ltd.). For the electrophoresis analysis, purified DNA extract was solubilized in 6X loading buffer (glycerol 30%, cyanol xylene 0.25%, bromophenol blue 0.25%) and DNA fragments were separated by migration on an agarose gel 0.7% dissolved in TBE buffer (Tris–Borate 89 mM, EDTA 2 mM, pH 8.3) in presence of ethidium bromide (0.5 μg/mL). DNA KiloBase

and Lambda-Pst1 was used as a marker. Migration was done during 17 h at 30 V using electrophoresis system (mini DNA SUB CELL, Bio-Rad, Mississauga, Canada). The DNA fragments were visualized under UV using a Gel Doc 1000 (Bio-Rad).

2.3. FT-IR analysis

A part of the extracted DNA was lyophilized using a rotary Evaporator (SpeedVac, Savant) during 3 h. Tablets (100 mg) composed of lyophilized DNA (3%) and anhydrous KBr were prepared with an hydraulic press (Carver Laboratory Equipment, Wabash, IN). FT-IR spectra were recorded with a Spectrum One (Perkin-Elmer Instruments, Norwalk, USA) equipped with a Universal Attenuated Total Reflectance (UATR) device for tablets analysis on the spectral region 1800–800 cm^{-1} with 256 scans at 4 cm^{-1} resolution. All spectra were normalized over the range using the Spectrum software 3.02.

3. Results

As reported previously by Lacroix and Lafortune [22] the detection of *P. agglomerans* was noted after 20 days of storage, in irradiated samples treated at a dose of 7 kGy suggesting the radiation tolerance of this bacterium. To investigate this phenomenon, the D_{10} determination of *P. agglomerans* isolated from carrots was carried out in parallel with *E. coli*, because these bacteria were classified in the same family (*Enterobacteriacea*). For *E. coli*, the D_{10} value required to reduce bacterial population by one log was about of 0.11 kGy and a dose of 0.9 kGy was necessary to decrease the level of this bacterium under the threshold level of detection (<10 CFU/mL, Fig. 1). In contrast, a high D_{10} value observed for *P. agglomerans* was 0.52 kGy and a dose necessary to decrease the bacterial population under the threshold level of detection was 4.5 kGy. These results suggest that the tolerance of *P. agglomerans* is five-fold higher than *E. coli*.
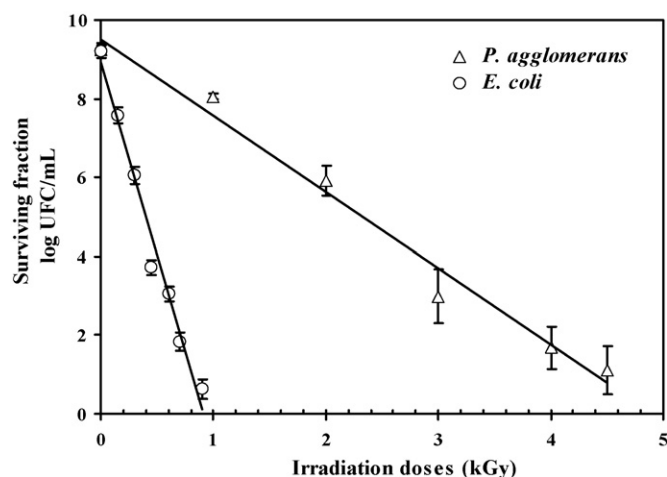

Fig. 1. Determination of D_{10} values of *Pantoea agglomerans* and *Escherichia coli* exposed at various doses of γ-irradiation.

3.1. FT-IR analysis of P. agglomerans DNA

In this experiment, DNA samples were analyzed under solid form, but no significant difference of the band positions between lyophilized DNA and DNA in solution was noticed (results not shown). Indeed, the choice to analyze the samples under solid state permits to eliminate the water bands in the spectrum, which can influence interpretations. Other advantage is to allow to obtain high quality FT-IR spectra with little sample.

Generally, FT-IR spectra analysis of DNA is divided in three principal regions [31]. The first region from 1750 to 1600 cm^{-1} is essentially due to C=O, C=N, C=C stretching and exocyclic –NH$_2$ bending vibrations in the DNA bases. The second region from 1600 to 1500 cm^{-1} results mostly from the purine and pyrimidine ring modes [32–34] and the last region from 1250 to 950 cm^{-1} correspond to the symmetric and asymmetric PO$_2{}^-$ groups of the phosphodiester-deoxyribose backbone [32,34].

3.2. Frequency region of nucleobases

For *P. agglomerans*, the untreated (non-irradiated) DNA spectrum in the spectral region 1750–1400 cm^{-1} shows four modes at 1692, 1650, 1605 and 1560 cm^{-1} (Fig. 2A). The absorption band at 1692 cm^{-1} could be assigned to an overlapping of carbonyl (C2=O2) stretching vibration of thymine and cytosine [33,35,36]. The band at 1650 cm^{-1} is contributed to carbonyl stretching of thymine (C4=O4), guanine (C6=O6) and C=N and C=C stretching vibrations [34], whereas the bands at 1605 and 1560 cm^{-1} are due mostly to NH$_2$ scissoring and N–H bending [31], respectively. In addition, the absorption bands at 1466 and 1488 cm^{-1} reflected to the purine and pyrimidine (DNA bases) ring modes [36].

The DNA isolated from the cells submitted to irradiation at doses <5 kGy showed distinct changes in some DNA vibrational bands (Fig. 2A). The irradiated DNA spectra show firstly an absorption increase of the band assigned to carbonyl which was slightly up shifted to high wavenumber from 1692 to 1696 cm^{-1}. Generally, this spectral region (1750–1550 cm^{-1}) contains absorption bands assigned to in-plane double bond stretching vibrations of bases, which were known to be particularly sensitive to base-pairing interactions [35]. In agreement with the proposed base-pairing scheme, changes in intensity of the vibrations from polar groups (i.e. C=O) result from alterations in external non-covalent interactions such as the loss of hydrogen bonds [37]. For this purpose, the increase in intensity and the up shifted to high wavenumber of carbonyl band are provisionally assigned to a free carbonyl (no hydrogen bonded) stretching vibration [38]. This phenomenon is in accordance with the increase of absorption bands of NH$_2$ scissoring (1605 cm^{-1}) and N–H bending vibration (1560 cm^{-1}) suggesting a number increasing of free NH$_2$ and N–H groups (non-paired).

Additionally, a very sensitive band around 1480–1460 cm^{-1} is assigned mainly to the imidazole ring vibration of purine, which depends on the N7C8 bending vibration [36]. Any modification in the position of this band will reflect an alteration of interactions on the N7C8 site [37]. Fig. 2A presents the untreated
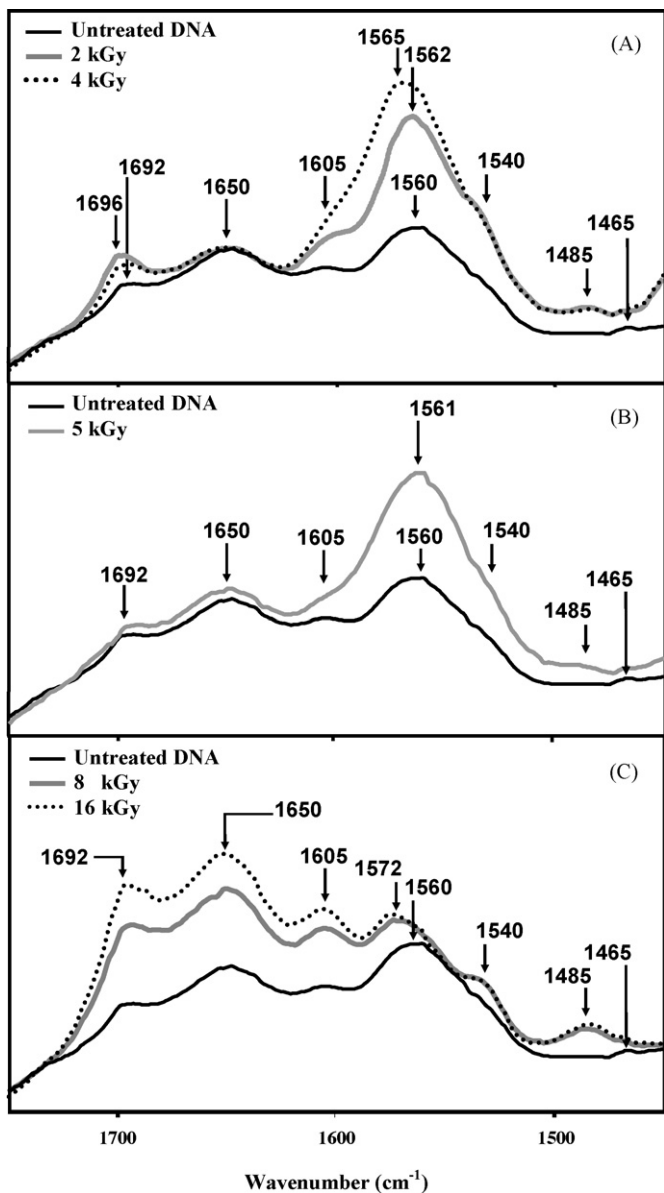
Fig. 2. FT-IR spectra of untreated and γ-irradiated DNA isolated from *P. agglom-erans* in frequency region assigned to nucleobases.

(non-irradiated) DNA, which show the N7C8 bending vibration located at 1465 cm^{-1}. When the DNA is submitted to irradiation, this band is slightly increased and up shifted to high wavenumber (1485 cm^{-1}) suggesting an alteration of interaction on this site due to the loss of hydrogen interaction, giving a free N7C8 site. However, no significant intensity change of the bands contributing for ring C=C and C=N (1650 cm^{-1}) was observed. Generally, the spectra of irradiated DNA at doses <5 kGy show an alteration of hydrogen interactions network between bases.

Similar observations with DNA irradiated at 5 kGy, but a slight increase of the absorption intensities of band contributing for ring C=C and C=N stretching vibrations (1650 cm^{-1}) was noticed (Fig. 2B). The intensity increase of this band suggests that there is not only an alteration of the interbase hydrogen networks, but probably a deterioration of base structures

(nucleobase damage). However, the increase in intensity remained weak.

At doses >5 kGy (8 and 16 kGy), the irradiated DNA spectra show an evident increase in intensity for the bands assigned to C=O (1696 cm^{-1}), ring C=N and C=C (1650 cm^{-1}) and exo-cyclic NH$_2$ (1605 cm^{-1}, Fig. 2C). However, the band located at 1560 cm^{-1} (mostly due to the N–H bending vibrations) is up shifted to high wavenumber at 1572 cm^{-1} (–NH$_2$ bending vibra-tion). The displacement was also observed for the band assigned for N7C8 (from 1465 to 1485 cm^{-1}). The explanation of these differences is based on the oxidative damage of nucleobases giv-ing several derivatives, as reported by numerous articles [39–42]. Indeed, the highly reactive •OH reacts with DNA by addition to double bonds of nucleobases and by abstraction of an H atom from the methyl group of thymine [42].

Several papers were reported that numerous products were detected in γ-irradiated pyrimidine bases such as 5-hydroxymethyluracil, 5-formyluracil, 5-hydroxycytosine, etc. [43–45]. With regard to the purine bases, damage reactions result in multiple products such as 8-hydroxyguanine, 2,6-diamino-4-hydroxy-5-formamido-pyrimidine, 8-hydroxyadenine, etc. [39,46]. These components present generally some more func-tional groups such as carbonyl and amine (i.e. 5-formyluracil, Fapy-Gua and Fapy-Ade, etc.) or new double bonded forma-tion (i.e 5-hydroxycytosine, 5,6-dihydroxycytosine, etc.), which explains the increase of absorption bands for irradiated DNA in the spectral region 1700–1600 cm^{-1}.

3.3. Frequency region of DNA backbone

This region reflects mostly the carbohydrate and phosphodi-ester, which constitute the backbone of DNA. Recent evidence has showed that the modification of DNA bases by •OH induces changes in the conformational structure of phosphodiester-deoxyribose moiety. These radicals are known to react directly with the phosphodiester-deoxyribose structure (i.e. by abstrac-tion a hydrogen atom from deoxyribose) resulting in strand breaks and the loss of phosphoric acid [47].

According to Lindqvist et al. [36], absorption bands arising from the phosphate backbone vibration dominate 1250–1200 cm^{-1} due to the asymmetric (asm) PO$_2$$^-$ stretching mode and around 1090–1070 cm^{-1} assigned to the symmetric (sm) PO$_2$$^-$ stretching mode. These bands are a characteristic marker for backbone conformational changes of DNA.

For DNA spectrum of untreated cells (Fig. 3), two absorp-tion bands at 1236 cm^{-1} and at 1070 cm^{-1} reflect, respectively, to asm PO$_2$$^-$ and sm PO$_2$$^-$. When DNA irradiated at doses 2 and 4 kGy, no significant change in intensity for asm and sm PO$_2$$^-$ was observed, but a slight shift toward high wavenumber (from 1070 to 1075 cm^{-1}) was noted for sm PO$_2$$^-$. This upper shift is indicative of change or rearrangement in the DNA back-bone structure, which could be associated to the alteration of the phosphate groups along the DNA backbone.

Major differences of the irradiated DNA at doses ≥5 kGy were observed. These differences are characterized by a slight increase of the absorption bands of the asm PO$_2$$^-$, whereas the sm PO$_2$$^-$ was up shifted from 1070 to 1088 cm^{-1} and widened
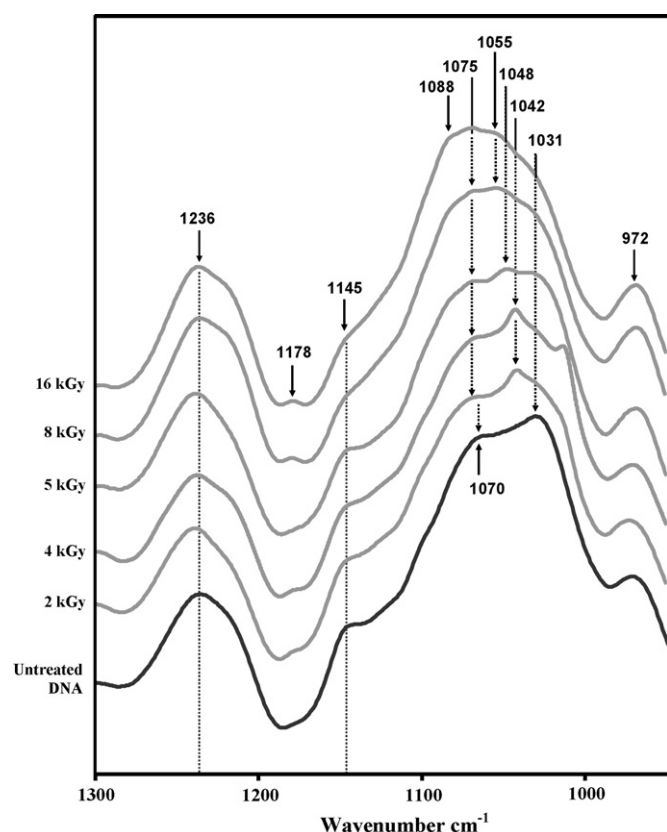
Fig. 3. FT-IR spectra of untreated and γ-irradiated DNA isolated from *P. agglomerans* in frequency regions of DNA backbone.

Fig. 4. Agarose gel (0.7%) electrophoresis of untreated and γ-irradiated (2–16 kGy) DNA isolated from *P. agglomerans*.

with a broad shoulder. It is worth to note that the shoulder is more evident at higher irradiation dose (16 kGy). One possible explanation is that there are substantial damages to the phosphodiester-deoxyribose structure, which seems to be connected with conformational changes in the position of phosphate groups in DNA. Additional evidence that supports this alteration is the decrease of the absorption band located at 1145 cm^{-1}, which is assigned to sm C–O–P stretching vibration [48,49]. This decrease is clearly noticed at high doses of irradiation suggesting the lost of phosphodiester bonds leading strand breaks, as reported by several authors [4,38].

In turn, the lost of phosphodiester bonds was also in part assigned to deoxyribosyl moieties, thus damaging of osidic structure, as revealed by the decrease in amplitude of the sm C–O–P band. Moreover, a new band appears at 1164 cm^{-1} contributed to the C–OH stretching vibration [49,50] is evident at high doses of irradiation. This appearance of C–OH band is probably resulted to the breakage of phosphodiester bonds and/or the ring-opening deoxyribose. According to Siddiqi and Bothe [51], series of reaction that lead to sugar modifications and strand breaks are initiated by radical formation at deoxyribose. This may result either from direct ionization by radiation or from attack of •OH, which are generated by water radiolysis. A detailed review of the mechanisms of these reactions can be found elsewhere [42,52].

In this supposition, the strand break was observed at high doses of irradiation (>5 kGy) suggesting there is DNA degra-

dation. To verify this phenomenon, agarose gel electrophoresis was used. Results have shown that there was no significant difference between the DNA irradiated at 2 kGy compared to the control DNA samples (non-irradiated samples, Fig. 4). However, DNA degradations were observed from 4 kGy and more clearly at doses 8 and 16 kGy. In addition, the appearance of a precipitate of irradiated DNA was observed in the wells of the agarose gel.

These agglomerates seem provisionally to be due to the cross-linking of part of DNA involving conversion to high molecular mass, which are unable to penetrate in the agarose gel. It is worth to mention that this event was not found in control and standard. The possible explanation of the DNA cross-linking during irradiation process is based on the formation of interstrand covalent bonds, as observed in the case of UV, which induced dimerization of pyrimidine bases [53].

4. Discussion

In the present study, FT-IR analysis of DNA isolated from irradiated cells of *P. agglomerans* show that there are important structural changes. At doses <5 kGy, results showed interbase hydrogen networks alteration without evidence base modifications. The phosphodiester-deoxyribose structure is also affected, which resulted to the breakage of phosphodiester bonds and/or the opening of ring-deoxyribose. However, moderate cleavages of DNA strands and damages of osidic structure were observed.

At doses ≥5 kGy, similar observations were recorded in nucleic base region, but additional increase of C=C and C=N bands is indicative of base modifications. DNA strand breaks and damages of osidic structure were obviously observed with distinct changes. These differences show that there are base

modifications and degradation of DNA, which are in correlation with analysis of agarose gel electrophoresis. Concerning the cross-linking phenomenon, until now, no extensive study has been reported on the DNA–DNA interstrand cross-linking induced by γ-irradiation. For instance, it is well documented that thymine- or cytosine-purine intrastrand cross-linking is the main product identified from γ-irradiated DNA [54,55]. Furthermore, several studies showed that γ-irradiation can induce the DNA protein cross-linking, which results in the combination between radicals of base and aromatic amino acid of proteins [42,56,57]. This phenomenon could be monitored by FT-IR, which showed an increase of bands at 1650 cm^{-1} and the appearance of new band located at 1540 cm^{-1}. These bands could be respectively assigned to amide band I and band II of protein backbone. This could be constituted an explanation why the absorption ratio 260/280 nm is slightly weak for DNA irradiated at high doses (1.6) compared to those irradiated with low doses (1.8). However, FT-IR spectra of DNA irradiated at 8 and 16 kGy show obviously these amide bands suggesting this phenomenon occurred at high doses of γ-irradiation.

In the present study, D_{10} determination showed that the radiotolerance of this bacterium (0.52 kGy) is five-fold higher than E. coli (0.11 kGy), although both belong to the family Enterobacteriacea. Several factors could be involved for explanation of bacterium radiotolerance. As mentioned above for D. radioduran, it is probable that P. agglomerans uses the same repair pathways or there are repair functions encoded among its genes [14]. These hypotheses emphasize repair of DNA damage caused by the direct effects of γ-photons and the indirect effects of reactive oxygen species (ROS) induced during irradiation.

Recently, Daly et al. [9] showed that the ring-like organization of the chromosomes is unlikely to play a role in radiation resistance. Instead, it is the very high intracellular concentration of manganese (Mn) ions relative to iron (Fe) that is critical. Rather than providing protection against the initial burst of radiation, high intracellular Mn might act against sudden increases in damaging ROS during the recovery from radical injury. No extensive study for P. agglomerans has been reported on the intracellular concentrations of Mn and Fe ions. For instance, Francis et al. [58] showed that P. agglomerans is able under anaerobic conditions of coupling acetate oxidation to dissimilatory metal reduction, mainly Mn and Fe. It is important to note that Mn is essential for the detoxification of ROS in most bacteria, principally as a co-factor for the Mn-dependent enzyme superoxide dismutase (Mn-SOD). In this context, it is possible that P. agglomerans uses this pathway of metal reduction to accumulate intracellular Mn ions, which react directly with ROS and/or indirectly as co-factor for enzyme defensive systems (i.e. SOD). This could be an important mechanism to explain the radiotolerance of P. agglomerans.

It is also interesting to mention that although P. agglomerans and E. coli belong to the family Enterobacteriacea, they occupy however different ecological niches. E. coli inhabits the intestinal tracts of humans or other vertebrates, whereas P. agglomerans is an epiphytic bacterium found primarily in soil, water, plants, insects, etc. Generally, epiphytic bacteria are subject to various environmental stresses, including extremes

of temperature and both UV and visible light irradiations. To survive, these bacteria have apparently evolved diverse adaptations, which enhance stress tolerance. Several studies [24–27,59] reported that the epiphytic bacteria have developed a superior stress tolerance, particularly P. agglomerans. This bacterium is able to synthesize yellow pigments, presumably carotenoids [24,59], which might serve to protect against ROS resulting from absorption of visible light by chlorophyll present in the host plant. Speculations about the possible role of carotenoids or other membrane pigment were equally reported. According to Lemee et al. [21], D. radiodurans strains containing carotenoids are more resistant to •OH than the colorless ones.

5. Conclusion

In conclusion, FT-IR spectroscopy is a useful method for investigation of radiation damages to the radiation resistance of bacteria. This very sensitive technique allows detection of the deleterious effects of γ-radiations and thus the phenomenon of DNA–protein cross-linking. Several damages to structural units of P. agglomerans DNA were detected by FT-IR at various doses of γ-irradiation. Generally, it appears that modifications of bases are the lethal consequences. The radiation resistance of P. agglomerans could be explained by various mechanisms to tolerate at a certain high dose of γ-irradiation. It is possible that this bacterium uses the conventional repair pathways with greater efficiency than E. coli. The accumulation of intracellular Mn ions constitutes also significant factors involving the antioxidative enzymes systems (e.g. Mn-SOD) and non-enzymatic systems such as carotenoids. Thus, infrared spectroscopy is becoming an interesting tool for the diagnosis of damage induced in any biological cell and for monitoring the sensitivity and/or the repair mechanism following injury. Further research on the radiation resistance of P. agglomerans should be emphasized on the FT-IR analysis of DNA isolated from post-irradiation reincubated cells, which allows to monitor the repair system effectiveness. Addition of protein synthesis inhibitor (i.e. chloramphenicol) seems equally interesting to highlight the resistant mechanism.

Acknowledgements

References

[1] E. Cadenas, Ann. Rev. Biochem. 59 (1989) 79–110.
[2] M.S. Cooke, M.D. Evans, M. Dizdaroglu, J. Lunec, FASEB J. 17 (2003) 1195–1214.

[3] D.C. Malins, N.L. Polissar, S.J. Gunselman, Proc. Natl. Acad. Sci. 93 (1996) 2557–2563.
[4] A.N. Melin, A. Perromat, G. Déléris, Arch. Biochem. Biophys. 394 (2001) 265–274.
[5] A.W. Anderson, H.C. Nordan, R.F. Cain, G. Parrish, D. Duggan, Food Technol. 10 (1956) 575–578.
[6] B.E.B. Moseley, A. Mattingly, H.J.R. Copland, J. Gen. Microbiol. 72 (1972) 329–338.
[7] C.C. Lange, L.P. Wackett, K.W. Minton, M.J. Daly, Nat. Biotechnol. 16 (1998) 929–933.
[8] K.W. Minton, Mol. Microbiol. 13 (1994) 9–15.
[9] M.J. Daly, E.K. Gaidamakova, V.Y. Matrosova, A. Vasilenko, M. Zhai, A. Venkateswaran, M. Hess, M.V. Omelchenko, H.M. Kostandarithes, K.S. Makarova, L.P. Wackett, J.K. Fredrickson, D. Ghosal, Science 306 (2004) 1025–1028.
[10] B.E.B. Moseley, Photochem. Photobiol. Rev. 7 (1983) 223–274.
[11] M.J. Daly, K.W. Minton, J. Bacteriol. 178 (1996) 4461–4471.
[12] M.T. Hansen, J. Bacteriol. 134 (1978) 71–75.
[13] B.E. Moseley, J. Bacteriol. 105 (1971) 976–983.
[14] Y. Liu, J. Zhou, M.V. Omelchenko, A.S. Beliaev, A. Venkateswaran, J. Stair, L. Wu, D.K. Thompson, D. Xu, I.B. Rogozin, E.K. Gaidamakova, M. Zhai, K.S. Makarova, E.V. Koonin, M.J. Daly, Proc. Natl. Acad. Sci. 100 (2003) 4191–4196.
[15] S. Levin-Zaidman, J. Englander, E. Shimoni, A.K. Sharma, K.W. Minton, A. Minsky, Science 299 (2003) 254–256.
[16] J.E. Repine, O.W. Pfenninger, D.W. Talmage, E.M. Berger, D.E. Pettijohn, Proc. Natl. Acad. Sci. 78 (1981) 1001–1003.
[17] J.A. Imlay, Annu. Rev. Microbiol. 57 (2003) 395–418.
[18] J.M. McCord, B.B. Keele Jr., I. Fridovich, Proc. Natl. Acad. Sci. 68 (1971) 1024–1027.
[19] P. Wang, H.E. Schellhorn, Can. J. Microbiol. 41 (1995) 170–176.
[20] A.M. Melin, A. Perromat, G. Deleris, Biospectroscopy 5 (1999) 229–236.
[21] L. Lemee, E. Peuchant, M. Clerc, M. Brunner, H. Pfander, Tetrahedron 53 (1997) 919–926.
[22] M. Lacroix, R. Lafortune, Radiat. Phys. Chem. 71 (2004) 79–82.
[23] J.M. Hamilton-Miller, S. Shah, Int. J. Antimicrob. Ag. 18 (2001) 81–83.
[24] R.W. Tuveson, R.A. Larson, J. Kagan, J. Bacteriol. 170 (1988) 4675–4680.
[25] B. Marthi, V.B. Fieland, M. Walter, R.J. Seidler, Appl. Environ. Microbiol. 56 (1990) 3463–3467.
[26] K.Y. To, E.M. Lai, L.Y. Lee, T.P. Lin, C.H. Hung, C.L. Chen, Y.S. Chang, S.T. Liu, Microbiology 40 (1994) 331–339.
[27] M. Wilson, S.S. Hirano, S.E. Lindow, Appl. Environ. Microbiol. 65 (1999) 1435–1443.
[28] W. Zeroual, C. Choisy, S.M. Doglia, H. Bobichon, J.F. Angiboust, M. Manfait, Biochim. Biophys. Acta 1222 (1994) 171–178.
[29] D. Naumann, D. Helm, H. Labischinski, Nature 351 (1991) 81–82.
[30] J. Marmur, J. Mol. Biol. 3 (1961) 208–218.
[31] S.H. Brewer, S.J. Anthireya, S.E. Lappi, D.L. Drapcho, S. Franzen, Langmuir 18 (2002) 4460–4464.
[32] M. Falk, K.A. Hartman, R.C. Lord, J. Am. Chem. Soc. 85 (1963) 391–394.
[33] J. Liquier, P. Coffinier, M. Firon, E. Taillandier, J. Biomol. Struct. Dyn. 9 (1991) 437–445.
[34] B. Zhou-Sun, J. Sun, S.M. Gryaznov, J. Liquier, T. Garestier, C. Helene, E. Taillandier, Nucl. Acids Res. 25 (1997) 1782–1787.
[35] F. Geinguenaud, J. Liquier, M.G. Brevnov, O.V. Petrauskene, Y.I. Alexeev, E.S. Gromova, E. Taillandier, Biochemistry 39 (2000) 12650–12658.
[36] M. Lindqvist, M. Sarkar, A. Winqvist, E. Rozners, R. Stromberg, A. Graslund, Biochemistry 39 (2000) 1693–1701.
[37] C. Dagneaux, J. Liquier, E. Taillandier, Biochemistry 34 (1995) 16618–16623.
[38] D.C. Malins, N.L. Polissar, S.J. Gunselman, Proc. Natl. Acad. Sci. 94 (1997) 3611–3615.
[39] K.C. Cheng, D.S. Cahill, H. Kasai, S. Nishimura, L.A. Loeb, J. Biol. Chem. 267 (1992) 166–172.
[40] H. Kamiya, H. Miura, N. Murata-Kamiya, H. Ishikawa, T. Sakaguchi, H. Inoue, T. Sasaki, C. Masutini, F. Hanaoka, S. Nishimura, E. Ohtsuka, Nucl. Acids Res. 23 (1995) 2893–2899.
[41] J. Cadet, M. Berger, T. Douki, J.L. Ravanat, Rev. Physiol. Biochem. Pharmacol. 131 (1997) 1–87.
[42] M.S. Cooke, M.D. Evans, M. Dizdaroglu, J. Lunec, FASEB J. 17 (2003) 1195–1214.
[43] L. Breimer, T. Lindahl, Biochemistry 24 (1985) 4018–4022.
[44] R. Téoule, Int. J. Radiat. Biol. 51 (1987) 573–589.
[45] M. Dizdaroglu, J. Laval, S. Boiteux, Biochemistry 32 (1993) 12105–12111.
[46] S.A. Weitzman, P.W. Turk, D.H. Milkowski, K. Kozlowski, Proc. Natl. Acad. Sci. 91 (1994) 1261–1264.
[47] D.C. Malins, N.L. Polissar, G.K. Ostrander, M.A. Vinson, Proc. Natl. Acad. Sci. 97 (2000) 12442–12445.
[48] G.I. Dovbeshko, N.Y. Gridina, E.B. Kruglova, O.P. Pashchuk, Talanta 53 (2000) 233–246.
[49] N. Gault, J.L. Poncy, J.L. Lefaix, Can. J. Physiol. Pharmacol. 82 (2004) 38–49.
[50] M. Jackson, H.H. Mantsch, Encyclopedia of Analytical Chemistry, vol. 15, J. Wiley, New York, 2000, pp. 131–156.
[51] M. Siddiqi, E. Bothe, Radiat. Res. 112 (1987) 449–463.
[52] K.B. Beckman, B.N. Ames, J. Biol. Chem. 27 (1997) 19633–19636.
[53] T. Douki, G. Laporte, J. Cadet, Nucl. Acids Res. 31 (2003) 3134–3142.
[54] S. Bellon, J.L. Ravanat, D. Gasparutto, J. Cadet, Chem. Res. Toxicol. 15 (2002) 598–606.
[55] Q. Zhang, Y. Wang, J. Am. Chem. Soc. 125 (2003) 12795–12802.
[56] M. Dizdaroglu, E. Gajewski, Cancer Res. 49 (1989) 3463–3467.
[57] S.M. Chiu, L.R. Friedman, N.L. Oleinick, Int. J. Radiat. Biol. 58 (1990) 235–247.
[58] C.A. Francis, A.Y. Obraztsova, B.M. Tebo, Appl. Env. Microbiol. 66 (2000) 543–548.
[59] K.L. Perry, T.A. Simonitch, K.J. Harrison-Lavoie, S.T. Liu, J. Bacteriol. 168 (1986) 607–612.

Separation and purification of verticine and verticinone from *Bulbus Fritillariae Thunbergii* by high-speed counter-current chromatography coupled with evaporative light scattering detection

Zhilan Liu[a], Yan Jin[a], Pingniang Shen[b],
Juan Wang[b], Yongjia Shen[a,*]

[a] *Laboratory for Advanced Materials, Institute of Fine Chemicals, East China University of Science and Technology, Shanghai 200237, China*
[b] *National Engineering Research Center for Traditional Chinese Medicine, Shanghai 201203, China*

Abstract

High-speed counter-current chromatography (HSCCC) coupled with evaporative light scattering detection (ELSD) was successfully applied to preparative separation and purification of verticine and verticinone from crude extracts of *Bulbus Fritillariae Thunbergii* by a one-step separation, using chloroform–ethanol–0.2 mol L^{-1} hydrochloric acid (3:2:2, v/v/v) as a solvent system. HPLC analysis of the fractions collected on the preparative HSCCC of 200 mg of crude extracts showed that the purity of verticine (25.6 mg) was 96.8% and that of verticinone (10.3 mg) was 95.4%. The chemical identities of these components were confirmed by ^{1}H NMR and EI–MS.
© 2006 Elsevier B.V. All rights reserved.

Keywords: Counter-current chromatography; *Bulbus Fritillariae Thunbergii*; Verticine; Verticinone; Evaporative light scattering detection

1. Introduction

Bulbus Fritillariae Thunbergii (Chinese name zhebeimu) is a famous Chinese medicine, which is derived from the bulbs of the genus *Fritillaria thunbergii* Miq. (Liliaceae) [1]. It has been used as one of the most important antitussive and expectorant drugs for more than 2000 years [2]. Extensive chemical studies have been conducted by many research groups [3–6]. A number of ingredients were found in *Bulbus Fritillariae Thunbergii* including isosteroidal alkaloids, steroidal alkaloids and non-alkaloids. Furthermore, pharmacological studies demonstrate that isosteroidal alkaloids are the primary active ingredients responsible for the antitussive activity. Among these alkaloids, verticine and verticinone (Fig. 1) are the most representative [7].

The conventional method of purifying verticine and verticinone was to utilize column chromatography, which required several steps, and resulted in low recovery yields [8]. High-speed counter-current chromatography (HSCCC), being as a support free liquid–liquid partition chromatography, eliminates irreversible adsorption of sample onto the solid support. This method has been successfully applied to the separation and purification of various natural products [9–12], and several reports have tried the HSCCC coupled with evaporative light scattering detection (ELSD) [13]. However, few studies have been focus on *Bulbus Fritillariae Thunbergii*. In this paper, high-speed counter-current chromatography is coupled with evaporative light scattering detection for separation and purification of verticine and verticinone from the extracts of *Bulbus Fritillariae Thunbergii* by a one-step HSCCC separation.

2. Experimental

2.1. Materials

Bulbus Fritillariae Thunbergii (Zhejiang, China) was purchased from Shanghai Kangqiao Medical Factory, authenticated by Shanghai Chinese Traditional Medicine Research Institute and fitted for Chinese Pharmacopoeia. All solvents used for the preparation of crude extracts and HSCCC separation were of

---

* Corresponding author. Tel.: +86 21 64252967; fax: +86 21 64252967.
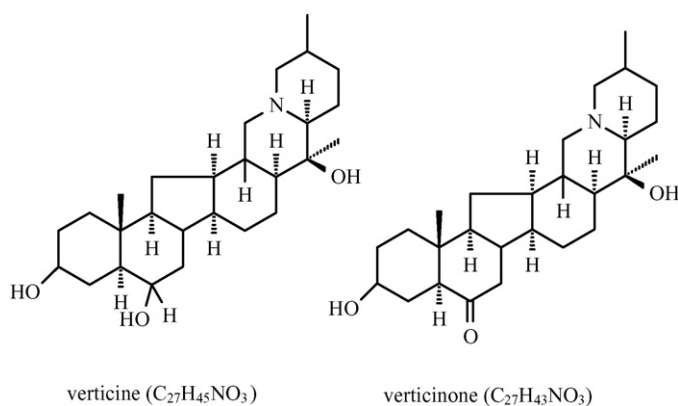 *E-mail address:* yjshen@ecust.edu.cn (Y. Shen).

Fig. 1. Chemical structures of verticine and verticinone.

analytical grade (Chinese Medication Group Shanghai Chemical Reagent Company, Shanghai, China). Methanol (Merck), acetonitrile (Merck) and pure water used for HPLC was treated with SAGA-30D Super Pure Water System (Saga Electronic Technology, Co., Ltd., Shanghai, China). Verticine and verticinone standard samples were purchased from National Institute for the Control of Pharamaceutical and Biological Products, Ministry of Health, Beijing, China.

2.2. Preparation of crude samples

The 100 g dried *Bulbus Fritillariae Thunbergii* was ground to powder (60 mesh) by a disintegrator (Shanghai Experimental Instrument Company, Shanghai, China) and loaded into microwave extractor (Model VIP 272, National Engineering Research Center for Chinese Traditional Medicine, Shanghai, China) and extracted at 680 W of microwave power in 90% ethanol (with a ratio of the powder to solvent 1:10) for 20 min. The extraction solution was filtered and concentrated to dryness by rotatory evaporator under reduced pressure and dried under vacuum (ZK 82J electrothermal vacuum desiccator, Shanghai Experimental Instrument Company). The residue was stored in a desiccator.

2.3. Selection of two-phase solvent system

The selection of the two-phase solvent system for the target compounds is the most important step in HSCCC, which may account for 90% of the entire work in HSCCC [14]. Two principles are generally followed. First, a suitable partition coefficient (K), which is the ratio of solute distributed between the mutually equilibrated two solvent phases. The suitable K-value for HSCCC are in the range of 0.5–1.0; second, higher retention of the stationary phase normally results in better peak resolution. If the setting time of the two-phase solvent system is less than 20 s, the solvent system would provide satisfactory retention of the stationary phase. A two-phase solvent system composed of chloroform–ethanol–0.2 mol L^{-1} hydrochloric acid (3:2:2, v/v/v) was chosen for the separation and purification of the crude extracts.

2.4. High-speed counter-current chromatography (HSCCC)

2.4.1. Instrumentation

The preparative HSCCC instrument (Model TBE-300A, Shanghai Tauto Biological Company, China) was equipped with three preparative coils connected in series (diameter of polytetrafluoroethylene (PTFE) tube, 2.6 mm; total volume, 119 mL) and a 10 mL sample loop. The revolution speed of the instrument is regulated with a speed controller in the range between 0 and 999 rpm. Constant temperature circulator (HX-1050, Beijing Boyikang Experimental Apparatus Company, China) was used to control the temperature. The solvent was pumped into the column with the AKTA purifier pump P-900 (Amersham, USA) at a flow rate of up to 10 mL/min and pressure up to 25 MPa. An optimum speed of 1.2 mL/min was used in the experiment. The continuous monitoring of the effluent was achieved with evaporative light scattering detection (Alltech ELSD 2000ES, Alltech, USA).

2.4.2. HSCCC separation procedure

The multiplayer coiled column was first fully filled with the upper phase (stationary phase) and lower phase (mobile phase) simultaneously at a flow rate of 10 mL/min. Then the lower phase alone was pumped at a flow rate of 1.2 mL/min. In the meantime, the HSCCC apparatus was rotated at 800 rpm, constant temperature was 25 °C. After 30 min, the lower phase emerged in the effluent and hydrodynamic equilibrium was established in the column. A sample solution containing 200 mg *Bulbus Fritillariae Thunbergii* extracts in 10 mL of the lower phase of the two-phase solvent system was injected through the injection valve. The effluent was continuously monitored by ELSD and each peak fraction was manually collected according to the chromatogram. After using thin layer chromatography (TLC) as a primary comparison with the standard sample of verticine and verticinone, HPLC analysis was carried out.

2.5. HPLC analysis, mass spectrometry and ^{1}H NMR identification of the fractions

HPLC analysis was performed with an Agilent/HP 1100 series (Agilent, USA) equipped with an Alltech ELSD 2000ES detector (Alltech USA). The Agilent/HP 1100 series HPLC was consisted of a vacuum degasser, quandary pump, thermostated column compartment, diode array detection and injection valve with a 20 μL loop. The crude extracts of *Bulbus Fritillariae Thunbergii* and each purified peak fraction from the preparative HSCCC separation were analyzed by HPLC (Agilent Exlipse XBD C$_{18}$ column, 5 μm, 4.6 mm × 150 mm), eluted with acetonitrile–water–diethylamine (70:30:0.3, v/v/v) at a flow rate of 1.0 mL/min, and column temperature was 30 °C. ELSD parameters were as follows: drift tube temperature, 90 °C; gas flow, 2.4 L min^{-1}; impactor, off. The purified fractions of verticine and verticinone obtained from the preparative HSCCC separation were analyzed by electron impact mass spectroscopy (EI–MS) (GC-TOFMS, Micromass, UK) and ^{1}H NMR (Bruker Advance 500 MHz spectrometer referenced to tetramethylsilane), respectively.

Table 1
The *K*-values of verticine and verticinone in different two-phase solvent systems

Solvent system	K-value	
	Verticinone	Verticine
n-Butanol–ethyl acetate–water (2:3:5, v/v/v)	18	15
n-Butanol–ethyl acetate–water (1:2:3, v/v/v)	16	14
n-Butanol–ethyl acetate–water (2:1:3, v/v/v)	16	15
n-Hexane–diethyl ether–ethanol–water (1:5:2:5, v/v/v/v)	1.68	3
Chloroform–ethanol–water (4:2:2, v/v/v)	1.67	2.06
Chloroform–ethanol–0.2 mol L^{-1} hydrochloric acid (2:3:2, v/v/v)	0.98	1.02
Chloroform–ethanol–0.2 mol L^{-1} hydrochloric acid (3:2:2, v/v/v)	0.87	1.16

Experimental procedure: 5 mL of each phase of the pre-equilibrated two-phase solvent system was poured in a 20 mL test tube and 10 mg of the sample was added. The tube was ultrasonic for 2 min and waited the solvent to separate completely. A 100 μL of each layer was taken out and evaporated. The residue was dissolved in 1 mL methanol and analyzed by HPLC for the *K*-value. The *K*-value was expressed as the peak area of target compound in the upper phase vs. in the lower phase.

3. Results and discussion

3.1. HSCCC separation of verticine and verticinone from the crude extract

In the HSCCC experiment, a good solvent system can provide an ideal partition coefficient (*K*) for the target compounds. The most suitable *K*-value of the target compounds is close to 1. In our experiment, two compounds want to be separated by one solvent system, so they must have different *K*-values. According to solubility of verticine and verticinone, preliminary HSCCC studies were carried out with seven different two-phase solvent systems, such as *n*-butanol–ethyl acetate–water (2:3:5, 1:2:3, 2:1:3, v/v/v), *n*-hexane–diethyl ether–ethanol–water (1:5:2:5, v/v/v/v), chloroform–ethanol–water (4:2:2, v/v/v) and chloroform–ethanol–0.2 mol L^{-1} hydrochloric acid (2:3:2, 3:2:2, v/v/v). The measured *K*-values are shown in Table 1. The two-phase solvent systems of *n*-butanol–ethyl acetate–water
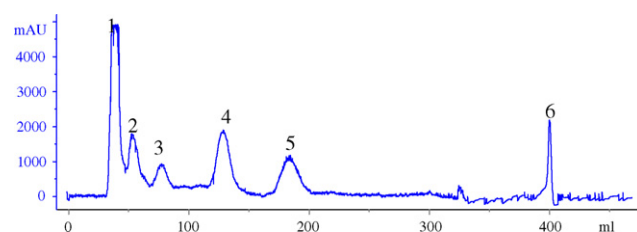
Fig. 2. Chromatogram of crude extracts of *Bulbus Fritillariae Thunbergii* by HSCCC. Peak 3, verticinone; peak 5, verticine. Experimental condition: two-phase solvent system; chloroform–ethanol–0.2 mol L^{-1} hydrochloric acid (3:2:2, v/v/v); stationary phase, upper phase; mobile phase, lower phase; flow-rate, 1.2 mL/min; rotary speed, 800 rpm; ELSD condition: drift tube temperature, 64.8 °C; gas flow, 2.1 L min^{-1}; impactor: off, sample size, 200 mg of crude extracts dissolved in 10 mL of the lower phase; retention of the stationary phase, 0.58; separation temperature, 25 °C.

and *n*-hexane–diethyl ether–ethanol–water did not give effective separation. The chloroform–ethanol–water system gave good result, however, it also led to emulsification. In the subsequent studies, this system was replaced with chloroform–ethanol–0.2 mol L^{-1} hydrochloric acid. After comparison of different ratios, chloroform–ethanol–0.2 mol L^{-1} hydrochloric acid (3:2:2, v/v/v) gave the best separation.

Other factors such as the revolution speed of the separation column, the flow rate of the mobile phase and the separation temperature, were also investigated. Emulsification seemed to occur when the revolution speed is higher than 800 rpm. Ultimately, a flow rate of 1.2 mL/min, a revolution speed of 800 rpm and separation temperature of 25 °C gave the best separation. Fig. 2 showed the preparative HSCCC separation chromatogram. A 25.6 mg of verticine and 10.3 mg of verticinone were obtained from the 200 mg crude extracts.

3.2. HPLC analysis

The method of HPLC analysis was referenced in Chinese Pharmacopoeia (2005). The crude samples and peak fractions separated by HSCCC were analyzed by HPLC under the analytical conditions described in Section 2.5. The chromatograms
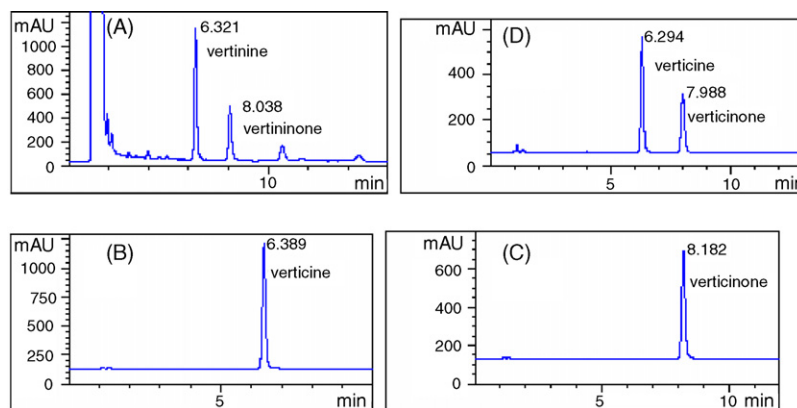
Fig. 3. HPLC chromatogram of crude extracts of *Bulbus Fritillariae Thunbergi* (A), peak 5 from preparative HSCCC (B), peak 3 from preparative HSCCC (C) and the standard sample of verticine and verticinone (D). Experimental condition: Aglient Exlipse XBD C$_{18}$ column (5 μm, 4.6 mm × 150 mm); mobile phase, acetonitrile–water–diethylamine (70:30:0.3); flow rate, 1.0 mL/min; temperature, 30 °C; ELSD condition: drift tube temperature, 90 °C; gas flow, 2.4 L min^{-1}; impactor, off.

were shown in Fig. 3. The purified samples of verticine and verticinone calculations were made by comparison of the peak area with the standard. The results showed that peak 3 corresponded to verticinone and peak 5 corresponded to verticine, and their purity were 95.4 and 96.8%, respectively.

3.3. Structural identification

The identities of peaks 3 and 5 in HSCCC were determined by electron impact mass spectroscopy (EI–MS) and ^{1}H NMR. Peak 3 ^{1}H NMR (CDCl$_3$) δ (ppm): 0.78 (s, 3H, 19-CH$_3$), 1.02 (s, 3H, 21-CH$_3$), 1.08 (d, $J = 7.0$ Hz, 3H, 27-CH$_3$), 3.58 (m, 1H, 3-CH); EI–MS: m/z, 429 (M$^+$), 414, 384, 372, 154, 124, 112 (100%). Peak 5 ^{1}H NMR (CDCl$_3$) δ (ppm): 0.82 (s, 3H, 19-CH$_3$), 1.05 (s, 3H, 21-CH$_3$), 1.10 (d, $J = 7.1$ Hz, 3H, 27-CH$_3$), 1.25 (m, 1H, 5-CH), 3.60 (m, 1H, 3-CH); EI–MS: m/z, 431 (M$^+$), 412, 386, 154, 112 (100%). Compared with the data given in reference [15], the compounds in peaks 3 and 5 were verticinone and verticine, respectively.

4. Conclusion

The overall results of our studies indicated that HSCCC coupled with evaporative light scattering detection was successfully used for separation and purification of verticine and verticinone from *Bulbus Fritillariae Thunbergii*. The present study also demonstrated that HSCCC coupled with ELSD is a powerful tool to monitor separation and purification of non-chromophoric active substances from natural medicines.

References

[1] Pharmacopoeia of the People's Republic of China, the first division of 2005 edition, China Chemical Industry Press, Beijing, 2005, p. 205.
[2] Z.J. Shang, X.L. Liu, Chin. J. Med. Hist. 25 (1995) 38.
[3] D.M. Xu, Y.J. Xu, Chin. Trad. Herbal Drugs 22 (1991) 132.
[4] G. Lin, Y.P. Ho, P. Li, X.G. Li, J. Nat. Prod. 58 (1995) 1662.
[5] P. Li, G.J. Xu, L.S. Xu, Y.X. Wang, Phytother. Res. 9 (1995) 460.
[6] P. Li, X.G. Li, G.J. Xu, J. Chin. Pharm. Univ. 21 (1990) 198.
[7] P. Li, H. Ji, S. Zhou, Chin. Trad. Herbal Drugs 24 (1993) 475.
[8] J.X. Zhang, G.E. Ma, A.N. Lao, R.S. Xu, Acta Pharm. Sin. 26 (1991) 231.
[9] F.Q. Yang, T.Y. Zhang, R. Zhang, Y. Ito, J. Chromatogr. A 829 (1998) 137.
[10] X.L. Cao, Y. Tian, T.Y. Zhang, X. Li, Y. Ito, J. Chromatogr. A 855 (1999) 709.
[11] T.H. Huang, P.N. Shen, Y.G. Shen, J. Chromatogr. A 1066 (2005) 239.
[12] J.H. Chen, F.G. Wang, F.S.C. Lee, X.R. Wang, M.Y. Xie, Talanta 69 (2006) 172.
[13] X. Cao, Y. Ito, J. Chromatogr. A 1021 (2003) 117.
[14] Y. Ito, J. Chromatogr. A 1065 (2005) 145.
[15] K. Kanwho, M. Tanaka, K. Haruki, Chem. Pharm. Bull. 28 (1980) 1345.

Voltammetric determination of glucose based on reduction of copper(II)–glucose complex at lanthanum hydroxide nanowire modified carbon paste electrodes

Li Liu[a], Jun-feng Song[a,*], Peng-fei Yu[b], Bin Cui[b]

[a] *Institute of Analytical Science, Northwest University, Xi'an 710069, China*
[b] *Department of Chemistry, Northwest University, Xi'an 710069, China*

Abstract

A novel voltammetric method for the determination of β-D-glucose (GO) is proposed based on the reduction of Cu(II) ion in $Cu(II)(NH_3)_4{}^{2+}$–GO complex at lanthanum(III) hydroxide nanowires (LNWs) modified carbon paste electrode (LNWs/CPE). In $0.1\ mol\,L^{-1}$ $NH_3 \cdot H_2O$–NH_4Cl (pH 9.8) buffer containing $5.0 \times 10^{-5}\ mol\,L^{-1}$ Cu(II) ion, the sensitive reduction peak of $Cu(II)(NH_3)_4{}^{2+}$–GO complex was observed at -0.17 V (versus, SCE), which was mainly ascribed to both the increase of efficient electrode surface and the selective coordination of La(III) in LNW to GO. The increment of peak current obtained by deducting the reduction peak current of the Cu(II) ion from that of the $Cu(II)(NH_3)_4{}^{2+}$–GO complex was rectilinear with GO concentration in the range of 8.0×10^{-7} to $2.0 \times 10^{-5}\ mol\,L^{-1}$, with a detection limit of $3.5 \times 10^{-7}\ mol\,L^{-1}$. A 500-fold of sucrose and amylam, 100-fold of ascorbic acid, 120-fold of uric acid as well as gluconic acid did not interfere with $1.0 \times 10^{-5}\ mol\,L^{-1}$ GO determination.
© 2006 Elsevier B.V. All rights reserved.

Keywords: Glucose; Lanthanum hydroxide nanowires; Carbon paste electrode; Glucose–copper(II) complex

1. Introduction

Quantitative determination of β-D-glucose (GO) is of great importance in clinical, biological and pharmacy samples as well as food processing and fermentation. The electrochemical technique for GO detection was introduced to achieve a low detection limit and low-cost equipment. Various electrochemical detection strategies have been designed, which continue to use essentially two ways. One way is based on the enzymatic reaction generally using glucose oxidase (GOD). Recently, metal and metal oxide [1,2], metal hexacyanoferrates [3–5], methyl viologen [6], metal–organic complexes [7–12], ferrocene derivatives [13–17], nanoparticles [18–23] and others are co-immobilized with GOD on electrode surface. These substances were used either as the catalyst to reduce the operation potential for monitoring the product of the enzymatic reaction, as the redox mediators to accelerate the enzymatic reaction or as electron transfer mediators to realize the direct electron transfer of GOD. But it still suffers from the problem of stability and biocompatibility due to the intrinsic nature of enzyme. The other way is based on the direct electro-oxidation of GO on different substrates such as metal [24–26], various alloys electrodes [27–31], metal–complex modified electrodes [32,33] and others [34] in strongly alkaline media. However, the practical application of these methods based on the direct electro-oxidation of GO is confined by low sensitivity and poor selectivity.

It has been proved that nanomaterials with many attractive properties such as carbon nanotubes have brought a series of advantages in developing sensing systems for biomolecule. Up to now, more attention has been paid to the functionalization of nanomaterials for further improving the function of nanomaterials. Prospectively, when nanomaterials with some additional properties were used as electrode materials, these properties would endow electrochemical methods with novel character.

Lanthanum(III) hydroxide nanowires (LNWs) as new rare earth nanaomaterial have some unique properties such as

---

optical, catalytic and magnetic properties [35,36]. In addition, it is known that La(III) and Cu(II) ions can coordinate with GO through deprotonated and free hydroxyl groups in alkaline media, respectively, and the coordination sites in GO are different, for La(III) ion the hydroxyl group at C-2 and C-3 or C-3 and C-4 [37,38], for Cu(II) ion most probably the hydroxyl group at C-1 and oxygen atom at C-5 [39–41]. By considering these, in this work, LNWs were immobilized in carbon paste electrode (CPE) to prepare LNWs modified carbon paste electrode (LNWs/CPE), Cu(II) ion in ammonium medium was used to transfer electroinactive GO into electroactive $Cu(II)(NH_3)_4^{2+}$–GO complex and the voltammetric behavior of the $Cu(II)(NH_3)_4^{2+}$–GO complex at LNWs/CPE has been investigated. The reduction peak current of the $Cu(II)(NH_3)_4^{2+}$–GO complex was greatly enhanced, and the related mechanism was discussed. Based on this, a sensitive and selective method for GO determination was proposed.

2. Experimental

2.1. Apparatus

A JP-303 polarographic analyzer (Chendu Instrument Factory, Chendu, China) is used for single sweep voltammetry and a CHI 660 electrochemical workstation (CH Instrument Inc., USA) is used for cyclic voltammetry. A three-electrode configuration includes a homemade LNWs/CPE working electrode, a platinum wire counter electrode and a saturated calomel reference electrode (SCE). All the potentials quoted in this work are referred to the SCE. All the measurements are carried out at room temperature.

2.2. Materials

GO was of analytical reagent grade (purity > 99%, Yixing Chemical Reagent Factory No. 3, Yixing, China). A 1.0×10^{-2} mol L^{-1} GO stock standard solution was prepared in aqueous solution. Working standard solutions were prepared by appropriate dilution of the stock standard solution with water. A 1.0×10^{-2} mol L^{-1} Cu(II) solution and 1.0 mol L^{-1} $NH_3 \cdot H_2O$–NH_4Cl buffer (pH 9.8) were prepared. All chemicals were of analytical reagent grade. Twice distilled water was used throughout. LNWs were prepared by hydro-thermal method [35,36], and were directly used without any further treatment. The transmission electron microscopy (TEM) micrograph of LNWs is showed in Fig. 1. As can be seen, that any impurities were hardly found, the LNWs had an average diameter of 15–20 nm.

2.3. Electrode preparations

Unmodified carbon paste electrode was prepared by mixing 1.0 g graphite powers and 0.2 mL paraffin oil adequately in agate mortar. A portion of the resulting paste was then packed firmly into the electrode cavity (2.6 mm diameter) of a PTFE sleeve. Electrical contact was established via a copper wire. Other modified CPEs were prepared in the similar manner. The LNWs/CPE
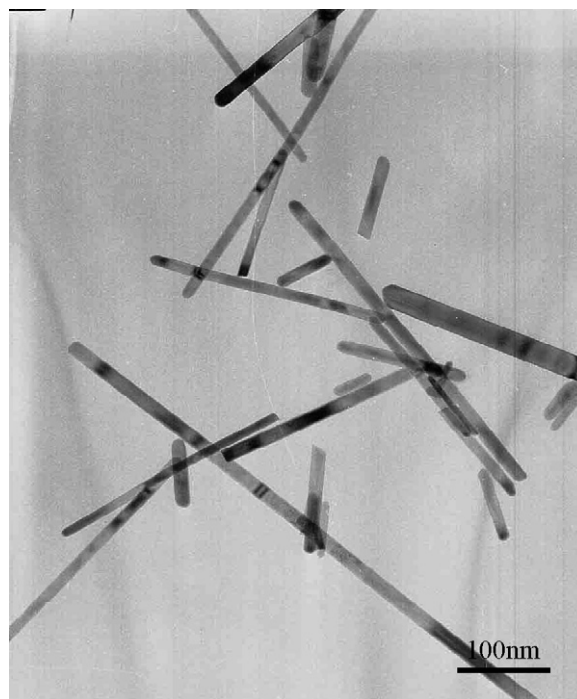
Fig. 1. TEM image of La(OH)$_3$ nanowires.

was prepared by mixing 0.98 g graphite powders, 0.02 g LNWs and 0.2 mL paraffin oil. The carbon nanotubes (CNT) modified CPE (CNT/CPE) was prepared by mixing 0.98 g graphite powders, 0.02 g CNT and 0.2 mL paraffin oil. And the La(NO$_3$)$_3$ modified CPE (La(NO$_3$)$_3$/CPE) was prepared as following: 0.02 g La(NO$_3$)$_3$ was dissolved in 2 mL water. Then the solution was mixed with 0.98 g graphite powders. After evaporating the solvent water at room temperature, La(NO$_3$)$_3$/CPE was prepared by mixing the obtained dry powers with 0.2 mL paraffin oil. The surface of all the modified and unmodified CPEs were carefully smoothed on weighing paper and rinsed with water prior to each measurement.

2.4. General procedure

After mixing appropriate GO and 5.0×10^{-5} mol L^{-1} Cu(II) ion in 0.1 mol L^{-1} $NH_3 \cdot H_2O$–NH_4Cl buffer (pH 9.8) for 35 min, the obtained solution was transferred into a voltammetric cell. The second-order derivative single sweep voltammogram was recorded by applying a cathode-going potential scan from 0.5 to −0.5 V at 100 mV s^{-1}. The second-order derivative reduction peak current i_p'' of the $Cu(II)(NH_3)_4^{2+}$–GO complex at −0.17 V was measured. The increment $\Delta i_p''$ of peak current was obtained by deducting the reduction peak current of the $Cu(II)(NH_3)_4^{2+}$ ion from that of the $Cu(II)(NH_3)_4^{2+}$–GO complex, the calibration curve was obtained by plotting the increment $\Delta i_p''$ of the reduction peak current versus GO concentration. Cyclic voltammetry was conducted under the same experimental condition.

After each measurement, the LNWs/CPE was regenerated by successive potential cycling in the range of 0.5 to −0.5 V in the $NH_3 \cdot H_2O$–NH_4Cl buffer (pH 9.8) several times until the stable background current was obtained. If necessary, the electrode

surface was renewed by pushing a folium (2–3 mm in thickness) of the carbon paste of the tube out, then polishing and washing with water.

2.5. Samples analysis

A 1.00 mL of GO injection (Xi'an Lijun Pharmaceutical Co. Ltd., China) was diluted in 250 mL volumetric flask with water. The determination of GO in the obtained sample solution was performed according to the general procedure mentioned above. The content of GO in the sample was calculated according to the calibration curve.

3. Results and discussion

3.1. Voltammetric behavior of GO at LNWs/CPE

Typical cyclic voltammetric curves at LNWs/CPE in $0.1 \, mol \, L^{-1}$ $NH_3 \cdot H_2O–NH_4Cl$ buffers (pH 9.8) are shown in

Fig. 2A, when GO was present alone, no voltammetric response was observed (Fig. 2A, curve a). When Cu(II) ion was present only, a pair of the well-defined redox peaks were observed (Fig. 2A, curve b). A reduction peak at −0.12 V was the reduction of $Cu(II)(NH_3)_4^{2+}$ ion, and an oxidation peak at −0.02 V was the oxidation of Cu(0). However, up adding GO, the reduction peak current of $Cu(II)(NH_3)_4^{2+}$ ion was greatly enhanced by about 620% accompanying with a potential shift of 50 mV in negative direction, whilst the oxidation peaks current of Cu(0) was also increased by about 180% accompanying with a potential shift of 30 mV in positive direction (Fig. 2A, curve c). The little shift of peak potential was attributed to the re-formation of the $Cu(II)(NH_3)_4^{2+}$–GO complex in ammonium buffer [32].

In order to check the reasons on great increase of the voltammetric responses, the voltammetric responses of $K_3Fe(CN)_6$ and $Cu(II)(NH_3)_4^{2+}$–GO complex at bare CPE, LNWs/CPE and CNT/CPE with the same geometrical surface were examined, respectively. As shown in Fig. 3, $K_3Fe(CN)_6$ exhibited a pair of redox peaks at bare CPE in pH 6.7 phosphate
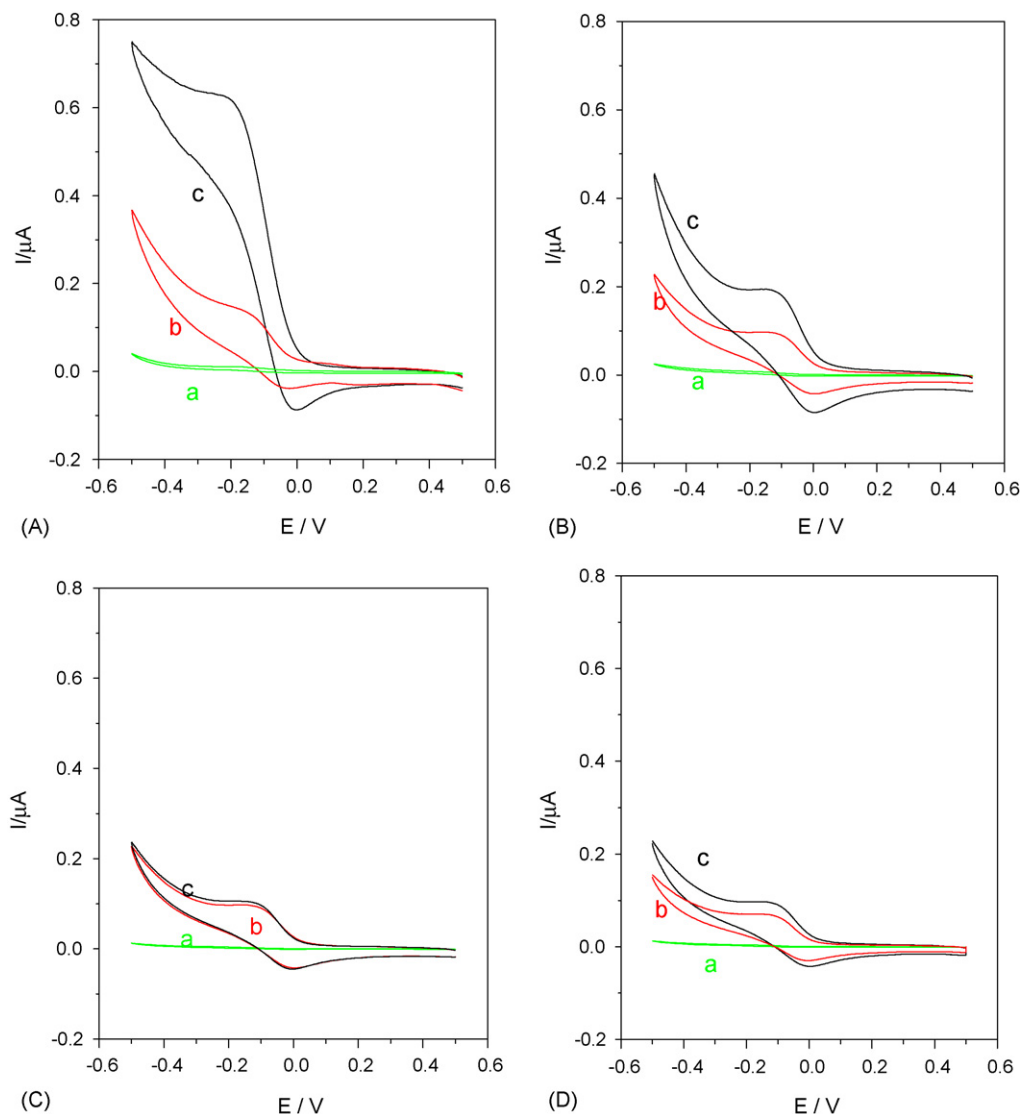

Fig. 2. Cyclic voltammograms at the LNWs/CPE (A), CNT/CPE (B), bare CPE (C) and La(NO_3)/CPE (D) in 0.1 mol L⁻¹ NH_3·H_2O–NH_4Cl buffer (pH 9.8) containing (a) 1.0 × 10⁻⁴ mol L⁻¹ GO, (b) 5.0 × 10⁻⁴ mol L⁻¹ Cu (II) and (c) 5.0 × 10⁻⁴ mol L⁻¹ Cu (II) and 1.0 × 10⁻⁴ mol L⁻¹ GO. Scan rate 0.1 V s⁻¹.
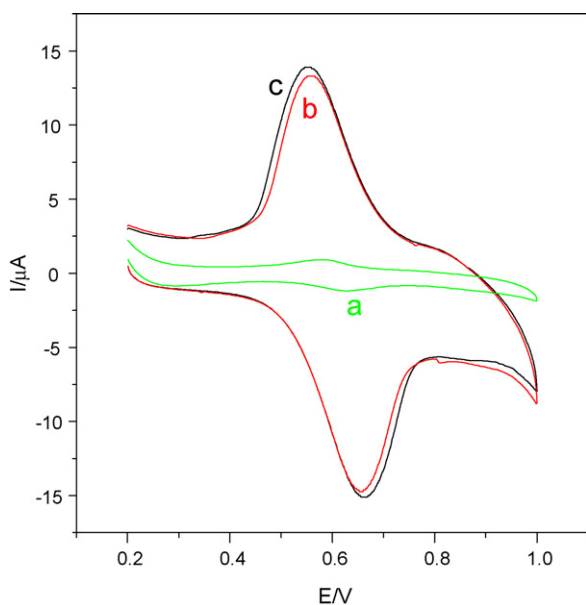
Fig. 3. Cyclic voltammograms (CV) of 1.0×10^{-3} mol L^{-1} K$_3$Fe(CN)$_6$ at bare CPE (a), CNT/CPE (b) and LNWs/CPE (c). Supporting electrolyte: phosphate buffer (pH 6.7), scan rate 0.1 V s^{-1}.

Fig. 4. Effect of pH value on reduction peak current of Cu(II)(NH$_3$)$_4{}^{2+}$–GO complex in NH$_3$·H$_2$O–NH$_4$Cl buffer containing 5.0×10^{-5} mol L^{-1} Cu(II) and 1.0×10^{-5} mol L^{-1} GO. Scan rate: 0.1 V s^{-1}.

buffer. The difference ΔE_p of peak potentials was about 90 mV and the ratio i_{Pa}/i_{Pc} of peak current was about 1 (Fig. 3, curve a). When LNWs/CPE was instead, the ΔE_p reduced to about 80 mV and the i_{Pa}/i_{Pc} still was about 1 (Fig. 3, curve c). Moreover, the voltammetric behavior of K$_3$Fe(CN)$_6$ at CNT/CPE was almost the same as that at LNWs/CPE (Fig. 3, curve b). The results demonstrated that the electrode process of K$_3$Fe(CN)$_6$ was reversible at bare CPE, CNT/CPE and LNWs/CPE. However, the peak currents at both CNT/CPE and LNWs/CPE were much higher than that at bare CPE. When scan rate ν increased from 50 to 500 m V s^{-1}, the peak current of the oxidation peak of K$_3$Fe(CN)$_6$ grown gradually, according to the Randles–Sevcik equation: $i_{pa} = 2.69 \times 10^5 n^{3/2} A C_0 D_R{}^{1/2} \nu^{1/2}$ and presuming the parameters such as n, C_0, D_R were constant, the linear regression equations were i_{pa} (μA) $= 0.0298 + 0.1188 \nu^{1/2}$ (mV s^{-1})$^{1/2}$, $r = 0.999$ for the bare CPE, i_{pa} (μA) $= 0.3082 + 1.010 \nu^{1/2}$ (mV s^{-1})$^{1/2}$, $r = 0.999$ for the LNWs/CPE, and i_{pa} (μA) $= 0.306 + 1.012 \nu^{1/2}$ (mV s^{-1})$^{1/2}$, $r = 0.998$ for the CNT/CPE, respectively. From the ratio of slopes of the three equations, the efficient electrode surfaces of the LNWs/CPE and CNT/CPE were about 10 times as large as that of bare CPE, and the efficient electrode surface of the LNWs/CPE was almost the same as that of CNT/CPE.

In 0.1 mol L^{-1} NH$_3$·H$_2$O–NH$_4$Cl buffers (pH 9.8) containing Cu(II) ion and GO, the reduction peak currents of the Cu(II)(NH$_3$)$_4{}^{2+}$–GO complex at LNWs/CPE (Fig. 2A, curve c) was higher about six times than that at CPE (Fig. 2C, curve c). The increase of the peak current was just related with the increase of the efficient electrode surface of LNWs/CPE in quatity, which was owing to the introduction and surface effect of LNW.

Additionally, the voltammetric responses in 0.1 mol L^{-1} NH$_3$·H$_2$O–NH$_4$Cl buffers (pH 9.8) containing Cu(II) ion with and without GO at CNT/CPE and LNWs/CPE with the same efficient electrode surface were compared. Without GO, the redox
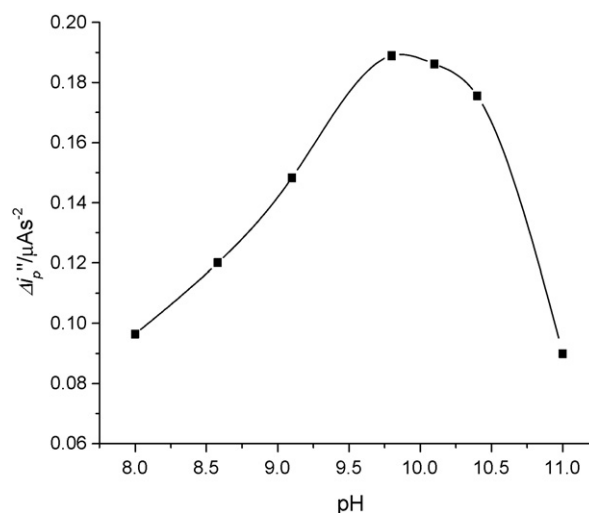
peak currents of Cu(II)(NH$_3$)$_4{}^{2+}$/Cu(0) couple at CNT/CPE were almost the same as that at LNWs/CPE (Fig. 2B, curve b). On adding the GO, the redox peak currents of Cu(II) ions increased (Fig. 2B, curve c). However, the peak currents of the Cu(II)(NH$_3$)$_4{}^{2+}$–GO complex at LNWs/CPE were higher about two times than that at CNT/CPE. Additionally, the voltammetric responses at La(NO$_3$)/CPE and CPE were also compared under the same condition. Up adding GO, the redox peak currents of the Cu(II)(NH$_3$)$_4{}^{2+}$–GO complex increased at both CPE (Fig. 2C, curve c) and La(NO$_3$)$_3$/CPE (Fig. 2D, curve c) to different extent. However, the increment of the peak current at La(NO$_3$)$_3$/CPE was higher than that at CPE. The increase resulted from the chemical coordination reaction of La(III) in LNWs with GO [30,31] because different coordination sites of La(III) and Cu(II) ions in GO made it possible for the Cu(II)(NH$_3$)$_4{}^{2+}$–GO complex to re-coordinate with La(III) and to be accumulated on the LNWs/CPE surface.

In summary, from these results mentioned above, it can be concluded that the great increase of the voltammetric responses of Cu(II)(NH$_3$)$_4{}^{2+}$–GO complex at LNWs/CPE resulted from both the surface and the chemical coordination function of LNWs.

With the reduction peak current of the Cu(II)(NH$_3$)$_4{}^{2+}$–GO complex at LNWs/CPE, a highly sensitive and selective method for GO determination was proposed. Single sweep second-order derivative voltammetry was employed used to record voltammogram as it can fast run and had good resolving power. The conditions were optimized.

3.2. Effect of pH values

Several alkaline supporting electrolytes such as Britton–Robinson, NH$_3$·H$_2$O–NH$_4$Cl buffers and NaOH solution were tested. The results showed that the second-order derivative reduction peaks of the Cu(II)(NH$_3$)$_4{}^{2+}$–GO complex were more stable and sensitive in NH$_3$·H$_2$O–NH$_4$Cl buffer than that in

other media. The effect of pH values on the second-order derivative reduction peak currents of the Cu(II)(NH$_3$)$_4^{2+}$–GO mixed complex was examined in the pH range of 8.0–11.0 (Fig. 4). The peak currents increased with the increase of pH values when pH value was less than 9.7, and kept almost unchanged between pH 9.7 and 9.8. When pH value was above 8.3, the reduction peak of the Cu(II)(NH$_3$)$_4^{2+}$–GO complex broadened and the peak current reduced, which might resulted from the change of the composition of the Cu(II)(NH$_3$)$_4^{2+}$–GO complex. Thus, 0.1 mol L^{-1} NH$_3$·H$_2$O–NH$_4$Cl buffer (pH 9.8) was chosen as supporting electrolyte. Meanwhile, with the increase of pH values, the peak potentials of reduction peak of the Cu(II)(NH$_3$)$_4^{2+}$–GO complex shifted positively, and obeyed the following equations: E_{pc} (V) = $-0.545 + 0.051$pH ($r = 0.997$). The shift of peak potential might depend on the different coordination states of the Cu(II)(NH$_3$)$_4^{2+}$–GO complex under different pH conditions.

3.3. Effect of Cu(II) ion concentration

As the measurement depended on the formation of the Cu(II)(NH$_3$)$_4^{2+}$–GO complex and the reduction of Cu(II) ion in the Cu(II)(NH$_3$)$_4^{2+}$–GO complex at LNWs/CPE, the effect of Cu(II) ion concentration was examined. The results showed that Cu(II) ion concentration was closely related to the peak current but hardly to the peak potential. As shown in Fig. 5, the peak current increased with Cu(II) ion concentration increasing in the range of $(0–4.0) \times 10^{-5}$ mol L^{-1}. When Cu(II) ion concentration was in the range of 4.0×10^{-5} to 5.0×10^{-5} mol L^{-1}, the peak current achieved a maximum value and was nearly unchanged. Accordingly, the final concentration of Cu(II) ion was 5.0×10^{-5} mol L^{-1}.

3.4. Effect of the mass radio of LNW in LNWs/CPE

Experimental results showed that the mass radio of LNW in LNWs/CPE had a significant influence on peak current but not on
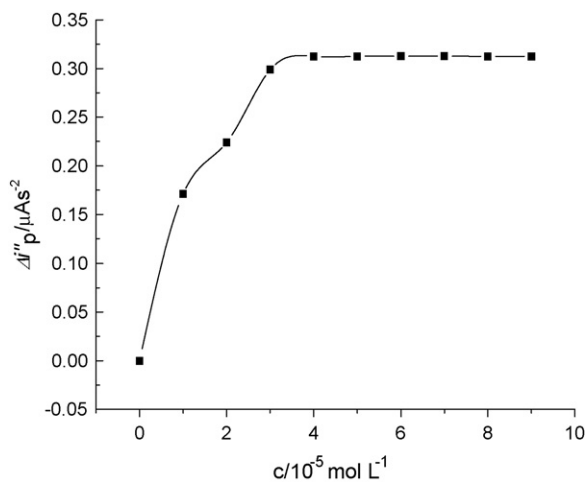
Fig. 5. Effect of Cu (II) concentration on reduction peak current of Cu(II)(NH$_3$)$_4^{2+}$–GO complex in NH$_3$·H$_2$O–NH$_4$Cl buffer (pH 9.8) containing 5.0×10^{-5} mol L^{-1} Cu (II) and 1.0×10^{-5} mol L^{-1} GO. Scan rate: 0.1 V s^{-1}.
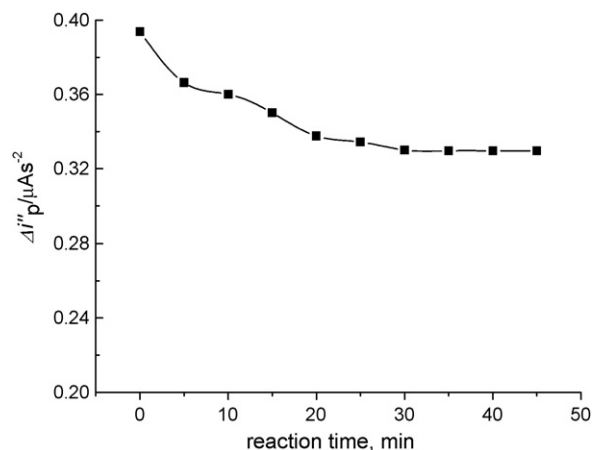
Fig. 6. Effect of reaction time on reduction peak current of Cu(II)(NH$_3$)$_4^{2+}$–GO complex in NH$_3$·H$_2$O–NH$_4$Cl buffer (pH 9.8) containing 5.0×10^{-5} mol L^{-1} Cu (II) and 1.0×10^{-5} mol L^{-1} GO. Scan rate: 0.1 V s^{-1}.

peak potential. The maximum peak current was obtained when the mass ratio of LNW and graphite power was 1:49. However, as the mass radio of LNW increased further, the peak current decreased. Presumably, more LNWs reduced the electronic conductance of the electrode.

3.5. Effect of reaction time

When GO was introduced into 0.1 mol L^{-1} NH$_3$·H$_2$O–NH$_4$Cl buffer (pH 9.8) containing Cu(II) ion, the peak current of the reduction peak of the Cu(II)(NH$_3$)$_4^{2+}$–GO complex was greater, and decreased gradually in half an hour and then it was nearly unchanged (Fig. 6). The reason of the decrease might be that GO first combined with more Cu(II)(NH$_3$)$_4^{2+}$ ions to form multinuclear oligomers, and the multinuclear oligomers then gradually transformed to be a more stable Cu(II)(NH$_3$)$_4^{2+}$–GO complex through a homogeneous ligand-exchange reaction between Cu(II)(NH$_3$)$_4^{2+}$ ion and GO.

4. Analytical performance

4.1. Calibration curve for GO

In 0.1 mol L^{-1} NH$_3$·H$_2$O–NH$_4$Cl buffer (pH 9.8) containing 5.0×10^{-5} mol L^{-1} Cu(II) ion, the relationship between the second-order derivative reduction peak current and GO concentration was examined by second-order derivative linear sweep voltammetry at scan rate of 0.1 V s^{-1}. The peak sharp of the second-order derivative reduction peak recorded was acute and easy to be measured (Fig. 7), and the increments $\Delta i_p''$ of the peak current were proportional to GO concentration over the range of 8.0×10^{-7} to 2.0×10^{-5} mol L^{-1}. The linear regression equation was $\Delta i_p''$ (μA s^{-2}) = $0.013 + 0.014 \times 10^6 C$ (mol L^{-1}), $r = 0.9996$. A detection limit of 3.5×10^{-7} mol L^{-1} was obtained (based on $3s_1/m$, where s_1 is the standard deviation of the intercept and m is the slope), which was lower than that of other electrochemical methods reported.

Table 1
Determination and recovery test of GO in GO injections

Samples (injection)	Found (g/250 mL)	R.S.D. (%)	Added (10^{-6} mol L^{-1})	Found (10^{-6} mol L^{-1})	Recovery (%)	R.S.D. (%)
GO	9.97	2.1	1.5	1.47	98.2	2.2
	10.01	1.9	3.0	3.07	100.2	2.9

4.2. Reproducibility

The proposed method showed good reproducibility, the relative standard deviation (R.S.D.) for eight successive determinations of 5.0×10^{-6} mol L^{-1} GO at a LNWs/CPE was 2.1%, and individual determination of 5.0×10^{-6} mol L^{-1} GO using five different LNWs/CPEs with the same surface area gave a R.S.D. of 2.8%.

4.3. Interferences

In order to further investigate the selectivity of LNWs/CPE, several potential interferences were tested. The tolerable limit was defined as the concentrations of foreign substances, which gave an error less than ±5.0% in the determination of 1.0×10^{-5} mol L^{-1} GO. The results showed that 500-fold of sucrose and amylam, 100-fold of ascorbic acid, as well as 120-fold of uric acid did not interfere with the determination. From the results, the selectivity of the method is good.

4.4. Determination of GO in clinic injections

The proposed method was applied to the determination of GO in clinic GO injections (10 g per 250 mL). The results (shown in Table 1) were in good agreement with the content marked in the label. The recovery experiments were carried out by standard addition method and the recovery ranged from 97.6 to 101.2%, which suggested acceptable accurate and precise of the method.
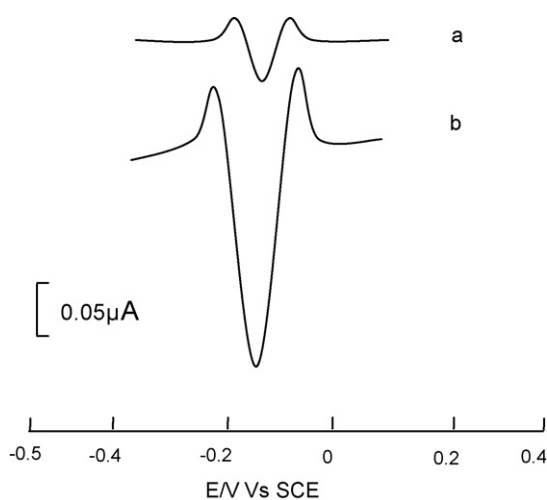
Fig. 7. Second-order derivative voltammetric curves in NH$_3$·H$_2$O–NH$_4$Cl buffer (pH 9.8) containing (a) 5.0×10^{-5} mol L^{-1} Cu (II); (b) a + 1.0×10^{-5} mol L^{-1} GO. Scan rate: 0.1 Vs^{-1}.

5. Conclusion

In this work, a novel strategy for GO determination was proposed without either enzymatic reaction or direct oxidation of GO. The LNWs as electrode material were provided with double function, not only increasing the electrode surface but also chemically coordinating with GO. The sensitive reduction peak of the Cu(II)(NH$_3$)$_4{}^{2+}$–GO complex at LNWs/CPE can be used for GO determination. Additionally, with the cathodic polarized operation, more easily oxidizable compounds were tolerated.

Acknowledgements

References

[1] D.R. Shankaran, N. Uehara, T. Kato, Biosens. Bioelectron. 18 (2003) 721–728.
[2] G.L. Luque, M.C. Rodrıguez, G.A. Rivas, Talanta 66 (2005) 467–471.
[3] F. Ricci, D. Mosconea, C.S. Tuta, G. Palleschi, A. Amine, A. Posciab, F. Valgimiglib, D. Messeri, Biosens. Bioelectron. 20 (2005) 1993–2000.
[4] D.W. Pan, J.H. Chen, L.H. Nie, W.Y. Tao, S.Z. Yao, Anal. Biochem. 324 (2004) 115–122.
[5] P.A. Fiorito, C.M.A. Brett, S.I.C.D. Torresi, Talanta 69 (2006) 403–408.
[6] M.E. Ghica, C.M.A. Brett, Anal. Chim. Acta 532 (2005) 145–151.
[7] S. Reiter, K. Habermuller, W. Schunmann, Sens. Actuators. B 79 (2001) 150–156.
[8] N.J. Forrow, S.J. Walters, Biosens. Bioelectron. 19 (2004) 763–770.
[9] Y. Nakabayashi, A. Omayu, S. Morii, S. Yagi, Sens. Actuators. B 66 (2000) 128–130.
[10] K. Yamamoto, H.S. Zenga, Y. Shen, M.M. Ahmed, T. Kato, Talanta 66 (2005) 1175–1180.
[11] T. Tatsuma, K. Saito, N. Oyama, Anal. Chem. 66 (1994) 1002–1006.
[12] J.J. Fei, K.B. Wu, F. Wang, S.S. Hu, Talanta 65 (2005) 918–924.
[13] H. Patel, X. Li, H.I. Karan, Biosens. Bioelectron. 18 (2003) 1073–1076.
[14] A. Gulce, H. Gulce, J. Biochem. Biophys. Methods 62 (2005) 81–92.
[15] Y.X. Huang, W.J. Zhang, H. Xiao, G.X. Li, Biosens. Bioelectron. 21 (2005) 817–821.
[16] I.L. Mattos, M.C.C. Areias, Talanta 66 (2005) 1281–1286.
[17] J. Wang, J.W. Mo, J. Porter, Anal. Chim. Acta 441 (2001) 183–189.
[18] H. Tang, J.H. Chen, S.Z. Yao, L.H. Nie, G.H. Deng, Y.F. Kuang, Anal. Biochem. 331 (2004) 89–97.
[19] M. Yemini, M. Reches, E. Gazit, J. Rishpon, Anal. Chem. 77 (2005) 5155–5159.
[20] Y. Liu, M.K. Wang, F. Zhao, Z.A. Xu, S.J. Dong, Biosens. Bioelectron. 21 (2005) 984–988.
[21] S.Q. Liu, H.X. Ju, Biosens. Bioelectron. 19 (2003) 177–183.
[22] J. Wang, M. Musameh, Anal. Chim. Acta 539 (2005) 209–213.
[23] J. Wu, Y.H. Zou, N. Gao, J.H. Jiang, G.L. Shen, R.Q. Yu, Talanta 68 (2005) 12–18.
[24] I.G. Casella, M. Gatta, M.R. Guascito, T.R.I. Cataldi, Anal. Chim. Acta 357 (1997) 63–71.
[25] S.B. Aoun, Z. Dursun, T. Koga, G.S. Bang, T. Sotomura, I. Taniguchi, J. Electroanal. Chem. 567 (2004) 175–183.

[26] P.F. Luo, S.V. Prabhu, R.P. Baldwin, Anal. Chem. 62 (1990) 752–755.

[27] S. Mho, D.C. Johnson, J. Electroanal. Chem. 500 (2001) 524–532.

[28] Y. Sun, H. Buck, T.E. Mallouk, Anal. Chem. 73 (2001) 1599–1604.

[29] D.J. Watson, G.A. Attard, Electrochim. Acta 46 (2001) 3157–3161.

[30] I.H. Yeo, D.C. Johnson, J. Electroanal. Chem. 484 (2000) 157–163.

[31] E. Scavetta, M. Berrettoni, R. Seeber, D. Tonelli, Electrochim. Acta 46 (2001) 2681–2692.

[32] M.D. Socorro, M. Quintino, H. Winnischofer, M. Nakamura, K. Araki, H.E. Toma, L. Angnes, Anal. Chim. Acta 539 (2005) 215–222.

[33] E. Garnier, C. Bachmann, K. Servat, K.B. Kokoh, K. Bamba, J.M. Leger, Electrochim. Acta 50 (2005) 3341–3346.

[34] J. Wang, M. Musameh, Anal. Chim. Acta 539 (2005) 209–213.

[35] X. Wang, Y.D. Li, Chem. Eur. J. 9 (2003) 5627–5635.

[36] X. Wang, X.M. Sun, Y.D. Li, Adv. Mater. 15 (2003) 1442–1444; H. Tsukube, S. Shinoda, H. Tamiaki, Coord. Chem. Rev. 226 (2002) 227–234.

[37] Y.M. Yang, S.F. Weng, J.G. Wu, G.X. Wu, Chem. J. Chin. Univ. 15 (1994) 646–650.

[38] J.H. Feng, X.J. Li, F.K. Pei, X. Chen, S. Li, Y.X. Nie, Anal. Biochem. 301 (2002) 1–7.

[39] G. Cerchiaro, A.C.S. Ana, M.L.A. Temperini, A.M.D.C. Ferreira, Carbohydr. Res. 340 (2005) 2352–2359.

[40] A. Diaz, I. Garcia, R. Cao, H. Beraldo, M.M. Salberg, D.X. West, L.G.E. Ochoa, Polyhedron 16 (1997) 3549–3555.

[41] J. Fan, Talanta 42 (1995) 317–321.

Spectral studies on the interaction of Amido black 10B with DNA in the presence of cetyltrimethylammonium bromide

Yun Fei Long [a,b], Cheng Zhi Huang [a,*]

[a] College of Chemistry and Chemical Engineering, Southwest University, Chongqing 400715, China
[b] Institute of Chemistry and Chemical Engineering, Hunan University of Science Technology, Hunan 411201, China

Abstract

The interaction of Amido black 10B (AB) with DNA in basic medium was studied in the presence of cetyltrimethylammonium bromide (CTMAB) based on the measurements of resonance light scattering (RLS), UV–vis, CD spectra, and RLS imaging. The interaction has been proved to give a ternary complex of CTMAB–DNA–AB in Britton–Robinson buffer of pH 11.55, which exhibits strong negative Cotton effect at 233.3 nm and 642.8 nm, and strong RLS signals characterized at 469 nm. Experiments showed that the enhanced RLS intensities (ΔI_{RLS}) against the mixture of AB and CTMAB are proportional to the concentration of fish sperm DNA (fsDNA) and calf thymus DNA (ctDNA), respectively over the range of 0.03–1.0 and 0.05–1.5 μg ml^{-1}, with the limits of determination (3σ) of 7.3 ng ml^{-1} for fsDNA and 7.0 ng ml^{-1} for ctDNA.
© 2006 Elsevier B.V. All rights reserved.

Keywords: Deoxyribonucleic acid (DNA); Amido black 10B (AB); Resonance light scattering (RLS); Cetyltrimethylammonium bromide (CTMAB)

1. Introduction

Investigation of the interaction of organic small molecules (OSMs) with DNA has been focused on the DNA studies since OSMs are generally employed as molecular structural probes of biopolymer, the clinic drug candidates targeted to nosogenetic genes, and the analogues in the study of protein-DNA recognition [1,2]. Thus, these investigations show high promise to find new OSMs as probes in order to therapeutically understand the mechanism of anticancer drug at molecular level, and to design new anticancer drugs for clinical use. In addition, the quantitative determinations of DNA are generally the basis in genetics. However, direct spectrofluorometry and spectrophotometry for DNA detection have been severely limited by poor sensitivity and serious interferences [3] for the low intrinsic absorption. Recently, a resonance light scattering (RLS) technique has attracted the attentions of chemist and biochemist, since it is highly sensitive to the binding properties of OSMs with biomolecules [4–8] and to the quantification of DNA in real and artificial samples using the probes such as cationic porphyrins [9,10], cationic dyes [5,11], metal complexes [12], and metal ion [13]. However, there

have been few investigations, in which anionic dyes are applied as reagents to determine DNA, due to the electrostatic repulsion between DNA and anionic dyes.

We found that a ternary complex could be formed if cationic surfactant such as CTMAB is present acting as a bridge of the interaction of DNA and anionic dye. Using Amido black 10B (AB, Fig. 1 displays the molecular structure), an anionic dye as an example, herein we report the formation and RLS emissions of a ternary complex of DNA, AB, and CTMAB.

2. Experimental

2.1. Apparatus

The RLS spectrum and the intensity were measured with a Hitachi F-4500 spectrofluorometer (Tokyo, Japan) fluorescence spectrometer by using 1.0 cm quartz fluorescence cell. Absorption and CD spectra were measured by a Hitachi U-3010 spectrophotometer (Tokyo, Japan) and a Jasco J-810 spectropholarimeter, respectively. A pHS-3C digital pH meter (Leici, Shanghai) was used to detect the pH values of the aqueous solutions. The RLS image was observed through an Olympus IX 70-141 inverted microscope system (Tokyo, Japan) excited with a 488 nm light beam emitted from an argon ion laser source (Ion Laser Technology, Shanghai, China).

* Corresponding author. Tel.: +86 23 68254659.
  E-mail address: chengzhi@swu.edu.cn (C.Z. Huang).
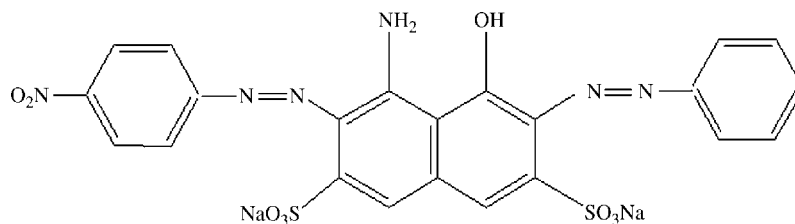
Fig. 1. Molecular structure of Amido black 10B (AB).

2.2. Reagents

Stock solutions of DNAs were prepared by dissolving commercially purchased calf thymus DNA (ctDNA, Shanghai Changyan Pharmaceutical factory, Shanghai, China) and fish sperm DNA (fsDNA, Shanghai Institute of Biochemistry, Chinese Academy of Sciences, Shanghai, China) in doubly distilled water. These stocks should be stored at 0–4 °C with occasional gentle shake. The concentration of DNAs is determined according to the absorbance values at 260.0 nm by using $\varepsilon_{DNA} = 6600\,M^{-1}\,cm^{-1}$ after establishing that the absorbance ratio of A_{260}/A_{280} was in the range 1.80–1.90 for DNA [14]. In this experiment, all working solutions of DNA were 20.0 mg l^{-1}. About 4.0×10^{-4} M stock solution of Amido black 10B (AB, Shanghai Chemical Reagents Co. Shanghai, China) was prepared by dissolving 0.0617 g of the commercial product in water in 250 ml volumetric flask. About 4.0×10^{-4} M stock solution of cationic surfactant cetyltrimethylammonium bromide (CTMAB, Merk, Germany) was prepared by dissolving 0.0364 g of the crystal product in water in 250 ml volumetric flask. Britton–Robinson buffer solution (pH 11.55) was used to control the acidity of the system. All chemicals used were analytical grade and double deionized distilled water was used throughout.

2.3. Procedures

To a 20.0 ml test tube, solutions were added in the sequence of 2.0 ml 4.0×10^{-4} M CTMAB, 2.0 ml Britton–Robinson buffer solution, an appropriate volume of DNA solution according to the concentration needed or sample solution, 0.5 ml 4.0×10^{-4} M AB. The mixture was diluted to 20.0 ml with water and mixed thoroughly, then kept still for 20 min prior to the RLS measurements. All RLS spectra were obtained by scanning simultaneously the excitation and emission monochromators with $\Delta\lambda = 0$ nm from 250.0 to 700.0 nm. The RLS intensity was measured at 469.0 nm in a quartz fluorescence cell with slit width at 5.0 nm for the excitation and emission.

3. Results and discussion

3.1. Feature of the resonance light scattering spectrum

It can be seen from Fig. 2 that AB, DNA, and CTMAB have weak RLS signals. The two binary mixtures, AB–CTMAB and DNA–CTMAB, have comparatively higher RLS signals, indicating that CTMAB could interact with AB or DNA

through electrostatic attraction. However, the ternary mixture of CTMAB–AB–DNA has much stronger RLS signals, indicating that CTMAB, DNA and AB could form ternary complex. The maximum RLS peak exhibit at 469.0 nm, with two shoulder peaks at 469.0 and 603.0 nm. Furthermore, the enhanced RLS intensities of AB–CTMAB–DNA system are in good proportion to the concentration of DNA at 469.0 nm.

3.2. Optimum condition of the interaction

The interaction of DNA, AB, and CTMAB is completed within 20 min, and the enhanced RLS signals (ΔI_{RLS}, the RLS intensity of CTMAB–DNA–AB against CTMAB–AB) remain stable in 2 h. All measurements were made after DNA, AB, and CTMAB were completely mixed for 20 min. In addition, it was found that the best order is to mix CTMAB and DNA first, and then AB.

Fig. 3 exhibits the effects of pH values on the ΔI_{RLS} signals of CTMAB–DNA–AB system. It can be seen that pH obviously affects the formation of CTMAB–DNA–AB ternary complex. ΔI_{RLS} keeps low and stable when pH is less than 11.34, and then increases till 11.45. Over the range of 11.45 to 11.90, ΔI_{RLS} reaches the maximum value and keeps stable again. In this work, the acidity of the aqueous medium was controlled with Britton–Robinson buffer of pH 11.55.

Fig. 4 displays the dependence of ΔI_{RLS} on the concentration of CTMAB. At low CTMAB concentration, ΔI_{RLS} is weak since the interaction only involves in the binding of CTMAB and
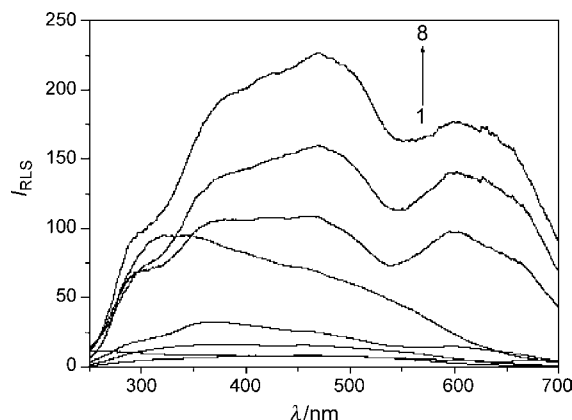
Fig. 2. Resonance light-scattering (RLS) spectra of AB and its interaction with DNA in the presence of CTMAB. Curves: 1, AB; 2, DNA–AB; 3, CTMAB; 4, CTMAB–AB; 5, DNA–CTMAB; 6–8, DNA–CTMAB–AB. Concentrations: c_{AB}, 1.0×10^{-5} M; c_{CTMAB}, 4.0×10^{-5} M; pH, 11.55; c_{DNA} (from 1 to 8): 0, 1.0, 0, 0, 1.0, 0.4, 0.8, 1.0 µg ml^{-1}.
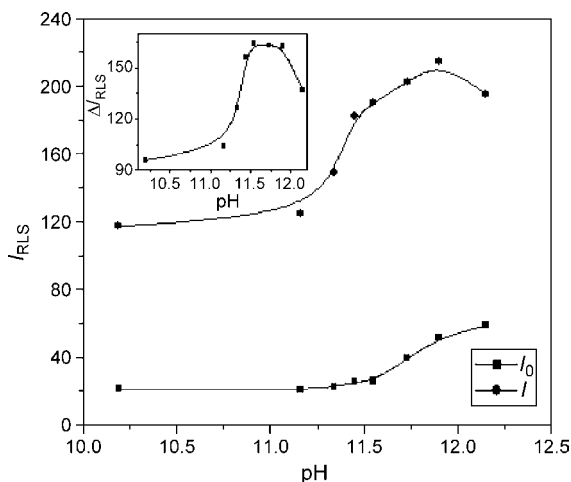
Fig. 3. The dependence of resonance light-scattering intensity on pH. Conditions: c_{DNA}, 1.0 µg ml^{-1}; c_{AB}, 1.0 × 10^{-5} M; c_{CTMAB}, 3.0 × 10^{-5} M.

DNA, and the binary complex of CTMAB–DNA could not bind with AB without excessive positive charges. With the increase of CTMAB, however, excessive positive charge of CTMAB gradually appears and the negatively charged AB could bind to the binary complex. Micelle will be formed when CTMAB concentration is higher than 4.0 × 10^{-5} M [15]. Thus, AB is dispersed into the micelle and hardly reacts with DNA, and the RLS signals decrease.

It was found that the AB concentration obviously effected ΔI_{RLS} of CTMAB–DNA–AB system. When the concentration of AB is within the range 1.0 × 10^{-5} to 1.2 × 10^{-5} M, the ΔI_{RLS} reaches maximum and keeps stable. So, 1.0 × 10^{-5} M AB is selected for further research.

About 1.0 mol l^{-1} NaCl solution was used to adjust the ionic strength. With the increasing NaCl concentration, RLS signal of CTMAB–AB keeps constant, whereas, that of AB–CTMAB–DNA decreases, indicating that electrostatic interaction exists between CTMAB–AB complex and DNA [16]. When NaCl concentration is higher than 0.07 M, the enhanced RLS signals keep constant and still strong, indicating
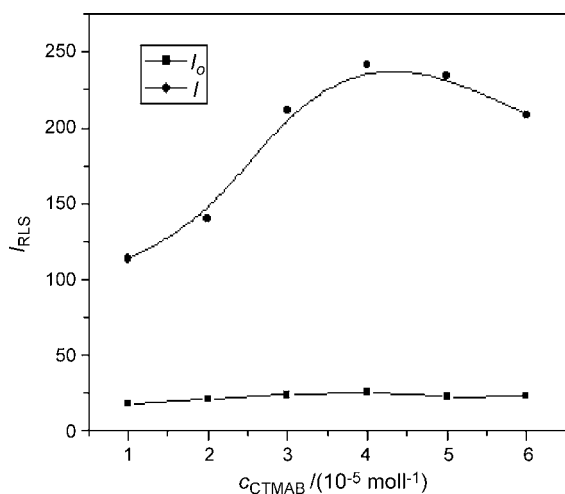
Fig. 4. The dependence of RLS intensity on concentration of CTMAB. Conditions: c_{DNA}, 1.0 µg ml^{-1}; c_{AB}, 1.0 × 10^{-5} M; pH 11.55.
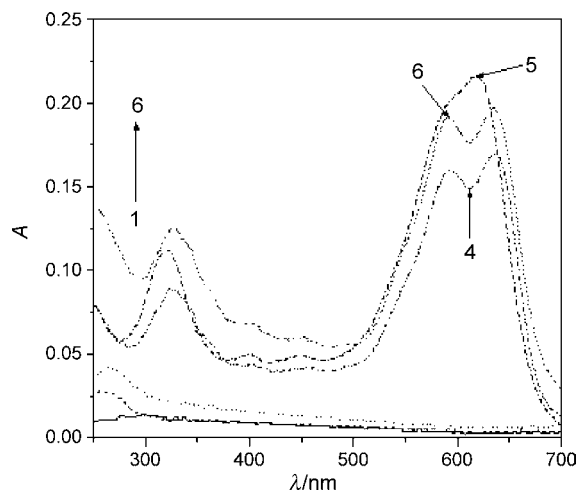
Fig. 5. The absorption spectra of AB and its interaction with DNA in the presence of CTMAB. Curve 1, CTMAB; curve 2, DNA; curve 3, DNA–CTMAB; curve 4, AB–CTMAB; curve 5, AB; curve 6, DNA–CTMAB–AB. Conditions: c_{DNA}, 1.5 µg ml^{-1}; c_{AB}, 1.0 × 10^{-5} M; c_{CTMAB}, 4.0 × 10^{-5} M; pH, 11.55.

that other kinds of interactions probably exist among CTMAB, DNA and AB.

3.3. Nature of the interaction of AB, CTMAB, and DNA

Generally, the interaction between OSMs and DNA involves in three modes, intercalative, groove, and electrostatic attraction [11]. It can be seen from Fig. 2 that coexistence of AB and DNA does not give rise to the enhanced RLS signals, indicating that the interaction of AB with DNA is impossible or very weak due to the electrostatic repulsion, whereas coexistence of CTMAB and DNA can result in enhanced RLS signals due to the formation of DNA–CTMAB complex. By introducing AB into DNA–CTMAB system, the RLS signals are enhanced markedly for AB, CTMAB, and DNA can form a ternary complex, which could be further manifested by UV–vis, CD spectra, and RLS imaging.

Fig. 5 shows that CTMAB and DNA have weak absorption band in violet region and no in visible region, while AB has the absorption band with the maximum at 618.5 nm (curve 5 in Fig. 5). The absorbance of DNA was enhanced over the wavelength range of 250–700 nm in the present of CTMAB, indicating that DNA can interact with CTMAB efficiently. On the other hand, when CTMAB is added to the AB solution, two new absorption bands at 637.5 nm and 592.0 nm could be observed at the expense of the AB absorption band (618.5 nm), implying that the interaction of CTMAB with AB occurs. The new absorption bands should possibly be ascribed to the aggregation of AB in the presence of CTMAB [17,18]. If DNA is added to the mixture of CTMAB and AB, however, strong hyperchromic effect at 637.5 nm and 592.0 nm could be observed, indicating that DNA can interact efficiently with the mixture of CTMAB and AB.

Fig. 6 shows the CD spectra. DNA, CTMAB, AB and CTMAB–DNA only exhibit weak CD signals, whereas, CTMAB–AB exhibits strong negative Cotton effect at 232.5 nm

Table 1
Analytical parameters of the determination

DNA	Linear range (μg ml^{-1})	Linear regression equation (μg ml^{-1})	Limit of determination (ng ml^{-1})	Correlation coefficient, r ($n=7$)
fsDNA	0.03–1.0	$\Delta I = -4.00 + 221.01c$	7.3	0.9955
ctDNA	0.05–1.5	$\Delta I = 7.25 + 228.93c$	7.0	0.9921

Conditions: c_{AB}, 1.0×10^{-5} M; c_{CTMAB}, 4.0×10^{-5} M; pH, 11.55.

Table 2
Interference of foreign substances

Foreign substances	Concentration (μM)	Change in I_{RLS} (%)
Na$^+$, Cl$^-$	200.0	−3.5
K$^+$, Cl$^-$	200.0	−1.7
Ba^{2+}, Cl$^-$	60.0	5.9
Ca^{2+}, Cl$^-$	20.0	2.1
Mg^{2+}, Cl$^-$	20.0	5.2
Cu^{2+}, Cl$^-$	20.0	−2.5
Zn^{2+}, Cl$^-$	20.0	6.0
Cd^{2+}, Cl$^-$	20.0	−3.8
NH$_4^+$, Cl$^-$	20.0	−0.4
Hg^{2+}, Cl$^-$	2.0	−8.6
Cr^{3+}, Cl$^-$	2.0	1.8
Co^{2+}, Cl$^-$	2.0	4.4
Pb^{2+}, NO$_3^-$	2.0	−7.8
Al^{3+}, Cl$^-$	2.0	4.5
Urea	100.0	−2.6
L-Leucine	40.0	−2.9
L-Glutamate	40.0	−5.3
L-Cysteine	40.0	−9.6
D,L-Cysteine	40.0	−7.3
Glucose	20.0	6.4
SDS[a]	4.0	−1.2
Sucrose	2.0	−9.5

Conditions: c_{DNA}, 1.0 μg ml^{-1}; c_{AB}, 1.0×10^{-5} M; c_{CTMAB}, 4.0×10^{-5} M; pH, 11.55.

[a] Represents sodium dodecanesulphonate.
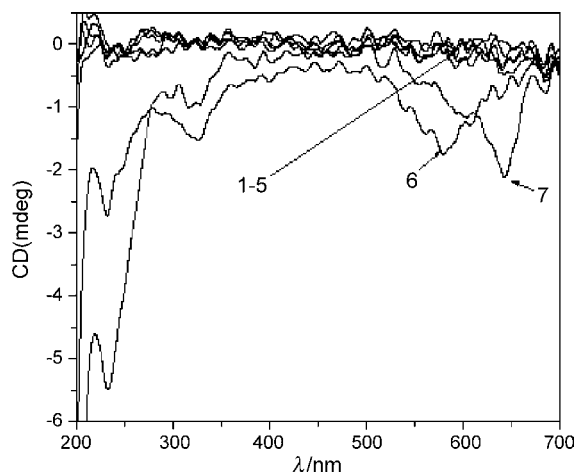
Fig. 6. The CD spectra of the system. Curve 1, CTMAB; curve 2, DNA; Curve 3, DNA–CTMAB; curve 4, AB–DNA; curve 5, AB; curve 6, AB–CTMAB; curve 7, DNA–CTMAB–AB. Conditions: c_{DNA}, 1.5 μg ml^{-1}; c_{AB}, 1.5×10^{-5} M; c_{CTMAB}, 4.0×10^{-5} M; pH, 11.55.
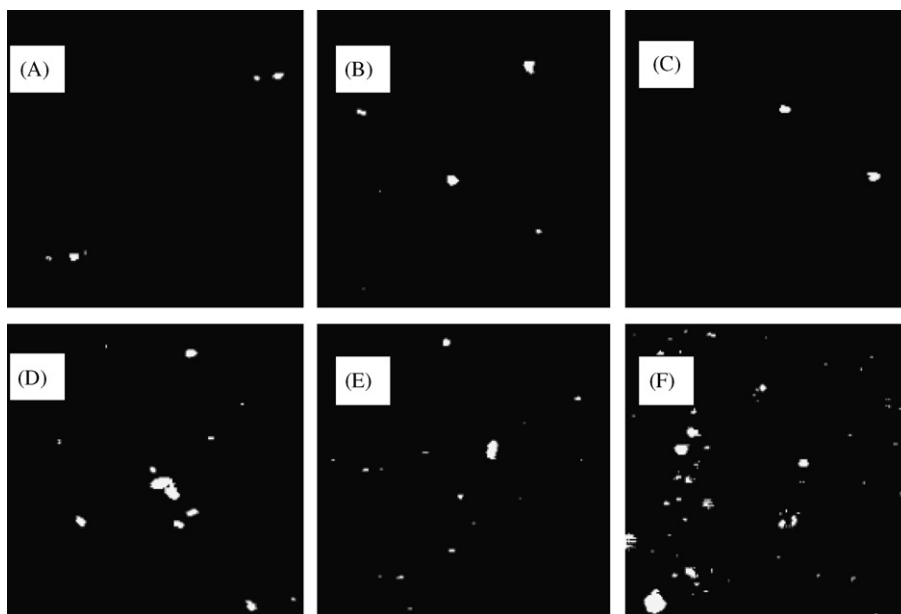
Fig. 7. Images of the system. (A) AB; (B) CTMAB; (C) DNA; (D) AB–CTMAB; (E) CTMAB–DNA; (F) CTMAB–DNA–AB. Conditions: c_{DNA}, 1.0 μg ml^{-1}; c_{AB}, 1.0×10^{-5} M; c_{CTMAB}, 4.0×10^{-5} M; pH, 11.55.

Table 3
Determination results of synthetic samples ($n = 5$)

Sample	Foreign substances	Found ($\mu g\,ml^{-1}$)	R.S.D. (%)	Added ($\mu g\,ml^{-1}$)	Total found ($\mu g\,ml^{-1}$)	R.S.D. (%)	Recovery (%)
1	Na$^+$, Zn^{2+}, L-leucine	0.252	0.9	0.500	0.739	0.9	97.4
2	Al^{3+}, Cr^{3+}, L-cysteine	0.329	0.7	0.500	0.800	0.8	94.2
3	Zn^{2+}, Mg^{2+}, L-glutamate	0.398	0.8	0.500	0.944	0.9	109.2

Conditions—(c, μM): AB, 10; CTMAB, 40; Al^{3+}, 5.0; K$^+$, 10.0; Co^{2+}, 0.5; Zn^{2+}, 1.0; Cr^{3+}, 0.5; Mg^{2+}, 5.0; L-cysteine, 2.0; L-leucine, 1.0; L-glutamate, 6.0; pH 11.55.

and 579.3 nm, indicating that CTMAB and AB can form complex. Compared with CTMAB–AB complex, CTMAB–DNA–AB complex exhibits much stronger negative Cotton effect at 233.3 nm, and simultaneously give rise to the new negative Cotton effect at 642.8 nm with red shift of 43.5 nm, further testifying that the complex of CTMAB–AB could react with DNA.

The RLS imaging graphs (Fig. 7) are obtained according to ref [19]. It can be seen that the RLS imaging counts (white point) are little when AB, DNA, and CTMAB exist alone, while, the counts are enhanced when CTMAB is mixed with AB or DNA, indicating that CTMAB can form the binary compound with AB or DNA. The RLS imaging counts of CTMAB–AB–DNA system are more than the total amount of CTMAB–AB and CTMAB–DNA, indicating that CTMAB, DNA and AB can form a ternary complex. These results are consistent with the results of the RLS, UV–vis, and CD spectra.

3.4. Calibration and analytical application

Under the optimum conditions, the dependence of ΔI_{RLS} on the concentration of DNA was determined. The analytical parameters of this method (Table 1) show that there is a good linear relationship between ΔI_{RLS} and the concentration of DNA over a relatively wide range.

Metal ions, amino acids, and other substances were examined as interference. The results were summarized in Table 2. It can be seen that most of the metal ions in biological systems, such as K$^+$, Na$^+$ and Ca^{2+} can be tolerated at high concentrations. This indicates that the method has the value of practical applications.

According to the calibration curves, three synthetic samples constructed on the basis of the interference of foreign substance are simultaneously determined under the same conditions. Their determination results are listed in Table 3. Table 3 shows that the values found in synthetic samples are credible, for the even recovery in the range of 94.2%–109.2%.

4. Conclusion

AB can aggregate on the surface of DNA through the bridged and synergistic effect of CTMAB, which results in the enhanced RLS signals of AB–CTMAB–DNA system. Thus, a RLS method for determining of DNA is proposed using AB, an anionic dye probe. This study enlarges the range of probe reagents for the determination of DNA. We believe that a valuable method for the quantitative determination of deoxyribonucleic acid (DNA) will be find through a serials anion dye probe studies. At the same time, the ternary complex of AB–CTMAB–DNA would become a new chiral material for it has CD properties.

References

[1] M.J. Waring, G.C. Roberts, Drug Action at the Molecular level, Macmillan, London, 1977, 167.
[2] M.J. Waring, K.R. Fox, S. Neidce, M.J. Waring, Molecular Aspects of Anti-Cancer Drug Action, Macmillan, London, 1983, 127.
[3] S. Udenfriend, P. Zaltzman, Anal. Biochem. 3 (1962) 49.
[4] R.F. Pasternack, P.J. Collings, Science 269 (1995) 935.
[5] H. Zhong, N. Li, F.L. Zhao, K.A. Li, Talanta 62 (2004) 37.
[6] S.F. Chen, Y.F. Li, C.Z. Huang, Talanta 70 (2006) 52.
[7] H. Zhong, J.J. Xu, H.Y. Chen, Talanta 67 (2005) 749.
[8] C.Z. Huang, X.B. Pang, Y.F. Li, Y.J. Long, Talanta 69 (2006) 180.
[9] S.P. Liu, Z.F. Liu, C.Z. Huang, Anal. Sci. 14 (1998) 799.
[10] C.Z. Huang, K.A. Li, S.Y. Tong, Anal. Chem. 68 (1996) 2259.
[11] R.T. Liu, J.H. Yang, X. Wu, T. Wu, Anal. Chim. Acta 448 (2001) 85.
[12] C.Z. Huang, K.A. Li, S.Y. Tong, Anal. Chem. 69 (1997) 514.
[13] C.X. Yang, Y.F. Li, P. Feng, C.Z. Huang, Chinese J. Anal. Chem. 30 (2002) 473.
[14] H.J. Karlsson, M. Eriksson, E. Perzon, B. Akerman, P. Lincoln, G. Westman, Nucleic Acids Res. 31 (2003) 6227.
[15] Y.J. Cheng, J.H. Yang, X. Wu, W. Cao, H.Y. Zhuang, Chinese Anal. Chem. 31 (2003) 1352.
[16] L.S. Ling, Z.K. He, Y.E. Zeng, Spectrochim. Acta A 55 (1999) 1297.
[17] S. Okada, H. Segawa, J. Am. Chem. Soc. 125 (2003) 2792.
[18] O.K. Kim, J. Je, G. Jernigan, L. Buckley, D. Whitten, J. Am. Chem. Soc. 128 (2006) 510.
[19] C.Z. Huang, Y. Liu, Y.H. Wang, H.P. Guo, Anal. Biochem. 321 (2003) 236.

ELSEVIER

Performance of a sound card as data acquisition system and a lock-in emulated by software in capillary electrophoresis

Marcos Mandaji [a], Tiago Buckup [b], Rafael Rech [b],
Ricardo Rego Bordalo Correia [b], Tarso Ledur Kist [c,*]

[a] *Centro de Biotecnologia, Universidade Federal do Rio Grande do Sul, Porto Alegre, RS, Brazil*
[b] *Instituto de Física, Universidade Federal do Rio Grande do Sul, Porto Alegre, RS, Brazil*
[c] *Instituto de Biociências, Universidade Federal do Rio Grande do Sul, Av. Bento Gonçalves,
9500, Caixa Postal 15093, 91501-970 Porto Alegre, RS, Brazil*

Abstract

The performance of fluorescence detectors in capillary electrophoresis is maximized when the excitation light intensity is modulated in time with optimal frequencies. This is especially true when photomultiplier tubes are used to detect the fluorescent light. The photomultiplier tube amplified raw output signal can in principle be captured directly by a personal computer sound card (PCSC) and processed by a lock-in emulated by software. This possibility is demonstrated in the present work and the performance of this new setup is compared with a traditional data acquisition system. The results obtained with this "PCSC and lock-in emulated by software" were of the same quality or even better compared to that obtained by conventional time integrators (Boxcars) and data acquisition boards. With PCSC the limits of detection (LOD) found for both naphthalene-2,3-dicarboxaldehyde-derivatized tyrosine and alanine were 3.3 and 3.5 fmol (injection of 5 nL of samples at 0.66 and 0.70 μmol/L), respectively. This is at least three times better compared to conventional systems when light emitting diodes (LEDs) are used as the excitation source in fluorescence detectors. The PCSC linear response range was also larger compared to conventional data acquisition boards. This scheme showed to be a practical and convenient alternative of data acquisition and signal processing for detection systems used in capillary electrophoresis.
© 2006 Elsevier B.V. All rights reserved.

Keywords: Light emitting diode; Capillary electrophoresis; PC sound card; Lock-in amplifier; Fluorescence

1. Introduction

It was recently shown that light emitting diodes (LED) are inexpensive alternatives to lasers in fluorescence detection systems used in capillary electrophoresis (CE) [1,2]. With the appearance of LEDs with high optical power, small spectral width, and the option of wavelength peaks ranging from UV to the near IR, the application of these devices increased significantly in fluorescence detection systems in capillary electrophoresis.

Several works demonstrated low limits of detection (LOD) for many analytes using LEDs as excitation sources in CE

[3–10]. Su et al. [3,5] analyzed riboflavin in beer and urine and obtained a LOD of 1–20 ng mL^{-1} with a blue LED in the detection system. Jong and Lucy [9] obtained the LODs of 50, 20, and 3 nM for riboflavin, eosin Y, and fluorescein, respectively. Yu et al. [4] also used a blue LED to analyze pathogen cells in fish fluid and obtained a LOD of 4.2×10^4 cells/mL. Tsai et al. [7] assembled a fluorescence detector with UV LED. According to these authors a LOD of 2.0×10^{-10} M and 3.0×10^{-8} M was obtained for NDA-derivatized reserpine and dopamine, respectively. Yang et al. [8] obtained a LOD of 10 nM for FITC-labeled phenylalanine. Zhang et al. [10] also obtained a LOD of 10 nM for FITC-labeled arginine.

In these works [3–9] the authors showed several optical setups and sample pre-concentration strategies to obtain low LODs. Zhang et al. [10] assembled the detector with dual modulation of the source light to enhance the signal-to-noise ratio. Several strategies are used to minimize the LODs. A few of these strategies are the use of an appropriate methodology of sample
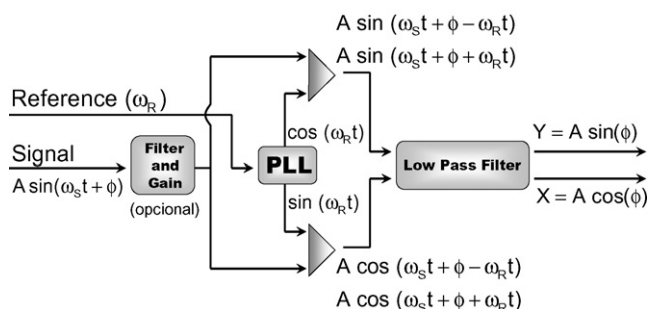

Fig. 1. Schematic diagram of a lock-in amplifier. Filtering and the phase-locked loop (PLL) were emulated by software written in Labview.

pre-concentration, good optical components, a good optical setup, LEDs with high optical output power, a sensitive light sensor, a good electronic system to filter the noise, and a data acquisition system with high resolution and sampling rate.

The LEDs' light intensity is easily modulated and this in turn leads to many new possibilities and strategies of signal processing and data acquisition. Usually, the source light is modulated and the signal is processed by a lock-in amplifier or a time integrator in fluorescence detectors for CE. This technique is widely used to detect low signal levels buried in high noise. Today several lock-in amplifiers are digital and the signal processing is made by a digital signal processor (DSP) with on-board software [11–13].

The scheme of a typical lock-in amplifier is shown in Fig. 1. A lock-in amplifier extracts frequency and phase information from a reference signal and generates a pure harmonic wave. This task is made by a digital phase-locked loop (PLL) circuit. The harmonic wave is mixed with a pre-amplified and pre-filtered signal. For each frequency component in the input signal, the mixer stage generates two output components: one with the frequency equal to the difference between the frequencies of the internal reference and the signal component ($\omega_R - \omega_S$) and another component equal to the sum of the two frequencies ($\omega_R + \omega_S$). Since the signal and internal reference have the same frequency then its difference will be a DC signal for a specific phase. It is usually referred as the X component and is proportional to the relative phase of the internal reference ($\cos\phi$) and signal amplitude. A low-pass filter, of sub-Hz cutoff frequency, will allow it to be detected, but the sum $\omega_R + \omega_S$ will be filtered out. If the steps of filtering and mixing are performed in quadrature, then the Y component can be extracted independently from the X component. In a lock-in amplifier the measurement and the comparison of these two components allows the amplitude and the relative phase of the signal to be determined.

The resolution (bits) and the sampling rate of analog to digital converters (A/D) installed on the data acquisition cards is another important parameter to achieve low limits of detection. A data acquisition card for CE usually has an A/D with a resolution of 14–16 bits and sampling rates higher than 50 kHz. Personal computers usually have two analog doors for data acquisition, they are the two channels of the on-board sound cards. The sound cards usually have high resolution A/Ds (16 or 24 bits) and sampling rate up to 192 kHz. These characteristics turn these devices

into very attractive data acquisition systems for slow varying signals (below 20 Hz), as is the case in capillary electrophoresis.

In this work the setup and performance of signal processing made by a lock-in emulated by software in a personal computer is tested. In addition, the data acquisition was made by a usual sound card installed on the mother board instead of a data acquisition card. This new setup was assembled in parallel with a traditional system to compare the performances.

2. Experimental

2.1. Electrophoresis parameters

The capillary was conditioned at the beginning of each run by rinsing it with NaOH 1 M for 2 min, followed by water for 1 min and running buffer (25 mM borate, pH 9.0, 15% methanol) for 2 min. The NaOH, boric acid, KCN and methanol were purchased from Merck (Darmstad, Germany), amino acids (Sigma–Aldrich) were derivatized with NDA (Sigma–Aldrich). The derivatization reaction was performed in 25 mM borate buffer pH 9.0 with KCN and NDA at concentrations 10 times higher than tyrosine and alanine.

2.2. Instrumentations

The CE instrument used in this work was built in our laboratory [2,14] and was equipped with a fused-silica capillary (Polymicro Technologies, Phoenix, AZ, USA) with an i.d. of 50 μm, o.d. of 363 μm, and a total length of 47 cm (42 cm to the detector). The high-voltage power supply (Series 205B; Bertan, Hicksville, NY, USA) has an output voltage ranging from 0 to ±30 kV.

An UV LED with emission maximum at 405 nm (10 mW) and a blue LED with emission maximum at 475 nm (5 mW) were used as the excitation sources for naphthalene-2,3-dicarboxaldehyde (NDA) derivatized amino acids and fluorescein, respectively.

Fig. 2 shows the instrumental setup of the CE instrument and of the two systems assembled in parallel used for data acquisition and signal processing. A function generator (CFG250; Tektronix, Beaverton, OR, USA) was used for both driving the LED and generating a trigger signal for the Boxcar integrator and a reference signal for the channel 1 of a personal computer sound card (PCSC). The signal from the photomultiplier tube (PMT) (Model E850-02; Hamamatsu, Bridgewater, NJ, USA) was enhanced by an adjustable pre-amplifier (13 AMP 003; Melles Griot, Boulder, CO, USA). The output of this pre-amplifier was send to two directions by a "T" like BNC connector. One branch was used to feed the time-integrator or Boxcar (model 132/164; Princeton Applied Research, Princeton, NJ, USA) called system A. In this system (system A) the signal was integrated by the Boxcar and recorded by means of a conventional data acquisition board (CIO-DAS08; Computer Boards Mansfield, MA, USA) using a home written HP VEE routine (HP VEE, Version 3.21). The second branch was used to feed the channel 2 of a PCSC (Vibra 128 PCI card, model CT4810, Chipset CT5880, Creative Labs) of a second
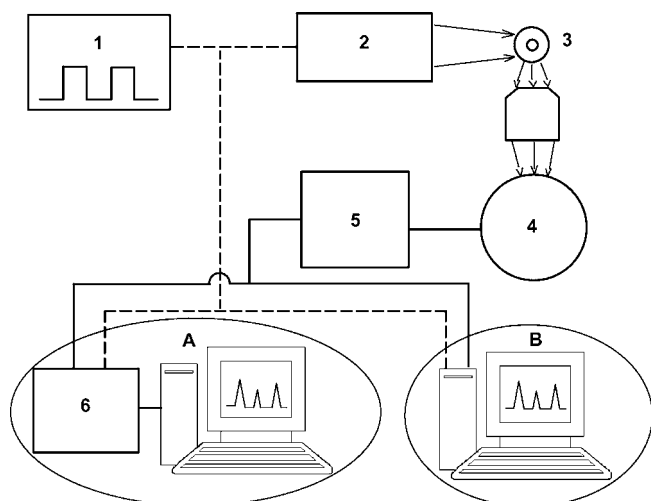
Fig. 2. Scheme of the experimental setup. The output of a function generator (1) is used to supply the LED, the Boxcar trigger, and the PCSC reference signal. The light of the LED (2) is collimated with lenses onto the capillary detection window (3) and the induced fluorescence light is detected by a PMT (4) after passing a spectral filter and a spatial filter (more details are shown in Ref. [2]). The PMT output signal is enhanced by the pre-amplifier (5). System A works with a time integrator (6) and a conventional data acquisition system, while the system B works with a PSCS and lock-in emulated by software. Both systems receive the same output signal from function generator (dashed line) and same output signal from pre-amplifier (solid line).

PC and was called system B. In this system (system B) the signal was processed by a Labview routine that emulates a lock-in and the results were recorded on this same PC where the PCSC is also installed. With this setup the data of a single CE run could be simultaneously processed and recorded by both systems and compared.

3. Results and discussion

Samples were run several times with 1, 2, 4 and 6 μM of derivatized tyrosine and alanine. They were injected at 1 kV for 30 s into the capillary and ran at 15 kV and 25 °C for LOD determination. The results are shown in Fig. 3. Considering the LOD as the concentration that produces a signal-to-noise ratio equal to 3, the LOD in system A was 9.1 and 10.6 fmol (injection of 5 nL of samples at 1.82 and 2.12 μmol/L) for NDA-derivatized tyrosine and alanine, respectively, while in system B the LOD was 3.3 and 3.5 fmol (injection of 5 nL of samples at 0.66 and 0.70 μmol/L), respectively. Therefore, system B showed to be about three times better (Fig. 4) than system A in this regard. These results show us that emulated lock-ins associated with a sound card have a performance as good as conventional lock-ins and data acquisition systems.

In general, enhancement of S/N comes from two aspects: A/D resolution and the intrinsic phase-sensitive detection mechanism [15]. The resolution of a lock-in can be estimated by the A/D card resolution. In the case of a sound card with a 16 bits A/D chip, the S/N that can be measured is at least around 48 dB. This is due to the PCSC high resolution and the ability of the emulated lock-in to make in-phase measurements (PLL). In this sense, the use of A/D cards with higher resolution and higher
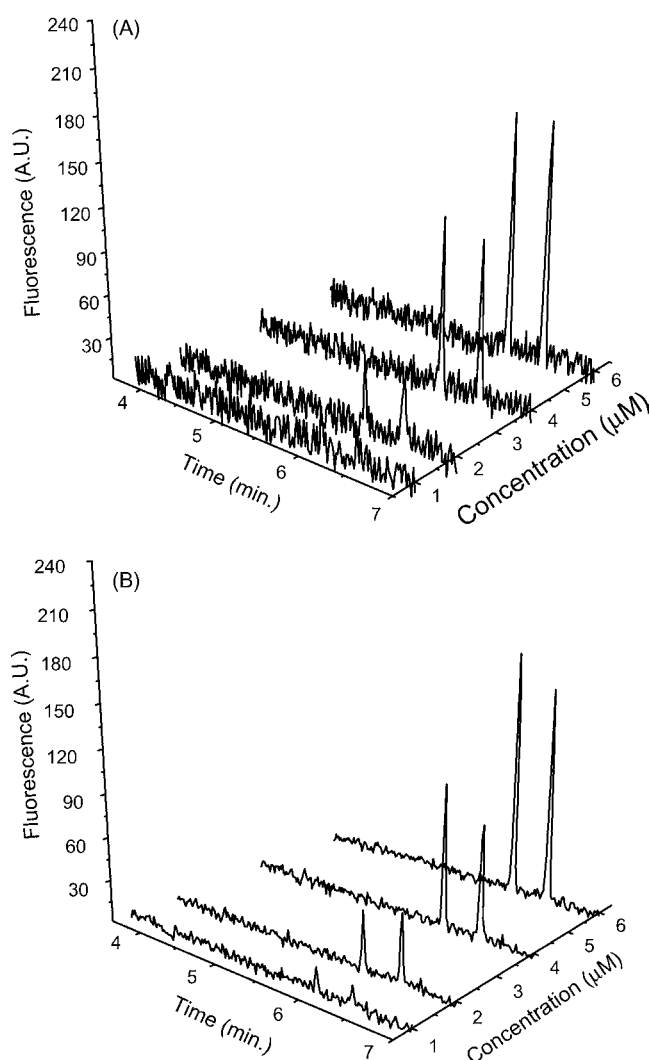
Fig. 3. NDA-derivatized tyrosine and alanine samples were diluted step-by-step and electrophoresed up to the LOD: (A) the results for system A and (B) for system B.
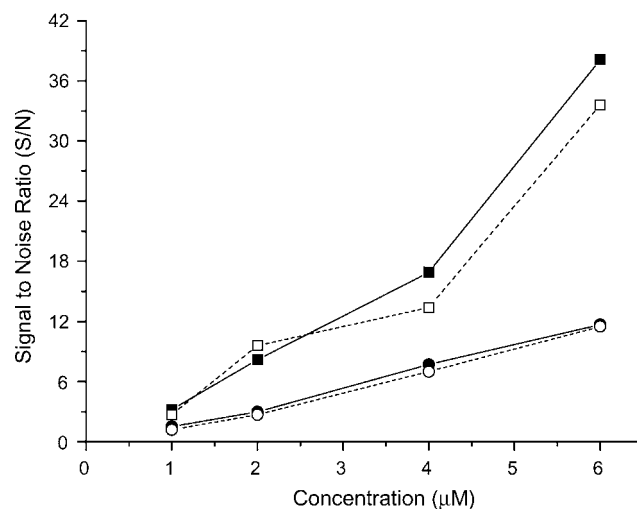
Fig. 4. Signal-to-noise ratio of NDA-derivatized tyrosine (filled symbols) and alanine (empty symbols) as a function of concentration measured by system A (circles) and system B (squares).

sampling rates would allow even lower LOD to be achieved. This is especially true in situations were strong noise components are present, i.e., the A/D scale is almost full: a one-count signal in a 24 bit (one in 2^{24} counts) A/D will be hardly detected in a 16 bit (one in 2^{16} counts) A/D because it does not have enough resolution depth. In our case, the A/D resolution did not play a strong role because the noise was not strong.

Sampling rate is another important parameter that must be optimized in order to maximize the S/N. According to the Nyquist Theorem [16], the sampling rate must be at least two times higher than the highest frequency observed in the signal. In our measurements, the signal (triggered LED) had a repetition rate of 0.5 kHz; therefore a sampling rate of at least 1.0 kHz should be used. However, sound cards can sample only in four available rates: 8, 11, 22, and 44 kHz. In our setup a sampling rate of 8 kHz was used. The S/N can be improved even more by using higher frequencies, as known from the literature [16]. These sampling rates are still low for multi-capillary systems, which limits its application to single capillary systems.

PCSC showed to be a good alternative to conventional data acquisition boards. For low analyte concentrations the PCSC exhibited excellent linear responses and linear regression variances, higher than 0.9741 for peak height and peak area in electropherograms shown in Fig. 3. The relative standard deviation of the four electrophoretic runs was less than 5% for all points using peak area and peak height. This shows that the use of a PCSC as data acquisition system with a lock-in emulated by software is a good alternative to traditional data acquisition boards.

Another point investigated was the range of linear response of the PCSC. For this, the UV LED was replaced by a blue LED (475 nm) and fluorescein was used as the analyte. For the test of linearity on the upper limit of the working range a solution of fluorescein was chosen to avoid solubility problems and instabilities that are frequently associated with NDA-derivatized amino acids at higher concentrations. The nonlinear behavior of both systems in the upper limit is examined in Fig. 5. The work-
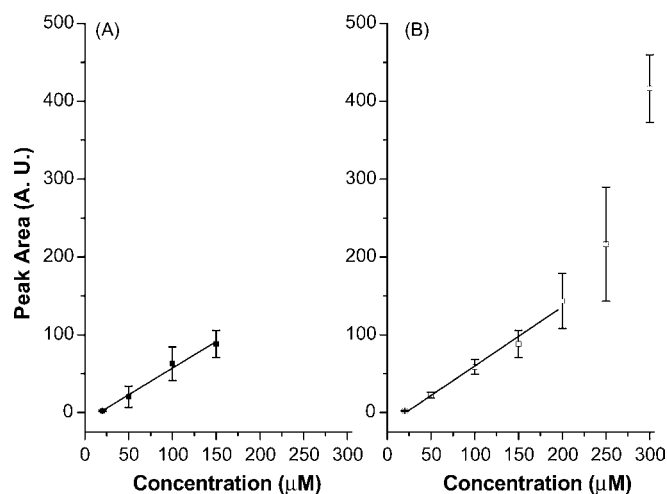
Table 1
Linear regression variance data of different fluorescein concentration ranges

Analyte[a] (μM)	Peak height		Peak area	
	System A	System B	System A	System B
20–150	0.9728	0.9819	0.9894	0.9983
20–200	n.a.[b]	0.9824	n.a.[b]	0.9870
20–250	n.a.[b]	0.9559	n.a.[b]	0.9694
20–300	n.a.[b]	0.7623	n.a.[b]	0.8641

[a] Analyte concentration range (fluorescein).
[b] Data not available (analog signal input overflow).

ing range of the A/D of system A was from 0 up to 10 V. The output signal of this system was linear with concentration from 0 to 150 μmol/L of fluorescein. Note that Fig. 5A shows the concentration of the samples against peak areas and not peak heights. According to the results shown in Fig. 5A we conclude that system A has a linear working range from 0 to 150 μmol/L of fluorescein. The working range of the A/D of system B was from −5 up to 5 V, but in practice only the range 0–5 V was used. Moreover, the limit signal of 5 V was only reached by 300 μmol/L of fluorescein. As shown in Fig. 5B, the output signal of this system was linear with concentration from 0 to 200 μmol/L of fluorescein. From Fig. 5A and B it is clear also that system B has a wider working range in concentration compared to system A. Moreover, by using an offset of −5 V in system B, the working range can easily be increased even more, from 0 to 400 μmol/L.

The linear regression variances of both systems in the upper limit interval are shown in Table 1. For higher concentrations the relationship is no longer linear, this saturation may be a result of many factors thus requiring a calibration curve for each device. However, by varying the detector's gain, the amplifier gain, or both parameters simultaneously allows the samples to be analyzed in a wider range of concentrations.

4. Conclusion

The PCSC with emulated lock-in showed a good performance and the ability to replace Boxcars and conventional data acquisition boards widely used in detection systems in capillary electrophoresis. This system showed to be more sensitive and exhibited a larger working range in concentration. The same performance was also observed for all analytes tested, which includes peptides, protein co-factors, carboxylic acids, and also indirect fluorescence detection of anions (data not shown). Moreover, the applicability of this setup (PCSC with emulated lock-in) is expected to work with all kind of excitation sources that can be modulated, for instance diode lasers and some lamps. Considering that the PCSC used in this work had an A/D with only 16 bits and maximum sampling rate of 44 kHz, it is possible to even improve the performance using PCSC with A/D of 24 bits or higher and with sampling rates of 96 kHz or higher. Therefore, the above tested setup and emulated lock-in showed a good cost-benefit ratio. This is also attractive for applications where low space is available, as all the data acquisition components already are present in entry level PC.

Fig. 5. Linear response of the peak area. Data obtained from system A was showed in (A) and from system B in (B). The averages and standard deviations of four repetitions are shown.

References

[1] M.L. Chabinyc, D.T. Chiu, J.C. McDonald, A.D. Stroock, et al., Anal. Chem. 73 (2001) 4491.
[2] S. Hillebrand, J.R. Schoffen, M. Mandaji, C. Termignoni, et al., Electrophoresis 23 (2002) 2445.
[3] A.K. Su, Y.S. Chang, C.H. Lin, Talanta 64 (2004) 970.
[4] L.J. Yu, L.L. Yuan, H.T. Feng, S.F.Y. Li, Electrophoresis 25 (2004) 3139.
[5] A.K. Su, C.H. Lin, J. Chromatogr. B 785 (2003) 39.
[6] F. Xu, M. Jabasini, B. Zhu, L. Ying, et al., J. Chromatogr. A 1051 (2004) 147.
[7] C.H. Tsai, H.M. Huang, C.H. Lin, Electrophoresis 24 (2003) 3083.
[8] B. Yang, F. Tan, Y. Guan, Talanta 65 (2005) 1303.
[9] E.P. Jong, C.A. Lucy, Anal. Chim. Acta 546 (2005) 37.
[10] T. Zhang, Q. Fang, S.-L. Wang, L.-F. Qin, P. Wang, Z.-Y. Wu, Z.-L. Fang, Talanta 68 (2005) 19.
[11] J. Gaspara, S.F. Chen, A. Gordillo, M. Hepp, P. Ferreyra, C. Marque, Microprocess. Microsys. 28 (2004) 157.
[12] M.O. Sonnaillona, F.J. Bonettob, Rev. Sci. Instrum. 76 (2005) 024703.
[13] A. Restelli, R. Abbiati, A. Geraci, Rev. Sci. Instrum. 76 (2005) 093112.
[14] T.B.L. Kist, C. Termignoni, H.P.H. Grieneisen, Braz. J. Med. Biol. Res. 27 (1994) 11.
[15] R.B. Northrop, Analog Electronic Circuits: Analysis and Applications, Addison-Wesley, 1989, 521 pp.
[16] M.J. Demler, High-Speed Analog-to-Digital Conversion, Academic Press, 1991, 182 pp.

Surface diffusion in reversed-phase liquid chromatography using silica gels bonded with C_1 and C_{18} ligands of different densities

Kanji Miyabe

Faculty of Engineering, University of Toyama, 3190 Gofuku, Toyama 930-8555, Japan

Abstract

Surface diffusion in reversed-phase liquid chromatography (RPLC) using silica gels bonded with C_1 and C_{18} alkyl ligands of different densities was studied from the viewpoints of two extrathermodynamic relationships, i.e., enthalpy-entropy compensation (EEC) and linear free energy relationship (LFER). First, according to the four methods proposed by Krug et al., the values of surface diffusion coefficient (D_s) were analyzed to confirm that an actual EEC resulting from substantial physico-chemical effects takes place for surface diffusion. Then, it was also demonstrated that a LFER is observed between surface diffusion and the retention equilibrium. The establishment of EEC and LFER suggests a mechanistic similarity of molecular migration by surface diffusion, irrespective of the alkyl chain length and the densities of C_1 and C_{18} ligands. Finally, a thermodynamic model for the LFER based on the real EEC was used to estimate D_s values under various RPLC conditions. The D_s values can be estimated with a mean square deviation of about 25–30%. The agreement between the D_s values estimated and those experimentally measured suggests that the total mass flux by surface diffusion consists of the two contributions due to C_1 and C_{18} ligands and that the contribution of each ligand is proportional to the ligand density.
© 2006 Elsevier B.V. All rights reserved.

Keywords: Reversed-phase liquid chromatography; Alkyl ligand bonded silica gel; Surface diffusion; Extrathermodynamics; Enthalpy-entropy compensation; Linear free energy relationship

1. Introduction

Recently, different types of separation media and systems have been developed to attain fast chromatography with high efficiency. Under linear isotherm conditions, band broadening depends on the mass transfer kinetics of several rate processes involved in columns and packing materials, that is, axial dispersion, external (fluid-to-particle) mass transfer, intraparticle diffusion, and adsorption/desorption kinetics [1–5]. Additionally, intraparticle diffusion is usually explained by assuming the parallel diffusion by pore diffusion and surface diffusion [1,2,4]. The band broadening is predominantly influenced by the mass transfer kinetics in the packing materials under high flow rate conditions. However, compared with ample works on the retention equilibrium, there are not so abundant studies on the mass transfer kinetics in the columns, especially in the stationary phases.

It has been reported that surface diffusion has an important contribution to the molecular migration in the stationary phase [1,2,6,7]. Most molecules migrate in intraparticulate space by surface diffusion. The manner of surface diffusion depends on the retention behavior of the molecules because they migrate on the stationary phase surface under adsorbed state. In principle, chromatographic separations rest on the difference in the attractive interaction of the sample molecules with the stationary phase surface. Surface diffusion should be correlated with some essential characteristics of chromatographic separations. It is expected that detailed analyses of surface diffusion would provide an important information about the mechanism of chromatographic separations.

About 40 years ago, the significance of surface diffusion had already been suggested as one of important mass transfer processes [8]. In the field of chromatography, however, surface diffusion itself and its contributions to the mass transfer kinetics in the stationary phase and to the column efficiency are still not sufficiently recognized. Even now, there are few kinetic studies on chromatographic separations with considering the predom-

Nomenclature

a	slope of the linear correlation between a thermodynamic property and C_n
A	slope of LFER
b	intercept of the linear correlation between a thermodynamic property and C_n
B	intercept of LFER
C	carbon content
C_n	carbon number in alkyl ligand
D_e	intraparticle diffusivity ($m^2 s^{-1}$)
D_m	molecular diffusivity ($m^2 s^{-1}$)
D_p	pore diffusivity ($m^2 s^{-1}$)
D_s	surface diffusion coefficient ($m^2 s^{-1}$)
D_{s0}	frequency factor of surface diffusion ($m^2 s^{-1}$)
E_s	activation energy of surface diffusion ($J mol^{-1}$)
ΔG	free energy change ($J mol^{-1}$)
h	planck constant (J s)
ΔH	enthalpy change ($J mol^{-1}$)
k_B	boltzmann constant ($J K^{-1}$)
k_f	external mass transfer coefficient ($m s^{-1}$)
k_h	hindrance parameter
k_t	tortuosity factor
K	retention equilibrium constant ($m^3 g^{-1}$)
MS	mean sum of squares
MSD	mean square deviation
N	number of data pairs (D_s^{cal} and D_s^{exp})
R	gas constant ($J mol^{-1} K^{-1}$)
ΔS	entropy change ($J mol^{-1} K^{-1}$)
T	absolute temperature (K)
T_c	compensation temperature (K)
T_{hm}	harmonic mean of experimental temperatures (K)

Greek letters

α_s	statistical level of significance
δ_s	D_s value normalized by σ ($m^2 s^{-1}$)
ε_e	column void fraction (external porosity)
ε_p	porosity of the stationary phase particle (internal porosity)
λ	distance between two equilibrium positions (m)
μ_1	first absolute moment (s)
μ_2'	second central moment (s^2)
ρ_p	particle density ($g cm^{-3}$)
σ	alkyl ligand density ($\mu mol m^{-2}$)

Subscripts

1	condition 1
2	condition 2
con	concurrence
C_1	contribution due to C_1 ligand
C_{18}	contribution due to C_{18} ligand
h	enthalpy change
noncon	nonconcurrence
ODS	measured using the column #5
s	entropy change
T_{hm}	at harmonic mean of experimental temperatures

TMS	measured using the column #6
ε	measurement errors

Superscripts

cal	calculated
exp	experimental
REF	reference
SMP	sample
*	thermodynamic parameters measured by analyzing temperature dependence of D_s

inant contribution of surface diffusion to the mass transfer in the stationary phase. We do not have yet enough information about the characteristics and mechanisms of surface diffusion in chromatography. Because of the quite important role of surface diffusion to intraparticle diffusion, the information is essential to develop superior packing materials for high performance and high speed separations.

This work deals with the characteristics and the mechanism of surface diffusion in reversed-phase liquid chromatography (RPLC) systems using silica gel particles bonded with C_1 and C_{18} ligands of different densities. First, the mechanism of surface diffusion was discussed from the viewpoints of enthalpy-entropy compensation (EEC) and linear free energy relationship (LFER). Detailed analyses of surface diffusion data based on the four approaches proposed by Krug et al. [9–11] demonstrated that a real EEC is observed for surface diffusion and originates from substantial physico-chemical effects. The results of these extrathermodynamic studies indicate that the mechanism of surface diffusion is the same irrespective of the modification densities of C_1 and C_{18} ligands. Then, it was attempted to use the results of the thermodynamic and extrathermodynamic studies on surface diffusion to predict D_s values under different RPLC conditions. The D_s values thus estimated agreed with those experimentally measured with a mean square deviation of 25–30%. This result suggests that the total flux by surface diffusion consists of the contributions of C_1 and C_{18} ligands and that the contribution of each ligand is proportional to its density or coverage on the stationary phase surface.

2. Experimental

2.1. Columns and reagents

Table 1 lists some physical properties of five C_{18}-silica gel columns and packing materials. They are synthesized by the chemical modification of C_{18} ligands on the surface of the same base silica gel with end-capping treatment. Regarding the C_{18}-silica gel #5, no substantial increase in the carbon content was observed upon the end-capping with trimethylsilyl ligands. The bonding density of C_1 and C_{18} ligands was intentionally changed. A column #6 was also used, which was packed with C_1-silica gel particles prepared using the same base silica gel. The six columns (6 mm id × 150 mm) were purchased from YMC

Table 1
Physico-chemical properties of RP stationary phases

Packing material/column no.	1	2	3	4	5	6
Main alkyl chain	C_{18}	C_{18}	C_{18}	C_{18}	C_{18}	C_1
Particle density, ρ_p (g cm^{-3})	0.67	0.69	0.71	0.79	0.86	0.74
Porosity, ε_p	0.65	0.61	0.57	0.50	0.46	0.62
Carbon content (%)						
Before end-capping	1.6	3.6	6.4	12.8	17.1	4.1
After end-capping	5.0	6.6	8.6	13.7	17.1	–
C_1 ligand	3.4	3.0	2.2	0.9	0	4.1
C_{18} ligand density, $\sigma_{C_{18}}$ (μmol m^{-2})[a]	0.26	0.58	1.1	2.3	3.2	–
C_1 ligand density, σ_{C_1} (μmol m^{-2})[b]	3.7	3.2	2.4	0.97	0	4.4

[a] Calculated from the carbon content before end-capping and the BET surface area of the base silica gel (290 m^2 g^{-1}).

[b] Calculated from the carbon content due to C_1 ligand and the BET surface area of the base silica gel (290 m^2 g^{-1}).

(Kyoto, Japan). Some items of the information in Table 1 were also obtained from the manufacturer. The average particle diameter of the base silica gel is 45 μm. As described later, this coarse base material was used in order to make it easier to quantitatively analyze band broadening phenomena and, more specifically, to estimate more accurate values of D_s from the chromatographic peak profiles experimentally measured.

The mobile phase was a mixture of methanol and water (70/30, v/v). Alkylbenzenes (ethylbenzene, *n*-butylbenzene, and *n*-hexylbenzene) were used as the sample compounds. They were all reagent grade and used without further purification. Sample solutions were prepared by dissolving the sample compounds into the mobile phase. The concentration of the sample solutions was 0.1 wt.% in most cases. Uracil and sodium nitrate were used as inert tracers to determine the internal porosity (ε_p) of the packing materials and the external porosity (void fraction) (ε_e) of the columns [12,13]. The internal porosity is the ratio of the intraparticulate pore volume to the volume of the stationary phase particles. The external porosity is the interparticle volume in the column divided by the column volume. Roughly speaking, the elution time of uracil provides an information about the sum of ε_p and ε_e. On the other hand, the value of ε_e is determined from the elution time of sodium nitrate because of the Donnan salt-exclusion effect [12]. The difference in the elution times of the two inert tracers gives ε_p.

2.2. Apparatus

A high performance liquid chromatograph system (LC-6A, Shimadzu, Kyoto, Japan) was used. A valve injector (Model 7125, Rheodyne, Cotati, CA, USA) was used to introduce a small volume of the sample solution (ca. 0.5–300 μL) into the mobile phase stream at the inlet of the columns. The column temperature was kept at intended levels by circulating temperature controlled water around the column. The concentration of the sample compound leaving from the column was monitored with an ultraviolet detector of the HPLC system (SPD-6A). The values of first absolute moment (μ_1) and second central moment (μ_2') were calculated from the elution peak profiles recorded by an integrator (C-R6A, Shimadzu, Kyoto, Japan).

2.3. Experimental procedure

Pulse response experiments (i.e., elution chromatography) were carried out at six different mobile phase flow rates between 1 and 2 cm^3 min^{-1}. The column temperature was adjusted at 288, 298, and 308 K. In this study, all the chromatographic data were measured under linear isotherm conditions because of the small amount of the sample compounds injected. The value of the retention equilibrium constant (K) and some information about the mass transfer kinetics were derived from μ_1 and μ_2' of the elution peaks, respectively [1–7].

2.4. Data analysis procedure

The values of D_s were derived from μ_2' by subtracting the contribution to the band broadening of some mass transfer processes taking place in the column, that is, axial dispersion, external mass transfer, and pore diffusion. Only the basic information about the derivation procedure of the D_s data is briefly explained in the following. Further details on the moment analysis method can be referred in other literature [1–7,14–16].

First, the contribution of the external mass transfer to the band spreading was subtracted beforehand. The equation proposed by Wilson–Geankoplis [17] was used for estimating the external mass transfer coefficient (k_f). The Wilke–Chang equation [3,18,19] was used for estimating the molecular diffusivity (D_m) of the sample compounds in the mobile phase solvent, which is necessary for the estimation of k_f and pore diffusivity (D_p) (see later). Then, the intraparticle diffusivity (D_e) was derived by taking advantage of the different flow rate dependence of the contribution to the band broadening of intraparticle diffusion and the axial dispersion. Finally, the value of D_s was calculated by subtracting the contribution of pore diffusion to intraparticle diffusion. Based on the parallel diffusion model [4,5], it is assumed that intraparticle diffusion consists of two parallel contributions of pore diffusion and surface diffusion. The D_p value was estimated from D_m, ε_p, the hindrance parameter (k_h), and the tortuosity factor (k_t) of the internal pores. The equation proposed by Satterfield et al. [20] was used for estimating k_h. The value of k_t was determined from the similar pulse response experiments

using uracil as the inert tracer. The contribution of the actual adsorption/desorption kinetics at adsorption sites to μ_2' is usually assumed to be negligible in the case of physisorption [4].

2.5. Corrections

Several corrections were made in order to accurately derive D_s values from μ_2'. These corrections are explained in detail.

2.5.1. Correction for extra-column tubes

The values of μ_1 and μ_2' experimentally measured contain the contributions of extra-column tubes between the injection valve and the column and between the column and the detector. These contributions were measured from the results of tracer experiments made without the column and were corrected to derive the values of K and D_s from μ_1 and μ_2', respectively.

2.5.2. Correction for asymmetrical peak profiles

Accurate values of μ_1 and μ_2' cannot be directly determined from the elution time and the width of elution peaks when they show asymmetrical profiles [21–23]. It is required to correct the influence of the peak distortion on the determination of accurate values of μ_1 and μ_2' (hence, K and D_s). The occurrence of asymmetrical (tailing or fronting) peaks has been explained based on several models [3]. In this study, the heterogeneity of the packing structure in the radial direction of the column was regarded as the only significant origin of the peak asymmetry. Although heterogeneous mass transfer kinetics on the stationary phase surface is considered as another possible cause of the peak skewness [3], it was not considered in this study because the surface of alkyl ligands bonded silica gels seems to be apparently homogeneous. For instance, when C_{18}-silica gels are used as the stationary phase: (1) the phase equilibrium isotherm is usually accounted for by the simple Langmuir model [2,3,24,25] and (2) both the enthalpy change due to retention and the activation energy of surface diffusion are nearly constant irrespective of the amount of sample molecules adsorbed [2]. These experimental observations imply the apparent uniformity of the surface of C_{18}-silica gels. This assumption is also supported by a theoretical analysis of the adsorption behavior of 2-phenylethanol and 3-phenylpropanol from an aqueous methanol solution onto a C_{18}-phase [26].

2.5.3. Correction for the injection volume of sample solution

The influence of μ_1 and μ_2' of the sample pulses to the values of μ_1 and μ_2' of the elution peaks was neglected because of the extremely small size of the sample solution injected. As described above, for instance, the injection volume of the sample solution of n-hexylbenzene was ca. 300 μL because of the low solubility of the compound into the mobile phase solvent. It is not small in comparison with the conventional sample injection volume in HPLC. However, the retention volume of n-hexylbenzene in the RPLC systems using 70 vol.%

methanol at 298 K is around 100 mL (column #5) and 10 mL (#6). It is larger than the sample injection volume by a factor of ca. 30–300. The retention of n-hexylbenzene is so strong that the volume of the sample solution injected provides substantially no influence on the moment analysis of the elution peaks.

2.5.4. Correction for the external mass transfer kinetics

As described above, the contribution of the external mass transfer resistance to μ_2' was subtracted beforehand for determining D_e. The accuracy of the D_s values is influenced by the error in the estimation of k_f. In this study, k_f was estimated by the Wilson–Geankoplis equation [17]. For instance, the value of k_f is estimated as 3.4×10^{-2} cm s^{-1} for the external mass transfer of benzene at 298 K when the superficial velocity of the mobile phase solvent is 0.12 cm s^{-1}. On the other hand, according to another equation proposed by Kataoka et al. [27], a slightly different value of k_f is estimated as 2.6×10^{-2} cm s^{-1} under the same conditions. Resulting values of D_s are 7.2×10^{-6} cm^2 s^{-1} and 5.8×10^{-6} cm^2 s^{-1}, respectively. These two values differ by ca. 25%. However, the estimation error of k_f would provide smaller influence on D_s values because the contribution of the external mass transfer resistance to μ_2' is almost of the same order of magnitude with the other two kinetic processes, i.e., the axial dispersion and intraparticle diffusion, in RPLC systems, except for the case that the retention of sample compounds is extremely strong [1,2,6,7].

2.5.5. Correction for pore diffusion

The estimation error of D_p also affects the accuracy of the D_s values because the contribution of D_p to D_e is corrected when D_s is calculated from D_e. As explained above, D_p is calculated from D_m, ε_p, k_h, and k_t. The accuracy in the estimation of D_m influences the accuracy in the estimation of D_s. In this study, the Wilke-Chang equation [3,18,19] was used for estimating the D_m values. It is reported that D_m values are estimated by the equation in error less than about 10% [18]. However, the uncertainty of the estimation of D_m provides little influence on D_s values because surface diffusion usually has the major contribution to intraparticle diffusion [1,2,6,7]. For example, the contribution of surface diffusion to the overall mass transfer inside C_{18}-silica gel particles was quite significant. Most molecules, as much as nearly 85–95% or more, migrate in intraparticulate space by surface diffusion [1,2,6,7]. Because of the predominant contribution of surface diffusion to intraparticle diffusion, the influence of small variation in D_p (hence in D_m) on the estimate of D_s is negligibly small.

In order to derive more accurate values of D_s, the corrections described above were made for some parameters affecting the original experimental data of μ_1 and μ_2'. These corrections are responsible for the error made in the determination of D_s, which is estimated at 5–10% [1,2]. Additionally, in this study, the pulse response experiments were carried out under such conditions that the influence of some sources on the peak broadening as described above is minimized. Because of the relatively large diameter of the packing materials, the experimental values of μ_2'

Fig. 1. Correlation between D_s and C.
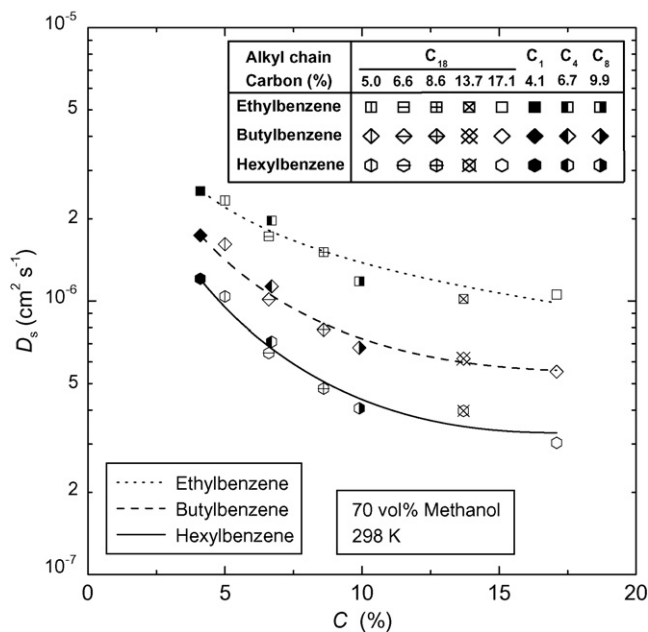
Fig. 2. Correlation between D_{s0} and E_s.

were originally large. This is the reason why the coarse silica gel particles were used in this study.

3. Results and discussion

3.1. Dependence of D_s on the retention

Fig. 1 illustrates the correlation of D_s experimentally measured against the carbon content (C) of the stationary phases, which depends on the density of C_{18} ligand and the alkyl chain length chemically bonded on the surface of the base silica gel. The D_s value gradually decreases with increasing C and tends to begin to plateau in the range of high value of C. The plots of D_s of the sample compounds fluctuate around each common curved line irrespective of the modification conditions of the stationary phase surface. These results in Fig. 1 seem to reflect two important characteristics of surface diffusion. First, the molecular migration by surface diffusion is restricted by the retentive interaction between the sample molecule and the stationary phase surface. Second, the mechanism of surface diffusion seems to be similar regardless of the density of C_{18} ligand and the alkyl chain length.

3.2. Enthalpy-entropy compensation of surface diffusion

It is well known that an equilibrium and/or a kinetic process is governed by a single mechanism when an EEC is established in a reaction system. In the following, some characteristics of surface diffusion are studied from the viewpoints of thermodynamics and extrathermodynamics. The temperature dependence of D_s was analyzed according to the Arrhenius equation.

$$D_s = D_{s0} \exp\left(\frac{-E_s}{RT}\right) \tag{1}$$

where D_{s0} and E_s are respectively the frequency factor and activation energy of surface diffusion, R the gas constant, and T the absolute temperature. The values of D_{s0} and E_s are calculated from the intercept and the slope of the conventional Arrhenius plot between $\ln D_s$ and the reciprocal of T.

Fig. 2 shows the plots between D_{s0} and E_s for each sample compound. They scatter around each straight line between $\ln D_{s0}$ and E_s, suggesting the existence of an EEC for surface diffusion. The results in Fig. 2 probably demonstrate the similarity in the mass transfer mechanism of surface diffusion. The slope of the parallel straight lines in Fig. 2 indicates a compensation temperature (T_c) of about 4.2×10^2 K for the sample compounds

Table 2
Compensation temperatures concerning surface diffusion

	$T_c^*(K)^a$	$T_c^*(K)^b$	$T_c^*(K)^c$		Confidence level $(1 - \alpha_s) \times 100\%$
			Minimum	Maximum	
Ethylbenzene	4.2×10^2	4.3×10^2	3.3×10^2	4.8×10^2	>90
n-Butylbenzene	4.2×10^2	4.3×10^2	3.1×10^2	5.2×10^2	>99
n-Hexylbenzene	4.2×10^2	4.2×10^2	3.5×10^2	4.8×10^2	>99

[a] T_c^* calculated from the slope of the linear correlation between in D_{s0} and E_s in Fig. 2.
[b] T_c^* calculated from the slope of the linear correlation between ΔH^* and ΔG_{Thm}^* in Fig. 4.
[c] Range of T_c^* at $(1 - \alpha_s) \times 100\%$ confidence level calculated by the estimation method proposed by Krug et al. [9].
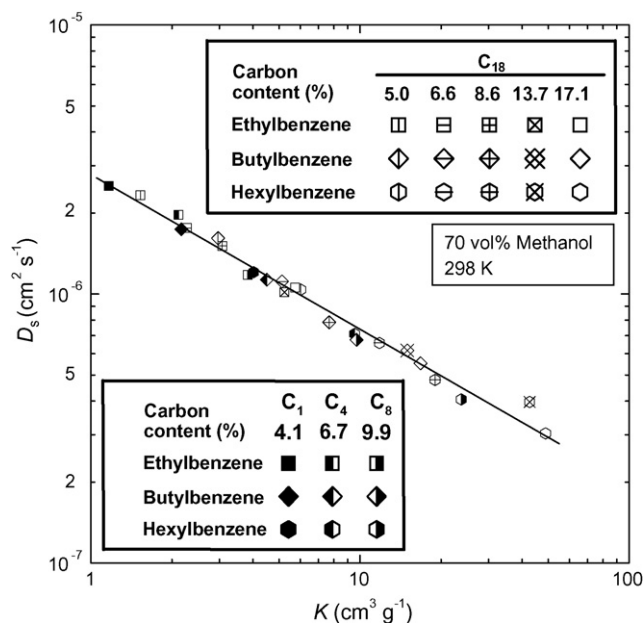
Fig. 3. Correlation between D_s and K.

(Table 2). This value of T_c is of the same order of magnitude as the previous results [28,29], although there is little information about the T_c values of surface diffusion in RPLC systems, i.e., ca. 3.7×10^2 K benzene derivatives and naphthalene in the RPLC system using a C_{18}-silica gel column and a mixture of tetrahydrofuran and water (50/50, v/v) [28] and ca. 6.0×10^2 K for *p*-alkylphenol derivatives in the RPLC system consisting of a C_{18}-silica gel column and an aqueous mixture of methanol (70 vol.%) [29].

3.3. Linear free energy relationships for surface diffusion

A linear free energy relationship is another extrathermodynamic relationship, which has also been used to demonstrate the mechanistic similarity of various chemical equilibria and/or kinetic processes. It is expected that a LFER is observed when an EEC is established. Fig. 3 illustrates a linear correlation at 298 K between $\ln D_s$ and $\ln K$. The plots gather around the single straight line, in spite of the variation in the C_{18} ligand density and the alkyl chain length. The results in Fig. 3 again suggest that the mechanism of surface diffusion is essentially identical irrespective of the modification conditions of the stationary phase surface. The linear line in Fig. 3 also provides a thermodynamic information about the mechanism of surface diffusion. The slope of the linear line between $\ln D_s$ and $\ln K$ is about -0.6. This means that the value of E_s is about three fifths of the enthalpy change due to the retention.

3.4. More detailed analyses of EEC of surface diffusion

The enthalpy change (ΔH) and the entropy change (ΔS) relating to a kinetic process are usually estimated from the temperature dependence of a rate coefficient on the basis of the Arrhenius equation. The values of ΔH and ΔS are conventionally calcu-

lated from the slope and intercept of a linear correlation between the logarithmic value of the rate coefficient and the reciprocal of T, respectively. When the two thermodynamic parameters are linearly correlated with each other, the existence of an EEC in the kinetic process is assumed and the value of T_c is estimated from the slope of the linear correlation between the two thermodynamic parameters. However, Krug et al. [9–11] pointed out some drawbacks of the ordinary procedure for deriving the two thermodynamic parameters and for discussing the existence of the EEC. They warned that the linear correlation between ΔH and ΔS thus measured by the conventional procedure does not directly demonstrate the establishment of the EEC. Even if no real EEC effect takes place, a linear correlation can be observed between ΔH and ΔS under certain circumstances. In such a case, this apparent EEC results from the errors made in the determination of the two thermodynamic parameters based on the linear regressions of the Arrhenius plots.

There are two essential problems in the conventional procedure based on the ordinary Arrhenius equation for deriving the thermodynamic parameters, i.e., ΔH and ΔS, and for analyzing the extrathermodynamic relationship, i.e., EEC. One is the dependence of ΔS on ΔH. The value of the intercept (i.e., ΔS) of the extrapolated Arrhenius plot varies depending on the change in the value of the slope (i.e., ΔH). The other is the long distance between the intercept of the extrapolation and the data points plotted at the experimental temperatures. Additionally, it is also significant that the distance is much longer than the usual experimental temperature range of RPLC. It seems that we can usually carry out RPLC measurements in the range from ca. 273 to 323 K, at maximum. The potential for the errors should be extremely high because the intercept at $1/T = 0$ is far from the experimental data points. Even if the variation of the slope of the ordinary linear Arrhenius plot is quite small, it would lead to a large fluctuation in the intercept.

Krug et al. [9–11] indicated that the slope and the correlation coefficient of the linear correlation between ΔH and ΔS are equal to the harmonic mean temperature (T_{hm}) and close to unity, respectively, in the case of an apparent EEC. They also proposed four different approaches to clarify whether the linear correlation between ΔH and ΔS originates from substantial physico-chemical effects or from the statistical compensation due to the experimental errors [9–11]. In the following, the four methods proposed by Krug et al. were applied to the experimental data of this study in order to demonstrate that a real EEC takes place for surface diffusion.

3.4.1. Plot of ΔH^* versus ΔG^*_{Thm}

The temperature dependence of D_s was analyzed using the following equation.

$$\ln D_s = -\frac{\Delta H^*}{RT} + \frac{\Delta S^*}{R} + \ln\left(\frac{\lambda^2 k_B T}{h}\right) \tag{2}$$

where the superscript * refers to the thermodynamic parameters measured by analyzing the temperature dependence of D_s. The parameters k_B and h are the Boltzmann and the Planck constants, respectively. According to the absolute rate theory [30], the dis-
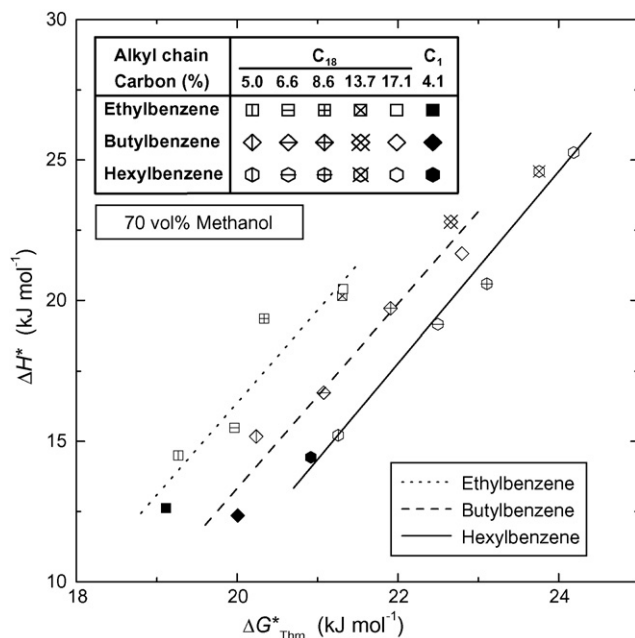
Fig. 4. Correlation between ΔH^* and G^*_{Thm}.

tance between two equilibrium positions (λ) was estimated as 3×10^{-10} m from the D_s values of various molecules, which are of the order of 10^{-10} m^2 s^{-1} in methanol/water (70/30, v/v) at 298 K [2,31].

Krug et al. [9–11] claimed that the value of ΔH^* should be linearly correlated with that of $\Delta G^*_{\mathrm{Thm}}$ (ΔG^* at T_{hm}) if there is a real EEC for surface diffusion. Because of the two major problems of the ordinary analytical procedure of the temperature dependence of D_s using the Arrhenius equation, they recommended that ln D_s should be plotted against $\{1/T - \langle 1/T \rangle\}$, rather than $1/T$. The brackets ($\langle \rangle$) means an average value. The values of ΔH^* and $\Delta G^*_{\mathrm{Thm}}$ for surface diffusion were respectively calculated from the slope and the intercept of the linear plot between ln D_s and $\{1/T - \langle 1/T \rangle\}$ [9–11].

$$\Delta H^* = -R\,(\text{slope}) - RT_{\mathrm{hm}} \tag{3}$$

$$\Delta G^*_{T_{\mathrm{hm}}} = -RT_{\mathrm{hm}}\,(\text{intercept}) + RT_{\mathrm{hm}}\,\ln\left(\frac{\lambda^2 e k_{\mathrm{B}} T}{h}\right) - RT_{\mathrm{hm}} \tag{4}$$

where e is the base of the natural logarithm. Fig. 4 illustrates the linear correlations between ΔH^* and $\Delta G^*_{\mathrm{Thm}}$ for each sample compound. As listed in Table 2, the compensation temperature of surface diffusion (T_c^*) is calculated from the slope of the straight lines in Fig. 4 as ca. $4.2–4.3 \times 10^2$ K for the sample compounds, according to $T_c = T_{\mathrm{hm}}/\{1 - 1/(\text{slope})\}$. The result is in agreement with the previous value of T_c, which was estimated from the slope of the linear line in Fig. 2.

3.4.2. Comparison of T_c^* with T_{hm} (hypothesis test)

Krug et al. claimed that T_c^* should be sufficiently different from T_{hm} (= 298 K) and that the null hypothesis, $T_c^* = T_{\mathrm{hm}}$, must be rejected when the EEC originates from substantial com-

pensation effects [9]. Table 2 lists the calculated values of T_c^* (minimum) and T_c^* (maximum). It is obvious that the hypothesis can be rejected for surface diffusion in the RPLC systems at the high confidence levels.

3.4.3. Convergence of the conventional Arrhenius plots at T_c^*

Fig. 5a–c illustrate the conventional Arrhenius plots of the sample compounds between ln D_s and $1/T$. The linear correlations properly intersect in a small region of the plane. It is suggested that almost the same values of D_s would be observed for each sample compound around the intersection points irrespective of the density of C_{18} and C_1 ligands. In addition, the intersection points seem to locate in the range of the reciprocal of T between ca. 2 and 2.5×10^{-3} K^{-1}. This means that the T_c values estimated from the intersection points in Fig. 5a–c range from ca. $4–5 \times 10^2$ K. This is properly close to the values of T_c^* listed in Table 2, which are estimated from the slope of the linear correlations between ln D_{s0} and E_s in Fig. 2 and that between ΔH^* and $\Delta G^*_{\mathrm{Thm}}$ in Fig. 4.

3.4.4. Probability for the intersection of the Arrhenius plots

The probability of the intersection of the conventional Arrhenius plots illustrated in Fig. 5a–c was compared with that of a nonintersection on the basis of the statistical data derived by an analysis of variance (ANOVA) procedure [11]. The probability of the nonintersection was also compared to the precision of the experimental data in the same manner. Table 3 lists the values of the mean sum of squares (MS) calculated. The MS values of the intersection (MS$_{\mathrm{con}}$) are more than one or two orders of magnitude larger than those of the nonintersection (MS$_{\mathrm{noncon}}$). The ratio MS$_{\mathrm{con}}$/MS$_{\mathrm{noncon}}$ for the three sample compounds is larger than the corresponding F-value, $F(1, 4, 1 - \alpha_s = 0.99) = 21.2$. These results indicate that the probability of the intersection is high enough in comparison with that of the nonintersection irrespective of the sample compounds. On the other hand, the absolute values of the ratio of MS$_{\mathrm{noncon}}$ to the mean sum of squares of the residuals (MS$_{\varepsilon}$) are smaller than the corresponding F-value, $F(4, 5, 1 - \alpha_s = 0.99) = 11.4$. Although the negative values of MS$_{\varepsilon}$ for butylbenzene and hexylbenzene are probably unreasonable, they seem to originate from calculation errors. The small absolute values of MS$_{\varepsilon}$ probably suggest that the variation due to the measurement errors is quite small. It is concluded that the variation due to the nonconcurrence is not greater than that due to the measurement errors at the $100\alpha_s\%$ level of significance.

3.5. Estimation of D_s

As described above, it is demonstrated that a real EEC based on substantial physico-chemical effects takes place for surface diffusion and that the LFER is established between the retention equilibrium and surface diffusion in the RPLC systems. These results suggest that the mechanism of surface diffusion of the sample compounds is the same irrespective of the alkyl chain length and the density of C_1 and C_{18} ligands on the stationary phase surface. It seems that the sample molecules migrate in parallel by surface diffusion on the patches bonded with C_1 lig-
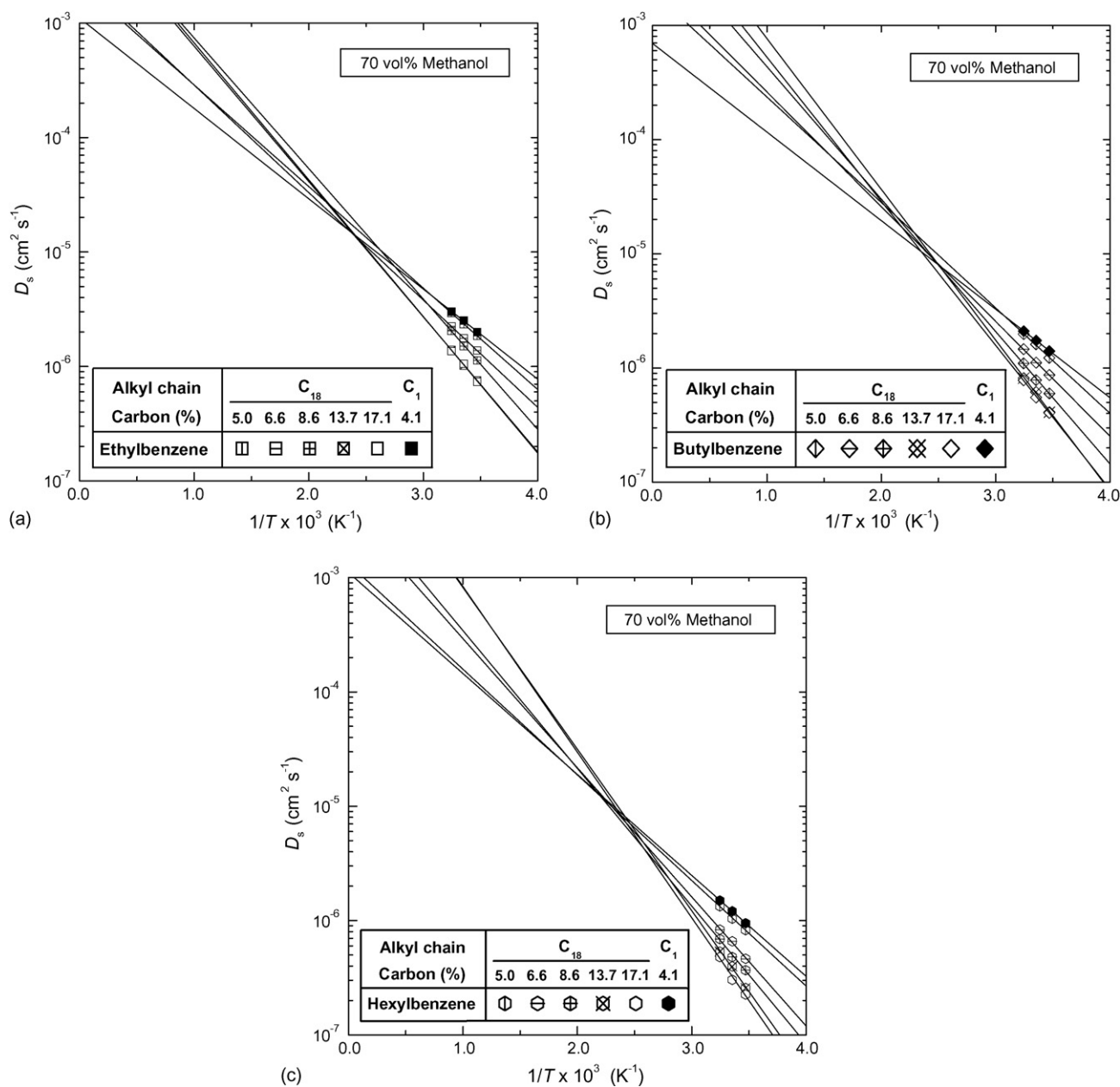
Fig. 5. Conventional Arrhenius plot of (a) ethylbenzene; (b) butylbenzene, and (c) hexylbenzene.

and and those with C_{18} ligand and that the total mass flux due to surface diffusion consists of the contributions of the molecular migration on the two types of alkyl ligands bonded areas. It is reasonable to assume that the contributions on the C_1 and C_{18} ligands modified surfaces are additive.

$$D_s = D_{s,C_1} + D_{s,C_{18}} \qquad (5)$$

where the subscripts C_1 and C_{18} respectively stand for the contribution of the mass flux by surface diffusion on the C_1 ligand bonded area and that on the C_{18} ligand bonded one to D_s. On the other hand, neither hydrophobic retention nor surface diffusion takes place when there is no alkyl ligand on the surface of the base silica gel. This means that, when the concentration gradient is the same, the higher the alkyl ligand density is, the larger

the mass flux due to surface diffusion per unit area and per unit time becomes. As a first approximation, it is assumed that D_s is proportional to the ligand density (σ).

$$D_{s,C_1} = \delta_{s,C_1}\sigma_{C_1} \qquad (6)$$

$$D_{s,C_{18}} = \delta_{s,C_{18}}\sigma_{C_{18}} \qquad (7)$$

where δ_s is the hypothetical surface diffusion coefficient, which is D_s normalized by σ. In other words, the value of δ_s would be measured by using silica gel particles chemically modified only with C_1 or C_{18} ligands of unit density. The values of δ_{s,C_1} and $\delta_{s,C_{18}}$ are respectively calculated as the ratio of D_s to σ from the values $D_{s,\text{TMS}}$ and $D_{s,\text{ODS}}$, which were measured using the columns #6 and #5 because the packing materials in the columns contain only C_1 and C_{18} ligands.

Table 3
ANOVA table for surface diffusion

Source of variation	DF[c]	SS[d]	MS[e]	Ethylbenzene ($p^{a}=6$, $q^{b}=3$)			n-Butylbenzene ($p^{a}=6$, $q^{b}=3$)			n-Hexylbenzene ($p^{a}=6$, $q^{b}=3$)		
				DF[c]	SS[d]	MS[e]	DF[c]	SS[d]	MS[e]	DF[c]	SS[d]	MS[e]
Total	$pq-1$	SS_T	MS_T	17	3.1	1.8×10^{-1}	17	4.5	2.6×10^{-1}	17	5.4	3.2×10^{-1}
Rows (samples)	$p-1$	SS_R	MS_R	5	2.2	4.5×10^{-1}	5	3.5	7.0×10^{-1}	5	4.3	8.6×10^{-1}
Columns (temperatures)	$q-1$	SS_C	MS_C	2	8.3×10^{-1}	4.1×10^{-1}	2	9.3×10^{-1}	4.7×10^{-1}	2	1.1	5.5×10^{-1}
Interactions	$(p-1)(q-1)$	SS_{RC}	MS_{RC}	10	7.4×10^{-2}	7.4×10^{-3}	10	1.7×10^{-2}	1.7×10^{-3}	10	8.6×10^{-3}	8.6×10^{-4}
Slope	$p-1$	SS_S	MS_S	5	2.0×10^{-2}	4.0×10^{-3}	5	3.0×10^{-2}	5.9×10^{-3}	5	3.8×10^{-2}	7.6×10^{-3}
Concurrence	1	SS_{con}	MS_{con}	1	1.8×10^{-2}	1.8×10^{-2}	1	2.8×10^{-2}	2.8×10^{-2}	1	3.8×10^{-2}	3.8×10^{-2}
Nonconcurrence	$p-2$	SS_{noncon}	MS_{noncon}	4	2.0×10^{-3}	5.0×10^{-4}	4	1.2×10^{-3}	3.1×10^{-4}	4	5.9×10^{-4}	1.5×10^{-4}
Residuals	$(p-1)(q-2)$	SS_L	MS_L	5	5.4×10^{-2}	1.1×10^{-2}	5	-1.3×10^{-2}	-2.6×10^{-3}	5	-3.0×10^{-2}	-5.9×10^{-3}

[a] p is the number of the stationary phases.
[b] q is the number of experimental temperatures.
[c] DF is the degree of freedom.
[d] SS is the sum of squares.
[e] MS is the mean sum of squares, MS = SS/DF, for each source of variation.
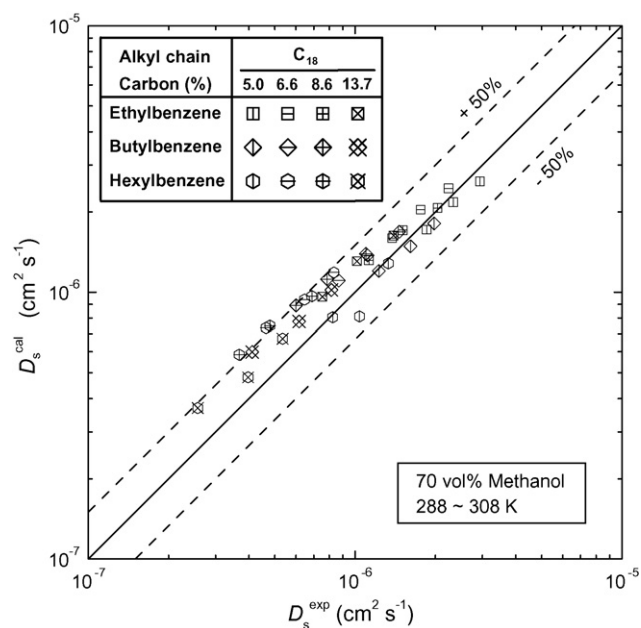
Fig. 6. Comparison of D_s^{exp} with D_s^{cal} estimated from the corresponding $D_{s,TMS}$ and $D_{s,ODS}$ values.

In Fig. 6, the values of D_s for the columns #1–#4 calculated, according to Eqs. (5)–(7), from δ_{s,C_1}, $\delta_{s,C_{18}}$, σ_{C_1}, and $\sigma_{C_{18}}$ are compared with those of D_s experimentally measured at 288, 298, and 308 K. The values of δ_{s,C_1} and $\delta_{s,C_{18}}$ at each temperature were calculated from the experimental values of $D_{s,TMS}$ and $D_{s,ODS}$ of the three sample compounds. The plots fluctuate in the vicinity of the diagonal line having the slope of unity. The mean square deviation (MSD) was calculated according to the following equation:

$$\text{MSD} = \left[\left(\frac{1}{N}\right)\sum\left[\left(\frac{D_s^{cal}-D_s^{exp}}{D_s^{exp}}\right)\right]^2\right]^{1/2} \tag{8}$$

where N is the number of data pairs of (D_s^{exp} and D_s^{cal}). The value of MSD was calculated as 0.30 for the plots in Fig. 6. The results in Fig. 6 demonstrate that the value of D_s can be estimated from δ_s and σ on the basis of Eqs. (5)–(7).

It was additionally attempted to estimate D_s values under given conditions of the C_1 and C_{18} ligand density, the sample compounds, and the column temperatures from a limited number of original experimental D_s data. The two arrows in Fig. 7 indicate the original D_s data of n-hexylbenzene at 298 K for the columns #6 (TMS) and #5 (ODS). All the D_s plots in Fig. 7 were calculated from the two original data (solid and open hexagonal symbols) plotted on the diagonal line. At first, the values of δ_{s,C_1} and $\delta_{s,C_{18}}$ of n-hexylbenzene at 298 K were calculated from the two original D_s plots. Then, the δ_{s,C_1} and $\delta_{s,C_{18}}$ values of the three sample compounds at given temperatures were calculated on the basis of a thermodynamic LFER model from molecular thermodynamic parameters and compensation temperatures. In a previous paper [32], surface diffusion phenomena on the surface of RP stationary phases bonded with alkyl ligands of different chain lengths (C_1, C_4, C_8, and C_{18}) were studied from

Fig. 7. Comparison of D_s^{exp} with D_s^{cal} estimated from only two experimental data of D_s of n-hexylbenzene on the stationary phases #5 and #6 at 298 K (indicated by the arrows).

Table 4
Molecular thermodynamic parameters

	a_s (kJ mol^{-1} K^{-1})	b_s (kJ mol^{-1} K^{-1})	b_h (kJ mol^{-1})
Ethylbenzene	2.2×10^{-3}	-3.9×10^{-2}	1.0×10^1
n-Butylbenzene	2.7×10^{-3}	-4.5×10^{-2}	9.7
n-Hexylbenzene	3.1×10^{-3}	-4.4×10^{-2}	1.1×10^1

Fig. 7 illustrates that the D_s values thus estimated are plotted around the diagonal line within the range of a relative error less than ca. 50%, respective of the RPLC conditions of the density of C_1 and C_{18} ligands, the sample compounds, and the temperatures. The value of MSD was calculated as 0.25 for the plots in Fig. 7. The results in Figs. 6 and 7 prove the assumption that the contributions of C_1 and C_{18} ligands to the molecular migration by surface diffusion are additive and that the contributions of the tw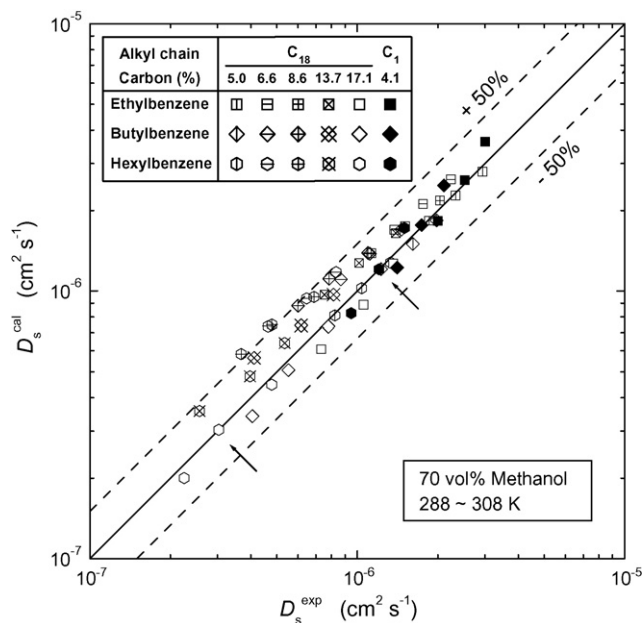o alkyl ligands are calculated as the product of δ_s and σ. It is also suggested that each contribution of C_1 and C_{18} ligands to surface diffusion can separately be evaluated from the experimental data of D_s.

4. Conclusion

Surface diffusion data in the RPLC systems using silica gels bonded with mixtures of C_1 and C_{18} alkyl ligands at different densities were analyzed from the viewpoints of two extrathermodynamic relationships, i.e., EEC and LFER. First, it was demonstrated that the real EEC of surface diffusion based on the substantial physico-chemical effects is observed. Surface diffusion data were analyzed in detail by applying the modified Arrhenius plot and the four tests proposed by Krug et al. The LFER between the retention equilibrium and surface diffusion is also observed irrespective of the chain length of alkyl ligands and of the density of C_1 and C_{18} ligands, suggesting the similarity in the mechanism of surface diffusion on the different alkyl ligands bonded silica gels.

Then, a new LFER model based on the real EEC was used to predict D_s values under different RPLC conditions. The values of MSD for the predictions range around 25–30% regardless of the simultaneous change of the RPLC conditions, i.e., the sample compound, the composition and density of the bonded ligands (C_1 and C_{18}), and the column temperature. These results allow us to assume that the contributions of C_1 and C_{18} ligands to surface diffusion are additive and that the contribution of each alkyl ligand is calculated as the product of δ_s and σ. It is also indicated that the LFER model (Eqs. (10) and (11)) provides a new information about the diffusive molecular migration on the stationary phase surface and is effective for explaining the change in the manner of surface diffusion under different RPLC conditions.

the viewpoints of thermodynamics and extrathermodynamics. The thermodynamic LFER model was proposed for representing the characteristics of a LFER concerning surface diffusion between two RPLC systems.

$$\ln \delta_{s T_2}^{SMP} = A \ln \delta_{s T_1}^{REF} + B \qquad (9)$$

The slope (A) and intercept (B) of the LFER are formulated as follows:

$$A = \frac{a_s^{SMP} T_1 (T_c^{SMP} - T_2)}{a_s^{REF} T_2 (T_c^{REF} - T_1)} \qquad (10)$$

$$B = \frac{1}{RT_2} \left[A \left(\frac{T_2}{T_1} \right) (b_h^{REF} - T_1 b_s^{REF}) - (b_h^{SMP} - T_2 b_s^{SMP}) \right]$$
$$+ (A - 1) \ln \left(\frac{h}{\lambda^2 k_B} \right) + (\ln T_2 - A \ln T_1) \qquad (11)$$

where T_1 and T_2 are the experimental temperatures. The values of a and b are the molecular thermodynamic parameters, which represent a linear correlation between the thermodynamic parameters, ΔH and ΔS, and the number of methylene unit (C_n) in the alkyl ligands [33,34]. The subscripts h and s denote ΔH and ΔS, respectively. The value of a_s is ΔS per unit value of C_n and those of b_h and b_s are respectively ΔH and ΔS at $C_n = 0$. The superscripts REF and SMP stand for the reference and sample systems, respectively. Table 4 lists the values of a_s, b_s, and b_h. The δ_{s,C_1} and $\delta_{s,C_{18}}$ values for each condition were calculated according to Eqs. (10) and (11). Finally, the values of D_s for all the columns were estimated on the basis of Eqs. (5)–(7) by adding the contributions of D_{s,C_1} and $D_{s,C_{18}}$, which were respectively calculated as the product of the value of δ_{s,C_1} and σ_{C_1} and that of $\delta_{s,C_{18}}$ and $\sigma_{C_{18}}$.

Acknowledgment

References

[1] K. Miyabe, G. Guiochon, J. Sep. Sci. 26 (2003) 155.

[2] K. Miyabe, G. Guiochon, Adv. Chromatogr. 40 (2000) 1.

[3] G. Guiochon, S. Golshan-Shirazi, A.M. Katti, Fundamentals of Preparative and Nonlinear Chromatography, Academic Press, Boston, 1994 (Chapters 2, 5, 6).

[4] M. Suzuki, Adsorption Engineering, Kodansha/Elsevier, Tokyo, 1990 (Chapters 4 and 6).

[5] D.M. Ruthven, Principles of Adsorption & Adsorption Processes, John Wiley and Sons, New York, 1984 (Chapters 5–8).

[6] K. Miyabe, A. Cavazzini, F. Gritti, M. Kele, G. Guiochon, Anal. Chem. 75 (2003) 6975.

[7] K. Miyabe, G. Guiochon, J. Sep. Sci. 27 (2004) 853.

[8] J.C. Giddings, Dynamics of Chromatography. Part I. Principles and Theory, Marcel Dekker, New York, 1965 (Chapter 6).

[9] R.R. Krug, W.G. Hunter, R.A. Grieger, J. Phys. Chem. 80 (1976) 2335.

[10] R.R. Krug, W.G. Hunter, R.A. Grieger, J. Phys. Chem. 80 (1976) 2341.

[11] R.R. Krug, Ind. Eng. Chem. Fundam. 19 (1980) 50.

[12] M.J.M. Wells, C.R. Clark, Anal. Chem. 53 (1981) 1341.

[13] L.C. Sander, S.A. Wise, CRC Crit. Rev. Anal. Chem. 18 (1987) 299.

[14] M. Suzuki, J.M. Smith, Chem. Eng. Sci. 26 (1971) 221.

[15] M. Suzuki, J. Chem. Eng. Jpn. 6 (1973) 540.

[16] M. Suzuki, J.M. Smith, Adv. Chromatogr. 13 (1975) 213.

[17] E.J. Wilson, C.J. Geankoplis, Ind. Eng. Chem. Fundam. 5 (1966) 9.

[18] R.C. Reid, J.M. Prausnitz, B.E. Poling, The Properties of Gases and Liquids, fourth ed., McGraw-Hill, New York, 1977 (Chapter 11).

[19] R.B. Bird, W.E. Stewart, E.N. Lightfoot, Transport Phenomena, second ed., John Wiley & Sons, New York, 2002 (Chapter 17).

[20] C.N. Satterfield, C.K. Colton, W.H. Pitcher Jr., AIChE J. 19 (1973) 628.

[21] K. Miyabe, G. Guiochon, J. Chromatogr. A 830 (1999) 263.

[22] K. Miyabe, G. Guiochon, J. Chromatogr. A 830 (1999) 29.

[23] K. Miyabe, G. Guiochon, J. Chromatogr. A 857 (1999) 69.

[24] K. Miyabe, G. Guiochon, Anal. Chem. 72 (2000) 5162.

[25] K. Miyabe, G. Guiochon, J. Chromatogr. A 890 (2000) 211.

[26] I. Quiñones, G. Guiochon, J. Chromatogr. A 796 (1998) 15.

[27] T. Kataoka, H. Yoshida, K. Ueyama, J. Chem. Eng. Jpn. 5 (1972) 132.

[28] K. Miyabe, S. Sotoura, G. Guiochon, J. Chromatogr. A 919 (2001) 231.

[29] K. Miyabe, G. Guiochon, Anal. Chem. 74 (2002) 5754.

[30] S. Glasstone, K.J. Laidler, H. Eyring, The Theory of Rate Processes, McGraw-Hill, New York, 1964 (Chapter 9).

[31] K. Miyabe, G. Guiochon, Anal. Chem. 73 (2001) 3096.

[32] K. Miyabe, G. Guiochon, J. Phys. Chem. B 109 (2005) 12038.

[33] A. Vailaya, C. Horváth, J. Phys. Chem. 100 (1996) 2447.

[34] B. Lee, Proc. Natl. Acad. Sci. U.S.A. 88 (1991) 5154.

As, Bi, Sb and Sn determination in atmospheric particulate matter by direct solid sampling-hydride generation-electrothermal atomic absorption spectrometry

Jorge Moreda-Piñeiro [a,*], Carmen Moscoso-Pérez [a], María Piñeiro-Iglesias [b], Purificación López-Mahía [a,b], Soledad Muniategui-Lorenzo [a], Esther Fernández-Fernández [a], Darío Prada-Rodríguez [a,b]

[a] *Department of Analytical Chemistry, Faculty of Sciences, University of A Coruña, Campus da Zapateira s/n, E-15071 A Coruña, Spain*
[b] *University Institute of Environment, University of A Coruña, Pazo de Lóngora, Liáns, E-15179 Oleiros, Spain*

Abstract

A novel, rapid and simple method by hydride generation-electrothermal atomic absorption spectrometry (HG-ETAAS) after direct As, Bi, Sb and Sn hydrides generation from untreated filters of atmospheric particulate matter (PM_{10} and $PM_{2.5}$) was optimised. PM_{10} and $PM_{2.5}$ were not subjected to any pre-treatment: circular portions between 0.28 and 6.28 cm^2 were directly placed into the reaction vessel of a batch mode generation system. A $2^8 \times 3/64$ Plackett–Burman design was used as a multivariate strategy for the evaluation of the effects of several variables affecting the hydride generation, trapping and atomisation efficiencies. Trapping temperature was the most statistically significant variable for As, Bi and Sn. Atomisation temperature was also statistically significant for Sb determination. Optimum values of significant variables were selected by using univariate optimisation approaches. An aqueous calibration method was used throughout. The developed method has been found to be precise with relative standard deviations of 6.2, 5.3, 9.1 and 7.5% for 11 determinations in a filter sample containing 0.7, 1.0, 1.4 and 1.7 $\mu g \, l^{-1}$ for As, Bi, Sb and Sn, respectively. Results obtained by direct solid sampling-HG-ETAAS have been found statistically comparable with those obtained after conventional method based on an acid digestion followed to ICP-MS. Absolute detection limits were 37, 15, 30, and 41 $ng \, l^{-1}$ for As, Bi, Sb and Sn, respectively. Detection limits referred to the air volume sampled (in the range of 0.020–0.050 $ng \, m^{-3}$) were low enough for the determination of several hydride-forming elements from PM_{10} and $PM_{2.5}$ samples collected in a non-polluted suburban area of A Coruña (NW Spain).
© 2006 Elsevier B.V. All rights reserved.

Keywords: Direct analysis; PM_{10} and $PM_{2.5}$; Hydride elements forming

1. Introduction

The close association between atmospheric particulate matter concentration and public health has been recently proved in epidemiological studies [1]. Thus, the characterisation of atmospheric aerosol composition is mandatory. Trace metals are a part of the atmospheric pollutants and their determination in the total suspended particles (TSP) as well as in the inhalable fraction (PM_{10} and $PM_{2.5}$) offers useful information when evaluating the interaction between air pollutants and public health [2,3]. The study of toxic element concentrations in inhalable fractions

(mean particulate matter which passes through a size-selective inlet with a 50% efficiency cut-off at 10 μm aerodynamic diameters for PM_{10} fraction or 2.5 μm aerodynamic diameters for $PM_{2.5}$ fraction) is more important than in TSP due to those fractions could reach the lower respiratory tract [4].

Although several techniques such as neutron activation analysis (NAA) and, recently, laser ablation (LA) and electrothermal vaporisation (ETV) coupled with inductively coupled plasma mass spectrometry (ICP-MS), do not require sample pre-treatment, their use have not been extensively applied to metal determination from particulate matter [5–11]. These techniques require instrumentation that has limited availability in many laboratories because of expense. On the other hand, atomic analytical methodologies require previous time-consuming sample pre-treatment such as acid mechanical

---

Table 1
Optimum spectrometer, hydride generation, and trapping and atomisation conditions for direct As, Bi, Sb and Sn determination from PM_{10} and $PM_{2.5}$ by HG-ETAAS

	Wavelength (nm)	Slit width (nm)	Lamp current (mA)
Spectrometer operating conditions			
As	193.7	0.7	380
Bi	223.1	0.2	382
Sb	217.6	0.2	410
Sn	286.3	0.7	325

	Circular portion area (cm^2)	[HCl] (mol l^{-1})	[NaBH$_4$] (%, w/v)	Reaction volume (ml)	Ar flow rate (mL min^{-1})
Hydride generation conditions					
As	0.28	0.5	1.0	5.0	50
Bi	2×3.14	0.5	1.0	5.0	50
Sb	0.28	0.5	1.0	5.0	50
Sn	2×3.14	0.5	1.0	5.0	50

	Step	Temperature (°C)	Ramp (s)	Hold (s)	Ar flow rate (mL min^{-1})
Trapping and atomisation conditions					
As	Collection	1000	1	30	250
	Atomisation	2000	0	3	100 (read)
	Cleaning	2500	1	3	250
Bi	Collection	100	1	30	250
	Atomisation	2000	0	3	0 (read)
	Cleaning	2300	1	3	250
Sb	Collection	400	1	30	250
	Atomisation	2100	0	5	0 (read)
	Cleaning	2300	1	3	250
Sn	Collection	1000	1	30	250
	Atomisation	2000	0	3	0 (read)
	Cleaning	2300	1	3	250

agitation, ultrasonic or microwave treatment [12–23], sequential leaching procedures [17,24,25] and acidified water sub-critical extraction [26]. Vapour generation techniques coupled to atomic absorption, atomic fluorescence and atomic emission detectors (VG-AAS [14,27], VG-AFS [13,15,24], VG-ICP-OES/MS [19,22,28]) have been also used for hydride forming elements determination in acid extracts from atmospheric particulate matter due to its simplicity, high sensitivity and relative freedom from interferences. Otherwise, these methodologies cannot be considered as environmentally friendly process due to the use of toxic reagents/acids at high concentrations during the sample pre-treatment.

Although chemical hydride generation has been used for the direct determination of hydride forming metals in slurred samples [29], the direct hydride generation from solid samples (without slurry preparation) has not been investigated. The avoidance of sample pre-treatment (short analysis time and corrosive and dangerous reagents removal) and the removal of sample contamination and analyte losses are the main advantages of the solid sampling technique, while the main drawback could be associated to the low vapour generation efficiency from the metal trapped into the solid particles. However, this drawback is negligible when PM_{10} and $PM_{2.5}$ are analysed, since hydride elements forming are contained into small particles (<10 and 2.5 μm). Therefore, these trace elements could easily pass

to the liquid phase and generate hydrides under conventional hydride generation conditions.

In this paper, we investigate the possibility of direct hydride generation from untreated PM_{10} and $PM_{2.5}$ samples. The target analytes As, Bi, Sb and Sn have been determined using hydride generation coupled to electrothermal atomic absorption spectrometry (HG-ETAAS). The main advantage and novelty of the proposed methods is that filters are not pre-treated, i.e. acid extraction or slurry preparation is not required.

2. Experimental

2.1. Apparatus

An Aanalyst 800 (Perkin-Elmer) equipped with electrodeless discharge lamps (System 2) was used to measure arsenic, bismuth, antimony and tin. The operating conditions are shown in Table 1. An MHS-10 hydride generation system (Perkin-Elmer) was used for hydride generation. The vapour-furnace sample transfer tube consists of quartz capillary (2 cm long × 1.3 mm o.d. × 0.5 mm i.d.). The tube is attached to a metal mount with a short piece of silicone rubber tubing, which in turn is attached to a PTFE tube. The metal mount of the FIAS furnace sample transfer tube was loaded into the spring clip at the end of the autosampler arm. A pyrolytic coated graphite tube with pyrolytic

Table 2
ICP-MS operating conditions for As, Bi, Sb and Sn determination from PM$_{10}$ and PM$_{2.5}$ by ICP-MS

Forward power (W)	1350
Gas flows (l min^{-1})	
Nebulizer	0.8
Auxiliary	0.9
Coolant	15.0
Nebulizer type	Cross flow
Data acquisition for quantitative analysis	Peak jump
Internal standard	^{115}In, ^{45}Sc, ^{205}Tl
Isotopes monitored	^{75}As, ^{209}Bi, ^{121}Sb, ^{120}Sn

platform treated with Ir was used [30]. An integrated absorbance signal was also used throughout.

An ICP-MS Plasma Quad II-SOption (Thermo Instruments, Austin, TX, USA) was used for digested PM$_{10}$ and PM$_{2.5}$ analysis. The operating parameters and the isotope masses employed are shown in Table 2.

2.2. Reagents

All solutions were prepared from analytical reagent grade chemicals using ultra-pure water, with a resistivity of 18 MΩ cm, which was obtained from a Milli-Q water purification system (Millipore, Bedford, MA, USA). Arsenic, bismuth, antimony and tin stock standard solutions, 1000 mg l^{-1} (Panreac, Barcelona, Spain) were used. Sodium tetrahydroborate (Aldrich) dissolved in 0.5% (w/v) of sodium hydroxide (Panreac) was used as reducing solution. This solution was prepared daily and filtered before use. Hydrochloric acid solution, prepared from hydrochloric acid solution, 37% (Panreac). Nitric acid 69–70% (Baker, Phillipsburg, PA, USA), hydrofluoric acid 48–51% (Baker) and perchloric acid 69–72% (Baker) were used for acid digestion. Argon C-45 purity (99.995%) (Carburos Metálicos, Barcelona, Spain) was used as purge gas.

2.3. Atmospheric particulate matter sample collection

Atmospheric particulate matter samples were collected in a non-polluted suburban area (Oleiros, latitude 43.2 °N, longitude 8.17 °W) of A Coruña, Spain in 2004. A Digitel Automatic High Volume Dust Sampler DA80 (recommended by the Commission of European Communities [31]), was used for PM$_{2.5}$ particulate matter collection on QF20 quartz fiber filters (15 cm diameter), Schleicher & Schuell, D-Dassel, Germany. The atmospheric particulate matter was collected by using an aspiration volume of 30 m^3 h^{-1} during 24 h. A Graseby–Andersen high volume sampler, which meet the requirements of UNE EN 12341 European Norm [32], was used for PM$_{10}$ particulate matter collection on QF20 quartz fiber filters (27 cm × 15 cm) by using an aspiration volume of 68 m^3 h^{-1} during 24 h. Preceding sampling, filters were pre-heated at 400 °C for 12 h and then, weighed after 48-h conditioning in a desiccator at constant temperature (20 ± 1 °C) and relative humidity conditions (50 ± 5) according to EN 12341 European Norm [30]. Afterwards, PM$_{10}$ and PM$_{2.5}$ samples were stored in a freezer (−18 °C) until further analysis.

2.4. Procedure for direct PM$_{10}$ and PM$_{2.5}$ samples measurements by HG-ETAAS

A circular portion of 0.28 cm^2 (for As and Sb determination) and two circular portions of 3.14 cm^2 (for Bi and Sn determination) were cut from the PM$_{10}$ and PM$_{2.5}$ using a hollow and sharp-edged steel cylinder (Selecta, Barcelona, Spain) when filters from suburban area were studied. Low circular portion areas (0.14 and 0.28 cm^2 for As and Sb and Bi and Sn determination, respectively) should be used for polluted urban areas. The spatial variability of the target metal concentrations was studied analysing several cutting position. Practically around 120 and 30 filter disks (the area of each filter disk is 3.14 cm^2) can be cut from the 27 cm × 15 cm and 15 cm diameter filters, respectively. A distribution pattern of the metals studied was not observed when all filter disks were analysed. Relative standard deviation obtained varied between 2.7% for Bi and 5.3% for Sb. Hydride generation has been directly produced from PM$_{10}$ and PM$_{2.5}$ circular portions. A 100 ml reaction vessel was used. The circular portions were placed into the reaction vessel with 5 ml of hydrochloric acid 1.0 M for As and Sb determination and 0.5 M for Bi and Sn determination. The tip of the quartz capillary tube was inserted automatically at the centre of the graphite tube. Then, the vapours have been generated by the addition of sodium tetrahydroborate [2.0% (m/v) for As, Bi and Sb and 1.0% (m/v) for Sn]. During the time period (40 s for As, Bi and Sb, and 20 s for Sn) for which the quartz capillary has been inserted onto graphite tube, the pump of the MHS-10 system placed the sodium tetrahydroborate solution into the vessel. Thus, the vapours are generated. These times are corresponding to the trapping times of the different metals studied. The purge gas flow rate for the analyte transfer to the furnace was 60 ml min^{-1}. Then, the quartz capillary moves out of the graphite tube. The trapped analyte was atomised during 3.0 s for As, Bi and Sn determination and 5.0 for Sb determination using maximum power heating and internal gas stop for all hydride elements studied except for As. An Ar flow rate of 100 ml min^{-1} during the atomisation was necessary for As determination due to the high arsenic content. The optimum vapour generation, trapping and atomisation conditions obtained for each species are shown in Table 1.

2.5. Procedure for PM$_{10}$ and PM$_{2.5}$ acid digests measurement by ICP-MS

Circular portions were digested following the validated method (by NIST 1648 and NIST 1649a reference materials analysing) described by Piñeiro-Iglesias et al. [33]: sample was transferred to a PFA bomb with the addition of 2.5 ml of nitric acid and 5 ml of hydrofluoric acid and heated at 90 °C in a closed bomb for 12 h. The mixture was driven to dryness after the addition of 2.5 ml of perchloric acid and 1 ml of nitric acid. Once total dryness was reached, 2.5 ml of nitric acid was added and

the solution made up to 25 ml. PM_{10} and $PM_{2.5}$ acid extracts were analysed by inductively coupled plasma atomic mass spectrometry (ICP-MS) by using the conditions shown in Table 2.

3. Results and discussion

3.1. Optimisation of the hydride generation and electrothermal atomic absorption detection conditions from untreated PM_{10} and $PM_{2.5}$

Different variables involved on the As, Bi, Sb and Sn hydride generation from atmospheric particulate filters and its determination by ETAAS were studied by using factorial designs (programs from Statgraphics Plus 4.0 routine, Statgraphics Graphics Corporation, Rockville, MD, USA).

Since published data in literature, hydrochloric acid and sodium tetrahydroborate concentration (affecting the hydride generation efficiency), trapping temperature and atomisation temperature (affecting the hydride atomisation efficiency) are the most reported main variables. However, other factors that could affect such as trapping time and Ar flow rate (affecting the hydride transport) have also been considered. The last variables (denoted as G and H), called dummy factor, were also taken into account in the study. Dummy factors are imaginary variables for which the change from one level to another is not supposed to cause any physical change. These variables are commonly used to evaluate the possible systematic error and/or the existence of an important variable that was not considered.

The responses, which in our study have been the metal recovery percentages, were obtained by changing the factors

Table 3
Experimental field definition for the PBD

Key	Parameter	Low (−)	High (+)
A	HCl concentration (mol l^{-1})	0.5	1.0
B	NaBH$_4$ concentration (%, m/v)	1.0	2.0
C	Ar flow rate (ml min^{-1})	25	50
D	Trapping temperature (°C)	400	800
E	Atomisation temperature (°C)	2000	2500
F	Trapping time (s)	30	60
G	Dummy factor	−	+
H	Dummy factor	−	+

from a low to a high level value from Table 3. The percentage recovery is calculated according to the following equation: $R(\%) = C_{\text{found}}/C_{\text{digested}} \times 100$, where C_{found} is the concentration obtained after each experiment (using direct hydride generation from and ETAAS) and C_{digested} is the value concentration measured by ICP-MS from digested PM_{10} and $PM_{2.5}$ using the validated method above commented [33]. Recoveries and concentrations shown in the tables throughout this work are mean recoveries. Each experiment was replicated ($n = 2$).

3.1.1. Plackett–Burman designs

The significance of the variables commented above was simultaneously evaluated by applying a $2^8 \times 3/32$ type III resolution design Plackett–Burman design (PBD), for eight factors, four degrees of freedom, twelve runs and two replicates. The experimental field definition for the PBD (high and low values for each factor) is shown in Table 3. The PBD matrix is shown in Table 4 together with the response (percentage recovery)

Table 4
PBD for the determination of significant parameters involved on As, Bi, Sb and Sn determination

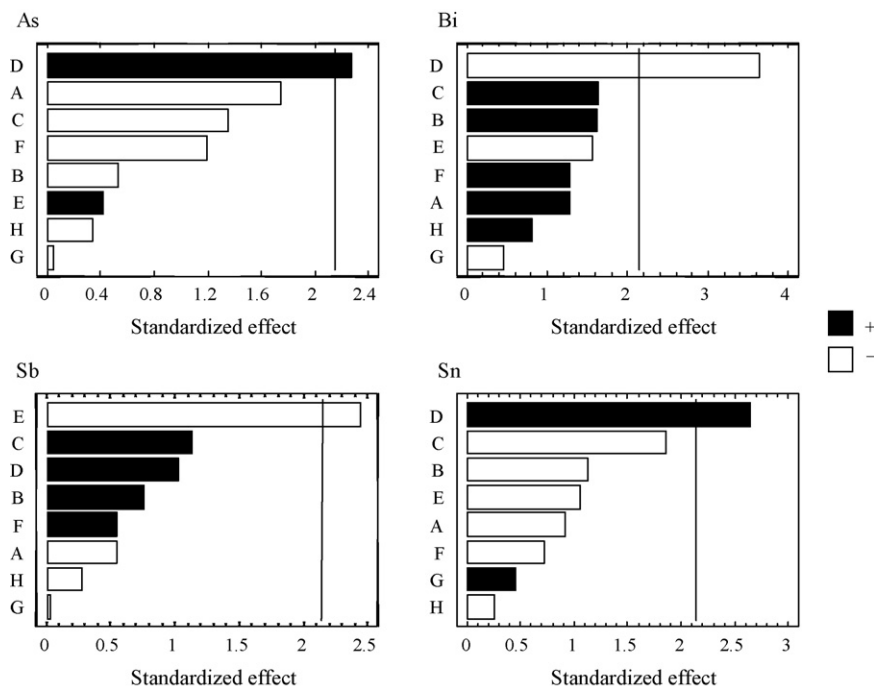| Run no.	Parameters								Analytical recovery (%)			
	A	B	C	D	E	F	G	H	As	Bi	Sb	Sn
1	+	−	+	−	−	−	+	+	60	86	90	72
2	+	+	−	+	−	−	−	+	55	93	70	68
3	−	+	+	−	+	−	−	−	57	92	70	61
4	+	−	+	+	−	+	−	−	64	73	89	71
5	+	+	−	+	+	−	+	−	98	39	72	85
6	+	+	+	−	+	+	−	+	53	93	59	41
7	−	+	+	+	−	+	+	−	72	85	79	68
8	−	−	+	+	+	−	+	+	71	62	58	59
9	−	−	−	+	+	+	−	+	92	48	71	86
10	+	−	−	−	+	+	+	−	41	94	55	54
11	−	+	−	−	−	+	+	+	59	86	87	72
12	−	−	−	−	−	−	−	−	81	65	62	75
13	+	−	+	−	−	−	+	+	64	85	68	78
14	+	+	−	+	−	−	−	+	50	89	68	62
15	−	+	+	−	+	−	−	−	56	88	85	56
16	+	−	+	+	−	+	−	−	61	70	92	76
17	+	+	−	+	+	−	+	−	93	41	71	89
18	+	+	+	−	+	+	−	+	52	94	56	43
19	−	+	+	+	−	+	+	−	63	75	77	71
20	−	−	+	+	+	−	+	+	69	60	65	65
21	−	−	−	+	+	+	−	+	90	52	73	96
22	+	−	−	−	+	+	+	−	36	94	50	50
23	−	+	−	−	−	+	+	+	65	87	83	67
24	−	−	−	−	−	−	−	−	83	66	61	68

Fig. 1. Standardized (*P* = 95.0%) main effect Pareto chart for the Plackett–Burman design for the As, Bi, Sb and Sn determination. (A) Hydrochloric acid concentration; (B) sodium tetrahydroborate concentration; (C) Ar flow rate; (D) trapping temperature; (E) Atomisation temperature; (F) trapping time; (G) dummy factor; (H) dummy factor.

obtained for each metal and each experiment. The high and low values (Table 3) were selected according to our prior experience and published or manufacturer data. Thus, high hydrochloric acid and sodium tetrahydroborate concentrations ranges were selected. The maximum trapping and atomisation temperatures values allowed were 1000 and 2500 °C, respectively. Therefore, the trapping temperature (D) was studied from 200 to 800 °C and the atomisation temperature (E) within the 2000–2500 °C range. High Ar flow rate could decrease the trapping efficiency onto Ir-treated graphite tube. Thus, this factor was studied in the 25–50 ml min^{-1} range. Finally, the trapping time (F) was studied within the 30–60 min range.

The statistical evaluation of results was attained at a 95.0% confidence interval from which a minimum *t*-value of 2.46, calculated by the Statgraphics routine trough an iterative process, was obtained. Variables which *t*-values higher than ±2.46 were considered as statistically significant factors. The analysis of the results leads the standardised (*P* = 95.0%) Pareto charts of main effects (Fig. 1). It can be seen that the variables trapping temperature (D) and atomisation temperature (E) are statistically significant for most of the elements. Concerning the trapping temperature (D), the effect of this variable was positive for As

and Sn. This means an increase on the trapping efficiency at high trapping temperature. Otherwise, a negative sign affected this variable for bismuth, increasing the trapping efficiency at low trapping temperatures. Atomisation temperature (E) was also significant for Sb. A negative sign affected this variable for Sb, decreasing the atomisation efficiency at high atomisation temperatures. Variables affecting hydride generation and transport conditions (hydrochloric acid concentration (A), sodium tetrahydroborate concentration (B) and Ar flow rate (C)) and trapping time (F) were not statistically significant in the studied ranges. The insignificance of the hydrochloric acid and sodium tetrahydroborate concentrations can be explained by the high concentrations of these reagents used. These concentration values are common when a batch vapour generation mode is used. The statistical insignificance of the trapping time (F) offers an important practical advantage due to the analysis time can be shortened.

3.1.2. Univariate optimisation

Screened out the variables that did not have a significant effect on the response, the remaining factor affecting the several hydride elements forming (trapping temperature for As, Bi

Table 5
Features of the determination methods

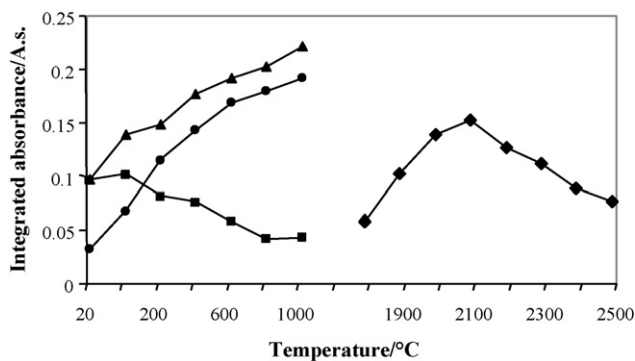|	Calibration[a]	Addition[a]	LOD (ng m^{-3})	LOQ (ng m^{-3})
As	$Q_A = 0.089 + 0.298[\text{As}]$	$Q_A = 0.174 + 0.310[\text{As}]$	0.050	0.170
Bi	$Q_A = 0.008 + 0.137[\text{Bi}]$	$Q_A = 0.083 + 0.121[\text{Bi}]$	0.020	0.065
Sb	$Q_A = 0.034 + 0.243[\text{Sb}]$	$Q_A = 0.161 + 0.230[\text{Sb}]$	0.045	0.150
Sn	$Q_A = 0.120 + 0.121[\text{Sn}]$	$Q_A = 0.215 + 0.119[\text{Sn}]$	0.055	0.180

[a] Values expressed in μg l^{-1}.

Fig. 2. Effect of trapping temperature (left) and atomisation temperature (right) on the integrated absorbance for: As (▲), Bi (■), Sb (♦), and Sn (●), respectively.

and Sn and atomisation temperature for Sb) were optimised by using univariate approaches. Fig. 2 shows result from the optimisation of those significant variables. Thus, the optimum values associated to each metal are shown in Table 1.

Given these findings, we decided to work with the optimum values obtained for the factors studied (Table 1). The fixed values for the insignificant factors (results from PBD) are also given in Table 1. The values for the insignificant factors were selected according to different aspects such as, reagents saving (low values for hydrochloric acid and sodium tetrahydroborate concentrations were chosen); analysis time saving (low value for trapping time was chosen) and graphite tube damage (low value for trapping and atomisation temperatures) and quartz capillary damage (low value for trapping temperature).

3.2. Features of the methods

Table 5 shows the calibration and addition equations obtained for several metals studied. Circular filter portions were spiked with 0.1, 0.2 and 0.4 $\mu g\,l^{-1}$ of As(III) or with 0.5, 1.0 and 2.0 $\mu g\,l^{-1}$ of Bi or with 0.5, 1.0 and 2.0 $\mu g\,l^{-1}$ of Sb(III) or with 0.5, 1.0, and 2.0 $\mu g\,l^{-1}$ of Sn for As, Bi, Sb and Sn determination, respectively. As we can see, for each determinant, the slopes of the calibration and standard addition graphs are statistically similar (*t*-test for a confidence level of 95.0%). Therefore, matrix effect is not important and the calibration method could be useful. In addition, low blank signals are obtained for all metal studied, except for As and Sn. This fact, in accordance with literature [34], is attributed to the high amount of sodium tetrahydroborate used in this hydride generation mode (batch mode). The within-batch precision (relative standard deviation for eleven replicate measurements) obtained for the different hydride generation procedures are good. R.S.D. (%) of 6.2, 5.3, 9.1 and 7.5% in a filter sample containing 0.7, 1.0, 1.4 and 1.7 $\mu g\,l^{-1}$ for As, Bi, Sb and Sn, respectively, were obtained. Absolute detection limits, defines as 3 and 10 S.D./*m*, respectively, where S.D. is the standard deviation of 11 measurement of a blank and *m* is the slope of the addition graphs, were 37, 15, 30, and 41 $ng\,l^{-1}$ for As, Bi, Sb and Sn, respectively. In addition, detection limits referred to the air volume sampled are also shown in Table 5.

Table 6
Mean concentrations (expressed as ng m⁻³) and S.D. [a] by direct sampling-HG-ETAAS and acid digestion-ICP-MS

PM₁₀ (μg m⁻³)	Sample code	As		Bi		Sb		Sn	
		Direct-HG-ETAAS	Acid digestion-ICP-MS	Direct-HG-ETAAS	Acid digestion-ICP-MS	Direct-HG-ETAAS	Acid digestion-ICP-MS	Direct-HG-ETAAS	Acid digestion-ICP-MS
22	08/03/2004	0.85 ± 0.01	1.05 ± 0.05	0.17 ± 0.01	0.12 ± 0.009	2.23 ± 0.2	1.77 ± 0.11	1.69 ± 0.05	2.01 ± 0.1
41	09/03/2004	0.94 ± 0.02	1.3 ± 0.08	0.21 ± 0.01	0.12 ± 0.008	0.95 ± 0.03	0.96 ± 0.04	1.57 ± 0.1	1.67 ± 0.1
17	10/03/2004	1.58 ± 0.10	1.8 ± 0.10	0.25 ± 0.01	0.19 ± 0.006	0.81 ± 0.02	0.72 ± 0.04	2.3 ± 0.2	2.15 ± 0.04
16	15/03/2004	0.87 ± 0.02	0.77 ± 0.10	0.26 ± 0.01	0.15 ± 0.013	1.11 ± 0.1	1.13 ± 0.08	1.77 ± 0.1	2.17 ± 0.4
22	16/03/2004	0.67 ± 0.01	0.92 ± 0.05	0.084 ± 0.005	0.11 ± 0.003	1.43 ± 0.09	1.33 ± 0.13	1.53 ± 0.1	1.84 ± 0.1
23	17/03/2004	0.67 ± 0.01	0.58 ± 0.09	0.092 ± 0.005	0.068 ± 0.003	0.54 ± 0.04	0.68 ± 0.05	0.93 ± 0.06	1.29 ± 0.2

PM₂.₅ (μg m⁻³)	Sample code	As		Bi		Sb		Sn	
		Direct-HG-ETAAS	Acid digestion-ICP-MS	Direct-HG-ETAAS	Acid digestion-ICP-MS	Direct-HG-ETAAS	Acid digestion-ICP-MS	Direct-HG-ETAAS	Acid digestion-ICP-MS
16	08/03/2004	0.61 ± 0.01	1.02 ± 0.08	0.13 ± 0.01	0.12 ± 0.008	0.69 ± 0.05	0.97 ± 0.04	1.44 ± 0.1	1.38 ± 0.1
25	09/03/2004	0.92 ± 0.01	0.79 ± 0.10	0.08 ± 0.006	0.1 ± 0.005	0.3 ± 0.01	0.31 ± 0.02	0.82 ± 0.04	0.9 ± 0.1
12	10/03/2004	0.48 ± 0.02	0.35 ± 0.05	0.073 ± 0.004	0.075 ± 0.003	<0.150	0.093 ± 0.05	1.36 ± 0.1	1.65 ± 0.3
10	15/03/2004	0.54 ± 0.02	0.66 ± 0.01	0.13 ± 0.01	0.11 ± 0.004	0.31 ± 0.02	0.38 ± 0.02	<0.18	0.17 ± 0.02
14	16/03/2004	0.81 ± 0.03	0.98 ± 0.14	0.086 ± 0.004	0.084 ± 0.012	0.33 ± 0.01	0.47 ± 0.06	2.91 ± 0.2	2.66 ± 0.6
16	17/03/2004	0.69 ± 0.03	0.57 ± 0.05	<0.065	<0.06	0.14 ± 0.01	0.16 ± 0.01	0.67 ± 0.04	0.73 ± 0.04

[a] Mean and S.D. of four measurements.

3.3. Validation and application to real samples

As, Bi, Sb and Sn were analysed in twelve atmospheric particulate matter filters, at one sampling station located in a non-polluted suburban area of A Coruña, Spain, during March 2004, using the proposed method (direct sampling-hydride generation from non-treated PM_{10} and $PM_{2.5}$ coupled to ETAAS) and a conventional acid digestion followed to ICP-MS quantification. The results (Table 6) from both methods were compared statistically in terms of metal concentrations. The hydride elements forming concentrations obtained after hydride generation-ETAAS and acid digestion-ICP-MS procedures were similar for all elements studied. Correlation coefficients (R^2, $n = 12$) of 0.7346, 0.7398, 0.9435 and 0.9105 for As, Bi, Sb and Sn, respectively, were obtained. The application of the paired t-test (95% confidence level and 11 degrees of freedom for As) gave a t_{cal} of 1.58, which are lower than the t_{crit} values of 2.20. For Bi, Sb and Sn the application of the paired t-test (95% confidence level and 10 degrees of freedom) gave a t_{cal} of 2.10, 0.22 and 1.56, respectively, which are also lower than the t_{crit} values of 2.23. Therefore, the direct hydride generation from PM_{10} and $PM_{2.5}$ leads to statistically similar concentrations for the studied elements to the conventional procedure based on acid digestion-ICP-MS. The high correlation coefficients corresponding to As and Sb leads us to conclude that pentavalent states of these elements (which are the predominant species [13,35]) can be reduced to arsine and stibine using the optimised conditions.

Concentration ranges of 0.67–1.58, 0.084–0.26, 0.54–2.23 and 0.93–2.3 ng m^{-3} for As, Bi, Sb and Sn, respectively, from PM_{10} and 0.48–0.92, <0.065–0.13, <0.15–0.69 and <0.18–2.91 ng m^{-3} for As, Bi, Sb and Sn, respectively, from $PM_{2.5}$ are shown in Table 6; which are in general agreement with reported data from a non-polluted suburban area. As can be seen, As, Sb and Sn are present in both fractions ($PM_{2.5}$ and PM_{10}), the high levels obtained corresponded to As and Sb in PM_{10} fraction. In addition, results indicated that As levels are below the 6 ng m^{-3} target value proposed by the European Commission (Directive 2004/107/EC [36]). Finally, considering that $PM_{2.5}$ is around 66% of PM_{10} fraction, the Bi percentages obtained in both fractions are similar. Around 74% of As and 80% of Sn in PM10 was present in the PM2.5 fraction. This proportion decreased down to 27% for Sb.

4. Conclusions

The direct hydride generation from atmospheric particulate matter filters (PM_{10} and $PM_{2.5}$) is a novel approach for As, Bi, Sb and Sn determination. Sample pre-treatment such as acid digestion or slurry preparation is avoided. The method only requires the cutting of PM_{10} and $PM_{2.5}$ previous to determination. Thus, the time for pre-treat the samples is hugely minimised. In addition, analytes losses and sample contamination is removed. The high hydride generation efficiency is possible because metals are trapped into lower than 10 and 2.5 μm particles sizes (collected in PM_{10} and $PM_{2.5}$, respectively). Therefore, metals hydrides are easily generated by using diluted hydrochloric acid. This implies an important reduction on wastes and the over-all pro-

cedure can be considered as an environmentally friendly process. The proposed methods allow an accurate and fast determination of As, Bi, Sb and Sn in PM_{10} and $PM_{2.5}$ atmospheric particulate matter.

References

[1] J. Schwartz, D.W. Dockery, L.M. Neas, J. Air Waste Manage. 46 (1996) 927.
[2] C.A. Pope, R.T. Burnett, M.J. Thun, E.E. Calle, D. Krewski, K. Ito, G.D. Thurston, J. Am. Med. Assn. 287 (2002) 1132.
[3] E. Rizzio, G. Giaveri, M. Gallorini, Sci. Total Environ. 256 (2000) 11.
[4] B.H. Mc Cormac, Introduction to the Scientific Study of Atmospheric Pollution, Reide, Dordrecht, Holland, 1971.
[5] T.r. Fogg, R.C. Seeley, Am. Lab. 16 (1984) 36.
[6] J.P. Pancras, J.M. Ondov, R. Zeisier, Anal. Chim. Acta 538 (2005) 303.
[7] Y. Narita, S. Tanaka, S.J. Santosa, J. Geophys. Res. 104 (1999) 26859.
[8] C. Ludke, E. Hoffmann, J. Skole, Fresenius J. Anal. Chem. 350 (1994) 272.
[9] C. Ludke, E. Hoffmann, J. Skole, M. Kriews, J. Anal. At. Spectrom. 14 (1999) 1685.
[10] C. Ludke, E. Hoffmann, J. Skole, Fresenius J. Anal. Chem. 359 (1997) 399.
[11] B.A. Bitterli, H. Cousin, B. Magyar, J. Anal. At. Spectrom. 12 (1997) 957.
[12] J. Tilch, C. Luedke, E. Hoffmann, Fresenius J. Anal. Chem. 355 (1996) 913.
[13] V. Oliveira, J.L. Gómez-Ariza, D. Sánchez-Rodas, Anal. Bioanal. Chem. 382 (2005) 335.
[14] F. Fernández-Álvarez, M. Ternero-Rodríguez, A.J. Fernández-Espinosa, A. Gutierrez-Daban, Anal. Chim. Acta 524 (2004) 33.
[15] C. Moscoso-Pérez, J. Moreda-Piñeiro, P. López-Mahía, S. Muniategui-Lorenzo, E. Fernández-Fernández, D. Prada-Rodríguez, Anal. Chim. Acta 526 (2004) 185.
[16] A. Limbeck, H. Rendl, H. Puxbaum, J. Anal. At. Spectrom. 18 (2003) 161.
[17] L. Fuechtjohann, N. Jakubowski, D. Gladtke, D. Klockow, J.A.C. Broekaert, J Environ. Monitor. 36 (2001) 681.
[18] J.C. Yu, K.F. Ho, S.C. Lee, Fresenius J. Anal. Chem. 369 (2001) 170.
[19] P.E. Rasmussen, K.S. Subramanian, B.J. Jessiman, Sci. Total Environ. 267 (2001) 125.
[20] M.B. Gómez, M.M. Gómez, M.A. Palacios, Anal. Chim. Acta 404 (2000) 285.
[21] I.A. Leal-Granadillo, J.I.G. Alonso, A. Sanz-Medel, Anal. Chim. Acta 423 (2000) 21.
[22] A. Chatterjee, R.N. Banerjee, Sci. Total Environ. 227 (1999) 175.
[23] P.K. Pandey, K.S. Patel, P. Subrt, Sci. Total Environ. 215 (1998) 123.
[24] M.M. Farinha, Z. Slejkovec, J.T. Elteren, H.Th. Wolterbeek, M.C. Freitas, J. Atmos. Chem. 49 (2004) 343.
[25] M. Bikke, K. Polak, J. Hlavay, J. Anal. At. Spectrom. 16 (2001) 74.
[26] J.J. Morales-Rifo, P. Richter, Anal. Bioanal. Chem. 380 (2004) 129.
[27] M. Sakata, K. Marumoto, Atmos. Environ. 36 (2002) 239.
[28] X. Feng, J.Y. Lu, D.C. Gregoire, Y. Hao, C.M. Banic, W.H. Schroder, Anal. Bioanal. Chem. 380 (2004) 683.
[29] H. Matusiewicz, Appl. Spectros. Rev. 38 (2003) 263.
[30] P. Bermejo-Barrera, J. Moreda-Piñeiro, A. Moreda-Piñeiro, A. Bermejo-Barrera, J. Anal At. Spectrom. 11 (1996) 1081.
[31] European Community, Council Decision 2004/470/EC of 29 April 2004 concerning guidance on a provisional reference method for the sampling and measurement of PM2.5, Off. J. L160 (2004) 53.

[32] European standard EN12341, Air quality – determination of the PM_{10} fraction of suspended particulate matter – reference method and field test procedure to demonstrate reference equivalence of measurement methods, 1998.

[33] M. Piñeiro-Iglesias, P. López-Mahía, S. Muniategui-Lorenzo, D. Prada-Rodríguez, X. Querol, A. Alastuey, Atmos. Environ. 37 (2003) 4171.

[34] J. Murphy, G. Schlemmer, I.L. Shuttler, P. Jones, S.J. Hill, J. Anal At. Spectrom. 14 (1999) 1593.

[35] J. Zheng, M. Ohata, N. Furuta, Analyst 125 (2000) 1025.

[36] European Community, Council Directive 2004/170/EC of 15 December 2004 relating to arsenic, cadmium, mercury, nickel and polycyclic aromatic hydrocarbons in ambient air. Off. J. L23 (2004) 3.

Effect of pH on the characteristics of potassium permanganate–luminol CL reaction in the presence of trace aluminum(III) and its analytical application

Jin Pan [a,b], Yuming Huang [a,*], Weiqun Shu [c], Jia Cao [c]

[a] College of Chemistry and Chemical Engineering, The Key Laboratory of the Three Gorges Reservoir Region's Eco-Environments,
Southwest University, Ministry of Education, Chongqing 400715, China
[b] School of River and Sea, Chongqing Jiaotong University, Chongqing 400074, China
[c] Department of Environmental Health, The Third Military Medical University, Chongqing 400038, China

Abstract

At pHs ≥ 11.45, trace Al was found to enhance the CL from luminol–KMnO$_4$ system. However, at pHs ≤ 10.42, it was found to inhibit strongly the CL from luminol–KMnO$_4$ system. The effect of pH, luminol and potassium permanganate concentrations on the kinetic characteristics of CL system was investigated in the presence of trace Al. On this basis, a flow injection inhibition chemiluminescence method was established for the determination of trace Al in this study. Under optimized conditions, the CL decreased linearly with Al(III) concentration in the range of 8–500 μg L^{-1} and the detection limit (3σ) of 2 μg L^{-1}. The relative standard deviation (R.S.D.) is 3.6% for 100 μg L^{-1} Al(III) ($n = 11$). The method has been applied to the determination of trace Al in real water samples with satisfactory results without the pretreatment of samples. The results given by the proposed method are in good agreement with those given by ICP-AES detection method.
© 2006 Elsevier B.V. All rights reserved.

Keywords: Aluminum; Chemiluminescence; Luminol; Environmental analysis

1. Introduction

Al had been thought to be a relative harmless element for a long time. Recent researches implicate that the proper level of aluminum can play a certain role in elements' metabolism in body, but excessive Al(III) has toxicity and can lead to various disorders, such as disturbing the metabolism of phosphorus to result in bone pathological changes. In particular, the bad effects on nerve center are most obvious, probably causing many mental diseases, such as dementia [1]. At present, the biologic toxicity of Al has been more and more concerned. Therefore, a development of fast, simple and sensitive method for trace Al determination is needed.

The published analytical methods for Al determination can be categorized two kinds. One is the direct method and the other the derivatization-based method. The former methods include atomic absorption spectrometry [2–7], and ICP-AES [8–10], and the latter do spectrophotometry [11–16], resonance Rayleigh scattering (RRS) [17] and fluorescence [18–25]. Chemiluminescent (CL) methods promise ultra sensitive detection limits (attomole-zeptomole), rapid assays, and a broad range of analytical applications with simple instruments (no monochromator required). CL-based analytical methods have been reported for metal analysis [26–32]. Regarding the determination of Al by chemiluminescence, however, there are limited literatures dealing with this issue to date [32]. Du and Huie [32] reported a chemiluminescence method for the determination of aluminum based on chemical excitation of fluorescent Al-lumogallion complex through hydrogen peroxide–peroxyoxalate system. Although high sensitivity and good selectivity were realized by above method, complex configuration and organic media were adopted for maximum of CL response. Direct chemiluminescence analysis of trace Al without derivatization has not been reported in literature.

In this paper, the feasibility of direct determination of trace Al by using FI-CL system was studied for the first

* Corresponding author. Fax: +86 23 68866796.
E-mail address: yuminghuang2000@yahoo.com (Y. Huang).

time. Experimental results show that at pHs ≥ 11.45, trace Al was found to enhance the CL from luminol–KMnO$_4$ system. However, at pHs ≤ 10.42, it was found to inhibit strongly the CL from luminol–KMnO$_4$ system. The investigations demonstrate that the luminol and potassium permanganate concentrations did not influence the pathway of CL reaction in the presence of trace Al. Based on above results, a flow injection inhibition chemiluminescence method was established for the determination of trace Al in this study. To the best of our knowledge, this is first report on direct CL determination of trace Al without derivatization by using common luminol system. The developed method was applied to the determination of Al contents in water samples with satisfactory results.

2. Experimental

2.1. Apparatus

Two two-channel peristaltic pumps (Wenzhou, China) and an eight-channel injector valve (Wenzhou, China) were used to construct the FI system. PTFE tubing (0.8 mm i.d.) was used to connect all components in the flow system. The chemiluminescence measurements were carried out with a Type IFFL-D Flow-Injection Chemiluminescence Analyzer (Reike, Xi'an). The ICP-AES determination of Al(III) was performed by Type TPS-7000 Atomic Emission Spectrophotometer (Puxi, Beijing, China). All the glass tubes and volumetric flasks were dipped in 20% (v/v) nitric acid, followed by thoroughly rinsing with double-distilled water prior to use. The pH measurements were made with a Model pHs-3C meter (Chengdu, China).

2.2. Reagents

All the reagents used were of analytical grade unless specified otherwise. Doubly deionized water was used throughout the study. All reagents were obtained from Chongqing Chemical Reagents Company (Chongqing, China) except for luminol (>95%) which was from Merck (Darmstadt, Germany). A stock solution of Al(III) (2500 μg mL^{-1}) was prepared by dissolving 3.4760 g Al(NO$_3$)$_3$·9H$_2$O in 100 mL of water and stored in refrigerator. Working standard solutions of Al(III) were prepared daily from the stocked solution by appropriate dilution with doubly deionized water. A 0.01 mol L^{-1} luminol solution was prepared by dissolving 0.1777 g luminol in 100 mL of 0.001 mol L^{-1} NaOH solutions. Potassium permanganate (GR grade) stock solution (1.0 × 10^{-2} mol L^{-1}) was prepared in brown bottle and kept in dark.

2.3. General experimental procedure for chemiluminescent determination

A schematic diagram of flow detection system used in this work is shown in Fig. 1. Two peristaltic pumps were used to deliver all solutions; one at a flow rate of 3.5 mL min^{-1} (pump1) for delivering sample and water carrier stream; the other for delivering CL reaction reagents at a flow rate of 3.5 mL min^{-1} (per tube, pump2). Flow lines were inserted into potassium per-
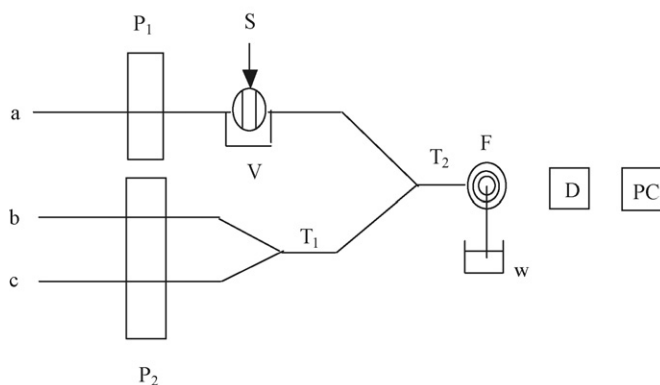

Fig. 1. Schematic diagram of the flow system for the determination of trace Al. a, H$_2$O; b, luminol; c, KMnO$_4$; S, sample; P$_1$ and P$_2$, peristaltic pump; V, eight-channel valve; T$_1$ and T$_2$, mixing tube; F, flow cell; W, wastewater; D, detector; PC, computer.

manganate, alkaline luminol solution, water carrier, respectively. One hundred eighty microlitres of sample solution was injected into water stream by an eight-way injection valve and then mixed with the mixture of luminescent reagents (potassium permanganate solution/luminol solution). The emitted CL was collected with a photomultiplier tube (operated at −800 V) of the Type IFFL-D Flow-Injection Chemiluminescence Analyzer. The signal was recorded using an IBM-compatible computer, equipped with a data-acquisition interface. Data-acquisition and treatment were performed with REMAX software running under Windows 98. For characterization of the chemiluminescent analysis system, aqueous standards were used. A series of working standard solution with different concentrations were prepared by diluting a concentrated fresh standard solution of Al(III) with water. The net CL emission intensity ($\Delta I = I_0 - I_1$, where I_1 is the CL intensity of sample solution, I_0 the blank solution.) versus Al(III) concentration were used for the calibration.

2.4. Procedure for water samples

Two tap water samples and two mineral water samples were collected from laboratory and local markets. The samples were stored at 4 °C in refrigerator to avoid exposure to light and air. For the determination of trace Al(III) in tap water sample, five-fold dilution was adopted. However, it is two-fold dilution for mineral water sample analysis.

3. Results and discussion

3.1. The characteristic of CL kinetic curves

Due to the nature of the luminol reaction, which is more favored under basic conditions, the kinetic curves at different pH in the presence of Al(III) were investigated. As shown in Fig. 2, the curves demonstrated one enhancing peak at 11.45 and 12.10 of pH, whereas one inhibiting peak at pH 9.40 and 10.42. It seems that the pH of solutions obviously influenced the pathways. The effect of luminol concentrations on CL kinetic curves of system
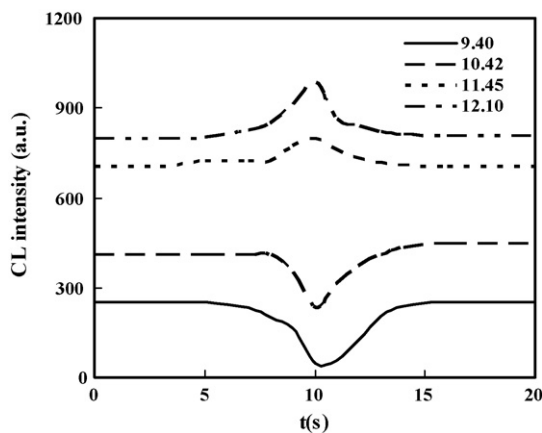
Fig. 2. The CL kinetic curves at different pH of luminol. Reaction conditions: Al(III), $100\,\mu g\,L^{-1}$; KMnO$_4$, $1.0 \times 10^{-4}\,mol\,L^{-1}$; luminol, $5.0 \times 10^{-5}\,mol\,L^{-1}$.

Fig. 3. Effect of pH on CL intensity. Reaction conditions: Al(III), $100\,\mu g\,L^{-1}$; KMnO$_4$, $1.0 \times 10^{-4}\,mol\,L^{-1}$; luminol, $5.0 \times 10^{-5}\,mol\,L^{-1}$.

was studied under pH of 9.40, 11.45 and 12.10, respectively. Experimental results demonstrate that only one inhibiting peak was observed with 1.0×10^{-6} to $1.0 \times 10^{-4}\,mol\,L^{-1}$ luminol at pH 9.40. However, only one enhancing peak was observed at pH 11.45 and 12.10. It is possible that luminol concentration did not influence the CL pathway.

The effect of concentrations of potassium permanganate on CL kinetic curves of the system was also studied under pH of 9.40. Experimental results demonstrate that only one inhibiting peak was observed with 1.0×10^{-6} to $2.0 \times 10^{-4}\,mol\,L^{-1}$ potassium permanganate. Similarly as luminol effect under high pH value, when the effect of concentrations of potassium permanganate on CL kinetic curves of the system were performed under pH 11.45 and 12.10, only one enhancing peak was observed. It is possible that potassium permanganate concentration did not influence the CL pathway. From above results, it can be concluded that the CL enhancement and inhibition of Al(III) depended the pH of the solutions.

3.2. Optimization of chemiluminescence reaction

As indicated above, luminol reacts with potassium permanganate to produce light emission in basic solution. Therefore, sodium hydroxide was added in a flow line to improve the sensitivity of reaction. The effect of pH on CL reaction was studied as shown in previous section. As can be seen from Fig. 3, in the pH range from 8.17 to 11.06, I_0 increases with increase of pH, however, in the presence of Al(III), inhibition CL signal was observed. So, from the results of pH effect we tested, it can be concluded that when pH $\leq$ 11.06, CL inhibition occurs in the presence of Al(III). When pHs $\leq$ 10.42, it was found to inhibit strongly the CL from luminol–KMnO$_4$ system. When pH is between 11.06 and 11.45, CL signal will from inhibition to background, then to enhancement. It was found from Fig. 3 that the ΔI increased with the increase of pH up to 9.4; however, the background level (I_0) also increases with pH value. So the signal/noise (S/N) ratio was used to evaluate pH effect. As can be seen from Fig. 3, the S/N ratio increases with pH value up
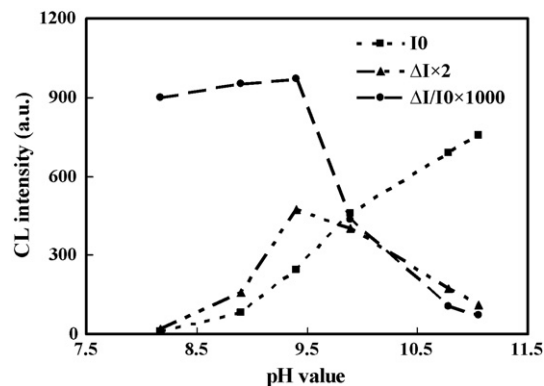
to 9.40, above which the S/N ratio decreases. As a compromise between the sensitivity and the background level, finally, pH value of 9.40 was selected for the present work. The effect of luminol concentration on the ΔI was investigated ranging from 1.0×10^{-6} to $1.0 \times 10^{-4}\,mol\,L^{-1}$. The experimental results showed that the S/N ratio increases with the concentration of luminol up to $5.0 \times 10^{-5}\,mol\,L^{-1}$, above which the S/N ratio decreases. So $5.0 \times 10^{-5}\,mol\,L^{-1}$ luminol was used in the following work. The effect of potassium permanganate concentration on the ΔI was investigated ranging from 1.0×10^{-6} to $2.0 \times 10^{-4}\,mol\,L^{-1}$. The results showed that ΔI increased with increase of potassium permanganate concentration, meanwhile, the base line also increased. The experimental results showed that the S/N ratio increases with the concentration of potassium permanganate up to $1.0 \times 10^{-4}\,mol\,L^{-1}$, above which the S/N ratio decreases. So $1.0 \times 10^{-4}\,mol\,L^{-1}$ potassium permanganate was used in the following work.

3.3. Effect of mixing tube length

The effect of mixing tube length was studied in the present study. The results demonstrate that the net CL response (ΔI) of FIA system increases with increasing of mixing tube T_1 to 48 cm, T_2 to 10 cm, respectively. Above which, the CL response decreases. Finally, 48 and 10 cm were selected as the optimum mixing tube length for T_1 and T_2, respectively.

3.4. Interference study

The effect of foreign substances was tested by analyzing a standard solution of Al(III) ($100\,\mu g\,L^{-1}$) to which increasing amounts of interfering substances was added. The tolerable concentration ratios with respect to $100\,\mu g\,L^{-1}$ Al(III) for interference at 5% level were over 1000 for Na$^+$, K$^+$, Cl$^-$, urea; 200 for Fe^{3+}; 100 for Ca^{2+}; 50 for Co^{2+}; 10 for Cr^{3+}, HCO$_3^-$; 5 for NH$_4^+$, CO$_3^{2-}$; 1 for Mg^{2+}, PO$_4^{3-}$, Ba^{2+}, respectively. From above results, it can be seen that some metals interfere with Al(III) determination. So, when performing the Al(III) analysis in real samples, the standard-addition method should be adopted in order to alleviate the matrix effects.
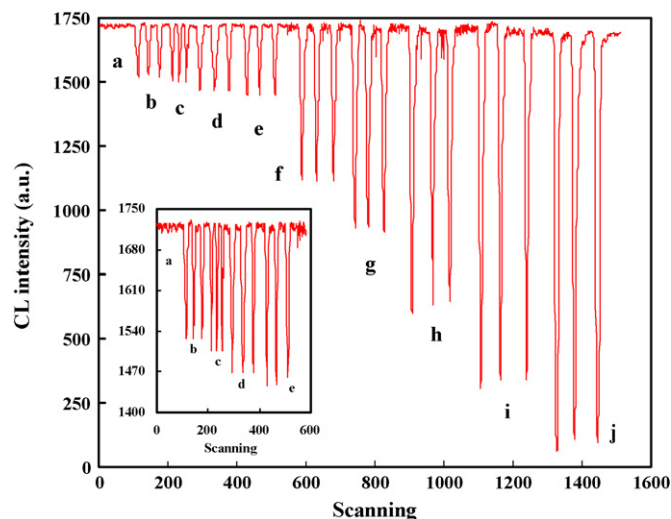
Fig. 4. A typical FIA chart from standard samples. Letters a–j represents Al(III) standard solutions with concentrations of: 0, 8, 10, 30, 50, 100, 200, 300, 400 and 500 μg L^{-1}, respectively. *Inset*: Amplification FIA chart from standard samples of a–e, respectively.

3.5. Working curves and detection limits

Under the selected conditions given above, the calibration graph of emission inhibition versus Al(III) concentration was linear in the 8–500 μg L^{-1} range ($\Delta I = 2924.7$ [Al(III)] (μg mL^{-1}) + 184; $r^2 = 0.9903$, $n = 9$) with a detection limit (3σ) of 2 μg L^{-1}. Relative standard deviation ($n = 11$) was 3.6% for 100 μg L^{-1} Al(III). The typical FIA chart from standard samples is given in Fig. 4.

The present method was compared to other published methods, as indicated in Table 1, for both detection limit and dynamic range. As can be seen that the detection limit of this method was generally same as those by UV [13,15], resonance Rayleigh scattering [17] and fluorescence [19,20]. Although the detection limit of this method was two-order magnitude higher than the Al-lumogallion complex-peroxyoxalate CL detection method [32] and three-order magnitude higher than the 8-hydroxyquinoline preconcentration-Al-lumogallion complex-Brij-35 fluorescence detection method [18], direct determination of trace Al(III)

without derivation can only be realized by the proposed method.

3.6. Application to the real samples

It is reported that Al(III) level is less than 50 μg L^{-1} in bottled mineral water [4] and is commonly between 10 and 140 μg L^{-1} range [24] in tap water. The proposed method can be used for Al(III) measurement due to its relatively high sensitivity. As an illustration of analytical application, the proposed method was applied to the determination of Al(III) at trace level in the tap water and mineral water samples. The procedure for pretreatment of each collected sample was described in Section 2.4. In order to alleviate the matrix effects, standard-addition method was adopted for Al(III) analysis when performing real sample analysis. The recovery tests were also carried out on the samples. The results are shown in Table 2 and Fig. 5. In order to examine the validity of the proposed method, the results obtained by ICP-AES method as a reference method were compared with those obtained by the proposed method (Table 2). The results show that the proposed method can be applied to the determination of Al(III) in tap water and mineral water samples with satisfactory results. Furthermore, the results given by the proposed method are in good agreement with those given by ICP-AES methods and the obtained recoveries were satisfactory. This suggests that the proposed method is sensitive, reliable and might be promising for determination of Al content in real samples.

3.7. Possible CL mechanism

It was found that the reaction of potassium permanganate with luminol could produce weak CL, which was inhibited by Al(III) at pHs ≤ 10.42 and enhanced by Al(III) at pHs ≥ 11.45. The fluorescence spectra of the potassium permanganate–luminol reaction in the absence and presence of Al(III) were measured at pH 9.40 and 12.00, respectively. All fluorescence spectra were almost identical with a maximum wavelength at about 425 nm, which indicated that the luminophor in the absence and presence of Al(III) at different pH conditions could be aminophthalate.

The UV–vis absorption spectra of the potassium permanganate–luminol-Al(III) CL reaction indicates that

Table 1
Comparison of the performance of the developed method for Al analysis with that of other methods

Method used	Dynamic range (μg L^{-1})	Detection limit (μg L^{-1})	References
Al-quercetin complex-HPLC–UV	2.7–2160	1.4	[13]
Al(III)-salicylaldehyde picolinoylhydrazone (SAPH) complex-UV	5–30	1.9	[15]
Al(III)–morin-surfactant complex resonance Rayleigh scattering	2.7–243	1.2–3.2	[17]
8-Hydroxyquinoline preconcentration-Al-lumogallion complex-Brij-35 fluorescence	–[a]	0.004	[18]
Al-lumogallion complex-fluorescence	0–999	0.10–1	[19]
Aluminum–morin complex fluorescence	50–1000	3	[20]
Al-lumogallion complex-peroxyoxalate CL	0.582–533	0.042	[32]
Luminol–potassium permanganate CL	8–500	2	This work

[a] Not given in the Ref. [18].

Table 2
The determination of Al(III) in real water samples

Sample	ICP-AES method		The proposed FI-CL method	
	Found[a] (μg mL^{-1})	Added (μg mL^{-1})	Found[a] (μg mL^{-1})	Recovery[a] (%)
A (tap water)	0.10 ± 1.60	0	0.12 ± 3.80	
		0.10	0.21 ± 2.93	92 ± 2.66
		0.15	0.29 ± 3.04	111 ± 2.38
B (tap water)	–[b]	0	0.12 ± 3.50	
		0.10	0.22 ± 3.22	104 ± 3.01
		0.15	0.26 ± 2.35	94 ± 2.33
C (mineral water)	0.04 ± 5.00	0	0.04 ± 2.50	
		0.04	0.08 ± 4.37	92 ± 3.27
		0.05	0.08 ± 3.82	93 ± 2.10
D (mineral water)	0.02 ± 4.20	0	0.04 ± 1.70	
		0.04	0.08 ± 2.08	94 ± 1.98
		0.05	0.09 ± 2.36	112 ± 2.85

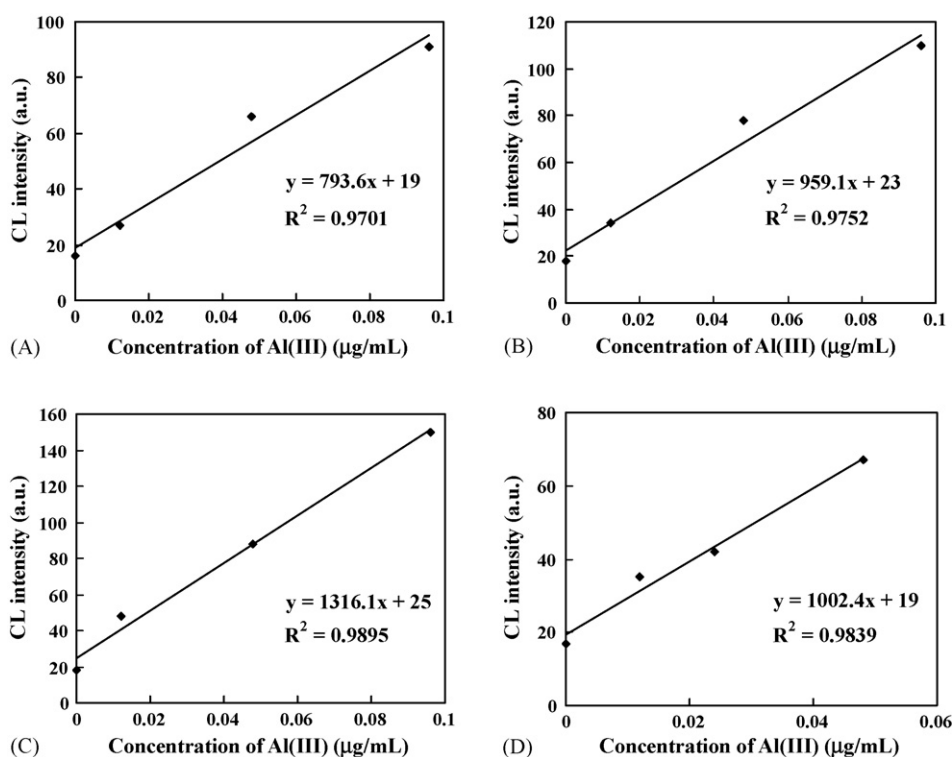[a] Averages of three determinations (R.S.D.%).
[b] Not analyzed.

Fig. 5. Results of standard-addition method for the determination of trace Al(III) level in real water samples. (A and B) The results from the tap waters; respectively. (C and D) The results from the mineral waters, respectively. Note that samples A and B were analyzed by dilution of 1:5; whereas samples C and D were analyzed by dilution of 1:2.

luminol was oxidized by potassium permanganate. However, there is no reaction between potassium permanganate and Al(III). Also there is no reaction between luminol and Al(III).

Based on the above discussion, the possible mechanism of the potassium permanganate–luminol-Al(III) CL reaction might be that aluminium(III) may form the hydroxide precipitate in mildly alkaline conditions, leading to the CL signal decrease due to turbidity occurring in mildly alkaline conditions. However, the hydroxide precipitate dissolves under strong alkali conditions, leading to enhancement CL signal.

4. Conclusion

The present study demonstrated, for the first time, the feasibility of employing the luminol–KMnO$_4$ CL reaction for the determination of trace Al via its inhibition effect on emission from potassium permanganate oxidation on luminol under relative lower basic pH. When compared to other analytical methods which employed FI for the detection of the Al, the sensitivity of the proposed method was same as those by fluorescence and resonance Rayleigh scattering. Moreover, the propose method

can reach direct chemiluminescence analysis of trace Al without derivatization. The method has been applied to the determination of trace Al in real water samples with satisfactory results without the pretreatment of samples. The results given by the proposed method are in good agreement with those given by ICP-AES detection method.

Acknowledgements

References

[1] R. Ren, D. Zhang (Eds.), Chemistry and Environment, Chemical Industry Press, Beijing, 2002.
[2] C.G. Magalhães, K.L.A. Lelis, C.A. Rocha, J.B.B. Silva, Anal. Chim. Acta 464 (2002) 323.
[3] J.L. Burguera, M. Burguera, R.E. Anton, J.-Louis Salager, M.A. Arandia, C. Rondon, P. Carrero, Y.P. de Pena, R. Brunetto, M. Gallignani, Talanta 68 (2005) 179.
[4] P. Maria, M. Agar, J. Food Compos. Anal. 8 (1995) 21.
[5] J.S. Verbeke, D. Verbeelen, D.L. Massart, Clin. Chim. Acta 108 (1982) 67.
[6] P. Allain, Y. Mauras, F. Khatchadourian, Anal. Chem. 56 (1984) 1196.
[7] E.A. Nater, R.G. Burau, M. Akeson, Anal. Chim. Acta 225 (1989) 233.
[8] G. Tanqen, T. Wickstr¢m, S. Lierhaqen, R. Vogt, W. Lund, Environ. Sci. Technol. 36 (2002) 5421.
[9] B. Fairman, A. Sanz-Medel, P. Jones, J. Anal. At. Spectrom. 10 (1995) 281.
[10] M. Luo, S. Bi, Environ. Chem. (Chin.) 22 (2003) 204.
[11] L. Sombra, M. Luconi, M.F. Silva, R.A. Olsina, L. Fernandez, Analyst 126 (2001) 1172.
[12] M. Luo, S. Bi, J. Inorg. Biochem. 97 (2003) 173.
[13] H. Lian, Y. Kang, S. Bi, Y. Arkin, D. Shao, D. Li, Y. Chen, L. Dai, N. Gan, L. Tian, Talanta 62 (2004) 43.
[14] O. Royset, Anal. Chem. 59 (1987) 899.
[15] G. Albendin, M.P. Manuel-Vez, C. Moreno, M. Garcia-Vargas, Talanta 60 (2003) 425.
[16] O.Yu. Nadzhafova, O.A. Zaporozhets, I.V. Rachinska, L.L. Fedorenko, N. Yusupov, Talanta 67 (2005) 767.
[17] X. Long, S. Bi, H. Ni, X. Tao, N. Gan, Anal. Chim. Acta 501 (2004) 89.
[18] J.A. Resing, C.I. Measures, Anal. Chem. 66 (1994) 4105.
[19] S.H. Sutheimer, S.E. Cabaniss, Anal. Chim. Acta 303 (1995) 211.
[20] S.M.Z. Al-Kindy, F.O. Suliman, S.B. Salama, Microchem. J. 74 (2003) 173.
[21] A. Alonso, M.J. Almendral, M.J. Porras, Y. Curto, C. García de María, Anal. Chim. Acta 447 (2001) 211.
[22] J. Zhang, H. Xu, J.L. Ren, Anal. Chim. Acta 405 (2000) 31.
[23] J.L. Ren, J. Zhang, J.Q. Luo, X.K. Pei, Z.X. Jiang, Analyst 126 (2001) 698.
[24] A.G. Howard, A.J. Coxhend, I.A. Potter, A.P. Watt, Analyst 111 (1986) 1379.
[25] J.F. Garcia Reyes, P. Ortega Barrales, A. Molina Diaz, Talanta 65 (2005) 1203.
[26] S. Satienperakul, T.J. Cardwell, S.D. Kolev, C.E. Lenehan, N.W. Barnett, Anal. Chim. Acta 554 (2005) 25.
[27] W.P. Yang, Z.J. Zhang, W. Deng, Anal. Chim. Acta 485 (2003) 169.
[28] S.M. Reza, J. Deepika, K.P. Jonathan, K.A. Hunter, Talanta 62 (2004) 924.
[29] P.L. Croot, L. Patrick, Anal. Chim. Acta 466 (2002) 261.
[30] B.X. Li, D.M. Wang, J.G. Lv, Z.J. Zhang, Talanta 69 (2006) 160.
[31] M.H. Sorouraddin, J.L. Manzoori, M. Iranifam, Talanta 66 (2005) 1117.
[32] M. Du, C.W. Huie, Anal. Chim. Acta 443 (2001) 269.

Determination of apparent reducing sugars, moisture and acidity in honey by attenuated total reflectance-Fourier transform infrared spectrometry

Luiz C.M. Pataca [a], Waldomiro Borges Neto [a], Maria C. Marcucci [b], Ronei J. Poppi [a,*]

[a] *Instituto de Química, UNICAMP, P.O. Box 6154, 13084-971 Campinas, SP, Brazil*
[b] *Universidade Bandeirante de São Paulo, Campus MC, Rua Maria Cândida, 1813, 02071-013 São Paulo, SP, Brazil*

Abstract

Attenuated total reflectance-Fourier transform infrared spectrometry, in conjunction with multivariate calibration, was used for determination of reducing sugars, humidity and acidity in honey bee samples. Multivariate calibration models were built using partial least squares (PLS) and were refined through variable selection per interval (iPLS) and genetic algorithms. The calibration models show satisfactory results for all parameters with average relative errors of 6% for acidity, 1% for reducing sugars and 2% for humidity. For the acidity and reducing sugars parameters, variable selection was irrelevant, but for humidity it was essential. For the humidity parameter, it was necessary to use two variable selection techniques (by intervals and genetic algorithm) concomitantly in order to obtain a satisfactory calibration model.
© 2006 Elsevier B.V. All rights reserved.

Keywords: Honey; Infrared spectroscopy; ATR; PLS

1. Introduction

Bee honey is a widely natural product used with production scattered all over the world. It is primarily used as a food, which therefore makes quality tests of utmost importance. Several agencies, such as Food and Agriculture Organization (FAO) and World Health Organization (WHO) of The United Nations through Condex Alimentarius Commission, which has become the global reference point for consumers, food producers and processors, national food control agencies and the international food trade, set quality parameters and methods of analysis for honey [1]. Some of these analytical methods are very time consuming, requiring intensive use of workforce and high execution costs.

The literature refers to some articles where vibrational spectroscopic techniques have been used for determination of some honey quality parameters. Several of them describe near-infrared spectroscopy (NIR) as the technique in the determinations.

Apparently, in literature there is no report of any application of the mid-infrared spectroscopy (MIR) to honey composition analysis. García-Alvarez et al. [2] had used NIR, combined with multiple linear regression (MLR), principal components regression (PCR) and modified partial least square (MPLS) to analyze fructose, glucose and moisture in honey. NIR was also used by Qiu et al. [3] in determination of moisture, fructose, glucose, sucrose and maltose but they did not obtain good results for free acid, lactone and hydroxymethylfurfural, which are trace components on honey. As on García-Alvarez article, Qiu used MLR, PCR and MPLS as statistical tools for data mining with best results being achieved using MPLS, except for moisture content, where the optimal calibration model was developed using PLS. It can be cited the work of Ha et al. [4] as another example of moisture, fructose, glucose and sucrose determination by NIR using PLS and MLR. Cho and Hong [5] have been used NIR combined with MLR and PLS to analyze moisture, inverted sugar, sucrose, hydroxymethylfurfural (HMF) and carbon stable isotope ratio (CSRI). Good results were obtained for moisture and CSIR, but for inverted sugar, sucrose and HMF validation results were considered to be insufficient for practical use implementation.

---

* Corresponding author. Tel.: +55 19 37883126; fax: +55 19 37883023.
 E-mail address: ronei@iqm.unicamp.br (R.J. Poppi).

Vibrational spectroscopy techniques, when combined with multivariate calibration, can be simple, of fast execution and low cost [6]. Mid-infrared spectroscopy displays more spectral information and better resolution of absorption bands than near-infrared spectrometry. The use of attenuated total reflectance (ATR) crystals greatly simplifies the process of spectra acquisition for viscous samples that contain humidity, such as honey samples.

Multivariate calibration is normally utilized to correlate spectral information with the property been studied (concentration of analytes). Multivariate calibration techniques using partial least squares (PLS) [7] have been widely utilized to obtain this correlation. Calibration models can be significantly improved through a process of variable selection. In this case, a set of spectral wavenumber is selected that will produce better prediction ability, based on errors of validation samples, in comparison with the full spectra. Therefore, techniques applying variable selection per interval (iPLS) [8] and genetic algorithm (GA) [9], with a view to obtain more accurate prediction values, have been used. The iPLS technique is based on the division of the spectrum into smaller intervals followed by the estimation of a PLS regression model for each interval. The root mean square error of cross-validation (RMSECV) is calculated for each model and compared to the value obtained for the whole spectrum. The region displaying the smallest value of RMSECV is then chosen [10]. The genetic algorithm is based on Darwin's theory of evolution and it is used for optimization processes. Each individual is composed of a set of "genes" (set of wavenumber) that are expressed in binary code. Each variable, or wavenumber, is given a binary representation of "1" or "0" (selected or not selected). The sets of variables that produce calibration models with the smallest value of the prediction error are selected in each generation and represent the most adapted individuals. New generations are produced by crossing between the most adapted individuals of the previous generation. Also mutations can be produced, which are utilized to give new "genetic" information to the population and to prevent its saturation with similar sets of genes (premature convergence). The disadvantages of variable selection by GA are: the possibility of generating a calibration model with overfitting (due to the number of generations or the dimension of the data matrix), the lack of reproducibility, because of its probabilistic nature, and computer running time. The last is becoming less relevant due to the evolution of computers [9]. With a view to avoid overfitting of the calibration model or even to obtain a calibration model with better prediction ability, the variables selected by the iPLS method can be used as input data in GA in an approach called GA–iPLS [11].

Apparent reducing sugars represent the great majority of the sugars in floral honey samples. In honeydew, however, the levels of these sugars are generally lower. A reducing sugar is a type of sugar with an aldehyde group. This allows the sugar to act as a reducing agent, for example, in the Benedict's test, which is used as method for determination of the presence of reducing sugars or more generally for the presence of aldehydes, in a solution. Benedict's reagent contains blue copper(II) sulfate $(CuSO_4)\cdot 5H_2O$ which is reduced to red copper(I) oxide by aldehydes, thus oxidizing the aldehydes to carboxylic acids. The copper oxide is insoluble in water and so precipitates. The colour of the final solution ranges from green to brick red depending on how many of the copper(II) ions are present. Reducing sugars on honey include mainly fructose and glucose. Significantly, sucrose is not a reducing sugar. The determination of this parameter is used for differentiating floral honey from honeydew. Another important parameter to describe honey quality is moisture, since honeys with high levels of water tend to ferment more easily. Acidity is an excellent indicator of the fermentation process, since there is an increase in the acidity of samples which are undergoing fermentation.

In this work, acidity, humidity and reducing sugars were determined in multi-floral honey samples through mid-infrared spectrometry using attenuated total reflection with a ZnSe crystal sampling accessory. Multivariate calibration based on PLS was used to built a model to establish a relation between the MIR spectra and the quality parameters obtained by standard methods. Finally, variable selection using iPLS, GA and a combination of both (GA–iPLS), were employed to improve the modeling performance.

2. Materials and methods

2.1. Samples

In this work, 48 authentic blossom honey samples, provided by Natural Labor, Campinas, Brazil, were employed. The parameters apparent reducing sugars, moisture and acidity had already been determined on these samples by Natural Labor. These values were used as reference values and they were determined by using official published methods. Apparent reducing sugars were determined following AOAC Official Method 920.183—sugars (reducing) in honey, which is based on a titrimetric redox method. Acidity was determined following the acid–base titrimetric AOAC Official Method 962.19—acidity (free, lactone and total) on honey. Moisture was determined following refractometer reading of honey at $20\,^{\circ}C$ (AOAC Official Method 969.38B—moisture in honey) [12].

2.2. Mid-IR spectroscopy

The MIR spectra were collected in triplicate using a ABB Bomem spectrometer, model MB100, with a DTGS detector and attenuated total reflectance with a ZnSe crystal sampling accessory. The spectrometer was operated with a resolution of $4\,cm^{-1}$ and 64 scans for each spectrum. Initially, spectra were taken by filling the sample holder with the honey sample. However, due to high sugar concentrations of honey, the spectra were very noisy and the absorbances showed values up to 3. To solve this problem, an area delimiter consisting of a plastic tube with 7.0 mm internal diameter and 10 mm length was constructed. The delimiter was placed onto the ZnSe surface in a fixed position (see Fig. 1). Spectra were taken with honey samples placed inside this delimiter. There was no laborious procedure for sample preparation before the spectra acquisition step. They were
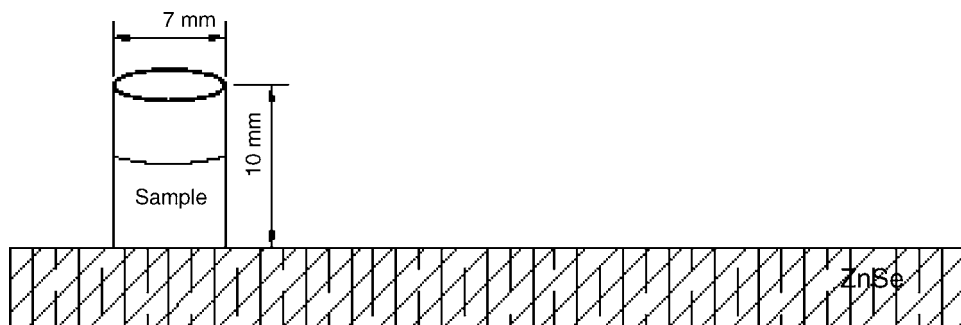
Fig. 1. Scheme of the plastic tube placed on the ATR crystal.

only heated for 2 h at 40 °C on a water bath to dissolve any crystals present.

2.3. Data sets

In the chemometric data treatment, the average of triplicate spectra was used. Samples were split into two groups, a calibration group and a validation group. Before sample group definition, the spectra were smoothed using the Savitzky–Golay algorithm [13] with 15 points in the filter (width) and a polynomial of order one. The groups were separated according to the Kennard–Stone algorithm [14] where samples are selected sequentially, spaced over the space defined by the variables. The first sample selected is the most different one based on the Euclidean distance. Each new sample is calculated using the distance from the previously selected samples. The algorithm will take always the farthest from the previously selected samples [14]. Partial least squares, based on factor decomposition of data set, was the base for all models developed, since it is the standard multivariate calibration methodology nowadays. PLS calibration models were built using a centered data set and the SIMPLS algorithm [15]. The number of significant latent variables was chosen using cross-validation based on the leave-one-out procedure.

For PLS multivariate calibration models, the PLS_Toolbox 3.5 from Eigenvector Research [16] was used. Variable selection based on iPLS was performed using the iToolbox for Matlab from Chemometrics Group-KVL, Copenhagen, Denmark [17]. The GA was performed using the GASELCTR routine from PLS_Toolbox 3.5, where it was minimized the cross-validation error for variable selection.

3. Results and discussion

Fig. 2 shows a typical honey infrared spectrum with vibrational assignments. As honey consists essentially of a watery solution of different sugars, predominantly fructose and glucose [18], MIR spectrum of honey is dominated by sugar and water absorptions. The main absorptions from sugars arise in the region from 800 to 1500 cm^{-1} [19]. Bands appearing between 1470 and 1150 cm^{-1} are due to bending modes of C–C–H, C–O–H, and O–C–H groups. The more intense peaks in the region 1150–900 cm^{-1} arise mainly from C–O and C–C stretching modes, with a peak around 1060–1020 cm^{-1} due to O–H

vibrations [20]. O–H and C–H stretching vibrations from sugars are expected to appear in the 3300–2820 cm^{-1} region [20]. The band frequencies of stretching and bending modes water appear at 3336 and 1635 cm^{-1}, respectively [21].

3.1. Acidity

Acidity reference values of the samples had values varying from 20.8 to 47.4 meq kg^{-1}. The samples were split into a calibration and a validation group with 32 and 16 samples, respectively. The PLS models created with these sample groups did not present good results, so it was done an outliers analysis following methodology described by Martens and Naes [22]. It was created a whole spectrum PLS model with all samples which presented eight outliers by residual analysis [22]. These outliers were removed and the remaining samples were split again into calibration and validation groups with 31 and 9 samples, respectively. A new PLS model was created and the predicted values for validation samples were determined using the PLS calibration model previously developed. From the predicted acidity values, the relative error for each sample was calculated, following the equation:

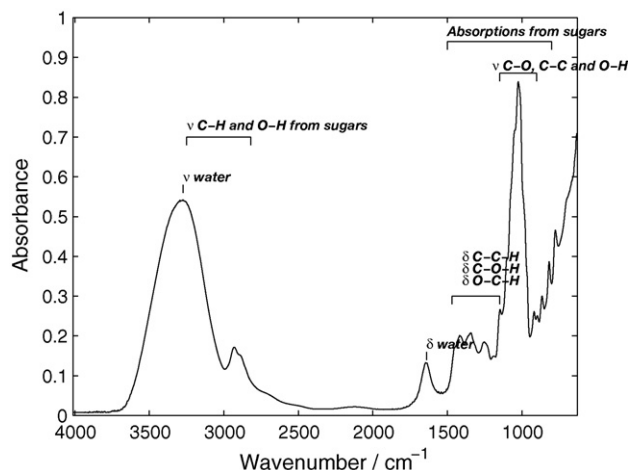$$\text{Relative error} = \sqrt{\frac{(y_p - y_r)^2}{y_r^2}} \times 100$$

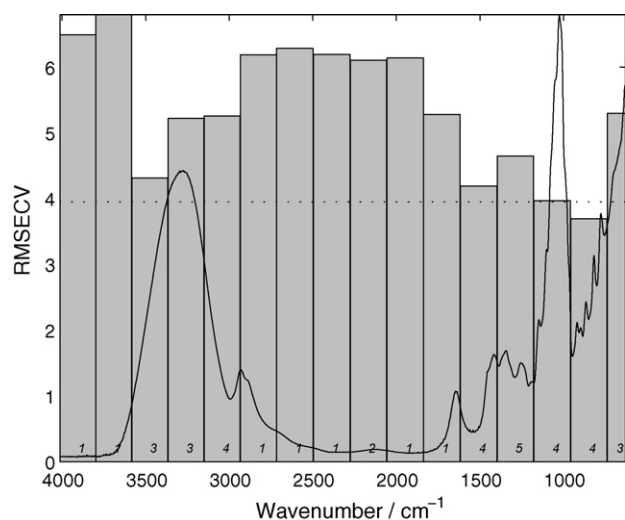Fig. 2. Infrared spectra of honey in the region of 4000–750 cm^{-1}.

Fig. 3. Cross-validated prediction errors (RMSECV) for 16 intervals (bars) for acidity determination and full spectrum of honey (line).

where y_p is predicted value by PLS model and y_r is reference value determined by AOAC method.

For accomplishment of iPLS, several sub-intervals division were initially tested in the range of 5–40 and the best results were reached when the spectrum was divided into 16 sub-intervals. In Fig. 3, the bar indicates the root mean square error of cross-validation for each interval model and the doted line corresponds to RMSECV for the global model (all variables) which was built with five latent variables (LV). The italicized numbers inside each error bar are the optimal number of latent variables for each interval model. The interval corresponding to wavenumbers from 738.7 to 956.6 cm^{-1} (second interval in Fig. 3) was chosen, since it produced the lowest RMSECV. The PLS model constructed with this interval of variables did not show lower root mean square error of prediction (RMSEP) values than the full spectrum PLS model (Table 1). Other interval combinations were tested, but none produced better prediction values. It is possible that the acidity information is spread on the whole spectral range and a variable selection per interval will automatically reduce the information and induce an increase of RMSEP compared with PLS.

The genetic algorithm was applied to the full spectrum (GA–PLS procedure) and to the iPLS interval region selected from 738.7 to 956.6 cm^{-1} (GA–iPLS procedure). The lower RMSEP was obtained using the whole spectrum as input for the GA. Table 1 shows the statistical indicators from PLS calibration models built for acidity. The correlation coefficient (R^2) in

Table 1
Statistical indicators for acidity calibration models

Indicator	PLS	iPLS	GA–PLS	GA–iPLS
Number of latent variables	5	4	4	4
RMSEP (%)	2.20	3.35	2.62	3.21
Minimum relative error (%)	0.37	1.45	0.55	2.07
Maximum relative error (%)	15.9	16.8	24.9	16.5
Mean relative error (%)	5.99	8.68	6.81	8.48
R^2	0.893	0.839	0.826	0.839

Table 2
Acidity reference and predicted values for validation samples

Reference values[a] (meq kg^{-1})	R.S.D.[b] (%)	Predicted values (meq kg^{-1})	Relative error (%)
20.8 ± 0.9	4.3	24.1	16
32.2 ± 0.6	1.9	31.0	3.8
38.2 ± 1.3	3.4	33.8	11
29.3 ± 1.2	4.1	27.4	6.6
33.3 ± 0.6	1.8	32.5	2.3
26.9 ± 0.8	3.0	27.6	2.7
32.7 ± 0.9	2.8	32.6	0.4
31.8 ± 0.6	1.9	29.3	7.8
32.7 ± 1.4	4.3	31.7	3.0

[a] Values determinated on triplicate.
[b] Relative standard deviation (R.S.D.).

Table 1 was computed from the regression line obtained between the predicted PLS values and the reference values obtained from the official method. Although the use of the whole spectrum (PLS procedure) yield the lowest values of RMSEP and mean relative error, there is no significant difference between this model and all other ones studied when comparing RMSEP values using an *F*-test at 95% of confidence. Therefore, no improvement in the results could be observed using any variable selection method. It was only possible to find a narrow spectral region (by using iPLS), related to sugar absorption (see Fig. 2) that can be used for acidity prediction.

Of the three parameters studied (acidity, reducing sugars and humidity), acidity presented the largest prediction errors using the calibration models developed. This might be explained by the uncertainty data of the reference values. For acidity, the reference values in the honey samples presented uncertainties with relative standard deviations of up to 9%. The reference method AOAC Official Method 962.19 – acidity (free, lactone and total) on honey, consists in the dissolution 10 g of honey on 75 mL CO_2 – free H_2O and titration with 0.05N NaOH at rate of 5.0 mL min^{-1}. Addition of NaOH is stopped at pH 8.50. Immediately, it is added 10 mL of 0.05N NaOH, and back-titration with 0.05N HCl in 10 mL buret is performed until pH 8.30. Changes in addition speed of the NaOH can affect the final results of the determination. The utilization of an automatic buret could improve the precision of the analyses. However, our laboratory did not possess such equipment. The low precision on acidity reference values led to high RMSEP values for the predictions. Table 2 presents results for acidity determination by AOAC Official Method 962.19 (in triplicate) and by PLS model.

3.2. Reducing sugars

Reducing sugars calibration PLS models were built in a similar way as for the acidity parameter. Residual analysis from the full spectrum PLS model did not show any outliers, so all samples were used, and calibration and validation groups produced by the Kennard–Stone algorithm had 32 and 16 samples, respectively. Reducing sugars values varied from 61.1 to 79.0% for all honey samples. On samples selected for validation, values were from 69.9 to 77.1%.
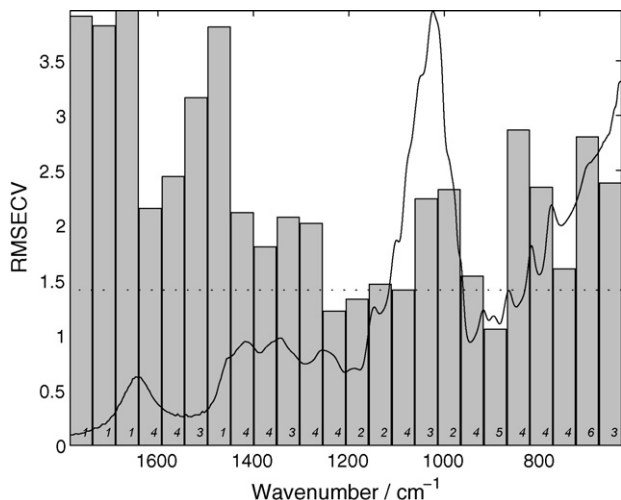
Fig. 4. Cross-validated prediction errors (RMSECV) for 24 intervals (bars) for reducing sugars determination and full spectrum of honey (line).

In the iPLS approach, the best results were achieved for division of the spectrum in 24 intervals. Others number of intervals and combinations of them were tried, but no improvement in the results was observed. Variable selection by intervals led to the choice of the wavenumber region from 869.8 to 916.1 cm^{-1}, which corresponds to the sixth interval in Fig. 4. The PLS model developed using this interval presented better prediction results but there is no significant difference between all models using a *F*-test at 95% of confidence. The utilization of the genetic algorithm again does not led to a better model in both GA–PLS and GA–iPLS models. Table 3 shows the statistical indicators of the PLS calibration models developed for the reducing sugar parameter. For the iPLS model, the results show a good correlation between reference values and values predicted by the model, indicated by a correlation coefficient of 0.920. Again using iPLS it was possible to find a narrow region for reducing sugar determination, in the range of 869.8–916.1 cm^{-1}, closed related to sugar absorption (see Fig. 2). Table 4 shows reference values which were determined by AOAC Official Method 920.183, on triplicate, and iPLS model predicted values for reducing sugars.

3.3. Humidity

As for the reducing sugars, there were no outliers for the humidity. Therefore, the data treatment was performed using the same steps as for the reducing sugars parameter. Once again, a group of calibration samples with 32 samples and another vali-

Table 4
Reducing sugars reference and predicted values for validation samples

Reference values[a] (%)	R.S.D.[b] (%)	Predicted values (%)	Relative error (%)
79.0 ± 0.3	0.38	78.7	0.40
74.6 ± 0.9	1.2	76.1	2.1
71.9 ± 0.9	1.2	72.7	1.2
74.2 ± 0.3	0.40	74.9	0.98
74.2 ± 0.3	0.40	74.6	0.61
74.4 ± 0.3	0.40	74.2	0.20
73.7 ± 0.3	0.41	73.7	0.00
75.0 ± 0.3	0.40	76.9	2.5
73.7 ± 0.3	0.41	72.7	1.4
74.2 ± 0.3	0.40	73.6	0.82
77.1 ± 0.3	0.39	76.0	1.5
74.6 ± 0.1	0.13	76.0	1.9
67.1 ± 0.1	0.15	68.3	1.8
74.6 ± 0.9	1.2	73.6	1.3
71.4 ± 0.1	0.14	73.1	2.4
76.3 ± 0.1	0.13	76.3	0.035

[a] Values determined on triplicate.
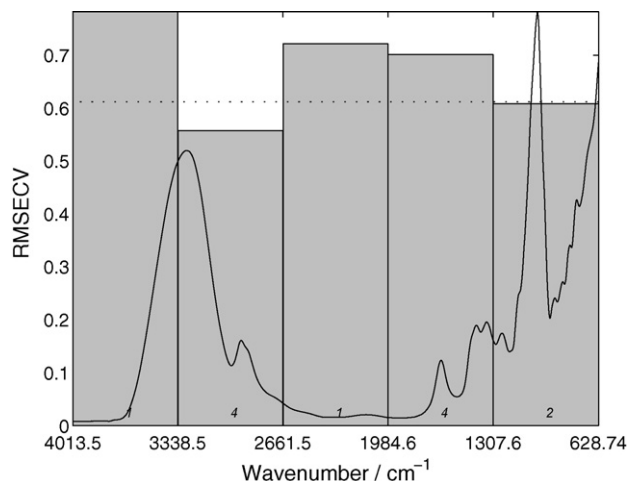[b] Relative standard deviation (R.S.D.).

Fig. 5. Cross-validated prediction errors (RMSECV) for five intervals (bars) for humidity determination and full spectrum of honey (line).

dation group with the rest of the samples were created according to the Kennard–Stone algorithm. The following calibration models: PLS, iPLS, GA–PLS and GA–iPLS, were developed.

In this case, the best results for iPLS were achieve when the spectrum was split in five intervals as shown in Fig. 5. The prediction results shown in Table 5 by PLS in the whole spectrum and GA–PLS calibration models were not satisfactory,

Table 3
Statistical indicators for reducing sugars calibration models

Indicator	PLS	iPLS	GA–PLS	GA–iPLS
Number of latent variables	7	5	5	4
RMSEP (%)	1.28	1.04	1.31	1.03
Minimum relative error (%)	0.26	0.0019	0.093	0.093
Maximum relative error (%)	3.60	2.47	3.89	2.21
Mean relative error (%)	1.44	1.184	1.37	1.24
R^2	0.762	0.846	0.755	0.843

Table 5
Statistical indicators for humidity calibration models

Indicator	PLS	iPLS	GA–PLS	GA–iPLS
Latent variables	3	4	7	7
RMSEP (%)	0.52	0.41	0.61	0.32
Minimum relative error (%)	0.49	0.029	0.25	0.17
Maximum relative error (%)	4.87	3.77	6.98	4.24
Mean relative error (%)	2.50	1.98	3.01	1.45
R^2	0.450	0.796	0.163	0.823

Table 6
Reference values and predicted values for humidity on validation samples

Reference values[a] (%)	R.S.D.[b] (%)	Predicted values (%)	Relative error (%)
17.6 ± 0.1	0.57	17.5	0.71
17.2 ± 0.3	1.7	17.4	1.3
16.9 ± 0.2	1.2	16.9	0.17
17.2 ± 0.1	0.58	17.6	2.6
17.1 ± 0.1	0.58	17.5	2.4
17.2 ± 0.1	0.58	17.4	0.96
17.7 ± 0.1	0.56	17.6	0.79
18.1 ± 0.1	0.55	17.8	1.5
17.7 ± 0.1	0.56	17.5	1.0
17.5 ± 0.1	0.57	17.3	1.2
18.3 ± 0.1	0.55	18.2	0.51
18.6 ± 0.2	1.1	18.2	2.2
17.2 ± 0.2	1.2	17.5	1.6
18.4 ± 0.2	1.1	18.3	0.27
19.0 ± 0.1	0.53	18.2	4.2
18.8 ± 0.1	0.53	18.5	1.7

[a] Values determined on triplicate.
[b] Relative standard deviation (R.S.D.).

presenting a correlation coefficient between prediction values and reference values of 0.671 and 0.404, respectively. Variable selection by intervals led to a significant improvement in the results, achieving a correlation coefficient of 0.907 for the GA–iPLS model. Frequency bands between 2665.4 and $3338.5 \, cm^{-1}$ (fourth interval in Fig. 5), which correspond to the beginning of the stretching band of the O−H bond of water, were utilized. Table 5 shows statistical indicators for the PLS calibration models developed for the humidity parameter. At first sight, it seems that the genetic algorithm may not be necessary as it makes only a small improvement in the results. Nevertheless, since humidity variation is relatively small in honey (15.6–19.3% for the samples in this study), this slight improvement became essential for the viability of the calibration model. An *F*-test performed at 95% of confidence indicated that the results for GA–iPLS are significantly different from the iPLS ones, showing the improvement when the variables selected by iPLS are inputted in the GA algorithm. For this parameter, the GA–iPLS has been selected only 15 variables for the model development. Table 6 shows reference values which were determined by AOAC Official Method 969.38B, on triplicate, and GA–iPLS model predicted values for humidity.

4. Conclusions

The utilization mid-infrared spectroscopy combined with multivariate calibration based on PLS with variable selection techniques make possible the development of calibration models that have satisfactory power of prediction for the quality parameters of honey studied: acidity, reducing sugars and humidity. The variable selection techniques studied produced irrelevant results in the case of acidity and reducing sugars, since for these parameters the information is spread on the whole spectral range and the use of a narrow region can reduce the information. Otherwise, for the humidity parameter, it was necessary to use the two variable selection techniques (by intervals and by genetic algorithm) concomitantly in order to obtain a satisfactory calibration model. In this case, the information is on the stretching band of the O−H bond of water.

References

[1] CODEX STAN 12, Revised Codex Standard for Honey, Rev. 2, 24th Session of the Codex Alimentarius in 2001, CODEX, Rome, 2001.
[2] M. García-Alvarez, J.F. Huidobro, M. Hermida, J.L. Rodríguez-Otero, J. Agric. Food Chem. 48 (2000) 5154.
[3] P.Y. Qiu, H.B. Ding, Y.K. Tang, R.J. Xu, J. Agric. Food Chem. 47 (1999) 2760.
[4] J. Ha, M. Koo, H. Ok, J. Near Infrared Spectrosc. 6 (1998) A367.
[5] H.J. Cho, S.H. Hong, J. Near Infrared Spectrosc. 6 (1998) A329.
[6] J.F.D. Kelly, G. Downey, V. Fouratier, J. Agric. Food Chem. 52 (2004) 33.
[7] P. Geladi, B.R. Kowalski, Anal. Chim. Acta 185 (1986) 1.
[8] L. Norgaard, A. Saudland, J. Wagner, J.P. Nielsen, L. Munck, S.B. Engelsen, Appl. Spectrosc. 54 (2000) 413.
[9] R. Leardi, J. Chemom. 14 (2000) 643.
[10] J. Paschoal, F.D. Barboza, R.J. Poppi, J. Near Infrared Spectrosc. 11 (2003) 211.
[11] R. Leardi, L. Norgaard, J. Chemom. 18 (2004) 486.
[12] M.A. Clarke, in: P. Cunniff (Ed.), Official Methods of Analysis of AOAC INTERNATIONAL, 16th ed., AOAC International, Gaithersburg, 1995, p. 22.
[13] A. Savitzky, M.J.E. Golay, Anal. Chem. 36 (1964) 1627.
[14] R.W. Kennard, L.A. Stone, Technometrics 11 (1969) 137.
[15] S. Dejong, Chemom. Intell. Lab. Syst. 18 (1993) 251.
[16] B.M. Wise, N.B. Gallagher, R. Bro, J.M. Shaver, W. Windig, R.S. Koch, PLS Toolbox 3.5 for use with MATLAB, Eigenvector Research Inc., Manson, 2005.
[17] L. Norgaard, iToolbox for Matlab, Chemometrics Group, Food Technology, KVL, Copenhagen, Denmark, 2004.
[18] L.W. Doner, J. Sci. Food Agric. 28 (1977) 443.
[19] F. Cadet, B. Offmann, Spectrosc. Lett. 29 (1996) 523.
[20] M. Hineno, Carbohydr. Res. 56 (1977) 219–227.
[21] J. Grdadolnik, Int. J. Vib. Spectrosc. (2004), http://www.ijvs.com/volume6/edition2/section3.html.
[22] H. Martens, T. Naes, Multivariate Calibration, John Wiley & Sons, Chichester, 1989.

ELSEVIER

Quantification of volatile PAHs present at trace levels in air flow by aqueous trapping—SPE and HPLC analysis with fluorimetric detection

F. Portet-Koltalo [a], K. Oukebdane [a], L. Robin [b],
F. Dionnet [b], P.L. Desbène [a,*]

[a] *Laboratoire d'Analyse des Systèmes Organiques Complexes, UPRES 3233 (SMS)-IRCOF et IFRMP, Université de Rouen,
55 rue Saint Germain, 27000 Evreux, France*
[b] *CERTAM, Technopole du Madrillet, 1 rue Joseph Fourier, 76800 Saint Etienne du Rouvray, France*

Abstract

In the context of a European project, a new approach of sampling of volatile polycyclic aromatic hydrocarbons (PAHs) from air was developed. In fact, the aim of this project was to test the efficiency of an air cleansing prototype reactor, which was operating by non-thermal plasmolysis. With an eye to model the atmosphere ejected by the prototype, we needed to vaporise the volatile PAHs in an air stream at concentrations as low as those recommended by European Directives (96/62/CE) for PAHs in ambient air (i.e. $1 \, \text{ng m}^{-3}$). Our strategy was based on the analysis of PAHs trapped in an aqueous medium, in order to avoid important losses of volatile compounds observed during the delicate desorption–concentration step when classical solid supports are used. Then a study was carried out to determine: the design of the collecting part, the flow-rate of the air sampling, the nature and concentration of chemical additives used to enhance PAH solubility in water. The very highly diluted aqueous media obtained after the bubbling step were concentrated by solid-phase extraction (SPE) on hydrophobic cartridges and analysed on-line by reversed-phase HPLC with UV and fluorimetric detections. Lastly, the sampling technique was directly applied to the outlet of the air cleansing prototype and the analysis after 3–6 h of non-thermal plasmolysis showed that the target volatile PAHs were not present in an air stream initially polluted by volatile organic compounds.
© 2006 Published by Elsevier B.V.

Keywords: Aerosol PAH analysis; Aqueous trapping; On-line SPE-HPLC coupling; Fluorimetric detection

1. Introduction

Polycyclic aromatic hydrocarbons (PAHs) are environmental pollutants formed during the incomplete combustion of carbonaceous materials at high temperature. Due to their toxic, carcinogenic and mutagenic effects, as well as their ubiquity in the environment (water, air and soils) these compounds received a great research interest [1–3]. Today strict legal controls are imposed in order to regulate production, use and emission of PAHs. According to the European Union requirements about ambient air quality assessment and monitoring (96/62/CE directive), a value of $1 \, \text{ng m}^{-3}$, considered as an annual mean of daily measurements, was recommended on September 1996 as a limit

value in ambient air for benzo(*a*)pyrene and $0.1 \, \text{ng m}^{-3}$ as a target value. The French National Health Council also issued on September 1997 a recommendation proposing $0.7 \, \text{ng m}^{-3}$ as a limit value and $0.1 \, \text{ng m}^{-3}$ as a target value. Although benzo(*a*)pyrene is essentially found in particulate matter, it is particularly carcinogenic and considered as the marker of all PAHs [4]. However, volatile and semi-volatile PAHs (containing less than five aromatic rings), which are known to be less carcinogenic, must be also considered because they are particularly abundant in the gas phase [5]. It is the case of naphthalene, phenanthrene, anthracene, fluoranthene and pyrene.

In the context of a European project, we developed a new approach of sampling of these volatile PAHs from an air flow emitted at the outlet of an air cleansing prototype. In fact the aim of this prototype was to eliminate pollutants present in the air, those initial pollutants being volatile organic compounds (VOC). Then we had to insure that the clean up process, consisting in

---

non-thermal plasmolysis generated by gliding arcs and catalysis [6], did not produce other harmful pollutants such as volatile PAHs.

Aerosol pollutants can be collected by means of high volume sampling apparatus (HVS), sampling rates ranging from 15 to $30\,m^3\,h^{-1}$, during about 10 h [7,8]. These apparatus are generally equipped with glass fiber filters or aluminium foils to trap the particulate matter and with polyurethane foams or XAD-2 sorbents to collect the PAHs present in the gas phase. However, low volume sampling impactors (LVS) are generally preferred, because the losses of volatile or semi-volatile PAHs which occur during the high-volume sampling are reduced [9,10]. For such impactors, sampling rates range only from 1 to $3\,m^3\,h^{-1}$ and consequently longer sampling periods, from a few days to a few weeks, are necessary to collect sufficient quantities of pollutants. Consequently this large time consuming technique also leads to significant losses of the more volatile PAHs whose molecular weights are less than that of phenanthrene [11,12]. Lastly an additional step is necessary before the chromatographic analysis of collected PAHs, namely the quantitative desorption of the analytes from the solid trapping matrix. Aerosol PAHs are traditionally extracted from a solid support by means of Soxhlet apparatus or by ultrasonication, sometimes by using microwave-assisted extraction (MAE) [13,14]. However, sample concentration by evaporation and clean up procedures are required prior to the chromatographic analysis. Now these steps are unfortunately very critical in order to achieve quantitative results concerning volatile PAHs.

For all these reasons, we chose to collect our target volatile PAHs (naphthalene, phenanthrene, anthracene, fluoranthene and pyrene) at the outlet of the air cleansing prototype directly into a liquid phase and not on a solid support, in order to avoid any sample loss after the extraction step and the inevitable concentration by evaporation. In fact the aqueous phase containing trapped PAHs could be directly analysed by reversed phase HPLC with UV and fluorimetric detection. Indeed most PAHs are inherently fluorescent and using a fluorescence detector can increase the detection sensitivity to the parts-per-billion level [15,16]. Moreover, if necessary, a preliminary quantitative concentration step by solid phase extraction (SPE), which can also be used as a sample clean up procedure [17], could be developed prior to the chromatographic analysis, in place of solvent evaporation, in order to reach parts-per-trillion level.

2. Experimental

2.1. Apparatus

2.1.1. HPLC analyses
The HPLC analyses were performed using a gold liquid chromatography system (pumps model 126, Beckman, Fullerton, USA) equipped with a diode array UV detector (model 168 Beckman). A Prostar fluorimetric detector from Varian was used on line (Varian, Palo Alto, USA). Reversed phase analyses were carried out using an octadecyl Ultrasphere column (250 mm × 4.6 mm i.d., $d_p = 5\,\mu m$) purchased from Beckman.

2.1.2. Solid phase extraction (SPE)
For liquid solid extractions, an empty steel column (30 mm × 4.6 mm) purchased from Alltech (Alltech France, Templemars, France) was filled with a trifunctional C_{18} solid phase ($d_p = 37$–55 μm) provided by Waters (Waters France, St. Quentin en Yvelines, France). We also tested a monofunctional C_{18} Ultrasphere precolumn (45 mm × 4.6 mm, $d_p = 5\,\mu m$) from Beckman. Functionality refers to the number of linear C_{18} side-chains emanating from a branch point on silica surfaces. The cation exchange cartridge Spherisorb SCX (30 mm × 4.6 mm, $d_p = 5\,\mu m$) was purchased from Waters. Finally a HPLC pump (model 510, Waters) was used for the percolation step.

2.1.3. Generation of gaseous PAHs
Nitrogen of Alpha gas 1 quality (Air Liquide, Ivry, France) was used as carrier gas. The heating resistance was purchased from Bioblock (Fisher Bioblock scientific, Illkirsh, France) whereas the temperature controller was provided by Corame (Mont Saint Aignan, France). When we tested the efficiency of the air cleansing prototype, a KNF Neuberger vacuum pump (Village-Neuf, France) was substituted to the generator of gaseous PAHs. The flowmeter used to control the aspiration flow-rate was provided by System C Industrie (Bourg Saint Andeol, France).

2.2. Solvents and samples

Water was purified and deionised using a Direct Q3 system from Millipore (Millipore France, Molsheim, France). Acetonitrile, methanol and isopropanol were of HPLC grade and purchased from SDS (Peypin, France). Diethanolamine (purity > 99%) came from Accros Organics (Accros Organics France, Noisy le Grand, France). Acetone, isopropanol and toluene, used as volatile organic compounds (VOC), came from Brenntag (Brenntag Nord, Wattrelos, France). Naphthalene (NAPH, purity > 99%), anthracene (ANT, purity > 99%), fluoranthene (FLUO, purity > 99%), phenanthrene (PHEN, purity > 96%) and pyrene (PYR, purity > 98%) were furnished by Sigma–Aldrich, France. Cetyl trimethyl ammonium bromide (CTAB, purity > 96%), Hexadecyl pyridinium chloride (HPC, purity > 99%), Octadecyl trimethyl ammonium bromide (OTAB, purity > 98%) and Sodium dodecyl sulfate (SDS, purity > 99%) were all purchased from Sigma–Aldrich, France. Brij 58 was furnished by Accros Organics France. At last, NaCl (purity > 99%) was obtained from Sigma–Aldrich, France.

2.3. Vaporization of PAHs and collection into an aqueous phase

PAH vaporization and trapping were performed by means of an experimental home-made apparatus, constituted on one hand of a flow-through generator of gaseous PAHs and on the other hand of two glass bubbling bottles containing an aqueous medium (capacity: 2 L) and an empty safety bottle. The two parts of the device were connected by a short PTFE tube and a heating wire was wrapped round this tube in order to minimize

Table 1
Wavelength programs as a function of time, used to detect the five target PAHs with UV and fluorescence detections, and limits of detection (LOD) and quantification (LOQ)

Detection	UV					Fluorescence				
Wavelength program	$t = 0$, $\lambda = 220$ nm (NAPH)[a] $t = 9.5$ min, $\lambda = 250$ nm (PHEN/ANT)[a] $t = 12.9$ min, $\lambda = 235$ nm (FLUO/PYR)[a]					$t = 0$, $\lambda_{ex} = 220$ nm, $\lambda_{em} = 330$ nm (NAPH)[a] $t = 9.5$ min, $\lambda_{ex} = 252$ nm, $\lambda_{em} = 370$ nm (PHEN/ANT)[a] $t = 12.9$ min, $\lambda_{ex} = 235$ nm, $\lambda_{em} = 420$ nm (FLUO/PYR)[a]				
	NAPH	PHEN	ANT	FLUO	PYR	NAPH	PHEN	ANT	FLUO	PYR
LOD (μg L^{-1})	4	9	5	14	15	0.3	0.2	0.2	0.7	0.8
LOQ (μg L^{-1})	14	29	16	46	50	0.9	0.8	0.5	2.2	2.5

[a] Compounds detected in the program segment.

the PAH condensation after vaporization. The temperature of this heating wire was kept constant at 180 °C by a temperature controller. Experiments were started by injecting 30 μL of PAH standard solutions (from 0.1 to 1 mg L^{-1}) into a round-bottom glass flask containing 10 mL of diethanolamine. Then, the flask was immersed into a pre-heated silicon bath (200 °C). This flask was connected to a flow-rate regulator and to a nitrogen pressure controller. Then the vaporized PAHs were carried away by the nitrogen through the second part of the device. The duration of the sampling test was generally equal to 3 h and the collecting recoveries were all determined in duplicate.

2.4. Trace enrichment

An empty column was filled with 180 mg of the trifunctional C$_{18}$ solid phase and was sonicated for a period of 10 min. Then this column was washed with water, at a flow-rate equal to 1 mL min^{-1} during 10 min, then with methanol (10 min) and lastly with water (10 min). After sonication (5 min), the aqueous medium containing the trapped PAHs was percolated through this cartridge. Such a cartridge was used approximately five times and was each time flushed by a sequence of 10 min with pure water, followed by 20 min of methanol and then 10 min of pure water, at a flow-rate equal to 1 mL min^{-1}.

2.5. HPLC analysis of target volatile PAHs

The separation of the five volatile target PAHs was achieved by using an octadecylsilane stationary phase and a mixture of acetonitrile and water 75:25 (v:v) as an isocratic mobile phase, the flow-rate being equal to 1 mL min^{-1} and the temperature set to 20 °C. In order to enhance the limits of detection, we determined the maximum UV absorption wavelengths for each studied compound and the optimal excitation (λ_{ex}) and emission wavelengths (λ_{em}) for fluorimetric detection. Segments of excitation/emission wavelength pairs were then programmed as a function of time as reported in Table 1. Lastly, we chose a 30 μL injection loop, without noticeable loss of chromatographic performances compared to those obtained in the case of classical 5 or 10 μL loops. Under such conditions the limits of detection (LOD, calculated as three times the background noise) and the limits of quantification (LOQ, calculated as 10 times the

background noise) could be calculated for UV and fluorimetric detections, as reported in Table 1.

2.6. Aqueous trapping at the outlet of the air cleansing prototype

Two bottles, containing silica gel, were added to the assembly described in part 2.3, to protect the flowmeter and the vacuum pump from humidity (see Fig. 1). Moreover, a collecting glass probe was connected to the first bubbling bottle. The heating wire was now wrapped round this collecting probe and was kept at 180 °C in order to minimize the condensation of PAHs. Indeed the temperature of the atmosphere coming from the outlet of the air cleansing prototype was measured and equalled approximately 190–200 °C.

The diameter of the air cleansing prototype exhaust pipe was equal to $D_1 = 60$ mm and the air flow-rate was approximately $Q_{v1} = 15$ m^3 h^{-1}. To operate at constant linear speed between the prototype (v1) and the home-made sampling apparatus (v2), it was necessary to solve the following equations:

$$v1 = v2 \Rightarrow \frac{Q_{v1}}{D_1{}^2} = \frac{Q_{v2}}{D_2{}^2} \Rightarrow Q_{v2} = 0.104 \, \text{m}^3 \, \text{h}^{-1}$$

with $D_2 = 5$ mm (internal diameter of the sampling probe and all glass tubings of the sampling system). Consequently the flowmeter placed before the vacuum pump was set to 0.1 m^3 h^{-1} during all the sampling time.

3. Results and discussion

3.1. Optimisation of trace enrichment by solid-phase extraction (SPE)

Five target volatile PAHs, having from two to four aromatic rings, were chosen to study the collecting procedure of volatile PAHs suspected to be present in a particular atmosphere without any particulate matter. Table 2 presents some physico-chemical properties of these five PAHs. Due to their relatively high vapor pressures compared to higher molecular weight PAHs, they generally occur in the gas phase of polluted atmospheres. We focused essentially on these aerosol PAHs because the atmosphere emitted by the air cleansing prototype was effectively devoid of any particulates but was supposed to eventually contain
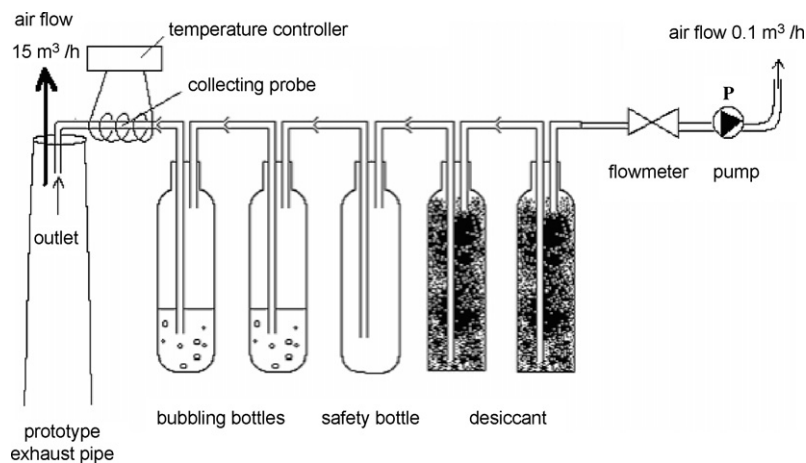
Fig. 1. Experimental assembly used for air sampling, each bubbling bottle containing 250 mL of aqueous medium; $T = 180\,^{\circ}C$ for the temperature controller.

non-degraded VOCs or other relatively small volatile molecules, larger ones being degraded by the plasmolysis process. Although the five target PAHs have a low aqueous solubility (see Table 2), we chose to collect them into an aqueous phase for the following reasons:

- Firstly, assuming that we could find good conditions to solubilize those PAHs in water, we could directly analyse the resulting aqueous medium by reversed phase HPLC. So this direct analysis would be free from the extraction step from a solid adsorbent, which is the case for usual HVS or LVS

Table 2
Some physico-chemical properties of the five studied volatile PAHs

PAHs	Chemical structure	Molar mass (g mol^{-1})	Vaporization temperature ($^{\circ}C$)	Vapor pressure at 25 $^{\circ}C$ (atm)[a]	Henry's law constant at 25 $^{\circ}C$[a] (L atm mol^{-1})	Aqueous solubility for gases at 25 $^{\circ}C$ (mol L^{-1})[a]
NAPH		128.6	217.9	3.7×10^{-4}	0.43	8.7×10^{-4}
PHEN		178.2	340	8.9×10^{-7}	0.026	3.5×10^{-5}
ANT		178.2	342	7.8×10^{-7}	0.023	3.3×10^{-5}
FLUO		202.3	375	7.8×10^{-7}	0.0105	8.3×10^{-6}
PYR		202.3	404	4×10^{-8}	0.0089	8.3×10^{-6}

[a] Ref. [31].

samplers and which can be critical for the quantification step;

- Secondly, we could envisage to concentrate traces of analytes using SPE, that is a quantitative technique, and not by means of solvent evaporation, generally used in classical extraction procedures but which is particularly critical for volatile PAHs.

The optimisation of a quantitative trace enrichment process was in fact necessary to decrease the UV and fluorimetric detection thresholds. Indeed the European Union requirements are of the nanogram per litre order of magnitude for PAHs. According to literature, several sorbents have been used in SPE for PAHs, but the one most currently used is certainly the C_{18} bonded silica [17–19].

At first, we tested off-line concentration, using a maximum percolation volume equal to 500 mL of a PAH aqueous solution. Although we could assume that PAHs should be completely solubilized in water at concentration levels below their limit of aqueous solubility, we decided to resort to an additive. In fact it was already suggested that ultra-trace enrichment with SPE was not an easy task because analytes may be lost by adsorption on the walls of tubings and vessels [20]. To solve this drawback, it was possible to add an organic co-solvent, but such an addition could decrease the adsorption capacity of PAHs on the C_{18} precolumn. Another possibility was to add a surfactant [21]. We could not choose a non-ionic surfactant because it has been demonstrated that on one hand it reduces the concentration efficiency on C_{18} cartridges and on the other hand it can mask the detection of PAHs having low retention times [22,23]. In fact, it is a cationic surfactant, the cetyl trimethyl ammonium bromide (CTAB) that was chosen in order to concentrate large volumes of highly diluted aqueous media without problems of solute adsorption on tubings. Then the influence of the percolating flow-rate was tested. It appeared that below $5\,mL\,min^{-1}$, the recovery yields of the five studied PAHs exceeded 92%. Above this limit, the operating time was decreased but the enrichment was not quantitative. Then the adsorbed PAHs had to be eluted with a volume of organic solvent which had to be minimized. Three solvents were tested and recovery yields increased in the order: methanol < acetonitrile < isopropanol. Then 5 mL of isopropanol were necessary to obtain quantitative results. Under such conditions, we could reach enrichment factors of 100. Consequently, it was possible to detect PAHs in aqueous phase at concentrations as low as 2–$8\,ng\,L^{-1}$ with the fluorescence detector. In view of the extremely weak rates recommended by the

European directives about PAHs in ambient air, those detection thresholds were still too high.

In such conditions, we decided to develop on-line SPE-HPLC coupling in order to avoid the dilution step due to the PAH elution by means of isopropanol. So the mobile phase required for the HPLC analysis was now used to elute the compounds concentrated into the C_{18} precolumn. Table 3 presents the recovery yields obtained after on-line SPE-HPLC coupling with two different C_{18} precolumns and CTAB in the aqueous phase. It can be seen from this table that the monofunctional C_{18} precolumn was not as efficient as the trifunctional C_{18} one to concentrate the heavier PAHs. This was probably due to the specificities of the trifunctional C_{18} stationary phase that possesses more hydrophobic boundary sites and is end-capped. When using the CTAB additive, it was effectively possible, as mentioned before, to eliminate the drawback of PAH adsorption on vials and tubings, even at lower concentrations, i.e. from nanograms to subnanograms per litre. Indeed relative standard deviations (R.S.D.) were now evaluated from four replicates at very low initial concentrations of PAHs ($6\,ng\,L^{-1}$). We obtained 6.1, 4.7, 7.1 and 6.9%, respectively for phenanthrene, anthracene, fluoranthene and pyrene. In fact, those R.S.D. were only slightly lowered when the tests were performed at higher initial PAHs concentrations. Such an observation showed that when the more diluted solutions were tested, the PAH adsorption on vessel walls was not really perceptible if CTAB was added to the aqueous solution. However, it should be noticed that results for naphthalene are not reported in Table 3. In fact, the presence of CTAB in aqueous phase was a drawback for the naphthalene quantification. Indeed although CTAB is not retained on the C_{18} stationary phase and is not detected using UV or fluorimetric detections, its large amount induces a peak tailing at dead volume which prevents us from quantitating the naphthalene. It should be mentioned that the percolating process on the C_{18} cartridge does not eliminate all the cationic species. A non-negligible quantity of CTAB remains on the C_{18} precolumn. Such an observation can be understood if one compare the large amounts of CTAB contained in 500 mL of percolating aqueous phase with the amounts of PAHs (10^6 times higher for CTAB). We will see later that one could not noticeably decrease the CTAB concentration because of its dominant role in the solubilisation process. Raising the PAHs retention times by increasing the percentage of water in the mobile phase used for the HPLC analysis was no more of a solution. Indeed a loss in efficiency of the SPE process was observed when the percentage of organic solvent used for PAH desorption was decreasing. So we attempted to eliminate the

Table 3

Comparison between two C_{18} stationary phases used in SPE on the recovery yields (%) of volatile PAHs obtained after on-line SPE-HPLC coupling

Cartridges (C_{PAH} ($ng\,L^{-1}$))	Monofunctional C_{18}			Trifunctional C_{18}		
	6	30	60	6	30	60
PHEN	94.5	94.5	94.5	94.8	94.2	99.8
ANT	63.3	88.4	96.2	88.2	97.6	94.1
FLUO	46.8	40.4	60.7	89.3	96.9	90.2
PYR	50.2	53.9	69.4	89.2	95.2	98.6

Experimental conditions: percolated volume: 500 mL, of the aqueous phase containing CTAB ($10^{-4}\,mol\,L^{-1}$), with variable initial PAH concentrations (C_{PAH}).

CTAB during the percolating step using a cation exchange cartridge. Unfortunately, it was not only ineffective to eliminate all the CTAB but also PAH recovery yields were poorer. Finally, we tried to eliminate the majority of CTAB before the analysis step, incorporating the cation exchange cartridge between the C_{18} concentration precolumn and the analytical column. Unfortunately this operation was not really effective in eliminating all the disturbing signals due to CTAB and the cation exchange cartridge introduced a dead volume that led to a very poor resolution for the anthracene/phenanthrene pair.

Despite the problems encountered for the naphthalene quantification, the excellent results showed for the other volatile PAHs should be underlined. As can be seen in Table 3, quantitative recovery yields were reached for the four other PAHs on the trifunctional C_{18} cartridge, even at initial PAH concentrations as low as $6 \, ng \, L^{-1}$. In light of these results, we succeeded in detecting the target volatile PAHs, solubilized in an aqueous medium, at concentrations ranging from 0.07 to $0.2 \, ng \, L^{-1}$ (for respectively anthracene and pyrene) with the fluorimetric detection.

3.2. Optimisation of the collection of PAHs from polluted atmospheres

To study the collection efficiency of PAHs with an appropriate aqueous medium, it was obviously necessary to develop an experimental device composed of:

- on one hand a dynamic flow-through gas generator of the target contaminants;
- on the other hand a collecting part containing the aqueous phase [24].

PAH vaporization was based on heating these compounds diluted in an organic solvent at 200 °C. Although PAHs have higher vaporization temperatures than 200 °C (see Table 2), their vapor pressures and their high Henry's law constants, quoted in Table 2, are favourable to a vaporization process at 200 °C. Indeed the obtained gas phase was progressively extracted from the organic solvent by means of a gas stream (flow-rate set to $0.1 \, m^3 \, h^{-1}$, see Section 2). It was obviously important to find an organic solvent which was not vaporized at 200 °C. Therefore we chose diethanolamine ($T_{vap} = 217 \, °C$ under 150 mmHg) not only for its thermal stability but also for its high viscosity which prevented any passage to the second section of the device.

The collecting part was inspired by French standards NFX 43–300, NFX 44–052 and XPX 43–304 about air quality and emissions from sources. So we used glass bottles in which contaminated air flow was bubbling for a few hours. At first, we tested the solubilization of PAHs in pure water. Fig. 2 shows the influence of the volume of water on trapping efficiencies when PAHs were tested above their solubilization limit. In such conditions, we could assume that it was not necessary to exceed 250 mL of water to enhance PAH solubility. Above this value, it would have taken more time to concentrate PAHs by SPE without any benefit on the PAH solubility. Nevertheless, we could see that recovery yields were very poor for anthracene, fluoran-
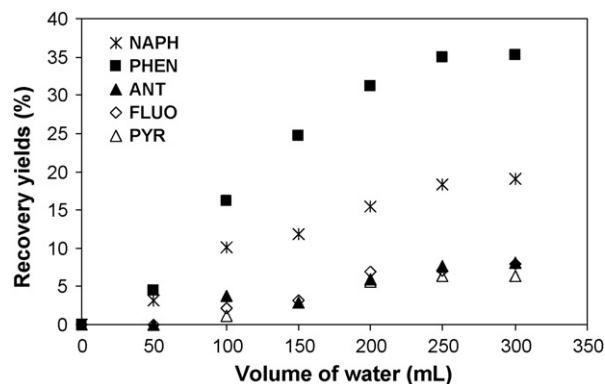

Fig. 2. Evolution of the recovery yields of PAHs as a function of the volume of pure water into the bubbling bottles (initial PAH quantity: 500 μg; bubbling time: 3 h).

thene and pyrene and only slightly better for naphthalene and phenanthrene. Given that the solubility is greater for naphthalene than for phenanthrene, we concluded from these results that the poorer recovery yield for naphthalene was due to its greater volatility (see Table 2) leading to an important loss of this compound during the experiment. For this reason, we chose to add a second bubbling bottle to recover the naphthalene. Lastly, we thought it could be beneficial to add a frit at the end of the bubbling tube with a view to breaking large bubbles and hence, increasing the surface of contact between the air and the aqueous medium. So we used glass or stainless steel frits with different pore diameters. In all cases, the recovery yields of the target PAHs were largely poorer, so we chose to work without any frit.

Next, with a view to improving the PAH solubilization and hence, the aqueous trapping, additives could be added to the water. It is well known that one way to enhance PAH solubility in water is to add surfactants at sufficiently high concentrations to form micelles. Non-ionic or anionic surfactants are generally used to solubilize PAHs [25–28]. However, we chose a cationic surfactant for the following reasons:

- Firstly, Brij 58 (critical micellar concentration (cmc) = $7.7 \times 10^{-5} \, mol \, L^{-1}$) was tried as a non-ionic surfactant and was effectively disturbing the SPE process and the quantification by reversed phase HPLC;
- Secondly, anionic surfactants were not chosen because they have a higher cmc than cationic ones. Now, if the solubility of the solute is directly enhanced above the surfactant cmc, foaming phenomenon is also increased, which is an important drawback for our application. Consequently, we needed to work with surfactant concentrations which were sufficiently low to avoid foaming. When trying the sodium dodecyl sulfate (SDS) as an anionic surfactant (cmc = $7.9 \times 10^{-3} \, mol \, L^{-1}$), we needed to work 80 times below its cmc to avoid important foaming and then overflowing problems. At this SDS concentration, PAH recovery yields were unfortunately lower than 50%.

Consequently we tested various cationic surfactants, the first one being the CTAB (cmc = $8.3 \times 10^{-4} \, mol \, L^{-1}$). Its effect on

Table 4

Comparison of the recovery yields (%) of the studied PAHs as a function of the cationic surfactants used for their solubilization

	CTAB[a]	OTAB[b]	HPC[b]
PAHs	8.3×10^{-4} [c]	2.1×10^{-4} [c]	5.6×10^{-4} [c]
PHEN	83.3	69.2	62.5
ANT	60.4	51.9	54.0
FLUO	54.5	53.6	53.4
PYR	54.4	50.1	51.3

Trace enrichment performed on the trifunctional C_{18} cartridge, percolated volume: 500 mL of aqueous phase containing CTAB at 10^{-4} mol L^{-1}, quantity of each studied PAH vaporized: 30 ng.

[a] $n = 8$ experiments.
[b] $n = 2$ experiments.
[c] cmc.

PAH solubility was studied for concentrations ranging from 10^{-5} mol L^{-1} to its cmc, but we noticed important foaming problems above 10^{-4} mol L^{-1}. So we chose to work below the cmc (10^{-4} mol L^{-1}), at concentrations where pre-micellar cores already forms but with only a low foaming phenomenon. We also tested two other cationic surfactants, with lower cmc than CTAB, i.e. octadecyl trimethyl ammonium bromide (OTAB) and hexadecyl pyridinium chloride (HPC) (see Table 4). As can be seen in this table, PAH recovery yields were not better than those obtained with CTAB, although the studied concentration (10^{-4} mol L^{-1}) was nearer from their cmc. So, we kept on working with CTAB at 10^{-4} mol L^{-1}. In such conditions, R.S.D. estimated from eight replicates equalled: 11% for phenanthrene, 12% for fluoranthene and pyrene and 15% for anthracene. These results took into account the overall process, i.e. PAH vaporization during three hours, PAH solubilization and trapping at the level of nanograms, concentration of 500 mL of aqueous medium by SPE followed by on-line HPLC analysis and quantification.

From these encouraging results, we still tried to enhance the PAH solubilization by adding some inorganic ions and organic compounds to CTAB [29]. Fig. 3 shows the effect of NaCl on PAHs recoveries. It was clear from these results that NaCl enhanced the PAH solubility into the aqueous medium contain-
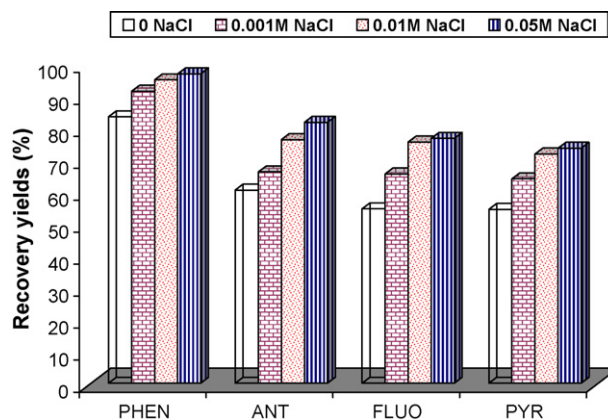

Fig. 3. Recovery yields of PAHs (%) as a function of NaCl concentration into the trapping aqueous phase. Initial quantity of each studied vaporized PAH: 30 ng; total volume of aqueous phase: 500 mL, containing CTAB (10^{-4} mol L^{-1}).
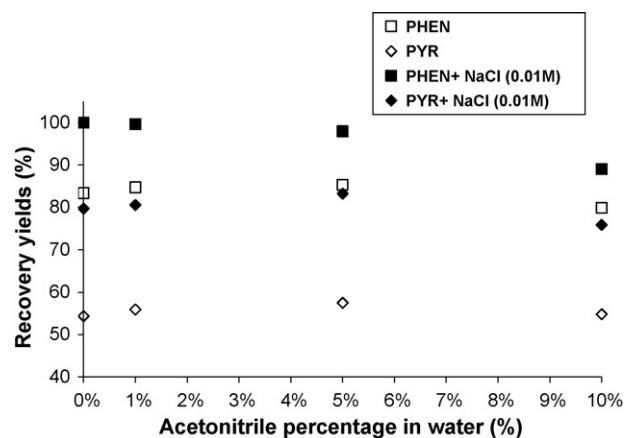

Fig. 4. Recovery yields of PAHs (%) as a function of acetonitrile percentage in water, with or without NaCl addition. Other operating conditions: see Fig. 3.

ing CTAB. Indeed the presence of electrolytes causes a decrease in the cmc, due to a reduction in the electrostatic repulsion between head charged groups [30]. It should be noticed that recovery yields were slightly better with 0.05 mol L^{-1} of NaCl than with 0.01 mol L^{-1} but the performance of the HPLC separation started to deteriorate. So the concentration of NaCl was set to 10^{-2} mol L^{-1}.

Another way to enhance the solubilization rates was to add organic additives. If the additive may be considered to be a co-solvent, the effects will be the result of changes in the solvent properties. A reduction in the dielectric constant of the solvent mixture can be favourable because it tends generally to decrease the cmc of ionic surfactants [30]. However, a too rich organic medium can become a disadvantage for the formation of cationic micelles, but also for the percolating process by SPE, which is not compatible with high levels of organic solvent. These trends could be noticed in Fig. 4, which presents the effect of acetonitrile addition into the aqueous medium, with or without NaCl, on the recovery yields of pyrene and phenanthrene. Acetonitrile addition increased the recovery yields up to 5% into the aqueous phase, the effect being negative above 5% (Fig. 4).

As a conclusion, we chose as an optimal aqueous phase for the bubbling process two bottles each containing 250 mL of a water:acetonitrile mixture 95:5 (v:v), the cationic surfactant CTAB being at a concentration equal to 10^{-4} mol L^{-1} and NaCl at 10^{-2} mol L^{-1}. Under these conditions, recovery yields of the volatile target PAHs all exceeded 90%. Table 5 shows the limits

Table 5

Limits of detection (LOD) and limits of quantification (LOQ) reached after flow-through vapor generation of the target PAHs, bubbling during 3 h into 500 mL of a water:acetonitrile 95:5 (v:v) mixture containing CTAB at 10^{-4} mol L^{-1} and NaCl at 10^{-2} mol L^{-1}; analysis by means of on-line SPE-HPLC coupling with fluorimetric detection

	PHEN	ANT	FLUO	PYR
LOD (ng L^{-1})	0.27	0.09	0.74	0.74
LOQ (ng L^{-1})	0.94	0.31	2.37	2.37

of detection and quantification that could be reached when the overall process was operating, i.e. bubbling during 3 h, enrichment by SPE and on-line analysis by HPLC.

3.3. PAH trapping at the outlet of the air cleansing prototype

As described in the experimental section, the pumped air flow-rate was set to $Q_{V2} = 0.1 \, \text{m}^3 \, \text{h}^{-1}$ at the air cleansing prototype outlet (see Fig. 1). In order to reach the extremely low rates required by the European directive about PAHs in ambient air, we should calculate the minimum collecting time necessary to detect the target PAHs, using the following equation:

$$t = \frac{Q_{m(PAH)}}{Q_{V2}[c]}$$

with $Q_{V2} = 0.1 \, \text{m}^3 \, \text{h}^{-1}$ (see Section 2), $[c] = 1 \, \text{ng} \, \text{m}^{-3}$ (value required by the European Directive 96/62/CE) and $Q_{m(PAH)}$ = minimal quantity (ng) of PAH detectable after enrichment by SPE and HPLC analysis with fluorimetric detection; $Q_{m(PAH)}$ ranged from 0.045 ng (for anthracene) to 0.37 ng (for fluoranthene and pyrene) in 500 mL of aqueous phase (see Table 5).

Finally, the minimum collecting time ranged from $t = 27$ min for anthracene to $t = 222$ min for fluoranthene and pyrene. Those values showed that it was not necessary to stay at the prototype outlet a few days with our low volume sampler to reach the
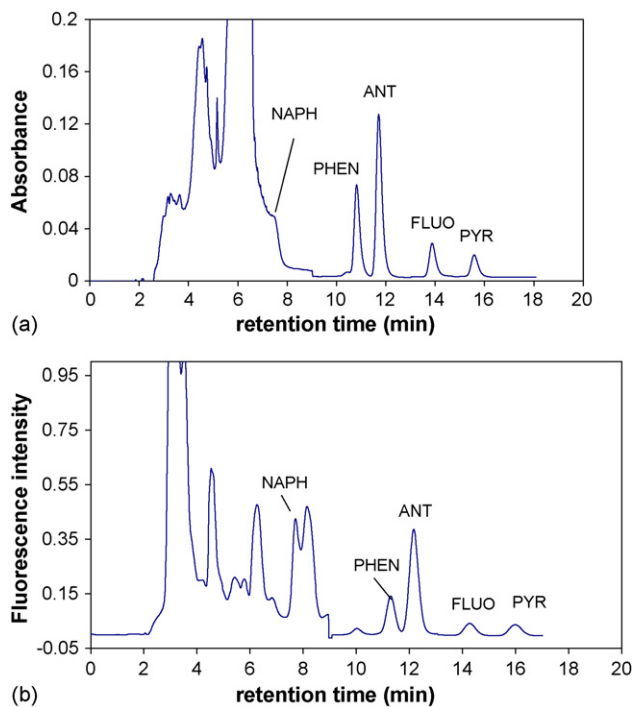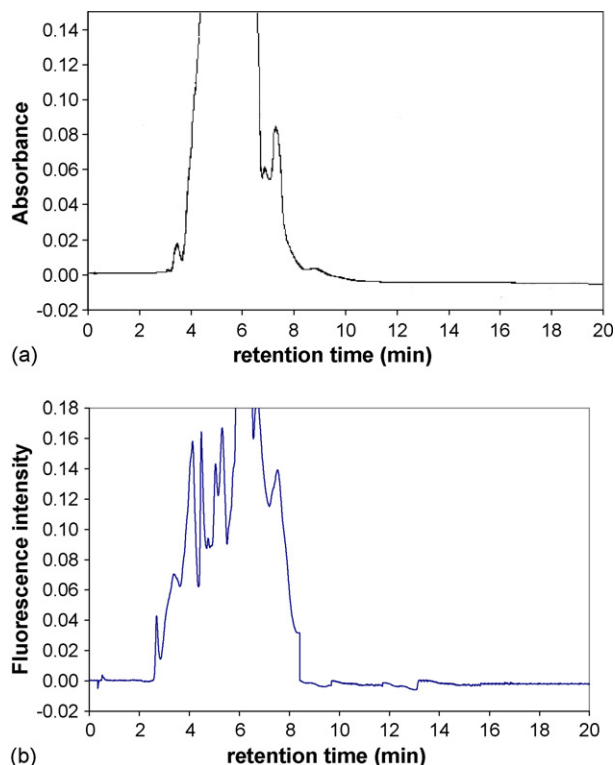

(a)

(b)

Fig. 6. Reversed phase HPLC analysis after sampling at the outlet of the air cleansing prototype; air initially polluted by toluene (0.1 g m^{-3}); decontamination by non-thermal plasmolysis and sampling during 6 h. Analytical conditions: see Fig. 5. (a) UV detection and (b) fluorimetric detection.

European directive. Then several experiments were carried out at the outlet of the air cleansing prototype, with an air initially polluted by acetone, isopropanol or toluene as VOCs (0.1 g m^{-3} in air).

In order to compare what we obtained after a sampling test where PAHs originated from our flow-through gas generation system and a sampling experiment at the outlet of the air cleansing prototype, we can examine the Figs. 5 and 6, which show examples of analysis with UV (a) and fluorescence (b) detections. The analysis reported in Fig. 6 corresponds to the result of 6 h of sampling at the outlet of the air cleansing prototype, with an air initially polluted by toluene. Fig. 6a and b shows that the target PAHs were not detected. If there was a doubt about one peak, like the peak at approximately 7.8 min on chromatograms reported on Fig. 6 (that could correspond to naphthalene), we compared the UV spectra recorded on-line with those stored in a personal library. In all cases, for all experiments with toluene, acetone or isopropanol as initial pollutants in air, neither retention times nor UV spectra corresponded to a target PAH. Therefore we concluded that one cannot detect any target volatile PAHs, in an atmosphere previously contaminated by VOCs, after air cleansing with a non-thermal plasma system, at following thresholds:

- for an air polluted by toluene, decontaminated and sampled during 6 h: no volatile PAHs were detected above levels ranging from 0.075 ng m^{-3} (anthracene) to 0.62 ng m^{-3} (fluoranthene and pyrene);

(a)

(b)

Fig. 5. Reversed phase HPLC analysis after the gas generation of 30 ng of the target PAHs, bubbling during 3 h at 0.1 m^3 h^{-1} in 500 mL of aqueous medium (water:acetonitrile 95:5 (v:v) containing CTAB (10^{-4} mol L^{-1}) + NaCl (10^{-2} mol L^{-1})) and finally SPE on the trifunctional C$_{18}$ cartridge. Analytical conditions: column C$_{18}$ ultrasphere (250 mm × 4.6 mm i.d., $d_p = 5$ μm); mobile phase: acetonitrile:water 75:25 (v:v); flow-rate: 1 mL min^{-1}. (a) UV detection and (b) fluorimetric detection.

- for an air polluted by isopropanol, decontaminated and sampled during 4 h 45 min: no volatile PAHs were detected above levels ranging from 0.095 ng m^{-3} (anthracene) to 0.78 ng m^{-3} (fluoranthene and pyrene);
- for an air initially polluted by acetone, decontaminated and sampled during 2 h 40 min: no volatile PAHs were detected above levels ranging from 0.17 ng m^{-3} (anthracene) to 1.39 ng m^{-3} (fluoranthene and pyrene).

4. Conclusion

An experimental home-made low volume sampler was developed with a view to trap aerosol PAHs from air into an aqueous medium, in order to avoid important losses of the volatile compounds observed using solid sorbents with classical LVS. The optimised aqueous phase, containing a mixture of water:acetonitrile 95:5 (v:v) with a cationic surfactant (CTAB at 10^{-4} mol L^{-1}) and NaCl (10^{-2} mol L^{-1}) was able to quantitatively trap vaporised PAHs at levels as low as those recommended by the European Union, that is at the parts-per-trillion level. This aqueous phase could then be directly and quantitatively concentrated and analysed by means of on-line SPE-HPLC coupling using the very sensitive fluorimetric detection. This new approach of sampling was then applied at the outlet of an air cleansing prototype that had to decontaminate, by means of non-thermal plasmolysis, an atmosphere initially polluted by VOCs. Then we showed that this prototype did not generate other harmful pollutants like volatile PAHs which could not be detected above 0.075 ng m^{-3} for anthracene and 0.62 ng m^{-3} for fluoranthene and pyrene. These very low levels, lower than those recommended by the European Union, could be reached in less than 6 h of sampling instead of a few days for classical LVS.

Acknowledgement

References

[1] M. Lipniak, J. Brandys, Polycycl. Aromat. Hydrocarb. 3 (1993) 111.
[2] G.R. Lotufo, Mar. Environ. Res. 4 (1997) 149.
[3] J. Santodonato, Chemosphere 34 (1997) 835.
[4] H.-L. Sheu, W.-J. Lee, S.J. Lin, G.-C. Fang, H.-C. Chang, W.-C. You, Environ. Pollut. 96 (1997) 369.
[5] J.-S. Park, T.L. Wade, S.S. Weet, Atmos. Environ. 35 (2001) 3241.
[6] D. Moussa, J.L. Brisset, J. Hazard. Mater. B 102 (2003) 189.
[7] N.T. Kim Oanh, L.B. Reutergardh, N.T. Dung, M.H. Yu, W.X. Yao, H.X. Co, Atmos. Environ. 34 (2000) 4557.
[8] G. Kiss, Z. Varga-Puchony, G. Rohrbacher, J. Hlavay, Atmos. Res. 46 (1998) 253.
[9] P. Kulkarni, C. Venkataraman, Atmos. Environ. 34 (2000) 2785.
[10] N. Yassaa, B.Y. Meklati, A. Cecinato, F. Marino, Atmos. Environ. 35 (2001) 1843.
[11] J. Oda, S. Nomura, A. Yasuhara, T. Shibamoto, Atmos. Environ. 35 (2001) 4819.
[12] K. Peltonen, T. Kuljukka, J. Chromatogr. A 710 (1995) 93.
[13] Y.Y. Shu, S.Y. Tey, D.K.S. Wu, Anal. Chim. Acta 495 (2003) 99.
[14] D. Ollivon, H. Blanchoud, A. Motelay-Massei, B. Garban, Atmos. Environ. 36 (2002) 2891.
[15] C. Mao, S.A. Tucker, J. Chromatogr. A 966 (2002) 53.
[16] E. Lazaro, M.P. San Andres, S. Vera, Anal. Chim. Acta 413 (2000) 159.
[17] R.M. Marcé, F. Borrull, J. Chromatogr. A 885 (2000) 273.
[18] J.L. Bernal, M.J. Nozal, L. Toribio, M.L. Serna, F. Borrull, R.M. Marcé, E. Pocurull, J. Chromatogr. A 778 (1997) 321.
[19] S.G. Nazarkina, A.V. Bulanova, O.G. Larionov, J. Anal. Chem. 56 (2001) 348.
[20] N. Li, H.K. Lee, J. Chromatogr. A 921 (2001) 255.
[21] D. Sicilia, S. Rubio, D. Perez-Bendito, N. Maniasso, E.A.G. Zagatto, Anal. Chim. Acta 392 (1999) 29.
[22] C. Madichie, G.M. Greenway, T. McCready, Anal. Chim. Acta 392 (1999) 39.
[23] R. Ferrer, J.L. Beltran, J. Guiteras, Anal. Chim. Acta 330 (1996) 199.
[24] R. Otson, J.M. Leach, L.T.K. Chung, Anal. Chem. 59 (1987) 1701.
[25] C.L. Chun, J.-J. Lee, J.-W. Park, Environ. Pollut. 118 (2002) 307.
[26] D.J.L. Prak, P.H. Pritchard, Water Res. 36 (2002) 3463.
[27] J.-L. Li, B.-H. Chen, Chem. Eng. Sci. 57 (2002) 2825.
[28] Y.-J. An, E.R. Carraway, M.A. Schlautman, Water Res. 36 (2002) 300.
[29] L. Zhu, S. Feng, Chemosphere 53 (2003) 459.
[30] D. Myers, Surfactant Science and Technology, 2nd ed., VCH publishers, New York, 1992.
[31] R.P. Schwarzenback, P.M. Gschwend, D.M. Imboden, Environmental Organic Chemistry, Wiley–Interscience, New York, 1993.

ELSEVIER

Molecularly imprinted polymer-based potentiometric sensor for degradation product of chemical warfare agents Part I. Methylphosphonic acid

K.P. Prathish [a], K. Prasad [a], T. Prasada Rao [a,*], M.V.S. Suryanarayana [b]

[a] *Inorganic Materials Group, Regional Research Laboratory (CSIR), Trivandrum 695 019, India*
[b] *Defence Research & Development Establishment (DRDE), Jhansi Road, Gwalior 474 002, India*

Abstract

A biomimetic potentiometric sensor for the specific recognition of methylphosphonic acid (MPA), the degradation product of nerve agents sarin, soman, VX, etc., was designed. This involves the preparation of MPA imprinted polymer particles and removal of the template by soxhlet extraction. Subsequently, the leached MIP particles were dispersed in 2-nitrophenyloctyl ether (plasticizer) and embedded in polyvinyl chloride matrix. The sensor responds to MPA in the concentration range 5×10^{-8} to 1×10^{-4} and 1×10^{-3} to 1×10^{-1} M with a detection limit of 5×10^{-8} M. The selectivity of the sensor has been tested with respect to chemical analogues such as phosphoric acid, sodium dihydrogen phosphate, organophosphorous pesticide and triazine herbicides. The utility of the sensor was tested for field monitoring of MPA in spiked ground water.
© 2006 Elsevier B.V. All rights reserved.

Keywords: Molecularly imprinted polymer membrane; Methylphosphonic acid; Potentiometric sensor; Ground waters

1. Introduction

The use of chemical weapons against civilians by terrorist groups or fanatic individuals is not just horror fiction any more, but an absolute real threat. Two sarin gas attacks in Matsumoto and Tokyo, Japan in 1994–1995 confirmed this horrible reality [1]. Nerve agents such as sarin, soman, Tabun and VX pose a large threat because they are fairly easy to manufacture and these can kill a person within 24 h even at very low concentrations. As the nerve agents are hydrolyzed in the environment, the detection of degradation product such as methylphosphonic acid (MPA) has been usually performed as the proof of the use of nerve agents [2,3]. There have been many innovations for the identification of MPA, including high performance liquid chromatography (HPLC), ion chromatography, HPLC–mass spectrometry, and gas chromatography [4,5]. Although these instruments do offer quantitative analysis, they are not optimal for rapid detection as they are plagued by several limitations such as expensive, require sophisticated and often extensive analysis procedures and non-portability [4,6,7]. The methods that meet the real-time analysis such as fibre-optic sensors [8], surface acoustic wave devices [9] or microbial biosensors [10] often lack selectivity and do not have an optimal alarm ratio.

Zhou et al. [11] reported for the first time MIP-based potentiometric sensor for MPA employing surface imprinting technique coupled with a nanoscale transducer, indium tin oxide. Undoubtedly, this device is selective as it mimics the function of ion channel in natural membrane by imprinting the templates on the surface of nanoscale transducer. However, the accuracy, precision and sensitivity are rather poor as there is significant response only in the range 10^{-2} to 10^{-1} M of MPA eventhough authors claim a detection limit of 5×10^{-5} M. We now propose a MIP-based potentiometric sensor for MPA present in spiked ground waters by casting a membrane after dispersing MPA imprinted polymer particles in 2-nitrophenyloctyl ether (NPOE) and embedding in polyvinyl chloride (PVC) matrix.

* Corresponding author. Tel.: +91 471 2515317; fax: +91 471 2491712.
E-mail address: tprasadarao@rediffmail.com (T.P. Rao).

2. Experimental

2.1. Reagents

Methylphosphonic acid (MPA), dichlorovos, parathion and 2,4-D were obtained from SUPELCO, USA. Stock standard solution of (0.1 M) MPA was prepared by dissolving 0.4801 g of MPA in 50 ml of deionized water and adjusted the pH to ~10.0 using HCl or NaOH after the addition of 5 ml of 1.0 M Tris buffer (E-Merck, India). The solutions of 1×10^{-8} to 1.0×10^{-2} M of MPA were prepared by serial dilution of the stock solution. Methacrylic acid (MAA), 4-vinylpyridine (VP), ethyleneglycoldimethacrylate (EGDMA), 2,2′-azobisisobutyronitrile (AIBN), 2-nitrophenyloctylether (NPOE), di-n-octylphthalate (DOP), bis(2-ethylhexyl) sebacate (BEHS), tris(2-ethylhexyl) phosphate (TEHP), and high molecular mass poly(vinyl chloride) (PVC) were purchased from Aldrich (Milwauke, USA). All other chemicals including NaH_2PO_4 and H_3PO_4 were of analytical reagent grade obtained from E-Merck, India. Deionized water was used throughout.

2.2. Preparation of MPA imprinted and non-imprinted polymer particles

MPA imprinted polymer particles were prepared by taking 1 mmol of MPA and 8 mmol MAA in 50 ml of round bottom flask and the mixture was left in contact for 5 min for prearrangement. Subsequently, EGDMA (32 mmol), AIBN (2 mmol) and 10 ml of 2-methoxyethanol were added. The mixture was purged with N_2 for 5 min and the flask was sealed under this atmosphere. It was then kept stirring in an oil bath maintained at 65 °C to start the polymerization process. After 1 h, the obtained polymer materials were ground and sieved, and the particles with sizes between 50 and 105 μm were collected. MPA and unpolymerized monomers were removed by soxhlet extraction with 100 ml of 1:1 methanol–acetic acid by refluxing for 12 h. Then, the particles were suspended in acetone and allowed to settle for 4 h. The sedimented particles were discarded and those not sedimented were collected by centrifugation. The particles collected were suspended in acetone again and allowed to settle for 4 h, followed by centrifugation. This procedure was repeated four times. The resulting MIP particles were dried to constant weight under vacuum at 60 °C and were used in the following experiments. Non-imprinted polymer (NIP) particles were prepared analogously without the addition of MPA during polymer material preparation.

2.3. Fabrication of the MPA sensor

The PVC membrane sensors were fabricated by following the general procedure mentioned below. MPA imprinted or non-imprinted polymer particles (90 mg) were dispersed in 0.2 ml of NPOE (DOP or BEHS or TEHP) and were added to 2.5 ml of THF containing 90 mg of PVC. The resulting solution was homogenized in a sonicator and then poured in a Teflon mould of 21 mm of internal diameter. The THF was allowed to evaporate at room temperature. The polymer membranes thus obtained have

a thickness of ~0.45 mm. A blank membrane was also prepared in a similar manner, maintaining the same composition without MPA imprinted or control polymer particles. The membranes were glued to one end of a pyrex glass tube with Araldite. The tube was then filled with an internal filling solution of 10^{-3} M of MPA. The sensor was kept in air when not in use.

2.4. Analytical procedure

The sensor was conditioned in 25 ml of 0.1 M Tris buffer with pH 10 for 30 min. The response of the sensor was examined by measuring the electromotive force (EMF) of the following electrochemical cell. Ag, AgCl 1.0×10^{-3} M MPA | PVC membrane | sample solution || KCl (saturated) | $HgCl_2$, Hg. The potential response of the sample solution containing varying amounts of MPA in 50 ml of 0.1 M Tris buffer (pH 10) was measured. The EMF was plotted as a function of MPA concentration.

2.5. Analysis of ground water samples

Ground water samples (after adjusting the pH to 10 in presence of 0.1 M Tris buffer with HCl or NaOH), spiked with known amounts of MPA were analysed by following the analytical procedure as described in Section 2.4 using the above fabricated MPA imprinted potentiometric sensor.

3. Results and discussion

Prasad et al. have developed Dy(III) ion selective electrode by dispersing Dy(III) ion imprinted polymer particles in NPOE and subsequently embedding in PVC, which selectively recognizes dysprosium(III) ion over several other alkali, alkaline earth and transition metal ions in the concentration range 8×10^{-6} to 1.0×10^{-1} M with a detection limit of 2×10^{-6} M [12]. In this paper, the suitability of MPA imprinted polymer particles dispersed in plasticizer and embedded in PVC to recognize MPA selectively has been examined.

3.1. Influence of functional monomer

The influence of functional monomer on the response characteristics of MIP-based potentiometric sensor for MPA was first investigated. In these studies, two such functional monomers, viz. MAA or VP were used for preparation of MIP particles as mentioned in Section 2.2, under exactly identical conditions including same concentration of cross-linking monomer–EGDMA. Sensors were fabricated using MAA- or VP-based MIP and corresponding NIP particles and response studies were conducted for MPA as per the procedure described in Section 2.3. The results obtained are shown in Table 1, from which it is clear that in all decade change of concentration, the response is higher for the sensor fabricated using MIP particles prepared from MAA as functional monomer compared to VP. This observation can be explained by the stronger H-bond interaction of MPA anion with MAA compared to electron rich VP in weakly alkaline solution. However, on comparing MIP with NIP particle-based sensors using MAA or VP as functional

Table 1
Response study of MPA sensor fabricated using MIP or NIP particles prepared using MAA and 4-vinyl pyridine as functional monomers

MPA (M)	Potential response (mV/decade)			
	NIP[a]	MIP[a]	NIP[b]	MIP[b]
10^{-6} to 10^{-5}	–	2	–	3
10^{-5} to 10^{-4}	–	2	–	8
10^{-4} to 10^{-3}	2	5	9	17
10^{-3} to 10^{-2}	35	43	48	59
10^{-2} to 10^{-1}	36	45	49	59

[a] 4-Vinylpyridine.
[b] MAA.

monomer showed imprinting effect in the entire concentration range. Hence, in all subsequent studies regarding optimization of response behaviour of MPA sensor, the MIP particles wherein, MAA is used as functional monomer is preferred.

3.2. Effect of membrane composition

Literature reports on conventional potentiometric sensors for inorganics show that the response behaviour of the sensor depends on various features of membranes such as the properties of the plasticizer, nature and amount of ion recognizing material used [13–15]. Thus, different aspects of the membrane preparation using MPA imprinted polymer particles were optimized on similar lines.

3.2.1. Nature of plasticizer

Addition of appropriate plasticizer leads to optimum physical properties and ensures high mobility of MPA ions in the membrane. These solvent mediators strongly influence the working concentration range of potentiometric sensors. As it is shown that the plasticizers improve the electrochemical properties of potentiometric sensors including dysprosium ion imprinted polymer-based sensors [12–15], the effect of different plasticizers on the performance of MPA sensor was first investigated. Fig. 1 shows the potential response of MPA sensor with different plasticizers NPOE, BEHS, TEHP and DOP. Of these, the membrane with NPOE offered higher sensitivity with a Nernstian response of 59.0 mV over the range 1×10^{-3} to 1×10^{-1} M and lower detection limit of 5×10^{-8} M. This observation is in tune with earlier report on conventional thallium (I)-selective PVC membrane electrode employing tetrathia macrocycle as ionophore [16]. Shamsipur et al. [17] have compared conventional lanthanum(III) PVC membrane electrodes constructed with three different plasticizers and found that the sensitivity can
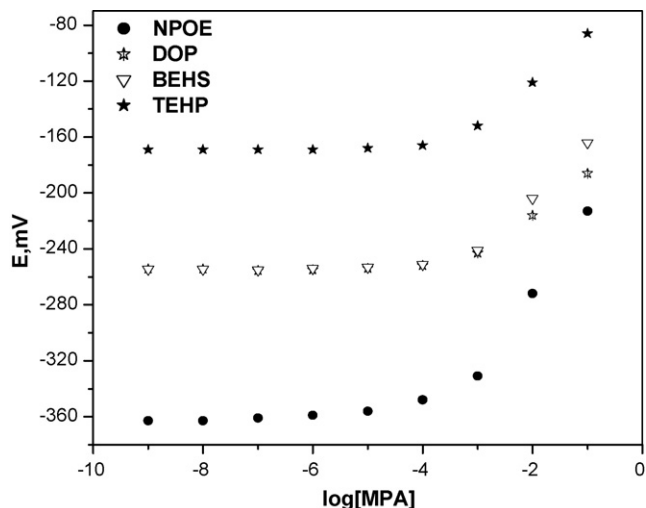

Fig. 1. Potential responses of the MIP-based MPA potentiometric sensor with different plasticizers.

be directly related to dielectric constant of the plasticizer. Thus, of the three plasticizers studied by above authors, acetophenone ($\in = 17.4$) gave better sensitivity compared to dibutylphthalate ($\in = 8.5$) and benzyl acetate ($\in = 5.1$). We have recently reported similar observation, i.e. the plasticizer NPOE having high dielectric constant of 24.0 giving better response characteristics that DOP ($\in = 5.0$), BEHS ($\in = 4.0$) and TEHP ($\in = 4.8$) in case of dysprosium(III) ion sensor. In a similar vein, MPA sensor gave narrower linear response range and poor detection limits with plasticizers like BEHS, TEHP and DOP compared to NPOE. It is pertinent to mention here that MPA membranes were found to be brittle in the absence of plasticizer and cannot be used for recording sensor performance.

3.2.2. Effect of MIP particles to PVC ratio

The ratio of ionophore to PVC influence the working concentration range, slope and response time in case of conventional ionophore-based sensors. This was evident from the accounts of several researchers in the past, for e.g., thallium(I) sensor reported by Singh and Saxena [16], yetterbium(III) and lanthanum(III) sensors reported by Ganjali et al. [18,19], etc. In case of imprinted polymer ion selective electrodes, viz. dysprosium(III) [12] and atrazine [20], we observed that the ratio of PVC to imprinted polymer particles was found to play a key role in the efficiency of sensors since the amount of imprinted polymer particles determines the number of binding sites available for recognition. Hence, a similar study was conducted with MPA sensor and the results obtained are shown in Table 2 from

Table 2
Effect of weight ratio of MPA imprinted polymer particles to PVC on MPA sensor response

Weight of MPA imprinted polymer particles (mg)	Weight of PVC (mg)	Weight ratio	Working concentration range (M)	Nernstian slope (mV/decade in the range 0.001–0.1 M)
45	90	0.5:1	10^{-5} to 10^{-2}	36.0 ± 0.3
90	90	1:1	5×10^{-8} to 10^{-1}	59.0 ± 0.5
180	90	2:1	5×10^{-8} to 10^{-1}	59.1 ± 0.6

which it is clear that the membrane having MIP particles to PVC ratio of 1:1 gave the best response. In case of membrane with the ratio 0.5:1, the total number of binding sites available for binding MPA are relatively lower for the membrane to respond effectively. On the other hand, during the preparation of membrane with the ratio 2:1, the MPA imprinted polymer particles are dispersed non-uniformly causing poor response behaviour. These observations are analogous to dysprosium(III) IIP sensor [12].

3.3. Effect of pH of test solution

The effect of pH of test solution on the performance of MPA sensor was studied by varying the pH in the range 9.0–11.0 in steps of 0.2 after addition of 5 ml of 1.0 M Tris–(hydroxymethyl)aminomethane (tris) buffer. The results show that the optimal pH for constant and maximum response characteristics over the entire concentration range of MPA (5×10^{-8} to 10^{-1} M) is 9.8–10.2. Hence, the pH of the test solution was adjusted to ~10 after the addition of 5 ml of 1.0 M Tris buffer.

3.4. Dynamic response time

Dynamic response time is yet another factor that measures the sensing ability of the sensor. The response time was recorded by changing the MPA concentration in test solution over a concentration range of 1×10^{-6} to 1×10^{-2} M (see Fig. 2). The actual potential versus time traces for MPA sensor depicted in Fig. 2 shows that 75% response was realized within 2 min and reaches equilibrium response in a time of about 5 min. To evaluate the reversibility of MPA sensor, a similar procedure in opposite direction was studied. The measurements performed in the sequence of high to low concentration (from 1×10^{-2} to 1×10^{-6} M) indicate that the MPA sensor was reversible analogous to conventional chemical and dysprosium IIP sensors.
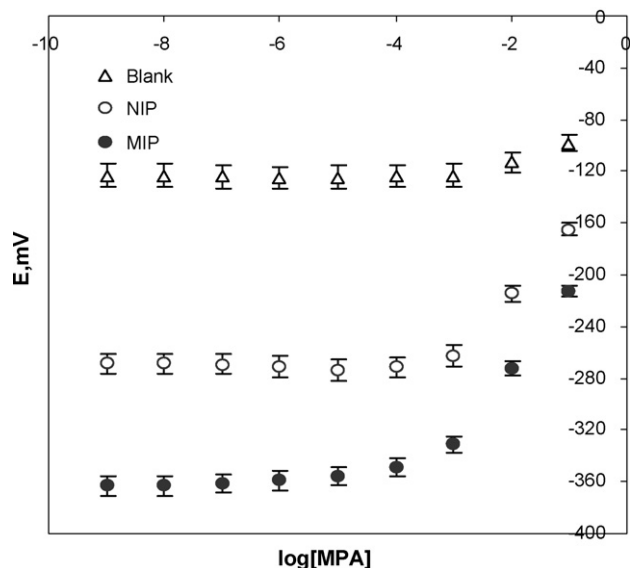
Fig. 3. Potential responses of potentiometric sensors with blank, NIP and MIP membranes.

3.5. Sensitivity and detection limit

The potential responses of MPA imprinted and control polymer and blank (without polymer particles) membrane sensors fabricated under optimal conditions, as obtained from the above studies, were checked and the results obtained are shown in Fig. 3. As seen from the figure, the plot obtained for MPA imprinted polymer sensor (based on triplicate measurements at each concentration) offers linear response in the ranges 5×10^{-8} to 1×10^{-4} M and 1×10^{-3} to 1×10^{-1} M. The limit of detection was calculated to be 5×10^{-8} M based on IUPAC definition [21]. On the other hand, the non-imprinted and blank membranes do not respond to MPA below 1×10^{-4} M and gave linear response for MPA in the concentration range 10^{-3} to 10^{-1} M, respectively. Better response characteristics of MPA imprinted sensor over non-imprinted polymer-based sensor in the entire concentration range is attributed to significant imprinting effect which has not been investigated in case of dysprosium(III) IIP sensor [12].

3.6. Sensor selectivity

The potentiometric output of the MIP-based MPA sensor alone was tested (as NIP do not respond at concentrations below 10^{-4} M) with some common compounds related to chemical warfare agents, pesticides, herbicides and chemicals like H_3PO_4 and NaH_2PO_4 that are most likely to interfere. The results obtained for change of the concentration from 10^{-5} to 10^{-4} M are shown in Fig. 4. It is clear from the figure that all these compounds did not give false positive readings except 2,4-D which gave 45% of MPA response. This observation can be explained by the similar basicity of 2,4-dichlorophenoxy acetate and methylphosphonate and weak basicity of PO_4^{3-} and $H_2PO_4^{-}$ anions and their differing interactions with MAA during rebinding.
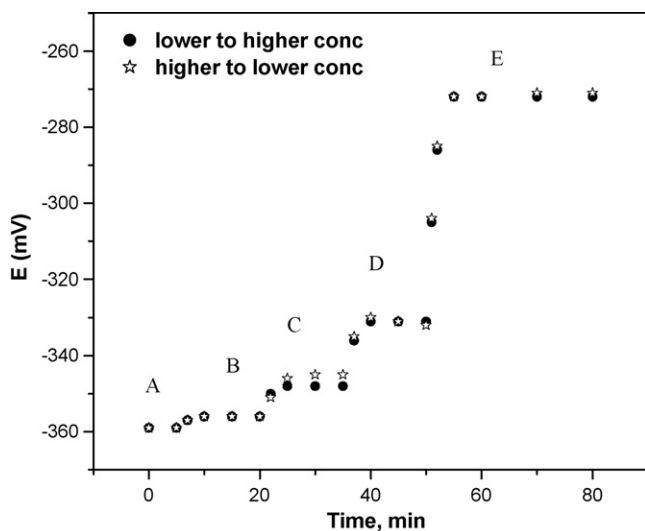

Fig. 2. Dynamic response time of the MIP-based MPA potentiometric sensor for stepwise concentration change of MPA. (A) 1×10^{-6} M; (B) 1×10^{-5} M; (C) 1×10^{-4} M; (D) 1×10^{-3} M; (E) 1×10^{-2} M.

Table 3
Analysis of natural water (45 ml of sample + 5 ml of pH 10.0 Tris buffer)

Sample	Interferent (100 μM)	Concentration of MPA (μM)		
		Added	Found[a]	
Natural water	–	–	–	–
	–	100	99.0	99.0 ± 1.0
	Dichlorovos + malathion	100	98.0	98.0 ± 1.0
	$H_3PO_4 + NaH_2PO_4$	100	98.5	98.5 ± 1.0
	Dichlorovos + malathion + $H_3PO_4 + NaH_2PO_4$	100	99.0	99.0 ± 1.5

[a] Average of three successive determinations.
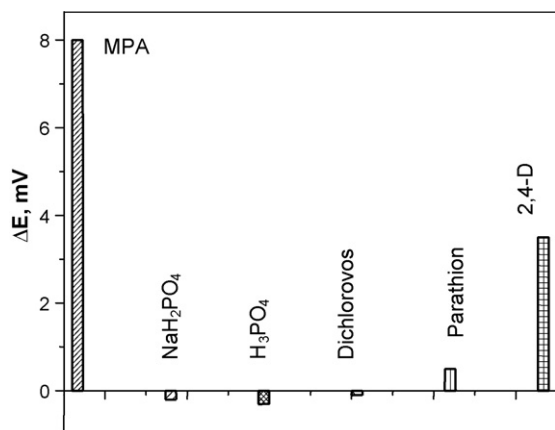
Fig. 4. Output of MIP-based MPA sensor to change of concentration of MPA and interferents from 1×10^{-5} to 1×10^{-4} M concentration.

3.7. Stability and reusability

The important criteria required for any sensing device in addition to sensitivity and selectivity is stability and reusability. The above developed MPA sensor was found to be stable (deviation less than 0.5 mV for 1×10^{-4} M of MPA) for 2 months and can be reused for more than 20 times without any loss in sensing ability. Furthermore, the MPA sensor do not require any conditioning unlike dysprosium(III) IIP sensor which requires 3 days of soaking in 10^{-3} M dysprosium(III) solution [12].

3.8. Analytical application

Since organophosphorus pesticides, H_3PO_4 and NaH_2PO_4 did not give false positive signals, it was decided to analyse natural water samples spiked with known amounts of MPA. The results obtained are shown in Table 3 from which it is clear that MIP-based MPA sensor can reliably be used for monitoring MPA in natural waters contaminated with organophosphorus pesticides or H_3PO_4 or Na H_2PO_4.

4. Conclusions

This report describes a simple and elegant way of designing potentiometric sensor for methylphosphonic acid compared to the one described by Zhou et al. [11] based on molecular imprinting concept. In addition to improved selectivity over structurally or chemically related compounds, the developed MIP sensor responds to MPA in a Nernstian manner over two decades unlike the sensor fabricated by Zhou et al. [11]. Again, the MPA sensor developed in this paper do not require conditioning unlike our previously reported dysprosium(III) IIP sensor [12]. The stability, reusability, portability and absence of memory effect enable the present sensor device to find ready use in field monitoring studies not only for MPA (demonstrated in the present work) but also to actual chemical warfare agents or their simulants.

Acknowledgement

References

[1] A.A. Tomchenko, G.P. Harmer, B.T. Marquis, Sens. Actuators B 108 (2005) 41.
[2] A.T. Tu, J. Mass Spectrom. Soc. Jpn. 44 (1996) 293.
[3] J.A. Ashley, C.H. Lin, P. Wlrsching, K.D. Janda, Angew. Chem. Int. Ed. Engl. 38 (1999) 1793.
[4] A.T. Tu, Natural and Selected Synthetic Toxins. American Chemical and Toxicological Properties, The Telford Press, Caldwell, New Jersey, 1987, p. 458.
[5] R.M. Black, R.J. Clarke, R.W. Read, M.T.J. Reid, J. Chromatogr. A 662 (1994) 301.
[6] M.T. Mesilaakso, Environ. Sci. Technol. 31 (1997) 518.
[7] A.E.F. Nassar, S.V. Lucas, S.A. Thomas, Anal. Lett. 32 (1999) 1023.
[8] A. Jenkins, O.M. Uy, G.M. Murray, Anal. Chem. 71 (1999) 373.
[9] M.S. Nieuwenhuizen, J.L.N. Harteveld, Sens. Actuators B 40 (1997) 167.
[10] A. Mulchandani, W. Chen, P. Mulchandani, J. Wang, Biosens. Bioelectron. 16 (2001) 225.
[11] Y. Zhou, B. Yu, E. Shiu, K. Levon, Anal. Chem. 76 (2004) 2689.
[12] K. Prasad, R. Kala, T. Prasada Rao, G.R.K. Naidu, Anal. Chim. Acta 566 (2006) 69.
[13] G.J. Moody, J.M. Slater, J.D.R. Thomas, Analyst 113 (1988) 699.
[14] S.S.M. Hassan, M.M. Ali, A.M.Y. Attawiya, Talanta 54 (2001) 1151.
[15] V.K. Gupta, R. Mangla, U. Khurana, P. Kumar, Electroanalysis 11 (1999) 573.
[16] A.K. Singh, P. Saxena, Talanta 66 (2005) 993.
[17] M. Shamsipur, M. Yousefi, M. Hosseini, M.R. Ganjali, Anal. Chem. 74 (2002) 5538.
[18] M.R. Ganjali, L. Naji, T. Pourasaberi, M. Shamsipur, S. Haghgoo, Anal. Chim. Acta 475 (2003) 59.
[19] M.R. Ganjali, A. Daftari, M. Rozapour, T. Puorasaberi, S. Haghgoo, Talanta 59 (2003) 613.
[20] K. Prasad, K.P. Prathish, J.M. Gladis, G.R.K. Naidu, T. Prasada Rao, Sens. Actuators B: Chem., in press.
[21] R.P. Buck, E. Lindener, Pure Appl. Chem. 66 (1994) 2527.

Evaluation of different mediator-modified screen-printed electrodes used in a flow system as amperometric sensors for NADH

Beatriz Prieto-Simón[*], Jorge Macanás, María Muñoz, Esteve Fàbregas

Grup de Sensors i Biosensors, Departament de Química, Universitat Autònoma de Barcelona, 08193 Bellaterra, Barcelona, Spain

Abstract

This work presents a comparative study between two different methods for the preparation of mediator-modified screen-printed electrodes, to be used as detectors in a reliable flow injection system for the determination of the nicotinamide adenine dinucleotide (NADH) coenzyme. The best strategy was selected for the final development of compact biosensors based on dehydrogenase enzymes. For the first immobilisation strategy, different redox mediators were electropolymerised onto the SPE surface. The second immobilisation strategy was carried out using polysulfone–graphite composites, which were deposited by screen-printing technology onto the screen-printed electrode (SPE) surface. Both methods achieved an effective and reliable incorporation of redox mediators to the SPE configuration. Finally, a flow system for ammonium determination was developed using a glutamate dehydrogenase (GlDH)-Meldola's Blue (MB)-polysulfone-composite film-based biosensor.

The stability of the redox mediators inside the composite films as well as the negligible fouling effect observed on the electrode surface improve the repeatability and reproducibility of the sensors, important features for continuous analysis in flow systems. Furthermore, the optimised bio/sensors, incorporated in a flow injection system, showed good sensitivities and short response times. Such a good analytical performance together with the simple and fast sensor construction are interesting characteristics to consider the polysulfone-composite films as attractive electrochemical transducer materials for the development of new dehydrogenase-based SPEs.
© 2006 Elsevier B.V. All rights reserved.

Keywords: SPE; Flow injection analysis; Polysulfone; Redox mediators

1. Introduction

Despite the wide range of available dehydrogenase enzymes, dehydrogenase-based biosensors have not been as widely developed as might be expected. The reason can be found in the fact that they relay on the amperometric detection of the NADH cofactor, process that involves some drawbacks. Actually, the development of a reliable system for the amperometric detection of NADH has been during years one of the main research subjects in electrochemical sensors. The problems related to the electrochemical oxidation of NADH involve high overpotentials [1] and the subsequent formation of byproducts that foul the electrode surface (i.e. dimerisation of NAD[•] radicals and other oxidation products) [2,3]. As a result, low selectivity and

stability are obtained. Much work has been related to the use of redox mediators [4]. These compounds allow the construction of more sensitive, selective and stable biosensors, since they permit to lower the overpotential and so prevent the electrode fouling [5]. However, the soluble, or partially soluble, mediating species may diffuse away from the electrode surface towards the bulk solution, especially when the sensor is used in multiple analyses, e.g. in a continuous flow system. In fact, sensors used as detectors in FIA systems are exposed to flowing buffer and, consequently, special attention must be given to the mediator immobilisation. If the mediator leaks from the sensor, significant current loss will occur and therefore the lifetime of the sensor will be considerably reduced. Different strategies to incorporate redox mediators into the electrochemical system involve either adding the mediator to the solution [6,7] or immobilising it within or on the electrode, producing compact chemically modified sensors [8,9]. The latter is achieved following different methodologies, such as the dispersion of the mediator in the bulk of a composite electrode [10,11] or its immobilisation on the electrode surface by physical adsorption [12,13], covalent attachment [14,15],

* Corresponding author at: Université de Perpignan, BIOMEM Group, 52 Avenue Paul Alduy, 66860 Perpignan Cedex, France. Tel.: +33 468662253; fax: +33 468662223.

E-mail address: beatriz.prieto-simon@univ-perp.fr (B. Prieto-Simón).

electropolymerisation [16,17], gel entrapment [18] or cross-linking [19]. Other immobilisation techniques involve the use of a polymeric film, where the mediator is covalently attached [20–23] or physically entrapped [24–26]. The chosen strategy will depend on the specific characteristics of the working system and the sensor performance under them, as the activity of the immobilised molecules depends on the immobilisation method, as well as, in the case of using an immobilising matrix [27], on its surface area, porosity and hydrophilic character.

In previous studies [28,29], the behaviour of different redox mediators, incorporated to the system by five different strategies was compared: in solution, incorporated inside a composite matrix, adsorbed or electropolymerised onto the electrode surface and incorporated inside polysulfone-composite films deposited on the electrode surface. This work was carried out with cylindrical-configuration electrodes based on epoxy–graphite composites. These new polysulfone-composite membranes were prepared by mixing polysulfone with graphite powder.

In the work reported here, two previously optimised immobilisation strategies have been used to prepare mediator-modified SPEs. Results show that electropolimerised mediators and mediator-modified polysulfone-composite films overcome one of the most critical points in the manufacture of thick-film sensors, such as the adhesion of the sensing layer to the transducer layer. The excellent stability of electron mediators immobilised inside polysulfone-composite materials together with the fact that they can be easily incorporated to the sensors through an additional layer in the screen-printing process, allow a massive production of disposable mediator-modified electrodes. Furthermore, the leakage absence and the negligible surface fouling ensure the feasibility to consider SPEs based on polysulfone-composite films as electrochemical detectors for flow injection systems. Finally, it has been demonstrated the usefulness of these sensors for the development of dehydrogenase-based biosensors to be used in FIA systems, showing as an example the performance of GlDH-mediator-polysulfone SPEs.

2. Experimental

2.1. Reagents

Polysulfone Ultrason nature 3120 was obtained from BASF. NADH, Meldola's Blue (MB), *o*-phenylenediamine (*o*-PDA), glutamate dehydrogenase (GlDH, EC 1.4.1.3 from bovine liver, 42 units/mg prot.) and α-ketoglutarate were purchased to Sigma. 3,4-dihydroxybenzaldehyde (3,4-DHB), *p*-benzoquinone (*p*-BQ) and *N,N*-dimethylformamide (DMF) were bought to Aldrich and dichlorophenolindophenol (DCPIP) to Fluka. Ammonium chloride, sodium dihydrogen phosphate and potassium chloride were purchased from Panreac. A platinum sheet (Ref. PT000251, Goodfellow, England) with 99.95% purity and 0.125-mm thick, a fibreglass support (Ariston), silver conductive resin 410E and the proper hardener (Epoxy Technology, Billerica, MA, USA) and epoxy diacrilate (Ebecril 600, UCB Chemicals) have been used for the construction of a planar-configuration platinum electrode. Clear polyester sheets, 0.5-

mm thick, were used as support for the SPEs. SPEs have been prepared by successive layer printing with inks supplied by Acheson: silver ink (Electrodag 418 SS), graphite ink (Electrodag 423 SS) and insulating ink (Electrodag 451 SS).

All solutions were prepared using deionized water obtained from a Milli-Q purification system, and they were de-aerated prior to their use.

2.2. Electrochemical measurements

Cyclic voltammetry was carried out using a multipotentiostat, AUTOLAB model PGSTAT10 (Eco Chemie) in a conventional electrochemical cell of 10-mL volume. Amperometrical studies were performed on a LC-4C potentiostat (BAS, USA) in a flow injection system. All experiments were carried out at room temperature, in a conventional three-electrode system with a planar-configuration platinum electrode or a SPE as working electrode. The auxiliary electrode was an epoxy–graphite composite electrode in a tubular configuration, and the reference electrode was a double-junction Ag/AgCl electrode (Orion 92-02-00), with a commercial inner filling solution (Thermo Orion 900002) and 0.1 M KCl as outer filling solution. The three electrodes were disposed along the flow system using methacrylate supports. The flow injection system consisted of a Gilson (Minipuls 3) peristaltic pump, interconnecting Teflon tubing (0.8 mm inner diameter) and a sample injection valve.

2.3. Electrode preparation

Glass fibre with photolithographed cooper tracks was used as conductive support for the construction of the planar-configuration platinum electrode. For this electrode, with an active surface area of $24\,mm^2$, the electric contact between the cooper and the platinum was achieved using a conductive silver resin, which allows the welding of both materials and, finally, the electrode was encapsulated with an epoxy resin.

A DEK 248 screen-printing system (DEK, UK) was used to fabricate the SPEs (with a geometrical area of $24\,mm^2$). The electropolymerisation process used for the preparation of the mediator-modified SPEs was previously described for conventional electrodes [28]. Briefly, the composite SPE surface was pre-treated by dipping it in phosphate buffer solution and performing cyclic voltammograms between −0.2 and +0.1 V for 10 min at $0.05\,V\,s^{-1}$ [16,30]. The aim of this pre-treatment was to enhance the reproducibility of the electrode surface characteristics. The second step was the electropolymerisation of the mediator on the SPE surface, by applying a constant potential to the electrode immersed in a redox mediator solution. The applied potential, as well as the mediator concentration and the electropolymerisation time, varied depending on the used mediator. Finally, the electrode surface was activated by recording 10 cyclic voltammograms at $0.05\,V\,s^{-1}$, using potential windows that depended on the mediator. On the other hand, for the preparation of the polysulfone–graphite composite-modified SPEs, a 7.5 wt% polysulfone solution was prepared in dry DMF. Once the solution was homogenised, 150 μL of this solution were mixed with 30 mg of graphite and 1.5 mg of redox mediator

Scheme 1. Sequence of reactions for the determination of ammonium.

(MB, 3,4-DHB, *p*-BQ, *o*-PDA or DCPIP). A thin film of this mixture was screen-printed onto the SPE surface. Immediately after printing, it was precipitated by phase inversion achieved by immersing the electrode in cold water (approximately 4 °C) or in a 0.477 units of GlDH/μL aqueous solution, depending on the kind of sensor to be prepared [31,29]. This process leads to a controlled phase change of the polysulfone-composite (cast onto the electrode surface) from liquid to solid. By controlling the initial state of phase transition, the membrane morphology can be controlled (i.e. porosity, thickness). Then, the polysulfone-composite SPEs were thoroughly rinsed with double-distilled water prior to use. The SPEs without enzyme were stored in air at room temperature, while the ones with enzyme were stored dried at 4 °C.

2.4. Analytical procedure

Cyclic voltammetry at a scan rate of $0.1\,\mathrm{V\,s^{-1}}$ was used to electrochemically characterise the evaluated SPEs. From these results, the appropriate working potential for each electrode was determined.

Electrochemical experiments were performed using two different background electrolyte solutions, depending on the assay: 0.05 M phosphate buffer solution with 0.05 M KCl at different pH or a solution containing 2.5 mM α-ketoglutarate and 0.2 mM NADH, freshly prepared in phosphate buffer at pH 7.3. These solutions, pumped at $0.9\,\mathrm{mL\,min^{-1}}$ flow rate, were used as carrier solutions in the flow injection system. Stock solutions of ammonium (1 M) and NADH (0.01 M) were prepared using phosphate buffer at pH 7.3 and 6.5, respectively. NADH solution must be freshly prepared prior to use. For the evaluation of both NADH sensors and GlDH-modified biosensors in flow system, 100 μL of various NADH or ammonium solutions, respectively, were injected once a stable baseline was reached. The applied potential (versus SCE) for the oxidation of NADH was dependent on the used mediator (Scheme 1).

All the measurements were based on the current peak height, calculated as the difference between the maximum current value after the injection and the current value for the baseline due to the carrier solution. Several calibration curves were performed with each electrode under the same conditions in order to study the evolution of the slope value, since this parameter will give information about the degree of alteration of the electrode surface.

For all the experiments at least three replicates were done, and the results given are the averages of all the measurements with the corresponding relative standard deviations (R.S.D.s).

3. Results and discussion

3.1. Evaluation of non-modified platinum planar-configuration electrode and SPEs used as NADH sensors in a flow injection system

In order to demonstrate the improved features of SPEs over platinum electrodes, the fouling effect on both surfaces was evaluated by measuring the current intensity after successive NADH injections. Results demonstrated that the SPEs slightly improved the repeatability compared to the platinum transducer, showing also a higher sensitivity value (i.e. the sensitivity values obtained from 10 successive calibration curves were $310\,\mu\mathrm{A\,M^{-1}}$ with a R.S.D. = 5% for a platinum electrode and $900\,\mu\mathrm{A\,M^{-1}}$ with a R.S.D. = 4% for a SPE). Even more important, the R.S.D.s for both electrodes were not only due to random oscillations among measurements, but they were more likely attributed to the decrease of sensitivity after successive calibration curves as a consequence of the fouling process of their surface. The SPEs slightly improved this loss of sensitivity, fact that agrees with previous studies carried out with platinum and graphite electrodes [32]. However, none of both is reliable for measuring NADH oxidation with time, as the SPEs lost around 40% of the signal for 20 injections of a 2×10^{-4} M NADH solution in different days, and the platinum electrode lost 60% (results not shown).

3.2. Development and characterization of redox mediator-modified screen-printed electrodes used as NADH sensors in a flow injection system

3.2.1. Amperometric studies
After choosing SPEs as working electrodes, the response to NADH oxidation was evaluated with calibration curves for

Table 1
Calibration parameters of NADH oxidation performed with SPEs based on electropolymerised mediators or mediator-modified polysulfone-composite films[a]

Redox mediator	Electropolymerised mediator		Mediator-modified polysulfone-composite film	
	E_w (V vs. SCE)	Sensitivity ($\mu\mathrm{A\,M^{-1}}$)	E_w (V vs. SCE)	Sensitivity ($\mu\mathrm{A\,M^{-1}}$)
MB	0.100	96 ± 29	−0.100	1009 ± 38
3,4-DHB	0.300	263 ± 17	0.350	727 ± 25
p-BQ	0.325	79 ± 8	0.175	753 ± 24
o-PDA	0.450	152 ± 12	0.300	640 ± 21
DCPIP	0.320	73 ± 13	0.150	761 ± 27

[a] Sensitivity values come from calibration curves where each point is the average of seven experimental data. The evaluated NADH concentration range was between 2×10^{-5} and 5×10^{-4} M. The carrier electrolyte solution was de-aerated 0.05 M phosphate buffer with 0.05 M KCl at pH 6.5, pumped at $0.9\,\mathrm{mL\,min^{-1}}$ flow rate.

Table 2

Evaluation of the repeatability of 20 successive injections of different NADH concentrations into a de-aerated carrier solution, using electropolymerised mediators or mediator-modified polysulfone-composite films

Redox mediator	E_w (V vs. SCE)	Current intensity (nA)	R.S.D. (%)
Electropolymerised mediator			
MB[a]	0.100	14	4
3,4-DHB[b]	0.300	61	3
p-BQ[b]	0.325	45	1
o-PDA[b]	0.450	33	5
DCPIP[a]	0.320	41	3
Mediator-modified polysulfone-composite film			
MB[b]	−0.100	206	1
3,4-DHB[b]	0.350	146	1
p-BQ[b]	0.175	151	2
o-PDA[b]	0.300	139	1
DCPIP[b]	0.150	159	1

[a] Injections of 100 μL of 5×10^{-4} M NADH.
[b] Injections of 100 μL of 2×10^{-4} M NADH.

the electrodes with electropolymerised mediators or mediator-modified polysulfone-composite films. Each point of the calibration curves is the average of the current intensity for a known NADH concentration after seven successive injections. All the electrodes showed linear calibration curves for the evaluated NADH concentration range, from 2×10^{-5} to 5×10^{-4} M. Table 1 shows that best sensitivity values were achieved with electrodes prepared using mediator-modified composite films. However, since the main drawback of non-modified electrodes is the fouling of the electrode surface by NADH oxidation byproducts, it was required a more thorough study. With this purpose, repeatability and reproducibility were evaluated for all the electrodes. The repeatability of the measurements was evaluated by measuring the current intensity values due to 20 successive injections of a known NADH solution. The reproducibility was evaluated by measuring the current intensity values due to injections of increasing NADH concentrations using the same electrode (calibration curves), in order to obtain the sensor sensitivity, and repeating it with the same electrode several times. The reproducibility of the sensitivity values (sensitivity R.S.D.) was done as the operational stability for the developed sensors.

Table 2 shows the results of repeatability for all the mediator-modified SPEs. The mediator presence, especially for composite films-based sensors, improves the R.S.D. compared to the results with a non-modified SPE (R.S.D. = 6%, *n* = 20). Table 3 shows the better reproducibility of the sensitivity values obtained with mediator-modified SPEs, pointing out how each electrode behaves after being used in successive calibration curves. The slight improvement of the reproducibility for the composite films-based sensors could be attributed to the different effect of the absorbed mediator. In electropolymerised mediator-based sensors, there is always a significant amount of adsorbed mediator that has a direct influence on the electrochemical characteristics. On the contrary, for the electrodes prepared with polysulfone, the amount of mediator still adsorbed after thoroughly rinsing the electrodes prior to use, can be neglected compared to the total amount of mediator retained in the polysulfone film. Thus, the electrochemical characteristics of these

Table 3

Evaluation of the reproducibility of five successive calibration curves obtained by injecting different NADH concentrations into a de-aerated carrier solution, using electropolymerised mediators or mediator-modified polysulfone-composite films

Redox mediator	E_w (V vs. SCE)	Sensitivity (μA M^{-1})	Sensitivity R.S.D.[a] (%)
Electropolymerised mediator			
MB	0.100	96	1
3,4-DHB	0.300	264	2
p-BQ	0.325	80	3
o-PDA	0.450	152	5
DCPIP	0.320	75	3
Mediator-modified polysulfone-composite film			
MB	−0.100	1035	1.5
3,4-DHB	0.350	695	0.4
p-BQ	0.175	751	0.7
o-PDA	0.300	640	1.3
DCPIP	0.150	769	0.7

[a] Reproducibility of the slope of five calibration curves. The evaluated NADH concentration range was between 2×10^{-5} and 5×10^{-4} M.

electrodes will mainly be dependent on the mediator entrapped inside the film. Furthermore, the minimisation of the electrode fouling for the electrodes based on polysulfone films, shown as an improvement of the reproducibility of the sensitivity values, could be explained from the better contact achieved between the mediator and the graphite particles.

Another important parameter is the response time, especially in flow systems, since it gives valuable information about the ability of the flow system to perform continuous measurements. As included in Table 4, all the mediator-modified SPEs had response times ($t_{95\%}$) from 12 to 30 s. All the electrodes showed response times that notably improved the response time ($t_{95\%}$), respect to non-modified electrodes, when a 2×10^{-4} M NADH solution was injected (>50 s).

Best sensitivity, repeatability and reproducibility were achieved using SPEs based on mediator-modified polysulfone-composite films. Moreover, the electrodes based on electropolymerised mediator were produced one by one through a process that requires about 30 min, while the electrodes based on polysulfone-composite films can be mass-produced by screen-

Table 4

Dynamic characteristics of the response obtained using electropolymerised mediators or mediator-modified polysulfone–graphite films[a]

Redox mediator	Response time ($t_{95\%}$, s)	
	Electropolymerised mediator	Mediator-modified polysulfone-composite film
MB	30 ± 1.2	17 ± 1.0
3,4-DHB	18 ± 0.4	20 ± 0.5
p-BQ	12 ± 1.3	19 ± 1.5
o-PDA	13 ± 0.4	20 ± 0.6
DCPIP	22 ± 2.8	26 ± 1.9

[a] Injections of 100 μL of 2×10^{-4} M NADH. Each given value is the average of three experimental values. The carrier electrolyte solution was de-aerated 0.05 M phosphate buffer with 0.05 M KCl at pH 6.5, pumped at 0.9 mL min^{-1} flow rate.

printing. As a result, mediator-modified polysulfone-composite film-based SPEs were chosen for the development of an ammonium biosensor, based on glutamate dehydrogenase enzyme (GlDH), to be implemented in a flow system.

3.2.2. Storage stability of the mediator-modified SPEs

The storage stability was calculated from the sensitivity of calibration curves obtained in different days with electrodes belonging to the same sheet, i.e. prepared at the same time. Consequently, firstly it was necessary to study the variability among electrodes belonging to the same sheet (36 electrodes/sheet). It was calculated from the values of current intensity for four electrodes belonging to the same sheet for 20 successive injections of a 2×10^{-4} M NADH solution. The R.S.D. for electrodes based on polysulfone-composite films varied from 4 to 9%, depending on the mediator. Since all mediators follow a heterogeneous catalysis mechanism, which implies that current intensity is proportional to both the surface area and the mediator coverage, it is inferred that the differences in both parameters, due to intrinsic limitations of the construction process, will notably increase the variability among the electrodes belonging to a same sheet. However, the high reproducibility observed may be due to the fact that the amount of mediator inside the polysulfone-composite membrane is high enough to ensure that small variations in mediator coverage do not induce important changes in the electrical signal. Once the inherent variability among NADH calibration curves for electrodes from the same sheet was known, it was possible to evaluate the storage stability. It was possible to conclude that the sensitivity values were affected only for the electrodes prepared with *p*-BQ and DCPIP during the first 15 days in a way that could not be attributed to the variability among the sheet.

3.3. Development, characterization and implementation of an ammonium biosensor based on GlDH-mediator-polysulfone–graphite SPE in a flow injection system

The behaviour of mediator-polysulfone-composite film-based sensors in front of some electroactive compounds that might interfere with the response of a dehydrogenase-based biosensor was evaluated. No interference was observed from common electroactive compounds, such as ascorbic and uric acids. Taking advantage of this good permselective behaviour, ammonium biosensors were developed using glutamate dehydrogenase (GlDH) enzyme incorporated into polysulfone-composite films placed onto SPEs. Based on previous studies about polysulfone membranes [29], this enzyme can be incorporated in the films during the phase inversion process that causes the precipitation of the polysulfone. Fig. 1 shows five successive calibration curves obtained using a GlDH-Meldola's Blue (MB)-polysulfone-composite film-based SPE in a flow system. MB was chosen as it was the mediator that offered the highest sensitivity. These biosensors showed a linear correlation for the evaluated ammonium concentrations ranging from 5×10^{-5} to 2×10^{-2} M under the working conditions described. The sensitivity to ammonium obtained for these biosensors in a flow system was $15 \, \mu A \, M^{-1}$ and the sensitivity R.S.D. was
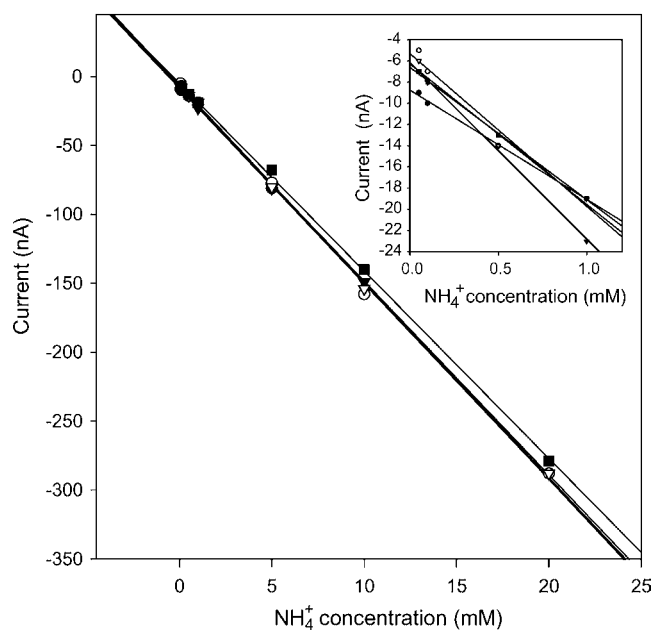

Fig. 1. Five successive calibration curves obtained from injections of different known ammonium concentrations in a flow system. A SPE based on GlDH-MB-polysulfone-composite film has been used as working electrode. De-aerated carrier solution: 0.05 M phosphate buffer with 0.05 M KCl, containing 2.5 mM α-ketoglutarate and 0.2 mM NADH, at pH 7.3. Working potential: −0.1 V vs. SCE. Flow rate: 0.9 mL min^{-1}.

1.9% ($n = 5$ consecutive calibration curves), corresponding to the operational stability. The reproducibility among biosensors belonging to the same sheet, meaning that they were prepared at the same time, was also studied, finding an R.S.D. associated to the slope of the calibration curves obtained with four of these electrodes of 4%. In addition, the storage stability was evaluated, proving that these biosensors can be stored at 4 °C at least for 1 month, showing a lost of sensitivity of 4%, being negligible as it is comparable to the sensitivity R.S.D. for different electrodes of the same sheet. Finally, the response time ($t_{95\%}$) for sample volumes of 100 μL was lower than 30 s, followed by a short recovery time, allowing an analysis time of 1 min. These results prove the usefulness of these biosensors for determining ammonium in flow, being able to be changed each day for a new electrode stored at 4 °C.

4. Conclusions

It has been demonstrated that both electropolymerised mediator-based SPEs and mediator-modified polysulfone-composite film-based SPEs, avoid problems related to the amperometric oxidation of NADH when used as detectors in a flow system, since they lower the high required overpotentials, thus minimising electrode fouling. Furthermore, both mediator-based strategies show good selectivities and low response times (<30 s) compared to the results for non-modified SPEs, indicating better electrocatalytic behaviour and allowing a higher number of NADH determinations in less time. Comparing the results for both types of sensors, it can be concluded that polysulfone-composite film-based sensors show the highest sensitivity, as

well as the best repeatability and reproducibility results. The latter parameter can be directly related to the operational stability, proving the absence of mediator leakage and electrode fouling, essential characteristics for electrodes to be used in flow systems. Finally, having considered the variability among electrodes belonging to a same sheet, it can be noticed that the electrodes based on MB, 3,4-DHB and *o*-PDA-polysulfone films kept 100% of their sensitivity at least during the first 15 days. These good performance characteristics demonstrated the usefulness of the mediator-modified polysulfone-composite films-based SPEs for the development of dehydrogenase-based biosensors and their further implementation in flow systems. Moreover, the simple and fast fabrication procedure allows their mass production. GlDH-MB-polysulfone-composite film-based SPEs have been shown to be reliable biosensors for the amperometric detection of ammonium in solution at a working potential of -0.1 V versus SCE, showing an excellent reproducibility among successive calibration curves (1.9%, $n = 5$). Thus, it can be concluded that a stable flow system for the determination of ammonium has been developed.

Acknowledgements

References

[1] C.O. Schmakel, K.S.V. Santhanam, P.J. Elving, J. Am. Chem. Soc. 97 (1975) 5083.
[2] J. Moiroux, P.J. Elving, Anal. Chem. 50 (1978) 1056.
[3] H. Jaegfeldt, J. Electroanal. Chem. 110 (1980) 295.
[4] A. Chaubey, B.D. Malhotra, Biosens. Bioelectron. 17 (2002) 441.
[5] P.N. Bartlett, P. Tebbutt, R.G. Whitaker, Prog. React. Kinet. 16 (1991) 55.
[6] T. Nakaminami, S. Kuwabata, H. Yoneyama, Anal. Chem. 69 (1997) 2367.
[7] K. Hirano, H. Yamato, K. Kunimoto, M. Ohwa, Sens. Actuators B 86 (2002) 88.
[8] R.W. Murray, A.G. Ewing, R.A. Durst, Anal. Chem. 59 (1987) 379A.
[9] H.D. Abruña, Coord. Chem. Rev. 86 (1988) 135.
[10] P.C. Pandey, Meth. Biotechnol. 6 (1998) 81.
[11] E.V. Ivanova, V.S. Sergeeva, J. Oni, C. Kurzawa, A.D. Ryabov, W. Schuhmann, Bioelectrochemistry 60 (2003) 65.
[12] A.B. Florou, M.I. Prodromidis, M.I. Karayannis, S.M. Tzouwara-Karayanni, Electroanalysis 10 (1998) 1261.
[13] V.S. Soukharev, A.D. Ryabov, E. Csöregi, J. Organomet. Chem. 668 (2003) 75.
[14] W.R. Everett, T.L. Welch, L. Reed, I. Fritsch-Faules, Anal. Chem. 67 (1995) 292.
[15] J. Lukkari, K. Kleemola, M. Meretoja, J. Kankare, Chem. Commun. (1997) 1099.
[16] F. Pariente, E. Lorenzo, H.D. Abruña, Anal. Chem. 66 (1994) 4337.
[17] S.L. Álvarez-Crespo, M.J. Lobo-Castañón, A.J. Miranda-Ordieres, P. Tuñón-Blanco, Biosens. Bioelectron. 12 (1997) 739.
[18] J. Wang, P.V.A. Pamidi, M. Jiang, Anal. Chim. Acta 360 (1998) 171.
[19] J. Razumiene, A. Vilkanauskyte, V. Gureviciene, V. Laurinavicius, N.V. Roznyatovskaya, Y.V. Ageeva, M.D. Reshetova, A.D. Ryabov, J. Organomet. Chem. 668 (2003) 83.
[20] A.P. Doherty, M.A. Stanley, J.G. Vos, Analyst 120 (1995) 2371.
[21] P.D. Hale, T. Inagaki, H.I. Karan, Y. Okamoto, T.A. Skotheim, J. Am. Chem. Soc. 111 (1989) 3482.
[22] N.C. Foulds, C.R. Lowe, Anal. Chem. 60 (1988) 2473.
[23] L. Ye, M. Hammerle, A.J.J. Olsthoorn, W. Schuhmann, H.-L. Schmidt, J.A. Duine, A. Heller, Anal. Chem. 65 (1993) 238.
[24] E. Tamiya, I. Karube, S. Hattori, M. Suzuki, K. Yokoyama, Sens. Actuators 18 (1989) 297.
[25] M. Vaillancourt, J.W. Chen, G. Fortier, D. Bélanger, Electroanalysis 11 (1999) 23.
[26] L. Gorton, E. Csöregi, E. Domínguez, J. Emnéus, G. Jönsson-Pettersson, G. Marko-Varga, B. Persson, Anal. Chim. Acta 250 (1991) 203.
[27] I. Willner, E. Katz, Angew. Chem. Int. Ed. 39 (2000) 1180.
[28] B. Prieto-Simón, E. Fàbregas, Biosens. Bioelectron. 19 (2004) 1131.
[29] B. Prieto-Simón, E. Fàbregas, Biosens. Bioelectron. 22 (2006) 131.
[30] C. Malitesta, F. Palmisano, L. Torsi, P.G. Zambonin, Anal. Chem. 62 (1990) 2735.
[31] C.A. Smolders, A.J. Reuvers, R.M. Boom, I.M. Wienk, J. Membr. Sci. 73 (1992) 259.
[32] W.J. Blaedel, R.A. Jenkins, Anal. Chem. 47 (1975) 1337.

A novel rapid method for preparation of sample solution for chemical characterisation of titanium minerals by atomic spectrometry

R. Radhamani [a,*], P. Murugesan [a], A. Premadas [b], P.K. Srivastava [a]

[a] *Atomic Minerals Directorate for Exploration and Research, Department of Atomic Energy, Nagpur 440001, India*
[b] *Atomic Minerals Directorate for Exploration and Research, Department of Atomic Energy, Bangalore 560072, India*

Abstract

A new rapid decomposition and dissolution method with a mixture of sodium di-hydrogen orthophosphate and di-sodium hydrogen orthophosphate as a novel flux is described. The minerals are fused with (1:1) mixture of the above salts (flux) and the melt is dissolved in distilled water. The solution is diluted to desired volume depending on the instrumental technique used for determination. ICP-OES is used for the determination of Al, Ca, Mg, Cr, V, Si, Fe and Ti without interference from titanium, iron and sodium phosphate (introduced as flux). All the elements except Si and V are also determined by AAS. The use of nitrous oxide–acetylene flame eliminates the depression due to titanium in the measurement of Mg, Mn, Cr and Fe in air–acetylene flame. Synthetic mixture conforming to ilmenite and rutile composition are analyzed by ICP-OES and AAS to check the validity of the method. The results are in good agreement. The proposed method has been applied to natural samples and the results are evaluated against the established decomposition method using potassium bisulphate. Both ICP-OES and AAS yielded comparable results. The R.S.D. of the proposed method in case of ICP-OES varies from 0.5 to 2%, whereas for AAS it varies from 1.5 to 3% for different elements ($n = 5$). The novelty of the proposed sample decomposition lies in its simplicity, ease and speed of fusion with minimal skills besides being eco-friendly unlike the reported tedious complicated decomposition procedures involving variety of fluxes and lot of hazardous chemicals.
© 2006 Elsevier B.V. All rights reserved.

Keywords: Titanium minerals; Decomposition with sodium phosphates; ICP-OES; AAS

1. Introduction

Ilmenite and rutile are the most economic titanium minerals found in the beach sands of India (east and west coast) in association with other heavy minerals such as zircon, monazite, sillimanite and garnet [1,2]. At different stages of exploration and exploitation, various mineral fractions are separated using gravity and magnetic separation methods. Among heavy minerals, ilmenite and rutile are valuable major minerals required for pigment industry and the feedstock that meets the tolerance level for Ca, Mg, Cr, V, Mn and Al is in great demand [3]. Ilmenite is chemically processed for the production of TiO_2. Above certain level, these elements affect the processing technology. Therefore, these minerals are frequently analyzed for above elements to ascertain its quality and suitability for process technology for production of titanium dioxide. A non-destructive instrumental technique, such as INNA or XRF spectrometry, has been used for the analysis of geological materials [4]. The INNA is virtually free from matrix effect, but it requires the access to a nuclear reactor to irradiate samples. The cost and inconvenience of this requirement restricts its application in routine analysis. Matrix interference is severe in XRF spectrometry. Proper matrix-matched reference materials covering the full concentration range of elements to be determined are required for accurate results. In addition, the certified results for major elements are available for SRM of a mineral, but the results for the minor constituents are not reported [5,6]. Further, the quantitative results for lightest elements (Mg, Al and Si) cannot usually be achieved, until the sample is fused with suitable flux to form homogeneous glass bead. The above limits its application to the analysis of minerals. Simple instrumental techniques such as ICP-OES and AAS (relatively less prone to matrix effect) involving solution for analysis are widely accepted alternate techniques for the analysis of geological samples.

---

* Corresponding author. Tel.: +91 7122564977; fax: +91 7122561438.
E-mail address: radhamani_mahanta@yahoo.com (R. Radhamani).

Sample solution preparation is the most important step in the chemical analysis prior to determination of various constituents. The titanium minerals are not decomposed completely with acid digestion involving combination of hydrofluoric and a mineral acid. Ortho-phosphoric acid is applied for decomposition and dissolution of ilmenite, and Ti, Fe, Mn, Ca, Mg, Cr, V and Mn are determined by ICP-OES [7,8]. However, rutile is not decomposed. A mixture of ortho-phosphoric acid and sodium pyrophosphate is also used for decomposition of other minerals such as biotite, garnet, chromite, olivine, bauxite, Fe and Mn ore [9,10]. Both glass and platinum wares are attacked during decomposition process.

Fusion with potassium bisulphate is most commonly used for decomposition of all the titanium minerals [11–15]. Lot of undesirable sulphur trioxide fumes is generated during the process. Lithium metaborate, lithium tetra borate and fused borax are also applied [15]. However, the fusion requires non-sticking Pt–Au crucibles and melt takes longer time for dissolution. In above fusion, the melt is dissolved in dilute sulphuric acid to prevent the hydrolysis of Ti. Large quantities of salt are introduced in to the solution, which affects the subsequent step of analysis. Therefore, there is a need of simple, rapid and economical method for the decomposition of both ilmenite and rutile, so that the constituents can be measured without much treatment. Various sodium salts of ortho-phosphoric acid melt at low temperature (600–700 °C) to form condensed phosphates, which have high ability to form complex with many cations in the pH range from 6 to 8.5 [16]. However, no application of these salts in decomposition of titanium mineral is reported. Keeping in view, the complexing ability and ease of fusion, decomposition of titanium minerals with these salts are tried. Investigation reveals that both the titanium minerals can be easily decomposed with liberation of water during the fusion and no hazardous fumes are generated unlike the potassium bisulphate fusion. Complexing ability of the condensed polyphosphate is utilized for the dissolution of the resulting melt in distilled water.

The aim of present work is to investigate the applicability of eco friendly flux comprising a mixture of $NaH_2PO_4 \cdot H_2O$ and Na_2HPO_4 (anhydrous) for decomposition and dissolution of both ilmenite and rutile, so that most of the above elements can be determined by ICP-OES or AAS.

2. Experimental

2.1. Instrumentation

ICP-OES, GBC model Integra XM (Dandenong, Vic., Australia) was used for measurement of V, Cr, Mg, Al, Fe, Mn, Ca

Table 1
ICP-OES operating parameters

Forward power (W)	1200
Reflected power (W)	<20
Observation height (mm)	15
PMT voltage[a] (V)	500–600
Coolant gas flow rate ($l min^{-1}$)	10
Auxiliary gas flow rate ($l min^{-1}$)	0.5
Sample gas flow rate ($l min^{-1}$)	0.5
Flush time (s)	10
Nebulizer	Concentric glass

Wavelength for measurement; Ti 334.941 nm, Fe 238.204 nm, Si 251.000 nm, Al 396.152 nm and Mg 279.553 nm, Cr 205.552 nm, Ca 393.366 nm, V 292.402 nm and Mn 257.610 nm.

[a] Varies from element to element.

and Si. The wavelengths and operating parameters are given in Table 1.

AAS, Model AA-Spectra-20B, Varian Techtron Australia was used for the measurement of Fe, Mg, Ca, Cr, Mn, Al and Ti. The wavelengths and operating parameters are given in Table 2.

Double beam spectrophotometer, Model 920 of GBC Equipment, Australia was used for spectrophotometric determination of Si, Ti, V and also to record the spectra of Fe and Ti complex.

2.2. Standards and reagents

Stock solution of all major oxides and trace elements V and Cr were prepared from High purity oxides (Alfa Aesar, A Johnson mathey company, London, UK).

Standard solution of titanium was prepared by fusing 0.5 g of TiO_2 with 8 g of 1:1 mixture of di-sodium hydrogen phosphate anhydrous and sodium di-hydrogen phosphate monohydrate. The melt was dissolved in distilled water and volume was made to 100 ml to give 5 $mg ml^{-1}$ of TiO_2 stock solution.

Standard solution of Fe was prepared similarly.

Blank solution was prepared by fusing 8 g of mixture and made up to 100 ml. The above solutions containing same quantity of P_2O_5 (40.6 $mg ml^{-1}$) are used for the interference studies in AAS measurements and the diluted solutions were used as calibration standards.

Other standards: Mn, Cr, V, Mg and Al, standards were prepared by fusing respective dried oxides (0.1 g for Mn, Cr, V, Mg and 0.2 g for Al) with the 4 g of 1:1 mixture of mono and di-hydrogen phosphate and dissolved in 100 ml-distilled water. Calcium carbonate (0.1 g) was used for preparation of Ca standard. These solutions were diluted further for use as calibration standards.

Table 2
AAS operating parameters

Particulars	Al	Ca	Mn	Fe	Cr	Ti	Mg
Lamp current (mA)	10	10	5	5	7	20	4
Wavelength (nm)	309.3	422.7	279.5	372.0	357.9	364.3	285.2
Spectral band width (nm)	0.5	0.5	0.2	0.2	0.2	0.5	0.5
Flame condition	C_2H_2–N_2O reducing	C_2H_2–N_2O reducing	C_2H_2–N_2O reducing	C_2H_2–N_2O reducing	C_2H_2–N_2O reducing	C_2H_2–N_2O reducing	C_2H_2–N_2O reducing

Silica standard: 0.05 g of quartz (GR, Merck, Germany) fused with 0.5 g of sodium carbonate and dissolved in water. The solution is neutralized with dilute ortho-phosphoric acid to pH 7 and diluted to 250 ml.

Di-sodium hydrogen phosphate anhydrous (Na_2HPO_4) and sodium di-hydrogen phosphate monohydrate ($NaH_2PO_4 \cdot H_2O$) were of GR grade (Merck, India).

2.3. Preparation of sample solution

2.3.1. Potassium bisulphate fusion

A 0.5 g-dried sample is fused with 10 g $KHSO_4$ in a silica crucible, which was preheated for dehydration. The fused melt was dissolved in dilute sulphuric acid and made up to 100 ml volume maintaining 10% (v/v).

2.3.2. Phosphate fusion

Four gram each of sodium di-hydrogen phosphate monohydrate and di-sodium hydrogen phosphate is mixed well in dry platinum crucible, heated slowly first on wire gauze and then strongly on the flame for the formation of condensed phosphate. Accurately weighed 0.5 g of sample is added to the cooled melt. The uncovered crucible is again heated on the flame for fusion. After 3–4 min, the crucible is covered with platinum lid. The crucible is swirled intermittently for complete decomposition, cooled and transferred in a 250 ml beaker containing distilled water. The beaker is heated on water bath for dissolving the melt. The crucible is removed from the beaker, washed thoroughly and the volume is made to 100 ml.

2.3.3. Measurements

A 10 ml of the master solution is further diluted to 100 ml for the determination of Cr, V, Al, Mn, Ca and Mg by ICP-OES. Ti and Fe are determined in further diluted solution depending on the minerals analyzed. Si is determined by ICP-OES only in the solution obtained after phosphate fusion.

Cr, Al, Mn, Ca and Mg, is determined in original solution. Ti and Fe are determined in further diluted solution by AAS.

The solution obtained by potassium bisulphate fusion was diluted similarly maintaining 10% acidity with respect to sulphuric acid. Blank were also prepared in same matrix.

Calibration standards were matched with the samples in respect of flux content.

3. Results and discussion

The various steps in a chemical analysis are decomposition, dissolution, separation and measurement. The most important step is decomposition and dissolution of the samples to get clear and stable solution, so that the constituents can be determined by ICP-OES or AAS without separation. Various aspects of the proposed method are discussed below.

3.1. Decomposition

Sodium di-hydrogen orthophosphate melts easily on heating and polymerizes to form poly cyclic *meta* phosphate $(NaPO_3)_n$
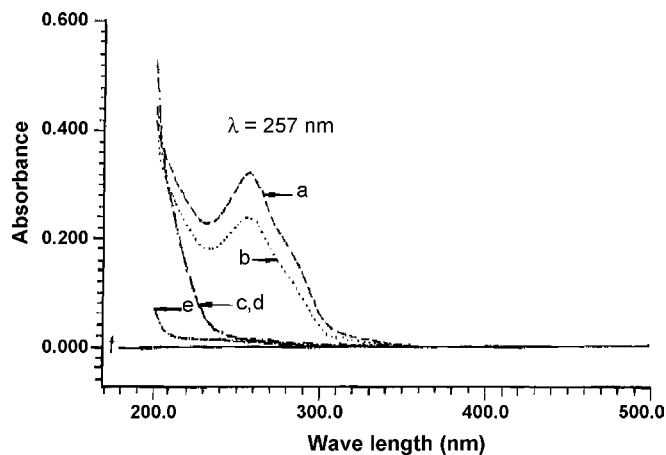
Fig. 1. Absorption spectra of TiO_2 (4 ppm)–polyphosphate complex under various condition: (a) solution obtained after fusion with $(NaPO_3)_n$ (5 g) and (b–d) are the solution obtained after fusion with the mixture of mono and di-sodium orthophosphate in the ratio of 4:1, 3:2 and 2.5:2.5 (5 g), respectively, (e) polyphosphate blank and (f) distilled water.

and mixture of sodium di-hydrogen phosphate and di-sodium hydrogen phosphate forms linear polyphosphate—$Na_{n+2}P_nO_{3n+1}$. Both linear and cyclic phosphates are stable in neutral and alkaline medium. Cyclic phosphate changes to linear phosphate in more alkaline medium. These condensed phosphates are excellent complexing agents and form complexes with most of the transitional and non-transitional metals ions [16].

Titanium and iron being the major constituent of titanium minerals, the decomposition studies of 0.1 g each of TiO_2 and Fe_2O_3 by fusion with 5 g flux containing different proportion of mono and di-sodium salts were carried out separately. Preliminary experiments show that sodium di-hydrogen orthophosphate is unable to decompose titanium dioxide but readily decomposes ferric oxide. It is further observed that the decomposition of TiO_2 is complete with addition of little quantity of di-sodium salt to it. The melt obtained is clear and soluble in water. Increase in di-sodium salt increases the efficiency of the flux, probably due to increase in alkalinity and melting temperature. It is difficult to fuse di-sodium hydrogen phosphate at normal burner temperature. Hence, this salt alone has not been tried.

In order to have the information regarding the complexes, the absorption spectra for Ti and Fe solutions obtained after fusion with various proportion of salts are shown in Figs. 1 and 2, respectively.

Ti complexes formed with (a and b) are of similar nature and absorb considerably at 257 nm. Probably, Ti forms complex with *meta* phosphate formed during the fusion. Further absorbance depends on the concentration of polyphosphate. The complexes obtained with (c and d) are different and may be because of formation of linear poly phosphate complex. No absorption peak at 257 nm is observed in the concentration range studied.

Iron complexes formed with (a–d) as shown in Fig. 2, have different absorption characteristics. The presence of different quantities of meta and linear poly phosphate in solution modify the absorption. There is clear-cut difference in (a and d). The complex with (d) absorbs at 280 nm and appears to be formed with linear poly phosphate. The complex with *meta* phosphate
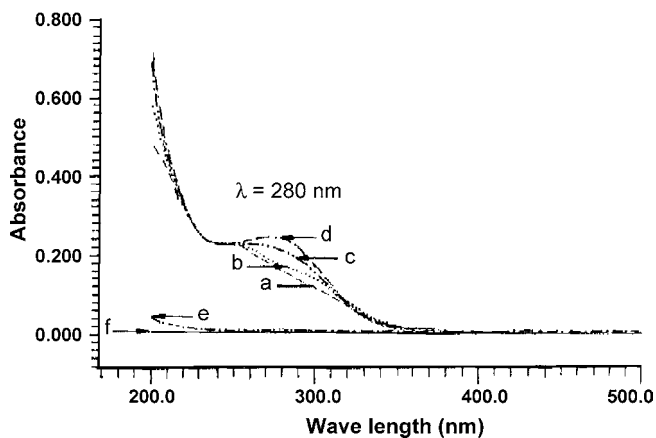
Fig. 2. Absorption spectra of Fe_2O_3 (4 ppm)–polyphosphate complex under various conditions: (a) solution obtained after fusion with $NaH_2PO_4·H_2O$ (5 g) and (b–d) are the solution obtained after the fusion with the mixture of mono and di-sodium orthophosphate in the ratio of 4:1, 3:2 and 2.5:2.5 (5 g), (e) polyphosphate blank and (f) distilled water.

(a) does not have absorption peak at 280 nm. Gradual change in shape of absorption curve is observed as the ratio of salts in flux is varied from (a to d).

Natural samples such as ilmenite and rutile, were taken for the decomposition studies with mixture of mono and di-sodium salts. Ilmenite and rutile obtained after beneficiation from beach sand are generally pure, but it is likely to be contaminated with traces of various associated minerals. Attempts were made to decompose a sample (0.10 g) containing ilmenite, sillimanite, zircon, garnet, rutile and monazite in equal proportion. The resulting melt was dissolved in distilled water and clear solution is obtained. Traces of combined silica (<2%) present in above minerals are easily decomposed. However, large quantity of silicate minerals such as zircon, sillimanite and quartz, if present, is partially attacked and silica precipitates as gel during dissolution in water. Thus, the 1:1 flux mixture is most suitable for the decomposition of both the Ti minerals ilmenite and rutile. It was observed that 8 g of flux is enough to decompose 0.5 g samples.

Based on the experimental observations, it is inferred that the formation of condensed poly phosphate during fusion are responsible for the effective attack and formation of the complexes soluble in distilled water. The solution is also very stable due to formation of metal complexes of poly phosphate. On acidifying the solution the complex break and titanium phosphate precipitates. Similarly, precipitation is observed after the addition of alkalis.

The proposed method is far superior compared to potassium bi-sulphate fusion in respect of sample to flux ratio, and the time required for decomposition.

3.2. ICP-OES measurement

ICP-OES is one of the most accepted instrumental analytical techniques of today. The solution obtained contains large quantity of salt in the form of sodium phosphate. It has been observed that there is no increase in nebulizer pressure when the diluted solution containing 0.8% sodium phosphate used for measurement of trace elements V, Cr, Mg, Al, Fe, Mn and Ca.
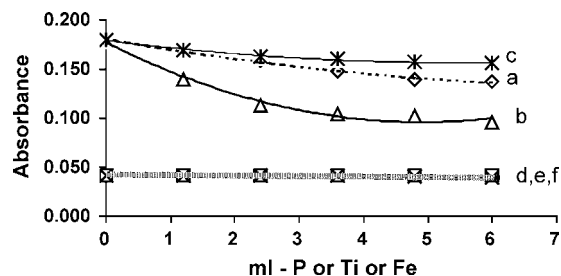
Fig. 3. Effect of P, Ti and Fe on Mn (a–c) show the effect of P, Ti and Fe, respectively, in air–acetylene flame while (d–f) shows the effect in $N_2O–C_2H_2$ flame.

3.3. Effect of P, Ti and Fe on measurement by AAS

Most of the required elements can be determined by AAS. Fe, Mg, Cr and Mn are determined usually in air–acetylene flame. But the resulting solution contains large quantity of phosphate salt, titanium (refractory element) and iron. Therefore, the effect of above on the measurement of Fe, Mg, Cr and Mn using air–acetylene flame is reinvestigated. The stock solutions of Ti, Fe and blank are used for interference studies of Ti, Fe and P, respectively. Keeping in view, the major matrix element composition of titanium minerals, a solution containing Ca: 0.8 ppm, Mg: 0.6 ppm, Cr: 3.42 ppm, Mn: 1.0 ppm and Fe: 7.0 ppm was taken for the study. The effect was studied separately for solution containing only Al (50 ppm). Nitrous oxide–acetylene burner was used for the interference studies.

The results of the interference studies obtained are shown in Figs. 3–6 for Mn, Mg, Cr and Fe, respectively. The quantities of P or Ti or Fe are represented on X-axis in "ml" because the volume used is common in all the cases. The detail of interferents added for the study is given in Table 3. The effect is discussed below. The degree of depressive effect due to phosphate decreases in the order of Mg, Mn, Cr and Fe in air–acetylene flame ("a" of Figs. 3–6). The depression is more severe in case of titanium ("b" of Figs. 3–6). This may be attributed to the formation of refractory compound of analyte with Ti in the flame. The depressive effect of iron as shown in the curve "c" of Figs. 3 and 4 is much less than phosphate. Curves "d–f" (Figs. 3–6) show the effect of P, Ti and Fe in nitrous oxide–acetylene flame, respec-
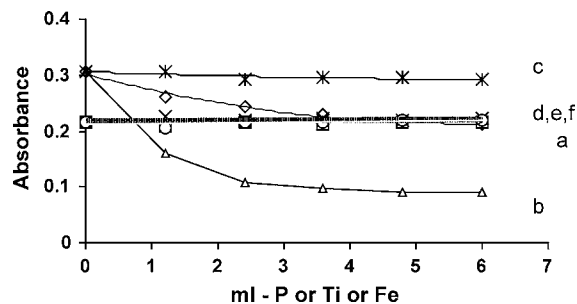
Fig. 4. Effect of P, Ti and Fe on Mg (a–c) show the effect of P, Ti and Fe, respectively, in air–acetylene flame while (d–f) shows the effect in $N_2O–C_2H_2$ flame.
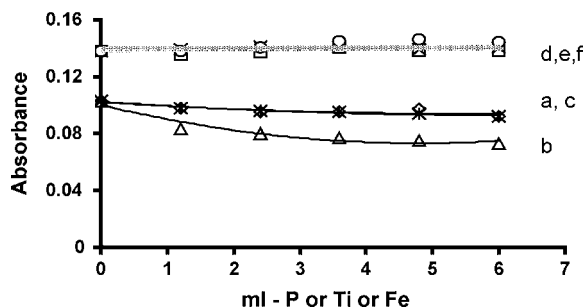
Fig. 5. Effect of P, Ti and Fe on Cr (a–c) show the effect of P, Ti and Fe, respectively, in air–acetylene flame while (d–f) shows the effect in N_2O–C_2H_2 flame.

Fig. 6. Effect of P and Ti on Fe (a and b) show the effect of P and Ti, respectively, in air–acetylene flame while (d and e) shows the effect in N_2O–C_2H_2 flame.

tively. The points on the curves merge each other. The curve (line) is parallel to X-axis, which implies that there is no ionization interference, probably due to suppression of ionization by the sodium present in the solution. The depression observed in air–acetylene for Mn, Mg, Cr and Fe, is eliminated. However, the sensitivity decreases for Mg, Mn and increases for Cr and Fe. No additional ionization suppressor is required.

Ca and Al are normally estimated using nitrous oxide–acetylene flame in concentrated solution. The effect of P, Ti and Fe is shown in Fig. 7. There is no effect of P, Ti and Fe on alu-

minium ("d–f" of Fig. 7) and Ca ("a–c" of Fig. 7). The effects are nullified with proper optimization of flame conditions and matrix matching in respect of flux content. Titanium, being the major constituents, no problem of salt concentration is observed in nitrous oxide flame because the solution can be diluted.

All the elements stated above are determined by AAS using nitrous oxide–acetylene flame. It is observed that burner clogging was more severe in case of bi-sulphate fusion.

In the absence of reference material, synthetic mixture conforming to rutile and ilmenite composition were analyzed by ICP-OES and AAS with matrix-matched standards to test the

Table 3
AAS interference studies—concentration of interfering elements

S.no.	Points on X-axis (ml)	P_2O_5 (mg ml^{-1})	TiO$_2$ solution		Fe$_2$O$_3$ solution	
			TiO$_2$ (mg ml^{-1})	P_2O_5 (mg ml^{-1})	Fe$_2$O$_3$ (mg ml^{-1})	P_2O_5 (mg ml^{-1})
1	0	0[a]	0	0[a]	0	0[a]
2	1.2	1.9	0.25	1.9	0.25	1.9
3	2.4	3.8	0.5	3.8	0.5	3.8
4	3.6	5.7	0.75	5.7	0.75	5.7
5	4.8	7.6	1.0	7.6	1.0	7.6
6	6.0	9.5	1.25	9.5	1.25	9.5

[a] Initial concentration of P_2O_5 is equal to 0.6 mg ml^{-1} shown as 0 in Figs. 3–7. Concentration of trace elements taken for the studies are—Ca: 0.8 ppm, Mg: 0.6 ppm, Cr: 3.42 ppm, Mn: 1.0 ppm, Fe: 7.0 ppm and Al: 50 ppm (studied separately).

Table 4
Comparison of results of synthetic mixture by the proposed method

Oxide	Synthetic mixture (rutile)[a]			Synthetic mixture (ilmenite)[a]		
	Quantity taken (mg)	Quantity found (mg)		Quantity taken (mg)	Quantity found (mg)	
		ICP-OES (mg)[b]	AAS (mg)[c]		ICP-OES (mg)[b]	AAS (mg)[c]
TiO$_2$	90.0	90.2	89.5	45	45.5	44.3
Fe$_2$O$_3$	5.0	4.80	4.90	45	44.8	44.9
Al$_2$O$_3$	2.5	2.45	2.60	2.5	2.45	2.54
MnO$_2$	1.5	1.51	1.48	1.5	1.5	1.56
MgO	1.5	1.45	1.44	1.5	1.51	1.48
CaCO$_3$	1.5	1.50	1.40	1.5	1.55	1.48
V$_2$O$_5$	1.5	1.45	1.49[d]	1.5	1.48	1.50[d]
Cr$_2$O$_3$	1.5	1.52	1.43	1.5	1.55	1.45
SiO$_2$	2.0	2.05	2.10[d]	2.0	1.95	1.95[d]

[a] The synthetic mixture conforming to ilmenite and rutile composition were prepared by mixing the various standard solution and diluting to 50 ml, so that the final concentration of flux is remains same.

[b] The ICP-AES measurement for Cr, V, Al, Si and Mg, (in both); Fe, Ca and Mn (in rutile) was taken in the dilute solution (dilution factor-10). Ti (in both); Fe, Mn and Ca (in ilmenite) are determined in further dilute solution (dilution factor-100).

[c] Measurement in concentrated solution (dilution factor-1) for minor elements and dilute solution for major elements (dilution factor-10 or 100).

[d] Determined spectrophotometrically by BPHA and molybdenum blue method.

Table 5
Comparison of results by the proposed method with potassium bisulphate fusion in natural samples

Sample	Fe_2O_3 (T)%				TiO_2%					MgO%			
	Phosphate		Bisulphate		Phosphate			Bisulphate		Phosphate		Bisulphate	
	A	B	A	B	A	B	C	A	B	A	B	A	B
Ilmenite-1	40.07	39.80	39.60	39.80	56.4	57.2	56.9	56.1	56.7	0.82	0.87	0.80	0.78
Ilmenite-2	50.30	50.64	50.40	50.80	48.9	49.2	49.1	48.9	49.5	0.05	0.05	0.04	0.05
Ilmenite-3	50.61	49.81	50.40	49.80	49.1	49.2	49.1	48.8	49.3	0.08	0.09	0.08	0.07
Ilmenite-4	50.00	50.41	50.10	50.50	49.7	49.9	49.4	50.1	49.4	0.05	0.06	0.06	0.05
Rutile-1	0.75	0.79	0.80	0.77	96.8	96.3	97.0	96.4	96.9	0.02	0.02	0.02	0.03
Rutile-2	1.01	0.95	0.96	1.10	96.4	95.8	96.8	95.5	96.3	0.02	0.02	0.03	0.02

	MnO%				CaO%				V_2O_5%			
	Phosphate		Bisulphate		Phosphate		Bisulphate		Phosphate		Bisulphate	
	A	B	A	B	A	B	A	B	A	C	A	C
Ilmenite-1	0.37	0.39	0.36	0.33	0.02	0.02	0.03	0.03	0.27	0.23	0.25	0.24
Ilmenite-2	3.50	3.70	3.60	3.50	0.08	0.08	0.07	0.08	0.68	0.66	0.65	0.64
Ilmenite-3	3.80	4.00	3.90	3.70	0.06	0.06	0.06	0.05	0.55	0.52	0.50	0.55
Ilmenite-4	3.60	3.90	3.70	4.00	0.07	0.06	0.07	0.06	0.07	0.06	0.06	0.06
Rutile-1	<0.01	<0.01	<0.01	<0.01	0.03	0.02	0.03	0.03	0.49	0.47	0.48	0.49
Rutile-2	<0.01	<0.01	<0.01	<0.01	0.03	0.04	0.04	0.03	0.49	0.46	0.48	0.46

	Cr_2O_3%				Al_2O_3%				SiO_2%	
	Phosphate		Bisulphate		Phosphate		Bisulphate		Phosphate	
	A	B	A	B	A	B	A	B	A	C
Ilmenite-1	0.17	0.18	0.19	0.18	1.14	1.29	1.21	1.30	0.77	0.79
Ilmenite-2	0.04	0.04	0.04	0.04	0.67	0.68	0.70	0.86	0.80	0.82
Ilmenite-3	0.01	0.01	0.01	0.01	0.89	0.87	0.86	0.85	0.94	0.90
Ilmenite-4	0.01	0.01	0.01	0.01	0.41	0.39	0.40	0.45	1.30	1.22
Rutile-1	0.23	0.22	0.22	0.23	0.31	0.37	0.30	0.35	1.60.	1.46
Rutile-2	0.21	0.22	0.22	0.23	0.46	0.48	0.48	0.45	0.79	0.70

A, ICP-OES; B, AAS; C, spectrophotometry: (1) vanadium by BPHA method, (2) Ti by hydrogen peroxide and (3) silica by molybdenum blue method after fusion with sodium hydroxide and aqueous extract was analyzed for silica content.

accuracy of the method. The results are compared in Table 4. The results are in excellent agreement.

On the basis of above observation the natural samples of ilmenite (4 nos.) and rutile (2 nos.) are analyzed several times ($n = 5$) to check the precision of the method. The results obtained by the proposed method are compared against the potassium bisulphate fusion in Table 5. In absence of reference materials, the results are checked further by the method of standard addition in above samples. The recovery found was in the range 98–102%.
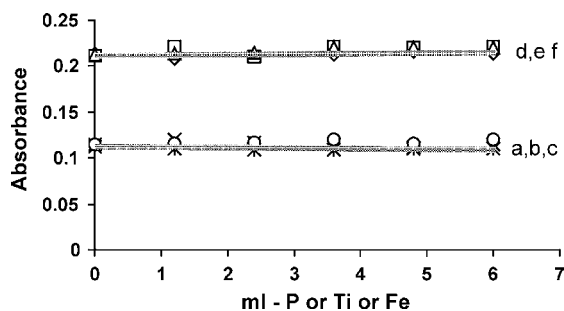
Fig. 7. Effect of P, Fe and Ti, in N_2O–C_2H_2 flame (a–c) show the effect of P, Ti and Fe, respectively, on Ca, and (d–f) shows the effect of P, Ti and Fe, respectively, on Al.

The R.S.D. of proposed method in case of ICP-OES varies from element to element in the range of 0.5–2% whereas for AAS it lies in the range 1.5–3% for different element ($n = 5$).

4. Conclusion

The proposed method for the decomposition and dissolution of titanium mineral is a new approach using sodium salts of ortho-phosphoric acid. The proposed method has following distinct advantages over the existing potassium bi sulphate decomposition procedures.

(1) There is no evolution of hazardous fume during decomposition.
(2) Both rutile and ilmenite can be decomposed with same flux.
(3) The melt is dissolved in water, which eliminates the use of harmful acids.
(4) The solution is very stable. The sample:flux ratio is lower in comparison to potassium bisulphate fusion.
(5) Further clogging of burner in AAS and, nebulizing efficiency in ICP-OES with Na salt is less in comparison of K salt.

(6) Addition of ionization suppressor is not required in AAS while using nitrous oxide–acetylene flame.

The method is simple, rapid, eco-friendly and being applied for the routine analysis of titanium mineral in the laboratory. The simple instrument like AAS can also be used for the determination of most of the desired elements such as Fe, Ti, Mn, Ca, Cr, Mg and Al. The R.S.D. in case of ICP-OES varies from element to element in the range 0.5–2% whereas for AAS it varies in the range 1.5–3% for different element ($n = 5$).

Acknowledgements

References

[1] K.K. Dwivedy, Keynote address International Workshop on Geology and Exploration of Platinum Group, Rare Metal and Rare Earth Elements, Calcutta, India, February 6, 1996.
[2] M.S. Nagar, Indian Mining Annu. Rev. (1995) 376.
[3] D.S. Rao, Miner. Met. Rev. (July (19)) (1990).
[4] Chris Riddle, Analysis of Geological Materials, Marcel Dekker Inc., New York, 1993, pp. 137–154.
[5] B. Lister, Geostandards Newslett. 2 (1978) 157–186.
[6] B. Lister, Geostandards Newslett. 10 (1986) 177–181.
[7] B. Jailson, De. Andrade, ICP Inf. Newslett. 21 (1995) 172.
[8] D.S. RMurthy, B. Gomathy, R. Bose, R. Rangaswami, Atom. Spectrosc. 19 (1) (1998) 14–17.
[9] J.A. Maxwell, Rock and Mineral Analysis, Interscience publishers, New York, 1968, p. 95, pp. 174–177.
[10] C.O. Ingamells, Talanta 2 (1959) 171–175.
[11] I.L. Marr, A Hand book of Decomposition Methods in Analytical Chemistry, International Textbook Co., Glasgow, UK, 1979, p. 80.
[12] W.R. Schoeller, A.R. Powell, The Analysis of Minerals and Ores of the Rarer Elements, Charles Griffin and Co., 42 Drury Lane, WC, London, 1955, pp. 119–131.
[13] W.F. Hillebrand, G.E.F. Lundell, Applied Inorganic Analysis, Interscience, New York, 1955, pp. 576–580.
[14] N. Howell Furman, Standard Methods of Chemical Analysis, D. Van Nostrand Company Ltd., Canada, 1963, 1096–1097.
[15] P.J. Potts, A Hand book of Silicate Rock Analysis, Blackie, New York, 1987, p. 53.
[16] F. Albert Cotton, G. Wilkinson, Advanced Inorganic Chemistry, A Comprehensive Text, Interscience, New York, 1967, pp. 512–515.

Gas chromatography mass spectrometry determination of acaricides from honey after a new fast ultrasonic-based solid phase micro-extraction sample treatment

R. Rial-Otero [*], E.M. Gaspar, I. Moura, J.L. Capelo

REQUIMTE, Departamento de Química, Faculdade de Ciências e Tecnología, Universidade Nova de Lisboa,
2829-516 Monte de Caparica, Portugal

Abstract

A method is reported for the determination of acaricides (amitraz, bromopropylate, coumaphos and fluvalinate) from honey by gas chromatography mass spectrometry after a new fast solid phase micro-extraction, SPME, procedure. Six different fibers were assessed for micro-extraction purpose studying the following variables: (i) SPME coating, (ii) extraction temperature, (iii) extraction time, (iv) desorption conditions and (v) agitation conditions. The new ultrasonic bath technology providing different sonication frequencies (35 and 130 kHz) and different working modes (Sweep, Standard and Degas) was studied and optimized for speeding up the acaricide micro-extraction. The best extraction results were achieved with the polyacrylate fiber. The extraction process was done in 30 min using the ultrasonic bath at 130 kHz in the Standard mode. Quality parameters of the proposed method show a good precision (<11%) and detection and quantitation limits lower than 6 and 15 ng/g, respectively, except for fluvalinate. Eleven Portuguese commercial honey samples were analyzed with the developed method in order to assess the performance of the method with real samples and to determine whether the concentration of acaricides in honey exceed their maximum residue levels (MRLs). Acaricide residues detected were lower than those established by the legislation.
© 2006 Elsevier B.V. All rights reserved.

Keywords: Acaricides; Honey samples; SPME; GC–MS

1. Introduction

The use of chemicals to combat honeybee's diseases or parasite infestations is a common practice among beekeepers that has led to contamination of honey and other hive products, ultimately affecting human health [1–3]. Amitraz, bromopropylate, coumaphos, cymiazole and fluvalinate are the most common acaricides used by the beekeepers to combat the parasitic mites *Varroa jacobsoni* and *Ascophera apis* [2,3]. In addition to the environmental concern, the presence of the aforementioned substances in honey decreases its quality. This situation has forced to the European Union, EU, and also to other countries to establish different regulations limiting maximum residual levels (MRLs) of acaricides in honey. For instance, the Council Regulation 2377/90/EEC of EU and their subsequent modifications

has established MRLs in honey for amitraz and coumaphos at 0.2 and 0.1 mg kg^{-1}, respectively [4]. Furthermore, the United States Environmental Protection Agency (USEPA) has established MRLs for amitraz, coumaphos and fluvalinate as follows: 1, 0.1 and 0.05 mg kg^{-1}, respectively [5]. No MRLs for bromopropylate in honey have been established for the USEPA or the EU regulations but some countries such as Germany and Switzerland have established their own MRLs for this compound at levels of 1 mg kg^{-1}. More restrictive limits for bromopropylate in honey have been fixed by the Italian legislation (0.01 mg kg^{-1}) [1].

To control pesticide residue levels in honey and their compliance with quality standards fixed by the UE and/or national regulations, rapid, robust and economic control methods must be developed. To date, analytical methods for the determination of acaricide residues in honey include commonly gas chromatography (GC) [2,6–16] or high-performance liquid chromatography (HPLC) [17–21] with selective detectors. Mass spectrometry detector (MS) is the universal and non-specific

---

* Corresponding author. Tel.: +351 21 294 9649; fax: +351 21 294 8550.
  E-mail address: raquelrial@dq.fct.unl.pt (R. Rial-Otero).

detector which allows not only to detect and to quantify the analytes present in the sample, but also to identify these compounds on basis on their structure. Because of this advances, it is every time more frequently used for pesticide determination [11,12,14,16].

Sample handling for acaricide extraction includes the following steps:

 (i) Honey dilution in water [2,7,9,12], methanol [8,13] or water mixtures such as ethanol/water [6,15] or methanol/water [11,14,21] in order to obtain a better sample homogenization.
(ii) After honey dilution, acaricides extraction is normally done by:
   (1) Solvent extraction, SE [7,9-11,18] with different extracting solvents or solvent mixtures such as dichloromethane [10,18], ethyl acetate [11], hexane/acetone [9], hexane/glacial acetic acid [7] or hexane/2-propanol [18].
   (2) Solid phase extraction, SPE [2,6,8,12–15,17,20,21], being the reversed phase C_{18} cartridge the most common choice for the extraction of acaricides from honey [2,12,14,15,17,21], although others sorbent phases such as C_8 [6], Florisil [8,13] and SCX-SPE [20] have been used with good results.

The solid phase micro-extraction technique, SPME, developed by Pawliszyn and co-workers [22,23] has become popular for the analysis of organic compounds. This technique presents several advantages over the above mentioned SE and SPE techniques such as:

  (i) total elimination of solvents;
 (ii) reduced blanks;
(iii) lower extraction times;
(iv) it does not require complete removal of the analyte from the liquid matrix.

In spite of the aforementioned advantages, to the best of our knowledge only Volante et al. [16] have purposed the use of the SPME with a 100 μm-polydimethylsiloxane fiber, PDMS-100, for acaricide extraction from honeys.

The use of sonication in the SPME procedure was reported by different authors with the following aims: (i) to increase the pass of volatile aromatic compounds to the headspace and reduce the extraction time required for SPME in the headspace [24–26], or (ii) to facilitate the desorption of the compounds adsorbed in the fiber into a solvent [27].

The aim of this work is to develop a rapid, robust and economic method for simultaneous determination of four acaricides (amitraz, bromopropylate, coumaphos and fluvalinate) in honey samples based on the SPME methodology plus GC–MS. Several commercially available coatings for SPME are tested and compared with the PDMS-100 fiber in terms of extraction efficiency. In addition, in the present work we report, to the best of our knowledge for first time, experimental data showing the importance of the new ultrasonic bath devices provided with

dual frequency of sonication, 35 and 130 kHz, and three different working modes, Sweep, Standard and Degas. Finally, the new methodology is applied to Portuguese commercial honey samples in order to assess the presence of acaricide residues and study their compliance with the legislation.

2. Experimental

2.1. Chemicals, solvents and disposables

Pestanal® grade standards of amitraz [CAS No. 33089-61-1], bromopropylate [18181-80-1], coumaphos [56-72-4] and tau-fluvalinate [102851-06-9] were purchased from Riedel-de-Haën (Seelze, Germany). Lindane [58-89-9] used as an internal standard was purchased from Aldrich (Steinheim, Germany). Purity was >93% for all of them. The individual stock solutions (ca. 500 mg/l) of each acaricide were prepared in acetone by weighing approximately 0.0125 g of the analyte into a 25 ml volumetric flask and diluting to volume. An intermediary mixed standard solution was prepared by dilution in acetone of the individual stock standard solutions to give a concentration of 1 mg/l of each acaricide. Stock standard solution of the internal standard (lindane) was prepared in the same way and working standard solution was prepared by dilution in acetone of the stock standard solution to give a final concentration of 5 mg/l. Stock and intermediary standard solutions were stored in the dark at −20 and −4 °C, respectively. Acetone Pestanal® grade was purchased from Fluka (Buchs, Switzerland); ultrapure water was obtained from an Milli-Q SP reagent water system (Millipore, Bedford, USA).

In the SPME procedure study six SPME fibers were considered: 7 μm polydimethylsiloxane (PDMS-7); 100 μm polydimethylsiloxane (PDMS-100); 85 μm polyacrilate (PA); 65 μm polydimethylsiloxane–divinylbenzene (PDMS/DVB); 65 μm carboxen–polydimethylsiloxane (CAR/PDMS); and 50/30 μm stable flex divinylbenzene–carboxen–polydimethylsiloxane (DVB/CAR/PDMS). The commercially available SPME device and fibers were purchased from Supelco (Bellefonte, PA, USA). Fibers were initially conditioned according to the manufacturer's instructions in order to remove contaminants and to stabilize the polymeric phase. For the SPME procedure, honey samples were placed in 40-ml EPA amber vials (Wheaton, USA) equipped with PTFE-coated magnetic bars and sealed with PTFE-faced silicone septum. Sample homogenization was done by stirring with a magnetic stirrer from Heidolph (Kelheim, Germany) or in an ultrasonic bath model transonic TL-H-5 from Elma (Singen, Germany).

2.2. Honey samples

Uncontaminated honey samples used for developing and characterizing the proposed method were purchased at local markets in Lisbon, Portugal. Spiked honey samples were prepared as follows: 40 g of honey was heated at 30 °C for a few minutes and then 2 ml of the mixed standard solution (1 mg/l of each acaricide, in acetone) were added. The sample was vigorously shaken and acetone was evaporated. Finally, aliquots of

spiked honey samples (3 g) were placed in a 40-ml EPA amber vials and samples was stored at $-20\,^{\circ}\text{C}$ for a maximum of 4 days, in order to avoid acaricide degradation processes [18].
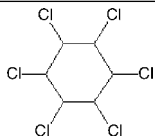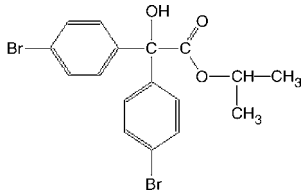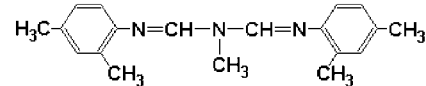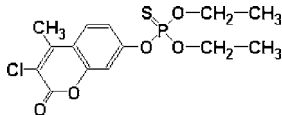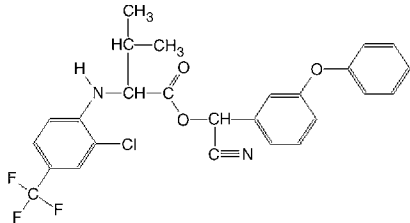
2.3. SPME extraction procedures

Honey samples (3 g) were placed into 40-ml EPA amber glass vials equipped with PTFE-coated magnetic bars. The samples were diluted with ultrapure water (30 ml) and capped with a PTFE-faced silicone septum. To each sample lindane was added as an internal standard (10 µl of the working standard solution of 5 mg/l) to correct the variability of the MS. The holder needle was inserted through the septum and the fiber was directly immersed into the sample. Solution was extracted for 30 min in an ultrasonic bath at 130 kHz in the Standard mode. After extraction, the fiber was withdrawn into the holder needle, removed from the vial and immediately introduced into the GC injector port for 3 min at $270\,^{\circ}\text{C}$ for thermal desorption of the analytes. Between sample and sample extraction the fiber was washed with water for 10 min and then it was conditioned in an extra injection port (split open) with hydrogen carrier gas for 10 min in order to avoid carryover processes.

2.4. GC–MS instrumentation and operating conditions

Analyses were carried out on a ThermoQuest (Rodano, Italy) TraceGC gas chromatograph equipped with a mass-selective detector Trace MS and linked to a computer running the Xcalibur™ Version 1.2 software program (Finnigan Corp., Italy). Chromatographic separations were performed using a BPX5 (30 m × 0.25 mm i.d., 0.25 µm film thickness) fused-silica capillary column from SGE (Darmstadt, Germany). The oven temperature was programmed as follows: $60\,^{\circ}\text{C}$ for 1 min ramped at $25\,^{\circ}\text{C/min}$ to $200\,^{\circ}\text{C}$ and held for 1 min, and ramped again at $8\,^{\circ}\text{C/min}$ to $310\,^{\circ}\text{C}$ and held for 10 min. A split/splitless injector was used in the splitless mode (3 min) with the split/column ratio equal to 50 ml/min. The carrier gas was helium with a constant flow of 1 ml/min. Injector temperature was $270\,^{\circ}\text{C}$, and source and transfer line temperatures were 200 and $275\,^{\circ}\text{C}$, respectively. MS detection was performed in single-ion monitoring mode (SIM) after a solvent delay time of 8 min; the ion energy used for the electron impact (EI) was 70 eV. The compounds that were analyzed by GC–MS and the selected mass/charge fragments (m/z) used for their quantification are listed in Table 1. Confirmation of the identity of acaricides in

Table 1
Retention time and quantification fragments of the acaricides analyzed by GC–MS

Acaricides	Structure	Retention time (min)	Quantification fragments (m/z) and relative intensities (%)
Lindane		9.74	181 (100), 183 (99.5), 219 (55.0)
Bromopropylate		16.66	185 (100), 183 (97.4), 341 (93.5)
Amitraz		17.71	162 (100), 132 (79.6), 293 (33.7)
Coumaphos		19.01	226 (100), 109 (97.6), 362 (96.0), 210 (77.5)
Fluvalinate		20.94	250 (100), 181 (34.0), 252 (30.0)
		21.02	250 (100), 181 (33.8), 252 (29.6)

honey samples was performed by direct comparison between the full mass spectral scans of the reference sample and the standard recorded within the same analytic conditions.

3. Results and discussion

3.1. SPME optimization

In order to develop the SPME described method for the extraction of acaricides from the honey matrix, the following variables were identified and studied:

(i) SPME coating;
(ii) effect of extraction temperature;
(iii) extraction time;
(iv) desorption conditions;
(v) agitation conditions.

Direct SPME was selected rather than headspace SPME due to the: (a) polarity of the studied analytes and (b) their affinity for the honey–water mixture, that is, due to their low volatility.

3.1.1. Fiber performance

As far as selection of the SPME fiber concerns, the nature of the analyte influences the SPME fiber selection. In this study, six SPME fiber sorbents were tested in order to obtain the best extraction efficiency of acaricides from honey. Fortified honey samples (3 g), spiked at levels of ca. 50 ng/g for each compound, were diluted with 30 ml of water and 10 µl of the internal standard solution (5 mg/l) was added. A volume of 30 ml of water (dilution ratio 1/10) was selected according to the protocol described by Volante et al. [16]. Samples were extracted at room temperature, 22 °C, for 50 min at a stirring speed of 750 rpm. Then, the analytes were thermally desorbed in the GC injector port at 250 °C for 3 min (splitless mode) for all fibers (*n* = 3). The results, expressed in areas, obtained for each fungicide with the different fibers and their standard deviations are shown in Fig. 1.
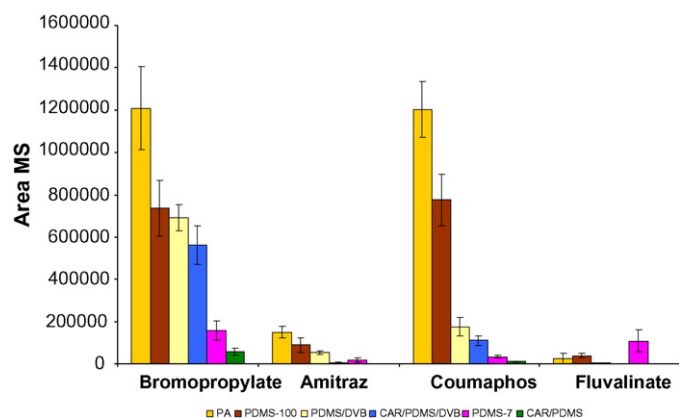
Fig. 1. Extraction efficiencies and standard deviations (±S.D.) of commercial SPME fiber coatings for sampling acaricides (*n* = 3). Spiked honey samples (50 ng/g for each compound) were extracted with different fibers for 50 min at room temperature under magnetic stirring (750 rpm) and then the analytes were desorbed into the GC injector port at 250 °C for 3 min.

Although, to the best of our knowledge, the PDMS-100 is the unique fiber recommended in the bibliography for the extraction of acaricides from honey [16], the results here reported show that other fibers can be used, being the recoveries obtained higher. As can be seen in Fig. 1, the best fiber for the extraction of amitraz, bromopropylate and coumaphos is the PA fiber. For the same experimental conditions, area increments between 55 and 68% are obtained when the PA fiber is compared with the PDMS-100 fiber. However, it must be remarked that in the case of fluvalinate the best results are obtained with the PDMS sorbents, namely PDMS-100 and PDMS-7. This finding can be explained taking into account the polarity of fluvalinate. Amitraz, bromopropylate and coumaphos are polar compounds for which polar fibers such as PA fiber enhances recoveries. On the contrary, the apolar phase of PDMS is more suitable for apolar compounds such as fluvalinate [28]. It must be pointed out that PDMS-7 showed ca. twice the recovery for fluvalinate than PDMS-100, this result was expected since PDMS-7 presents better extraction efficiency for high molecular weight compounds [29]. On basis of the previous results the PA fiber was chosen for method optimization.

3.1.2. Selection of the extraction temperature

The extraction temperature has two different effects on the SPME technique. On the one hand, increasing the temperature enhances the diffusion coefficient of analytes; on the other hand, as adsorption is an exothermic process, increasing temperature reduces the distribution constant of the analyte, limiting the extraction capability of the fiber [30]. To study the effect of temperature on analyte recovery, the acaricides spiked up to 50 ng/g in honey samples, were extracted with the PA fiber as follows: (i) at room temperature and (ii) using a water bath at 40 °C. Forty degree celsius was chosen because higher temperatures could decompose the acaricides. Results showed that, with the exception of amitraz, recoveries for all pesticides were virtually the same regardless the temperature studied. In the case of amitraz, the recovery was lowered ca. 75% when the extraction temperature was increased up to 40 °C. This finding can be linked to amitraz degradation caused by heating it in an acid medium. For next experiences, room temperature was chosen as optimum.

3.1.3. Selection of the extraction time

The sorption time profile for the PA fiber was obtained by plotting the detector response versus the extraction time for each acaricide in order to obtain the partition equilibrium curve (Fig. 2). Honey samples spiked at 50 ng/g were used. Sorption time profiles for bromopropylate and coumaphos indicated that a sampling time higher than 90 min is necessary to reach the equilibrium, while amitraz and fluvalinate reach the equilibrium at 60 and 30 min, respectively. However, when the equilibrium is not reached in a time as long as 90 min, an alternative is to develop the extraction in non-equilibrium conditions, which needs shorter extraction times. Ai [31,32] proposed a dynamic model of SPME adsorption, in which the amount of analyte adsorbed from the sample onto the fiber is proportional to the initial analyte concentration in the sample matrix, if the agitation and the sampling time are held constants among samples. Therefore, according to Ai, SPME quantitation is feasible at non-
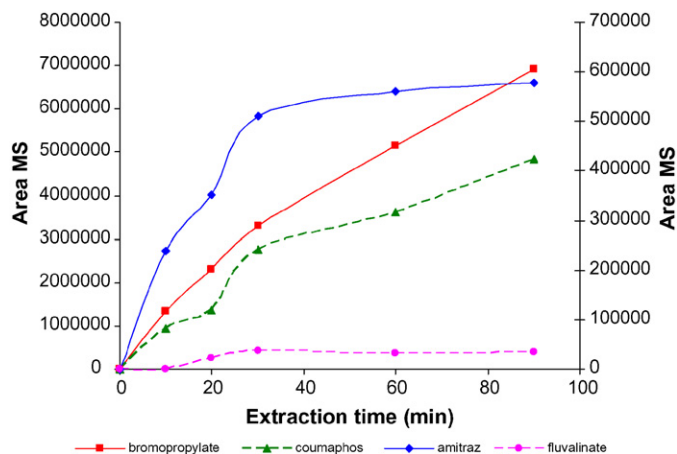
Fig. 2. Extraction time profiles of target acaricides from honey with the PA fiber ($n = 3$). In the figure bromopropylate and coumaphos areas are represented in the left axis and amitraz and fluvalinate areas are represented in the right axis. Spiked honey samples (50 ng/g for each compound) were extracted with the PA fiber for increasing times at room temperature under magnetic stirring (750 rpm) and then the analytes were desorbed into the GC injector port at 250 °C for 3 min.
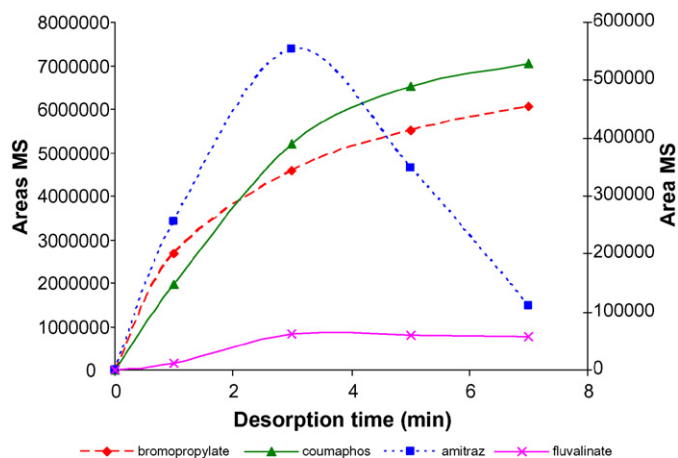
Fig. 3. Desorption time profiles of target acaricides ($n = 3$). In the figure bromopropylate and coumaphos areas are represented in the left axis and amitraz and fluvalinate areas are represented in the right axis. Spiked honey samples (50 ng/g for each compound) were extracted with the PA fiber for 40 min at room temperature under magnetic stirring (750 rpm) and then the analytes were desorbed into the GC injector port at 270 °C for increasing times.

equilibrium conditions. Hence, a time of 40 min was chosen as a compromise, since fluvalinate gives the highest signal at this extraction time, amitraz more than 90% of the signal obtained with 90 min, coumaphos gives ca. 60% of the maximum signal and bromopropylate ca. 50%.

3.1.4. Selection of the desorption parameters

The temperature of the GC injector and desorption time were tested in order to guarantee the complete desorption of the acaricides and to avoid carryover processes. Temperatures ranging between 220 and 290 °C were tested. Higher desorption temperatures can be used to enhance the desorption process but they can also degrade the analytes. As can be seen in Table 2, desorption temperatures lower than 250 °C were not enough for the complete desorption of the analytes. The best recoveries were obtained for bromopropylate, coumaphos and fluvalinate at 290 °C but in the case of amitraz thermal degradation was observed at temperatures higher than 270 °C. For this reason, in the following experiments a desorption temperature of 270 °C was selected as optimum.

Desorption time was investigated in the range of 0–7 min. As can be seen in Fig. 3, this parameter is limited by the compound amitraz, since times higher than 3 min leads to its rapid degradation in the GC injector port. Accordingly a desorption time of 3 min was chosen for further experiences.

3.1.5. Selection of the agitation conditions

Agitation is normally used to achieve faster equilibrium because it enhances the diffusion of analytes toward the fiber. Agitation can be produced by magnetic stirring or by sonication [30]. Comparative studies between magnetic stirring and sonication were realized over spiked honey samples (50 ng/g for each compound). In the case of sonication, low (35 kHz) and high (130 kHz) ultrasonic frequency were tested and also three operation modes (Sweep, Standard and Degas) were evaluated. In the Standard mode, the ultrasonic frequency is regulated against the chemical resonance of the ultrasound transformer which optimizes the performance in the distributed maxima. The Sweep function causes a continued shifting of the sound pressure maxima, which ensures that the sound field distribution is more homogeneous in the bath than during Standard operation. During the Degas function the set power is interrupted for a short period so that the air bubbles are not retained by the ultrasonic forces and the liquid is degassing which optimizes the ultrasonic effect. It must be remarked that ultrasonic baths with dual frequency of ultrasonication are relatively new at the Analytical Laboratory. As a matter of fact, to the best of our knowledge, only Pena-Farfal et al. have reported a study in which the frequency of the ultrasonic bath was found to be critical for the enhancement of enzymatic extraction of metals from mussel tissue [33]. In addition, the possibilities given by the three modes in which the ultrasonic bath can be used, Sweep, Standard and

Table 2
Effect of the desorption temperature in the acaricide extraction by SPME with a PA fiber (area MS/1000 ± S.D.)

Acaricides	220 °C	240 °C	250 °C	270 °C	290 °C
Bromopropylate	1525 ± 6	3915 ± 4	3899 ± 10	4588 ± 11	5547 ± 6
Amitraz	289 ± 10	635 ± 11	495 ± 4	545 ± 16	218 ± 3
Coumaphos	459 ± 12	2721 ± 3	3232 ± 14	4983 ± 12	5719 ± 8
Fluvalinate	–	–	28 ± 3	63 ± 2	75 ± 10

Spiked honey samples (50 ng/g for each compound) were extracted with the PA fiber for 40 min at room temperature under magnetic stirring (750 rpm) and then the analytes were desorbed into the GC injector port for 3 min ($n = 3$).
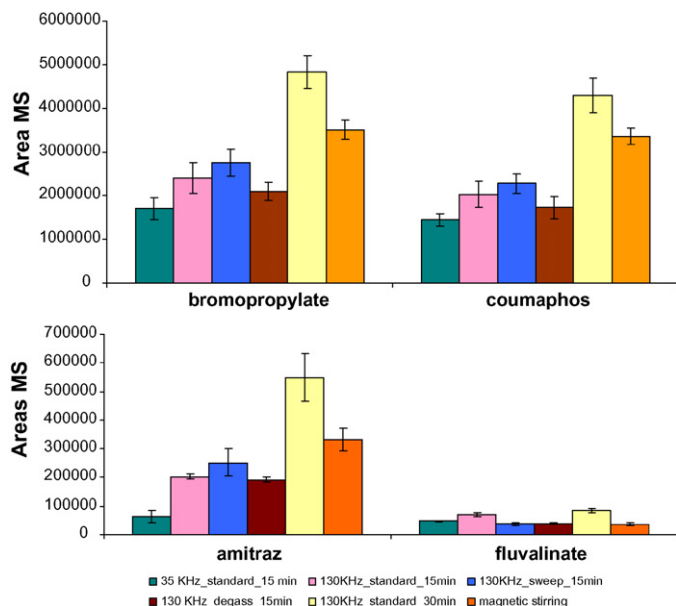
Fig. 4. Effect of ultrasounds on the extraction of acaricides from honey (area MS ± S.D.). Spiked honey samples (50 ng/g for each compound) were extracted with the PA fiber for 15 or 30 min at room temperature under magnetic stirring or in a ultrasonic bath and then the analytes were desorbed into the GC injector port at 270 °C for 3 min.

Degas, are fully exploited in this work for first time in analytical literature. As can be seen in Fig. 4, the use of low ultrasonic frequency, 35 kHz, provide worst results than the utilization of the high frequency, 130 kHz, especially in the case of amitraz. It was stated throughout our experiences that amitraz was the most unstable compound in our conditions. Therefore, it can be easily concluded that the cavitation effects produced by the ultrasonic bath at 35 kHz were enough to decompose amitraz in the acidic media. Thus, the recovery obtained for amitraz was significantly different (t-test, $P = 0.05$, $n = 3$), when the 130 kHz is compared with 35 kHz, both in the Standard operation mode and with 15 min of ultrasonic application. It must be pointed out that the cavitation effects are directly linked to the sonication frequency. The lower the frequency the higher the cavitation effects for the same amplitude [34]. It must be also stressed that for the same extraction time, 15 min, the recoveries obtained at 130 kHz for bromopropylate, and coumaphos were higher than using the 35 kHz frequency. Moreover, the Sweep mode was the best way to use the ultrasonic bath for those compounds. However, for fluvalinate the best mode was the standard one, with which twice more was recovered than with the other modes. For this reason, the Standard mode was selected for further experiences, since in this mode all the compounds showed good recoveries. Finally, the sonication time was studied also for 30 min, showing an increase of 100%, for all compounds except fluvalinate, for which the maximum recovery is achieved in 15 min. In addition, when extraction with sonication was compared with extraction with magnetic stirring, the recoveries obtained for sonication were higher and statistical differences were observed (t-test, $P = 0.05$, $n = 3$). For this reason, extraction with sonication for 30 min was selected as the optimum agitation condition for further experiments.

Table 3
Optimum conditions for the SPME procedure for the extraction of target acaricides from honey samples

SPME fiber	Polyacrilate (85 μm)
Extraction temperature	Room temperature
Agitation conditions	Sonication in a ultrasonic bath (130 kHz frequency, 100% amplitude, Standard mode)
Extraction time	30 min
Desorption conditions	3 min (splitless mode), 270 °C

3.2. Method performance

With the optimum conditions for the SPME procedure shown in Table 3, quality parameters of the SPME/GC–MS method such as precision, limits of detection (LODs) and quantitation (LOQs) were calculated.

The repeatability of the SPME/GC–MSD method was assessed by analyzing five spiked honey samples on the same day ($n = 5$). All samples were spiked at a concentration of 50 ng/g for each acaricide. Results are reported in Table 4. The relative standard deviation (R.S.D.%) was about 7% for all compounds except for amitraz (11%). These values allow to confirm the good precision of the proposed method.

Limits of detection and quantitation were evaluated on the basis of the signal obtained with the analysis of unfortified honey samples ($n = 7$), following the recommendations of the ACS [35]. As tested experimentally detection and quantitation limits were lower than 6 and 15 ng/g, respectively, except for fluvalinate (Table 4). LOQs obtained for amitraz and coumaphos are 10 times lower than the MRLs established by the EU Council Regulation 2377/90/EEC and their subsequent modifications. Furthermore, LOQ for bromopropylate are 200 times lower than MRLs established by the Germany and Switzerland legislation and 2 times lower than those fixed by the Italy legislation. Also, it must be taken into account that LOQ obtained for fluvalinate with the polyacrilate fiber (39 ng/g) is lower than the MRLs of the EU regulation, in spite of the fact that PA fiber is not the best option for fluvalinate extraction from honey as was explained above.

Matrix effect was also studied. For this, three honey samples (honey a, used during method performance; honey b and honey c) free of the considered acaricide traces, as found by previous analysis, were spiked at levels of 40 ng/g for each compound and analyzed by duplicate with the PA fiber under the experimental

Table 4
Recoveries, repeatabilities, limits of detection (LODs) and limits of quantitation (LOQs) of the optimized method

Acaricides	Relative recovery ± repeatability[a] (% ± R.S.D.)	LOD[b] (ng/g)	LOQ[b] (ng/g)
Bromopropylate	100 ± 7	2	4
Amitraz	100 ± 11	6	15
Coumaphos	100 ± 7	3	7
Fluvalinate	100 ± 8	18	39

[a] ($n = 5$) mean of determinations.
[b] ($n = 7$).
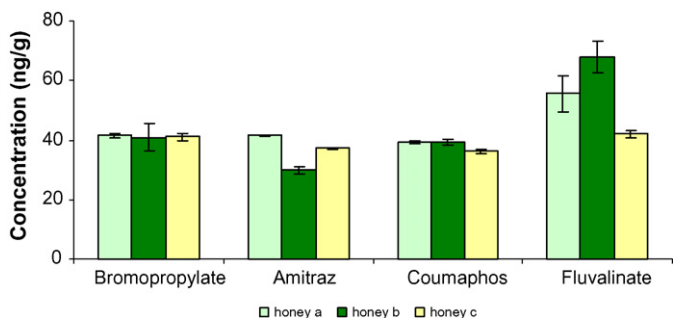
Fig. 5. Measured concentrations and standard deviations of target acaricides in spiked honey samples (40 ng/g of each acaricide). Samples were extracted by duplicate with the PA fiber for 30 min at room temperature in an ultrasonic bath (130 kHz, standard mode) and then the analytes were desorbed into the GC injector port at 270 °C for 3 min.

conditions summarized in Table 3. As can be seen in Fig. 5, significant differences were found between concentrations obtained in honey b and honey c samples respect to concentrations determined in honey a for amitraz and fluvalinate. These differences can be attributed to matrix effects and were also detected by other authors as was reviewed recently [1]. The honey matrix can affect the extraction efficiency for pesticides but can also affect the detector by increasing or decreasing its response [1]. Bromopropylate and coumaphos were less affected by matrix effects. As a conclusion, the standard addition method was used in the quantitation process in order to solve this problem. That is, the calibration curve was done using the honey previously fortified with the target acaricides. Hence, the real sample and standard-spiked real samples are processed in the same way and, in this case, the influence of the honey matrix is the same in samples and standards. Therefore, the relative recovery is about 100% (Table 4).

When the values obtained for the quality parameters were compared with the data reported in previously published papers it was observed that the detection and quantification limits obtained were comparable to those obtained for Volante et al. [16] using the fiber PDMS-100. In addition, were also similar to those obtained by the conventional SE and SPE procedures

[2,10,12]. The most important disadvantage and limitation of the SPME method proposed by Volante et al. for the same analytes were the low recoveries and the high R.S.D.% (<56%) values obtained for some compounds [16]. On the contrary, the method described in this work overcomes this problem because of its good precision (<11%) and relative recovery (ca. 100%). The better precision may be related with the use of sonication during the extraction procedure, since the homogenization of the honey sample solution is better than using stirring conditions.

3.3. Analysis of Portuguese commercial honey samples

Finally, in order to test the applicability of the proposed method, a total of 11 Portuguese commercial honey samples were analyzed. Three honey samples (A–C) were produced in Alentejo (Portugal), two honey samples (D and E) were produced in Serra do Malcata (Portugal), four honey samples (F–I) were dietetic products and two honey samples (J and K) were imported honey samples.

When the developed method was applied to the commercial honey samples, in some cases, one peak was observed in the chromatograms at the same retention time of coumaphos. The presence of this peak can induce a false positive for coumaphos or an error in its quantification by overestimation. It was observed that the main m/z fragment for this peak was 226. Due to, since this moment, the fragment 226 was removed from the quantification fragments list used for coumaphos determination.

Due to the existence of matrix effects the standard addition method was used in the quantitation process in order to avoid this problem. Standard addition method was applied as follows: honey samples were directly analyzed twice and subsequently two standard additions of the target acaricides were performed into the honey samples at levels of 10 and 20 ng/ml for further analysis. The four-point calibration equation was calculated in order to estimate the acaricide concentration in honey as well as the corresponding error according to Miller and Miller [36].

The results obtained for the Portuguese commercial honey samples analyzed are summarized in Table 5. Residues of

Table 5
Analysis of acaricides in 11 Portuguese commercial honey samples with the proposed method

	Honey sample	Bromopropylate	Amitraz	Coumaphos	Fluvalinate
Alentejo	A	–	–	–	
	B	<LOQ	–	–	–
	C	–	–	<LOQ	–
Serra do Malcata	D	<LOQ	–	–	–
	E	–	–	–	–
Dietetic products	F	–	–	–	–
	G	–	–	–	–
	H	–	–	–	–
	I	<LOQ	–	–	–
Imported samples	J	–	–	15 ng/g	–
	K	–	–	–	–

(–) Not detected.
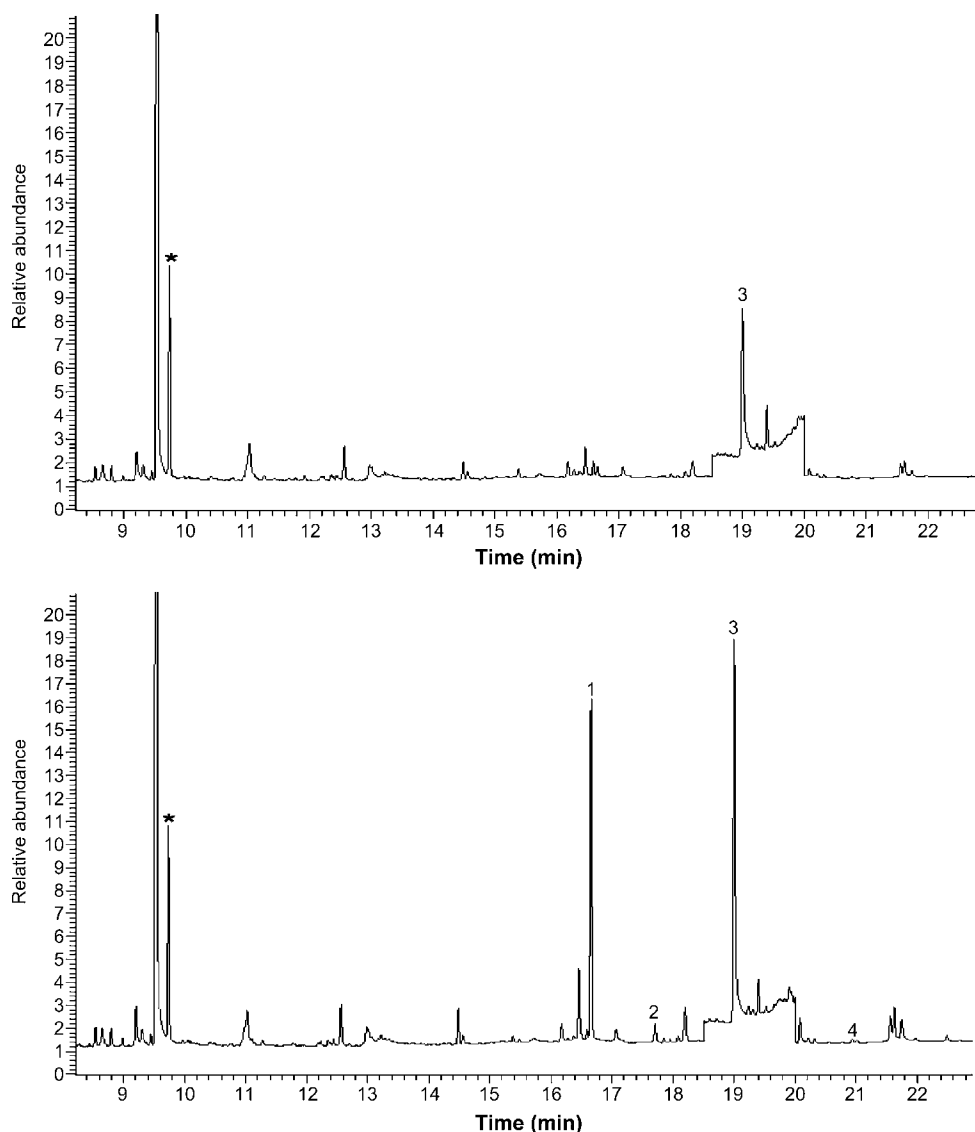
Fig. 6. SPME/GC–MS chromatograms registered in SIM mode for the direct analysis of the Portuguese commercial honey samples J (up) and for the Portuguese commercial honey sample J spiked at 20 ng/g (down) at the optimized and validated conditions. Peaks: (*) internal standard, lindane, (1) bromopropylate, (2) amitraz, (3) coumaphos and (4) fluvalinate.

coumaphos at levels lower than 15 ng/g were detected in 2 of the 11 honey samples which represent values more than 10 times lower than the MRL fixed by the European Council Regulation for this compound. In addition, bromopropylate residues were also detected in three honey samples at levels lower than the quantification limit (4 ng/g). It must be remarked that amitraz and fluvalinate residues were not present in none of the samples analyzed. The chromatograms obtained from the direct analysis and the standard addition of 20 ng/g for the Portuguese commercial honey sample J are shown in Fig. 6. These values permit to confirm the good quality of the Portuguese honeys in terms of acaricides presence and their compliance with the MRLs fixed by the legislation. Bromopropylate and coumaphos residues at levels of 5–60 and 110–260 ng/g, respectively, were also found by other authors in honey samples analyzed in Spain and France in 1997 and 2002 [2,18].

4. Conclusions

The developed method based on the solid phase microextraction of pesticides from honey followed by gas chromatographic determination is suitable for the determination and quantification of acaricide residues of amitraz, bromopropylate, coumaphos and fluvalinate in honey samples. The PA fiber was found to be the most appropriate to extract all analytes quantitatively. The use of sonication during the SPME extraction increases the recoveries of acaricides from honey when compared with extraction with magnetic stirring. In addition, the extraction time was reduced ca. 25%. Non-equilibrium conditions were adopted in order to reduce the total extraction time. Matrix effects can be avoided with the use of the standard addition method for quantification. This method permits the simultaneous detection of some of the most common aca-

ricides used to combat the parasitic mites *V. jacobsoni* and *A. apis* with high sensitivity, good precision and accuracy. This point represents an important advance over the SPME method previously published for acaricides extraction from honey samples, because the developed method is suitable for screening purposes but also can be used as a quantification method.

No important residues of acaricides were found when 11 Portuguese commercial honey samples were analyzed. In some honey samples, an interfering compound with mass 226 was observed at the same retention time of coumaphos. In order to avoid false positives for coumaphos the mass 226 was removed from the list of quantification fragments for coumaphos in the instrumental method.

Acknowledgements

References

[1] R. Rial-Otero, E.M. Gaspar, I. Moura, J.L. Capelo, Talanta 71 (2007) 503–514.
[2] M.A. Fernandez, M.T. Sancho, J. Simal, J.M. Creus, J.F. Huidobro, J. Simal, J. Food Prot. 60 (1997) 78.
[3] M. Fernández, Y. Picó, J. Mañes, J. Food Prot. 65 (2002) 1502.
[4] Council Regulation No. 2377/90/EEC of 26 June 1990 (OJ L 224 18.08.1990, p. 1) laying down a community procedure for the establishment of maximum residue limits of veterinary medicinal products in foodstuffs of animal origin.
[5] Food and Drug Administration of the United States, Pesticides Tolerances (http://www.cfsan.fda.gov).
[6] A.D. Tsigouri, U. Menkissoglu-Spiroudi, A. Thrasyvoulou, Pest Manag. Sci. 57 (2001) 467.
[7] S.M. Waliszewski, V.T. Pardio, K.N. Waliszewski, A. Ochoa, R.Mª. Infanzon, J. Sci. Food Agric. 77 (1998) 149.
[8] J.L. Bernal, J.J. Jiménez, Mª.J. del Nozal, M. Higes, J. Llorente, J. Chromatogr. A 882 (2000) 239.
[9] J.J. Jimenez, J.L. Bernal, J. Atienza, Chromatographia 42 (1996) 130.
[10] U. Menkissoglu, G.C. Diamantidis, V.E. Georgiou, A.T. Thrasyvoulou, J. AOAC Int. 83 (2000) 178.
[11] M.V. Russo, B. Neri, Chromatographia 55 (2002) 607.
[12] M.A. Fernández, J. Simal, Analyst 118 (1993) 1519.
[13] J.J. Jiménez, J.L. Bernal, Mª.J. del Nozal, L. Toribio, M.T. Martín, J. Chromatogr. A 823 (1998) 381.
[14] B. Albero, C. Sanchez-Brunete, J.L. Tadeo, J. Agric. Food Chem. 52 (2004) 5828.
[15] S. Bogdanov, V. Kilchenmann, A. Imdorf, J. Apicult. Res. 37 (1998) 57.
[16] M. Volante, R. Galarini, V. Miano, M. Cattaneo, I. Pecorelli, M. Bianchi, M.T. Marinoni, L. Cossignani, P. Damiani, Chromatographia 54 (2001) 241.
[17] E. Korta, A. Bakkali, L.A. Berrueta, B. Gallo, F. Vicente, J. Chromatogr. A 930 (2001) 21.
[18] A.C. Martel, S. Zeggane, J. Chromatogr. A 954 (2002) 173.
[19] J. Atienza, J.J. Jiménez, J.L. Bernal, M.T. Martín, J. Chromatogr. A 655 (1993) 95.
[20] D. Blanco Gomis, A. Castaño Fernández, V. Megido Bernardo, M.D. Gutiérrez álvarez, Chromatographia 39 (1994) 602.
[21] D.B. Gomis, J.J. Mangas, A. Castaño, Mª.D. Gutiérrez, Anal. Chem. 68 (1996) 3867.
[22] D. Louch, S. Motland, J. Pawliszyn, Anal. Chem. 64 (1992) 1187.
[23] C.L. Arthur, K. Pratt, J. Motlagh, J. Pawliszyn, J. High Resolut. Chromatogr. 15 (1992) 741.
[24] J.H. Lee, J.H. Kang, D.B. Min, J. Food Sci. 68 (2003) 844.
[25] J.H. Lee, R. Diono, G.Y. Kim, D.B. Min, J. Agric. Food Chem. 51 (2003) 1136.
[26] P. Kusch, G. Knupp, J. Sep. Sci. 25 (2002) 539.
[27] R. Batlle, A. Colmsjo, U. Nilsson, Fresenius J. Anal. Chem. 371 (2001) 514.
[28] R. Rial Otero, C. Yagüe Ruiz, B. Cancho Grande, J. Simal Gándara, J. Chromatogr. A 942 (2002) 41–52.
[29] M.J.M. Wells, Principles of extraction and the extraction of semivolatile organics from liquids, in: J.D. Winefordner, S. Mitra (Eds.), Chemical Analysis: A Series of Monographs on Analytical Chemistry and its Applications, vol.162, John Wiley & Sons Inc., New Jersey, USA, 2003, pp. 37–138.
[30] M.F. Alpendurada, J. Chromatogr. A 889 (2000) 3–14.
[31] J. Ai, Anal. Chem. 69 (1997) 1230.
[32] J. Ai, Anal. Chem. 69 (1997) 3260.
[33] C. Pena-Farfal, A. Moreda-Pineiro, A. Bermejo-Barrera, P. Bermejo-Barrera, H. Pinochet-Cancino, I. de Gregorio-Henríquez, Anal. Chem. 76 (2004) 3541–3547.
[34] J.T. Mason, Sonochemistry, Oxford University Press, Oxford, UK, 1999, p. 11.
[35] American Chemical Society (ACS) Subcommittee on Enviromental Analytical Chemistry, Anal. Chem. 52 (1980) 2242–2249.
[36] J.C. Miller, J.N. Miller, Statistics for Analytical Chemistry, Ellis Horwood Ltd., Chichester, UK, 1988.

Feasibility of using solid sampling graphite furnace atomic absorption spectrometry for speciation analysis of volatile and non-volatile compounds of nickel and vanadium in crude oil

Márcia M. Silva [a,*], Isabel C.F. Damin [a], Maria Goreti R. Vale [a], Bernhard Welz [b]

[a] *Instituto de Química, Universidade Federal do Rio Grande do Sul, Av. Bento Gonçalves 9500, 91501-970 Porto Alegre, RS, Brazil*
[b] *Departamento de Química, Universidade Federal de Santa Catarina, 88040-900 Florianópolis, SC, Brazil*

Abstract

A method for the direct determination of volatile and non-volatile nickel and vanadium compounds in crude oil without previous treatment using direct solid sampling graphite furnace atomic absorption spectrometry is proposed. The crude oil samples were weighed directly onto solid sampling platforms using a microbalance and introduced into a transversely heated solid sampling graphite tube. In previous work of our group losses of volatile nickel and vanadium compounds have been detected, whereas other nickel and vanadium compounds were thermally stable up to 1300 and 1600 °C, respectively. In order to avoid this problem different chemical modifiers (conventional and permanent) have been investigated. With 400 µg of iridium as permanent modifier, the signal started to drop already after two atomization cycles, possibly because of an interaction of nickel (which is a catalyst poison) with iridium. Twenty micrograms of palladium applied in each determination was found to be optimum for both elements. The palladium was deposited on the platform and submitted to a drying step at 150 °C for 75 s. After that the sample was added onto the platform and submitted to the furnace program. The influence of sample mass on the linearity of the response and on potential measurement errors was also investigated using four samples with different nickel content. For the sample with the lowest nickel concentration the relationship between mass and integrated absorbance was found to be non-linear when a high sample mass was introduced. It was suspected that the modifier had not covered the entire platform surface, which resulted in analyte losses. This problem could be avoided by using 40 µL of 0.5 g L^{-1} Pd with 0.05% Triton X-100. Calibration curves were established with and without modifier, with aqueous standards, oil-in-water emulsions and the certified reference material NIST SRM 1634c (trace metals in residual fuel oil). The sensitivity for aqueous standards and emulsions was close to that for SRM 1634c, making possible the use of aqueous standards for calibration. The limits of detection and quantification obtained for nickel and vanadium under this condition were found to be 0.02 and 0.06 µg g^{-1}, respectively, for both elements, based on 10 mg of sample. Nickel and vanadium were determined in the samples with (total Ni and V) and without the use of Pd (thermally stable compounds), and the concentration of volatile compounds was calculated by difference. The results were compared with those obtained by high-resolution continuum source graphite furnace atomic absorption spectrometry by emulsion technique; no significant differences were found for total Ni and V at the 95% confidence level according to a Student's *t*-test.
© 2006 Elsevier B.V. All rights reserved.

Keywords: Nickel and vanadium in crude oil; Solid sampling; Graphite furnace atomic absorption spectrometry; Volatile porphyrin complexes; Chemical modifiers

1. Introduction

Crude oil represents a complex mixture of organic compounds. It also contains a wide variety of trace elements at concentrations varying from mg kg^{-1} to low µg kg^{-1} levels. They may be present in very different chemical forms, such as organic complexes, salts of organic acids or as inorganic compounds. The determination of trace elements in crude oil is difficult due the complex nature of the sample and the several different forms in which the metals can be found. Information on trace metal concentrations in crude oil is getting increasingly important for the geochemical characterization of source rocks and basins and also to allow corrective actions during petroleum production and refining, e.g. prevention of scale formation and catalyst poisoning, corrosion and pollution control [1].

---

* Corresponding author. Tel.: +55 51 3316 6278; fax: +55 51 3316 7304.
E-mail address: mmsilva@iq.ufrgs.br (M.M. Silva).

In the petroleum industry there is increasing interest not only in total trace element content but also in speciation analysis. The stability of many species during extraction or storage has been studied [2]. Nickel and vanadium are among the most important trace elements in crude oil [3–6], but it should be stressed that the separate determination of the volatile fraction of both elements in addition to the total content is very important, as it is certainly this volatile fraction that is preferentially transported through crude oil refining processes, acting as a catalyst poison, and appearing again in intermediate products, such as naphtha or petroleum condensate. The use of chromatographic techniques coupled with spectrometric detection for speciation analysis of trace metals in petroleum products has been reported [7].

In recent reviews about trace metal determination in crude oil [8] and in petroleum products [7], it is pointed out that the main techniques utilized lately for this analysis are graphite furnace atomic absorption spectrometry (GF AAS), flame atomic absorption spectrometry (F AAS), inductively coupled plasma optical emission spectrometry (ICP OES) and inductively coupled plasma mass spectrometry (ICP-MS). The advantage of the spectrometric techniques is that only a minimum pretreatment of the samples is required, avoiding ashing or digestion procedures as those are time consuming and might be affected by analyte losses. The techniques based on nebulization for sample introduction generally require significant dilution in an appropriate organic solvent previous to aspiration of the highly viscous samples. Problems related to the overloading of the plasma with solvent vapors making it unstable by changing its physical characteristics and energy, and, consequently, affecting the overall performance of the technique have been reported [9]. In ICP-MS, the presence of solvent vapor in the plasma causes carbon deposition on the cooler surfaces of the sampler and skimmer cones and on the ion lens, affecting the transport efficiency of ions. In addition, polyatomic interferences caused by carbon–argon species seriously limit the quantification of some elements. In order to minimize these problems, special introduction tools have been applied, such as ultrasonic nebulization [1], flow injection analysis [10], gas chromatography [11] and electrothermal vaporization [12–14]. For F AAS, although the flames used are quite tolerant to most organic solvents, the main problem remains the low and different sensitivity observed for the various organic compounds [15–17]. Graphite furnace AAS appears to be an alternative since the introduction is not really affected by the differing physical characteristics of the sample, the heating program allows the elimination of the majority of the matrix, but problems with low stability of the analyte in standards and diluted samples have been reported [3,4,18,19].

The formation and analysis of emulsions or microemulsions instead of a dilution of the crude oil sample with an organic solvent has been proposed for GF AAS [4,5,20,21], ICP-MS [22–24] and for ICP OES [18,25]. This technique allows the use of aqueous standards for calibration instead of expensive and instable organometallic standards. Better stability for a number of elements in standards and emulsified samples has been reported in all papers.

Our group has carefully investigated the determination of nickel in crude oil using the emulsion technique. Using high resolution continuum source (HR-CS) GF AAS it was found that up to 50% of the nickel might be lost during the pyrolysis stage already at temperatures above 400 °C, whereas the rest of the nickel was thermally stable up to about 1400 °C [4]. Based on literature data [26] it has been assumed that it was the non-polar porphyrin complexes that were lost, whereas the highly polar non-porphyrins were retained in the graphite tube to high temperatures. The same behavior was also found for vanadium [6]. The unsurpassed background correction capability of HR-CS GF AAS allows pyrolysis temperatures as low as 300 °C to be used even with such a complex matrix as crude oil. Hence, total nickel and vanadium have been determined using a pyrolysis temperature of 400 °C, and "thermally stable" compounds using a pyrolysis temperature of 800–1000 °C. The volatile fraction, which is largely nickel and vanadyl porphyrin complexes, was calculated by difference. For the application of this method in conventional GF AAS, the use of palladium as a modifier has been proposed to stabilize the volatile compounds. A mass of 20 μg of palladium, introduced into the graphite tube and thermally pretreated prior to the injection of the emulsion, was found to efficiently prevent any low-temperature losses of nickel and vanadium from crude oil samples up to pyrolysis temperatures of 1200 and 1450 °C, respectively [5]. In this approach the total nickel and vanadium was determined using palladium and the "thermally stable" compounds were determined without a modifier at the same pyrolysis temperature. The advantage of this procedure was that kind of fractionation was obtained with a relatively simple sample preparation and without any chromatographic pre-separation. It should be stressed that if the presence of volatile compounds is not taken into consideration, even using relatively low pyrolysis temperatures, GF AAS might actually be a source of severe systematic errors.

One aspect that should receive major attention when performing speciation analysis is to retain all species of interest in their original form during sample preparation. The condition of a minimal pretreatment procedure must be applied to attain accurate results [27]. Obviously, no sample preparation at all would be kind of an ideal situation. In the case of crude oil "light" oils are highly viscous, and very difficult to pipette, whereas "heavy" oils are essentially solid. This means that conventional liquid sampling techniques cannot be used for the direct analysis of crude oils.

The use of direct solid sampling (SS) GF AAS has been increasing in the last years manly because rugged and reliable accessories for direct SS-GF AAS became available in the late 1990s [28]. The main advantages of the technique are extremely low detection limits because of the absence of any dilution and a minimal risk of contamination. Among the limitations mentioned in connection with SS-GF AAS are the difficulties of calibration and of using chemical modifiers. Nevertheless, in a recent review about this subject [28] it has been shown that calibration against aqueous standards has been used by many authors for very different kind of samples and the use of chemical modifiers, including permanent modifiers, has also been shown to be feasible by several authors [29–33].

The goal of this work was the differential determination of volatile and non-volatile compounds of nickel and vanadium

Table 1
Graphite furnace temperature program for the determination of nickel and vanadium in crude oil

Program step	Temperature (°C)	Ramp (°C s^{-1})	Hold time (s)	Gas flow rate (L min^{-1})
Drying 1	150	10	50	2.0
Drying 2	300	5	30	2.0
Pyrolysis	1400[a,b]	100	20[a], 40[b]	2.0
Atomization	2400[a], 2600[b]	1500	5[a], 9[b]	0
Cleaning	2600	100	4	2.0

[a] Nickel.
[b] Vanadium.

using direct analysis of crude oil by SS-GF AAS. The expected advantage of this procedure would be that kind of a fractionation analysis could be obtained without any sample preparation and without any chromatographic or other pre-separation. This way there would be no change in the sample and no risk of losses during digestion or a pre-separation step; there would also be no adsorption in the flasks after dilution with solvents, hence minimizing all these sources of error. The main difficulties associated with this procedure, such as weighing errors, calibration and the use of chemical modifiers were investigated in detail.

2. Experimental

2.1. Instrumentation and operation

All measurements were carried out using a Model AAS5 atomic absorption spectrometer (Analytik Jena AG, Jena, Germany) with deuterium background correction, equipped with a transversely heated graphite tube atomizer. NARVA hollow cathode lamps for nickel and vanadium (GLE, Berlin, Germany) were used as the radiation source with a current of 6.0 mA. Due to high sensitivity of SS-GF AAS and the relatively high concentration of Ni in crude oil, the analytical line at 234.6 nm, which is about four times less sensitive compared to the primary line, was used in all the measurements, with a spectral bandwidth of 0.5 nm. For vanadium the main analytical line at 318.4 nm and a spectral bandwidth of 0.8 nm were used. The spectrometer was interfaced to an IBM PC/AT-compatible computer. All experiments were carried out using solid sampling platforms (Analytik Jena Part No. 407-152.023) and solid sampling tubes without dosing holes (Analytik Jena Part No. 07-8130325). An SSA 5 manual solid sampling accessory (Analytik Jena AG) was used for introduction of the platform into the graphite tube. Emulsions, aqueous standards and modifier solution were injected manually on the SS platform using a micropipette. The crude oil samples were weighed on an M2P microbalance (Sartorius, Göttingen, Germany). The accurate sample mass, typically around 1 mg, was automatically transmitted to the instrument's computer to calculate the 'normalized integrated absorbance' (integrated absorbance calculated for 1 mg of sample) after each measurement. This normalized integrated absorbance is commonly used in SS-GF AAS to compare signals, as it is practically impossible to introduce always exactly the same sample mass in a series of measurements. Argon with a purity of 99.996%

(White Martins, São Paulo, Brazil) was used as the purge gas. Integrated absorbance (peak area) was used exclusively for signal evaluation and quantification. The optimized graphite furnace temperature program is given in Table 1. In case when a chemical modifier was used, the modifier solution containing 20 µg of palladium with or without Triton X-100 was introduced first into the graphite platform, and the first two steps of the temperature program were executed in order to dry and condition the modifier. Then the program was stopped, and the furnace allowed cool before the sample was introduced, and the entire temperature program executed.

For the measurements with the permanent modifier, the SS graphite platforms were treated by pipetting 10 times 40 µL of a 1000 mg L^{-1} Ir standard solution and submitting the platform after each injection to the following heating program: 130 °C/40 s, 160 °C/50 s, 1000 °C/25 s and 1400 °C/5 s. After the last treatment, when a total of 400 µg of Ir had been applied, the platform was heated to 2000 °C for 5 s.

The standard calibration technique using aqueous standards was used for most of the determinations. Calibration using oil-in-water emulsions and by weighing different masses of a suitable reference material was also investigated for comparison under the same experimental conditions. The reference material and the crude oil samples were analyzed weighing at least six replicates each.

A Unique-Thorton Model USC-2850 ultrasonic bath (Thorton, São Paulo, Brazil) operated at a frequency of 37 ± 3 kHz, with temperature control up to 80 ± 5 °C, was used for preparation of the emulsions.

2.2. Reagents

Analytical grade reagents were used throughout. Distilled, deionized water (DDW) with a specific resistivity of 18 MΩ cm, from a Milli-Q water purification system (Millipore, Bedford, MA, USA), was used for the preparation of the standards. All containers and glassware were soaked in 3 mol L^{-1} nitric acid for at least 24 h and rinsed three times with DDW before use. The nitric acid (Merck, Germany) used in this work for standards preparation was further purified by sub-boiling distillation in a quartz sub-boiling still (Kürner Analysentechnik, Rosenheim, Germany). Aqueous stock solutions of nickel and vanadium (1000 mg L^{-1}) were prepared from Titrisol concentrates (Merck). The working standards were prepared by serial dilution of the stock solutions with the addition of 0.014 mol L^{-1}

nitric acid. The emulsion standards were prepared by serial dilution of the aqueous stock solutions with the addition of base mineral oil (BMOMS, High Purity Standards, Charleston, SC, USA), Xylene (Merck) and Triton X-100 (Union Carbide). The composition of the oil-in-water emulsion and the mode of its preparation were optimized using a multivariate approach, described in previous work [5].

The following solutions were used as chemical modifiers: a palladium stock solution with 1000 mg L^{-1} Pd in 5 mol L^{-1} nitric acid and 1000 mg L^{-1} of Ir (as the chloride) stock solution (both from Merck).

2.3. Reference materials and samples

The NIST Certified Reference Material SRM 1634c, Trace Elements in Fuel Oil (National Institute for Standards and Technology, Gaithersburg, MD, USA) was used for method validation. The samples analyzed in this work were acquired from local refineries of Petrobras, most of them are from the state of Bahia, Brazil.

3. Results and discussion

3.1. Temperature program and modifiers

Losses of volatile nickel and vanadium compounds in crude oil at pyrolysis temperatures above 400 °C have been detected in previous work of our group [4,6]. Palladium, deposited on the platform and dried prior to the introduction of the emulsified oil sample, was found to efficiently prevent any low-temperature losses of nickel and vanadium [7]. Carrying out the same analysis without and with the addition of palladium even made possible a differential determination of the volatile and non-volatile analyte compounds from crude oil samples [7]. Obviously, the injection of a modifier solution and its thermal pretreatment in the graphite tube prior to each sample introduction is a significant complication of the analytical procedure, and the use of a permanent modifier would offer clear advantages. For this reason, iridium and ruthenium, the platinum group metals with the highest melting points (besides osmium, which was not considered because of the extreme volatility and toxicity of its tetroxide), were investigated in this work as permanent modifiers in addition to palladium, added in the conventional way.

The attempt of using ruthenium (400 μg) as permanent modifier was not successful at all. The signal for nickel in aqueous standards and an oil sample (OB3) was reduced to about 25%, compared to the palladium modifier, and the absorption pulse showed a very irregular profile, even when higher atomization temperatures were used. This modifier was therefore not further investigated. The use of iridium (400 μg) as permanent modifier appeared to be more successful, as at least for aqueous nickel standards the same sensitivity was obtained as with the palladium modifier (and without modifier). However, when an oil sample (OB3) was used, a rapid drop in sensitivity by about 40% was observed over the first three atomization cycles, as shown in Fig. 1, after which the sensitivity remained
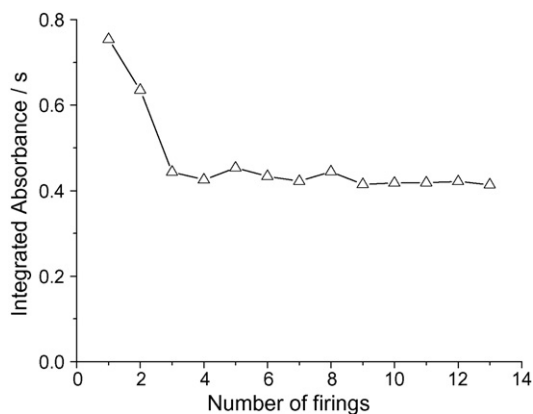
Fig. 1. Integrated absorbance signals obtained for nickel in OB3 crude oil over 14 consecutive atomization cycles using a platform tube treated with 400 μg Ir. $T_p = 1400$ °C and $T_a = 2400$ °C.

stable at this low level, a phenomenon that will be discussed later.

Before the pyrolysis stage of the heating program could be investigated, it was found necessary to optimize the "drying stage". While this stage is straight-forward when aqueous solutions are used, and it might even be omitted in the analysis of solid samples, it requires special attention in the case of oil samples. In order to achieve a smooth and complete removal of all the volatile components from up to 10 mg of crude oil, it was found necessary to apply two "drying" steps with relatively high temperature (150 and 300 °C), slow ramp rates and long hold times, as shown in Table 1.

Pyrolysis curves were established for aqueous and emulsified nickel standards and for a crude oil sample: without the use of a modifier, with the addition of 20 μL of a 0.1% (m/v) palladium solution (20 μg Pd) and with iridium (400 μg Ir) as a permanent modifier. The pyrolysis curves for 2 ng of nickel in aqueous and emulsified standards are shown in Fig. 2a, and those for a crude oil sample under the various conditions are shown in Fig. 2b. The integrated absorbance signals obtained for the crude oil were 'normalized' for 1 mg of sample. Not all of the pyrolysis curves are shown in Fig. 2a, but essentially the same sensitivity was obtained for aqueous and emulsified standards, without modifier and in the presence of the palladium or iridium modifier. The same maximum pyrolysis temperature (1400 °C) was found for the aqueous and the emulsified nickel standard without modifier and with the palladium modifier, whereas a slightly higher pyrolysis temperature (1600 °C) could be used in the presence of iridium.

However, a significantly different behavior was observed for the crude oil sample, as shown in Fig. 2b. In agreement with our previous work [5] there is a very significant difference in sensitivity for nickel in the presence and in the absence of palladium, which shows that this modifier is very efficient in preventing losses of volatile compounds, most likely nickel porphyrin complexes [26], while the lower signal without modifier is due to the thermally stable nickel compounds only. The curve with 400 μg of iridium as permanent modifier (obtained after the experiments for Fig. 1) was essentially identical with that obtained without a modifier, except that a higher pyrolysis tem-

(a)

(b)

Fig. 2. Pyrolysis curves for nickel without modifier and using different modifiers and modes of preparation: (a) 2 ng of standard and (b) crude oil (OB3). $T_a = 2400\,^\circ C$.
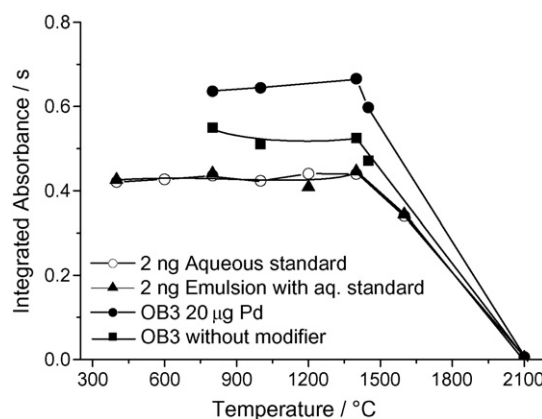

Fig. 3. Pyrolysis curves for vanadium. The data for OB3 crude oil curves are in 'normalized integrated absorbance' (integrated absorbance calculated for 1 mg of sample). $T_a = 2600\,^\circ C$.

3.2. Influence of sample mass

In solid sampling analysis a small amount of sample, typically in the range of 0.1–10 mg, is used and has to be weighed with high precision. In order to evaluate the weighing errors, 'light' crude oils, which are liquid and of relatively low viscosity and 'heavy' crude oils, which are highly viscous or almost solid, were investigated. In the case of 'light' crude oils that contain a volatile fraction (light hydrocarbons), a small drop in weight with time was observed due to volatilization. However, keeping the temperature in the laboratory around 20–25 °C, this effect could be minimized. The strategy we used to weigh such samples was to record the first weight, not considering the weight loss with time. Table 2 shows the standard deviation of the measurements for four samples with different characteristics and nickel contends. The samples OB7 and OB8 are almost solid, whereas OB12 is more liquid (with a volatile fraction). The NIST SRM 1634c, a fuel oil, was also investigated in this experiment. As can be seen, the precision was good and similar to values reported for solid sample analysis [34,35], showing that precision was not affected by the strategy used for weighing the sample. Actually, in contrast to our expectation, precision for OB12 was the best one of all, although this sample was most affected by evaporation of volatile hydrocarbons. It appears that the lower viscosity of this sample, which facilitates its transfer to the platform, is of greater importance than a potential weighing error due to volatilization losses. On the other hand the nickel content that limited the mass of sample that could be weighed to give a signal within the linear range, although a less sensitive line was used,

perature (1600 °C) could be used, as was the case for aqueous standards. This finding, together with the observations made in Fig. 1, strongly suggests that iridium looses its stabilizing power for the volatile nickel compounds within a few determinations. The reason for that could be an interaction of nickel, which is a well known catalyst poison, with iridium, blocking the active sites that are responsible for preventing losses of volatile nickel porphyrin complexes.

Based on the above experience the idea of using a permanent modifier for this kind of application was abandoned, and the use of 20 μg of palladium, applied prior to each determination, was considered the best choice, as it efficiently prevents low-temperature losses of nickel from crude oil samples up to pyrolysis temperatures of 1400 °C. Hence, only this modifier was investigated for the determination of vanadium in crude oil. The pyrolysis curves shown in Fig. 3 for the crude oil sample OB3 with and without 20 μg of palladium showed the same behavior as for nickel, proving the efficiency of this modifier also to prevent low-temperature losses of vanadium from crude oil samples. The best pyrolysis temperature for vanadium in all situations (aqueous standard, stable and total vanadium in crude oil) was 1400 °C. A pyrolysis temperature of 1400 °C was therefore chosen for the determination of nickel and vanadium in all further experiments.

Table 2
Relative standard deviation for crude oil samples (with 20 μg Pd as modifier)

Sample	Concentration ($\mu g\,g^{-1}$)	Mass range (mg)	R.S.D. (%) ($n=6$)
OB7	2.81[a]	2.043–3.332	3.3
OB12	10.4[a]	0.526–0.647	2.5
OB8	59.1[a]	0.043–0.054	10
SRM 1634c	17.5	0.525–0.656	8.6

[a] From ref. [5].

appears to have a greater influence on the precision, similar to the experience with direct solid sampling analysis.

The homogeneity of the samples was also investigated. For this purpose the samples were warmed to 40 °C on a water bath and then mixed vigorously with a glass rod before sampling. The standard deviation for 10 measurements for these 4 samples before and after this procedure was not significantly different showing that the analyte content in these samples is homogeneous.

The influence of sample mass on the linearity of the response and on potential measurement errors was also investigated using four samples with significantly different nickel concentration. For the sample with the lowest nickel concentration (OB7), for which a sample mass between 0.5 and 4.0 mg was used for analysis, the relationship between mass and integrated absorbance was found to be non-linear. Even for samples with higher nickel concentration (OB12 and SRM 1634c), with analyzed masses between 0.1 and 0.7 mg, the same behavior was observed. Only for the sample with the highest concentration (OB8), for which only less than 0.1 mg could be introduced, the relationship between mass and integrated absorbance was found to be linear. An attempt of increasing the amount of palladium did not result in a linear relationship for the affected samples. Hence, it was suspected that the problem was associated with the surface coverage of the modifier, which has not been added together with the sample, but before. Most likely, 20 μL of an aqueous solution will not cover the entire platform surface, and the Pd modifier, after the drying stage, will only be found in the central part. Crude oil, however, might be expected to spread over the entire platform surface upon heating, which means that part of the sample, depending on the sample mass introduced, will not be in contact with the modifier, resulting in losses of volatile compounds. To clarify and eventually solve this problem, a greater volume (40 μL) of a lower concentration of palladium (0.5 g L^{-1}) was injected, and 0.05% Triton X-100 was added in order to assist spreading of the solution over the entire platform surface. After this modification the relationship between mass and integrated absorbance was found to be linear for all samples investigated, even with high sample mass. The curves using 20 μL of 1.0 g L^{-1} Pd and 40 μL of 0.5 g L^{-1} Pd with 0.05% Triton X-100, respectively, for two different samples are shown in Fig. 4. The loss of sensitivity of about 35 and 25% observed for the highest sample mass for OB12 and SRM 1634c, respectively, using the more concentrated modifier solution, was completely eliminated using the greater volume of the more diluted modifier with the addition of Triton X-100.

3.3. Figures of merit

Using the previously optimized conditions, calibration curves were established using: (i) aqueous standards, (ii) aqueous standards emulsified with xylene and Triton X-100 as it was successfully used in the determination of nickel and vanadium in crude oil emulsified in the same way [7] and (iii) using the certified reference material NIST SRM 1634c. However, calibration using one or more CRM, besides being expensive and not recommended for routine analysis, was found to contribute
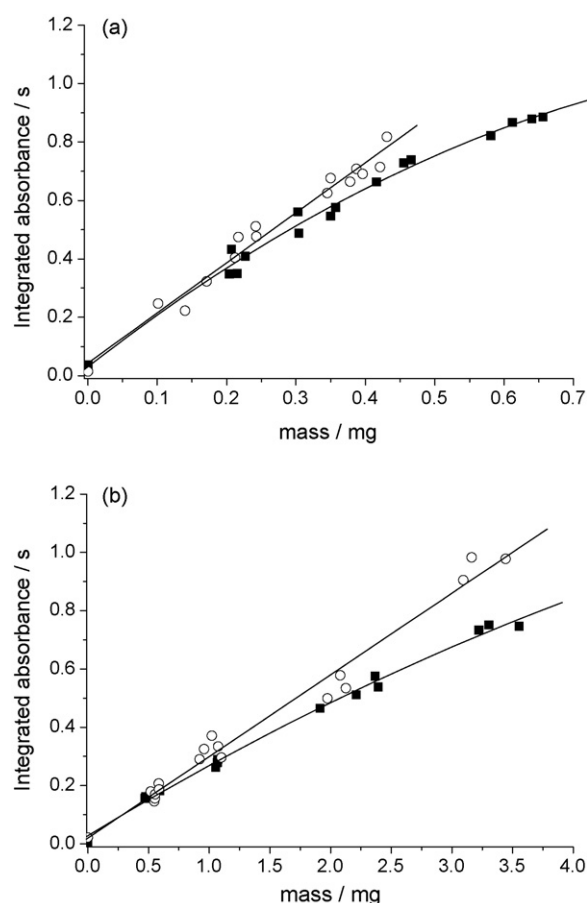
Fig. 4. Influence of sample mass on the linearity of the response using two different ways of applying the modifier. (a) SRM 1634c and (b) crude oil sample OB7; (■) 20 μL of 1.0 g L^{-1} Pd and (○) 40 μL of 0.5 g L^{-1} Pd with 0.05% Triton X-100.

significantly to imprecision, as the uncertainty of the certified value is fully introduced into the calibration [35,36]. The calibration curves were established with and without modifier. As can be seen in Table 3 the sensitivity was similar for all nickel curves, although a slightly lower characteristic mass was obtained for the emulsions. The SRM 1634c without modifier resulted in the highest characteristic mass, which is most likely due to the fact that the volatile nickel compounds present in this material were lost during the heating program. The most important result in our opinion was the similarity in the characteristic mass values obtained for aqueous solutions and the SRM, which strongly suggested the simplest solution, i.e., the use of aqueous standards for calibration. Another feature is that the calibration curve could be established without a modifier, and the same curve could be used for the determination of thermally stable Ni (analyzing the samples without modifier) and total nickel (analyzing the samples with modifier), and the volatile Ni being calculated by difference. Fig. 5 shows in addition the absorbance signals for nickel and vanadium in aqueous standards and in crude oil with and without palladium + Triton X-100 as the modifier. The peak profiles are very similar in the different situations, supporting the possibility that aqueous standards can be used for the determination of nickel and vanadium in crude oil with the proposed technique.

Table 3
Analytical figures of merit for the determination of nickel and vanadium in crude oil using emulsions, aqueous standard and certified reference material for calibration, without and with the addition of palladium as chemical modifier

Analyte	Method	Linear regression equation	r	m_0 (pg)
Ni	SRM 1634C	$A = 0.01892 + 0.08109m$	0.9992	44
	SRM 1634C[a]	$A = 0.06913 + 0.09800m$	0.9925	38
	Emulsion	$A = 0.07437 + 0.09788m$	0.9927	27
	Emulsion[a]	$A = 0.06848 + 0.09941m$	0.9904	28
	Aqueous standard	$A = 0.02313 + 0.09294m$	0.9964	40
	Aqueous standard[a]	$A = 0.02235 + 0.09297m$	0.9968	34
V	Emulsion	$A = 0.0205 + 0.1768m$	0.9922	20
	Aqueous standard	$A = 0.01018 + 0.1858m$	0.9966	21

[a] 20 µg Pd + Triton X-100.

Table 4
Analytical results obtained for nickel in a certified reference material and in various crude oil samples with (total Ni) and without (stable Ni) the addition of 20 µg Pd as modifier. The volatile analyte fraction was determined by difference

Sample	Total Ni (mg kg^{-1})			Stable Ni (mg kg^{-1})		Volatile Ni (mg kg^{-1})	
	HR CS AAS[a]	GF AAS[a]	SS-GF AAS	GF AAS[a]	SS-GF AAS	GF AAS[a]	SS-GF AAS
SRM 1634c[b]	17.4 ± 0.3	17.7 ± 0.5	17.1 ± 1.2	17.1 ± 1.1	16.9 ± 1.3	0.6 ± 1.2	0.2 ± 1.8
OB2	21.8 ± 0.5	24.5 ± 0.2	23.7 ± 1.1	18.9 ± 0.2	18.9 ± 2.8	5.6 ± 0.3	4.8 ± 3.0
OB3	5.3 ± 0.4	4.9 ± 0.1	4.3 ± 0.5	3.5 ± 0.1	2.5 ± 0.2	1.4 ± 0.1	1.8 ± 0.5
OB4	1.3 ± 0.1	1.1 ± 0.1	1.2 ± 0.1	0.7 ± 0.1	0.6 ± 0.03	0.4 ± 0.1	0.6 ± 0.1
OB6	34.0 ± 2.1	36.7 ± 1.1	31.2 ± 2.4	24.2 ± 0.7	28.3 ± 1.1	12.5 ± 1.3	2.9 ± 2.6
OB7	2.9 ± 0.5	2.8 ± 0.1	2.8 ± 0.3	2.4 ± 0.1	2.5 ± 0.6	0.4 ± 0.1	0.3 ± 0.7
OB8		59.1 ± 1.9	80.2 ± 7.8	61.4 ± 2.2	76.6 ± 9.2	–	3 ± 12
OB12		10.4 ± 0.2	10.6 ± 0.7	5.4 ± 0.1	5.4 ± 0.5	5.0 ± 0.2	5.2 ± 0.9
OB13		14.8 ± 0.6	16.2 ± 2.4	8.5 ± 0.4	10.5 ± 0.5	6.3 ± 0.7	5.7 ± 2.5
OB15		16.6 ± 0.7	16.8 ± 1.2	10.5 ± 0.6	13.0 ± 0.3	6.1 ± 0.9	3.8 ± 1.2

[a] From ref. [5].
[b] SRM 1634c certified value 17.5 ± 0.21 mg kg^{-1}.

The limits of detection (LOD) and limits of quantification (LOQ), based on the 'zero mass response' [34], i.e., 3 times and 10 times the standard deviation, respectively, of 10 readings obtained from the "atomization" of an empty platform, were found to be 0.017 and 0.056 mg kg^{-1}, respectively, for nickel and 0.018 and 0.062 mg kg^{-1}, respectively, for vanadium, based on 10 mg of sample. This mass was considered for calculations as it was close to the maximum amount of crude oil that could be analyzed. The LOD of nickel was comparable with literature values for emulsion and microemulsion techniques [5,18] and with those for SS-GF AAS [37,38], but it should be stressed that about four times better results could be obtained for this

Table 5
Analytical results obtained for vanadium in a certified reference material and in various crude oil samples with (total V) and without (stable V) the addition of 20 µg Pd as modifier. The volatile analyte fraction was determined by difference

Sample	Total V (mg kg^{-1})			Stable V (mg kg^{-1})			Volatile V (mg kg^{-1})		
	HR CS AAS[a]	GF AAS[b]	SS-GF AAS	HR CS AAS[a]	GF AAS[b]	SS-GF AAS	HR CS AAS[a]	GF AAS[b]	SS-GF AAS
SRM 1634c[c]	29.3 ± 1.0	27.2 ± 1.2	27.2 ± 2.4	25.6 ± 1.3	23.2 ± 2.0	22.9 ± 1.3	3.4 ± 2.5	4.0 ± 2.3	4.3 ± 2.7
OB2	30.2 ± 0.4	28.7 ± 0.9	24.5 ± 1.5	18.5 ± 0.7	23.3 ± 0.5	21.1 ± 0.7	11.6 ± 1.3	5.4 ± 1.0	3.4 ± 1.7
OB3	3.18 ± 0.07	3.2 ± 0.1	3.8 ± 0.3	2.28 ± 0.2	2.0 ± 0.3	2.9 ± 0.3	1.01 ± 0.3	1.2 ± 0.3	0.9 ± 0.4
OB4	0.29 ± 0.04	0.24 ± 0.03	0.21 ± 0.01	0.16 ± 0.05	0.16 ± 0.02	0.12 ± 0.02	0.07 ± 0.1	0.08 ± 0.04	0.09 ± 0.1
OB6	8.51 ± 0.2	8.4 ± 0.1	8.9 ± 0.5	6.91 ± 0.4	6.4 ± 0.2	7.9 ± 0.3	1.84 ± 0.7	2.0 ± 0.2	1.0 ± 0.6
OB7	<0.04	<0.06	<0.02	< 0.04	<0.06	<0.02	–	–	–
OB8	0.75 ± 0.06	<0.06	0.47 ± 0.04	0.73 ± 0.02	<0.06	0.42 ± 0.05	n.d.[d]	–	n.d.[d]
OB12	12.3 ± 0.3	12.1 ± 1.2	10.1 ± 1.2	9.25 ± 0.1	8.9 ± 0.8	6.2 ± 0.6	2.95 ± 0.4	3.2 ± 1.0	3.9 ± 1.3
OB13	–	18.5 ± 1.3	15.5 ± 2.1	–	13.7 ± 0.4	12.6 ± 0.6	–	4.8 ± 1.2	2.9 ± 2.2
OB15	–	16.2 ± 0.9	19.9 ± 1.2	–	14.0 ± 0.3	16.8 ± 1.2	–	2.2 ± 0.9	3.1 ± 1.7

[a] From ref. [6].
[b] From ref. [5].
[c] SRM 1634c, 28.5 ± 0.40 mg kg^{-1}.
[d] n.d., no statistical difference between the results for total and stable vanadium according to the confidence interval.

element using the most sensitive line. For vanadium, the LOD was also comparable with literature values for emulsion and microemulsion techniques [5,6,18]. The relatively high LOD obtained is due to the fact that vanadium is one of the refractory elements that form stable carbides, requiring a high atomization temperature. Even using the maximum temperature seems to be not sufficient for rapid atomization, as can be seen in Fig. 5.

3.4. Analytical results

The use of palladium as a modifier allows the determination of the total concentration of nickel and vanadium in crude oil, and a determination without modifier, using the same pyrolysis temperatures, results in the concentration of the "thermally stable" fraction so that the volatile fraction can be determined

by difference. The calibration curves established with aqueous standards without a modifier were used for quantification of both elements and species. The results for the certified reference material SRM 1634c and a number of Brazilian crude oil samples are shown in Tables 4 and 5 for nickel and vanadium, respectively, and compared with the emulsion technique developed in our previous work [5,6]. In order to have a comparison with an independent procedure, the reference values established for total Ni and V with HR-CS AAS, using no modifier and a pyrolysis temperature of only 400 °C in order to avoid losses, are also included in Tables 4 and 5. The results of stable vanadium obtained using no modifier and a pyrolysis temperature of 1400 °C with HR-CS AAS as well as the volatile fraction are also included. There was no significant difference between the results on a 95% confidence level, using a paired Student's *t*-test. The results obtained for the CRM also showed no significant
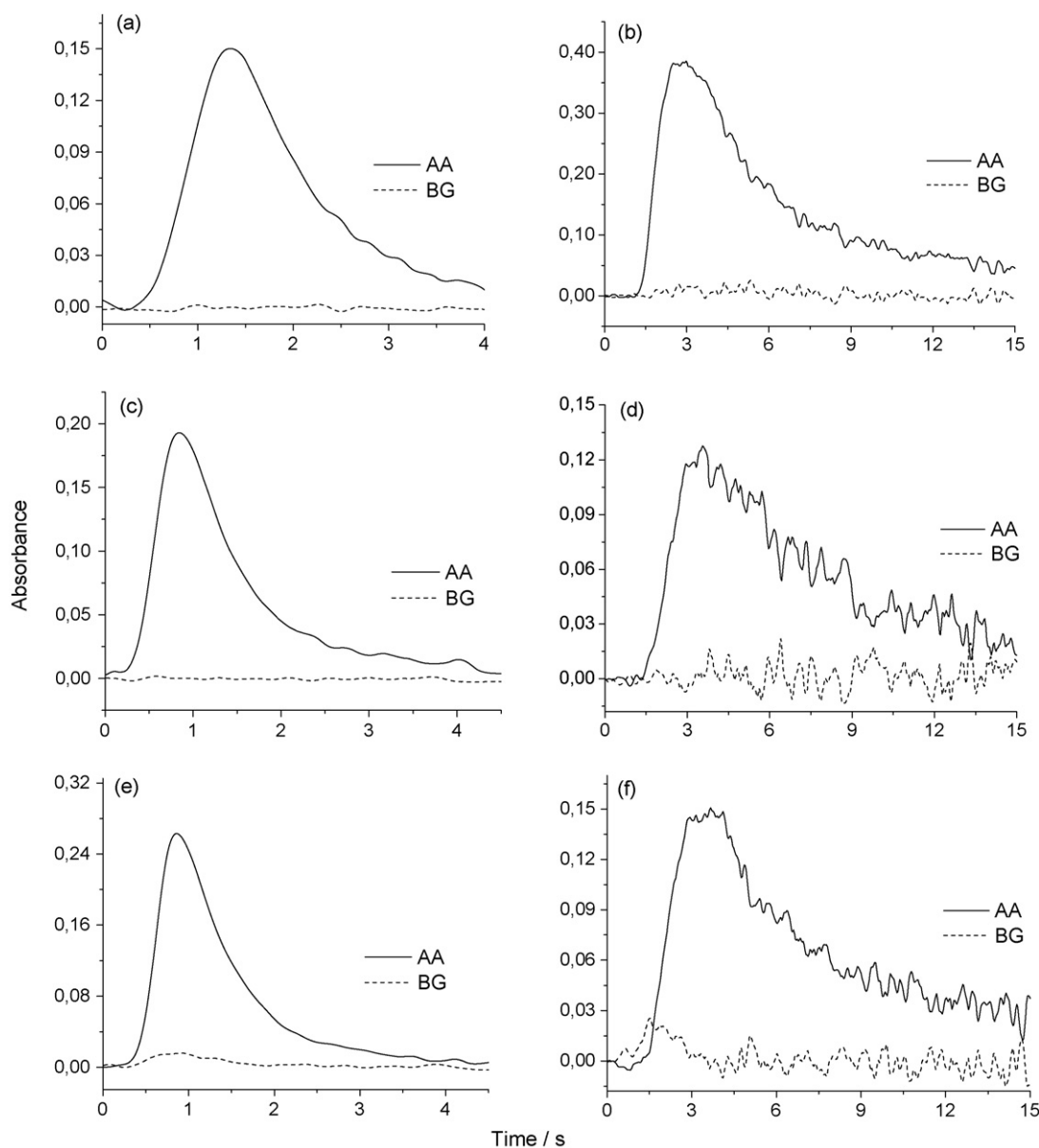
Fig. 5. Absorbance signals for nickel (a, c and e) and vanadium (b, d and f) in aqueous standard: 2 ng for Ni and 10 ng for V (a and b); OB3 crude oil without modifier (c and d); OB3 crude oil with 20 μg Pd + Triton X-100 as modifier (e and f).

difference at the 95% confidence level from the certified value for both elements.

Unfortunately, as the content of volatile compounds had to be determined by difference, it is suffering from the uncertainty of both measurements, total and thermally stable compounds. This fact has been taken into consideration in the calculation of the standard deviation in Tables 4 and 5. In cases where the total content is very close to the 'stable' content, as in SRM 1634c, the volatile fraction might be hidden within the uncertainty of the measurement.

The results obtained in this work provide several interesting information. Firstly, there was one crude oil sample that did not contain any detectable vanadium, i.e., less than $0.062\,mg\,kg^{-1}$, and another one with a very low content ($0.21\,mg\,kg^{-1}$, which is quite unusual, as the content of this element is typically $>1\,mg\,kg^{-1}$) [8,15]. Secondly, the volatile porphyrine fraction was found to be between about 5 and 50% of the total nickel and vanadium content, and there was no correlation between the volatile fraction and the total content for both elements.

4. Conclusion

The proposed procedure makes possible an accurate determination of total nickel and vanadium and of the thermally stable fraction in crude oil using the same graphite furnace program. The volatile fraction, which most likely consists of the non-polar nickel and vanadyl porphyrin complexes, could be determined by difference. This selective determination without any sample preparation, together with the use of aqueous standards for calibration, makes the procedure suitable for routine application. The separate determination of the volatile fraction of both elements in addition to the total content is considered to be of particular importance, as it is for sure predominantly this type of species that is transported in the distillation process to intermediate products, such as naphtha and petroleum condensate, and acts as catalyst poison. The quality of a crude oil might therefore be much better characterized by its content of volatile nickel and vanadium than by its total content, which is not correlated to the former ones. The only disadvantage of this approach is that the most important fraction is determined by difference and suffers from the imprecision of both measurements.

Acknowledgements

References

[1] C. Duyck, N. Miekeley, C.L.P. Silveira, P. Szatmari, Spectrochim. Acta Part B 57 (2002) 1979.
[2] B. Fairman, M.W. Hinds, S.M. Nelms, D.M. Penny, P. Goodall, J. Anal. At. Spectrom. 16 (12) (2001) 1446.
[3] R.Q. Aucélio, A. Doyle, B.S. Pizzorno, M.L.B. Tristão, R.C. Campos, Microchem. J. 78 (2004) 21.
[4] M.G.R. Vale, I.C.F. Damin, A. Klassen, M.M. Silva, B. Welz, A.F. Silva, F.G. Lepri, D.L.G. Borges, U. Heitmann, Microchem. J. 77 (2004) 131.
[5] I.C.F. Damin, M.G.R. Vale, M.M. Silva, B. Welz, F.G. Lepri, W.N.L. dos Santos, S.L.C. Ferreira, J. Anal. At. Spectrom. 20 (2005) 1332.
[6] F.G. Lepri, B. Welz, D.L.G. Borges, A.F. Silva, M.G.R. Vale, U. Heitmann, Anal. Chim. Acta 558 (2006) 195.
[7] C.P. Lienemann, Oil Gas Sci. Technol.-Rev. de l Institut Francais du Petrol. 60 (6) (2005) 951.
[8] C. Hardaway, J. Sneddon, J.N. Beck, Anal. Lett. 17 (37) (2004) 2881.
[9] S.J. Kumar, S. Gangadharan, J. Anal. At. Spectrom. 14 (1999) 967.
[10] H.M. Al-Swaiden, Talanta 43 (1996) 1313.
[11] G.R. Peters, D. Beauchemin, J. Anal. Chem. 65 (1993) 97.
[12] T.D. Saint'Pierre, L.F. Dias, S.M. Maia, A.J. Curtius, Spectrochim. Acta Part B 59 (4) (2004) 551.
[13] T.D. Saint'Pierre, L.F. Dias, D. Pozebon, R.Q. Aucelio, A.J. Curtius, B. Welz, Spectrochim. Part B 57 (12) (2002) 1991.
[14] M.P. Escobar, B.W. Smith, J.D. Winefordner, Anal. Chim. Acta 320 (1) (1996) 11.
[15] B. Welz, M. Sperling, Atomic Absorption Spectrometry, third ed., Wiley-VCH, Weinheim, NY, 1999, p. 531.
[16] M. Sperling, B. Welz, J. Hertzberg, C. Rieck, G. Marowsky, Spectrochim. Acta Part B 51 (9–10) (1996) 897.
[17] J.L. Hammond, Y.L. Lee, C.O. Noble, J.N. Beck, C.E. Proffitt, J. Sneddon, Talanta 47 (1998) 261.
[18] R.M. de Souza, A.L.S. Meliande, C.L.P. da Silveira, R.Q. Aucélio, Microchem. J. 82 (2006) 137.
[19] C. Bruhn, V. Cabalin, Anal. Chim. Acta 147 (1983) 193.
[20] R.Q. Aucélio, A.J. Curtius, B. Welz, J. Anal. At. Spectrom. 15 (2000) 1389.
[21] J.L. Burguera, R.M. Avila-Gomez, M. Burguera, R.A. Salager, J.L. Salager, C.L. Bracho, M. Burguera-Pascu, C. Burguera-Pascu, R. Brunetto, M. Gallignani, Y.P. Pena, Talanta 61 (2003) 353.
[22] H.M. Al-Swaidan, Talanta 43 (1996) 1313.
[23] H.M. Al-Swaidan, At. Spectrosc. 14 (1993) 170.
[24] R.A. Reimer, A. Miyazaki, Anal. Sci. 9 (1993) 157.
[25] M. Murillo, J. Chirinost, J. Anal. At. Spectrom. 9 (1994) 237.
[26] N. Márquez, F. Ysambertt, C. De la Cruz, Anal. Chim. Acta 395 (1999) 343.
[27] A.K. Das, R. Chakraborty, M.L. Cervera, M. De la Guardia, Mikrochim. Acta 122 (1996) 209.
[28] M.G.R. Vale, N. Oleszczuk, W.N.L. dos Santos, Appl. Spectrosc. Rev. 41 (2006) 377.
[29] M.G.R. Vale, M.M. Silva, B. Welz, É.C. Lima, Spectrochim. Acta Part B 56 (10) (2001) 1859.
[30] M.G.R. Vale, M.M. Silva, B. Welz, R. Nowka, J. Anal. At. Spectrom. 17 (1) (2002) 38.
[31] A.F. da Silva, B. Welz, A.J. Curtius, Spectrochim. Acta Part B 57 (12) (2002) 2031.
[32] C.S. Nomura, C.S. Silva, A.R.A. Nogueira, P.V. Oliveira, Spectrochim. Acta Part B 60 (5) (2005) 673.
[33] A.F. da Silva, D.L.G. Borges, F.G. Lepri, B. Welz, A.J. Curtius, U. Heitmann, Anal. Bioanal. Chem. 382 (8) (2005) 1835.
[34] U. Kurfürst, in: U. Kurfürst (Ed.), Solid Sample Analysis, Springer, Berlin/Heidelberg/New York, 1998, pp. 21–127.
[35] U. Kurfürst, A. Rehnert, H. Muntau, Spectrochim. Acta Part B 51 (1996) 229.
[36] M. Berglund, D.C. Baxter, Spectrochim. Acta Part B 47 (14) (1992) 1567.
[37] V. Krivan, M.D. Huang, Anal. Chem. 70 (24) (1998) 5312.
[38] M. Hornung, V. Krivan, Anal. Chem. 70 (16) (1998) 3444.

Determination of chromium(III) and total chromium using dual channels on glass chip with chemiluminescence detection

Waraporn Som-Aum [a,b], Jirasak Threeprom [a], Haifang Li [a], Jin-Ming Lin [a,*]

[a] *The Key Laboratory of Bioorganic Phosphorus Chemistry & Chemical Biology, Department of Chemistry, Tsinghua University, Beijing 100084, China*
[b] *Department of Chemistry, Faculty of Science, Mahidol University, Rajathavi, Bangkok 10400, Thailand*

Abstract

A simple, rapid and sensitive method for the determination of chromium(III) and total chromium using the simple dual T channels on glass chip with negative pressure pumping system and chemiluminescence (CL) detection is presented. The CL reaction was based on luminol oxidation by hydrogen peroxide in basic aqueous solution catalyzed by chromium(III). Total chromium in form of chromium(III) was achieved after chromium(VI) was completely reduced by acidic sodium hydrogen sulfite. Total chromium could then be determined with the same strategy as the chromium(III). The CL reagent was composed of 1.0×10^{-4} mol/L luminol, 1.0×10^{-2} mol/L hydrogen peroxide and 0.10 mol/L sodium bromide in 0.050 mol/L carbonate buffer (pH 11.00). The 1.0×10^{-2} mol/L ethylenediaminetetraacetic acid was added into the sample solution in order to improve the selectivity. Chromium(III) could be detected at a notably concentration of 1.6×10^{-16} mol/L and a linear calibration curve was obtained from 1.0×10^{-15} to 1.0×10^{-13} mol/L. The sample and CL reagent consumption were only 15 and 20 µL, respectively. The analysis time was less than 1 min per sample with the precision (%R.S.D.) was 4.7%. The proposed method has been applied successfully to the analysis of river water, mineral waters, drinking waters and tap water. Its performance was verified by the analysis of certified total chromium-reference materials and by recovery measurement on spiked synthetic seawater sample.
© 2006 Elsevier B.V. All rights reserved.

Keywords: Chromium (III); Total chromium; Chemiluminescence; Microchip; Luminol

1. Introduction

Chromium is a metal which occurs in oxidation states ranging from −2 to +6. However, as far as the environmental protection is concerned, only two most stable oxidation states namely trivalent chromium (Cr(III)) and hexavalent chromium (Cr(VI)), needed to be considered.

Cr(III) and Cr(VI), are drastically different in charge, physicochemical properties as well as chemical and biochemical reactivity. Cr(III) is well known as an essential trace element for humans, required for the maintenance of normal glucose, cholesterol, and fatty acid metabolism. On the other hand, water soluble Cr(VI) is highly irritating and toxic to humans and animals [1]. It is carcinogenic owing to its ability to oxidize other species and has adverse effects on the lung, liver, and kidneys [2]. Therefore,

chromium speciation is of considerable interest to the scientific community.

Although the Environmental Protection Agency (EPA) of USA has set the maximum level of total chromium allowed in drinking water at 100 µg/L [3], the chromium content is normally presented at very low concentration in natural waters, where typical concentrations are in the 0.1–0.5 µg/L range. Therefore, the direct determination of trace chromium species in environmental samples demands very sensitive analytical techniques.

Many detection protocols of chromium have been utilized including spectrometry [4], flame atomic absorption spectrometry (FAAS) [5,6], electrothermal atomic absorption spectrometry (ETAAS) [7–11], inductively coupled plasma-atomic emission spectrometry (ICP-AES) [12,13], liquid chromatography with UV detection (LC-UV) [14–16], liquid chromatography with chemiluminescence detection (LC-CL) [17], capillary electrophoresis with UV detection (CE-UV) [18], capillary electrophoresis with inductively coupled plasma mass spectrometry (CE-ICPMS) [19] and capillary electrophoresis with chemilumi-

* Corresponding author. Fax: +86 10 62841953.
E-mail addresses: jmlin@mail.tsinghua.edu.cn, jmlin@mail.rcees.ac.cn (J.-M. Lin).

nescence detection (CE-CL) [20,21]. However, the procedures are complex, time consuming and/or need preconcentration step in these methods.

In the recent decade, extensive work has been directed toward miniaturization of analytical methods since this concept was first introduced in 1990s by Manz et al. [22]. Its results from the short analysis time, as well as small reagent and sample requirements [23]. Numerous reports have appeared on the use of this fashion for the metal analysis [24–33]. Among them it showed only a few reports on the determination of chromium using microfluidic device. Xu et al. [29,30] firstly reported the use of glass micromachined device for the quantitative detection of Cr(III) with CL detection. A micromachined reactor was employed in a continuous flow injection set-up. The linear range for Cr(III) determination was in the range 10^{-6} to 10^{-4} mol/L. The detection limit was below 10^{-7} mol/L. This system was simple and sensitive, however, only Cr(III) could be monitored. The CL detection integrated with a microchip capillary electrophoresis system that fabricated in poly(dimethylsiloxane) for separation of Cr(III) and other metal ions was demonstrated by Liu et al. [31]. A detection limit down to submicromolar concentrations was achieved with good reproducibility and symmetric peak shape. Again, only Cr(III) was focused in this work. The interfacing of microchip based electrophoresis separation system with inductively coupled plasma mass spectrometry for chromium speciation was recently introduced by Song et al. [32,33]. Hydrodynamic sample injection was accomplished by a flow injection mode through an externally controlled gravity pump and a three-way valve. Cr(III) and Cr(VI) could be separated in acidic solution within 30 s. The limit of detection for Cr(III) and Cr(VI) was 3.7 and 2.5 μg/L, respectively. Although the Cr(III) and Cr(VI) could be individually detected with this procedure, the system was complex.

The aim of the present work is, therefore, to firstly propose the determination of Cr(III) and total chromium utilizing microfluidic device with CL reaction. The CL as a method of detection for microchip has the advantage of high sensitivity and simple instrumentation compared with spectrophotometric techniques due to the exclusion of an external light source. This method is based on the Cr(III)-catalyzed oxidation of luminol by hydrogen peroxide in a basic aqueous solution. In this case Cr(III) can be determined selectively in the presence of Cr(VI) and other metal ions in the aqueous environment [34,35]. Total chromium can be determined with the same strategy as Cr(III) after Cr(VI) is completely reduced to Cr(III) with acidic sodium hydrogen sulfite. Cr(VI) can then be calculated by the difference.

2. Experimental

2.1. Reagents

All chemicals were of analytical grade and used without further purification. All reagents were prepared with ultrapure water purified by a Barnstead EASY pure LF system (Dubuque, IA, USA).

All chemicals were obtained from Beijing Chemical Reagents Co., Ltd. (China) except the luminol and hydrogen per-

oxide. Luminol (3-aminophthalhydrazide) was purchased from Merck (Darmstadt, Germany). Thirty percent volume hydrogen peroxide was obtained from Shantou Xilong Chemical Co., Ltd. (China).

Stock solution of luminol (1.0×10^{-2} mol/L) was prepared by dissolving 0.8860 g of luminol in 1.75 mL of 1.0 mol/L NaOH solution and diluting to 50.00 mL with water. Stock solution of 0.10 mol/L H_2O_2 was prepared by sequential dilution of 30% H_2O_2 with water. Stock solution of 1.0 mol/L NaBr was prepared by dissolving 5.1445 g of NaBr in 50.00 mL of water. The CL reagent was 1.0×10^{-4} mol/L luminol, 1.0×10^{-2} mol/L H_2O_2 and 0.10 mol/L NaBr in 0.050 mol/L NaHCO$_3$–Na$_2$CO$_3$ buffer, pH 11.00. This solution was prepared and left to stand for 15 min before used.

The reductant reagent was 1.0×10^{-2} mol/L NaHSO$_3$ dissolved in 1.0×10^{-2} mol/L HCl solution. This solution was always prepared immediately prior to use.

Standard solutions of Cr(III) and Cr(VI) were prepared by appropriate dilution from 1.0×10^{-3} mol/L stock solution made from chromium trichloride and potassium dichromate, respectively. Ethylenediaminetetraacetic acid (EDTA) was added to all sample solutions to remove the interference of other metal ions with the CL analysis [34]. The working standard chromium/sample solutions were prepared in 1.0×10^{-2} mol/L EDTA prior to use.

All glassware were cleansed with 10% (v/v) nitric acid for 48 h and subsequently rinsed with ultrapure water before used.

The natural water tested was Certified Reference material SLRS-4 from NRC-CNRC (Canada) with the certified Cr-content value of 0.33 ± 0.02 μg/L.

The synthetic seawater was prepared by dissolving 33.80 g NaCl, 10.92 g MgSO$_4$·7H$_2$O and 0.22 g NaHCO$_3$, respectively, making the solution up to 2000 mL with ultrapure water, this matrix corresponds to the composition of coastal seawater [36,37] used for internal calibration.

2.2. Microchip design and fabrication

The glass microchip was fabricated by a standard photolithography, wet chemical etching and heat bonding techniques [38]. The design for the template was drawn using a standard Illustrator software package (Adobe Systems). The borosilicate glass wafers with Cr$_2$O$_3$/Cr film (145 nm thick) and positive photoresist (AZ 1350, 0.6 μm thick) was purchased from Shaoguang Microelectronics Corporation (Changsha, China). The plastic reservoirs were finally glued to the top plate with epoxy.

The scheme of the channel structure in the glass microchip was shown in Fig. 1. A channel pattern from Nelstrop et al. [39] reported was modified. A reverse T design accomplished the parallel dual channels was designed for detection. At each T channel, two reservoirs (A–A′ and B–B′) acted as reagents wells. Another reservoir (C and C′) not only acted as the waste reservoir but also the reservoir to which negative pressure was applied to move the reagents through the microreactor. A further reservoir was utilized as a reaction well. The identical channel dimension of 150 μm wide and 50 μm deep for the T line was prepared.
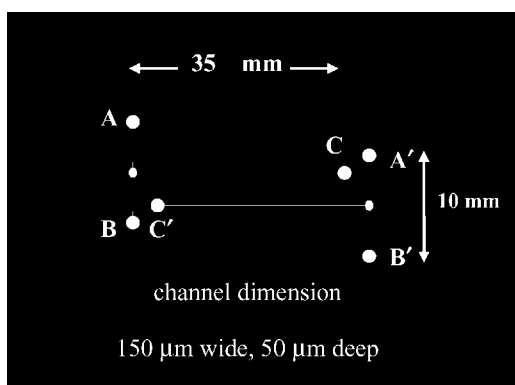
Fig. 1. Schematic structure of the microchip.

The channel length was 35.0 mm from the reaction well to the waste reservoir and 5.0 mm from reaction well to each reagent reservoir. The reaction well was ellipse shape which has volume capacity of 60 nL.

2.3. Microchip operation

The scheme of the set-up system was depicted in Fig. 2. In this work the negative pressure pumping system was utilized with the reagents being loaded into the reservoirs by microsyringe. This method produced negligible backpressure on the microreactor channels and non-discriminatory movement of reagents in varying reaction conditions [39,40]. The negative pressure was applied to the waste reservoirs and sucked the solutions through the channels by means of a lab-made microsyringe pump. Separated controllable syringe pump was connected to each waste reservoir which allowed the operation done at different time. The reagents met at the reaction well and were mixed together along the length of the channel. The flow rate of the solutions through the channel was optimized to be 160 μL/min. Reservoir A and A′ contained 20 μL of CL reagent (luminol, H_2O_2, and NaBr solutions in carbonate buffer). Reservoir B contained
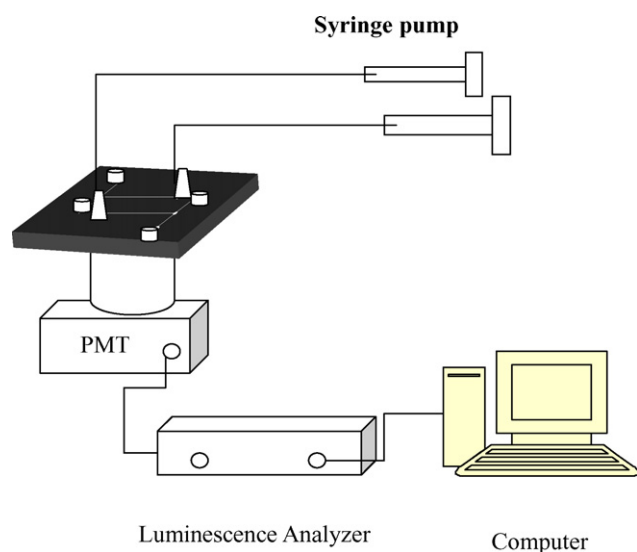
Fig. 2. Schematic diagram of the complete experimental set-up.

15 μL of standard Cr(III)/sample in EDTA solution and 5 μL of water. Reservoir B′ contained 15 μL of standard Cr(VI)/sample in EDTA solution and 5 μL of reductant. The A, B, C – T line was used for Cr(III) determination while the A′, B′, C′ – T line was served in total chromium determination. The determination of Cr(III) was firstly operated. After 15 s the total chromium determination was subsequently done. Between each run, the channels were flushed with carbonate buffer and then air for two times.

The back of the microchip was packed with black adhensive tape except the reaction well and stem T. The microchip was fixed above the PMT of Ultra-Weak Luminescence Analyzer (Institute of Biophysics Academia Sina, China) in black box. The voltage of PMT was set at −850 V. The CL signals were measured in every 0.2 s and recorded by a computer.

3. Results and discussion

3.1. Sample injection and operational procedure

The luminol reaction is rapid with the maximum peak height of the transient CL signal being reached in approximately 50 s [41]. The complete CL emission profile versus time can be obtained in 2–3 s. Therefore, the flow rate of reagents applied is critical which contributed to the mixing of the reagents and producing the signal. In this work, the negative pressure was applied to control the flow rate of reagents in order to eliminate the back pressure produced in the channels and to reduce the number of syringe pumps used. Only two syringe pumps were satisfied to manipulate the reagent flowed, which made the system simplicity. Unfortunately, the flow rates of sample and CL reagent were not exactly controllable independently as a result of negative pumping. With symmetric T-shape pattern, however, liquid flow seemed to be divided in half almost equally. The flow rate of solutions in the interval of 80–200 μL/min was varied and investigated by adjusting the speed of suction. The effect of flow rate on the intensity signal was illustrated in Fig. 3. Low speed of flow rate could not be supported the rapid CL reaction, resulting in the low sensitivity. On the other hand, high flow rate applied was not provided sufficient time in the reaction. Therefore, the flow rate of 160 μL/min was chosen and adopted in this work.
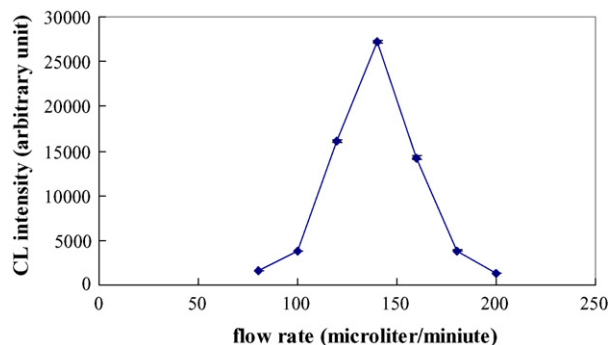
Fig. 3. Effect of sample and reagent flow rate on CL intensity. Cr(III) 1.0×10^{-9} mol/L was in 1.0×10^{-2} mol/L EDTA (mean ± S.D., $n = 3$). CL reaction solution: 1.0×10^{-4} mol/L luminol, 1.0×10^{-2} mol/L H_2O_2, 0.10 mol/L NaBr in 0.075 mol/L carbonate buffer, pH 11.50.
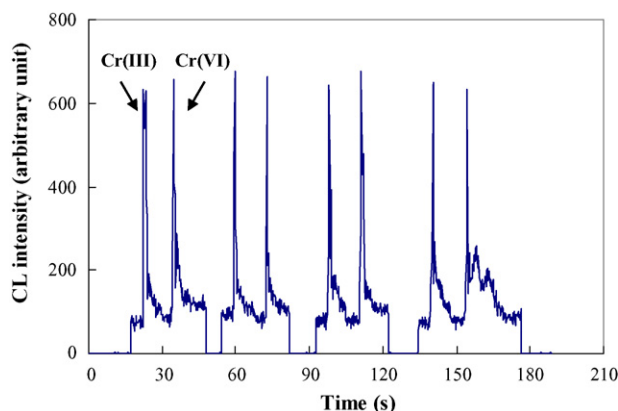
Fig. 4. Peak signal of four consecutive runs of Cr(III) and Cr(VI) at 1.0×10^{-15} mol/L. Cr(III) and Cr(VI) were in 1.0×10^{-2} mol/L EDTA. CL reaction solution: 1.0×10^{-4} mol/L luminol, 1.0×10^{-2} mol/L H_2O_2, 0.10 mol/L NaBr in 0.050 mol/L carbonate buffer, pH 11.00. Reductant solution: 0.010 mol/L $NaHSO_3$ in 0.010 mol/L HCl.

In order to get the two well resolved peaks corresponded to Cr(III) and total chromium, the negative pressure was applied with different time at reservoir C and C′, respectively. The delay time between these two operations was needed. In addition, this step was utilized for leaving the reductant to react with Cr(VI) prior to the analysis. The delay time between 5 and 20 s was examined and found that 15 s was sufficient for this purpose as could be seen clearly in Fig. 4.

Before inject the CL reagent into the reservoirs, the reagent was left to stand with time for 15 min due to an initiation time was needed for carbonate to enhance the CL signal after mixing with H_2O_2 [42]. For standard and sample solutions, after mixing with EDTA the solutions were immediately injected into the respective reservoirs. No initiation time was required as a result of fast complexation reactions of most metals with EDTA as contrast to the complexation of Cr(III) by EDTA, which is kinetically slow [43].

3.2. Optimization of the experimental conditions

A series of experiments were carried out to establish the optimum conditions for use, employing a Cr(III) concentration of 1.0×10^{-12} mol/L.

3.2.1. Effect of luminol concentration

The effect of luminol concentration on the CL intensity was shown in Fig. 5. The hydrogen peroxide concentration was kept constant at 1.0×10^{-2} mol/L while luminol concentration was varied from 1.0×10^{-6} to 1.0×10^{-3} mol/L. The intensities were slightly decreased with decreasing luminol concentrations. Consequently concentration of 1.0×10^{-4} mol/L was selected for subsequently analyses.

3.2.2. Effect of pH of carbonate buffer

The carbonate buffer which reported to enhance the CL signal in luminol–H_2O_2 system [40] was chosen and used in the preparation of CL solution. Since Cr(III) catalyzed the luminol with H_2O_2 in alkaline solution, the effect of CL reagent
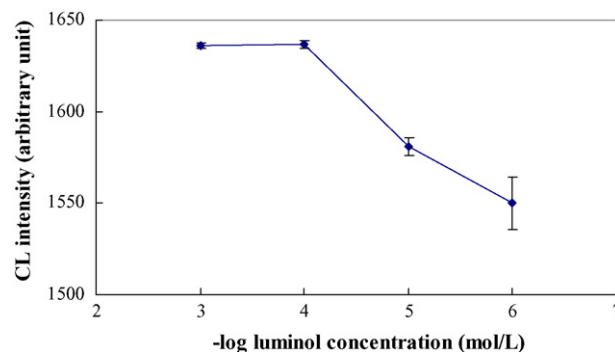
Fig. 5. Effect of luminol concentration on CL intensity. Cr(III) 1.0×10^{-12} mol/L was in 1.0×10^{-2} mol/L EDTA (mean ± S.D., $n = 3$). CL reaction solution: 1.0×10^{-2} mol/L H_2O_2, 0.10 mol/L NaBr in 0.075 mol/L carbonate buffer, pH 11.50.

pH was needed to investigate. Under investigation the concentration of carbonate buffer was fixed at 0.10 mol/L while its pH was varied between 10.13 and 12.00 by varying the composition of $NaHCO_3$ and Na_2CO_3 or adding the NaOH solution. The effect of carbonate reagent pH was shown in Fig. 6. The results showed that the CL signal reached a maximum intensity and was stable within the pH range of 10.60–12.00. Therefore, the pH value of 11.00 was chosen for subsequent determinations.

3.2.3. Effect of carbonate buffer concentration

The effect of carbonate buffer concentration was then examined by keeping the pH constant at 11.00. The concentration of carbonate buffer was varied between 0.010 and 0.10 mol/L. The results showed that a concentration of carbonate buffer greater than 0.025 mol/L achieved maximum CL intensity. A 0.050 mol/L was chosen as the optimal concentration of carbonate buffer.

3.2.4. Effect of NaBr concentration

NaBr was added to the luminol solution in carbonate medium in order to enhance the CL signal [42,44,45]. In the presence of bromide, the hydroxyl radical is converted into bromide radical
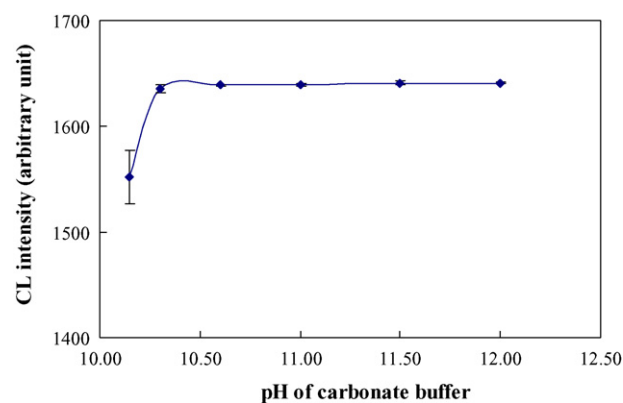
Fig. 6. Effect of carbonate reagent pH on CL intensity. Cr(III) was in 1.0×10^{-2} mol/L EDTA (mean ± S.D., $n = 3$). CL reaction solution: 1.0×10^{-4} mol/L luminol, 1.0×10^{-2} mol/L H_2O_2, 0.10 mol/L NaBr in 0.075 mol/L carbonate buffer.

with selectively reacts with luminol yielding the luminol radical [42]. Bromide enhances the CL intensity by selectively increasing the steady-state concentration of luminol radical and facilitates its decomposition to give more excited luminol ions [44]. The addition of bromide significantly enhanced the CL signal under our investigation with agreed well with the report of Chang and Patterson [44]. Under exactly the same conditions with and without bromide ion, the linear regression equation in calibration range of 1.0×10^{-13} to 1.0×10^{-11} Cr(III) are $y = 2241.5 \log C + 41035$ ($r^2 = 0.9984$) and $y = 277.5 \log C + 4809.8$ ($r^2 = 0.9951$), respectively, where y is the CL intensity and $\log C$ is the concentration in logarithm function expressed in mol/L. Concentration of NaBr in the range of 0.010–0.20 mol/L was investigated. The CL intensity was slightly increased when the concentration of bromide was increased. In this work, 0.10 mol/L NaBr was adopted.

3.2.5. Effect of reductant concentration on reduction of Cr(VI) to Cr(III)

The choice of reductant is very important for the Cr(VI) to be completely reduced to Cr(III). In this work, NaHSO$_3$ was selected for this purpose due to its rapid reaction and high efficiency [20]. It can completely reduce Cr(VI) to Cr(III) in acidic solution. The concentration of NaHSO$_3$ prepared in 0.01 mol/L HCl was studied from 0.0050 to 0.10 mol/L. A measurement of standard Cr(VI) 1.0×10^{-12} mol/L solution without NaHSO$_3$ added in the system showed a low signal related to Cr(VI). The signal was dramatically increased when NaHSO$_3$ added into the system. The complete reduction was achieved in the range of concentration studied. A concentration at 0.010 mol/L NaHSO$_3$ was then chosen as the optimum.

A concentration of HCl solution was then studied and found that HCl concentration in the range of 0.010–0.10 mol/L gave the maximum response. Therefore, 0.010 mol/L HCl was adopted in this work. The signal belonged to Cr(VI) after complete reduction was exhibited in Fig. 4.

The influence of varying concentration ratios of Cr(VI) in Cr(III) for quantitative reduction of Cr(VI) was also investigated. The results showed that at any concentration of Cr(VI) in the presence of Cr(III) was not interfere in the reduction yield.

3.3. Investigation of interferences

Interferences from coexisting metal ions were considered in order to achieve a desired degree of selectivity. In this work, EDTA was added to all solutions to remove the interference of the other metal ions with the CL catalysis. Complexation of Cr(III) by EDTA is kinetically slow. As a result, shortly after the addition of EDTA to the sample, the only potentially chemiluminescent metal species in solution is the free Cr(III) ion [34]. The effect of foreign metal ions was tested by analyzing a standard solution of 1.0×10^{-12} mol/L Cr(III) to which increasing amounts of interfering substances had been added. The 1.0×10^{-2} mol/L EDTA was used as masking reagent. The tolerable concentration ratio for a 5% signal change was investi-
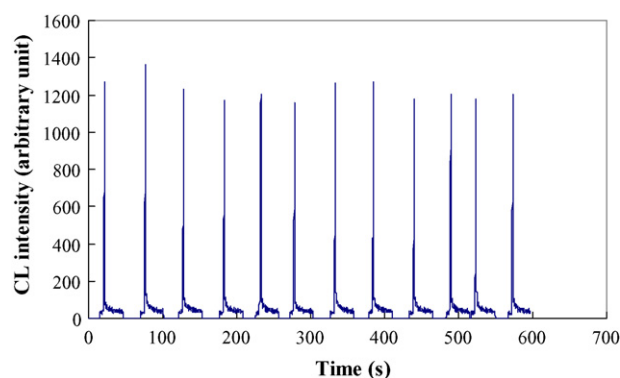
Fig. 7. Signal intensity of 12 consecutive runs of 1.0×10^{-13} mol/L Cr(III). Cr(III) was in 1.0×10^{-2} mol/L EDTA. CL reaction solution: 1.0×10^{-4} mol/L luminol, 1.0×10^{-2} mol/L H$_2$O$_2$, 0.10 mol/L NaBr in 0.050 mol/L carbonate buffer, pH 11.00.

gated with some metal ions. It was found that Cd^{2+}, Co^{2+}, Cu^{2+} and Pb^{2+} did not interfere as a ratio of 100:1, where as Fe^{2+}, Fe^{3+}, Al^{3+}, Zn^{2+} and Ni^{2+} did not interfere at a ratio of 10:1 under the same conditions.

It could be seen that most interfering species might be interfere in this condition. Their tolerance concentration was a level that potentially could be encountered in natural waters. Other masking or complexing agents such as tartaric acid, nitrilotriacetic acid, and citric acid might be added to support the EDTA function. However, any interference effects could be minimized by using the standard addition procedure for quantification which was adopted in this work.

3.4. Linearity, precision and limit of detection

The linearity, repeatability and limit of detection were measured from Cr(III). The linearity range was from 1.0×10^{-15} to 1.0×10^{-13} mol/L Cr(III) with correlation coefficient value of 0.9970. A definition of detection limit in this work was based on the analyte concentration which gives the response signal (Y) three times that of the standard deviation of the blank (S.D.$_b$) plus response signal (Y_b); $Y = Y_b + 3$S.D.$_b$ [46]. The detection limit for Cr(III) was found to be 1.6×10^{-16} mol/L which notably has not been reported. The even low determination limit achieved in our work study might be attributed to (i) utilization of the carbonate and bromide enhancement, (ii) recognition of the importance of the initiation times after mixing H$_2$O$_2$ and carbonate, (iii) flow pattern and reaction take place in microchannel. For the latter reason, the flow regime on microchip was encountered. The flow in this pressure driven system is laminar due to the low Reynolds numbers [47]. The two liquids met at the intersection point and a parallel side-by-side laminar flow formed in the microchannel. The reaction of CL reagents and Cr(III) proceed as the continuous reacting mixture flowed along the microchannel. This effect was brought about an increase in the interface area which leaded to enhanced mass transfer as well as of chemical reaction.

The relative standard deviation (%R.S.D.) of the system was examined by making 12 consecutive runs with Cr(III) concentration of 1.0×10^{-13} mol/L (Fig. 7) and was found to be 4.7%.

Table 1
Determination of Cr contents in CRM SLRS-4, spiked synthetic seawater, mineral waters, drinking waters and tap water

Sample	Certified value (mol/L)			Amount found (mol/L) ($n = 3$, ±S.D.)		
	Total Cr	Cr(III)	Cr(VI)	Total Cr	Cr(III)	Cr(VI)
SLRS-4	1.0×10^{-15}	1.0×10^{-15}	–	$(0.9 \pm 0.2) \times 10^{-15}$	$(0.9 \pm 0.6) \times 10^{-15}$	ND[a]
SLRS-4 (spiked with Cr(VI))	3.0×10^{-15}	1.0×10^{-15}	2.0×10^{-15}	$(3.7 \pm 1.0) \times 10^{-15}$	$(0.9 \pm 0.6) \times 10^{-15}$	$(2.7 \pm 1.2) \times 10^{-15}$
Synthetic seawater	5.0×10^{-15}	2.0×10^{-15}	3.0×10^{-15}	$(5.1 \pm 0.6) \times 10^{-15}$	$(2.2 \pm 0.1) \times 10^{-15}$	$(2.9 \pm 0.6) \times 10^{-15}$
Mineral water 1				$(2.6 \pm 0.3) \times 10^{-13}$	$(2.5 \pm 0.4) \times 10^{-13}$	ND
Mineral water 2				$(8.2 \pm 0.5) \times 10^{-13}$	$(7.7 \pm 1.8) \times 10^{-13}$	ND
Drinking water 1				$(1.2 \pm 0.4) \times 10^{-13}$	$(1.3 \pm 0.3) \times 10^{-13}$	ND
Drinking water 2				$(2.1 \pm 0.3) \times 10^{-13}$	$(2.5 \pm 0.5) \times 10^{-13}$	ND
Tap water				$(2.1 \pm 0.3) \times 10^{-12}$	$(1.7 \pm 0.7) \times 10^{-12}$	ND

[a] ND is referred to non-detectable.

3.5. Evaluation of the system and analytical application

The accuracy of the method was firstly checked by analyzing a certified reference material SLRS-4, river water reference material for trace metals. The certified Cr-content was stated to be 0.33 ± 0.02 μg/L. Before analysis the reference standard was diluted until a concentration of 1.0×10^{-15} mol/L of Cr was obtained.

The Cr(III) was determined directly by the proposed CL method. Total chromium was determined after reduction of Cr(VI) to Cr(III) by $NaHSO_3$. Cr(VI) was then calculated by the difference between total chromium concentration and that of Cr(III). All the determinations were performed by using three-level standard addition for calibration. Three replicate measurements were made on each sample. The results were shown in Table 1.

As shown in Table 1, the result achieved from the SLRS-4 reference material was in good agreement with the recommended value. No content of Cr(VI) was found in the CRM. The result found might be due to the fact that all Cr originally present was as in the state of Cr(III). Conventionally, dilute nitric acid is used to preserve natural samples in order to prevent the adsorption of trace elements in solution on to the walls of the container, and this is case in this instance, where SLRS-4 has been acidified with ultrapure nitric acid to pH 1.6. However, in the presence of organic materials, as one might expect to find in natural samples, it has been reported that Cr(VI) under acidic conditions can be reduced to Cr(III) [2,48,49]. With the SLRS-4 sample being stabilized with nitric acid, the Cr-content, therefore, is very likely exclusively Cr(III). This assumption was checked by spiking the sample with 2.0×10^{-15} mol/L of Cr(VI). A reasonable recovery of 2.7×10^{-15} mol/L of Cr(VI) was found. Then a synthetic seawater sample spiked with Cr(III) and Cr(VI) at a concentration level of 2.0×10^{-15} and 3.0×10^{-15} mol/L, respectively, were analyzed. Again, the very satisfactory recovery was found. This method has proven to be most reliable for determination of Cr.

Using the proposed method, the Cr(III) and total chromium contents in water samples were further determined. The Cr contents measured were summarized in Table 1. The amount of Cr(VI) calculated from the amount difference between total chromium and Cr(III) was determined within 95% confidence interval. It was found that there was no significant difference between total chromium and Cr(III) amounts found in each sample tested. Only Cr(III) could be detected in mineral waters, drinking waters and tap water, respectively. The result found might be due to some minerals reduced Cr(VI) to Cr(III).

4. Conclusions

We have firstly presented the successful use of dual channels on glass chip with CL detection system used for the determination of Cr(III) and total chromium in water samples. Cr(III) was determined by measuring the light emitted as a result of the Cr(III)-catalyzed reaction between luminol and hydrogen peroxide. Total chromium was achieved after Cr(VI) was reduced to Cr(III) using acidic sodium hydrogen sulfite. The simple dual T channels and the utilizing of negative pressure pumping system make possible very quickly and seems to be very attractive and convenient method for chromium species analysis. The analysis time was less than 1 min per sample. The system is simple, extremely sensitive and high efficient. The calibration curve for Cr(III) was linear in the range between 1.0×10^{-15} and 1.0×10^{-13} mol/L and the excellent limit of detection was low as 1.6×10^{-16} mol/L. This strategy described has proven to be reliable for the determination of Cr(III) and total chromium in water samples with no need of separation and preconcentration. This perspective is not limited for only chromium determination-not the least because it offers possibility for the determination of other analytes involving similar chemistries.

Acknowledgements

References

[1] J.O. Nriagu, E. Nieboer, Chromium in the Natural and Human Environment, Wiley, New York, 1988.
[2] J. Kotaś, Z. Stasicka, Environ. Pollut. 107 (2000) 263.

[3] http://www.epa.gov/OGWDW/mcl.html.
[4] A.A. Mohamed, A.T. Mubarak, Z.M.H. Marstani, K.F. Fawy, Talanta 70 (2006) 460.
[5] D.G. Themelis, F.S. Kika, A. Economou, Talanta 69 (2006) 615.
[6] M.V. Balarama Krishna, K. Chandrasekaran, S.V. Rao, D. Karunasagar, J. Arunachalam, Talanta 65 (2005) 135.
[7] W. Som-Aum, S. Liawruangrath, E.H. Hansen, Anal. Chim. Acta 463 (2002) 99.
[8] F.A. Silva, C.C. Federici Padilha, L.E. Pezzato, M.M. Barros, P.M. Padilha, Talanta 69 (2006) 1025.
[9] R.A. Gil, S. Cerutti, J.A. Gásquez, R.A. Olsina, L.D. Martinez, Talanta 68 (2006) 1065.
[10] L.A. Pereira, I. Amorim, J.B. Borba da Silva, Talanta 68 (2006) 771.
[11] J. Chwastowska, W. Skwara, E. Sterlińska, L. Pszonicki, Talanta 66 (2005) 1345.
[12] T. Sumida, T. Ikenoue, K. Hamada, A. Sabarudin, M. Oshima, S. Motomizu, Talanta 68 (2006) 388.
[13] Y.K. Agrawal, K.R. Sharma, Talanta 67 (2005) 112.
[14] J. Threeprom, S. Purachaka, L. Potipan, J. Chromatogr. A 1073 (2005) 291.
[15] J.S. Wang, K.-H. Chiu, Anal. Sci. 20 (2004) 841.
[16] J. Threeprom, R. Meelapsom, W. Som-Aum, J.-M. Lin, Talanta 71 (2007) 103–108.
[17] B. Gammelgaard, Y.-P. Liao, O. Jøns, Anal. Chim. Acta 354 (1997) 107.
[18] F. Priego-Capote, M.D. Luque de Castro, J. Chromatogr. A 1113 (2006) 244.
[19] C.-F. Yeh, S.-J. Jiang, J. Chromatogr. A 1029 (2004) 255.
[20] W.-P. Yang, Z.-J. Zhang, W. Deng, J. Chromatogr. A 1014 (2003) 203.
[21] W.-P. Yang, Z.-J. Zhang, W. Deng, Anal. Chim. Acta 485 (2003) 169.
[22] A. Manz, D.J. Harrison, E. Verpoorte, C. Fettinger, H. Ludi, H.M. Widmer, Chimia 45 (1991) 103.
[23] A. Manz, D.J. Harrison, E. Verpoorte, H.M. Widmer, Adv. Chromatogr. 33 (1993) 1.
[24] S.C. Jacobson, A.W. Moore, J.M. Ramsey, Anal. Chem. 67 (1995) 2059.
[25] J.P. Kutter, R.S. Ramsey, S.C. Jacobson, J.M. Ramsey, J. Microcol. Sep. 10 (1998) 313.
[26] K. Tsukagoshi, M. Hashimoto, R. Nakajima, A. Arai, Anal. Sci. 16 (2000) 1111.
[27] X.-J. Huang, Q.-S. Pu, Z.-L. Fang, Analyst 126 (2001) 281.
[28] X.Y. Huang, J.N. Wang, L. Chen, J.C. Ren, Chin. Chem. Lett. 15 (2004) 683.
[29] Y. Xu, F.G. Bessoth, J.C.T. Eijkel, A. Manz, Analyst 125 (2000) 677.
[30] Y. Xu, F.G. Bessoth, A. Manz, Chin. J. Anal. Chem. 28 (2000) 876.
[31] B.-F. Liu, M. Ozaki, Y. Utsumi, T. Hattori, S. Terabe, Anal. Chem. 75 (2003) 36.
[32] Q.J. Song, G.M. Greenway, T. McCreedy, J. Anal. At. Spectrom. 18 (2003) 1.
[33] Q.J. Song, G.M. Greenway, T. McCreedy, J. Anal. At. Spectrom. 19 (2004) 883.
[34] W.R. Seitz, W.W. Suydam, D.M. Hercules, Anal. Chem. 44 (1972) 957.
[35] A. Townshend, Analyst 115 (1990) 495.
[36] S. Nielsen, E.H. Hansen, Anal. Chim. Acta 366 (1998) 163.
[37] S. Nielsen, S. Stürup, H. Spliid, E.H. Hansen, Talanta 49 (1999) 1027.
[38] D.J. Harrison, A. Manz, Z. Fan, H. Lüdi, H.M. Widmer, Anal. Chem. 64 (1992) 1926.
[39] L.J. Nelstrop, P.A. Greenwood, G.M. Greenway, Lab Chip 1 (2001) 138.
[40] M.L. Grayeski, Anal. Chem. 59 (1987) 1243A.
[41] A.A. Alwarthan, A. Townshend, Anal. Chim. Acta 196 (1987) 135.
[42] C. Xiao, D.W. King, D.A. Palmer, D.J. Wesolowski, Anal. Chim. Acta 415 (2000) 209.
[43] R. Escobar, Q. Lin, A. Guiraúm, F.F. de la Rosa, Analyst 118 (1993) 643.
[44] C.A. Chang, H.H. Patterson, Anal. Chem. 52 (1980) 653.
[45] A. Economou, A.K. Clark, P.R. Fielden, Anal. Commun. 35 (1998) 389.
[46] J.C. Miller, J.N. Miller, Statistic for Analytical Chemistry, 3rd ed., Ellis Horwood Limited, 1993.
[47] M. Kakuta, F.G. Bessoth, A. Manz, Chem. Rec. 1 (2001) 395.
[48] J. Lameiras, M.E. Soares, M.L. Bastos, Analyst 123 (1998) 2091.
[49] S. Matsuoka, Y. Tennichi, K. Takehara, Analyst 124 (1999) 787.

Sequential injection spectrophotometric determination of zinc(II) in pharmaceuticals based on zinc(II)–PAN in non-ionic surfactant medium

Wish Thanasarakhan [a], Saisunee Liawruangrath [a,*], Sunanta Wangkarn [a], Boonsom Liawruangrath [b]

[a] *Department of Chemistry, Faculty of Science, Chiang Mai University, Chiang Mai 50200, Thailand*
[b] *Department of Pharmaceutical Chemistry, Faculty of Pharmacy, Chiang Mai University, Chiang Mai 50200, Thailand*

Abstract

A sequential injection analysis (SIA) spectrophotometric method for the determination of trace amounts of zinc(II) with 1-(2-pyridylazo)-2-naphthol (PAN) is described. The method is based on the measurement of absorbance of the zinc(II)–PAN chelate solubilized with a non-ionic surfactant, Triton X-100, no extraction procedure is required in the proposed method, yielding a pink colored complex at pH 9.5 with absorption maximum at 553 nm. The SIA parameters that affect the signal response have been optimized in order to get the better sensitivity and minimum reagent consumption. A linear relationship between the relative peak height and concentration was obtained in the concentration range of $0.1–1.0 \,\mu g \, ml^{-1}$. The limit of detection (LOD, defined as 3σ) and limit of quantification (LOQ, defined as 10σ) were 0.02 and $0.06 \,\mu g \, ml^{-1}$, respectively. The sample throughput about 40 samples/h was obtained. The repeatability were 1.32 and 1.24% ($n = 10$) for 0.1 and $0.5 \,\mu g \, ml^{-1}$, respectively. The proposed method was successfully applied to the assay of zinc(II) in three samples of multivitamin tablets. The results were found to be in good agreement with those obtained by flame atomic absorption spectrophotometric method and with the claimed values by the manufactures. The *t*-test showed no significant difference at 95% confidence level.
© 2006 Published by Elsevier B.V.

Keywords: Sequential injection analysis; PAN; Zinc(II); Triton X-100

1. Introduction

Zinc(II) is an essential element in many other living beings. It plays many important roles in all replications, protein synthesis, gene expression, cell division and in the metabolism of nucleic acids, and acts as a cofactor in numerous enzymes. Zinc(II) acts predominantly as a Lewis acid, and is found in many metalloenzymes such as carboxypeptidase and carbonic anhydrase [1]. The wound healing effect of zinc(II)—containing ointments had been already known in the ancient world, and zinc(II) has increasingly been used as a remedy for growth disorders due to malnutrition, interactions between zinc(II) and growth hormones [2]. Zinc(II) deficiency may also cause a variety of other symptoms such as a lack of appetite, a reduced sense of taste,

an enhanced disposition for inflammations and an impairment of the immune system [3]. Furthermore, zinc compounds have bactericidal activity since they can precipitate and denature several bacterial proteins. Thus, they have been employed in dermatology, mouthwashes and ophthalmic solutions as antiseptic and disinfectant agents. In addition, zinc(II) is present in multivitamin and multimineral preparations [4]. For this reason, the determination of zinc(II) in pharmaceutical preparations is an important analytical field.

Various spectrophotometric methods were proposed for determination of zinc(II) contents in pharmaceutical preparations by using complexing reagents such as 7-(4-nitrophenyl azo)-8-hydroxyquinoline-5-sulfonic acid (ρ-NIAZOXS) [5], 2-(5-nitro-2-pyridazo)-5-(*N*-propyl-*N*-sulfopropylamino)phenol (nitro-PAPS)[6], 1-(phenyl-2-pyridyl)carbilidene-5-resorcilidene thiocarbohydrazone (PPRT) [7], 3-(5′-mercapto-1′,2′4′-triazole-3′-azo)-2,4-dihydroxybenzoic acid (METRIA-REZ-γ) [8], 2-(2′,4′-dihydroxyphenylazo-1′) benzimidazole
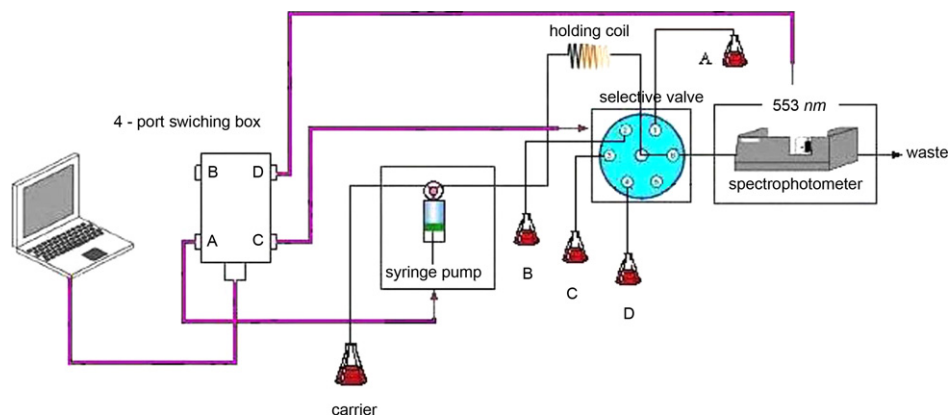
Fig. 1. SI manifold for the determination of zinc(II): (A) (valve 1) a combined buffer solution and masking agent; (B) (valve 2) Triton X-100; (C) (valve 3) sample; (D) (valve 4) PAN solution and 150 cm/0.7 mm (length/i.d.) holding coil.

(BIAR) and 3-mercapto-5-(2′-hydroxynaphtylazo-1′)-1,2,4,-triazole (METRIAN) [9], 2,2′-dipyridyl-2-pyridylhydrazone (DPPH)[10], xylenol orange [11], 1-(2-tiazolylazo)-2-naphthol(TAN) [12], 4-(pyridyl-2-azo)-resorcinol (PAR) [13,14], 3-acetylformazans [15] and 1-(2-pyridylazo)-2-naphthol [16,17].

PAN is a sensitive reagent used for determining several transition metals. It is practically insoluble in water and reacts with zinc(II) to yield a non-polar pink color complex, generally extracted into an organic solvent such as ether or chloroform [18]. This method took an unacceptably long time and tedious to measure the absorbance of the organic phase with gradually changing the pH of the aqueous phase for the complex of reagents processing high distribution constant [19]. Recently, the use of micelles in analytical chemistry involving the beneficial alteration of metal ion–ligand complex spectral properties via surfactant association is growing [20,21–25].Usually, the metal-complexes formed in the micellar systems, a pseudo-single-phase formed by surfactant micelles in an aqueous solution, are more stable than those formed in the absence of micelles. Surfactants and micellar systems stabilized water-insoluble complexes, and the size of micelles provided the equilibrium to be attained quickly with a change in pH. Currently, surfactant system used in development of many spectrophotometric methods for determining micro amounts of metal ions to improve the sensitivity for these methods [26].

Several flow injection analysis (FIA) methods for pharmaceutical assays have been reported in recent reviews [27,28]. Although they are superior to the batch-wise methods in that they provide relatively high sample throughput, low reagents and sample consumptions, low analysis time and cost effectiveness. Some of which typically uses high reagent consumptions and makes a large amount of waste especially dealing with expensive chemicals, hazardous reagents, or online/remote site applications. Thus, the FIA technique is a relatively expensive method by comparison with the second generation termed sequential injection analysis (SIA).

SIA has been introduced in 1990, as a new concept automatic sample analysis. It is simple, rapid, low sample and

reagent consumption. Additionally, it is fully automated system to make it fast and efficient that is important to many routine tasks. In SIA, there is no need for special system reconfiguration of manifold to apply different chemicals into the systems, while all major parameters such as reagents and sample volumes, flow rate, order of mixing and reaction time can be optimized by computer-control. It is compatible with both optical and electrochemical detectors. SIA has been used for pharmaceutical assays that were highlighted in recent reviews [29].

This paper proposes the use of a SIA method for the spectrophotometric determination of zinc(II), using PAN as chromogenic reagent. To avoid the extraction procedure, it was found that Zn(II)–PAN complex can be solubilized by a non-ionic surfactant, Triton X-100. Because of the high sensitivity inherent in the use of PAN, it was decided to investigate solubilization of Zn(II)–PAN complex as the basis to develop a novel method for zinc(II) determination with Triton X-100. The pink colored Zn(II)–PAN complex in micellar media is detected spectrophotometrically at 553 nm. NaF and KCN were used as masking agents for Fe(III), Mn(II) and Cu(II). The proposed method has been successfully applied to the determination of zinc(II) in pharmaceutical preparations.

2. Experimental

2.1. Instrumentations

The developed SIA manifold (Fig. 1) was arranged using the following equipment: a FIAlab® 3000 system (FIAlab® Instruments, USA) consists of a syringe pump (syringe reservoir 2.5 ml) and a six-port selection cheminert valve (Valco Instrument Co., USA), which is connected to a four-port switching box. The four ports undergo the following functions:

- Port A is connected to a syringe control (CAVRO XL 3000 stepper motor-driven syringe pump).
- Port B is available for other instruments (where necessary).
- Port C is connected to a valve control unit.
- Port D is connected to Jenway 6400 Spectrophotometer.

A Jenway 6400 Spectrophotometer (Jenway, Dunmow, Essex, UK) with a model QS1.000 (Hellma, Germany) flow cell (10 mm path length, 120 μl inner volume) over the wavelength range 360–800 nm. The flow system used PTFE tubes as the liquid channels. The holding coil was constructed by winding the PTFE tubing around the small test tube. An absorbance signal can be retrieved directly from a Jenway 6400 spectrophotometer via the RS-232 interface. The absorbance of the colored Zn(II)–PAN complex was monitored at 553 nm through a 10 mm path length flow cell. All electrical devices of the manifold were computer controlled by means of a home-made program written in Microsoft Visual Basic 6.0.

2.2. Reagents and solutions

All chemicals were of analytical reagent grade, and used without further purification. Distilled deionised water was used throughout which was prepared by passing distilled water through a Milli-Q system (Millipore, USA).

Standard zinc(II) solution was prepared by dissolving an appropriate weight of $ZnCl_2$ in distilled deionised water. The stock solution was standardized by EDTA titration, it contains $1000\ \mu g\ ml^{-1}$ of Zn^{2+}. The working standard solutions were prepared just before use by an appropriate dilution of the stock solution.

PAN (Aldrich) stock solution ($1 \times 10^{-2}\ mol\ l^{-1}$) was prepared from the pure product by dissolving an appropriate weight using ethanol/water mixtures (9:1) as solvent.

Triton X-100 (Sigma) solution was prepared by an appropriate dilution with distilled deionised water.

Combined masking agent-buffer solution was prepared by adding 85 ml of 0.20 M Na_2CO_3 to 15 ml of 0.20 M $NaHCO_3$ solution (pH 9.5) followed by $1.2 \times 10^{-3}\ mol\ l^{-1}$ KCN and $5 \times 10^{-3}\ mol\ l^{-1}$ NaF solutions.

2.3. Sequential injection method

A four-port RS 232 switching box receives an activation command from the PC through master port. When the system is initialized, it activates port A (Fig. 1) move the piston of the syringe to zero position. It also activates port C to actuate with the valve at position 6. Then, it activates port A to drive the syringe to aspirate the carrier (water) with the desired volume. After that, it activates port C to actuate the valve at position 1 (combined masking agent-buffer solution). Then, it activates port A to drive the syringe to aspirate the desired volume of combined solution. It again activates port C to actuate the valves at position 2 (Triton X-100), 3 (sample) and 4 (PAN reagent), respectively followed by activating port A to drive the syringe to aspirate the desired volume of solution. While the PC is sending the empty syringe command through port A, it activates port D and receives absorbance signals from the spectrophotometer and drives the plot module to plot the SIA grams on the screen. The maximum peak heights were also detected at 553 nm and displayed in this process. The time required to analyze one sample is approximately 1.5 min. Table 1 lists the steps of the procedure entered to the FIAlab for windows software.

Table 1
Experimental protocol as shown in the FIAlab for Windows software

Loop Start (#) 3
  Fill Syringe
    SyringePump Flowrate ($\mu l\ s^{-1}$) 100
    SyringePump Valve In
    SyringePump Delay Until Done
    SyringePump Aspirate (μl) 1500
    SyringePump Valve Out
    SyringePump Delay Until Done

  Standard to holding coil
    Valve port 1
    SyringePump Valve Out
    SyringePump Flowrate ($\mu l\ s^{-1}$) 25
    SyringePump Aspirate (μl) 30
    SyringePump Delay Until Done

    Valve port 2
    SyringePump Valve Out
    SyringePump Flowrate ($\mu l\ s^{-1}$) 25
    SyringePump Aspirate (μl) 30
    SyringePump Delay Until Done

    Valve port 3
    SyringePump Flowrate ($\mu l\ s^{-1}$) 25
    SyringePump Aspirate (μl) 50
    SyringePump Delay Until Done

    Valve port 4
    SyringePump Flowrate ($\mu l\ s^{-1}$) 25
    SyringePump Aspirate (μl) 30
    SyringePump Delay Until Done

  Send sample to detector
    Valve port 6
    SyringePump Valve Out
    SyringePump Flowrate ($\mu l\ s^{-1}$) 40
    SyringePump Empty
    SyringePump Delay Until Done

  Clean detector
    SyringePump Flowrate ($\mu l\ s^{-1}$) 100
    SyringePump Valve In
    SyringePump Delay Until Done
    SyringePump Aspirate (μl) 250
    SyringePump Valve Out
    SyringePump Delay Until Done

    Valve port 6
    SyringePump Valve Out
    SyringePump Empty
    SyringePump Delay Until Done

Loop End

2.4. Preparation of pharmaceutical sample solutions for zinc(II) determination

Ten Centrum From A to Zinc® multivitamin and multimineral tablets were weighed, ground, placed in a conical flask and treated with 50 ml of $0.1\ mol\ l^{-1}$ HCl. The solution was shaken mechanically and filtered, the precipitate was thoroughly washed with deionized water, then the combined filtrate was transferred into a 1000 ml volumetric flask and diluted to the mark with deionised water, the final concentration of zinc(II) ions was about $6\ \mu g\ ml^{-1}$.
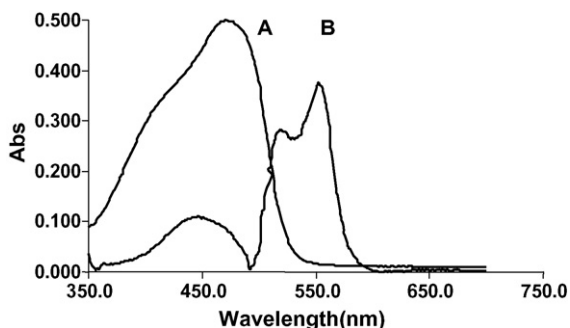
Fig. 2. Absorption spectra of Zn(II) complex and its reagent blank curve. (A) PAN-Triton X-100, (B) Zn(II)–PAN-Triton X-100. The concentration of Zn(II) = 5 $\mu g \, ml^{-1}$, PAN = 1.0×10^{-4} mol l^{-1}, and Triton X-100 = 1%, respectively; in carbonate buffer solution pH 9.0.

Fig. 3. Influence of the pH on response and precision.

2.5. Atomic absorption spectrometric method

Flame atomic absorption spectroscopy was performed with an AA-680 atomic absorption spectrophotometer (Shimadzu, Japan). The Centrum *From A to Zinc*® multivitamin and multi-mineral samples were prepared as described above. For FAAS measurements, the absorption value of zinc was measured at 213.9 nm with hollow cathode lamp.

3. Results and discussion

Preliminary experiments revealed that suitable conditions for dissolving Zn(II)–PAN complex in aqueous solution could be achieved by adding some non-ionic surfactants such as Tween-80, Triton X-100, poly(vinylalcohol) were successively at different concentrations (0.1–1.0%, v/v) into the reaction medium. Preliminary experiments pointed out those cationic surfactants could not be used for this purpose. In fact, the analytical signal was not observed in the presence of cetyltrimethylammonium or cetrypriridinium chloride, in view of the hydration caused by the ionic group [30] that reduced the molecular forces impairing the dissolution, thus the establishment of the organized medium. Cationic surfactants were then not investigated further. Among the different non-ionic surfactants tested, Triton X-100 was selected because the attainable sensitivity was the highest.

3.1. Spectral characteristics

The absorption spectra of PAN and its zinc(II) complex in the presence of Triton X-100 are shown in Fig. 2. In the presence of surfactant, the pink color of zinc(II) complex formed at pH 9.0 showing maximum absorbance of 0.368 at 553 nm (spectrum B), the blank (PAN-Triton X-100) shows the maximum absorbance of 0.498 at 474 nm (spectrum A). Hence, further measurements were made at 553 nm because at this wavelength the bank signal was found to be minimum (see Fig. 2).

3.2. Optimum conditions for the reaction

The parameters that influence the sensitivity, accuracy and reproducibility of the proposed method for determining the ana-

lyte of interest, zinc(II) were studied in order to establish the optimum working configurations. In all cases both the mean relative peak height (for $n = 4$ repetitive determinations) and the relative standard deviation were used as a criteria for establishing the most appropriate parameters. All the optimization steps were carried out with a chosen zinc(II) concentration of 0.5 $\mu g \, ml^{-1}$, with the fixed concentrations of 0.5% (v/v) Triton X-100, and 1×10^{-5} mol l^{-1} PAN.
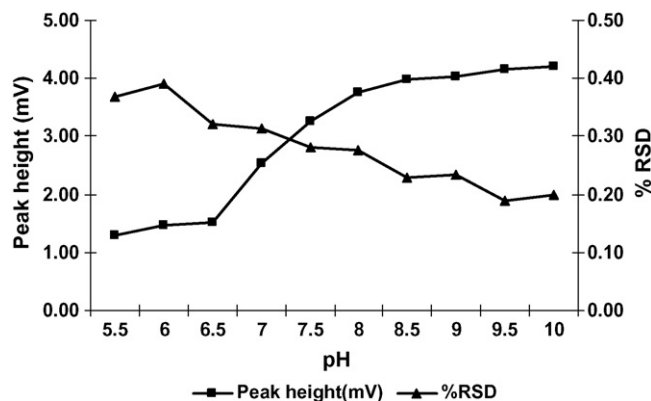
3.2.1. Effect of pH

The influences of pH on the absorbance (as peak height in mV) of zinc(II) complexes were studied over the pH range 5.5–10 at 553 nm (Fig. 3). The pH was adjusted to the desired values using carbonate buffer. It was found that, the chelate was completed at pH values higher than 7, the peak height became significant when the pH exceeded about 10. A pH 9.5 was chosen as the optimum for these reasons and because the carbonate–bicarbonate buffer system has maximum buffer capacity at this pH. The effect of carbonate buffer concentration was studied over the range 0.01–0.1 mol l^{-1}. The results demonstrate that it slightly increases in the range 0.01–0.05 mol l^{-1}. Further increment of the buffer concentrations the peak heights remain constant over the concentration range 0.05–0.1 mol l^{-1}. Thus, the concentration 0.05 mol l^{-1} of carbonate buffer was chosen for subsequent experiments.

3.2.2. Aspiration order of reagents and sample

In reactions involving multiple zone penetrations, it is essential to examine the aspiration order of reagents and sample [31]. Several aspiration orders have been designed using the SI set-up shown in Table 2. It was found that, the order of the aspiration of the sample and reagent was proved be critical. The appropriate order for aspiration of reagents and sample are as follows: combined masking agent-buffer solution, Triton X-100, sample and PAN reagent, respectively because it provides the highest signal (mean peak height of 5.54 mV, $n = 4$) with the best repeatability (R.S.D. = 0.24%) and hence this aspiration order is chosen for subsequent measurements.

3.2.3. Flow rate

In any flow-based analysis procedure the response is dependent on the reagents and sample flow rates and thus it is necessary

Table 2
Aspiration orders of sample and reagent

Aspiration order	Peak height (mV) (mean ± S.D.)
Sam./Triton.[a]-masking buffer[b]-PAN	3.38 ± 1.07
Masking buffer-PAN-Sam./Triton.[a]	3.53 ± 0.31
Masking buffer-Sam./Triton[a].-PAN	3.72 ± 0.42
Masking buffer-Sam.[c]-Triton.[d]-PAN	5.02 ± 0.78
Masking buffer-Triton.[d]-Sam.[c]-PAN	5.54 ± 0.24
Masking buffer-Triton.[d]-PAN-Sam.[c]	4.84 ± 0.85
Sam.[c]-masking buffer-Triton.[c]-PAN	4.77 ± 1.23
Sam.[c]-Triton.-masking buffer-PAN	4.58 ± 0.93
Sam.[c]-masking-PAN-Triton.	3.91 ± 0.78

[a] Sample (Zn(II) 1 ppm) in 0.5% (v/v) Triton X-100.
[b] Combined masking agent and buffer solution pH 9.5.
[c] Sample (Zn(II) 0.5 $\mu g\,ml^{-1}$).
[d] 0.5% (v/v) Triton X-100.

to optimize them to achieve the greatest sensitivity, reproducibility, sample throughput, etc.

3.2.3.1. Optimization of sample and reagents flow rates.
It was obvious that the flow rate of aspiration of sample and reagent were significant with the peak height. The reagent and sample flow rates were investigated from 15 to 50 $\mu l\,s^{-1}$ at every 5 $\mu l\,s^{-1}$ interval while the flow rate of sending sample to detector kept constant at 50 $\mu l\,s^{-1}$. As the flow rate increases the peak height increases up to 35 $\mu l\,s^{-1}$, where after it tends to level off. The flow rate chosen for yielding the best results was 25 $\mu l\,s^{-1}$ (best precision) and best for Triton X-100 aspiration cause faster aspirate the bubble can occur in the line of stream.

3.2.3.2. Flow rate of sending sample to detector.
The flow rates of sending the sample to detector were investigated from 15 to 50 $\mu l\,s^{-1}$ at every 5 $\mu l\,s^{-1}$ intervals the flow rate of aspiration of sample and reagent were kept constant at 25 $\mu l\,s^{-1}$. It was observed that the peak height increased with increasing in the flow rate up to 40 $\mu l\,s^{-1}$ and then it decreased with provision of the faster flow rates. Thus, a flow rate of 40 $\mu l\,s^{-1}$ was chosen and used for subsequent measurements due to its highest peak height and precision.

3.2.4. Sample and reagents aspiration volumes optimizations
To minimize the consumption of reagent volumes while maintaining the best results, both of sensitivity (peak height) and precision, of the procedure, thus these parameters were optimized. The volume of buffer solution, sample and PAN reagent were studied. When varying the volume of solution of interest whereas the others were kept constant at 50 μl^{-1}. The results are given in Table 3.

3.2.4.1. Buffer solution aspiration volume.
The influence of the buffer volume was investigated in the range of 10–100 μl at every 10-μl interval. There was no significant difference in the response when the volume increases. A buffer solution volume of 30 μl was chosen as optimum due to the precision and minimum volume of buffer solution consumed.

3.2.4.2. Sample and reagent volumes.
The influence of the sample and PAN reagent volumes were studied between 10 and 100 μl at every 10 μl interval. The volumes of buffer solution and surfactant were kept constant at 30 μl. It was found that the maximal response was obtained at a volume of 50 μl for sample volume and it gave the best precision (0.20% R.S.D.). For PAN reagent volume, it was found that as the aspiration volume increased the peak height increased up to 30 μl and remained almost constant afterwards. A volume of 30 μl was chosen as an optimum reagent volume for subsequent measurements. In addition, this volume gave a fine base line in SIA grams.

3.2.5. The effect of PAN concentration
The effect of PAN concentration was studied in the range 1.0×10^{-5} to $2.0 \times 10^{-6}\,mol\,l^{-1}$. The peak height increases with increasing concentration up till $5 \times 10^{-5}\,mol\,l^{-1}$ and started leveling off (Fig. 4). The concentration of PAN at 5.0×10^{-5} and $10 \times 10^{-5}\,mol\,l^{-1}$ have the best peak heights but the %R.S.D. at $5.0 \times 10^{-5}\,mol\,l^{-1}$ is lower than that obtained at 10×10^{-5} hence the $5 \times 10^{-5}\,mol\,l^{-1}$ PAN was chosen for further works.

3.2.6. The effect of concentration of Triton X-100
Without addition of surfactant, Zn(II)–PAN complex cannot be dissolved in aqueous phase thus in the system the precipitate

Table 3
Influence of aspiration volume on peak height (sensitivity) and precision

Parameters	Volume (μl)									
Buffer solution	10	20	30	40	50	60	70	80	90	100
Mean RPH[a]	4.05	4.08	4.07	4.09	4.09	4.07	4.07	4.06	4.08	4.09
%R.S.D.[b]	0.86	0.97	0.20	0.44	1.06	0.40	0.90	1.26	1.06	1.10
Sample	10	20	30	40	50	60	70	80	90	100
Mean RPH[a]	3.68	3.79	4.04	4.07	4.20	4.19	4.19	4.18	4.18	4.19
%R.S.D.[b]	0.91	0.59	0.83	1.08	0.20	0.46	0.64	0.54	0.43	0.70
PAN reagent	10	20	30	40	50	60	70	80	90	100
Mean RPH[a]	3.98	4.06	4.25	4.22	4.22	4.19	4.17	4.21	4.17	4.18
%R.S.D.[b]	0.95	0.90	0.17	0.54	0.66	0.46	1.10	0.54	0.81	1.06

[a] Mean relative peak height ($n = 4$ repetitive determinations).
[b] Percentage relative standard deviation.

Fig. 4. Influence of the concentration of reagent, PAN on response and precision.

Table 4
Tolerance limits of interferences ions on the determination of 1 μg ml^{-1} zinc(II) at optimum conditions

Ion	Tolerated ration of interferences ions to zinc(II)
Ca^{2+}, Mg^{2+}, Al^{3+}	500[a]
Cu^{2+}, Co^{2+}, Ni^{2+}	750[a]
Fe^{3+}, Mn^{2+}	50
Cd^{2+}	75
Pb^{2+}	250[a]
Cr^{2+}, Ag^{+}, Hg^{2+}	550
I^{-}, Cl^{-}	1000

[a] More than this amount of ions cause precipitation.

can accumulate on the tubing inner wall and flow cell, impairing the instrumentation of the method. Concentration of this surfactant plays an important role in the system designed. For concentration higher than 0.0130% (v/v) (critical micelle concentration), the products formed aggregated themselves. The influence concentration of Triton X-100 was studied over the range 0.1–1.0% (v/v) and the volume of surfactant was kept constant at 30 μl. The response increased with an increase in concentration, the 1.0% (v/v) concentration was chosen for the best peak height and precision of the method (Fig. 5). The higher concentration than 1.0% (v/v) did not recommend because it caused high viscosity and the peak height did not related with sample concentration.

3.2.7. Effect of reaction coil dimensions

The effect of reaction coil diameter on peak height was studied from 0.51 to 1.60 mm (all lengths were 150 cm) at five different diameters based on availability. A coil diameter of 0.7 mm gave the highest signal. As the diameter increased beyond 0.70 mm the relative peak height decreased and also worst precision was obtained.

3.2.8. Interferences

The effect of metallic ion interferences on the determination of 1 μg ml^{-1} zinc(II) using the proposed method were tested. Results are summarized in Table 4. The tolerance limit was taken

as the concentration of added ion causing less than 3% relative error.

Fe(III), Mn(II) and Ca(II) are possible interfering species in this method. The interfering species were eliminated by using appropriate masking agent and pH values Fe(III) by the addition of sodium fluoride and Mn(II) and Ca(II) by addition of potassium cyanide as masking agent, and the careful control of the pH of the buffer solution.

3.3. Figures of merit

Using the optimized parameters listed in Table 5, the SIA system was evaluated for its response for different concentrations of standard zinc(II) solutions. Under the optimum conditions, the calibration curve was linear between 0.1 and 1.0 μg ml^{-1} with the following calibration equation: $Y = 56.835X + 0.895$, with a correlation coefficient (R^2) of 0.9997, where Y and X represent SIA signal as peak height in mV, and zinc(II) concentrations in μg ml^{-1}, respectively. The detection limit was calculated (S/N = 3σ, σ is the standard deviation of the blank ($n = 10$)) is 0.02 μg ml^{-1}. The quantification limit was calculated (S/N = 10σ) is 0.06 μg ml^{-1}. The repeatability of the method was checked for 0.1 and 0.5 μg ml^{-1} standard solution, the R.S.D. values of 1.32 and 1.24, respectively, were registered ($n = 10$ measurements in each case). The sample throughput was 40 h^{-1}.

Table 5
Optimization parameters

Parameters	Optimized value
pH of carbonate buffer solution	9.5
Flow rate	
Flow rate of aspiration of sample and reagents	25 μl s^{-1}
Flow rate of sending sample to detector	40 μl s^{-1}
Buffer aspiration volumes	30 μl
Triton X-100 aspiration volumes	30 μl
Sample aspiration volumes	50 μl
PAN reagent aspiration volumes	30 μl
PAN concentration	5×10^{-5} mol l^{-1}
Triton X-100 concentration	1% (v/v)
Reaction coil diameter	0.7 mm
Wave length	553 nm
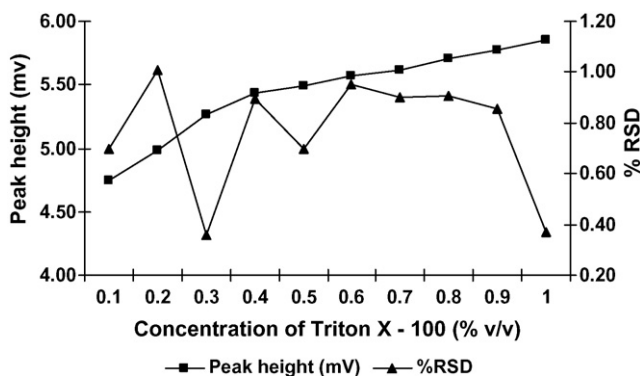
Fig. 5. Influence of concentration of Triton X-100 on response and precision.

Table 6
Determination of zinc(II) in pharmaceutical preparations sample with the propose SIA method and flame atomic absorption spectrophotometric method

Sample	SIA (mg/tablet) ($n = 6$)	FAAS (mg/tablet) ($n = 6$)	Calculated t-test value	% labeled amount
Tablet 1	15.06 ± 0.21	14.89 ± 1.25	0.60	100.40
Tablet 2	14.90 ± 0.95	15.01 ± 0.60	0.27	99.33
Tablet 3	15.08 ± 0.60	15.11 ± 1.18	0.13	100.53

The claimed value for all samples was 15 mg/tablet.

3.4. Determination of zinc(II) in pharmaceutical samples

The developed SIA method has been satisfactorily applied to the determination of zinc(II) in three commercial pharmaceutical preparations. Centrum tablets were analyzed. Comparative determination of zinc(II) in the same sample solutions by atomic absorption spectrophotometry (AAS) was also carried out. The zinc(II) content found in pharmaceutical preparations by the proposed SIA procedure and AAS was compared and then the results were given in Table 6. The null hypothesis was used and t-test with multiple samples (paired by difference) was applied to examine whether the two methods differ significantly at 95% confidence level. The t calculated values for samples tablet 1, 2 and 3 are 0.60, 0.27 and 0.13, respectively, for SIA and AAS methods. The tabulated critical value of t at 95% confidence level and five degrees of freedom is 2.57 [32]. Since the calculated values is less than the critical value, the null hypothesis cannot be rejected and it follows that there is no statistically significant difference between the two methods.

4. Conclusions

The proposed SIA system for zinc(II) in pharmaceutical preparation analysis respects to sensitivity, detection limit, simplicity, repeatability. Using non-ionic surfactant, Triton X-100, reduce the time for complex extraction into organic phase prior to analysis by spectrometric method. Moreover, it uses microlitres of the reagent and solutions per analytical cycle. The system is fully automated and is able to determine zinc(II) concentration at a frequency of 40 samples/h with a relative standard deviation <1.5%. The calibration graph is linear between 0.1 and $1.0 \, \mu g \, ml^{-1}$ of zinc(II) with a detection limit $0.02 \, \mu g \, ml^{-1}$. The method is suitable for routine analysis of zinc(II) in not only pharmaceuticals but also in environmental samples.

References

[1] R.W. Hay, Bio-inorganic Chemistry, Ellis Horwood Series Chemical Science, University of Stirling, Scotland, 1984.
[2] B.C. Cunningham, M.G. Mulkerrin, J.A. Wells, Science 253 (1991) 545.
[3] W. Kaim, B. Schwederski, Bioinorganic Chemistry: Inorganic Elements in the Chemistry of Life: An introduction and Guide, John Wiley & Sons, England, 1994.
[4] R. Matíes, F. Jiménez, J.J. Arias, Anal. Lett. 30 (1997) 2059.
[5] M.G.A. Korn, A.C. Ferreira, L.S.G. Teixeira, C.S. Costa, J. Braz. Chem. Soc. 10 (1999) 46.
[6] T. Makino, Clin. Chim. Acta 187 (1991) 209.
[7] G. Gonzales, R. Beltran, J.L. Gomez Ariza, A. Guiraum Perez, Quim. Anal. 8 (1989) 81.
[8] S. Zanęba, Farm Pol. 48 (1992) 575.
[9] S. Zaręba, Pharm. Acta Helvetiae 70 (1995) 195.
[10] D.G. Themelis, P.D. Tzannavaras, A.A. Liakou, H.D. Tzanavaras, J.K. Papadimitriou, Analyst 125 (2000) 2106.
[11] J.K.F. van Staden, M. Tsanwani, Fres. J. Anal. Chem. 371 (2001) 376.
[12] L.S.G. Teixeira, F.R.P. Rocha, M. Karn, B.F. Reis, S.L.C. Ferreira, A.C.S. Costa, Anal. Chim. Acta 383 (1999) 309.
[13] J. Karpińska, M. Kulikowska, J. Pharm. Biomed. Anal. 29 (2002) 153.
[14] D.S. de Jesus, R.J. Cassella, S.L.C. Ferreira, A.C.S. Costa, M.S. de Carvalno, R.E. Santelli, Anal. Chim. Acta 366 (1998) 263.
[15] A.S. Amin, Y.M. Issa, J. Pharm. Biomed. Anal. 31 (2003) 491.
[16] P.L. Mulvankar, V.M. Slinde, Analyst 116 (1991) 1081.
[17] M.J.A. Caňada, M.I.P. Requera, A.M. Díaz, Anal. Chim. Acta 375 (1998) 71.
[18] L. Cheng, K. Ueno, T. Imamura, Hand Book of Organic Analytical Reagents, CRC Press, Boca Taton, FL, 1982.
[19] A.V. Drozed, I.M. Baskir, J. Anal. Chem. 57 (2002) 16.
[20] H. Watanabe, Talanta 21 (1974) 295.
[21] M. Benamor, K. Belhamel, M.T. Praa, J. Pharm. Biomed. Anal. 23 (2000) 1033.
[22] A.S. Amin, Micro Chem. J. 65 (2000) 261.
[23] A.S. Amin, Anal. Lett. 34 (2001) 163.
[24] A.S. Amin, I.S. Ahmed, M.E. Moustafa, Anal. Lett. 34 (2001) 749.
[25] A.S. Amin, Y.M. Issa, J. Pharm. Biomed. Anal. 31 (2003) 491.
[26] F.M. El-Zawawy, M.F. El-Shahat, A.A. Mohamed, M.T. Zaki, Analyst 120 (1995) 549.
[27] P. Solich, H. Sklenářová, M. Polášek, R. Karliček, J. Flow. Inject. Anal. 18 (2001) 13.
[28] P. Solich, H. Sklenářová, M. Polášek, R. Karliček, J. Flow. Inject. Anal. 18 (2001) 118.
[29] P. Solich, M. Polášek, J. Klimundrá, J. Ruzika, Trends Anal. Chem. 22 (2003) 116.
[30] A.C.B. Dias, J.M.T. Carneiro, E.A.G. Zagatto, Talanta 63 (2004) 245.
[31] N.W. Beyene, J.F.V. Staden, R.I. Stefan, Anal. Chim. Acta 521 (2004) 223.
[32] J.C. Miller, J.N. Miller, Statistics for Analytical Chemistry, 3rd ed., Ellis Horwood, Chichester, 1984.

Application of gallium film electrode for elimination of copper interference in anodic stripping voltammetry of zinc

Katarzyna Tyszczuk, Mieczyslaw Korolczuk*, Malgorzata Grabarczyk

Faculty of Chemistry, Maria Curie-Sklodowska University, 20-031 Lublin, Poland

Abstract

For elimination of copper interference in anodic stripping determinations of zinc at mercury and bismuth film electrodes gallium ions are usually added to the supporting electrolyte. In the presented studies novel ex situ formed gallium film electrode was applied for this purpose. The proposed electrode is less toxic than mercury one while the detection limit for zinc was lower than for bismuth film electrode following the same deposition time. The calibration graph for deposition time of 60 s was linear from 5×10^{-8} to 2×10^{-6} mol L^{-1}. The determinations of zinc were carried out from undeaerated solutions. The proposed procedure was applied to zinc determination in certified reference material and tap water sample.
© 2006 Elsevier B.V. All rights reserved.

Keywords: Gallium film electrode; Zinc; Determination; Stripping voltammetry

1. Introduction

Anodic stripping voltammetry (ASV) is an accepted method for trace metal determinations, including zinc. For zinc determinations by the method a HMDE, a mercury film, a bismuth film and amalgam electrodes were used. Determination of zinc by ASV, especially at the mercury film and bismuth film electrodes, is affected by the presence of copper in the analysed samples. In the course of deposition of zinc, copper was deposited simultaneously on the electrode, from typically used supporting electrolytes, and an intermetallic compound between copper and zinc was formed. In the stripping step the compound was oxidised at a potential close to that of copper and as a consequence the zinc peak decreased and the copper peak increased, compared to these peaks obtained from solutions containing these ions separately. The problem of a copper interference on a zinc determination by ASV is discussed in a number of papers [1–8] while typical approaches to solve the problem are summarised in [9–11]. Addition of Ga(III) ions to a sample solutions is often recommended to minimise or eliminate copper interference on zinc determination. Ga(III) ions are reduced to a metallic state during the deposition step and preferentially reacts with copper.

As a result of this reaction an amount of zinc in the form of an intermetallic compound with copper decreases. Addition of Ga(III) ions to eliminate copper interference was often used for measurements carried out at mercury film electrode [4–6] and bismuth film electrode [12]. In the case of bismuth film electrode the calibration plot for zinc is linear in the narrow range of zinc concentrations [13].

In this paper a new type of film electrode, gallium film electrode is proposed to eliminate copper interference on zinc determination by ASV. The principle of elimination of copper interference at gallium film electrode was the same as in the case of mercury or bismuth film electrodes. Additionally calibration graph obtained at gallium film electrode was linear in a wider range of zinc concentrations than in the case of bismuth film electrode.

2. Experimental

2.1. Apparatus

Measurements were performed using μAutolab Electrochemical Analyser, Eco Chemie, The Netherlands. The classical three-electrode quartz cell, volume 10 mL, consisting of a glassy carbon electrode, a Pt electrode, and Ag/AgCl reference electrode was used. A glassy carbon electrode of diameter 1 mm

---

was polished daily using 0.3 μm alumina slurry on the Buehler polishing pad. UV irradiation of water samples was carried out in a quartz tube using UV-digester made by Mineral, Poland.

2.2. Reagents

0.5 mol L^{-1} acetate buffer (pH 4.6) was prepared from Suprapure CH$_3$COOH and NaOH·H$_2$O, both obtained from Merck. 0.01 mol L^{-1} Ga(NO$_3$)$_3$ was prepared from Ga(NO$_3$)$_3$ obtained from Johnson & Matthey. Standard solution of zinc at concentration 1 g L^{-1} was obtained from Fluka. Certified reference material TMRAIN-95 was obtained from the National Research Council, Canada. Other reagents were obtained from POCh Poland, and used as received. All solutions were prepared with Milli-Q water.

2.3. Sample preparation

Tap water sample was acidified to pH ca. 2 using Suprapure HNO$_3$. Acidified water samples were digested by UV irradiation for 3 h.

2.4. Standard procedure of measurements

Gallium film electrode was prepared ex situ by electrolytic deposition of gallium from stirred solution 0.05 mol L^{-1} CH$_3$COONa + 0.05 mol L^{-1} CH$_3$COOH + 1 × 10^{-4} mol L^{-1} Ga(NO$_3$)$_3$. At first the potential of 0.5 V for 5 s was applied to clean the electrode after preceding measurement. Then the potential was changed to −1.75 V for 60 s and gallium film was formed.

Such a prepared gallium film electrode was used for Zn(II) determination from solution 0.05 mol L^{-1} CH$_3$COONa + 0.05 mol L^{-1} CH$_3$COOH + Zn(II). The potential of the electrode was changed in the following sequence −1.75 V for 5 s and −1.45 V for 60 s. At potential −1.75 V the gallium film, which can be oxidised as a result of contact with air, was reduced to the metallic state. Experiments show that the short polarisation time of the electrode at potential −1.75 V leads to most reproducible Zn(II) signal. During both steps zinc was deposited while the solution was stirred using a magnetic stirring bar. Then, after a rest period of 5 s a square wave voltammogram was recorded at frequency 20 Hz in the potential range −1.25 to −0.75 V. The amplitude was 25 mV. The measurements were carried out from undeaerated solutions.

3. Results and discussion

Taking into account disadvantages of application of mercury and bismuth film electrodes for ASV of Zn(II) mentioned in Introduction it seemed desirable to find and alternative electrode material for elimination of cooper interference in zinc determination. Preliminary experiments indicate that ex situ plated gallium film electrode can be exploited for Zn(II) determination in the presence of Cu(II) by ASV, so optimisation of the parameters of determinations was carried out.
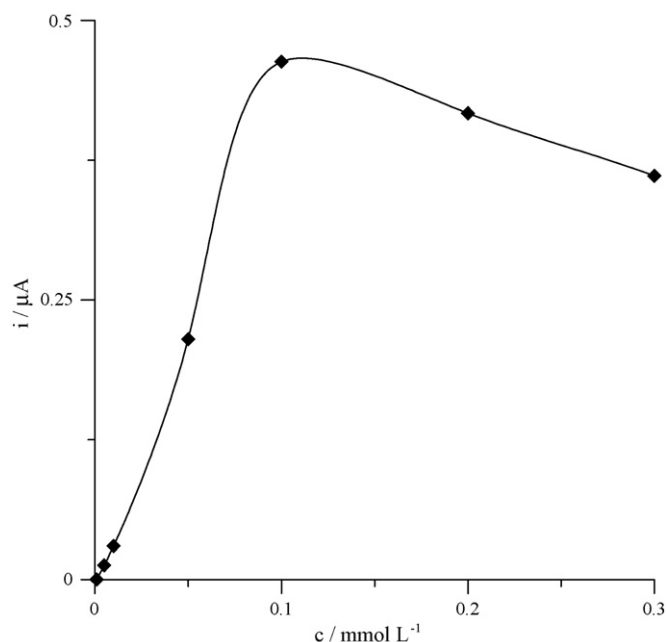
Fig. 1. The influence of gallium concentration in plating solution of pH 4.6 on the Zn(II) peak current in subsequent measurement. Concentration of Zn(II): 2 × 10^{-7} mol L^{-1}. Deposition time of gallium and zinc was 60 s. Deposition potential −1.75 V for gallium and −1.45 V for zinc.

3.1. Optimisation of experimental conditions of gallium film formation

Three parameters were optimised: concentration of Ga(III) ions in a plating solution, the potential of film formation and time of film formation. The influence of these parameters on zinc peak current obtained in subsequent measurement was studied. It was observed that the change of concentration of Ga(III) ions from 0 to 1 × 10^{-4} mol L^{-1} led to an increase of zinc peak current while further increase of Ga(III) concentration led to a slight decrease of zinc peak current, as shown in Fig. 1. For further study, a Ga(III) concentration of 1 × 10^{-4} mol L^{-1} in plating solution was chosen. The influence of the potential of gallium film formation on zinc peak current is presented in Fig. 2. For further study potential of gallium film formation equal to −1.75 V was chosen. The influence of time of gallium film formation on zinc peak current is shown in Fig. 3. For further study the time of film formation of 60 s was chosen.

3.2. Optimisation of conditions of zinc deposition

Influence of deposition potential and deposition time was studied for solution containing 4 × 10^{-7} mol L^{-1} Zn(II). Deposition potential was changed from −1.1 to −1.6 V and the results obtained are presented in Fig. 4. The results indicate that the efficiency of zinc deposition is acceptable as the deposition potential is more negative than −1.2 V. For further study an deposition potential of −1.45 V was chosen.

Next, the effect of deposition time on the current of stripping peak of zinc was investigated and it was observed that the stripping peak height for zinc increased linearly with an increase of
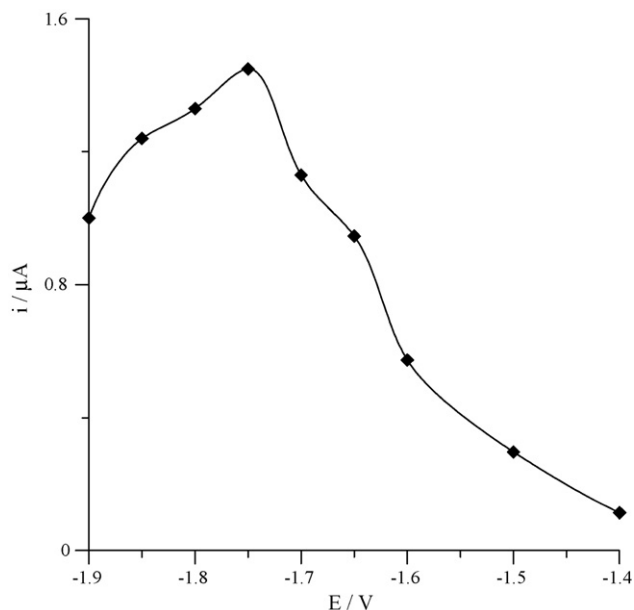
Fig. 2. The influence of potential of gallium film formation on the Zn(II) peak current. Concentration of Zn(II): 5×10^{-7} mol L^{-1}. Concentration of Ga(III): 1×10^{-4} mol L^{-1}. Other conditions as in Fig. 1.

the deposition time from 15 to 120 s. For further study, the deposition time of 60 s was chosen, although for zinc determinations at concentrations close to a detection limit a longer time of zinc deposition is recommended.

3.3. Analytical parameters

The calibration graph for deposition time of 60 s was linear from 5×10^{-8} to 2×10^{-6} mol L^{-1} and obeyed the equation
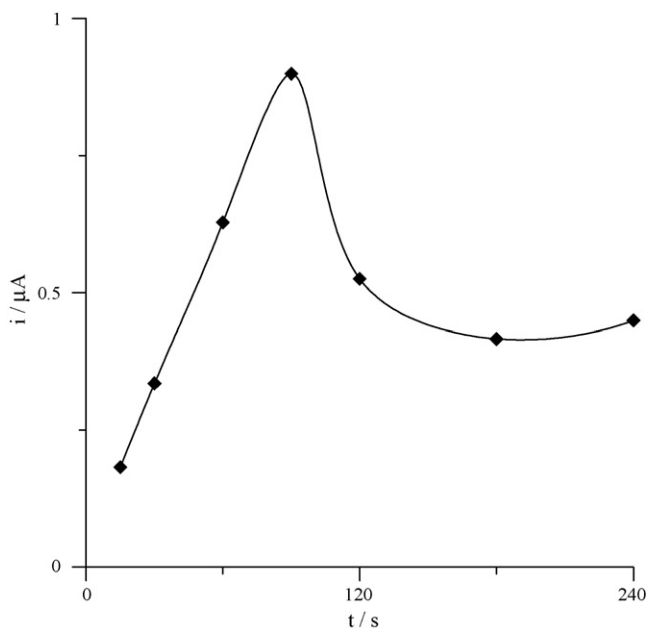
Fig. 3. The influence of time of gallium film formation on Zn(II) peak current. Concentration of Zn(II): 2.5×10^{-7} mol L^{-1}. Concentration of Ga(III): 1×10^{-4} mol L^{-1}. Other conditions as in Fig. 1.
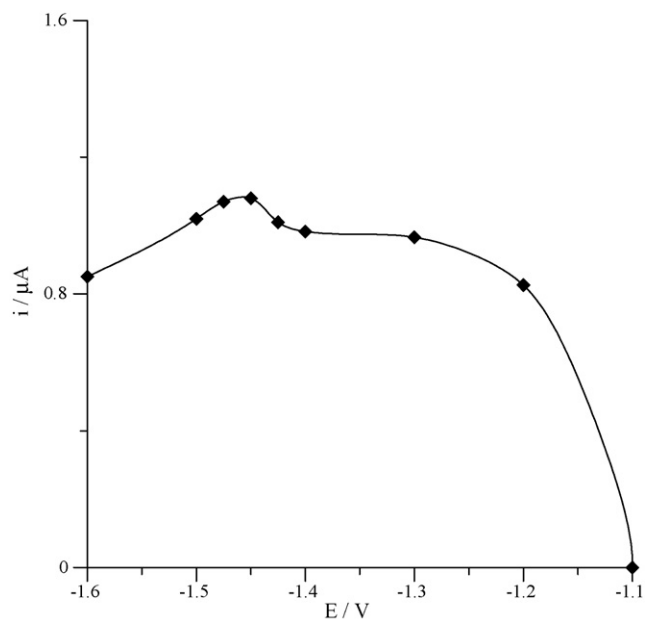
Fig. 4. The influence of zinc deposition potential on its peak current. Concentration of Zn(II): 4×10^{-7} mol L^{-1}. Other conditions as in Fig. 1.

$y = 3.12x - 1.1$, where y and x are peak current (nA) and Zn(II) concentration (nmol L^{-1}), respectively. The linear correlation coefficient was 0.9994. The relative standard deviation for a Zn(II) concentration 5×10^{-7} mol L^{-1} was 4.8% ($n = 7$). The detection limit estimated from 3σ for Zn(II) concentration 5×10^{-8} mol L^{-1} and deposition time of 60 s was about 1.2×10^{-8} mol L^{-1}. Comparable detection limit was reported for bismuth film electrode, however, following deposition time of 600 s [14]. The voltammograms obtained for low concentrations of Zn(II) are shown in Fig. 5. Additionally measurements for the calibration graphs for Zn(II) in the presence of 5×10^{-7} and 2×10^{-6} mol L^{-1} of Cu(II) were performed. Calibration graph for Zn(II) obtained for solution
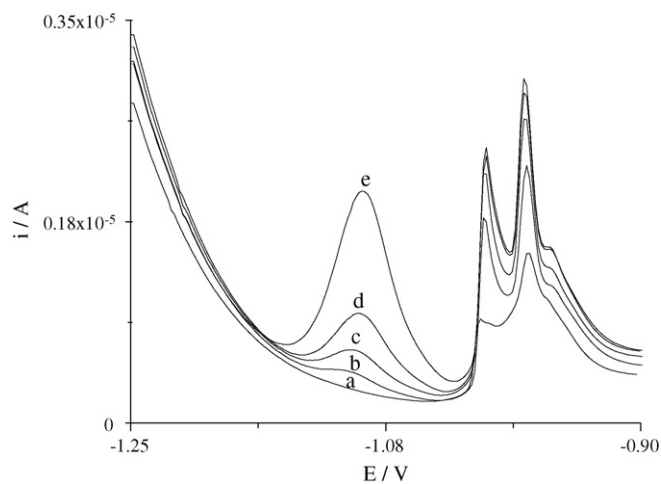
Fig. 5. Square wave voltammograms for various Zn(II) concentrations: (a) blank; (b) 5×10^{-8} mol L^{-1}; (c) 1×10^{-7} mol L^{-1}; (d) 2×10^{-7} mol L^{-1}; (e) 5×10^{-7} mol L^{-1}. Deposition time for zinc was 60 s.
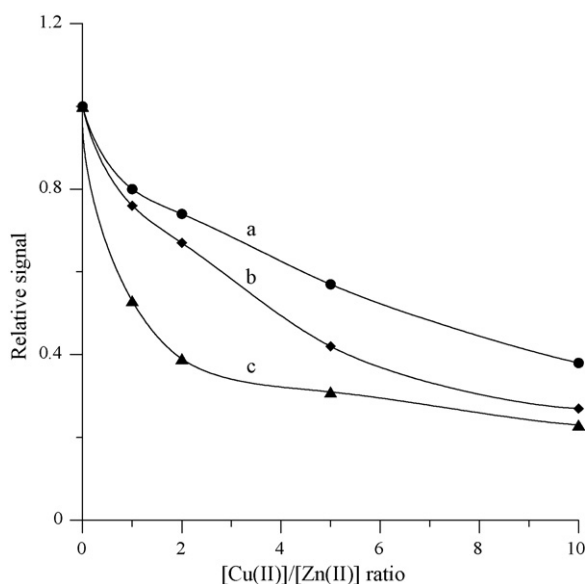
Fig. 6. The influence of [Cu(II)]/[Zn(II)] ratio on the relative signal in the presence and absence of Cu(II). Zn(II) concentrations: (a) 1×10^{-7} mol L^{-1}; (b) 3×10^{-7} mol L^{-1}; (c) 1×10^{-6} mol L^{-1}. Deposition time for zinc: (a) 120 s; (b and c) 60 s.

containing 5×10^{-7} mol L^{-1} Cu(II) was linear from 5×10^{-8} to 2×10^{-6} mol L^{-1} and obeyed the equation $y = 1.28x - 0.49$. The linear correlation coefficient was 0.9996. Calibration graph for Zn(II) obtained for solution containing 2×10^{-6} mol L^{-1} Cu(II) was linear from 2×10^{-7} to 2×10^{-6} mol L^{-1} and obeyed the equation $y = 0.88x - 0.10$. The linear correlation coefficient was 0.9995. Such results are better than those reported for bismuth film electrode where the linear calibration plot in the range from 5×10^{-7} to 3×10^{-6} mol L^{-1} was obtained [13].

3.4. Copper interference

Special attention was paid to the copper interference and it was studied for Zn(II) concentrations of 1×10^{-7}, 3×10^{-7} and 1×10^{-6} mol L^{-1}. The results obtained are presented in Fig. 6. The results show that zinc peak current decreases as Cu(II) concentration increases. However, zinc peak is measurable even in the presence of 10-fold excess of Cu(II) for all studied Zn(II) concentrations.

3.5. Analytical applications

The proposed method was applied for Zn(II) determination in rain water certified reference material, tap water and tap water spiked with Cu(II). Determinations were performed using the method of standard additions. Results from Zn(II) determinations were compared with the certified value and with that obtained by flame AAS, these are presented in Table 1. The results obtained show that the proposed method can be

Table 1
Results of Zn(II) determination in certified reference material and tap water sample

Sample	Zn(II) concentration (μg L^{-1} ± S.D.)	
	Proposed method	Reference value
CRM TMRAIN-95	10.6 ± 0.6	11.1 ± 2.33[a]
Tap water	1920 ± 130	1880 ± 43[b]
Tap water spiked with 10 mg L^{-1} Cu(II)	1850 ± 110	

S.D.: standard deviation ($n = 5$).
[a] Certified value.
[b] Result obtained by AAS.

successfully applied for determination of Zn(II) in natural water samples.

4. Conclusions

It has been shown that novel ex situ plated gallium film electrode can be applied for Zn(II) determination by ASV even in the presence of 10-fold excess of Cu(II). Such electrode can replace mercury film electrode usually used for Zn(II) determination by ASV. The calibration graph at the gallium film electrode is linear in the wider range of Zn(II) concentrations as compared to the results reported for bismuth film electrode [13]. Advantage of the proposed electrode is also lower toxicity of gallium as compared to mercury [15]. Preliminary results show that the electrode can be used for determination of other metal ions (e.g. Pb(II)). Research in our laboratory is progressing towards expanding the scope and applications of gallium film electrodes.

References

[1] M.S. Shuman, G.P. Woodward, Anal. Chem. 48 (1976) 1979.
[2] D.A. Roston, E.E. Brooks, W.R. Heineman, Anal. Chem. 51 (1979)1728.
[3] A.L.B. Marques, G.O. Chierice, Talanta 38 (1991) 735.
[4] E.Ya. Nieman, L.G. Petrova, V.I. Ignatov, G.M. Dolgopolova, Anal. Chim. Acta 113 (1980) 277.
[5] T.R. Copeland, R.A. Osteryoung, R.K. Skogerboe, Anal. Chem. 46 (1974) 2093.
[6] M.I. Abdullah, B. Reusch, R. Kilmex, Anal. Chim. Acta 84 (1976) 307.
[7] J. Wang, P.A.M. Farias, D.B. Luo, Anal. Chem. 56 (1984) 2379.
[8] J. Obiols, R. Devesa, A. Malet, Analyst 113 (1988) 1529.
[9] C.M.A. Brett, M.B.Q. Garcia, L.F.C. Lima, Anal. Chim. Acta 339 (1997) 167.
[10] J. Wang, Stripping Analysis: Principles, Instrumentation and Applications, VCH, Florida, 1985.
[11] J.-M. Zen, H.-Y. Lin, H.-H. Yang, Electroanalysis 13 (2001) 505.
[12] J. Wang, J. Lu, U.A. Kirgoz, S.B. Hocevar, B. Ogorevc, Anal. Chim. Acta 434 (2001) 29.
[13] Z. Guo, F. Feng, Y. Hou, N.J. Renault, Talanta 65 (2005) 1052.
[14] G. Kefala, A. Economou, A. Voulgaropoulos, M. Sofoniou, Talanta 61 (2003) 603.
[15] I. Moschen, K. Schweizer, C.A. Wagner, J. Geis-Gerstorfer, F. Lang, J. Dent. Res. 80 (2001) 1753.

ELSEVIER

Simultaneous determination of traces of heavy metals by solid-phase spectrophotometry

J. Vuković [a,*], S. Matsuoka [b], K. Yoshimura [b],
V. Grdinić [a], R. Jurišić Grubešić [a], O. Županić [a]

[a] *Faculty of Pharmacy and Biochemistry, University of Zagreb, A. Kovačića 1, Zagreb, Croatia*
[b] *Faculty of Sciences, Kyushu University, Ropponmatsu, Chuo-ku, Fukuoka 810-8560, Japan*

Abstract

A coupling sensitive solid phase spectrophotometric (SPS) procedure for determination of traces of heavy metals (*Me-SPS*) and multicomponent analysis by multiple linear regressions (MA), a simple methodology for simultaneous determination of metals in mixtures was inaugurated. The *Me-SPS* procedure is based on sorption of heavy metals on *PAN*-resin and direct absorbance measurements of colour product *Me-PAN* sorbed on a solid carrier in a 1-mm cell. This methodology (*Me-SPS-MA*) was checked by simultaneous determination of metals in synthetic mixtures with different compositions and contents of metals important in pharmaceutical practice: Zn, Pb, Cd, Cu, Co, and Ni. Good agreement between experimental and theoretical amounts of heavy metals is obtained from the recovery test (78.3–110.0%). The proposed method enables determination of particular metal ion at the ng mL^{-1} level and it was successfully applied to the determination impurities from heavy metal traces in pharmaceutical substances (Cu in ascorbic acid, Pb in glucose, and Zn in insulin). The proposed procedure could be possible contribution to the development of pharmacopoeial methodology for a heavy metals test.
© 2006 Elsevier B.V. All rights reserved.

Keywords: Heavy metals; Multicomponent analysis; Solid-phase spectrophotometry; 1-(2-Pyridylazo)-2-naphthol; Heavy metal limit test

1. Introduction

Detection and determination of heavy metals in the area of analytics and control of medicines are very important and demanding tasks, and, therefore, drug analysis and quality control have required increasingly better analytical methods and procedures for solving specific problems in pharmaceutical and in industrial production of medicines. Today, instrumental techniques like atomic absorption spectrometry, X-ray fluorescence spectrometry, and inductively coupled plasma-optical emission spectrometry are widely used in the pharmaceutical and food industry, as well as in other industrial branches, for the specific determination of metal traces.

According to most pharmacopoeias [1–4], the heavy metal limit test, based on sulphide precipitation in a weakly acidic medium and comparison with a lead solution at a concen-

tration that is usually 10 ppm, has been employed for about 100 years [5]. This method is simple and has the advantage of distinguishing a variety of heavy metal ions such as bismuth, copper, gold, lead, mercury, ruthenium, silver(I), and tin(II) with different colours. Furthermore, in addition to testing for heavy metals in general, pharmacopoeias [1,2] also require specific testing for a number of individual heavy metals, such as nickel in polyols and hardened fats, lead in sugars, and iron in diverse substances. Clearly, the purpose now is to detect contamination caused by toxicologically significant heavy metals coming from manufacturing equipment and processes. The experimental conditions chosen show that the focus of interest was on lead and cooper, two elements which formerly were widely used in factory equipment. In practice, however, the heavy metal limit test has several serious limitations: it is non-selective and barely semi-quantitative. The total amount of heavy metals is expressed against lead, although metals react with different sensitivity. Moreover, a comparison with the dark brown lead sulphide is not very expedient, apart from the colour of the sulphide formed, and there is no

* Corresponding author. Tel.: +385 1 49 200 89; fax: +385 1 49 200 89.
E-mail address: jadranka@pharma.hr (J. Vuković).

information about the identity of the ion which causes the possible positive reaction. The major difference between methods in particular pharmacopoeias is the source of the sulphide ion [6]: thioacetamide [1,3] or sodium sulphide [4] as precipitating reagents.

Although various suggestions for improvements have been made, including abolition and replacement by more sophisticated analytical methods [7,8], the test has held its ground, mainly due to the lack of an alternative that provides the required information with comparable ease and simplicity. A simple test for heavy metals in aqueous solutions, which yields a measure for the overall amount of heavy metals present, as well as the identity of the contaminating ions was suggested by Brozovic-Pohl et al. [9]. The procedure was based on treatment of solutions with diethyldithiocarbamic acid and determination of the total amount of metal ions and identification of metals by TLC. The main limitation of this method is that it is unspecific measure for the total amount of the ions and does not specify the content of particular metal ions.

Since simple, sensitive, low cost solid phase spectrophotometry (SPS) [10–12] has an important role in quantitative analysis of inorganic [13–16] and organic traces [17–19], the usefulness of this methodology can be extended to the microanalysis of heavy metals in pharmaceutical samples to meet the need to introduce novel methods into pharmacopoeia.

The aim of this work is to develop simple and sensitive SPS procedure coupled with powerful multicomponent analysis [20] that could be used for investigation of total and particular heavy metal contents in pharmaceutical samples. The multivariate calibration methods for multicomponent analysis in SPS are reported and used in several papers related to inorganic [21,22] and mainly organic analysis [23–27].

The basic idea of the SPS method for determination of nickel with PAN (1-(2-pyridylazo)-2-naphthol) presorbed resin has already been proposed by Yoshimura et al. [28]. Since the procedure was extended to the simultaneous determination of other metals, some experimental conditions were changed and therefore the optimization of the Me-SPS procedure was done to obtain good performance characteristics for the selected method. Different solid phase extractors including ion exchange resins [29–32], alumina [33], and polymeric membranes [34,35] impregnated with PAN are used as systems for the preconcentration of different analytes. The trace species preconcentrated on PAN impregnated solid carriers are determined by different instrumental techniques [30,33,34,36–38]. Quality control and standardization of the Me-SPS procedure were performed by using a comprehensive prevalidation strategy proposed by Grdinić and Vuković [39].

2. Experimental

2.1. Apparatus

A double beam UV-Visible Spectrophotometer Cary 50 Bio (Varian, Inc., Palo Alto, USA) with 1 mm quartz cells was used for all absorbance measurements.

2.2. Reagents

All chemicals were of analytical-reagent grade and doubly distilled water was used throughout this work. Working standard solutions of metals with desired concentrations were prepared by appropriate dilution of the standard stock solution of each metal: Zn, Pb, Cd, Cu, Ni, and Co (Kishida, Japan). A 0.1% PAN solution was prepared daily by dissolving 0.1 g of PAN (Kemika, Croatia) in 100 mL of methyl alcohol. For preparation of $0.5\,mol\,L^{-1}$ of HEPES buffer solution (pH 8.0), a 30 g of HEPES (Dojin, Japan) was dissolved in 250 mL of doubly distilled water and the pH was adjusted with $1\,mol\,L^{-1}\,NH_3$.

Thirty grams of cation exchanger AG 50W-X2-H$^+$ (150–300 μm) (Bio-Rad Laboratories, USA) was added to about 100 mL of solution containing 24 mL of 0.1% PAN and the mixture was stirred. After 1 h of stirring, the PAN-resin was converted into the sodium form by addition of $1.0\,L$ of $0.5\,mol\,L^{-1}$ NaOH, and the mixture was stirred for another 1 h. The resins were washed with water and dried in the air. The prepared resin was kept in a container at +4 °C.

2.3. General measurement procedure

Into a 200 mL solution containing $0.05–1.0\,\mu mol\,L^{-1}$ of target heavy metal ions and 20 mL of the 0.5 M HEPES buffer solution (pH 8.0), 0.20 g of *PAN-resin* was added; and the mixture was stirred for 30 min. The absorbances of sample (A_S) and blanks (A_B), at the absorption maximum of the reaction product *Me-PAN* in the resin phase (λ_1) and in the range where only the resin absorbs light (λ_2), were measured in a 1-mm optical path length quartz cell (Table 1). The net absorbance of the product species *Me-PAN* in the resin phase was calculated according to Eq. (1):

$$A_{net} = A_S - A_B = (A_{S\lambda_1} - A_{B\lambda_1}) - (A_{S\lambda_2} - A_{B\lambda_2}) \qquad (1)$$

The difference in absorbances at absorption maximum and non-absorption wavelengths was used to give better results for the determination of traces of metals.

2.4. Methodological model for multicomponent analysis

2.4.1. Establishment of absorptivity matrix **K**

The first step in the multicomponent analysis is establishment of the absorptivity matrix **K**, where the matrix elements, which are the absorptivities of the m components at the n wavelengths, can be obtained from the spectra of the pure components. Therefore, a concentration-normalized spectrum of each system containing $1\,\mu mol\,L^{-1}$ of a particular metal in the wavelengths range from 530 to 750 nm was measured according to Section 2.3. The elements of the **K** matrix are treated as the independent

Table 1
Characteristic wavelengths of analytical systems

	Zn-SPS	Pb-SPS	Cd-SPS	Cu-SPS	Ni-SPS	Co-SPS
λ_1	554	554	554	554	565	625
λ_2	750	750	750	750	750	750

variables and the number of wavelengths must be at least equal to or greater than the number of components. Matrix elements were apparent molar absorptivities ε (L μmol^{-1} mm^{-1}) calculated at 13 wavelengths from recorded spectra of each metal. The order of the matrix ($m \times n$) used for multicomponent analysis depends on the number of metals in mixture. For example, for determination of metals in six-component system, the absorptivity matrix $\mathbf{K}$ (6×13), i.e., six components at 13 wavelengths, was used as shown in Eq. (2):

$$\mathbf{K} = \begin{matrix} Zn & Pb & Cd & Cu & Ni & Co \\ \begin{pmatrix} \varepsilon_{1Zn} & \varepsilon_{1Pb} & \varepsilon_{1Cd} & \varepsilon_{1Cu} & \varepsilon_{1Ni} & \varepsilon_{1Co} \\ . & . & . & . & . & . \\ . & . & . & . & . & . \\ \varepsilon_{13Zn} & \varepsilon_{13Pb} & \varepsilon_{13Cd} & \varepsilon_{13Cu} & \varepsilon_{13Ni} & \varepsilon_{13Co} \end{pmatrix} & \begin{matrix} \lambda_{530} \\ . \\ . \\ \lambda_{650} \end{matrix} \end{matrix} \quad (2)$$

2.4.2. Determination of metals in the synthetic mixtures

The proposed procedure (*Me-SPS* with multicomponent analysis, *Me-SPS-MA*) was checked by simultaneous determination of metals in synthetic mixtures with different composition and contents of metals. Analytical systems investigated were: S1 (Zn, Co), S2 (Zn, Ni, Co), S3 (Zn, Pb, Cd), S4 (Zn, Pb, Cu, Co), S5 (Zn, Pb, Cu, Ni, Co), and S6 (Zn, Pb, Cd, Cu, Ni, Co). The concentrations of particular metals in investigated mixtures were varied from 0.05 to 1.0 μmol L^{-1}. Measurements were performed according to Section 2.3. Calculations were performed using an appropriate absorptivity matrix $\mathbf{K}$ and a set of equations for multiple linear regression [20,40]. To meet the need for faster calculations, software for multicomponent analysis of mixtures by multiple linear regressions called SPIS was recently developed by the authors.

2.5. Procedures for the determination of metals in pharmaceutical substances

2.5.1. Determination of copper in ascorbic acid

A 2.0 g substance to be examined was dissolved in 25 mL of 0.5 mol L^{-1} HEPES buffer solution. Such a prepared sample was diluted with water up to 200 mL and Section 2.3 was performed. The content of copper was determined according to Section 2.4.

2.5.2. Determination of lead in glucose

A 20.0 g substance to be examined was dissolved in 100 mL water. To the 50.0 mL of sample, 20 mL of 0.5 mol L^{-1} HEPES buffer solution were added, the solution was diluted to 200 mL with water and Section 2.3 was performed. The content of lead was determined according to Section 2.4.

2.5.3. Determination of zinc in insulin

A 50.0 mg substance to be examined was dissolved in 5 mL of 0.01 mol L^{-1} hydrochloric acid and diluted to 25 mL with water. To the 0.25 mL of solution, 20 mL of 0.5 mol L^{-1} HEPES buffer solution was added, the solution was diluted to 200 mL with water, and Section 2.3 was performed. The content of zinc was determined according to Section 2.4.

2.6. Distribution measurement

In order to determine distribution ratio D (mol of product sorbed per g of ion exchanger/mol of product per mL of solution) of the target metal ions between the resin and aqueous solution, 200 mL (V_{sol}) of aqueous solution containing an appropriate amount of metal (C_1) and 20 mL of 0.5 mol L^{-1} HEPES buffer solution were equilibrated with 0.5 g (m_r) of *PAN-resin*. After 30 min of equilibration, the ion exchanger (m_r) was separated from the solution by filtration and the net absorbance, A_1, of the solid phase was measured (Section 2.3). To the filtrate, an additional amount of resin (0.5 g) was added and the solution was stirred for 30 min. The net exchanger absorbance, A_2, was measured again according to Section 2.3. The distribution ratio, D, was calculated from the following equation [41]:

$$D = \frac{[C_1 - (C_1 A_2 / A_1)]/m_r}{(C_1 A_2 / A_1)/V_{sol}} = \left(\frac{A_1}{A_2} - 1 \right) \frac{V_{sol}}{m_r} \quad (3)$$

2.7. Execution of prevalidation

The prevalidation strategy included a total of 24 measurements (n) divided into 6 analytical groups (j) of 4 experiments each (i) related to measured and blank values. Standards and blanks were measured in a standard working range of 1 power of 10 ($1.0x_U = x_1 = 0.50$ μmol, upper level of analyte, $0.8x_U = x_2 = 0.40$ μmol, $0.6x_U = x_3 = 0.30$ μmol, $0.4x_U = x_4 = 0.20$ μmol, $0.2x_U = x_5 = 0.10$ μmol, and $0.1x_U = x_6 = x_L = 0.05$ μmol, lower level of analyte), alternately in the following group sequence: 1, 6, 2, 5, 3, 4. Working standard solutions for the prevalidation procedure were prepared by an appropriate dilution of the standard stock solution, and measurements were performed according to Section 2.3. Blank solutions were prepared and absorbances were identically measured, but without the analyte. Mathematical/statistical tests included: characterization of groups 1–6, checking of groups 1 and 6, testing of data homogeneity, estimation of calibration and analytical evaluation functions, outlier recognition, and estimation of limiting values. The prevalidation strategy was systematically explained in the paper [39]. The prevalidation expert system was applied for evaluation and quality control of the *Me-SPS* procedure. Analytical and instrumental parameters were presented in Table 2.

3. Results and discussion

A fast and sensitive one-step SPS-procedure, using a sensitive but not selective PAN reagent, was optimized and used for determination of heavy metals which are important in pharmaceutical practice (Zn, Pb, Cd, Cu, Co, and Ni). In this SPS procedure, the resin presorbed with PAN reagent was used as a resinous reagent (*PAN*-resin) [28]. The reagent concentration on the resin was constant, irreversibly sorbed on a cation-exchange resin and developed a coloured complex with a small amount of different metals in the resin phase. The excess of uncomplexed PAN was not desorbed during the equilibration.

Table 2

Analytical and instrumental parameters

Parameters	Zn-SPS system
Analytical	
Analyte	Zinc
Analyte working range (μmol)	0.05–0.50
Reagent	PAN
Total volume (mL)	200
Matrix	–
Instrumental	
Method	Solid phase spectrophotometry
Instrument	UV-Visible Spectrophotometer Cary 50 Bio
Wavelength (nm)	
λ_1	554
λ_2	750
Cell ($l = 1.0$ cm)	Quartz cell with spacer
Optical path length (cm)	0.1

3.1. Spectral characteristics in the resin phase

The majority of the products *Me-PAN* (*Zn-PAN*, *Pb-PAN*, *Cd-PAN*, *Cu-PAN*, and *Ni-PAN*) sorbed on resin phase showed maximum absorbance in the range from 554 to 560 nm (Fig. 1). In the same wavelengths range, the absorbance of the reagent blank was fairly small. Products *Zn-PAN* and *Ni-PAN* possessed a second maximum around 520 nm. Absorption spectra of *Co-PAN* significantly differed from the others and showed two maxima at 584 and 625 nm.

Above 700 nm, the products fixed in the resin phase did not absorb light. The fixation and preconcentration of the coloured species in the small volume of the ion-exchange resin were influenced by this noticeable increase in sensitivity. The apparent molar absorptivities of Zn, Pb, Cd, Cu, Ni, and Co were 1.26×10^7, 3.02×10^6, 3.73×10^6, 7.08×10^6, 1.32×10^7, and 5.42×10^6 L mol^{-1} cm^{-1}, respectively. These results pointed to the high sensitivity of proposed SPS method. The distribution ratios (D) of metal ions were determined according to Section 2.6. Four replicate determinations were performed for each metal and the results were presented in Table 3.

Very high values of distribution ratios show that all metals can be almost completely sorbed on the resin from the surrounding solution.
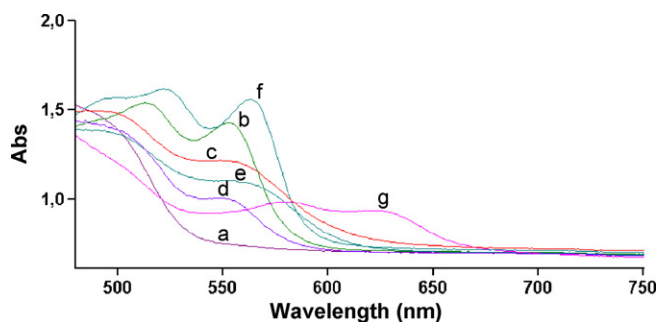
Fig. 1. Absorption spectra of products *Me-PAN*. Reaction conditions: 0.20 g of PAN-resin; $V_{sample} = 200$ mL, optical cell length: 1 mm; *a*: blank; *b*: 0.8 μmol L^{-1} Zn; *c*: 0.9 μmol L^{-1} Pb; *d*: 0.5 μmol L^{-1} Cd; *e*: 0.5 μmol L^{-1} Cu; *f*: 1 μmol L^{-1} Ni; and *g*: 0.5 μmol L^{-1} Co.

Table 3

Distribution ratios of the products *Me-PAN*

Metal	c (nmol mL^{-1})	D ($\times 10^4$ mL g^{-1})
Zn	1	1.90
Pb	1	1.34
Cd	1	0.26
Cu	1	1.55
Ni	1	4.00
Co	1	4.52

3.2. Optimization of experimental conditions

The parameters optimized in a series of experiments for the establishment of optimum analytical working conditions were: pH-dependence of colour development, time-dependence of colour development, the amount of resin, and stability of sorbed *Me-PAN* products.

A study of the effect of pH on the product formation and sorption on resin revealed that the pH-range from 7.0 to 8.0 is the most convenient for all metals investigated. The pH could be satisfactorily adjusted by addition of 20 mL 0.5 mol L^{-1} HEPES buffer solution (pH 8.0). The influence of the amount of resin on sensitivity was studied with quantities from 0.05 to 0.5 g of resin. The amount of resin, 0.2 g, which gave the highest absorbance and greatest ease in handling, was used in all measurements. The optimum stirring time to reach completion in the ion-exchange step within a short time was 30 min in the case of all investigated metals. The sorbed *Me-PAN* species were stable for at least 24 h after equilibration.

3.3. Analysis of prevalidation results

Starting prevalidation data were: the amount of zinc (x) within the working range from 0.05 to 0.50 μmol, absorbances obtained from measurements of the blank (B) and the sample (y), as well as the corrected absorbance (S) obtained by simple calculation of $y - B$. The results of complete prevalidation confirmed the validity of the *Me-SPS* procedure which is characterized with favourable metrological characteristics summarized in Table 4.

3.3.1. Characterization of groups 1–6

Standard and relative standard deviations of absorbances obtained from measurements of the blank (S_{rB} from $\pm 1.71\%$ to $\pm 3.85\%$), sample (S_{ry} from $\pm 0.68\%$ to $\pm 2.52\%$), and corrected absorbances (S_{rs} from $\pm 0.68\%$ to $\pm 4.15\%$) showed that a high level of precision was attained for the *Me-SPS* procedure in accordance with strict prevalidation criteria ($S_r < \pm 5\%$) [39]. Measures of particular sensitivities ($A_n = S_n/x_n$) were from 1.385 to 1.622, with relative standard deviations from $\pm 0.68\%$ to $\pm 4.15\%$, respectively.

3.3.2. Checking of limiting groups 1 and 6

In the *Me-SPS* procedure, the blank signal is significantly lower than the gross signal at lower analyte levels, significant influence of blank dispersions on S_M is not expected

Table 4
Prevalidation characteristics of *Me-SPS* procedure

Parameter	Me-SPS procedure					
Working range (μmol)	0.05–0.50					
Information value range (absorbance units)	0.069–0.811					
Analyte–signal relationship	$r = 0.9981$					
Calibration function	$\hat{S} = 1.606x$					
Analytical evaluation function	$\hat{x} = 0.62S$					
Standard deviation of procedure	± 0.0064					
Limit of detection, L_D (μmol)	0.004					
Limit of quantitation, L_Q (μmol)	1.011					
Groups data						
Actual (μmol)	0.500	0.400	0.300	0.200	0.100	0.050
Found (μmol)	0.505	0.397	0.302	0.194	0.094	0.043
Random deviations						
$S_{\hat{x}}$ (μmol)	± 0.003	± 0.006	± 0.005	± 0.004	± 0.002	± 0.002
$S_{r\hat{x}}$ (%)	± 0.67	± 1.43	± 1.65	± 2.11	± 2.07	± 4.15
Systematic deviations, $\Delta\bar{x}$						
Absolute (μmol)	+0.005	−0.003	+0.002	−0.006	−0.006	−0.007
Relative (%)	+0.95	−0.73	+0.83	−3.06	−6.33	−13.80

($S_{rB1} = \pm 3.85\%$, $S_{rB6} = \pm 2.44\%$) and the determination limit is expected to be below x_6. Relative standard deviation values for gross and corrected measurements at x_U and x_L lie below $\pm 2.5\%$ ($S_{ry1} = \pm 0.68\%$, $S_{rs1} = \pm 0.68\%$) and $\pm 25\%$ ($S_{ry6} = \pm 2.52\%$, $S_{rs6} = \pm 4.15\%$), respectively. Furthermore, gross and blank signals could be readily distinguished ($R = 15.00$). Even the preliminary linearity check, as applied to particular sensitivity values, showed that a linear calibration function was not expected ($R = 8.11$), so complete and systematic evaluation of calibration function was necessary.

3.3.3. Testing of data homogeneity

Analysis of variance applied to the six groups of blank values in the *Me-SPS* procedure indicated a high homogeneity of blank values ($R = 0.59$). Additional checking of blank homogeneity showed that the influence of blank values is not negligible since information obtained for the grand blank mean is not small enough in relation to information obtained at the upper analyte level. Homogeneity testing applied to S and S_r values for blanks (B), gross signals (y), corrected signals (S), and particular sensitivity values (A), as well as to the values of the apparent mass of the analyte ($\hat{x}$), using the very valuable Bartlett test, pointed to a strongly homogenous standard and relative standard deviations of all investigated values ($R = 2.37$–8.39). Furthermore, the total S_r value for blank measurements was below $\pm 50\%$ ($S_{rBN} = \pm 3.12\%$). Favourable homogeneity testing results impose the need to correct each y value with the grand blank mean in the *Me-SPS* procedure.

3.3.4. Signal–concentration relationship

The characteristic data evaluated by method of the least squares for preliminary inspection of the relationship between signal values and content of analyte were: determination coefficient ($r^2 = 0.9997$), slope of a line ($b = 1.6451$), intercept of a line ($a = -0.0140$), errors in the slope ($S_b = \pm 0.0427$), and intercept ($S_a = \pm 0.0004$). For the *Me-SPS* system, a statistical *t*-test showed that significant correlation does exist ($R = 180.84$). Systematic evaluation of analytical functions in the complete analyte working range, using a standardized mathematical/statistical procedure [39], showed that both ideal calibration and analytical evaluation function were found (Table 4). Other characteristic data were mean errors of calibration ($S_V = \pm 0.0069$) and analytical evaluation constants ($S_V = \pm 0.0027$), as well as the standard deviation of the analytical procedure ($S_M = \pm 0.0064$) in the given working range. From the final calibration and analytical evaluation function, apparent signal values ($\hat{S}$) and apparent amounts of analyte ($\hat{x}$) were evaluated.

3.3.5. Outlier recognition

Testing for the regression outliers in the prevalidation process revealed no influence on the homogeneity of the data, since no outlying value is observed in the investigated procedure.

3.3.6. Estimation of limiting values

According to recently adopted concepts of limiting values [42], the estimated values of the limit of detection ($L_D = 0.004\ \mu$mol) and quantitation ($L_Q = 0.011\ \mu$mol) were significantly lower then the amount of analyte at the lower analyte level. These calculated values being below the respective x_6 level confirmed the quality of the measurements.

Analysis of variance, the Bartlett test, reality of linear analytical evaluation function, agreement of actual amounts of analyte (x), and appropriate found values ($\hat{x}$), as well as random and systematic deviations confirmed the quality and usefulness of the *Me-SPS* system, which is characterized with favourable metrological characteristics. The extensive prevalidation metrological characteristics are summarized in Table 4.

Table 5
Content of particular metal in mixtures

Metal	Added (μmol L^{-1})	Found (μmol L^{-1})	Recovery (%)	Matrix
Zn	0.125	0.123	98.4	Pb, Cd
	1.000	1.085	108.5	Co
Pb	0.250	0.250	100.0	Zn, Cu, Co
	0.300	0.290	96.7	Zn, Cu, Ni, Co
Cd	0.500	0.488	97.6	Zn, Pb
Cu	0.750	0.730	97.3	Zn, Pb, Co
Ni	0.100	0.104	104.0	Zn, Pb, Cu, Co
	0.125	0.125	100.0	Zn, Co
	0.125	0.132	105.6	Zn, Pb, Cd, Cu, Co
Co	0.250	0.253	101.2	Zn, Pb, Cd, Cu, Ni
	1.000	1.000	100.0	Zn

3.4. Applicability of Me-SPS-MA procedure

3.4.1. Synthetic mixtures

Simultaneous determination of heavy metals in analytical systems with different composition and content of metals was performed to check the usefulness of the *Me-SPS-MA* procedure. Although *Me-PAN* complexes sorbed on resin showed similar absorption spectra, there are some differences in spectral characteristics and sensitivity. The difference in absorption spectra together with powerful multicomponent analysis made simultaneous determination of metals in mixture possible. An appropriate absorptivity matrix **K** was obtained according to a procedure for the *establishment of absorptivity matrix* **K**, and determination of particular metal in the mixture, as well as total amount of metals in mixtures was performed according to a procedure for the *determination of metals in the synthetic mixtures*. A good agreement between experimental and theoretical amounts of heavy metals, as well as favourable recoveries confirmed the validity of this methodological approach (Tables 5 and 6).

3.4.2. Pharmaceutical samples

The inaugurated procedure was applied for the determination of copper in ascorbic acid, lead in glucose, and zinc in insulin (Tables 7–9). For all pharmaceutical substances, the European Pharmacopoeia [1] recommends determination of particular heavy metals. For samples of ascorbic acid and glucose examined, measurable quantities of Cu and Pb were not found.

Table 6
Content of total metals in mixtures

Analytical system	Added (μmol L^{-1})	Found (μmol L^{-1})	Recovery (%)
S1 (Zn, Co)	0.750	0.744	98.7
	1.000	1.000	100.0
S2 (Zn, Ni, Co)	0.750	0.750	100.5
S3 (Zn, Pb, Cd)	1.050	1.083	103.1
S4 (Zn, Pb, Cu, Co)	0.700	0.712	101.7
S5 (Zn, Pb, Cu, Ni, Co)	1.000	0.977	97.7
S6 (Zn, Pb, Cd, Cu, Ni, Co)	1.300	1.232	94.8

Table 7
Copper in ascorbic acid

Sample	Amount of Cu (μmol L^{-1})		S_r (%)	Recovery (%)
	Added	Found		
Ascorbic acid	0.080	0.082	3.78	102.1
	0.480	0.487	0.79	101.4
	0.800	0.792	0.27	99.0

Table 8
Lead in glucose

Sample	Amount of Pb (μmol L^{-1})		S_r (%)	Recovery (%)
	Added	Found		
Glucose	0.150	0.149	3.09	99.5
	0.300	0.296	0.85	98.5
	0.900	0.903	1.28	100.4

Table 9
Zinc in insulin

Sample	Amount of Zn (μmol L^{-1})		S_r (%)	Recovery (%)
	Added	Found		
Insulin	0	0.098	4.41	–
	0.050	0.152	1.25	108.0
	0.100	0.200	7.63	102.0
	0.300	0.403	2.83	101.7

The sample of insulin contained 0.098 μmol L^{-1} of zinc, that is, 2.6 mg Zn per g of insulin.

In order to check the accuracy of the proposed method, recovery experiments for different amounts of metals were carried out. The results confirmed the validity of the proposed method.

4. Conclusions

Combining a sensitive SPS-technique and a sensitive but non-selective PAN reagent, procedure for the determination of heavy metals important in pharmaceutical practice has been developed. This simple, fast, sensitive, and low-cost procedure enables determination of particular metal ion at the ng mL^{-1} level. Optimal working conditions were: PAN-resin, 0.2 g, pH 8.0, time colour development, 30 min, and sample volume, 200 mL. The prevalidation strategy confirmed the quality of the *Me-SPS* system which was characterized with acceptable metrological characteristics. A combination of sensitive *Me-SPS* procedure and a chemometric algorithm of multicomponent analysis by multiple linear regressions was used for development of this sensitive and fast methodological approach for the simultaneous determination of heavy metals in a mixture without previous concentration or separation (*Me-SPS-MA*). Although PAN reagent is sensitive but non-selective, differences in sensitivity and spectral characteristic of *Me-PAN* complexes were used to establish this methodological approach. The proposed *Me-SPS-MA* procedure was checked by determination of total and particular amounts of metals in synthetic mixtures with different

compositions and contents of metals. Good agreement between experimental and theoretical amounts of heavy metals, as well as favourable recoveries confirmed the validity of this methodological approach. The proposed methodology was successfully applied to the determination of heavy metal traces as impurities in pharmaceutical substances (Cu in ascorbic acid, Pb in glucose, and Zn in insulin). Inaugurated *Me-SPS-MA* procedure gives new impetus to the investigations and development of analytical procedures for the needs of pharmacopoeia, as well as drug quality control in general and could be applied to routine pharmaceutical analysis.

References

[1] European Pharmacopoeia, 4th ed., Council of Europe, Strasbourg, 2002, p. 187.
[2] British Pharmacopoeia, British Pharmacopoeia Commission, Norwich, 2001, p. 10.
[3] The United States Pharmacopeia, United States Pharmacopeial Convention, Rockville, 2002.
[4] The Japanese Pharmacopoeia, 14th ed., The Society of Japanese Pharmacopoeia, Tokyo, 2001, pp. 43–44 http://www.jpdb.nihs.go.jp/jp14e/.
[5] R. Ciciarelli, D. Jäkel, E. König, R. Müller-Käfer, M. Röck, M. Thevenin, H. Ludwig, Pharmacopoeial Forum 21 (1995) 1638–1640.
[6] K.B. Blake, Pharmacopoeial Forum 21 (1995) 1632–1637.
[7] Pharmeuropa 15 (2003) 359–361.
[8] Pharmacopoeial Forum 24 (1998) 6460–6461.
[9] K. Brozovic-Pohl, H. Altorfer, X. Perlia, Fresenius J. Anal. Chem. 343 (1992) 348–351.
[10] K. Yoshimura, H. Waki, S. Ohashi, Talanta 23 (1976) 449–454.
[11] K. Yoshimura, H. Waki, Talanta 32 (1985) 345–352.
[12] S. Matsuoka, Y. Tennichi, K. Yoshimura, J. Ion Exchange 14 (2003) 313–316.
[13] M.F. Molina, M. Nechar, J.M. Bosque-Sendra, Anal. Sci. 14 (1998) 791–797.
[14] L.S.G. Teixeira, A.C. Spínola Costa, J.C. Rosa Assis, S.L. Costa Ferreira, M. Korn, Mikrochim. Acta 137 (2001) 29–33.
[15] M.C. Valencia, E. Arana Nicolas, L.F. Capitán-Vallvey, Talanta 49 (1999) 915–921.
[16] A.S. Amin, Anal. Chim. Acta 437 (2001) 265–272.
[17] P. Ortega-Barrales, G. Pellerano, F.A. Vazquez, A. Molina-Diaz, Anal. Lett. 35 (2002) 1491–1504.
[18] I. Nukatsuka, S. Nakamura, K. Watanabe, K. Ohzeki, Anal. Sci. 16 (2000) 269–273.
[19] A. Ruiz Medina, M.L. Fernández de Córdova, A. Molina Diaz, J. Pharm. Biomed. Anal. 20 (1999) 247–254.
[20] D.L. Massart, B.G.M. Vanderginste, L.M.C. Buydens, S. de Jong, P.J. Lewi, J. Smeyers-Verbeke, Handbook of Chemometrics and Qualimetrics: Part A, Elsevier Science, Amsterdam, 1997.
[21] L.S.G. Texeira, A.C.S. Costa, S. Garrigues, M. De la Guardia, J. Braz. Chem. Soc. 13 (2002) 54–59.
[22] L. Hejazi, D.E. Mohammadi, Y. Yamini, R.G. Brereton, Talanta 62 (2004) 185–191.
[23] L.F. Capitán-Vallvey, M.D. Fernandez, I. de Orbe, J.L. Vilchez, R. Avidad, Analyst 122 (1997) 351–354.
[24] A. Ruiz Medina, M.L. Fernandez de Cordova, A. Molina Diaz, J. Pharm. Bopmed. Anal. 21 (1999) 983–992.
[25] L.F. Capitán-Vallvey, M.K.A. Deheidel, I. Orbe Paya, R. Avidad, Analyst 124 (1999) 49–53.
[26] L.F. Capitán-Vallvey, M.D. Fernandez, I. de Orbe, R. Avidad, Talanta 47 (1998) 861–868.
[27] S. Ortega-Algar, N. Ramos-Martos, A. Mooina-Diaz, Talanta 60 (2003) 313–323.
[28] K. Yoshimura, Y. Toshimitsu, S. Ohashi, Talanta 27 (1980) 693–697.
[29] P. Bermejo-Barrera, N.A. Martínez, C. López Díaz, A. Bermejo Barrera, Microchim. Acta 142 (2003) 101–108.
[30] I. Narin, M. Soyalk, Talanta 60 (2003) 215–221.
[31] N. Malcik, O. Oktar, M.E. Ozser, P. Caglar, L. Bushby, A. Vaughan, B. Kuswandi, R. Narayanaswamy, Sens. Actuators B: Chem. 53 (1998) 211–221.
[32] I. Narin, M. Soylak, K. Kayakirilmaz, L. Elci, M. Dogan, Anal. Lett. 36 (2003) 641–658.
[33] F. Shemirani, B.T.S. Akhavi, Anal. Lett. 34 (2001) 2179–2188.
[34] D.L. Giokas, E.K. Paleologos, M.I. Prodromidis, M.I. Karayannis, Talanta 56 (2002) 491–498.
[35] M. Soylak, N.D. Erdogan, L. Elci, J. Chin. Chem. Soc. 51 (2004) 703–706.
[36] O.P. Kalyakina, O.N. Kononova, S.V. Kachin, A.G. Kholmogorov, Bull. Korean Chem. Soc. 24 (2003) 173–177.
[37] M.C. Yebra, A. García, N. Carro, A. Moreno-Cid, L. Puig, Talanta 56 (2002) 777–785.
[38] I.M.M. Kenawy, M.A.H. Hafez, M.A. Akl, R.R. Lashein, Anal. Sci. 16 (2000) 493–500.
[39] V. Grdinić, J. Vuković, J. Pharm. Biomed. Anal. 35 (2004) 489–512.
[40] J.N. Miller, J.C. Miller, Statistics, Chemometrics for Analytical Chemistry, Pearson Education Limited, Essex, 2000.
[41] T. Nakashima, K. Yoshimura, H. Waki, Talanta 37 (1990) 735–739.
[42] M. Thompson, S.L.R. Ellison, R. Wood, Pure Appl. Chem. 74 (2002) 835–855.

Development of a mild mercaptoethanol extraction method for determination of mercury species in biological samples by HPLC–ICP-MS

Wang Meng [a,b], Feng Weiyue [a,*], Shi Junwen [a,b], Zhang Fang [a,b], Wang Bing [a,b],
Zhu Motao [a,b], Li Bai [a], Zhao Yuliang [a,b], Chai Zhifang [a,c,d]

[a] *Laboratory for Bio-Environmental Health Sciences of Nanoscale Materials and Key Laboratory of Nuclear Analytical Techniques,
Institute of High Energy Physics, Chinese Academy of Sciences, Beijing, China*
[b] *Graduate School of the Chinese Academy of Sciences, Beijing, China*
[c] *Institute of Nuclear Technology, Shenzhen University, Shenzhen, China*
[d] *Institute of Nanochemistry and Nanobiology, Shanghai University, Shanghai, China*

Abstract

A mild, efficient and convenient extraction method of using 2-mercaptoethanol contained extractant solution combined with an incubator shaker for determination of mercury species in biological samples by HPLC–ICP-MS has been developed. The effects of the concentration of 2-mercaptoethanol, the composition of the extractant solution and the shaking time on the efficiency of mercury extraction were evaluated. The optimization experiments indicated that the quantitative extraction of mercury species from biological samples could be achieved by using 0.1% (v/v) HCl, 0.1% (v/v) 2-mercapoethanol and 0.15% (m/v) KCl extractant solution in an incubator shaker for shaking overnight (about 12 h) at room temperature. The established method was validated by analysis of various biological certified reference materials, including NRCC DOLT-3 (dogfish liver), IAEA 436 (tuna fish), IAEA MA-B-3/TM (garfish filet), IAEA MA-M-2/TM (mussel tissue), GBW 08193 (bovine liver) and GBW 08572 (prawn). The analytical results of the reference materials were in good agreement with the certified or reference values of both methyl and total mercury, indicating that no distinguishable transformation between mercury species had occurred during the extraction and determination procedures. The limit of detection (LOD) for methyl (CH_3Hg^+) and inorganic mercury (Hg^{2+}) by the method are both as $0.2\,\mu g\,L^{-1}$. The relative standard deviation (R.S.D.s) for CH_3Hg^+ and Hg^{2+} are 3.0% and 5.8%, respectively. The advantages of the developed extraction method are that (1) it is easy to operate in HPLC–ICP-MS for mercury species determination since the extracted solution can be directly injected into the HPLC column without pH adjustment and (2) the memory effect of mercury in the ICP-MS measurement system can be reduced.

1. Introduction

Mercury (Hg) is one of the most hazardous pollutants in the environment. It has been introduced into the environment as three major forms, elemental Hg^0, inorganic Hg^{2+} and organic Hg. The inorganic mercury (Hg^{2+}) and monomethylmercury (CH_3Hg^+) are the two major species generally found in various biological samples [1]. The differences of mercury species in bioavailability and toxicity make it important to develop a method to simultaneously determine mercury species in biological samples with high sensitivity, good accuracy and convenience.

Nowadays the reliable analysis of mercury species has been mainly achieved by hyphenated techniques, including gas chromatography (GC), high performance liquid chromatography (HPLC) coupled with a mercury-selective detection technique, such as atomic fluorescence spectrometry (AFS), atomic emission spectrometry (AES), atomic absorption spectrometry (AAS) and inductively coupled plasma-mass spectrometry (ICP-MS) [1–3]. Among the methods mentioned above, the coupling of HPLC to ICP-MS appears to be one of the most common methods for mercury speciation analysis because of its easiness of sample preparation, simplicity of the interface to the detector, availability of the isotope ratio information

* Corresponding author. Tel.: +86 10 88233209; fax: +86 10 88233186.
E-mail address: fengwy@mail.ihep.ac.cn (W. Feng).

and specificity of the signal intensity of the determined element [4].

In spite of significant progress in mercury analytical instruments, reliable results are mainly dependent upon sample preparation. The extraction of mercury species from the sample matrix is recognized as one of the most crucial steps before determination. The traditional extraction methods include acid leaching [5], alkaline digestion [6] and stream distillation [7]. The drawbacks of these methods include complicated procedure, low efficiency, high solvent consumption and mercury loss during pretreatment. Additionally, various extraction techniques, such as distillation, acid and alkaline extraction, have been demonstrated to have tendency to form artificial methylmercury from inorganic mercury during sample preparation [8,9]. Recently, microwave- [10] and ultrasound-assisted extraction [11] have been used to elevate the efficiency of mercury extraction. However, there still exist some problems for such methods. The concentrated acid or alkali, high temperature and high pressure still have to be used. After extraction, most of the methods need a further derivatization treatment or pH adjustment of the extracted solution for GC or HPLC separation. Consequently, there is still an increasing possibility of transformation between mercury species during sample preparation. This possibility may be due to the oxidative energy creation during the sonolysis of solvent [12] or the high temperature and pressure during the microwave-assisted extraction [13]. Qvarnstrom and Frech [14] showed that significant transformation took place during ultrasound-assisted alkaline digestion of biological samples.

A successful extraction procedure for speciation analysis requires high extraction efficiency, and more importantly, all original species must keep intact prior to analysis. In order to lower the possibility of mercury transformation during pretreatment, a mild extraction method by using of a 2-mercaptoethanol contained extractant solution combined with an incubator shaker is developed to quantitatively extract inorganic and methylmercury from biological samples in this work. The effects of the concentration of 2-mercaptoethanol, the composition of the extractant solution and the shaking time on the extraction efficiency of mercury were carefully evaluated. After extraction, total mercury and mercury species were determined by ICP-MS and HPLC–ICP-MS, respectively. The developed method was validated by analysis of various biological certified reference materials.

2. Experimental

2.1. Instrumentation

An incubator shaker was supplied by Donglian Electronic & Technology Development Company (Harbin, PR China).

The high performance liquid chromatography system used for the separation of methyl and inorganic mercury consisted of a Waters metal-free 626 gradient pump, a Rheodyne 7725 injector with a 50 μL sample loop and a reverse phase column (Symmetry Shield RP$_{18}$ column, 150 mm × 3.9 mm, 5 μm, Waters). The

Table 1
Operating conditions of Thermo X7 ICP-MS

Plasma conditions	
Forward power (W)	1300
Plasma gas flow rate (L min^{-1})	13.5
Auxiliary gas flow rate (L min^{-1})	0.75
Nebulizer gas flow rate (L min^{-1})	0.84
Nebulizer	Glass concentric
Spray chamber	Quartz impact bead
Measurement parameters	
Acquisition mode	Continuous[a] or time resolved analysis[b]
Isotope monitored	^{202}Hg
Dwell time per point (ms)	10[a], 100[b]
Replicates	3[a], 1[b]
Total analysis time (s)	35[a], 800[b]

[a] For total mercury analysis.
[b] For mercury speciation analysis.

mobile phase flow rate was 1 mL/min. The outlet of the column was directly connected to the nebulizer of an ICP-MS system by a PEEK tubing (Ø = 0.13 mm).

The determination of mercury was carried out on a Thermo X7 ICP-MS (Thermo Electron Corp., Waltham, USA) through all the experiment. The mass calibration of the ICP-MS instrument was tuned daily with a tuning solution of 5 μg L^{-1} Be, Co, In and U in 5% (v/v) methanol for speciation analysis or in the extraction solution for total mercury analysis. The optimal operation conditions and data acquisition parameters are given in Table 1.

2.2. Reagents and materials

The guaranteed grade hydrochloric acid, HPLC grade methanol, analytical grade potassium chloride and ammonium acetate were obtained from Beijing Chemical Reagents Company (Beijing, China). The guaranteed grade 2-mercaptoethanol was supplied by Nacalai Tesque Inc. (Kyoto, Japan). Ultra-pure water (18.2 MΩ cm^{-1}) from a Milli-Q water purification system (Millipore, MA, USA) was used.

A standard solution of 1000 mg Hg L^{-1} of Hg^{2+} in 10% (v/v) HNO$_3$ was purchased from AccuStandard Inc. (Connecticut, USA). The methylmercury chloride (CH$_3$HgCl) was supplied by Riedel-de Haën (Seelze, Germany) and a stock solution of 1000 mg Hg L^{-1} was prepared by dissolving CH$_3$HgCl in 10% (v/v) HNO$_3$. All the stock standard solutions were protected from light and stored at 4 °C. The mercury working standards were prepared daily by proper dilution with the extractant solution.

The HPLC mobile phase containing 5% (v/v) methanol, 0.1% (v/v) 2-mercaptoethanol and 0.06 mol L^{-1} ammonium acetate was used.

Several certified reference materials (CRMs), including NRCC DOLT-3 (dogfish liver), IAEA 436 (tuna fish), IAEA MA-B-3/TM (garfish muscle), IAEA MA-M-2/TM (mussel tissue), GBW 08193 (bovine liver), GBW 08572 (prawn) and GBW 07601 (human hair), were used for method validation.

2.3. Procedure

The sample (about 100 mg) was accurately weighed into a 10 mL capped polyethylene centrifuge tube. Then, 5 mL of the extractant solution were added. Subsequently, the mixture solution was put into an incubator shaker for shaking overnight (about 12 h) at room temperature. Afterwards, the supernatant was collected by centrifugation at 3000 rpm for about 10 min. The residue was vortexed with another 5 mL extraction solution for about 1 min, and then centrifuged. The two portions of the resulting supernatant solution were mixed together and passed through a 0.45 μm filter prior to analysis. Blanks were prepared along with the samples in each batch. The total mercury concentration in the extracted solution was analyzed by ICP-MS in a continuous mode and mercury species were analyzed by HPLC–ICP-MS in time resolved analysis (TRA) mode.

3. Results and discussion

3.1. Effect of extractant solution composition

The composition of extractant solution was a significant factor to affect extraction efficiency of mercury species. Westöö first developed a classic protocol to extract methylmercury from fish by 6 mol L^{-1} hydrochloric acid [5]. Later, many modifications of Westöö's method were proposed to extract mercury species by a strong acidic medium containing NaCl, KBr or iodoacetic acid [1]. However, all the above procedures have two main disadvantages when coupled with HPLC–ICP-MS for mercury speciation analysis. Firstly, considering a compatible pH value for the reverse phase column, a laborious procedure usually has to be adopted to adjust appropriate pH of the extracted solution prior to injection into HPLC, especially in the case of using concentrated acids. Secondly, it might be prone to form artificial mercury species when using concentrated acids. Rahman and Kingston indicated that the 11 mol L^{-1} HNO$_3$ or 5 mol L^{-1} HCl contained extractant might be unsuitable for mercury speciation analysis in soil and sediment samples because the complete or significant transformation from methylmercury to inorganic mercury could occur [15].

In order to improve extraction efficiency of mercury species at low acidity, some extractant solution, such as 0.05% (m/v) L-cysteine–0.05% (v/v) 2-mercaptoethanol [16] or diluted HNO$_3$ (5–20%, v/v)–thiourea (0.02–0.2%, v/v) [17] have been used to extract mercury species from both biological and soil samples in combination with microwave- [16] or ultrasound-assisted method [17]. Since mercury had a high affinity to sulphydryl group, therefore, in many studies one kind of sulphydryl reagent was usually used as a component in an extraction system.

In this work, 2-mercaptoethanol was used as an ion-pair reagent in the mobile phase for HPLC study. In order to simplify the subsequent HPLC operation, 2-mercaptoethanol was considered to use as a component of the extractant solution as well. The effect of different 2-mercaptoethanol concentrations (0%, 0.05%, 0.1%, 0.15% and 0.2%, v/v) in 0.15% (m/v) KCl and 0.1% (v/v) HCl contained extractant solution
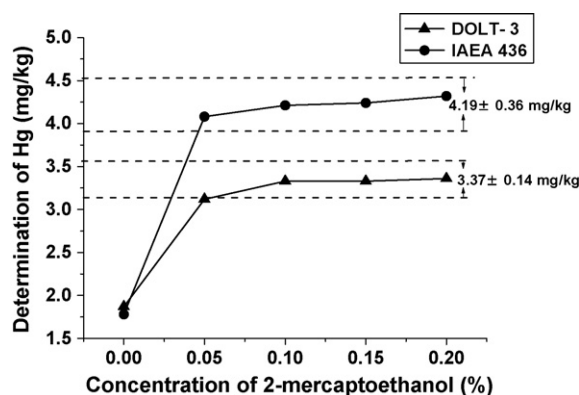
Fig. 1. Effect of the concentration of 2-mercaptoethanol on the extraction of total mercury from NRCC DOLT-3 and IAEA 436. The extractant solution contained 2-mercaptoethanol, 0.1% (v/v) HCl and 0.15% (m/v) KCl. The samples were shaken overnight (about 12 h) at room temperature. The certified values of mercury in NRCC DOLT-3 and IAEA 436 are 3.37 ± 0.14 and 4.19 ± 0.36 mg kg^{-1}, respectively.

on the extraction efficiency of mercury in two certified reference materials, NRCC DOLT-3 and IAEA 436 was studied. Total mercury in the extracted solution was determined by ICP-MS. The results are presented in Fig. 1. The data indicated that the extraction efficiency of mercury increased with the increase of 2-mercapoethanol concentration. Compared with the certified values, the results showed that when the concentration of 2-mercaptoethanol was 0.1% (v/v), the extraction efficiencies reached 98.8% and 100.5% for the two references materials, respectively. Whereas, when higher concentration of 2-mercaptoethanol was used, no significant increase of the extraction efficiency was found. Some researchers reported that the retention time of mercury species in HPLC increased with the increase of 2-mercapoethanol concentration in the mobile phase when using a reverse column [16]. Therefore, the extractant solution containing 0.1% (v/v) 2-mercaptoethanol was chosen to use in the following experiments.

Fig. 2 shows the extraction efficiency of mercury in NRCC DOLT-3 and IAEA 436 by four extractant solution, 0.1% (v/v) 2-mercaptoethanol alone; 0.1% (v/v) 2-mercaptoethanol–0.1% (v/v) HCl; 0.1% (v/v) 2-mercaptoethanol–0.15% (m/v) KCl and 0.1% (v/v) 2-mercaptoethanol–0.15% (m/v) KCl–0.1% (v/v) HCl. The results indicated that quantitative extraction of mercury could not be achieved by using 0.1% (v/v) 2-mercaptoethanol alone. In order to enhance the extraction efficiency, HCl and KCl were added into the extractant solution. It was reported that the addition of 0.15% (m/v) KCl into the extractant could improve the extraction efficiency of mercury [18]. An acid medium is helpful for the quantitative extraction of mercury species from biological matrices. Considering a compatible pH value for the reverse phase column, 0.1% (v/v) HCl was added to keep the pH of the extracted solution at about 2; thus, the solution could be directly injected into the column.

Our results indicated that the extractant solution of 0.1% (v/v) HCl, 0.1% (v/v) 2-mercaptoethanol and 0.15% (m/v) KCl could quantitatively extract total mercury from the two reference materials.
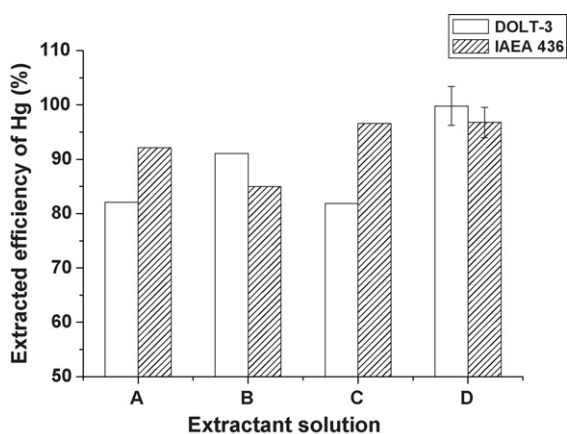
Fig. 2. Effect of the composition of the extractant solution on mercury extraction from NRCC DOLT-3 and IAEA 436. Extractant solution: (A) 0.1% 2-mercaptoethanol; (B) 0.1% 2-mercaptoethanol + 0.1% HCl; (C) 0.1% 2-mercaptoethanol + 0.15% KCl; (D) 0.1% 2-mercaptoethanol + 0.15% KCl + 0.1% HCl ($n = 4$). The samples were shaken overnight (about 12 h) at room temperature.

3.2. Effect of shaking time

The effects of different shaking time, 1, 2, 4, 8, 12, 16 and 24 h on the extraction efficiency of mercury from biological matrices are presented in Fig. 3. Two certified reference materials, NRCC DOLT-3 and IAEA 436, were used for the optimization experiments. The samples were processed according to the procedure described in Section 2. The optimal extractant solution, 0.1% (v/v) 2-mercapoethanol, 0.1% (v/v) HCl and 0.15% (m/v) KCl, was used. As shown in Fig. 3, when the shaking time was over 2 h, the extraction efficiency of mercury could reach over 90%. When the shaking time was about 12 h, the efficiency could be higher than 95%. Therefore, in order to guarantee all the mercury completely extracted from samples, the optimal shaking time was conveniently selected as 12 h (overnight).

3.3. Validation of the extraction method

The developed extraction method was validated by determination of seven certified reference materials, including NRCC
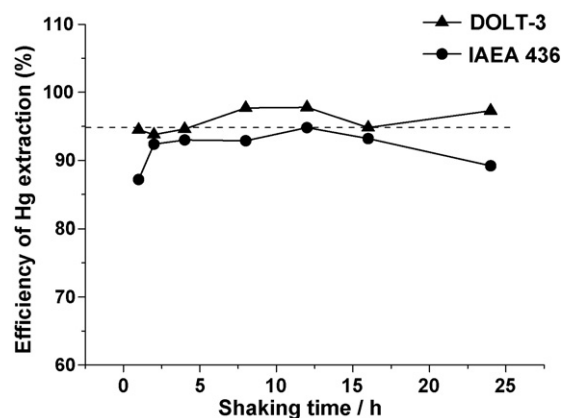
Fig. 3. Effect of shaking time on the extraction efficiency of mercury from NRCC DOLT-3 and IAEA 436. Extractant solution: 0.1% 2-mercaptoethanol + 0.15% KCl + 0.1% HCl.

DOLT-3 (dogfish liver), IAEA 436 (tuna fish), IAEA MA-B-3/TM (garfish filet), IAEA MA-M-2/TM (mussel tissue), GBW 08193 (bovine liver), GBW 08572 (prawn) and GBW 07601 (human hair). The procedure was the same as described in Section 2. In all the determined samples, only two mercury species, inorganic and methylmercury could be detected. Compared with the certified or reference values, the data showed that the extraction method could quantitatively extract total mercury from the various biological samples, except for human hair sample (GBW 07601). In the hair samples (GBW 07601), only about 60% of total mercury was extracted. The reason might be due to the different matrices of human hair from animal tissues. For the tissues which composed of strong structural protein, i.e. keratin, such as hair and nail, only high concentration of acid should be used for efficient extraction, however, as for the loose freeze-dried tissue samples, the mild extractant solution could achieve the extraction purpose. The results summarized in Table 2, except for the data of human hair (GBW 07601), were in good agreement with the certified or the reference values of both total mercury and methylmercury, indicating that the transformation of mercury species during sample preparation could be negligible.

Based on the mercury standard solution measurements, the response of methyl and inorganic mercury by HPLC–ICP-MS determination are both linear up to $100\,\mu g\,L^{-1}$. The limit of detection (LOD) for methyl and inorganic mercury by HPLC–ICP-MS are the same as $0.2\,\mu g\,L^{-1}$ (defined as three times of the standard deviation of the blank). Precision was determined using six injections of a standard solution containing CH_3Hg^+ and Hg^{2+} ($10\,\mu g\,Hg\,L^{-1}$, respectively). The relative standard deviations of the peak area were 3.0% and 5.8% for CH_3Hg^+ and Hg^{2+}, respectively. The relative standard deviation of the retention time was found to be 0.5% and 0.8% for CH_3Hg^+ and Hg^{2+}, respectively.

3.4. Elimination of memory effect of mercury in ICP-MS system

Many previous studies reported that determination of total mercury in biological samples using classic wet digestion method followed by ICP-MS, in contrast to many other elements, suffered from serious memory effect [19,20]. The appearance of mercury in the instrumental system is attributed to the fact that the ionic mercury species in the digested solution are prone to adhere to the walls of the spray chamber and the transfer tubing in the sample introduction system. The memory effect will result in non-linear calibration graphs, long washing time and poor detection sensitivity [20].

In this experiment, mercury species extracted from biological samples could coordinate with 2-mercaptoethanol to form a stable mercury-sulphur complex in the extraction system. Then, the mercury complex was directly aspirated into ICP-MS. An investigation was conducted to compare the memory effect of the developed extraction solution with the commonly used 2% HNO_3 solution in ICP-MS system. A mixed solution containing inorganic mercury ($50\,\mu g\,L^{-1}$) and rhodium ($50\,\mu g\,L^{-1}$) in the optimal extractant was aspirated into ICP-MS in time resolved analysis (TRA) mode for about 2 min. Afterwards, the sampling

Table 2
Hg^{2+}, CH$_3$Hg$^+$ and total Hg in biological reference materials using the developed extraction method[a]

Samples	Determination by HPLC–ICP-MS			Determination by ICP-MS	Certified or reference values of CH$_3$Hg$^+$ (mg kg^{-1})	Certified values of total Hg (mg kg^{-1})
	CH$_3$Hg$^+$ (mg kg^{-1})	Hg^{2+} (mg kg^{-1})	Total Hg[b] (mg kg^{-1})	Total Hg (mg kg^{-1})		
GBW 080193 bovine liver	<LOD[c]	0.176 ± 0.001	0.176 ± 0.001	0.193 ± 0.004	–	0.18[d]
IAEA MA-M-2 mussel tissue	0.068 ± 0.001	0.865 ± 0.007	0.932 ± 0.007	0.939 ± 0.008	0.068 ± 0.006 [21]	0.93 ± 0.16
NRCC DOLT-3 dogfish liver	1.50 ± 0.03	1.87 ± 0.04	3.39 ± 0.06	3.36 ± 0.06	1.59 ± 0.12	3.37 ± 0.14
GBW 05872 prawn	0.181 ± 0.002	<LOD[c]	0.181 ± 0.002	0.201 ± 0.008	0.178 ± 0.005 [22]	0.201 ± 0.004
IAEA MA-B-3 garfish filet	0.443 ± 0.007	0.050 ± 0.004	0.493 ± 0.011	0.489 ± 0.012	0.434 ± 0.015 [21], 0.434 ± 0.021 [22]	0.51 (0.47–0.61)
IAEA 436 tuna fish	3.48 ± 0.12	0.562 ± 0.034	4.04 ± 0.14	4.06 ± 0.12	3.67 ± 0.42	4.19 ± 0.36
GBW 07601 human hair	0.153 ± 0.008	0.059 ± 0.004	0.211 ± 0.008	0.208 ± 0.010	0.146 ± 0.006 [22]	0.36 ± 0.05

[a] Values are means ± S.D. of three determinations (n = 3).
[b] Total Hg = CH$_3$Hg$^+$ + Hg^{2+}.
[c] <LOD: below the limit of determination.
[d] Information value.
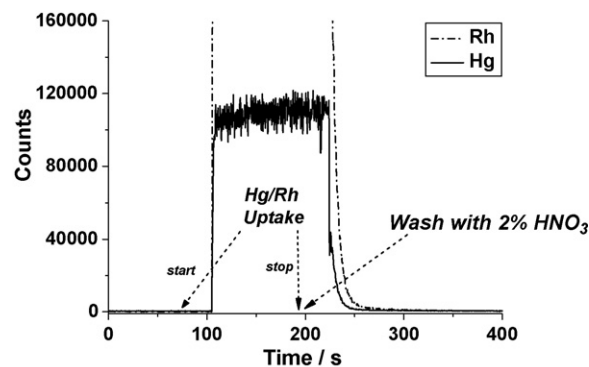
Fig. 4. Signal profile of mercury at *m/z* 202 and rhodium at *m/z* 103 in the time resolved analysis mode. The aspirated solution contained inorganic mercury (50 µg L^{-1}) and rhodium (50 µg L^{-1}) in 0.1% 2-mercaptoethanol–0.15% KCl–0.1% HCl extractant mixture. The washing solution was 2% (v/v) HNO$_3$.
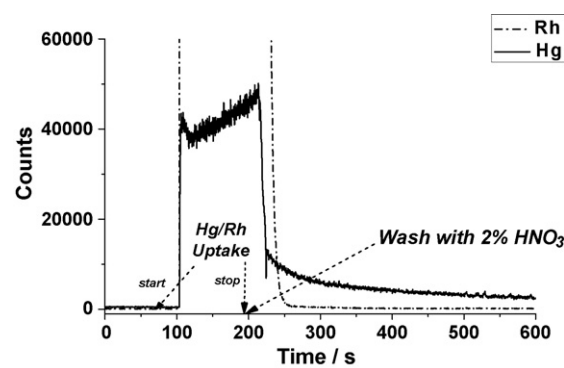
Fig. 5. Signal profile of mercury at *m/z* 202 and rhodium at *m/z* 103 in the time resolved analysis mode. The aspirated solution contained inorganic mercury (50 µg L^{-1}) and rhodium (50 µg L^{-1}) in 2% (v/v) HNO$_3$. The washing solution was 2% (v/v) HNO$_3$.

tube was removed from the mixed solution and placed into 2% (v/v) HNO$_3$ for washing. The intensities of mercury and rhodium were recorded with the proceeding time by ICP-MS. The signal peak profiles for analysis of mercury and rhodium using the developed extractant solution are shown in Fig. 4. The signal of mercury returned to the baseline level at almost the same time as rhodium. The similar results could be obtained when analyzing mercury in the certified reference materials by using the developed extraction method. However, when the mixed standard was in the conventional 2% (v/v) HNO$_3$ solution with the same proceeding, the mercury signal was difficult to return to the baseline even after 6 min of washing time (Fig. 5). These results clearly demonstrated that the memory effect of mercury in the ICP-MS system could be effectively eliminated by using the developed extraction method.

4. Conclusions

A mild, efficient and convenient extraction method followed by ICP-MS and HPLC–ICP-MS for determination of total mercury and mercury species in biological samples has been established. Quantitative extraction of total mercury was achieved by using the optimal extractant solution of 0.1% (v/v) HCl, 0.1% (v/v) 2-mercapoethanol and 0.15% (m/v) KCl. The complete

extraction should be assisted by shaking overnight (about 12 h) at room temperature.

The developed extraction method offers the following advantages: (1) high extraction efficiency under a mild condition; (2) no distinguishable transformations between mercury species; (3) conveniently direct injection into the column of HPLC without pH adjustment; (4) the memory effect of mercury in ICP-MS system can be eliminated.

Acknowledgements

References

[1] M. Leermakers, W. Baeyens, P. Quevauviller, M. Horvat, Trends Anal. Chem. 24 (2005) 383.
[2] E. Bramanti, C. Lomonte, M. Onor, R. Zamboni, A. D'Ulivo, G. Raspi, Talanta 66 (2005) 762.
[3] P. Tajes-Martinez, E. Beceiro-Gonzalez, S. Muniategui-Lorenzo, D. Prada-Rodriguez, Talanta 68 (2006) 1489.
[4] B. Michalke, Trends Anal. Chem. 21 (2002) 142.
[5] G. Westöö, Acta Chem. Scand. 20 (1966) 2131.
[6] N.S. Bloom, Can. J. Fish. Aquat. Sci. 49 (1992) 1010.
[7] M. Horvat, K. May, M. Stoppler, A.R. Byrne, Appl. Organomet. Chem. 2 (1988) 515.
[8] H. Hintelmann, R. Falter, G. Ilgen, R.D. Evans, Fresen. J. Anal. Chem. 358 (1997) 363.
[9] A.I.C. Ortiz, Y.M. Albarran, C.C. Rica, J. Anal. At. Spectrom. 17 (2002) 1595.
[10] G.M.M. Rahman, H.M. Kingston, J. Anal. At. Spectrom. 20 (2005) 183.
[11] S. Rio-Segade, C. Bendicho, J. Anal. At. Spectrom. 14 (1999) 263.
[12] J.L. Luque-Garcia, L. de Castro, Trends Anal. Chem. 22 (2003) 41.
[13] C.M. Tseng, A. deDiego, F.M. Martin, O.F.X. Donard, J. Anal. At. Spectrom. 12 (1997) 629.
[14] J. Qvarnstrom, W. Frech, J. Anal. At. Spectrom. 17 (2002) 1486.
[15] G.M.M. Rahman, H.M. Kingston, Anal. Chem. 76 (2004) 3548.
[16] C.S. Chiou, S.J. Jiang, K.S.K. Danadurai, Spectrochim. Acta Part B 56 (2001) 1133.
[17] M.V.B. Krishna, M. Ranjit, D. Karunasagar, J. Arunachalam, Talanta 67 (2005) 70.
[18] A. Collasiol, D. Pozebon, S.M. Maia, Anal. Chim. Acta 518 (2004) 157.
[19] Y.F. Li, C.Y. Chen, B. Li, J. Sun, J.X. Wang, Y.X. Gao, Y.L. Zhao, Z.F. Chai, J. Anal. At. Spectrom. 21 (2006) 94.
[20] C.F. Harrington, S.A. Merson, T.M.D. D'Silva, Anal. Chim. Acta 505 (2004) 247.
[21] M. Horvat, Water Air Soil Poll. 56 (1991) 95.
[22] M. Wang, W.Y. Feng, F. Zhang, B. Wang, J.W. Shi, B. Li, Z.F. Chai, Y.L. Zhao, Chin. J. Anal. Chem. 33 (2005) 1671.

Evanescent wave infrared chemical sensor possessing a sulfonated sensing phase for the selective detection of arginine in biological fluids

Yeu K. Wei, Jyisy Yang *

Department of Chemistry, National Chung-Hsing University, Taichung 402, Taiwan

Received 12 July 2006; received in revised form 15 September 2006; accepted 15 September 2006
Available online 27 October 2006

Abstract

This paper describes a new infrared (IR) sensing scheme for the determination of arginine (Arg). In this method, the surface of an IR evanescent wave sensing element was modified with sulfonic acid groups to selectively interact with Arg through specific interactions with its guanidine moiety. The sulfonated sensing phase was prepared using a two-layer modification approach. To demonstrate that this assembly could be used for selective infrared sensing, a large number of amino acids were subjected to analysis. Although the sulfonate groups on the surface of the sensing element did interact selectively with the guanidine groups of Arg species, lysine and histidine units caused some interference; this problem could be minimized because of the unique IR absorption bands of the guanidine moiety of Arg. To optimize the detection conditions, we studied the effects of both the pH and the composition of the polymer. The most intense signal was obtained at pH 9. We observed different adsorption rates for the detection of Arg at different values of pH, which we attribute to changes in the accessibility of the analytes to the pore structures of the sensing phase. The composition of the base polymer was also optimized; 60% PVBC (w/w) provided a water-stable, sensitive phase for the detection of Arg in aqueous solution. Under the optimized conditions, we obtained a linear range of detection up to 0.1 mM with a detection limit of ca. 5 μM.
© 2006 Elsevier B.V. All rights reserved.

Keywords: Evanescent wave; Infrared; Sulfonic acid group; Guanidine moiety; Arginine

1. Introduction

Amino acids, the building blocks of peptides and proteins, play many vital roles in the metabolic processes within living bodies. Among the amino acids, arginine (Arg) is the most basic natural amino acid, having the highest proton affinity [1]. On the surfaces of proteins, Arg and two other relatively weakly basic amino acids, lysine and histidine, often play crucial roles in protein recognition [2]. Arg residues are important components for biological peptide and protein recognition and for protein folding processes. The guanidine moiety – a strongly basic functional unit responsible for the majority of this amino acid's interactive behavior – provides a site for strong electrostatic interactions and/or hydrogen bonding with anionic functional units [3]. Arg is also of considerable interest in human nutrition and health; it is present in significant amounts in many agricul-

tural products [4]. Measuring the concentration of Arg in blood serum is a fairly effective approach toward identifying diseases, such as disorders related to amino acid metabolism, and determining the clinical states of patients having unbalanced nutrition [5]. Also, the concentration of Arg can be used to measure the maturity of peanuts and grapes, and the degree of fermentation of musts and wines. Thus, techniques for the rapid determination of the concentration of Arg in biological fluids remain in demand.

A large number of methods have been proposed to analyze the levels of Arg in biological samples, including those using HPLC [6], amino acid analyzers [7], capillary electrophoresis [8], voltammetry [9], and fluorometric methods [10]. These methods suffer from a number of disadvantages, including they being highly time-consuming and complicated in terms of the need for sample pretreatment. Although colorimetric-based analyses – e.g., the Staron–Allard and Voges–Proskauer methods [11], and Sakaguchi reaction methods [12] – are widely used because of their simplicity, such wet chemical reactions generally lack simplicity and, sometimes, specificity. The application of the

* Corresponding author. Tel.: +886 422840411x514; fax: +886 422862547.
E-mail address: jyisy@dragon.nchu.edu.tw (J. Yang).

arginase enzyme for the determination of Arg has also been reported [13,14]; this method is, however, rather slow (60 min per sample) and, furthermore, it is useless if urea or ammonia is present in the sample. The enzymatic end-point analysis method proposed by Mira de Orduna [15] is simple, but it consumes a large amount of material.

To improve upon these existing methods, we propose a new Arg sensing scheme based on an evanescent wave infrared (IR) sensor. Because of the short depth of penetration (d_p) of evanescent waves, such infrared sensors are highly suitable for the detection of organic compounds in aqueous solutions [16]. The d_p varies in the IR region from a few tenths of a micron to a few microns; these small values of d_p limit the sensitivity of this type of detection. After suitable treatment of hydrophobic thin films on the surfaces of the evanescent wave sensing elements, the sensitivity can be increased through the attraction of target compounds toward the evanescent field [17]. The ability

of hydrophobic thin films to attract polar compounds is, however, limited. To improve the attraction toward polar compounds while maintaining the water stability of the sensing phase, we have devised a two-layer modification method. In this approach, a reactive hydrophobic thin film is first treated on the surface of the IRE; the desired polar functional groups are subsequently covalently bound to the surface of the hydrophobic thin film [18–22]. In this manner, water-stable sensing phases can be produced with the potential for enhanced sensitivity.

To produce a sensitive infrared sensor for the specific detection of Arg, we chose to modify the sensing phase with sulfonic acid groups. Several advantages exist for using sulfonic acid groups to attract Arg species. First, the sulfonic acid group is easily deprotonated; the group bears a negative charge at most values of pH. This property is highly useful in terms of attracting positively charged Arg units through electrostatic interactions. Secondly, the sulfonic acid group exhibits only a few infrared absorption bands, which are located mainly around $1000 \, cm^{-1}$. Because these absorption bands exist far from the characteristic bands of amino acids, spectral interference is minimized. Furthermore, as demonstrated by Schug et al. [23] and Friess and Zenobi [2], sulfonic acid groups are capable of interacting selectively with amino acids possessing guanidine moieties because of their mutual forklike structures (Fig. 1A). Therefore, we believed that integrating these features with IR sensing technology would provide access to selective and sensitive IR sensors. To prepare the desired sulfonated sensing phase, we utilized the reaction scheme displayed in Fig. 1B. We used poly(vinylbenzyl chloride) (PVBC) as a reactive hydrophobic polymer with which to treat the surface of the sensing element. Through suitable reactions with thio compounds and their subsequent oxidation, a sensing phase presenting sulfonic acid groups was prepared for the direct sensing of Arg units.

2. Experimental

2.1. Chemicals

Poly(ethylene) (PE) and PVBC were obtained from Aldrich Chemical and used as received. Toluene (Acros Organics, Geel, Belgium) and p-xylene (Shimakyu Chemicals, Osaka, Japan) were used as solvents for the polymer solutions. Sodium iodide and potassium permanganate were obtained from Shimakyu Chemicals. Acetonitrile was obtained from TEDIA (Fairfield, Ohio). 1,3-Propanedithiol was purchased from Lancaster Chemicals. Tributylamine was obtained from Acros Organics. All reagents were of reagent grade and used as received without further purification. Deionized water was used to prepare all of the aqueous solutions.

2.2. Apparatus

The experimental setup is presented in Fig. 2A. The dimensions of the sample cell were $30 \, mm \times 30 \, mm \times 20 \, mm$; 15 mL of the aqueous sample could be loaded. A 45° trapezoidal ($55 \, mm \times 4 \, mm \times 2 \, mm$) zinc selenide internal reflection element, purchased from International Crystal Laboratory
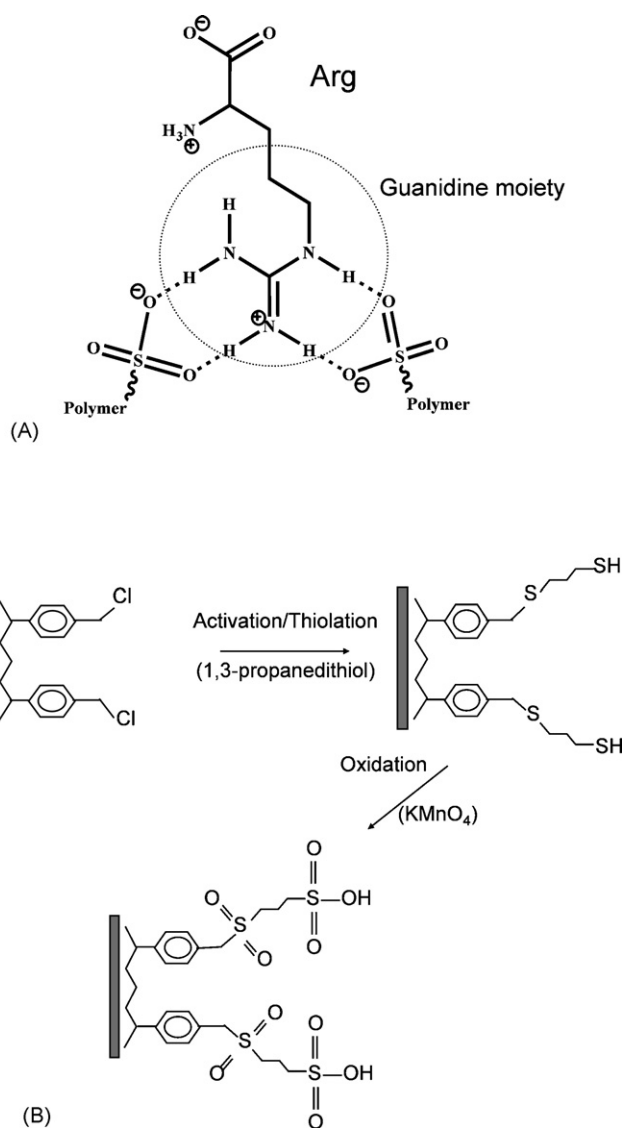
Fig. 1. (A) Schematic illustration of the interaction between two sulfonate groups and the guanidine group of Arg. (B) Procedures used in the preparation of the water-stable sulfonate sensing phase.
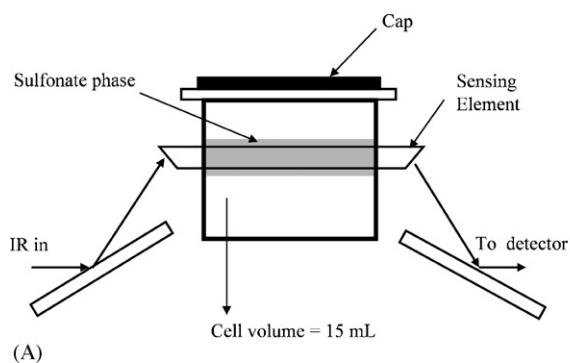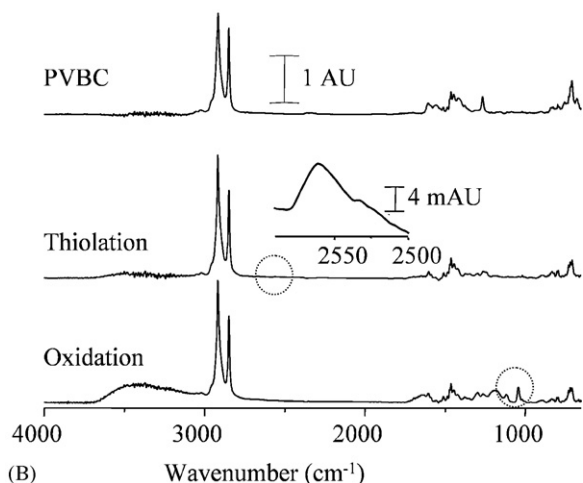
Fig. 2. (A) Schematic illustration of the sensing device used in this study. (B) Typical spectra of the polymer coating [PVBC/PE; 60/40 (w/w)], the thiol-modified polymer phase, and the sulfonated sensing phase.

(Garfield, New Jersey), was placed at the center of the sample cell. The sample cell was placed in the sample compartment of a Jasco 460 plus FT-IR spectrometer (Jasco Co., Tokyo, Japan), equipped with a medium range mercury-cadmium-telluride detector. All of the spectra were acquired by co-adding of 64 scans at $4 \, cm^{-1}$ resolution. To remove the small baseline variation caused by water vapor, a mean-value smooth function with a bandwidth of $5 \, cm^{-1}$ was applied to each spectrum before calculation of the peak intensities.

2.3. Preparation of sensing phase

Different concentrations of the polymer solutions were prepared by dissolving different weights of PVBC and PE in p-xylene at 80 °C. The prepared polymer solution (30 μL) was coated directly onto the surface of the sensing element. After air-drying for at least 1 h, the coated sensing element was placed into a solution containing 2% (w/v) sodium iodide in acetonitrile and heated to 60 °C for 24 h. This sensing phase was thiolated by soaking it in a solution containing 5% (v/v) 1,3-propanedithiol and 2.5% (v/v) tributylamine in toluene for 10 min at room temperature. Following oxidation of the attached thiol compounds (0.1 M $KMnO_4$, 10 min), the sulfonated sensing phase was obtained.

3. Results and discussion

3.1. Characterization of sulfonated sensing phase

To ensure that a suitable sulfonated sensing phase was synthesized, the reaction products from each step were monitored using an IR spectrometer; Fig. 2B displays these spectra. We
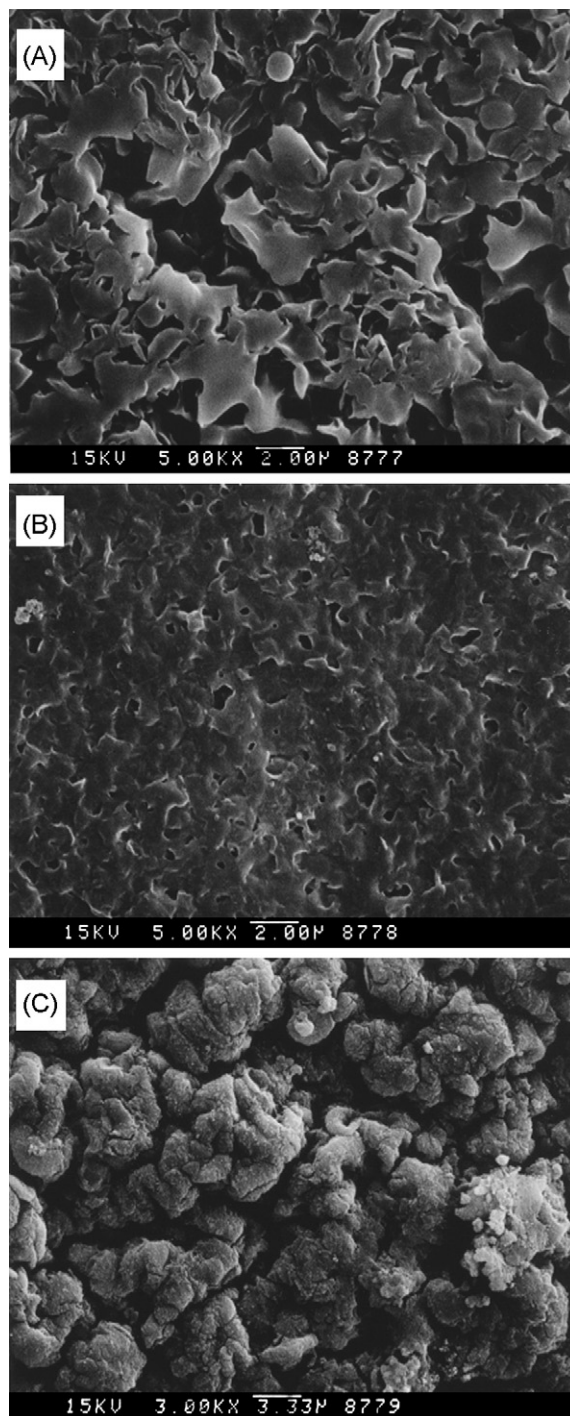
Fig. 3. Scanning electron micrograph images of the sensing phase at different stages of its preparation: (A) PVBC/PE polymer; (B) thiol-modified polymer; and (C) sulfonated sensing phase.

observe that PVBC was successfully thiolated after treatment with 1,3-propanedithiol for 10 min, as indicated by the weak absorption located at ca. $2550\,cm^{-1}$ for SH stretching. To produce the sulfonic acid groups on the surface, the thiolated phase was oxidized in $KMnO_4$ solution; strong absorption bands were generated at ca. $1100\,cm^{-1}$, representing the symmetric and asymmetric stretching bands of sulfonate units. Based on these features, it was clear that the sulfonated sensing phase was obtained successfully.

To provide further information about the changes in the morphologies of the sensing phase during each step of the synthesis, a scanning electron microscope (SEM) was used to obtain the images presented in Fig. 3. The hydrophobic thin film of PVBC exhibited a dense phase containing macropores, which are visible in Fig. 3A. After thiolation, the sensing phase appeared as a denser film possessing smaller pore sizes on its surface; in addition, the surface has a relatively more uniform structure than did the unmodified PVBC film. After oxidation, the surface of the sensing phase became rougher and looser, as indicated in Fig. 3C. These features suggested that a more rapid rate of sensing of the target molecules might occur because of the higher surface area present after oxidation.

3.2. Effect of pH on the sulfonated sensing phase

The functional groups attached to the sensing phase were in the form of $-SO_3H$ units under acidic conditions. In contrast, in a basic solution, they were deprotonated. To determine whether any spectral interference of sulfonic acid group would occur when detecting the amino acids, the synthesized phases were subjected to aqueous solutions at various values of pH. The pK_a for the dissociation of the second proton of sulfonic acid is ca. 1.92 [23]. Assuming that the immobilized sulfonic acid groups in the sensing phase would exhibit behavior similar to that of sulfonic acid, we expected the synthesized sensing phase to be insensitive to pH changes at values of pH higher than 3; i.e., it should remained deprotonated in solutions having values of pH above 3. To confirm this hypothesis, we subjected the sulfonated sensing phase to aqueous solutions having values of pH in the range from 4 to 11. Fig. 4 displays the corresponding IR spectra, indicating the major absorption band region of the sulfonic acid groups. These spectra were acquired after soaking the samples for 30 min with a background obtained at pH 7. Several bands were affected slightly by the changes of the pH. For example, the absorption bands of the $-SO_3^-$ groups ($1042\,cm^{-1}$) were shifted to 1050 and $1038\,cm^{-1}$ at pH 4 and 11, respectively. The small shift in this band's position indicates that the synthesized sensing phase existed mainly in the form of deprotonated sulfonic acid groups (i.e., sulfonate ions), but small variations in the local electron densities occurred at different values of pH. In terms of quantitative analysis, this small variation restricts the use of the spectral region at ca. $1000\,cm^{-1}$. Fortunately, no intense bands for amino acids exist around this region and, therefore, the performance of the sulfonated sensing phase for the detection of amino acids should not suffer from any degradation.
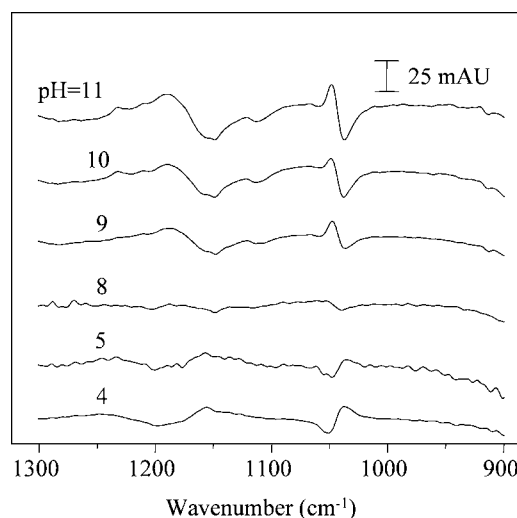
Fig. 4. Variation of the sulfonate sensing phase at different values of pH. An aqueous solution at pH 7 was used to obtain the background spectrum.

3.3. Effect of pH on the chemical properties of Arginine in water

Each amino acid contains two common functionalities: amino and carboxylic acid groups. The chemical form of an amino acid is, therefore, strongly influenced by the pH of the sample solution. To determine the chemical form most suited to detection by the sulfonated sensing phase, we first examined the detection of Arg. The chemical equilibria between the different chemical species of Arg can be expressed as shown in Fig. 5A. To determine the relative abundance of each species of Arg, we calculated their mole fractions at various values of pH based on the corresponding literature values of pK_a [24]; Fig. 5B provides a plot of the results. Four chemical forms of Arg exist; for simplicity, we name these chemical forms R^{2+}, R^+, R, and R^- based on their net charges. In terms of the electrostatic interactions, R^{2+} should interact most effectively with the sulfonate groups; the negatively charged R^- is the species least likely to be detected because of electrostatic repulsion. Based on the calculated mole fractions of each species of Arg at different values of pH, we predicted that its adsorption should be favored at values of pH below 11 to reduce the effects of charge repulsion.

To observe the variation in the IR absorption bands upon changing the pH, we prepared solutions of 100 mM Arg at various values of pH and examined them using the bare sensing element. Fig. 5C indicates that several intense bands appeared at 1670, 1640, 1630, 1580, 1525, and $1400\,cm^{-1}$. Based on literature values [25,26], the bands located at 1580 and $1400\,cm^{-1}$ are assignable to the asymmetric and symmetric stretches of the carboxylate group. The guanidine group in Arg is responsible for the two absorption bands at 1670 and $1640\,cm^{-1}$, which correspond to the asymmetric and symmetric stretches, respectively, of this unit. The absorption bands of the α-amine group (NH_3^+) are responsible for the two bands at 1630 and $1525\,cm^{-1}$ (asymmetric and symmetric deformations, respectively). The absorption bands representing the guanidine group were observable at each value of pH with similar intensities. The absorption bands of the
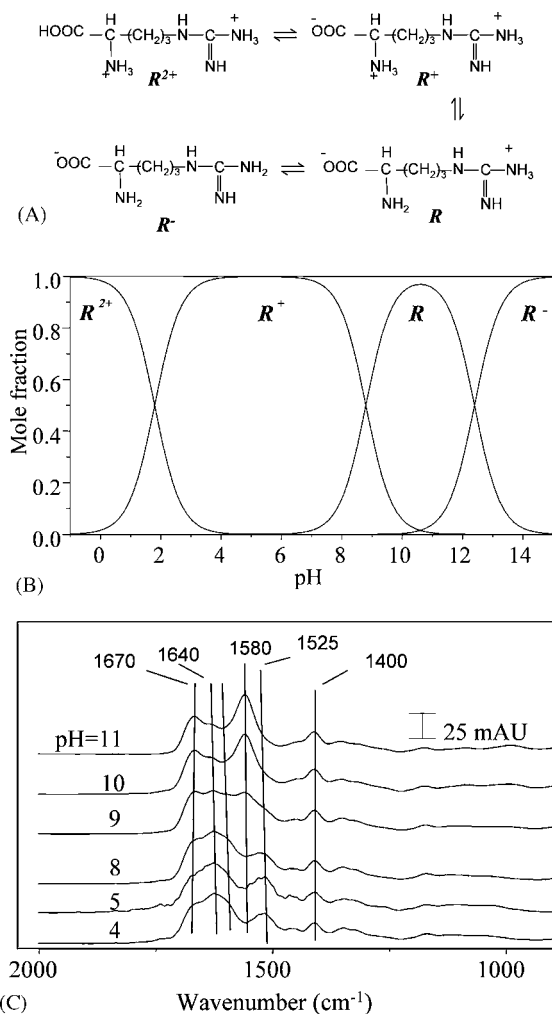
Fig. 5. (A) The chemical equilibria between the different chemical species of Arg. (B) Calculated mole fractions of the Arg species at different values of pH. (C) Infrared spectra of solutions of 100 mM Arg in water at different values of pH. Bare ZnSe was used to obtain these spectra.

Fig. 6. (A) Infrared spectra of Arg adsorbed to the sulfonate film from a 0.1 mM aqueous Arg solution at different values of pH. (B) Response time profiles for solutions containing 0.1 mM Arg at values of pH of 10 (●), 9 (■), 8 (▲), and 5 (▼).

carboxylate group were more intense at values of pH higher than 10. This observation agrees with our calculated mole fractions of Arg. For instance, at values of pH higher than 10, the major forms of Arg are R and R^-, i.e., those with deprotonated carboxylic acid groups. At pH 9, the spectrum indicates that the Arg solution contains the species R and R^+ because of the broad absorption extending from 1680 to 1630 cm^{-1}. At values of pH in the range from 4 to 8, the predominant form of Arg is R^+. The absorption band of the symmetric deformation of the α-amino group (NH_3^+) was observed at 1525 cm^{-1} at low pH, but its asymmetric stretching, which is commonly observed at 1626 cm^{-1}, was seriously obscured by the presence of other absorption bands in this region. The symmetric absorption band of the α-amino group disappears at high pH (e.g., pH >9) because of its deprotonation.

3.4. Effect of pH on the detection of Arginine by sulfonated sensing phase

To optimize the conditions for sensing Arg in aqueous solution and to determine the species that can most effectively interact with the sulfonated sensing phase, we prepared a series of 100 μM Arg solutions having various values of pH. Although the concentrations of these Arg solution were 1000 times lower than those used in the previous set of experiments, the IR signals remained intense, as indicated in the typical spectra plot presented in Fig. 6A. Based on the intensities of the band of the guanidine group at 1665 cm^{-1}, we calculated the response time profiles (Fig. 6B). As indicated in Fig. 6A, the pH affected the chemical form of Arg and, as a consequence, the appearance of the signals varied with respect to the pH; the most intense signals appeared at pH 9. Note that only the intensities of the bands varied in the IR spectra, not their wave numbers, at the different values of pH. Relative to the spectra in Fig. 5B, the spectra in Fig. 6A exhibited absorption features similar to those of the neat spectra at lower values of pH, but with some slight differences. For example, both stretching absorption bands of the carboxylate group shifted to higher frequency when compared with those in the neat spectrum of Arg measured at low pH. This observation suggests that, in the presence of the modified surface, the carboxylate groups interacted with protons to partially
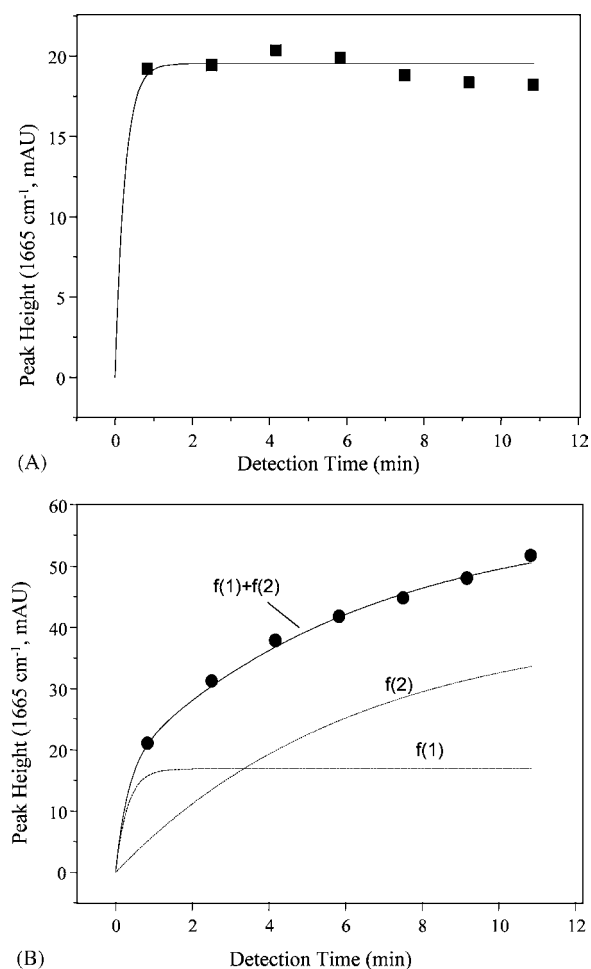
Fig. 7. (A) One exponential growth function fitted to the data for the detection time profile obtained at pH 5. The fitted curve is the solid line and the symbols represent the measured data. (B) Two exponential growth functions fitted to the data for the detection time profile obtained at pH 9. The solid line in this plot is the summation of the fitted values from the fitted curves; the symbols are the measured values.

reduce their electron density. Also, the absorption band of the α-amino group was observed at 1525 cm⁻¹ in all of the spectra, indicating that this functional group remained protonated over the examined pH range.

In terms of the sensitivity of the detection of Arg, the observed signals were most intense in the pH range from ca. 8–9, as indicated in Fig. 6B, after extended detection times. In terms of the speed of detection, the signals reached their maximum intensities during relatively short detection times for the sample solutions having values of pH of ca. 5 and ca. 10. On the other hand, the rate of detection of Arg was relatively much lower at pH 9. Based on the shape of the detection time profile at pH 9, it is highly probably that two mechanisms exist for the adsorption of Arg. To simplify the system, we examined the time profiles at pH 5 and 9 only; the results are plotted in Fig. 7A and B, respectively. In Fig. 7A (pH 5), we observe that one exponential growth function fits the experimental data well for the detection time profile. For the time profile detected at pH 9, two exponential growth functions fit the curve ($R^2 > 0.99$). Based on these observations, the behavior of the detection of

Arg at pH 5 appears to be based mainly on one type of surface adsorption, and the speed of detection is extremely high. For the detection of Arg at pH 9, a second adsorption mechanism exists at a rate that is ca. 10 times slower than that of the first. Comparing the intensities for the first adsorption process at pH 5 and 9, we find that the intensities were slightly weaker for the signals obtained at pH 9. This behavior can be explained by considering the concentration of the positive charged species R^+. For example, the mole fraction of R^+ (refer to Fig. 5A) is ca. 100% at pH 4–7 and it decreases when the pH is increased, eventually disappearing completely at a value of pH of ca. 11. Based on the fitted result for the curve obtained at pH 5, we believe that R^+ can interact effectively with the surface sulfonate groups under these conditions such that the time required for attraction can be shorter than 1 min (Fig. 7A). Based on fitted values for this faster process, the signal of pH 5 is indeed more intense than that obtained at pH 9; in addition, a second, slower process for the adsorption of Arg occurs at pH 9. This behavior is most likely caused by the nature of the pores on the sensing phase (refer to the SEM image in Fig. 3C), which contain active sites that are more readily accessed at pH 9 than at pH 5. These pores may not be easy to access once the surface of the sensing phase is rapidly covered with R^+ units, as we observed at pH 5. Further access to these pores is restricted because the layer of adsorbed R^+ units hinders the movement of other species into the pores. At pH 9, half of the Arg molecules exist in the R form, which has neutral charge and can penetrate deeper more readily, through the first adsorbed Arg layers and into the surface of the sensing phase. Based on the IR spectrum recorded at pH 9, the adsorbed chemical form is similar to that obtained at pH 5; this result indicates that the adsorbed R form of the molecules can further bond to a proton from the environment so that the chemical system re-equilibrates. On the other hand, although the R form of Arg must also access the active sites positioned in pores at deeper layers, the adsorption of Arg favors the positively charged form, i.e., R^+. The signals observed at pH 10 and 11 agree with these deductions. At pH 10, the amount of R^+ in solution is quite low and, as a consequence, weaker-intensity signals are observed. At pH 11, the amount of R^+ is negligible and, hence, only very weak analytical signals are observed.

3.5. Selection of polymer film thickness and composition

Because evanescent wave penetrates only a short distance, the thickness of the polymeric film must be optimized. Meanwhile, controlling the degree of sulfonation is also important in terms of optimizing the sensitivity, water stability, and speed of detection. To examine the effect that the thickness had on detection, polymer solutions containing PVBC and PE [60:40 (w/w)] were prepared in *p*-xylene at concentrations of 0.1, 0.25, 0.5, and 1.0% (w/v). After coating 30 μL of each of these prepared solutions onto the ATR crystal, polymeric films of different thicknesses were obtained. Fig. 8A provides the corresponding time profiles for the detection of 100 μM Arg at pH 9. We observed that the intensities of the signals increased as the thickness of the polymer film increased, but the speed of detection of Arg decreased accordingly, presumably because the inner pores
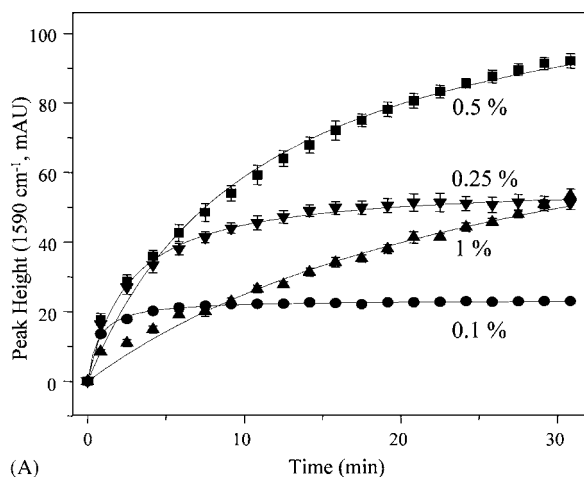
(A)
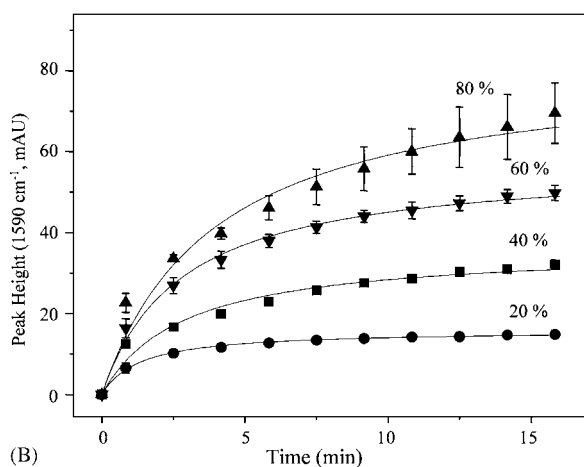
(B)

Fig. 8. (A) Detection time profiles of 100 μM Arg at pH 9 using the sulfonated sensing phases prepared from different polymer concentrations; 1% (■), 0.5% (●), 0.25% (▲), and 0.1% (▼). The polymer solutions were prepared by mixing PVBC and PE [6:4 (w/w)]; *p*-xylene was used to dilute the mixed polymers to desired concentrations. (B) Detection time profiles of Arg (100 μM) provided by sensing phases prepared from base polymer (PVBC/PE) mixtures in which the PVBC contents were 80 wt% (■), 60 wt% (●), 40 wt% (▲), and 20 wt% (▼).

within the thicker polymer were somewhat less accessible. For rapid practical detection in our further studies, we chose to use the polymer solution having a concentration of 0.25% (w/v).

Because sulfonate groups are charged and highly water-soluble, a high degree of derivatization with sulfonate groups will decrease the stability of the sensing phase in water. In contrast, a low degree of derivatization of the sensing phase will limit the sensitivity of the detection. To determine the optimal conditions, we mixed nonreactive polyethylene with PVBC to form polymer films containing 20, 40, 60, and 80 wt% PVBC. The amount of PE limits the degree of derivatization of the polymer films. We examined the sensing of a 100 μM Arg solution at pH 9; Fig. 8B displays the results as detected adsorption time profiles. The speed of detection was similar for each polymer film composition, but the signals were more intense at higher PVBC contents. Meanwhile, the standard deviations between runs were also higher at higher PVBC contents. Based on these results, we found that a 60 wt% PVBC solution produced the optimal sensing phase.
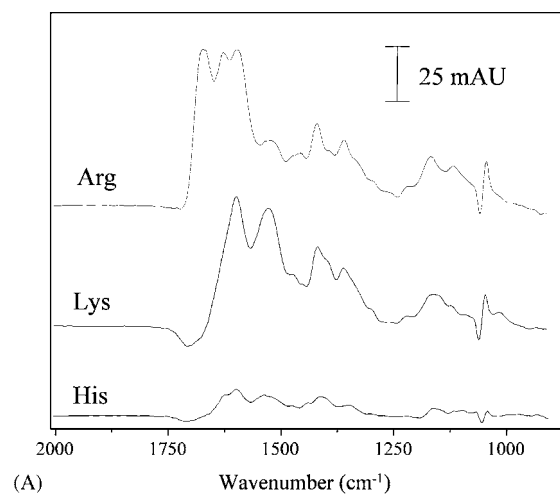
(A)
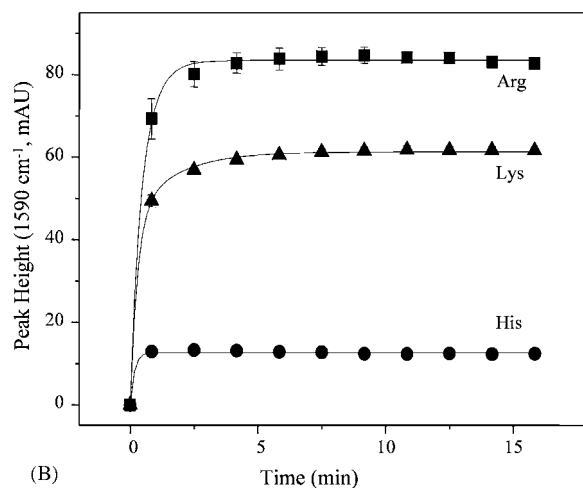
(B)

Fig. 9. Typical (A) detected spectra and (B) calculated detection time profiles of Arg, Lys, and His. The concentrations of these amino acids were 1 mM (pH 9).

3.6. Selectivity of the amino acid sensor

To investigate the selectivity of the prepared sensing phase toward the detection of Arg, we examined the analysis of other amino acids – lysine, histidine, alanine, valine, proline, glycine, serine, aspartic acid, and glutamic acid (1 mM each) – using the sulfonated sensing phase. Fig. 9A indicates that only the cationic amino acids – Arg, Lys, and His – were detectable at pH 9; the speeds of their detection were similar (Fig. 9B). The other amino acids – alanine, valine, proline, glycine, serine, aspartic acid, and glutamic acid – were not detectable. These results indicate that the prepared, sulfonated sensing phase was selective toward the basic amino acids. To distinguish the signal of Arg from those of the other cationic amino acids, we can use the unique absorption band of the guanidine group located at 1665 cm^{-1}.

3.7. Quantitative aspects

To study the linearity and detection limits in the detection of Arg by the sulfonated sensing phase, we examined Arg solutions of different concentrations prepared at pH 9. Fig. 10A presents
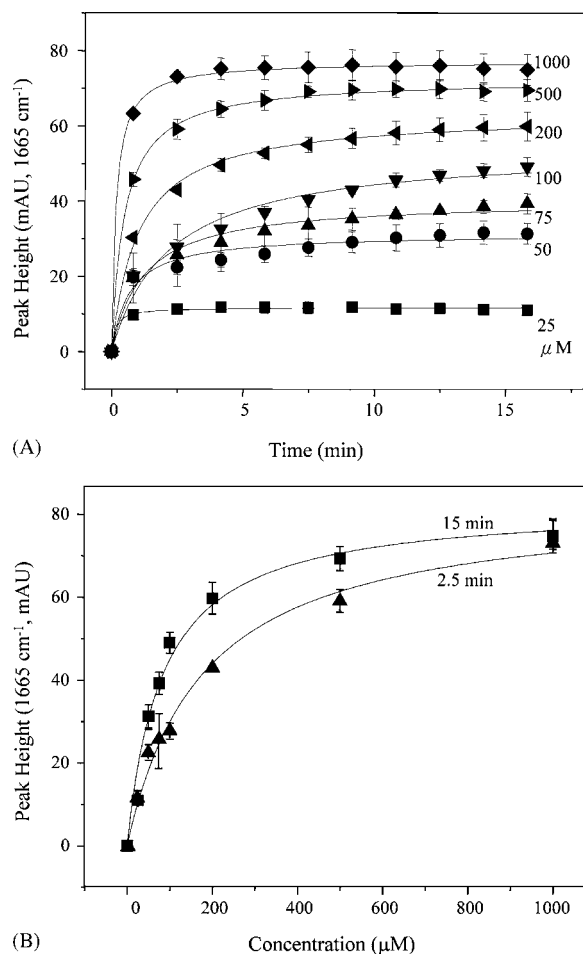
Fig. 10. (A) Adsorption isotherm of Arg at different concentrations (pH 9). (B) Standard curves generated at detection times of 2.5 min (▲) and 15 min (■).

the detected time profiles. The time required to reach the maximal signal was typically less than 5 min. Two standard curves were generated based on the detected signals at 2.5 and 15 min (Fig. 10B). We note that the curve generated at the shorter of detection time exhibited a higher range of linearity. These standard curves both fit well to Langmuir isotherms (Fig. 10B), indicating that the detection process occurred mainly through surface adsorption; the linear range of detection occurred up to a concentration of Arg of 0.1 mM. Based on three times of noise level, the calculated detection limit was ca. 5 μM.

4. Conclusion

In this study, we prepared an Arg-selective sensing phase based on the derivatization of sulfonic acid group onto a PVBC/PE polymer mixture. Two mechanisms existed for the adsorption of Arg onto the prepared sensing phase. The first process was rapid and we believe that it was due to adsorption at the outer surface of the sensing phase. The second adsorption process was relatively slower; we believe that it was due to the adsorption by the sulfonate groups located within pores. An IR spectroscopic study into the effects of pH indicated that the adsorbed Arg was in the R$^+$ form and that the most-intense

signals were obtained at a pH close to 9. The composition of the polymer film was also optimized to match the requirements of both sensitivity and water-stability; we found that a 60 wt% PVBC polymer mixture provided the best compromise. From a study of the selectivity of the detection process, we found that only cationic amino acids, such as Lys and His, were detectable. Fortunately, the unique IR absorption bands of the guanidine moiety of Arg can be used to eliminate interference from these two amino acids. In terms of quantitative aspects, the prepared sensing phase can be used to detect Arg through surface adsorption over a short linear range (up to 100 μM). Under the optimized conditions, the detection limit was ca. 5 μM with a linear range up to 0.1 mM.

Acknowledgment

References

[1] K.A. Cox, S.J. Gaskell, M. Morris, A. Whiting, J. Am. Soc. Mass Spectrom. 7 (1996) 522.
[2] S.D. Friess, R. Zenobi, Mass Spectrom. 12 (2001) 810.
[3] K.A. Schug, W. Lindner, K. Lemr, J. Am. Soc. Mass Spectrom. 15 (2004) 840.
[4] G. Wu, S.M. Morris JR., Biochem. J. 336 (1998) 1.
[5] H. Okamoto, A.R. Timerbaev, T. Hirokawa, J. Sep. Sci. 28 (2005) 522.
[6] M.L. Patchett, C.R. Monk, R.M. Daniel, H.W. Morgan, J. Chromatogr. 425 (1988) 269.
[7] A. Bastone, L. Diomede, R. Parini, F. Carnevale, M. Salmona, Anal. Biochem. 191 (1990) 384.
[8] D.L. Olson, M.E. Lacey, A.G. Webb, J.V. Sweedler, Anal. Chem. 71 (1999) 3070.
[9] L.Z. Wang, C.S. Ma, X.L. Zhang, Z.S. An, J. Indian Chem. Soc. 76 (1999) 116.
[10] T. Miura, M. Kashiwamura, M. Kimura, Anal. Biochem. 139 (1984) 432.
[11] M.J. Micklus, I.M. Stein, Anal. Biochem. 54 (1973) 545.
[12] M.A. Parniak, G. Lange, T. Viswanatha, J. Biochem. Bioph. Methods 7 (1983) (1983) 267.
[13] A. Alonso, M.J. Almendral, M.D. Baez, M.J. Porras, C. Alonso, Anal. Chim. Acta 308 (1995) 164.
[14] J. Hutzler, L-Lysine, Methods of Enzymatic Analysis, L-Arginine, L-Histidine, L-Ornithine and L-Tyrosine: Colorimetric Method with Fluorodinitrobenzene, Verlag Chemie, Weinheim, Germany, 1974.
[15] R. Mira de Orduna, J. Agric. Food Chem. 49 (2001) 549.
[16] N.J. Harrick, Internal Reflection Spectroscopy, Wiley, New York, 1967.
[17] R. Krska, R. Kellner, U. Schiessel, M. Tacke, A. Katzir, Appl. Phys. Lett. 63 (1993) 1868.
[18] G. Huang, J. Yang, Anal. Chem. 75 (2003) 2262.
[19] G. Huang, J. Yang, Biosens. Bioelectron. 21 (2005) (2005) 408.
[20] J. Yang, H.J. Lin, H.Y. Huang, Anal. Chim. Acta 527 (2004) 27.
[21] J. Yang, H.J. Lin, H.Y. Huang, Anal. Chim. Acta 530 (2005) 213.
[22] J. Yang, S.C. Liang, Anal. Chim. Acta 537 (2005) 385.
[23] K.A. Schug, W. Lindner, Chem. Rev. 105 (2005) 67.
[24] C.R. Cantor, P.R. Schimmel, Biophysical Chemistry. Part I. The conformation of biological macromolecules, W.H. Freeman, San Francisco, 1980, p. 49.
[25] K. Rahmelow, W. Hubner, Th. Ackermann, Anal. Biochem. 257 (1998) 1.
[26] A.D. Roddick-Lanzilotta, P.A. Connor, A.J. McQuillan, Langmuir 14 (1998) 6479.

Determination of total fluoride in HF/HNO$_3$/H$_2$SiF$_6$ etch solutions by new potentiometric titration methods

Wenke Weinreich, Jörg Acker*, Iris Gräber

IFW Dresden, Institute for Solid State Analysis and Structural Research, P.O. Box 270116, D-01171 Dresden, Germany

Abstract

In the photovoltaic industry the etching of silicon in HF/HNO$_3$ solutions is a decisive process for cleaning wafer surfaces or to produce certain surface morphologies like polishing or texturization. With regard to cost efficiency, a maximal utilisation of etch baths in combination with highest quality and accuracy is strived. To provide an etch bath control realised by a replenishment with concentrated acids the main constituents of these HF/HNO$_3$ etch solutions including the reaction product H$_2$SiF$_6$ have to be analysed. Two new methods for the determination of the total fluoride content in an acidic etch solution based on the precipitation titration with La(NO$_3$)$_3$ are presented within this paper. The first method bases on the proper choice of the reaction conditions, since free fluoride ions have to be liberated from HF and H$_2$SiF$_6$ at the same time to be detected by a fluoride ion-selective electrode (F-ISE). Therefore, the sample is adjusted to a pH of 8 for total cleavage of the SiF$_6{}^{2-}$ anion and titrated in absence of buffers. In a second method, the titration with La(NO$_3$)$_3$ is followed by a change of the pH-value using a HF resistant glass-electrode. Both methods provide consistent values, whereas the analysis is fast and accurate, and thus, applicable for industrial process control.
© 2006 Elsevier B.V. All rights reserved.

Keywords: Fluoride determination; La(NO$_3$)$_3$; Potentiometric titration; Ion-selective electrode; Glass-electrode

1. Introduction

The determination of the fluoride concentration using an ion-selective electrode (F-ISE) either by direct potentiometry or by potentiometric titration with La(NO$_3$)$_3$ is known for numerous applications, e.g. pharmaceutical products [1] or potable water [2]. Detailed studies about interferences have shown no influence of any of the common anions such as chloride, nitrate, sulphate or phosphate [3]. The only significant interaction has to be referred to the hydroxide ion if its concentration is in the range of the fluoride content or higher [3,4].

The direct potentiometry with a F-ISE is carried out after calibration and addition of TISAB-buffer. A robust and more exact method, especially, for the determination of the fluoride concentration is the use of the F-ISE as end-point indication during the titration of fluoride with lanthanum nitrate solution leading to precipitated lanthanum fluoride (Eq. (1)).

$$3F^- + La^{3+} \rightarrow LaF_3 \tag{1}$$

The dependence of the titration on the pH-value was studied thoroughly using different systems of buffered and unbuffered solutions. The largest potential change was determined for neutral solutions without any addition of buffer. A lower pH-value adjusted by various buffer systems leads to a decrease of the potential change due to the formation of protonated fluoride species [5] that cannot be detected by the F-ISE. Although, the titration of neutral and unbuffered solution provides the best results these conditions are hardly to stabilize, mainly, because La(NO$_3$)$_3$ undergoes an acid hydrolysis. Buffering with acetate–acetic acid is necessary to set a solution permanently to a neutral pH. A problem going along with the use of acetate buffer is the shift of the equivalence point (EP) according to the amount of buffer that forms soluble lanthanum–acetate complexes. In contrast, there is no direct interference of the acetate-ion with the LaF$_3$ crystal of the F-ISE [4–7].

An increase of the sensitivity can be achieved by working in organic solvents. This affects the solubility of the precipitated LaF$_3$ due to the altered polarity of the solvent. Mainly, dipolar aprotic solvents, a variety of alcohols and their mixtures with slight amounts of water [5,8] contribute to an extension of the detection limit to nanomolar quantities of fluoride [9].

* Corresponding author. Tel.: +49 351 46 59 694; fax: +49 351 46 59 452.
E-mail address: j.acker@ifw-dresden.de (J. Acker).

Recently, the F-ISE was applied for the determination of the total fluoride content in acidic etch solutions of silicon consisting of nitric acid (HNO_3), hydrofluoric acid (HF) and the reaction product hexafluorosilicic acid (H_2SiF_6) [10]. The more exact and efficient titration with $La(NO_3)_3$ has not yet been performed for such strong acidic solutions. Hence, two different new titration methods for the determination of fluoride on the basis of $La(NO_3)_3$ are described in this paper. The methods are applicable for acidic solutions containing bounded fluoride species. One titration method uses the F-ISE for end-point detection and the other one is performed with a HF resistant glass-electrode. These methods combine several important advantages like excellent recovery, low relative standard deviation (R.S.D.), as well as the adherence of essential pH-values and the decomplexation of fluoride both without the use of buffer solution. Additionally, the determination of fluoride can be realised after the analysis of other important constituents of silicon etch solutions [10] right in the same aliquot and this approach leads to a minimal R.S.D.

2. Experimental

For the preparation of the synthetic etch solutions analytic grade acids were used. Acidic etch solutions for silicon contain the remaining educts nitric acid (HNO_3, 65 wt.%, Merck) and hydrofluoric acid (HF, 40 wt.%, Merck) and the reaction product hexafluorosilicic acid (H_2SiF_6, 35 wt.%, Fluorchemie Dohna). The exact concentrations of the used acids were additionally verified by titration. All used volumes of the acids in the synthetic sample solutions were weighed at first (AT 200, Mettler-Toledo AG) and then mixed with 40 mL deionized water in a polyethylene (PE)-beaker. Each titration was performed four times and the analysing was based on mass. The volumes of the studied sample solutions range between 0.5 and 1 mL.

The titrant for acid–base titrations was $0.5\ mol\ L^{-1}$ sodium hydroxide (NaOH, diluted from $1\ mol\ L^{-1}$ Titrisol, Merck). Back-titration was realised with $1\ mol\ L^{-1}$ hydrochloric acid (HCl, $1\ mol\ L^{-1}$ Titrisol, Merck). The 0.033 and $0.167\ mol\ L^{-1}$ equimolar fluoride titrant was made from lanthanum nitrate hexahydrate ($La(NO_3)_3 \cdot 6H_2O$, Merck) from which the titer was obtained by titration of dried sodium fluoride (NaF, Suprapur®, Merck).

For the preparation of the acetate–acetic acid buffer 30 mL glacial acetic acid (100 wt.%, Merck) were dissolved in 750 mL deionized water. Afterwards, $8\ mol\ L^{-1}$ NaOH (made from NaOH pellets, Merck) was added up to a pH-value of 6 and the mixture was filled up with deionised water to a volume of 1 L.

The fluoride concentration was determined by a fluoride ion-selective electrode (Mettler-Toledo). The electrode was regularly conditioned in $10^{-2}\ mol\ L^{-1}$ fluoride solution. The detection of the pH-value was realised with a HF resistant glass-electrode of the type InLab429 (Mettler-Toledo AG).

All titrations were performed by an automated titrator of the type DL 70 (Mettler-Toledo AG) with suitable equilibration adjustments corresponding to the performed titration; acid–base and precipitation titration, respectively. The analysing of the resulting data was done by the titration software LabX (Mettler-

Toledo). The equivalence point received from the F-ISE was evaluated as the maximum of the first derivative of the voltage signal. Due to the segmented pH–titration curve the EP from the glass-electrode was set at the maximum of the second derivative of the voltage signal.

3. Results and discussion

3.1. Titration of fluoride with $La(NO_3)_3$ and F-ISE for end-point detection

Etch solutions of silicon consist of HF and HNO_3 plus the reaction product H_2SiF_6. At the typical pH-values < 1 of such mixtures fluoride is existent as H_2F_2 and as protonated solution species of $SiF_6{}^{2-}$ (the speciation of H_2SiF_6 is not yet fully resolved [11]) in the etch solution. For the precipitation with $La(NO_3)_3$ and for the detection with the F-ISE free fluoride is mandatory, so that the performed analysing methods require special preparation approaches. To obtain deprotonated fluoride species the pH-value of the solution has to be larger than five. At a pH-value around 8 [12] the cleavage of the hexafluorosilicic anion, $SiF_6{}^{2-}$, occurs. Additionally, the interference of hydroxide ions with the F-ISE has to be considered, hence, the pH-value must not exceed 8. A common and a new developed titration method using the F-ISE as end-point detector are discussed in the following paragraphs.

3.1.1. With buffer
A first and common way for stabilising the pH-value is the use of buffer systems like acetate–acetic acid buffer. Among the fixation of the pH-value the buffer solution is capable of releasing the fluoride ion from its compounds. Due to the large amount of HNO_3, the investigation of real etch solutions requires a high buffer volume that is necessary to receive a pH-value larger than 5. In Table 1, examples for compositions of synthetic acidic etch solutions and the pH-value realised with a certain amount of buffer are shown.

Exemplarily, the titration of such a mixture (50 μL HF and 50 μL H_2SiF_6) under addition of a slight amount of buffer solution (20 mL) with $0.033\ mol\ L^{-1}\ La(NO_3)_3$ yields to a recovery of 102.2% that presents a slight excess. The shift of the EP to higher volume is due to the presence of acetate buffer [4].

The requirement of high buffer volume to adjust the essential pH-value reveals that the shifting of the EP and therefore, the recovery for real etch solutions would be exceeding. The use of acetate buffer and thus, the common method for titra-

Table 1

Volume of buffer solution that is necessary to achieve a pH of 5 in an aliquot with the composition of a characteristic acidic etch solution

Composition	Buffer (mL)	pH
50 μL H_2SiF_6	10	5.28
100 μL H_2SiF_6	15	5.14
50 μL H_2SiF_6 + 50 μL HF	20	5.20
0.05 mL HNO_3 + 0.05 mL HF + 0.05 mL H_2SiF_6	25	5.05
0.5 mL HNO_3 + 0.05 mL HF + 0.05 mL H_2SiF_6	80	4.99

tion of fluoride with $La(NO_3)_3$ is not applicable for acidic etch solutions.

3.1.2. *Without buffer*

For an accurate analysis of the total fluoride content in acidic etch solutions by titration with $La(NO_3)_3$ the development of a new method without the use of buffer solution is unavoidable.

The determining approach of that method is the adjustment of the pH-value at the beginning of the titration that has to be 8 as upper limit for the F-ISE and for the cleavage of SiF_6^{2-}. The pH of 8 is achieved by the potentiometric titration with NaOH. Secondly, the titrated aliquot has to be diluted concerning the amount of fluoride and the corresponding volume of acidic $La(NO_3)_3$ so that the pH-value does not fall below 5 during the titration. By means of this method a recovery of 98.8% was achieved for the titration of 50 µL H_2SiF_6.

To improve the obtained results and to ensure a complete decomposition of SiF_6^{2-} the titration with NaOH should be expanded. Before the $La(NO_3)_3$-titration is started an acid–base titration according to Henßge et al. [13] without the optimised dilution steps is performed whereas free fluoride ions exist at the end of the titration at a pH around 12. Afterwards, the pH of 8 is attained by back-titration with HCl. The recovery of such an approach lies at 99.5% for the titration of 50 µL H_2SiF_6. The mean R.S.D. was found to 1.10%. Synthetic etch solutions consisting of HNO_3, HF and H_2SiF_6 were titrated with this method and a mean recovery of 99.7% and a mean R.S.D. of 1.04% were achieved.

The new titration method with $La(NO_3)_3$ is a precise procedure for the determination of fluoride in acidic etch solutions. In Fig. 1, the improvement of that method compared to the common method with buffer solution is shown. One advantage of the new method is the higher potential change leading to an improved analysing of data. Moreover, more precise recovery results can be achieved without the use of acetate buffer since there is no shift of the EP.
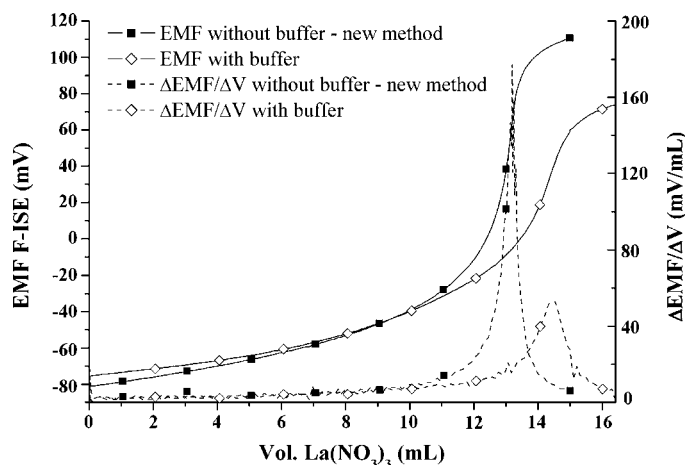
Fig. 1. Comparison of two different preparation methods for the titration of synthetic etch solutions (30 µL HNO_3, 40 µL H_2SiF_6, 30 µL HF) with 0.033 mol L^{-1} $La(NO_3)_3$: (◇) addition of 20 mL acetate–acetic acid buffer, common method, (■) titration with NaOH to pH 12 and back-titration with HCl to pH 8, new approach.
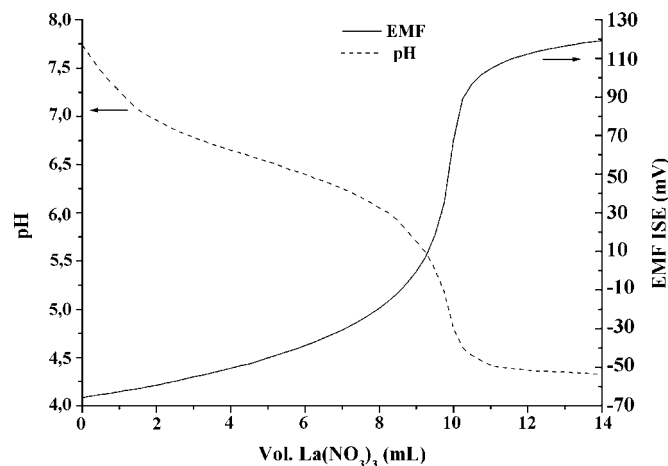
Fig. 2. Titration of 50 mg NaF with 0.033 mol L^{-1} $La(NO_3)_3$ solution and detection of the pH by glass-electrode and of the fluoride concentration by F-ISE.

3.2. *Titration of fluoride with $La(NO_3)_3$ and glass-electrode for end-point detection*

After the acid–base titration with NaOH, the fluoride of HF and H_2SiF_6 is converted to NaF that dissociates in aqueous solution. In the aqueous sample solutions a hydrolysis reaction according to Eq. (2) occurs.

$$F^- + H_2O \rightarrow HF + OH^- \qquad (2)$$

In contrast, the lanthanum ion undergoes an acidic hydrolysis in aqueous solution (Eq. (3)) [9].

$$\tfrac{1}{3}La^{3+} + H_2O \rightarrow \tfrac{1}{3}La(OH)_3 + H^+ \qquad (3)$$
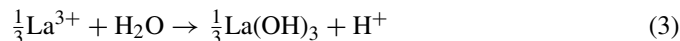
Due to both hydrolysis reactions during the titration of fluoride with La^{3+} a change of the pH-value can be observed that is detectable by a glass-electrode. A resulting titration curve is shown in Fig. 2. An amount of 50 mg NaF in 40 mL deionized water with a pH of 8 adjusted by NaOH was titrated with $La(NO_3)_3$ and the potentiometric detection was done with the F-ISE and the glass-electrode at the same time. The development of the pH-value can be interpreted as segmented titration curve with an explicit EP that is analysed as the maximum of the second derivative of the voltage signal. Both equivalence points of direct fluoride concentration and of the pH show a good congruence.

In Table 2, a comparison between pH-method (glass-electrode) and fluoride-method (F-ISE) for the titration with $La(NO_3)_3$ is given. Two different amounts of fluoride from a stock solution of 10 g L^{-1} NaF were titrated starting at a pH of 8. Two aliquots of each amount of NaF were analysed one detected

Table 2
Comparison of recoveries achieved by detection with glass-electrode and with ISE

NaF stock solution (10 g L^{-1}) (mL)	Recovery (%)	
	pH	ISE
3	100.9	98.9
5	101.7	99.8

Table 3

Fluoride recoveries of synthetic etch solutions (0.3 mL HNO_3, 40 μL H_2SiF_6, 30 μL HF) for titration with $La(NO_3)_3$ and detection by glass-electrode starting at different pH-values

Starting pH	Recovery (%)
5	87.3
6.3	98.6
8.3	104.5

Table 4

Recoveries of the fluoride concentration in various synthetic acidic etch solutions determined by titration with $La(NO_3)_3$ using a glass-electrode for end-point detection

HNO_3 (μL)	H_2SiF_6 (μL)	HF (μL)	Recovery (%)	R.S.D. (%)
300	40	20	101.9	0.66
300	40	40	99.0	0.69
300	40	50	98.0	1.22
300	20	30	97.0	1.25
300	30	30	98.2	1.34
300	50	30	98.0	1.01

by glass-electrode and one by F-ISE. The resulting recoveries coincide.

The end-point detection of the fluoride titration by glass-electrode can also be applied after the acid–base titration of silicon etch solutions with NaOH (Section 3.1.2) [13]. An important parameter for the accuracy of the fluoride titration in this case is the pH-value at the beginning of the titration. A potential change in the titration curve originates only if the titration is performed around a pH of 7. Accordingly, the exactness of this titration method shows a dependence on the starting pH that is produced by the addition of HCl after the acid–base titration. This dependence of the recovery is listed in Table 3 for aliquots mixed of 0.3 mL HNO_3, 40 μL H_2SiF_6 and 30 μL HF. A low pH causes an obvious low recovery and a starting pH higher than 8 yields to an exceeding one. Therefore, the pH at the beginning of the $La(NO_3)_3$ titration should be around 7. In Fig. 3, the resulting titration curves of the three different starting pH-values are shown and the well analysable equivalence points are labelled.

According to the obtained results different mixtures of the main components of acidic etch solutions were titrated starting at a pH around 7. After the acid–base titration with NaOH and the back-titration with HCl to a pH of 7 the titration with $La(NO_3)_3$ followed and the resulting recoveries of the fluoride concentration are listed in Table 4. The R.S.D. of the titration is under 1.5% and only for small amounts of fluoride (20 mg) the deficiency is smaller than 2%.

The pH-value of the sample solution is not only dependent on fluoride and lanthanum, but also influenced by $NaNO_3$

and NaCl that originate from the former titrations with NaOH and HCl. For the investigation of the effect of these salts a titration with NaF was performed and equivalent amounts of $NaNO_3$ and NaCl according to the titration of etch solutions were added (Fig. 4). No influence of the added salts on the recovery could be observed. Thus, neither the content of HNO_3, nor the back-titration with HCl does have any effect on the determination of the fluoride concentration by titration with $La(NO_3)_3$ and detection of the equivalence point by glass-electrode.

The application of the fluoride titration for industrial etch solutions has to comply with several requirements. On the one hand, the performance of the analysis has to be very fast and accurate and on the other hand, samples with high amounts of fluoride have to be analysed. In contrast, due to the precipitation reaction and the long response time of the F-ISE either a longer break between two additions of titrant or a low concentration of the titrant is required. Both alternatives are not practicable for industrial application because of an increasing analysing time. The presented new potentiometric titration method of fluoride with glass-electrode detection allows the utilisation of higher concentrated titrants (0.167 mol L^{-1} $La(NO_3)_3$) simultaneously with quick titration times because of the short response time of the electrode. The resulting titration curves for a high and a low amount of fluoride titrated with 0.167 mol L^{-1} $La(NO_3)_3$ are shown in Fig. 5. For both amounts excellent recoveries of 99.2 and 100.7% could be achieved.

Fig. 3. Titration of synthetic etch solutions (0.3 mL HNO_3, 40 μL H_2SiF_6, 30 μL HF) with 0.033 mol L^{-1} $La(NO_3)_3$ detected by glass-electrode after acid–base titration with NaOH and back-titration with HCl to different starting pH-values: (···) 5, (—) 6.3, (- - -) 8.3; the EP is calculated from the second derivative and labelled by a vertical line.
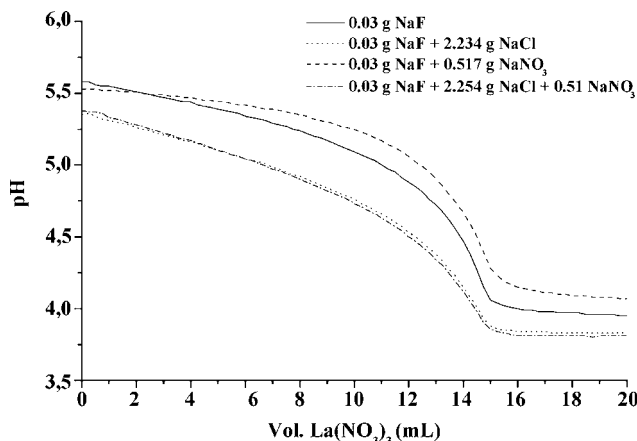
Fig. 4. Effect of additional components of acidic etch solutions on the pH-value during the titration of NaF with 0.033 mol L^{-1} $La(NO_3)_3$.
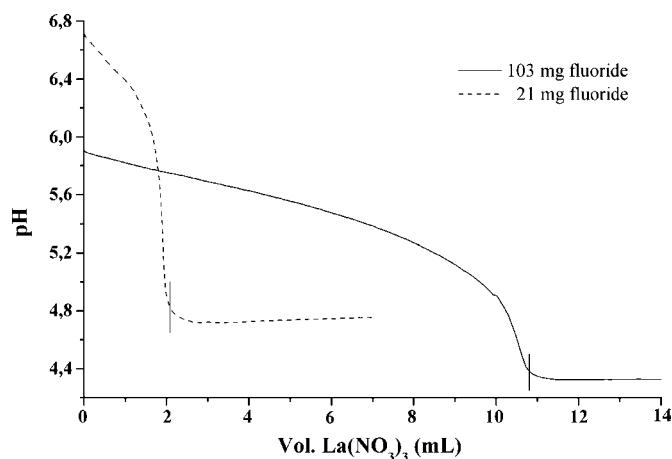
Fig. 5. Titration of synthetic acidic etch solutions with $0.167 \, mol \, L^{-1}$ La(NO$_3$)$_3$ and end-point detection by glass-electrode after acid–base titration with NaOH and back-titration with HCl: (- - -) 21 mg fluoride (20 μL H$_2$SiF$_6$, 30 μL HF, 0.3 mL HNO$_3$), (—) 103 mg fluoride (100 μL H$_2$SiF$_6$, 150 μL HF, 0.3 mL HNO$_3$); the EP is calculated from the second derivative and labelled by a vertical line.

4. Conclusions

Two new potentiometric titration methods for the determination of fluoride in acidic solutions are presented. Based on the titration with La(NO$_3$)$_3$ and the F-ISE common approaches have been adapted to strong acidic etch solutions. Furthermore, the use of a glass-electrode for the detection of the EP in the fluoride titration has been established. This new method makes it possible to determine all important components of acidic etch solutions of silicon with only one analysing method, the titration, and in only one sample solution right one after another. That is an important advantage with regard to fast and accurate application in the industry.

References

[1] B.F. Abramovic, F.F. Gaál, Talanta 39 (1992) 511–515.
[2] T.S. Light, R.F. Mannon, K.S. Fletcher III, Talanta 16 (1969) 1441–1443.
[3] M.S. Frant, J.W. Ross Jr., Science 154 (1966) 1553–1555.
[4] P.A. Evans, G.J. Moody, J.D.R. Thomas, Lab. Practice 20 (1971) 644–652.
[5] J.J. Lingane, Anal. Chem. 39 (1967) 881–887.
[6] R. Ding, S.A. Wood, Water-Rock Interactions, Ore Deposits, and Environmental Geochemistry, Special Publication No. 7, 2002, pp. 209–227.
[7] A. Sonesson, Acta Chem. Scand. 12 (1958) 165–181.
[8] J.F. Coetzee, M.W. Martin, Anal. Chem. 52 (1980) 2412–2416.
[9] E. Heckel, P.F. Marsh, Anal. Chem. 44 (1972) 2347–2351.
[10] A. Henßge, J. Acker, Talanta, submitted for publication.
[11] E.T. Urbansky, Chem. Rev. 102 (2002) 2837–2854.
[12] L. Gmelin, Gmelins Handbuch der anorganischen Chemie, Bd. 15, 8. Aufl., Verlag Chemie, Weinheim, 1956.
[13] A. Henßge, J. Acker, C. Müller, Talanta 68 (2006) 581–585.

ELSEVIER

Fluorescent peptide sensor for the selective detection of Cu^{2+}

Brianna R. White, James A. Holcombe *

*Department of Chemistry and Biochemistry, University of Texas at Austin, Austin,
TX 78712, United States*

Abstract

A new fluorescent peptidyl chemosensor for Cu^{2+} ions with fluorescence resonance energy transfer (FRET) capabilities has been synthesized via Fmoc solid-phase peptide synthesis. The metal chelating unit, which is flanked by the fluorophores tryptophan (donor) and dansyl chloride (acceptor), consists of the amino acids glycine and aspartic acid (Gly-Gly-Asp-Gly-Gly-Asp-Gly-Gly-Asp-Gly-Gly-Asp-Gly-Gly). Coordination of the Cu^{2+} ions to the metal chelating unit results in fluorescent quenching of both the donor and acceptor fluorophores. Although it was determined that Cu^{2+} binding causes no change in FRET efficiency, emission and Cu^{2+}-induced quenching of the acceptor dye can be used to monitor the concentration of the copper ions, with a detection limit of 32 μg L^{-1}. The sensor also demonstrated sensitivity, reversibility and selectivity towards Cu^{2+} in a transition metal matrix at pH 7.0.
© 2006 Elsevier B.V. All rights reserved.

Keywords: Copper peptidyl chemosensor; Fluorescence; FRET; Quenching; Solid phase peptide synthesis; Metal binding peptide

1. Introduction

The significance of in situ determination of low level concentrations of metals such as Ca^{2+}, Cu^{2+} and Zn^{2+} in environmental and biological samples has prompted research into the development of fluorescent chemosensors [1–7]. These chemosensors are typically composed of two structural subunits intramolecularly connected through a linking bridge: a fluorophore (for signal transduction) and an ionophore (for selective recognition of the metal ion). When designing these sensors, intense effort is put into maximizing the selectivity of the metal chelating unit. Early fluorescent chemosensors focused on using chelating units composed of organic molecules, but synthesis was rigorous and binding was not always reversible [3,8–18]. Peptide motifs from metal binding proteins proved to be a viable alternative since they often maintained the protein's metal selectivity, could be easily synthesized via fluorenylmethoxycarbonyl (Fmoc)-solid phase peptide synthesis (SPPS) [19,20] and were useable in aqueous solutions. One of the first examples was the use of a small peptide sequence (25 residues) based on the zinc finger protein by Walkup and Imperiali [21]. Other motifs, such as the Cu^{2+} binding tripeptide growth factor [22] and the Cu^{2+} and Ni^{2+} binding ACTUN [23–26] have also been used successfully.

Typically, metal binding is detected by the quenching of a single fluorophore such as dansyl chloride [8,12,15,23–25,27,28], lucifer yellow [29] or anthracence [9,30–32]. Although concentration dependent quenching mechanisms have proven successful, it is inherently less sensitive than methods that *produce* fluorescence as a result of binding [33]. Also, it is often difficult to distinguish analyte response from sensor degradation when quenching is relied upon for quantitation.

It was our initial intent to link a fluorophore to each end of the chelating unit to observe an increase in fluorescence resonance energy transfer (FRET [34–36]) with metal binding. Conceptually, if the chelating unit folds around the metal as it binds, the fluorophores are brought closer together, causing increased transfer of energy from the donor fluorophore to the acceptor fluorophore. Because it is a distance-dependent interaction, FRET can also be used as a diagnostic to understand the conformation and mechanism of metal binding to the chelating unit. In comparison to conventional fluorescence, FRET can

---

* Corresponding author.
E-mail address: holcombe@mail.utexas.edu (J.A. Holcombe).

generate a larger wavelength separation between the excitation and emission wavelengths thereby permitting lower resolution wavelength isolation devices (e.g., filters).

This paper reports on the synthesis of a new peptide motif with FRET capabilities for the selective detection of Cu^{2+}, a trace metal that is essential to sustain life, but is toxic in excess amounts [37–40]. The 15 residue peptide (sequence: Dansyl-Gly-Gly-Asp-Gly-Gly-Asp-Gly-Gly-Asp-Gly-Gly-Asp-Gly-Gly-Trp-$CONH_2$) was not based on any metal binding proteins in an attempt to illustrate the potential of constructing a selective chelator using a short peptide without the need for a biological starting point. The FRET pair (tryptophan as donor and dansyl chloride as acceptor) were conveniently attached during SPPS, eliminating the need for labeling reactions. Each of the four aspartic acid residues, which have an affinity for hard acid metals such as Cu^{2+} [41], were separated by two glycine residues in hopes of exploiting the preference of Cu^{2+} for a square planar coordination and thus resulting in an increase in FRET. Prior to this, two examples of FRET-based fluorescent peptidyl chemosensors for Cu^{2+} have been attempted in the literature, but the addition of Cu^{2+} to the peptide solution resulted in the quenching of one or both fluorophores and no increase in FRET [26,42]. Unfortunately, these previous studies were unable to provide definitive evidence that a change in FRET was occurring due, in part, to the strong influence of the quenching phenomena.

2. Materials and methods

2.1. Chemicals

All chemicals were reagent grade unless noted, and deionized distilled water was used to prepare solutions. All glassware was soaked overnight in $4\,mol\,L^{-1}$ HNO_3 prior to use. Peptide synthesis reagents N-Dansyl-N'-Fmoc-ethylenediamine-MPB-AM (Dansyl NovaTag®) resin (100–200 mesh; $0.38\,mmol\,g^{-1}$), Wang resin (100–200 mesh, $1.2\,mmol\,g^{-1}$), glycine (Fmoc-Gly-OH), aspartic acid (Fmoc-Asp(t-butyl ester (OtBu))-OH), tryptophan (Fmoc-Trp(Boc)-OH), 2-(1H-benzotriazole-1-yl)-1,1,3,3-tetramethylaminium hexafluorophosphate (HBTU), and 1-hydroxybenzotriazole (98%) (HOBt) were used as received from Novabiochem. All the amino acids were of L-configuration. Stock solutions of $1000\,\mu g\,mL^{-1}$ Cd^{2+} (Anderson Laboratories), Cu^{2+} (SCP Science), Na^+ (Sigma–Aldrich), Ni^{2+} (SCP Science), and Zn^{2+} (Acros) atomic absorption standards were used to prepare metal solutions for fluorescence measurements. For Ca^{2+} and Mg^{2+} (J.T. Baker), the stock solutions were prepared from standardized solutions of the reagent grade nitrate salt in 1% (v/v) HNO_3 and 1% (v/v) HCl. A $0.05\,mol\,L^{-1}$ (N-[hydroxyethyl] piperazine-N'-[2-ethanesulfonic acid]) (HEPES) (Aldrich) buffer was prepared and adjusted to pH 7.0 with ammonium hydroxide (Fisher). Other reagents used include trifluoroacetic acid (99%) (TFA), triisopropylsilane (99%) (TIPS), ethyl ether (Fisher), (ethylenedinitrilo)-tetraacetic acid (EDTA) (EM Science), N-methylmorpholine (NMM) (Fisher), N-methylpyrrolidone (NMP) (Fisher) and piperidine (99%).

2.2. Apparatus

A Photon Technologies International Quanta Master Spectrofluorimeter (model QM-4/2005) was used for all fluorescence measurements.

2.3. Peptide synthesis

A peptide consisting of the sequence Dansyl-Gly-Gly-Asp-Gly-Gly-Asp-Gly-Gly-Asp-Gly-Gly-Asp-Gly-Gly-Trp-$CONH_2$ (**P1**) was synthesized on Dansyl NovaTag® resin and a peptide consisting of the sequence Gly-Gly-Asp-Gly-Gly-Asp-Gly-Gly-Asp-Gly-Gly-Asp-Gly-Gly-Trp-$CONH_2$ (**P2**) was synthesized on Wang resin by Fmoc-solid phase peptide synthesis using a Ranin Symphony Quartet automated peptide synthesizer. The peptides were double coupled (each amino acid coupling reaction was performed twice) in order to increase reaction efficiency and peptide integrity. Cleavage of the peptides from the resin was conducted with TFA/TIPS/H_2O (95/2.5/2.5) for 2.5 h. The solution was then suction filtered, isolated using ether, and lyophilized. The peptide masses (1510.7 for **P1** and 1234.1 for **P2**) were confirmed using electrospray mass spectrometry and the purity of each sequence (63% for **P1** and 71% for **P2**) was determined by reverse phase-HPLC. For both **P1** and **P2**, no other single component was present in excess of 15%.

2.4. Fluorescence studies

2.4.1. Cu^{2+} response studies

Fluorescence emission spectra were collected from $10\,\mu mol\,L^{-1}$ solutions of **P1** and **P2** (pH 7.0, $50\,mmol\,L^{-1}$ HEPES). A range of Cu^{2+} concentrations (1–$20\,\mu mol\,L^{-1}$) were added to each peptide solution from a $0.002\,mol\,L^{-1}$ stock solution. Both FRET studies (monitoring emission of Trp and dansyl, $\lambda_{ex} = 290\,nm$, $\lambda_{em} = 300$–$574\,nm$) and single fluorophore studies (monitoring emission of dansyl, $\lambda_{ex} = 348\,nm$, $\lambda_{em} = 425$–$600\,nm$) were conducted on **P1**. Single fluorophore studies (monitoring emission of Trp, $\lambda_{ex} = 290\,nm$, $\lambda_{em} = 300$–$425\,nm$) were conducted on **P2**. When determining signal intensity for dansyl chloride emission, an average of intensities in the wavelength region 545–550 nm was used due to the broad emission peak. For tryptophan emission, intensities at 348 nm were used.

2.4.2. Multi-metal response studies

A $10\,\mu mol\,L^{-1}$ **P1** and $10\,\mu mol\,L^{-1}$ (each) Cd^{2+}, Co^{2+}, Mn^{2+}, Ni^{2+} and Zn^{2+} solution (pH 7.0, $50\,mmol\,L^{-1}$ HEPES) was prepared. A range of Cu^{2+} concentrations (1–$20\,\mu mol\,L^{-1}$) was added to the **P1**/metal solution from a $0.002\,mol\,L^{-1}$ stock solution to determine **P1**'s response to Cu^{2+} in a transition metal matrix ($\lambda_{ex} = 348\,nm$, $\lambda_{em} = 425$–$600\,nm$).

A $10\,\mu mol\,L^{-1}$ **P1** and $5\,\mu mol\,L^{-1}$ Cu^{2+} solution (pH 7.0, $50\,mmol\,L^{-1}$ HEPES) was prepared. $400\,mg\,L^{-1}$ stock solutions of Ca^{2+}, Cd^{2+}, Mg^{2+}, Na^+, Ni^{2+} and Zn^{2+} were prepared and $100\,\mu L$ aliquots were added to the **P1**/Cu^{2+} solution. Metal interferant concentration versus %error in

Cu signal was plotted in Origin 7.0® and the polynomial fit function was used to determine the concentration of each metal that would cause a 10% error in the **P1** response to Cu^{2+} ($\lambda_{ex} = 348$ nm, $\lambda_{em} = 425$–600 nm). This procedure was repeated for a 10 μmol L^{-1} **P1** and 10 μmol L^{-1} Cu^{2+} solution (pH 7.0, 50 mM HEPES).

2.5. FRET measurement

In order to determine the initial distance (r) between the fluorophores before metal was added, Eq. (1) [34] was used.

$$E = \frac{R_0^6}{R_0^6 + r^6} \tag{1}$$

For the measurement of the FRET efficiency (E), the emission of **P2**, which contains only tryptophan (I_D), has been compared to the emission of **P1**, which contains both tryptophan and dansyl chloride ($I_{D/A}$). Eq. (2) [34] was used to calculate FRET efficiency.

$$E = 1 - \frac{I_{D/A}}{I_D} \tag{2}$$

The Forster distance, R_0, for tryptophan/dansyl chloride has been previously determined to be 21 Å [35] and their spectral overlap has been illustrated [43,44]. The distance between the dyes is 62 Å if **P1** is completely elongated.

3. Results and discussion

3.1. Existence of FRET and fluorescence quenching by Cu^{2+}

The fluorescence of **P1** ($\lambda_{ex} = 348$ nm) is shown in Fig. 1A where only dansyl chloride is excited. With excitation of the Trp donor ($\lambda_{ex} = 290$ nm, Fig. 1B), the emission spectra of dansyl chloride is again observed, thus verifying FRET. The dansyl chloride emission decreased noticeably when the pH was lowered to 3.5, but was restored to its original intensity when the pH was returned to 7.0, illustrating the robustness of the peptidyl system.

For **P1**, the fluorescence emission intensity of both fluorophores decreased with the addition of Cu^{2+} (Fig. 1), suggesting quenching, and this quenching was easily reversed by the addition of excess EDTA to the peptide solution. Fig. 1B suggests that dansyl chloride quenching might be a simple consequence of the reduction of FRET excitation. However, Fig. 1A again shows Cu^{2+} quenching of dansyl at $\lambda_{ex} = 348$ nm when there is no excitation of Trp and therefore no chance of FRET. Thus, Cu^{2+} quenches both of these fluorophores. This is further supported by the more strongly dependent quenching of dansyl on Cu^{2+} when FRET is the primary excitation mode for Trp (see Fig. 1A and B). This is demonstrated in a slightly different presentation in the isotherms shown in Fig. 2.

Fig. 2 also shows that the maximum Cu:peptide binding ratio is approximately one. This suggests that there is probably only one Cu binding site that is responsible for both quenching
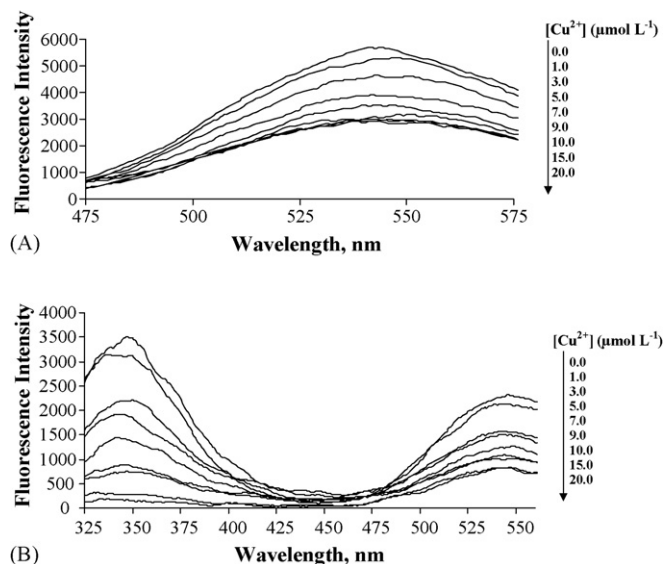
Fig. 1. Relationship of the fluorescence of **P1** to the concentration of Cu^{2+} (50 mmol L^{-1} HEPES, pH 7.0). Response of **P1** (10 μmol L^{-1}) to the addition of Cu^{2+} with excitation at (A) 348 nm and (B) 290 nm (from top to bottom 0.0, 1.0, 3.0, 5.0, 7.0, 9.0, 10.0, 15.0 and 20.0 μmol L^{-1} Cu^{2+}). All spectra were smoothed using Savitzky–Golay least squares smoothing routine with a 21 point window (Origin).

phenomena. The quenching of dansyl is likely due to Cu^{2+} complexation with the dansyl sulfonamide, which has been modeled and shown to cause quenching in other peptide systems [24,25]. At pH 7, the Cu^{2+} coordination to the N-terminal amine of Trp may account for its quenching interaction [45].

At 1 equiv Cu^{2+}, **P1** quenched to 57.5% of its initial value when excited at 290 nm and 41.5% of its initial value when excited at 348 nm. As is seen in Figs. 1 and 2, only a nominal decrease in fluorescence was observed after this point. As expected, a larger amount of quenching occurred when excitation was at 290 nm because dansyl chloride is losing emission by
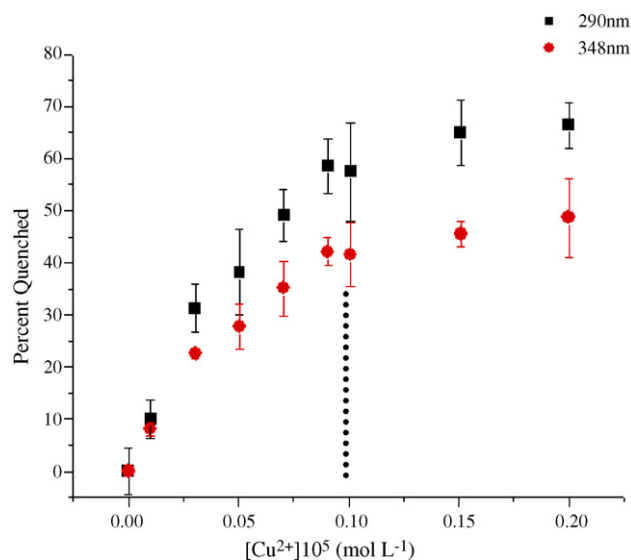
Fig. 2. Fluorescent binding isotherms of **P1** with Cu^{2+} (excitation at 290 and 348 nm). A 1:1 copper to peptide binding ratio is observed.

both copper quenching and loss of FRET. Studies by Zheng and coworkers on short Cu^{2+} binding peptides based on the ACTUN motif showed almost 100% quenching of dansyl chloride at 1 equiv Cu^{2+} when the sulfonamide group was directly involved in Cu^{2+} binding. Incomplete quenching was seen when the dansyl chloride was located on a side chain and not close enough to the binding event to signal it completely [25]. In the case of **P1**, where dansyl chloride is located on the C-terminus, the incomplete quenching may be due to the shared Trp/ dansyl binding site. Also, as will be discussed later, **P1** exhibited excellent metal selectivity towards Cu^{2+} whereas Zheng and coworkers witnessed more nonspecific binding when dansyl chloride did not quench completely.

The log K of **P1**-Cu^{2+} was calculated by the method of Conners [46] to be 4.90. This value is much smaller than that of metal binding proteins, such as the zinc finger (log K = 9) [47] or ACTUN (log K = 17) [48], probably as a consequence of the peptide carboxylates not actually actively involved in Cu^{2+} binding in this system, as will be discussed in greater detail in Section 3.3.

3.2. Cu^{2+} determination

Calibration curves were constructed from the fluorescence spectra to illustrate the quantitative dependence of the fluorescence on Cu^{2+} concentration. Detection limits at both excitation wavelengths were calculated for **P1** complexation with Cu^{2+}. The detection limit was 129 $\mu g\,L^{-1}$ at 290 nm and 32 $\mu g\,L^{-1}$ at 348 nm. Due to the lower detection limit and better precision, subsequent studies using mixed-metal matrix were conducted with excitation only at 348 nm.

3.3. Impact of peptide chain's functionalities in Cu^{2+} binding

Using equation (1), the FRET efficiency without Cu^{2+} was determined to be 80 ± 4%, which corresponds to a distance of only 17 ± 1 Å between the fluorophores, indicating that **P1** (62 Å when completely elongated) is already tightly coiled or folded even before the addition of metal. As a result of this small separation, it again is reasonable that both the dansyl sulfonamide and the N-terminal amine may be participating in the same binding site, yielding the 1:1 binding ratio.

Even though the fluorophores are initially separated by only 17 Å, it is possible that the peptide chelating unit changes conformation when Cu^{2+} binds. Typically, an increase in FRET efficiency (E) denoted by an increase in the acceptor's fluorescence is used to indicate a conformational change. In the case of **P1**, both fluorophores are being quenched, making the determination of a change in E less straightforward. Monitoring and comparing the emission intensity of two peptide sequences, one containing both fluorophores (i.e., **P1**) and one containing just the donor (i.e., **P2**) is required. An increase in E due to Cu^{2+} binding should quench **P1**'s Trp emission more than **P2**'s because it is losing energy from the FRET process *and* Cu^{2+} quenching. Tryptophan quenching for both **P1** and **P2** were plotted (Fig. 3) and found to overlap, indicating that no change in E occurred.
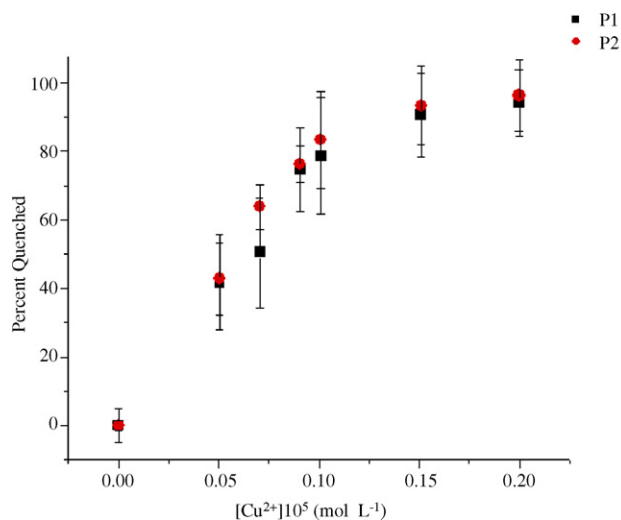
Fig. 3. Plots of tryptophan quenching in **P1** and **P2**. The overlapping curves suggest that no change in FRET efficiency (E) is occurring. The fluorescence intensity has been normalized and expressed in terms of percent quenched. Excitation is at 290 nm.

It is known that Cu^{2+} has a propensity to coordinate with carboxylates [41], such as that contained within the peptide chain of **P1**. However, previous results suggest that Cu^{2+} coordination with amines is stronger than Cu^{2+} coordination with carboxylates, with Cu^{2+} able to deprotonate nitrogens on the peptide backbone [49]. The fact that a 2 fold excess of Cu^{2+} did not significantly alter the FRET signal suggests that minimal binding to the peptide carboxylates is occurring. If binding had occurred with such an excess, then the dansyl-Trp distance would have likely changed as a result of the conformational change of the peptide unit. This should have produced an increase or decrease in the dansyl fluorescence because of an alteration in E. This was not observed. Because the fluorophores are only separated by 17 Å before the addition of metal, it is likely that the peptide is significantly coiled in the absence of Cu^{2+}. Thus, the carboxyl ligands in the chain may be inaccessible or geometrically misaligned for chelation with Cu^{2+}, allowing coordination with the N-terminal amine, the dansyl sulfonamide and perhaps nitrogens located on the peptide backbone instead.

3.4. Evaluation of selectivity

The selectivity of **P1** towards Cu^{2+} was demonstrated in a pH 7.0 HEPES solution containing several transition metal ions (Fig. 4). Initially, when the transition metal ions Cd^{2+}, Co^{2+}, Mn^{2+}, Ni^{2+} and Zn^{2+} (each is 1 equiv) were added to **P1**, there was no significant change in the fluorescence intensity. However, after 1 equiv of Cu^{2+} was added to the solution, the fluorescence intensity quenched to 55.1% of its initial intensity. This is a statistically similar value to what was observed for Cu^{2+} quenching of **P1** in the absence of other metal ions. It is not clear at this point how important the peptide link is in providing the proper Cu^{2+} binging geometry for dansyl and Trp, both of which appear to be involved in the complex.
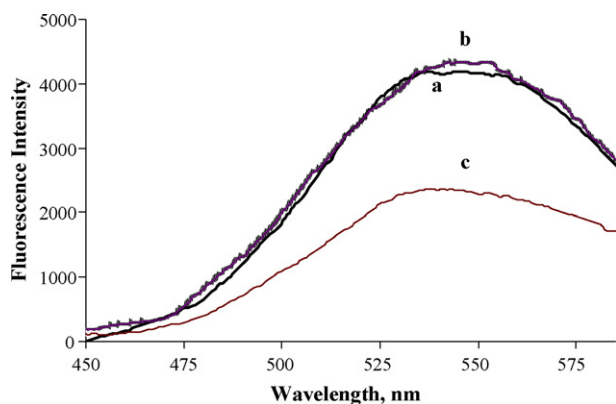
Fig. 4. Fluorescent selectivity of **P1** toward copper ions (50 mmol L^{-1} HEPES, pH 7.0). (a) Free **P1** (10 μmol L^{-1}), (b) **P1** and mixed metal solution containing 10 μmol L^{-1} each of Cd^{2+}, Co^{2+}, Ni^{2+}, Mn^{2+}, and Zn^{2+}, and (c) **P1**, mixed metal solution and Cu^{2+} (10 μmol L^{-1}). Excitation wavelength is 348 nm.

Table 1
Concentration (in mg L^{-1}) of various cations and the concentrations that produce a 10% increase in the fluorescent signal for 0.3 and 0.6 mg L^{-1} Cu^{2+}

Interfering ion	0.3 mg L^{-1} Cu^{2+}	0.6 mg L^{-1} Cu^{2+}
Ca^{2+}	23	27
Cd^{2+}	15	16
Na$^+$	28	32
Mg^{2+}	37	42
Ni^{2+}	15	16
Zn^{2+}	12	13

The effect of six metal interferents commonly found in Cu^{2+} contaminated areas [37] on **P1**'s fluorescence signal in the presence of Cu^{2+} was determined. These metals caused an increase in **P1**'s fluorescence signal (i.e., less quenching of **P1** as a result of Cu^{2+} displacement by non-quenching metals) and Table 1 lists the concentrations required to cause a 10% error in the fluorescence signal at two different Cu^{2+} concentrations. Zn^{2+} proved to have the greatest effect on **P1**'s fluorescence signal, but needs to be present at a 22 times excess to do so.

Curiously, when the amount of Cu^{2+} in the solution doubles, the interfering metal concentration needed to cause a 10% error in signal changed very little. Several binding models with varying number of binding sites and log K values were constructed in an attempt to simulate this observation. At this time, no explanation is available.

4. Conclusion

A new fluorescent peptidyl chemosensor consisting of the amino acids glycine and aspartic acid for the detection of Cu^{2+} was designed. The amino acid sequence used was not based on any metal binding proteins, which suggests the potential utility of short peptides in designing selective detectors where a biological starting point may not be available. The sensor had a detection limit of 32 μg L^{-1} for Cu^{2+} and exhibited a statistically similar response to Cu^{2+} among other possible interfering metals in a pH 7.0 buffer. Although the sensor was designed to utilize the signal enhancement capabilities of FRET, which was

observed; in this particular system fluorescence quenching of both fluorophores occurred and proved to be the most sensitive means of quantifying the results. The lack of a change in FRET efficiency indicates that the conformation of the peptide in this system is not changing as metal concentrations in the solution are altered.

References

[1] A.W. Czarnik, Fluorescent Chemosensors for Ion and Molecule Recognition, vol. 538, American Chemical Society, Washington, DC, 1993.
[2] L. Fabbrizzi, M. Licchelli, P. Pallavicini, L. Parodi, A. Taglietti, in: J.P. Sauvage (Ed.), Transition Metals in Supramolecular Chemistry, Wiley, Chichester, 1999, pp. 93–134.
[3] R. Kramer, Angew. Chem. Int. Ed. Engl. 37 (1998) 772.
[4] J.P. Desvergne, A.W. Czarnik, Chemosensors of Ion and Molecular Recognition, vol. 492, Kluwer Academic Publishers, Dordrecht, The Netherlands, 1997.
[5] A.P. de Silva, H.Q. Nimal Gunaratne, T. Gunnlaugsson, A.J.M. Huxley, C.P. McCoy, J.T. Rademacher, T.E. Rice, Chem. Rev. 97 (1997) 1515.
[6] R.P. Haugland, Handbook of Fluorescent Probes and Research Chemicals, sixth ed., Molecular Probes, Inc., Eugene, 1996.
[7] F. Pina, A. Bernardo, E. Garcia-Espana, Eur. J. Inorg. Chem. 20 (2000) 2143.
[8] R. Corradini, A. Dossema, G. Galaverna, R. Marchelli, A. Panagia, G. Sartor, J. Org. Chem. 62 (1997) 6283.
[9] G. De Santis, L. Fabbrizzi, M. Licchelli, C. Mangano, D. Sacchi, N. Sardone, Inorg. Chim. Acta 257 (1997) 69.
[10] J. Yoon, N.E. Ohler, D.H. Vance, W.D. Aumiller, A.W. Czarnik, Tetrahedron Lett. 38 (1997) 3845.
[11] K.A. Mitchell, R.G. Brown, D. Yuan, S.-C. Chang, R.E. Utecht, D.E. Lewis, J. Photochem. Photobiol. A 115 (1998) 157.
[12] L. Prodi, F. Bolletta, M. Montalti, N. Zaccheroni, Eur. J. Inorg. Chem. (1999) 455.
[13] M. Beltramello, M. Gatos, F. Mancin, P. Tecilla, U. Tonellato, Tetrahedron Lett. 42 (2001) 9143.
[14] G. Klein, D. Kaufmann, S. Schurch, J.-L. Reymond, Chem. Commun. (2001) 561.
[15] L. Prodi, M. Montalti, N. Zaccheroni, F. Dallavalle, G. Folesani, M. Lanfranchi, R. Corradini, S. Pagliari, R. Marchelli, Helv. Chim. Acta 84 (2001) 690.
[16] J. Bourson, F. Badaoui, B. Valeur, J. Fluoresc. 4 (1994) 275.
[17] E.U. Akkaya, S. Turkyilmaz, Tetrahedron Lett. 38 (1997) 4513.
[18] J. Kawakami, H. Itoh, H. Mitsuhashi, S. Ito, Anal. Sci. 15 (1999) 617.
[19] R.B. Merrifield, J. Am. Chem. Soc. 85 (1963) 2149.
[20] E. Atherton, R.C. Sheppard, Solid Phase Peptide Synthesis: A Practical Approach, IRL Press, Oxford, 1989, pp. 131–148.
[21] G.K. Walkup, B. Imperiali, J. Am. Chem. Soc. 118 (1996) 3053.
[22] Y. Zheng, Q. Huo, P. Kele, F.M. Andreopoulos, S.M. Phan, R.M. Leblanc, Org. Lett. 3 (2001) 3277.
[23] A. Torrado, G.K. Walkup, B. Imperiali, J. Am. Chem. Soc. 120 (1998) 609.
[24] Y. Zheng, K.M. Gattas-Asfura, V. Konka, R.M. Leblanc, Chem. Commun. 20 (2002) 2350.
[25] Y. Zheng, X. Cao, J. Orbulescu, V. Konka, F.M. Andreopoulos, S.M. Pham, R.M. Leblanc, Anal. Chem. 75 (2003) 1706.
[26] D.A. Pearce, G.K. Walkup, B. Imperiali, Bioorg. Med. Chem. Lett. 8 (1998) 1963.

[27] S. Bhattacharya, M. Thomas, Tetrahedron Lett. 41 (2000) 10313.

[28] A. Singh, L. Yao, W.C. Still, D. Sames, Tetrahedron Lett. 41 (2000) 9601.

[29] T. Mayr, T. Werner, Analyst 127 (2002) 248.

[30] P. Jiang, Z. Guo, Coord. Chem. Rev. 248 (2004) 205.

[31] L. Fabbrizzi, M. Licchelli, P. Pallavicini, A. Perotti, A. Taglietti, D. Sacchi, Chem. Eur. J. 2 (1996) 75.

[32] L. Fabbrizzi, M. Licchelli, P. Pallavicini, A. Perotti, D. Sacchi, Angew. Chem. Int. Ed. Engl. 33 (1994) 1975.

[33] M.Y. Chae, A.W. Czarnik, J. Am. Chem. Soc. 114 (1992) 9704.

[34] T. Forster, Ann. Phys. 2 (1948) 55.

[35] B.W. Van Der Meer, G. Coker III, S.Y.S. Chen, Resonance Energy Transfer: Theory and Data, VCH Publishers, Inc., New York, 1994, p. 157.

[36] C.G. dos Remedios, P.D.J. Moens, in: A.A. Demidov (Ed.), Resonance Energy Transfer, John Wiley and Sons, New York, 1999, pp. 1–54.

[37] United States E.P.A., Ambient Water Quality Criteria for Copper, 1980, http://www.epa.gov/ost/pc/ambientwqc/copper80.pdf.

[38] M. DiDonato, B. Sarkar, Biochim. Biophys. Acta 1360 (1997) 3.

[39] B. Sarkar, J. Inorg. Biochem. 79 (2000) 187.

[40] M.A. Deibel, W.D. Ehmann, W.R. Markesbery, J. Neurol. Sci. 143 (1996) 137.

[41] E. Gutierrez, T.C. Miller, J.R. Gonzalez-Redondo, J.A. Holcombe, Environ. Sci. Technol. 33 (1999) 1664.

[42] A. Mokhir, A. Kiel, D.-P. Herten, R. Kraemer, Inorg. Chem. 44 (2005) 5661.

[43] B.M. Dunn, C. Pham, L. Raney, D. Abayasekara, W. Gillespie, A. Hsu, Biochemistry 20 (1981) 7206.

[44] M. Gustiananda, J.R. Liggins, P.L. Cummins, J.E. Gready, Biophys. J. 86 (2004) 2467.

[45] C.K. Luk, Biopolymers 10 (1971) 1229.

[46] K.A. Conners, Binding Constants: The Measurement of Molecular Complex Stability, John Wiley & Sons, New York, 1987, pp. 339–343.

[47] J.M. Berg, D.L. Merkle, J. Am. Chem. Soc. 111 (1989) 3759.

[48] M.J.A. Rainer, B.M. Rode, Inorg. Chim. Acta 92 (1984) 1.

[49] H. Sigel, R.B. Martin, Chem. Rev. 82 (1982) 385.

Study on the separation of amino acids in modified poly(dimethylsiloxane) microchips

Yan Xiao, Xiao-Dong Yu, Kai Wang, Jing-Juan Xu, Jun Huang, Hong-Yuan Chen *

*The Key Laboratory of Analytical Chemistry for Life Science, School of Chemistry and Chemical Engineering,
Nanjing University, Nanjing 210093, China*

Abstract

A mixture of five amino acids including arginine, histidine, phenylalanine, serine and glutamic acid was successfully separated in microchip capillary electrophoresis and detected with laser-induced fluorescence (LIF) detector. These amino acids were labeled with 5-(4, 6-dichloro-*s*-triazin-2-ylamino) fluorescein (DTAF). The analyses were performed on two kinds of modified poly(dimethylsiloxane) (PDMS) microchips. One kind of chip was simply treated with oxygen plasma (OP-chip), and the other was further modified by coating double layers of non-ionic polymer poly(vinyl alcohol) (PVA) after plasma oxidization (PVA-chip). The derivatization condition of amino acids by DTAF was optimized. The properties of the two modified PDMS microchips were studied and separation conditions, such as the buffer pH, buffer concentration and separation voltage, were also optimized. The column efficiencies of the two microchips were in the range of 193,000–1,370,000 plates/m. The DTAF-labeled amino acids were sufficiently separated within 50 s and 90 s in 2.5 cm channels on OP-chip and PVA-chip, respectively.
© 2006 Elsevier B.V. All rights reserved.

Keywords: Poly(dimethylsiloxane); Modified PDMS microchips; DTAF; Amino acids; Poly(vinyl alcohol)

1. Introduction

Over the past decade, microfluidic-based analytical methods have been developed dramatically because of low sample consumption and rapid analysis [1–4]. The production of microfluidic devices made of glass or silicon is expensive and time-consuming. Polymers such as poly(dimethylsiloxane) (PDMS), poly(methylmethacrylate) (PMMA), and polycarbonate (PC) have been employed increasingly as device substrates [5–7]. These substrates are less fragile, cost-effective and suitable for mass production. Among these polymers, PDMS was the most widely used one in the last few years because of its well-known good properties such as easy fabrication using a replica molding process, high chemical resistance, optical transparency, nontoxicity and good elasticity. However, its application in microfluidics has been limited due to its hydrophobic nature and adsorption of samples. Fortunately, many modification approaches have been employed on the PDMS microchannels to increase its hydrophilic property in order to reduce analytes adsorption. The surface treatment methods of PDMS have been reviewed in recent years [8–10]. Using oxygen plasma to treat the PDMS microchip is an effective approach to create hydrophilic surfaces and to irreversibly bind the PDMS microchip together [11–18]. However, the short effective lifetime of OP-chips remains a problem [19]. One solution for this problem is attaching hydrophilic group onto the PDMS surface. For example, acrylic acid [20], 2-acrylamido-2-methyl-1-propanesulfonic acid (AMPS) [21], polyacrylicamide [22], poly(ethylene glycol) (PEG)[23], PVA [24] and some surfactants [25] have been used to enhance the surface properties of PDMS.

Amino acids as a kind of the main components in organism play an essential role in physical procedures such as transfer nerve information, regulation metabolic activity, biosynthesis protein and peptide. Therefore, to establish rapid and simple method for the analysis of amino acids is of importance. Microfluidic devices have been successfully used in the separation of amino acids on glass chips [2,26–32], PMMA chips [33–37], CaF₂ chip [38], PDMS chips and PDMS-glass hybrid chips [39–41].

The detection methods for amino acids include electrochemical detection, chemiluminescence detection, infrared

---

detection and fluorescence detection. Among all these methods, laser-induced fluorescence (LIF) detection is an ideal method in the miniaturized analytical system because of its high sensitivity and low background noise. Some compounds without fluorophore can be detected by derivatization with appropriate fluorescent labeling agent. Fluorescein isothiocyanate (FITC) has been used to label amino acids in microchip capillary electrophoresis, while the derivatization reaction was time-consuming and some amino acids derivatized by FITC could not be efficiently separated [40,41].

Recently, a fluorescent labeling reagent, 5-(4, 6-dichloro-*s*-triazin-2-ylamino) fluorescein (DTAF), which was introduced by Blakeslee in 1976 [42,43], has been receiving much attention due to its low cost, high purity and relatively fast labeling reaction in mild condition. The maximum excitation wavelength of DTAF is 492 nm, and the maximum emission wavelength is 520 nm [44]. So the commercially available argon-ion laser ($\lambda_{max} = 488$ nm) could be used to induce DTAF and its derivatives to emit fluorescence. In capillary electrophoresis (CE), DTAF has been used as pre-column or on-column labeling reagent for amino acids and biogenic amines [45], phosphorus containing amino acid [46,47], ephedrine and pseudoephedrine [48] and aniline metabolites [49]. Also, it has been used to label licorice-derived compounds [50] and biogenic amines [51] in microchip capillary electrophoresis. However, the methods for the separation of DTAF-labeled amino acids on PDMS microchips have not been reported.

In this paper, two kinds of modified poly(dimethylsiloxane) (PDMS) chips were prepared. One chip (OP-chip) was simply modified by oxygen plasma treatment, and the other one (PVA-chip) was modified by coating with double layers of non-ionic polymer poly(vinyl alcohol) (PVA) after the plasma oxidization. Properties of the modified PDMS microchips were studied. Five amino acids including arginine, histidine, phenylalanine, serine and glutamic acid labeled with DTAF were separated on these modified PDMS microchips and detected by LIF detection.

2. Experimental

2.1. Chemicals and solutions

DTAF (>99.0%) and PVA (Mr = 49,000) were products of Fluka (Buchs, Switzerland). Arginine, histidine, phenylalanine, serine and glutamic acid, sodium dodecyl sulphate (SDS) and polyoxyethylene dodecanol (Brij35, 30% aqueous solution) were purchased from Sigma–Aldrich (St. Louis, MO, USA). Sylgard 184 was obtained from Dow Coring (Midland, MI, USA). Dimethyl sulfoxide (DMSO), cetyltrimethylammonium bromide (CTAB) and $Na_2B_4O_7 \cdot 10H_2O$ were from Nanjing Reagent Plant (Nanjing, China). DMSO was distilled and dried by molecular sieves before use. All reagents were of analytical grade. Stock solutions (10 mM) of amino acids were prepared with distilled water (stored at 4 °C). A 10 mM DTAF stock solution was prepared in DMSO (stored at −20 °C in the dark). A 50 mM borate buffer (adjusted to the desired pH with HCl and diluted to proper concentration with distilled water) was used as

derivatization buffer and electrophoresis buffer. All buffer solutions were filtered through a 0.22 μm filter before introduction into the chip.

2.2. Microchip fabrication

A straight separation PDMS microchannel with cross-sampling channels was made based on a master composed of a positive relief structure of GaAs for the channels microfabricated in No. 55 Electronic Institution (Nanjing, China) by using standard microphotolithographic technology. The PDMS was weighed, degassed, and poured over the channel master. After curing at 80 °C for 2 h and cooling at room temperature, the PDMS was stripped from the master, producing a pattern of negative relief channels and reservoirs in the PDMS. Then it was cut into suitable size and punched holes of 4 mm in diameter. A thin piece of PDMS substrate was obtained by casting the polymer mixture in a glass box. The sampling channel was 30 μm in width, 18 μm in depth and the separation channel was 50 μm in width and 18 μm in depth, respectively. The PDMS chip and PDMS substrate were ultrasonically cleaned with acetone, methanol and water for 20 min, respectively. Then they were dried under an infrared lamp. The total length of the separation channel was 3.0 cm. The LIF detection length of the separation channels was all fixed at 2.5 cm from the intersection along the separation channel.

2.3. Apparatus

As shown in Fig. 1, the simple and effective homemade non-confocal LIF detector was greatly improved compared with the one described in our previous paper Ref. [52]. An air-cooled argon ion laser (Sanle Optical Company, Nanjing, China) with a 488 nm excited wavelength was adjusted to focus the laser on the microchannel with an incident angle of 45° by a precisely three-dimensional adjustor (Shanghai Lian Yi Instrument Factory of Optical Fiber and Laser, China) with the precision of ±1 μm in each direction. The adjustor was fixed on a slab staged under a stereoscopic microscope (XTB-1; Jiangnan Optical Instrument Factory, Nanjing, China). The fluorescence emission signal was collected by an optical fiber of 2 mm diameter connected with an inverted microscope via a 40× objective, and then passing through a 535 nm band-pass filter amplified by a photomultiplier tube (PMT, 750 V) equipped with an amplifier. A homemade signal-recording system was used to control the power supply and the PMT. Meanwhile, it was used to record the amplified output signals from the PMT. A homemade power supply provided a stable and continuously variable high voltage ranging from 0 to 5000 V.

2.4. Derivatization procedure

A 2 μL DTAF solution (10 mM), 10 μL stock solutions of each amino acid (10 mM) and 8 μL borate buffer solutions (10 mM, pH 9.2) were transferred to 1 mL vials sequentially. The solutions were centrifuged for 1 min to mix well (TGL-16G, Shanghai Anting Science Instrument Co.) and kept to
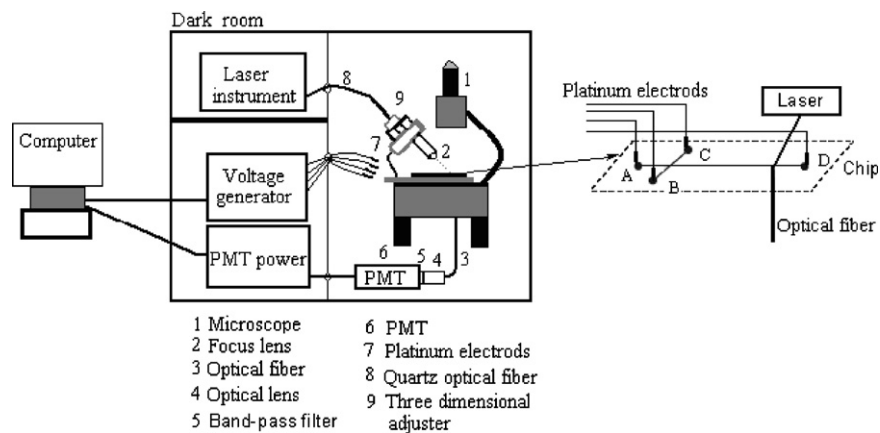
Fig. 1. Schematic of the PDMS microchip system integrated with LIF detection (left) and structure of the PDMS microchip (right). Reservoirs are (A) buffer reservoir, (B) sample reservoir, (C) sample waste reservoir, and (D) waste reservoir.

react in a water-bath (38 °C) for 30 min. After cooling to room temperature, the solutions were stored at −20 °C in the dark before use. Prior to analysis, the derivatization solutions were diluted with running buffer to the desired concentrations. These solutions can be used for 3 days without fluorescence decreasing.

2.5. Microchips treatment

The OP-chip was prepared as follows: the structured PDMS piece and PDMS substrate were treated by oxygen plasma (PDC-32G, NY, USA) for 1 min. Then the two parts were immediately sealed and the irreversible bonding was obtained after they joined together. All reservoirs were filled with distilled water and then the channels were filled with water automatically and completely due to capillary action (if no plasma treatment, the solution was forced through the channel by a vacuum pump).

The PVA-chip was similarly prepared according to Ref. [24]. Simply, the oxygen plasma treated chip was filled with PVA aqueous solution (1%, w/w) and then placed at room temperature for 10 min. After that, the reservoirs and channels were emptied by a vacuum pump. The PVA coated chip was dried by heating at 115 °C for 10 min. The above steps were repeated once. Finally, the coating was thermally immobilized in an oven with the temperature was increased from 115 °C to 140 °C at 1 °C/min and then maintained for 20 min at 140 °C. After that, the chip was allowed to cool down to room temperature inside the oven. For ATR-FT-IR measurement, the upper face of flat PDMS was immersed in PVA solution for 10 min, and the other procedure was the same as that in coating PDMS channels.

2.6. Characteristic measurement of PDMS

Fourier-transform infrared absorption by total attenuated reflection (ATR-FT-IR) spectra of PDMS on a wedged germanium crystal were obtained using a Bruker IFS 66/S spectrometer with a DTGS detector. A freshly cleaned germanium crystal surface was recorded as a reference. All spectra were obtained at 45° angle of incidence for 50 scans with a resolution of 4 cm^{-1} in the range of 2000–4000 cm^{-1}.

2.7. Electrophoretic experiments

All the reservoirs filled with water on OP-chip were emptied and loaded with 2 μl buffer solutions. Then, the chip was placed onto the slab and the platinum electrodes were put into four reservoirs. The cross injection was carried out by applying high-voltage to the sample reservoir for several seconds through Pt electrodes connected to the power supply, with the sample waste reservoir grounded and the other two reservoirs floating. Once the injection was finished, the separation voltage was applied to the buffer reservoir with the waste reservoir grounded and the other two reservoirs floating. As for the PVA-chip, the same injection procedure was used on such chip except that the electrodes were reversedly placed.

2.8. Measurement of EOF

EOF was detected using a new current monitoring method as our group reported previously [53]. Briefly, the separation channel and detection cell were filled with buffer. Then the injection sample channel and separation channel were rinsed with this buffer in sequence for 10 min, respectively. After that, a diluted buffer (buffer:water = 8:2) was placed in the same reservoir. The peak was monitored at 0 V with a single carbon fiber cylindrical electrode, which was placed in the end of the separation channel. The diluted buffer would lead to an increase of peak current. Migration time of EOF was rapidly obtained. The EOF was calculated according to the equation of $\mu_{eof} = (L/t)E^{-1}$, where L is the effective length of the microchannel, t the migration time of the diluted buffer in the separation channel, and E is the electric field strength. Electrochemical detection was performed using "amperometric i–t curve" mode with a CHI630A electrochemical analyzer (CHI Co., Shanghai, China).

3. Results and discussion

3.1. Derivatization conditions

Fig. 2 shows the scheme of the derivatization reaction between DTAF and amino compounds. The derivatization conditions between DTAF and amino acids had been reported in
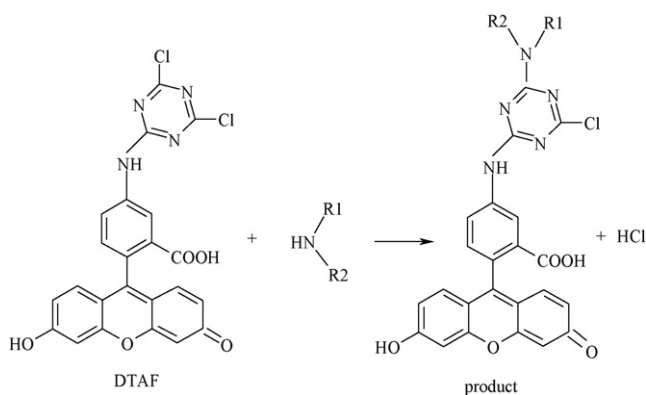
Fig. 2. Scheme of the derivatization reaction between DTAF and amino compounds.

Ref. [30]. The derivatization conditions were mild and the reaction time was short. In this study, the reaction temperature 38 °C, reaction time 40 min and reaction medium pH 9.2 borate buffer (10 mM) were selected for the derivatization. In addition, it was found that the hydrolysate of DTAF had much higher signals than those of samples. So, several changes were introduced to enhance the sample signals and also suppress the hydrolyzation, namely: (1) the sample dilution was carried out after the derivatization reaction instead of before the derivatization reaction to decrease the DTAF hydrolysis. (2) The different molar ratios between DTAF and amino acids (5:1, 1:1, 1:5 and 1:10) were tested. It was found that the signal intensities of DTAF-labeled amino acids were increased with the increasing amount of amino acids. Considering the use of smaller sample amount, the best molar ratio 1:5 between DTAF and amino acids for derivatization was chosen instead of 1:10.

3.2. Properties of modified chips

3.2.1. ATR-FT-IR characteristic

In the ATR-FT-IR spectrum of the native PDMS there was no infrared absorption between 3030 and 4000 cm^{-1} (Fig. 3A),
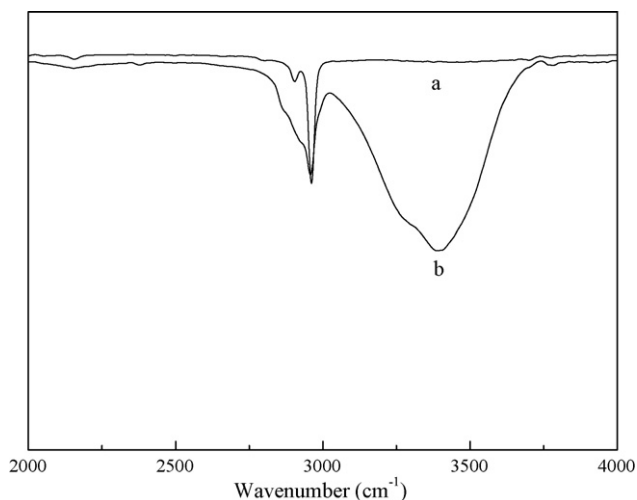
Fig. 3. ATR-FT-IR spectra of (A) native PDMS and (B) plasma oxidized PDMS coated with two-layer PVA.

while in the spectrum of the PVA treated PDMS a band at ca. 3390 cm^{-1} was observed (Fig. 3B), which was attributed to O–H stretch vibration of PVA. It is well-known that the –OH group of polymer (solid and liquid) is found at 3500–3250 cm^{-1} and the dominant group –OSi (–CH$_3$)$_2$O– has no infrared absorption in the range of 3100–3700 cm^{-1}. This indicated that PVA had been successfully coated on the PDMS surface.

3.2.2. EOF

EOF is a useful parameter to investigate surface modification and the stability of modified layers. Fig. 4A showed the relationship between EOF and pH (in basic condition) on the modified chips and native PDMS chip in 10 mM borate buffer. The pH greatly influenced the EOF of OP-chip and native PDMS microchip. The EOF of OP-chip increased with the increase of pH as a whole and enhanced doubly than that of native PDMS chip. The EOF of PVA-chip was more stable in tested pH values and was suppressed by three times than that of native PDMS
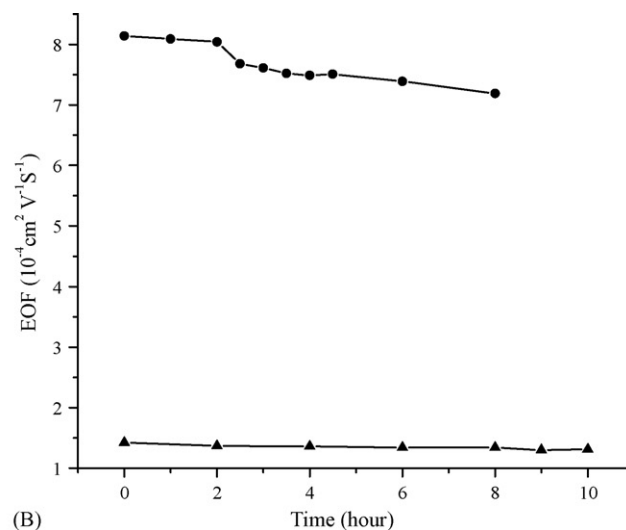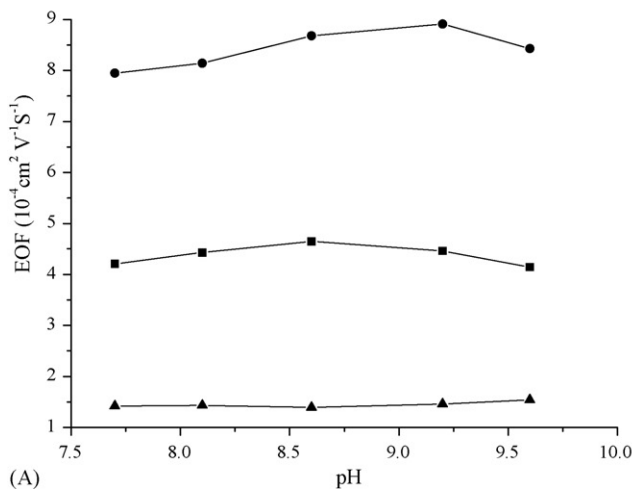
Fig. 4. (A) Effect of pH on EOF of the native PDMS chip (■), OP-chip PVA-chip (●) and PVA-chip (▲) and (B) the stability of EOF on the OP-chip (●) and PVA-chip (▲).

chip. The relative standard deviation (R.S.D.) of EOF for native PDMS chip was 1.31% ($n = 3$), and 0.29% and 0.45% ($n = 3$) for OP-chip and PVA-chip in pH 8.1, respectively. Fig. 4B showed the stability of EOF in 10 mM buffer (pH 8.1). The EOF of OP-chip decreased obviously after 2 h, reduced by 6% 2.5 h later, then changed little within 2 h, and last decreased slowly after this period of time. The EOF of PVA-chip was relatively more stable and decreased by 6% 6 h later.

Fig. 5 showed the electropherograms of the separation of amino acids on native PDMS chip, OP-chip and PVA-chip, respectively. On native PDMS chip, the DTAF-labeled amino acids and hydrolysate of DTAF were strongly adsorbed and the separation of amino acids could not be observed. While on both OP-chip and PVA-chip, base-line separation of DTAF labeled amino acids was achieved. The suppressed adsorption and the good separation efficiency attributed to the hydrophilic functional groups such as silanol, hydroxyl and carboxyl which were generated after oxygen plasma treatment on the PDMS surface and the highly hydrophilic non-ionic polymer PVA layer on PDMS. As can be seen in Fig. 5C, the peak sequence of analytes on PVA-chip was in the reversed order in comparison with that on OP-chip shown in Fig. 5B, which was due to thatthe the EOF of PVA-chip was suppressed greatly as shown in Fig. 4, then in this experiment all the analytes on PVA-chip were detected at the anode with the reversed migration order accordingly. In addition, all the analytes were successfully separated within 50 s and 90 s on OP-chip and PVA-chip, respectively.

3.3. Optimization of electrophoresis conditions

3.3.1. Effect of buffer pH value

The pH value of running buffer, which can influence the mobility of analytes by adjusting the velocity of EOF and the charge of the analyte molecule, has been acknowledged as one of the most important parameters for electrophoretic separation. Furthermore, the buffer pH value can influence the substance fluorescence intensity [54]. The fluorescence intensities of compounds labeled with DTAF were commonly high at basic condition. Therefore, the effects of borate buffer system pH ranged from 7.6 to 9.2 on the separation of amino acids on OP-chip and PVA-chip were mainly tested. The results showed that the pH greatly influenced the separation of histidine and phenylalanine. Fig. 6 showed the effect of pH on the resolution (based on equation: $R = 1.18((t_2 - t_1)/(w_{1/2(2)} + w_{1/2(1)}))$) of the two kinds of amino acids. As can be seen in Fig. 6, the resolution deceased with the increase of pH on both chips. And the efficient separation of histidine and phenylalanine were achieved from pH 7.6 to 8.2 on OP-chip. Above pH 8.2, histidine and phenylalanine could not be separated efficiently. Further increasing the pH, the resolution between histidine and phenylalanine decreased to zero. Although the efficient separation could be obtained at pH 7.8, the signal intensities of analytes at this pH value were much lower than that at pH 8.0. Therefore, running buffer pH 8.0 was selected for separation on OP-chip. It also can be seen from Fig. 6 that histidine and phenylalanine were separated except at pH 9.2 on PVA-chip. At
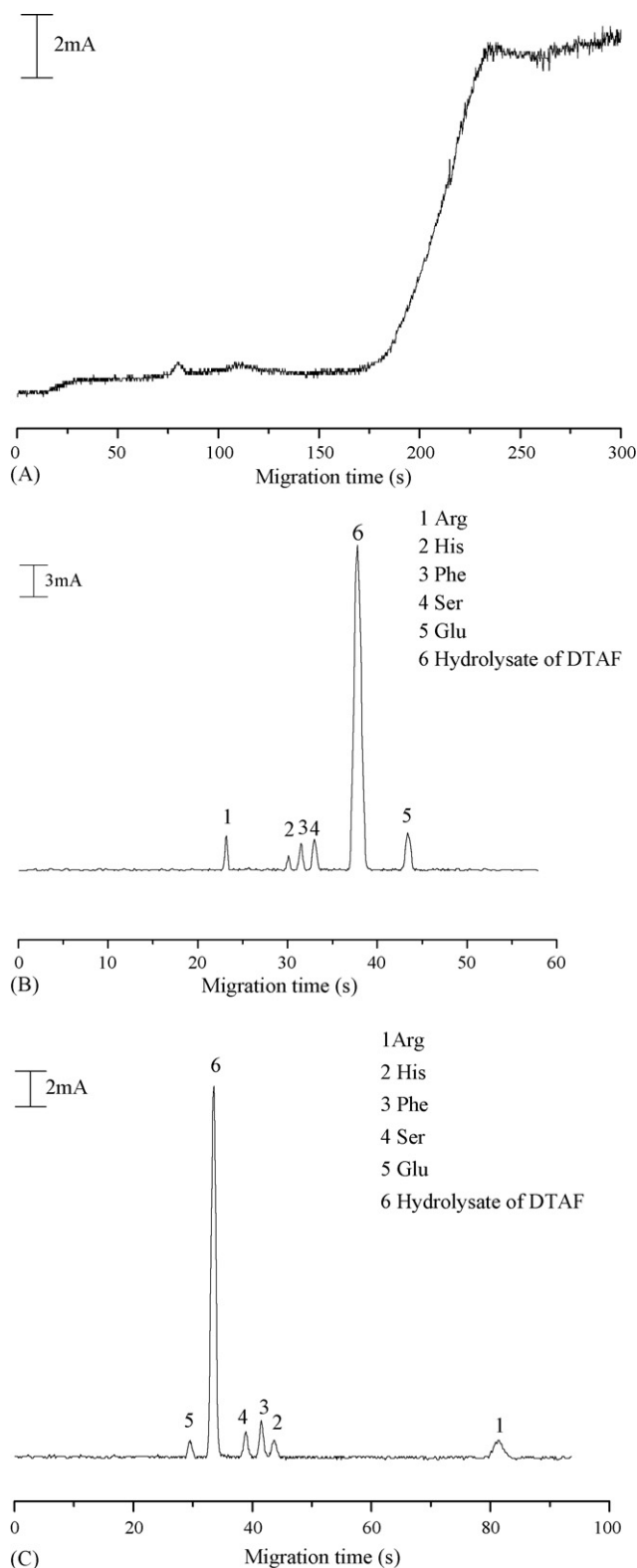
Fig. 5. Electropherogram of the separation of DTAF-labeled amino acids on native PDMS chip (A), OP-chip (B) and PVA-chip (C). Separation conditions: 10 mM borate buffer (A and C), 15 mM borate buffer (B), pH 8.0; separation voltage 800 V (A), 1000 V (B and C); 3 cm separation length; 2.5 cm detection length; 10 μM for each amino acid.
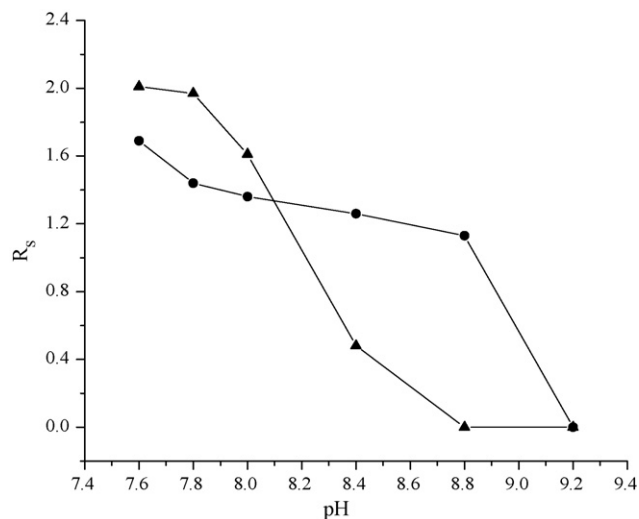
Fig. 6. Effect of running buffer pH on the resolution of DTAF-labeled histidine and phenylalanine on OP-chip (▲) and PVA-chip (●). Separation conditions: 10 mM borate buffer; separation voltage, 800 V (▲) and 1000 V (●); other conditions as in Fig. 5.

pH 8.0, the signal intensities of analytes were high; therefore, running buffer pH 8.0 was selected for separation on PVA-chip.

3.3.2. Effect of borate buffer concentration

The effect of borate buffer concentration on separation was investigated in the range of 5–20 mM at pH 8.0. To select the optimal buffer concentration for separation, the resolutions between histidine, phenylalanine and serine were calculated and the results were shown in Table 1. It can be seen that the borate sodium concentration (15 mM) was the best one for the separation of amino acids on OP-chip. Though the best resolutions can be obtained both in buffer concentration 10 mM and 20 mM on PVA-chip, the signal intensities of analytes were much lower in 20 mM buffer than those in 10 mM buffer. So, the buffer concentration 10 mM was chosen as the separation concentration on PVA-chip.

3.3.3. Effect of applied voltage

The effect of applied voltage on separation was investigated in the range of 800–1400 V on OP-chip and 800–1200 V on PVA-chip. The resolutions between histidine, phenylalanine and serine were calculated and the results were shown in Table 2. According to the data, the best separation was obtained with 1000 V separation voltage on OP-chip. The separation efficiency on PVA-chip decreased with the increase of voltage. When the

Table 1

The resolutions of amino acids in different buffer concentration on OP-chip and PVA-chip

Buffer concentration (mM)	OP-chip		PVA-chip	
	$R_{His,Phe}$	$R_{Phe,Ser}$	$R_{Ser,Phe}$	$R_{Phe,His}$
5	1.2	1.2	1.5	1.3
10	1.8	1.6	2.2	1.7
15	1.8	1.8	2.1	1.4
20	1.5	1.7	2.2	1.7

Table 2

The resolutions of amino acids at different separation voltage on OP-chip and PVA-chip

Separation voltage (V)	OP-chip		PVA-chip	
	$R_{His,Phe}$	$R_{Phe,Ser}$	$R_{Ser,Phe}$	$R_{Phe,His}$
800	1.7	1.7	1.8	1.7
1000	2.1	2.0	1.7	1.6
1200	1.8	1.8	1.4	1.3
1400	1.9	1.5		

separation voltage 800 V was used, the signal intensities of analytes were low. So, a voltage of 1000 V was applied for separation of amino acids on PVA-chip.

3.3.4. Effect of surfactants

Different kinds of surfactants including SDS, Brij35 and CTAB were tested in order to change the electroosmotic flow to obtain more kinds of amino acids separation in such shorter channel on OP-chip. Unfortunately, the added surfactants cannot efficiently increase the resolutions between histidine, phenylalanine and serine, but induce the baseline raise [55]. Therefore, no surfactants were added in this experiment.

3.4. The separation reproducibility

Under the optimal separation condition, the separation reproducibility on the modified microchips was tested based on the R.S.D of the migration time and the peak height of the analytes. The results were shown in Table 3. The results showed good reproducibility achieved on OP-chip and on PVA-chip. In addition, more than 40 and 60 runs with good resolution were performed continuously on OP-chip and PVA-chip, respectively.

3.5. The Linear range and detection limit

Under the selected conditions, a linear relationship was obtained between the height of detection signal with non-confocal LIF and the concentration of analyte. The linear range and detection limit on modified microchips were shown in Table 4. The results showed that the wider linear range was obtained on PVA-chip. We speculated that the wider linear range obtained on PVA-chip attributed to two aspects, one was the stable EOF of PVA-chip and the other was the efficient suppression of the adsorption especially in high concentration conditions.

Table 3

The reproducibility of migration time and peak height on the modified chips

	R.S.D. (%) of the migration time ($n = 3$)		R.S.D. (%) of the peak height ($n = 3$)	
	OP-chip	PVA-chip	OP-chip	PVA-chip
Arg	0.58	2.0	3.8	3.9
His	0.84	1.0	3.7	4.6
Phe	0.81	1.2	1.4	3.6
Ser	0.61	1.0	0.64	1.4
Glu	0.66	0.53	2.5	3.7

Table 4
The linear range and detection limit on modified chips

	Linear range (μM)		Detection limit (μM, S/N = 3)		Correlation coefficients	
	OP-chip	PVA-chip	OP-chip	PVA-chip	OP-chip	PVA-chip
Arg	2.0–75.0	8.0–100.0	1.6	5.0	0.9951	0.9948
His	8.0–90.0	10.0–150.0	3.0	5.5	0.9966	0.9949
Phe	5.0–150.0	4.0–150.0	2.0	2.0	0.9998	0.9984
Ser	8.0–80.0	4.0–100.0	2.0	2.0	0.9971	0.9976
Glu	6.0–70.0	10.0–92.0	5.0	7.0	0.9911	0.9937

Table 5
The column efficiency of amino acids on OP-chip (N^a) and PVA-chip (N^b)

Theoretic plate number (plates/m)	Arg	His	Phe	Ser	Glu
N^a	1.03×10^6	1.26×10^6	1.37×10^6	9.65×10^5	7.42×10^5
N^b	4.28×10^5	5.20×10^5	7.79×10^5	6.84×10^5	1.93×10^5

The column efficiencies (based on equation: $N = 5.54(t_R/w_{1/2})^2$) were also calculated based on Fig. 5 and the results were shown in Table 5. It can be seen that high column efficiencies were obtained on both microchips. The efficiency is similar to those on PDMS/glass [41] and PMMA [35] chips with confocal LIF detection. The theory plate numbers were 7.9×10^5, 2.7×10^5 and 6.4×10^4 plates/m for FITC labeled Arg, Phe and Glu on PDMS/glass chip, respectively [41], and 2.1×10^5, 3.7×10^5 and 1.4×10^5 plates/m for NBD labeled Ser, Glu and Phe on PMMA chip, respectively [35].

4. Conclusions

In this paper, two kinds of modified PDMS chips – OP-chip and PVA-chip have been successfully used for the complete separation of five DTAF derivatized amino acids including arginine, histidine, phenylalanine, serine and glutamic acid. Compared to native PDMS microchips, the adsorption of solute reduced greatly on these modified microchips. Both modified microchips have high column efficiencies, which were in the range of 193000–1370000 plates/m. Comparing the two modified microchips, OP-chip exhibited higher separation efficiencies, good reproducibility and shorter analysis times while PVA-chip had relatively wider linear range and long lifetime stable EOF.

Acknowledgements

References

[1] D.J. Harrison, K. Fluri, K. Seiler, Z.H. Fan, C.S. Effenhauser, A. Manz, Science 261 (1993) 895.
[2] C.S. Effenhauser, A. Manz, H.M. Widmer, Anal. Chem. 65 (1993) 2637.
[3] S.C. Jacobson, R. Hergenroder, L.B. Koutny, J.M. Ramsey, Anal. Chem. 66 (1994) 1114.
[4] A.T. Woolley, R.A. Mathies, Anal. Chem. 67 (1995) 3676.
[5] A. de Mello, J. Lab. Chip. 2 (2002) 31N.
[6] H. Becker, L.E. Locascio, Talanta 56 (2002) 267.
[7] T.D. Boone, Z.H. Fan, H.H. Hooper, A.J. Ricco, H. Tan, S.J. Williams, Anal. Chem. 74 (2002) 78.
[8] H. Makamba, J.H. Kim, K. Lim, N. Park, J.H. Hahn, Electrophoresis 24 (2003) 3607.
[9] D. Belder, M. Ludwig, Electrophoresis 24 (2003) 3595.
[10] A. Pallandre, B. de Lambert, R. Attia, A.M. Jonas, J.L. Viovy, Electrophoresis 27 (2006) 584.
[11] J.L. Fritz, M.J. Owen, J. Adhesion 54 (1995) 33.
[12] J.Y. Lai, Y.Y. Lin, Y.L. Denq, S.S. Shyu, J.K. Chen, J. Adhesion Sci. Technol. 70 (1996) 231.
[13] J. Hyun, A. Chilkoti, J. Am. Chem. Soc. 123 (2001) 6943.
[14] A.D. Stroock, S.K. Dertinger, G.M. Whitesides, A. Ajdari, Anal. Chem. 74 (2002) 5306.
[15] J. Heo, K.J. Thomas, G.H. Seong, R.M. Crooks, Anal. Chem. 75 (2003) 22.
[16] D.M. Cannon, T.C. Kuo, P.W. Bohn, J.V. Sweedler, Anal. Chem. 75 (2003) 2224.
[17] Zh.Y. Wu, N. Xanthopoulos, F. Reymond, J.S. Rossier, H.H. Girault, Electrophoresis 23 (2002) 782.
[18] G.B. Lee, Ch.H. Lin, K.H. Lee, Y.F. Lin, Electrophoresis 26 (2005) 4616.
[19] D.C. Duffy, J.C. McDonald, O.J.A. Schueller, G.M. Whitesides, Anal. Chem. 70 (1998) 4974.
[20] S.W. Hu, X.Q. Ren, M. Bachman, C.E. Sims, G.P. Li, N. Allbritton, Anal. Chem. 74 (2002) 4117.
[21] B.E. Slentz, N.A. Penner, F.E. Regnier, J. Chromatogr. A 948 (2002) 225.
[22] D.Q. Xiao, T. Van-Le, M.J. Wirth, Anal. Chem. 76 (2004) 2055.
[23] A. Papra, A. Bernard, D. Juncker, N.B. Larsen, B. Michel, E. Delamarche, Langmuir 17 (2001) 4090.
[24] D.P. Wu, Y. Luo, X.M. Zhou, Zh.P. Dai, B.Ch. Lin, Electrophoresis 26 (2005) 211.
[25] C.D. Garcia, B.M. Dressen, A. Henderson, C.S. Henry, Electrophoresis 26 (2005) 703.
[26] J.A. Lapos, A.G. Ewing, Anal. Chem. 72 (2000) 4598.
[27] N.J. Munro, Z.L. Huang, D.N. Finegold, J.P. Landers, Anal. Chem. 72 (2000) 2765.
[28] C.T. Culbertson, S.C. Jacobson, J.M. Ramsey, Anal. Chem. 72 (2000) 5814.
[29] J. Wang, G. Chen, Talanta 60 (2003) 1239.
[30] J. Wang, S. Mannino, C. Camerad, M.P. Chatrathi, M. Scampicchio, J. Zima, J. Chromatogr. A 1091 (2005) 177.
[31] J.A. Lapos, D.P. Manica, A.G. Ewing, Anal. Chem. 74 (2002) 3348.
[32] R.G. Su, J.M. Lin, K. Uchiyama, M. Yamada, Talanta 64 (2004) 1024.
[33] R.T. Kelly, A.T. Woolley, Anal. Chem. 75 (2003) 1941.

[34] M. Kato, Y. Gyoten, K.S. Kato, T. Nakajima, T. Toyo'oka, Anal. Chem. 76 (2004) 6792.
[35] M. Kato, Y. Gyoten, K.S. Kato, T. Nakajima, T. Toyo'oka, Electrophoresis 26 (2005) 3682.
[36] M. Kato, Y. Gyoten, K.S. Kato, T. Toyo'oka, J. Chromatogr. A 1013 (2003) 183.
[37] R.T. Kelly, T. Pan, A.T. Woolley, Anal. Chem. 77 (2005) 3536.
[38] T. Pan, R.T. Kelly, M.C. Asplund, A.T. Woolley, J. Chromatogr. A 1027 (2004) 231.
[39] J.J. Xu, Y. Peng, N. Bao, X.H. Xia, H.Y. Chen, J. Chromatogr. A 1095 (2005) 193.
[40] G.T. Roman, T. Hlaus, K.J. Bass, T.G. Seelhammer, C.T. Culbertson, Anal. Chem. 77 (2005) 1414.
[41] Y. Mourzina, A. Steffen, D. Kalyagin, R. Carius, A. Offenhässer, Electrophoresis 26 (2005) 1849.
[42] D. Blakeslee, J. Immunol. Meth. 13 (1976) 305.
[43] D. Blakeslee, J. Immunol. Meth. 17 (1977) 361.
[44] G.Z. Chen, X.Z. Huang, Z.Z. Zheng, J.G. Xu, Z.B. Wang, Fluorescence Analysis Method, 2nd ed., Science Press, Beijing, 1991, 287.
[45] M. Molina, M. Silva, Electrophoresis 23 (2002) 2333.
[46] M. Molina, M. Silva, Electrophoresis 23 (2002) 1096.
[47] X. Liu, Y.Q. Hu, L. Ma, Y.T. Lu, J. Chromatogr. A 1049 (2004) 237.
[48] W.P. Wang, C.H. Li, Y. Li, Zh.D. Hua, X.G. Chen, J. Chromatogr. A 1102 (2006) 273.
[49] E. Orejuela, M. Silva, Electrophoresis 26 (2005) 2991.
[50] A.W. David, C.H. Li, Paul, Anal. Chim. Acta 507 (2004) 107.
[51] N.P. Beard, J.B. Edel, A.J. deMello, Electrophoresis 25 (2004) 2363.
[52] Y. Zhang, N. Bao, X.D. Yu, J.J. Xu, H.Y. Chen, J. Chromatogr. A 1057 (2004) 247.
[53] J.J. Xu, N. Bo, X.H. Xia, Y. Peng, H.Y. Chen, Anal. Chem. 76 (2004) 6902.
[54] G.Z. Chen, X.Z. Huang, Z.Z. Zheng, J.G. Xu, Z.B. Wang, Fluorescence Analysis Method, 2nd ed., Science Press, Beijing, 1991, p. 83.
[55] B.C. Giordano, L. Jin, A.J. Couch, J.P. Ferrance, J.P. Landers, Anal. Chem. 76 (2004) 4705.

Application of microwave-assisted desorption/headspace solid-phase microextraction as pretreatment step in the gas chromatographic determination of 1-naphthylamine in silica gel adsorbent

Cheing-Tong Yan [a], Jen-Fon Jen [b,*], Tung-Sheng Shih [c]

[a] Department of Occupational Safety and Health, Chung-Shan Medical University, Taichung 402, Taiwan
[b] Department of Chemistry, National Chung Hsing University. Taichung 402, Taiwan
[c] Institute of Occupational Safety and Health, Council of Labor Affair, Executive Yuan, Sijhih City, Taipei County 221, Taiwan

Abstract

Pretreatment of silica gel sample containing 1-naphthylamine by microwave-assisted desorption (MAD) coupled to in situ headspace solid phase microextraction (HS-SPME) has been investigated as a possible alternative to conventional methods prior to gas chromatographic (GC) analysis. The 1-naphthylamine desorbs from silica gel to headspace under microwave irradiation, and directly absorbs onto a SPME fiber located in a controlled-temperature headspace area. After being collected on the SPME fiber, and desorbed in the GC injection port, 1-naphthylamine is analyzed by GC-FID. Parameters that influence the extraction efficiency of the MAD/HS-SPME, such as the extraction media and its pH, the microwave irradiation power and irradiation time as well as desorption conditions of the GC injector, have been investigated. Experimental results indicate that the extraction of a 150 mg silica gel sample by using 0.8 ml of 1.0 M NaOH solution and a PDMS/DVB fiber under high-powered irradiation (477 W) for 5 min maximizes the extraction efficiency. Desorption of 1-naphthylamine from the SPME fiber in GC injector is optimal at 250 °C held for 3 min. The detection limit of method is 8.30 ng. The detected quantity of 1-naphthylamine obtained by the proposed method is 33.3 times of that obtained by the conventional solvent extraction method for the silica gel sample containing 100 ng of 1-naphthylamine. It provides a simple, fast, sensitive and organic-solvent-free pretreatment procedure prior to the analysis of 1-naphthylamine collected on a silica gel adsorbent.
© 2006 Elsevier B.V. All rights reserved.

Keywords: 1-Naphthylamine; Microwave-assisted desorption; Headspace SPME; Silica gel; Workplace monitoring

1. Introduction

1-Naphthylamine is an important industrial material, used as a chemical intermediate for certain dyes, rubber and in the synthesis of a large number of chemicals such as certain herbicides [1,2]. Although the International Agency for Research on Cancer (IARC) states there is inadequate evidence of 1-naphthylamine being a human carcinogen, however, occupational exposure to commercial 1-naphthylamine containing 4–10% of 2-naphthylamine is strongly associated with bladder cancer. Therefore, it has been regulated as 1 of 13 carcinogens under the General Industry Standard, 29 CFR 1910.1004 by

OSHA [3]. 1-Naphthylamine in workplace is thus monitored to protect workers from exposure [4].

For monitoring 1-naphthylamine in workplace air, sulfuric acid-treated glass fiber filters are used to collect samples in the occupational safety and health administration (OSHA) method [5]. After desorption and phase transfer, the analysis is performed by reaction the amine with heptafluorobutyric acid anhydride (HFAA) and analyzing the resulting derivative by GC-ECD [5]. Although this method is sensitive and precise, it requires organic solvent and complicate process for derivatization. Silica gel is used as a mediator to collect naphthylamines in air in NIOSH method [4]. As in other environmental samples [6–9], appropriate pretreatment of the silica gel sample is required including desorption with 2-propanol and enrichment by evaporation prior to chromatographic analysis [5]. Although these procedures yield good results, they are relatively time-consuming, hazardous to health due to the organic solvents, and

very expensive with respect to the disposal of solvents. Therefore, pretreatment procedures that take a short time and use little or no organic solvents have led to the recent developed techniques.

In the past 10 years, solid-phase microextraction (SPME) has been used as an alternative to collect samples in environmental matrices prior to GC analysis [10–14]. With advantages of SPME, Zhu et al. [15] applied a SPME sampling method to collect 1-naphthylamine. Later, the headspace SPME (HS-SPME) was developed and applied to prevent matrix effects and eliminate interference for volatile analytes [10,16–17]. However, HS sampling is only suited for volatile analytes, or it will take a long time to finish the sampling and obtain a bad sensitivity.

In this decade, microwave energy was applied to accelerate sample digestion [18], extraction [19,20] and derivatization [21,22] in chemical analyses. Under microwave irradiation, the temperature of system rises within a very short-time period. Therefore, microwave heating also applied to improve the SPME sampling [23–26].

In our recent studies, the microwave-assisted HS-SPME has been developed to achieve the one-step in situ headspace sampling of semi-volatile organic compounds in aqueous samples, vegetables, and soil before GC analysis [27–31]. Besides, the HS-SPME sampling coupled with microwave-assisted desorption (MAD) has also been developed successfully and applied to collect aniline from silica gel adsorbent [32]. Because the boiling point (301 °C), pK_a (3.40) and polarity of 1-naphthylamine are much different from those of aniline (boiling point 184 °C, pK_a 4.19), the application of the MAD/HS-SPME technique as an alternative pretreatment step for 1-naphthylamine collected on silica gel adsorbent is still required to investigate.

In this work, the MAD in situ on-line HS-SPME was systematically investigated to be a simple, fast, sensitive and solvent-free pretreatment process for the gas chromatographic analysis of 1-naphthylamine collected in silica gel adsorbent.

2. Experimental

2.1. Chemicals and reagents

Deionized water was produced using a Barnstead Nanopure water purification system (Barnstead, NY, USA) for all aqueous solutions. All chemicals and solvents were of ACS reagent grade. 1-Naphthylamine was purchased from Fluka (Buchs, Switzerland). Ethanol (95%), iso-propyl alcohol (IPA), and acetic acid were purchased from J.T. Baker (Phillipsburg, NJ, USA). Acetone was obtained from Mallinckrodt (Paris, Kentucky, USA), sodium hydroxide was from Tedia (Fairfield, Ohio, USA) and hydrochloric acid (36.5%) was from Fisher Scientific International (USA). A standard stock solution of 1-naphthylamine (0.5 mg/ml) was prepared by dissolving 5 mg 1-naphthylamine in 10 ml iso-propanol containing 0.05% acetic acid; the solution was stored at 4 °C in silanized brown glass bottle with Teflon-lined cap. Fresh working solutions were prepared by appropriately diluting the stock solution with the iso-propanol containing 0.05% acetic acid. Silica gel (grade 12, 20/40 mesh) and silica gel sampling tubes (100 mg/50 mg, ORBO^{TM}-52) were obtained from Supelco (Bellefonte, PA, USA). Highly pure nitrogen (99.9995%) and hydrogen (99.9995%) were obtained from Lien-Hwa (Taichung, Taiwan).

2.2. GC/FID system

The GC employed herein was a Hewlett-Packard 6890 system (Pennsylvania, USA) equipped with a flame ionization detector (FID), and a split/splitless injector. Separations were performed using a fused silica CP-WAX 52 CB capillary column
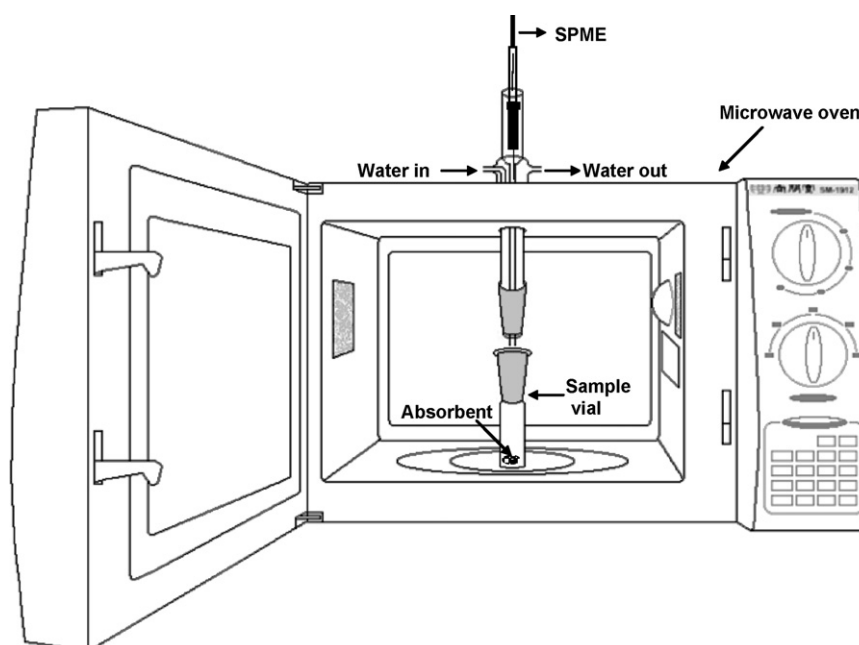
Fig. 1. The assembly of MAD-HS-SPME apparatus.

(30 m × 0.53 mm i.d., 1.0 μm film thickness) (Agilent Technologies, PA, CA). Separation was conducted isothermally at 210 °C with the carrier gas (N_2) at a flow-rate of 20 ml/min. The injector was held at 250 °C to desorb the 1-naphthylamine in SPME for 3 min, and the FID was maintained at 350 °C. A Chem-Lab Data system (Chem-Lab. Co.,Taipei, Taiwan) was used to obtain the chromatogram and perform data calculations.

2.3. MAD/HS-SPME system

The microwave oven was a modified home-used SM-1912 system (2450 MHz, MIDEA, Thailand) with a maximum power of 700 W. After modification, the effective powers of microwave were 95, 172, 255, 345 and 477 W for weak, medium-low, medium, medium-high and high irradiation, respectively. The headspace sampling apparatus included a water jacket condenser (21 mm o.d., 215 mm length, with inner-tube of 3 mm i.d., 5 mm o.d. and 180 mm length) connected to a temperature-controlled circulating water bath (9D-610, DENG YNG, Taiwan) to control the sampling zone temperature. The proposed MAD-HS-SPME system was set up as shown in Fig. 1. Aluminum foil was tacked onto the inner and outer wall of the microwave oven in the interface between the microwave body and the headspace sampling apparatus to prevent microwaves from leaking. A MD-2000 microwave leak detector (Less EMF Inc., NY, USA) was employed to check the safety of the set-up through the experiment.

The SPME device, consisting of the holder and the fiber assembly for manual sampling, was purchased from Supelco and used without modification. The fibers used herein were 1 cm length and coated with 65 μm PDMS/DVB, 100 μm PDMS, 75 μm CAR/PDMS, 65 μm CW/DVB, 85 μm PA, 50/30 μm DVB/CAR/PDMS and 85 μm CAR/PDMS. They were conditioned before they were used as the procedures recommended by supplier before they were used. The needle on the SPME manual holder was set to its maximum length of 4 cm in the GC injector port. A desorption temperature of 250 °C, held for 3 min, was set to generate the highest sensitivity to 1-naphthylamine. All analyses were conducted using a 20 ml vial containing 150 mg of silica gel sample and 0.8 ml of 1.0 M NaOH.

2.4. Preparation of the silica gel spiked sample (surrogate sample)

Several portions of 3 g of silica gel were individually spiked with 0.01–1.0 ml of 1-naphthylamine standard solution (10 μg/ml) and 1.0 ml of *iso*-propanol. After mixed thoroughly, the *iso*-propanol was removed to dryness through an evaporator. Silica gel samples spiked with 0.005–0.5 μg of 1-naphthylamine per 150 mg were obtained, respectively.

2.5. Procedure

Silica gel or silica gel-spiked surrogate samples (150 mg) were added with 0.8 ml of 1.0 M NaOH to a 20 ml sample vial. After swirling, the vial was placed in the microwave oven and connected to the HS-SPME system. A SPME device with a

fiber was inserted into the hollow part of the condenser connected to a water circulator to control the sampling temperature. The 1-naphthylamine was absorbed onto the SPME fiber in the headspace directly under 477 W of microwave irradiation for 5 min. After 1-naphthylamine was collected on fiber, the SPME fiber was desorbed in the GC injector and analyzed using the GC system.

3. Results and discussion

In order to obtain the optimum conditions of the MAD-HS-SPME pretreatment for 1-naphthylamine adsorbed in silica gel, factors that affected the extraction efficiency, including the microwave power and its irradiation time (fiber sampling time), the extraction solution and its pH, the fiber used and sampling temperature, as well as the desorption conditions, were studied thoroughly.

3.1. Selection of SPME fiber coating

Seven commercial SPME fiber-coatings (65 μm PDMS/DVB, 100 μm PDMS, 75 μm CAR/PDMS, 65 μm CW/DVB, 85 μm PA, 50/30 μm DVB/CAR/PDMS and 85 μm CAR/PDMS) were evaluated for the MAD-HS-SPME sampling. A fortified aqueous sample (2 μl of 10 μg/ml 1-naphthylamine spiked in 0.8 ml of 1.0 M NaOH solution) was analyzed in triplicate using each fiber. After 5 min of MAD-HS-SPME sampling at 477 W of microwave irradiation and GC-FID determination, the results were shown in Fig. 2. It is obvious that the mixed PDMS/DVB fiber and the CW/DVB fiber absorbed 1-naphthylamine more efficient than others, and the mixed PDMS/DVB fiber was therefore used herein.

3.2. Microwave irradiation conditions

The influences of microwave irradiation power (95, 172, 255, 345 and 477 W) and irradiation time (from 1 to 9 min)
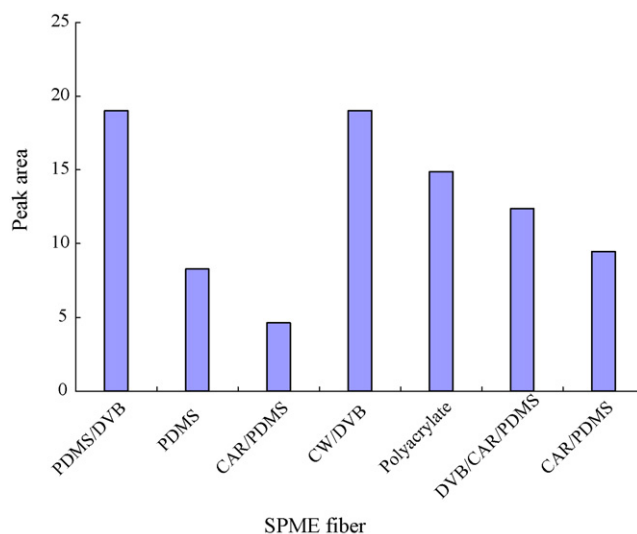
Fig. 2. The extraction efficiency on various SPME fibers.

on the extraction of 1-naphthylamine from the silica gel sample were investigated. Silica gel (150 mg) spiked with 0.1 µg of 1-naphthylamine was used as the test sample. From a series of tests, the results indicated that the peak area increased with the power of irradiation and with the irradiation time (same as sampling time), reaching an optimum at 5 min and then leveling, of 477 W microwave irradiation. It revealed that microwave irradiation at high irradiation power (477 W) for 5 min has enough to achieve the best extraction efficiency of HS-SPME.

3.3. Effect of sodium hydroxide addition on extraction efficiency

In this study, 150 mg silica gel spiked with 0.1 µg of 1-naphthylamine was used as the spiked surrogate sample. In the proposed method, microwave irradiation tended to increase the temperature and thus the partition ratio of 1-naphthylamine between headspace and silica gel. However, an insignificant signal of 1-naphthylamine was observed in the chromatogram by direct microwave-assisted desorption of silica gel and in situ headspace SPME. It implied that the energy absorbed by the silica gel was not enough to desorb 1-naphthylamine into headspace. Polar water was thus added into the silica gel sample to enhance the energy absorption during microwave irradiation. Moreover, the acidic silica gel turns 1-naphthylamine into its protonated form (1-naphthylaminium ion), which does not favor evaporation. Therefore, 1.0 M NaOH was used to neutralize the acidity of the extraction medium and increase the pH to keep 1-naphthylamine in its neutral form for evaporation. The effect of NaOH addition was thus examined. Results indicated that the peak area of 1-naphthylamine increased with the volume of NaOH addition until 0.8 ml, beyond which volume the area decreased slightly due to the dilution effect. Therefore, 0.8 ml of 1.0 M NaOH was used to extract 1-naphthylamine from silica gel in the MAD-HS-SPME process.

3.4. Temperature of sampling system

A 150 mg of silica gel spiked with 10 µg/ml of 1-naphthylamine 2 µl was added to a 20 ml vial containing 0.8 ml of 1.0 M NaOH to elucidate the effect of sampling temperature (from 15 to 90 °C) on the recovery of 1-naphthylamine. The results indicated that the peak area increased with the sampling temperature, reaching a maximum at 80 °C, and then declining slightly. Thus, the sampling temperature was controlled at 80 °C to enable 1-naphthylamine to be absorbed on the SPME fiber.

3.5. Thermal desorption of 1-naphthylamine from SPME fiber

The optimal temperature and duration time for desorbing 1-naphthylamine in the hot GC injector were investigated from 190 to 270 °C for 1–5 min, respectively. After a series of tests, results demonstrated that the peak area (desorption efficiency) increased with the injector temperature, reaching a maximum at 250 °C, and then declined slightly. It also implied 1-naphthylamine is unstable at high temperature. Only one min

was sufficed for the thermal desorption of 1-naphthylamine from the SPME fiber. To ensure complete desorption and regenerate the fiber, the fiber was desorbed in the hot injector for 3 min at 250 °C. Thereafter, no significant signal was observed for the re-injection.

3.6. Features of the method

To examine the applicability of the proposed MAD-HS-SPME method as an alternative pretreatment process in the quantitative determination of the absorbed 1-naphthylamine in silica gel by GC-FID, silica gel spiked with 1-naphthylamine was used for calibration, following complete treatments involving MAD-HS-SPME and thermal desorption from the fiber into the chromatographic system. Fig. 3 shows a FID chromatogram of 1-naphthylamine in surrogate sample obtained under the conditions described previously. The peak appeared at 5.07 min is 1-naphthylamine and at 0.43 min is the solvent signal. A calibration plot was established over the concentration of 20–500 ng/150 mg silica gel with equation of $Y = 0.57X + 10.68$. The linear relationship between the peak area and the spiked quantity was in good agreement with a correlation coefficient (R^2) of 0.9955. The standard deviation of the slope (S_m) is 0.0084 and of the intercept (S_b) is 0.39. The detection limit was calculated by dividing three times the average background noise by the detection sensitivity (slope of calibration plot), which was 8.30 ng. The precision was 1.56% R.S.D. estimated by performing four extractions of 1-naphthylamine spiked in silica gel at the concentration of 100 ng per 150 mg of silica gel, prepared as described in Section 2. The calibration plot of 1-naphthylamine established over the concentration of 0.5–100 ng by direct injection of standard solutions was specified with equation of $Y = 13.87X + 5.13$ ($R^2 = 0.9997$, $S_m = 0.25$ and $S_b = 0.022$). When spiked 20–500 ng of 1-naphthylamine in 0.8 ml of 1.0 M NaOH and with the MA-HS-SPME pretreatment process to determine quantities of 1-naphthylamine, a calibration plot was also obtained with equation of $Y = 0.88X + 16.51$ ($R^2 = 0.9978$, $S_m = 0.016$ and $S_b = 0.21$). Because the slope of a calibration plot represents the detection sensitivity of analyte which related to the efficiency of operation process, thus desorption efficiency of 1-naphthylamine from silica gel into aqueous solution can
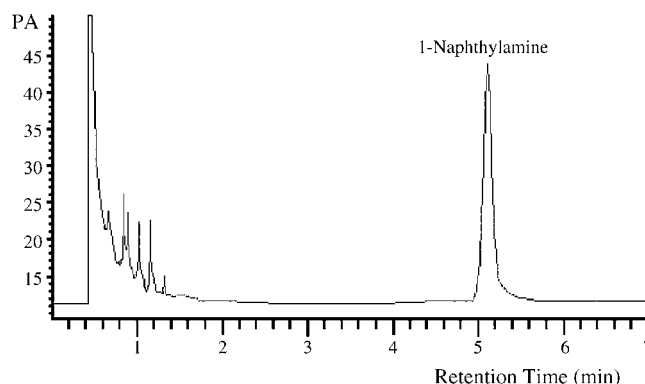
Fig. 3. Chromatogram of 1-naphthylamine spiked in silica gel with the proposed method.

Flow-injection on-line oxidizing fluorimetry and solid phase extraction for determination of thioridazine hydrochloride in human plasma

Zhi-Qi Zhang [a,*], Jian Ma [a], Ying Lei [b], Yue-Mei Lu [b]

[a] School of Chemistry and Materials Science, Shaanxi Normal University, Xi'an 710062, China
[b] Xi'an Mental Health Center, Xi'an 710061, China

Abstract

A simple, sensitive and specific fluorimetric method has been developed for the determination of thioridazine hydrochloride in human plasma involving solid phase extraction (SPE). In a flow-injection system, thioridazine hydrochloride is on-line oxidized into a strongly fluorescent compound with a lead dioxide solid-phase reactor and the fluorescence intensity is measured with a fluorescence detector (λ_{ex} = 349 nm, λ_{em} = 429 nm). A comparison of plasma sample pretreatment between SPE procedure and precipitation method was made and the results showed that SPE procedure was better than precipitation method. Under the optimum conditions, the fluorescence intensity is proportional to the concentration of thioridazine hydrochloride in the range from 0.015 to 2.000 $\mu g\,mL^{-1}$. The detection limit is 5.5 $ng\,mL^{-1}$ of thioridazine hydrochloride and the relative standard deviation is 1.06%. This method has been applied to determination of thioridazine hydrochloride in real patients plasma samples with the results compared with those obtained by HPLC method.
© 2006 Elsevier B.V. All rights reserved.

Keywords: Flow-injection analysis; Fluorimetry; Solid phase extraction; Thioridazine hydrochloride; Human plasma

1. Introduction

Thioridazine hydrochloride, the hydrochloride of 10-[2-(l-methyl-2-piper-idyl)ethyl]-2-methylthiophenothiazine, is a phenothiazine neuroleptic drug used for the treatment of schizophrenia and other psychiatric disorders [1]. It is also used for the short-term treatment of adults with major depression who have varying degrees of associated anxiety [2] and in other aspects [3]. Pharmacology research showed that thioridazine increases the rate of Ca^{2+} accumulation into synaptic plasma membrane vesicies [4]. Due to the clinical importance of thioridazine hydrochloride, it is significant to establish a simple and sensitive method for its determination in human plasma.

Several analytical methods have been described for determination of thioridazine hydrochloride. Among the methods, UV spectrophotometry and conventional high performance liquid chromatography (HPLC) [5–11] are most often used. UV spectrophotometry is also regulated by China Pharmacopoeia [12]

as the official method for assay of thioridazine hydrochloride in tablets. Electrochemistry [13,14], Capillary electrophoresis [15] and chemiluminescent method [16–18] have been reported for the determination of thioridazine hydrochloride. Supercritical fluid chromatography [19] and HPLC combined with other techniques [20–23] were also reported for determination of thioridazine hydrochloride and its main metabolites or derivatives. Some of these methods lack adequate sensitivity, and some are expensive and time consuming. Although chemiluminescent method is characterized by its high sensitivity and simple instrumentation, this method suffers serious interferences.

Fluorimetry is a simple and highly sensitive method widely applied to the assay of drugs [24–28], protein [29] and drug–protein interaction [30,31]. Recently, a spectrofluorimetric method was reported for simultaneous determination of thioridazine hydrochloride and its derivatives [32]. The method was based on oxidizing the studied drugs with cerium (IV) in presence of sulfuric acid and monitoring the fluorescence of the formed cerium (III) at λ_{ex} = 254 nm and λ_{em} = 355 nm. The linearity range was from 0.05 to 1.30 and the limit of detection was 0.035 $\mu g\,mL^{-1}$. Because this method is non-directly

---

* Corresponding author. Tel.: +86 29 85303939; fax: +86 29 85310230.
  E-mail address: zqzhang@snnu.edu.cn (Z.-Q. Zhang).

determination of thioridazine hydrochloride through measuring the fluorescence intensity of cerium (III) produced from reduction of cerium (IV), the reductive substances in samples would present certain interference.

Solid phase extraction (SPE) [33–35] and precipitation [36,37] are two ordinary isolation procedures for pretreatment of plasma sample. The aim of this work was to develop a simple, rapid, sensitive and selective fluorimetric method combined with pretreatment techniques for determination of thioridazine hydrochloride in human plasma.

2. Experimental

2.1. Instrumentation

An eight-channel Model IFIS-C intellectual flow injector (Xi'an Ruike Electronic, China) was employed in this system. The fluorescence spectra of thioridazine hydrochloride and its oxidized product were measured with a Model 970CRT fluorescence spectrophotometer (Shanghai Analytical Apparatus Factory, China). Fluorescence intensity was measured in flow-injection system with Waters 2475 Multi λ fluorescence detector (Waters Corporation, USA) equipped with a 150-W continuous xenon lamp and a flow cell of 8 μL. The experimental temperature was controlled with a Model 88-2 thermostatic bath (Gongyi Yuhua Experimental Apparatus Factory, China).

The thioridazine hydrochloride reference values in real patient plasma samples were obtained with a Waters (Waters Corporation, USA) liquid chromatography apparatus consisting of a model 1525 pump and a model 2996-photodiode array detector operating at 262 nm. A reversed-phase Hypersil VP-ODS C_{18} column (5 μm, 150 mm × 4.6 mm i.d.,) was used and 20-μL sample solution was injected into the chromatographic system.

2.2. Reagents and solutions

All the chemicals used were of analytical-reagent grade or better. Water purified with Milli-Q deionization system (Millipore, USA) was used throughout.

The thioridazine hydrochloride standard was purchased from the Chinese National Institute for the Control of Pharmaceutical and Biological Product, and prepared as a 0.100 mg mL^{-1} stock solution by dissolution of 10.0 mg in 20.0 mL absolute ethanol and dilution to 100 mL volumetric flask with Milli-Q water. Working standard solution was obtained daily by appropriate dilution stock solution with ethanol solution of 20.0% (v/v).

1.0 mol L^{-1} phosphoric acid and 20.0% (v/v) ethanol solutions were prepared as usual.

Chromatographic mobile phase was prepared as reference [38,39]. Acetonitrile, methanol, methylene chloride, hexane and tetrahydrofuran (THF) were HPLC grade purchased from Dikma Co. (DIMA Technology Inc., USA). Diethylamine, analytical grade, were purchased from Xi'an reagent factory.

2.3. Solid-phase reactor preparation

The solid-phase reactors containing different oxidant were prepared using the way as reference [26]. Cellulose acetate (0.25 g) was dissolved in 0.5 mL formamide and 3.0 mL acetone. With stirring, 5.0 g of oxidant powder was then added slowly to the solution. Ten minutes later, rigid polyester solid was obtained. After air-drying, the polyester was cut into 250–300 μm particles and the solid-phase reactors were constructed by filling polyester particles in different length (2.0 mm i.d.) of glass tubes.

2.4. Sample and preparation

Real plasma samples were taken from anonymous epileptic patients under therapy with thioridazine hydrochloride at the Xi'an Mental Health Center. Four hours after the first daily drug administration, patient blood samples were collected and then treated into plasma. Drug-free plasma samples were also taken from the Xi'an Mental Health Center.

2.4.1. Precipitation method

As reference [36,37], transfer 1.0 mL of drug-free human plasma into a disposable polypropylene micro centrifuge tube, add different amount of 2 μg mL^{-1} thioridazine hydrochloride solution and 20.0% ethanol solution in order to obtain a plasma solution of 2 mL and final thioridazine hydrochloride concentration of 0.1, 0.5, and 1.0 μg mL^{-1}, respectively. Shake well for 3 min and add 3 mL of acetonitrile to precipitate deproteination. Shake the mixture on a vortex for 30 s, and centrifuge for 5 min at 3000 rpm in a micro centrifuge. Transfer the protein free supernatant into a 10 mL standard flask and then prepare as an ethanol solution of 20.0%. Carry out a blank experiment adopting the above procedure.

2.4.2. Solid phase extraction (SPE) procedure

SPE procedure of thioridazine hydrochloride from human plasma was performed with Sep-Pak C_{18} cartridges (Waters Corporation, Milford, MA, USA) preconditioned with methanol (1 mL) and washed with Milli-Q water (1 mL). For the comparison of plasma sample pretreatment methods, make 1 mL of drug-free plasma, as precipitation method, up to 2 mL solution that contains thioridazine hydrochloride concentration of 0.1, 0.5, and 1.0 μg mL^{-1}, respectively. Then the sample solution was applied to the cartridge and forced out slowly by air pressure with a 2 mL pipet until the cartridge appeared dry and no more water droplets came out. The cartridge was sequentially washed with 2 mL of 5% (v/v) methanol solution, and analyte was eluted twice with 2 mL of eluent (1.0 mol L^{-1} phosphoric acid solution containing 20.0% ethanol) and collected into a standard flask, finally diluted to 10 mL with 20.0% ethanol solution. For the real patient plasma samples analysis, mix 500 μL of patient plasma and 500 μL of 20.0% ethanol solution into sample solution, and then apply the above SPE procedure.

2.5. Flow-injection procedure

As reference [26,31], a flow-injection system with two channels was employed. After sampling for 30 s, the valve switched from sampling position into the injection position and the sample solution (300 μL) was injected into carrier. Sample solution injected mixed with other acidic reaction medium flow (each at a flow rate of 0.6 mL min⁻¹) and then passed through the solid-phase reactor, in which thioridazine hydrochloride was oxidized by immobilized oxidant. The fluorescent intensity of the oxidization product was measured in a flow-through cell (8 μL) at an excitation wavelength of 349 nm and an emission wavelength of 429 nm. Sixty seconds later, the valve was switched back to the sampling position for next determination.

3. Results and discussion

3.1. Fluorescence spectra

Thioridazine hydrochloride has various oxidation products by side chain oxidation resulting in the formation of thioridazine 2-sulfoxide (THD 2-SO) and thioridazine 2-sulfone (THD 2-SO$_2$) and by ring sulfoxidation leading to thioridazine 5-sulfoxide (THD 5-SO) [1]. However, thioridazine hydrochloride showing weak native fluorescence can become a strong fluorescence compound when it is oxidized suitably [32]. As shown in Fig. 1, the product resulted from the oxidization by lead dioxide in an acid medium has the maximum excitation wavelength of 349 nm and emission wavelength of 429 nm, respectively.

3.2. Optimization of oxidization conditions

In flow-injection system, the oxidization conditions for thioridazine hydrochloride were optimized to achieve maximum sensitivity.
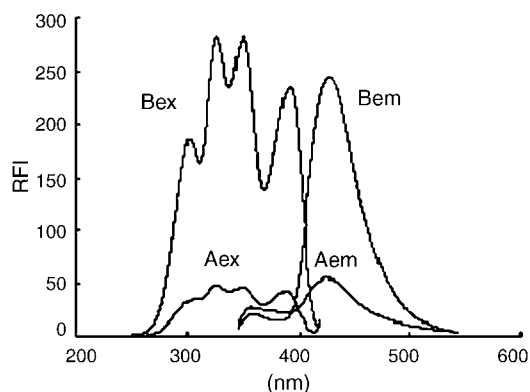

Fig. 1. Fluorescence spectra of thioridazine hydrochloride and its oxidization product for 0.1 μg mL⁻¹ thioridazine hydrochloride in 0.5 mol L⁻¹ phosphoric acid. Aex and Aem, excitation and emission spectra of thioridazine hydrochloride; Bex and Bem, excitation and emission spectra of its oxidation product.

Studies have indicated that different acidic media have a critical effect on the on-line oxidation of thioridazine hydrochloride. Reaction medium was optimized for lead dioxide, sodium bismuthate and manganese dioxide solid-phase reactor, respectively. As shown in Fig. 2, when oxidization reaction runs in the medium of phosphoric acid and sulfuric acid, fluorescence intensity of the oxidization product were much higher than in the medium of hydrochloric acid, acetic acid and nitric acid. The highest fluorescence intensity was obtained in 0.1 mol L⁻¹ of phosphoric acid medium for lead dioxide reactor (Fig. 2(A)), in 0.1 mol L⁻¹ of sulfuric acid medium for sodium bismuthate reactor (Fig. 2(B)) and in 0.25 mol L⁻¹ of sulfuric acid medium for manganese dioxide reactor (Fig. 2(C)), and the signals produced by lead dioxide reactor were much higher than that produced by sodium bismuthate reactor and manganese dioxide reactor as well. So, a lead dioxide reactor was adopted in subsequent work and a 0.1 mol L⁻¹ solution of phosphoric acid selected as acidic reaction medium.
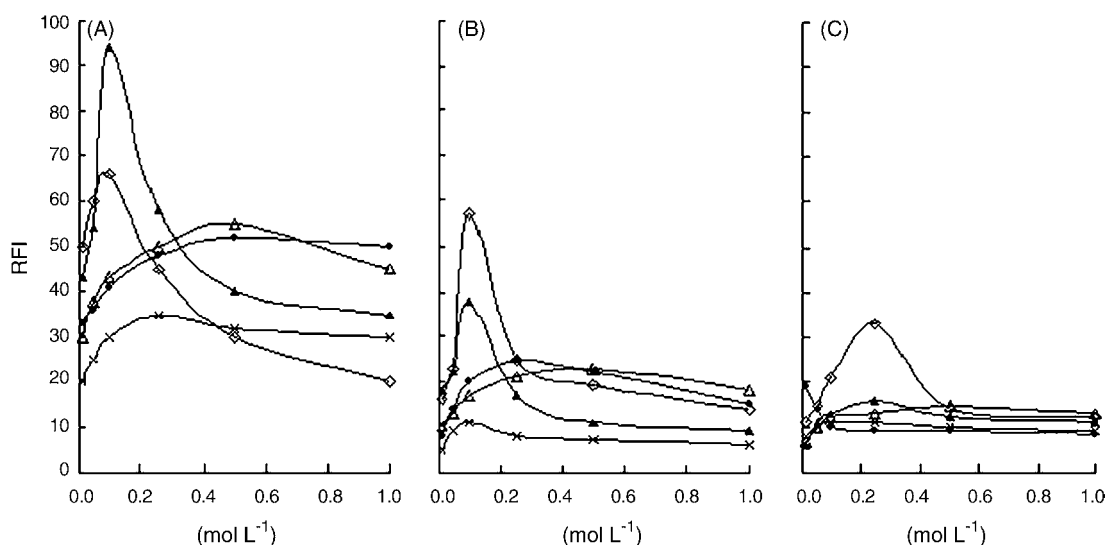

Fig. 2. Influence of reaction medium and acidity on fluorescence intensity: (A) with lead dioxide reactor; (B) with sodium bismuthate reactor; (C) with manganese dioxide reactor. (▲) H$_3$PO$_4$, (◇) H$_2$SO$_4$, (△) HAc, (●) HCl, and (×) HNO$_3$.
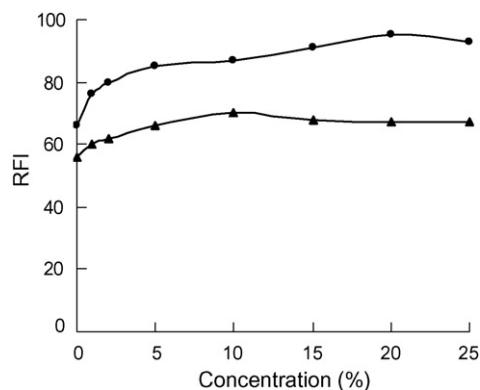
Fig. 3. Effect of solvent on fluorescence intensity. (▲) Acetone and (●) ethanol.

The effect of reaction temperature was studied in the range of 10–80 °C. The fluorescence intensity increased with temperature up to 50 °C and decreased gradually with further increasing temperature. When the temperature approached to 80 °C, fluorescence intensity suddenly decreased near to zero. Thus, the solid-phase reactor was placed in a water bath to control reaction temperature at 50 °C.

It has been reported [40] that the organic solvents such as acetone and ethanol could sensitize the fluorescence intensity of some compounds because of solvent effect. An investigation was made into the effect of acetone and ethanol by taking a certain concentration of solvent as carrier. As shown in Fig. 3, ethanol solution was better than acetone. The fluorescence signals increased slowly with the increasing of the ethanol concentration up to 20%. Finally, 20% ethanol solution used as carrier and sample solution that could enhance the sensitivity to about 40%.

3.3. Optimization of flow system parameters

The flow system variables studied were length of solid-phase reactor, sample volume to be injected and flow rate.

The influence of reactor length was studied in 1–20 cm range with an inner diameter of 2.0 mm. The results showed that the signal was gradually increased with increasing reactor length and highest fluorescence intensity was obtained with a reactor length of 15 cm, then the signal decreased with further increasing length of reactor because thioridazine hydrochloride was over oxidized. Consequently, a 15 cm length of lead dioxide solid-phase reactor was chosen.

The effect of sample volume to be injected was studied in 100–400 µL range. The results showed that fluorescence intensity increased with increasing sample up to different volumes according to the reactor length. As to a 15 cm length of reactor, 300 µL sample volume was optimum, over which fluorescence intensity was not significantly increased but analytical time was lengthened. Thus, a 300 µL of sample volume was selected.

The flow rate was checked over the range of 0.2–1.0 mL min^{-1}. Experiment results showed that the fluorescence intensity increased slightly with increasing flow rate up to 0.6 mL min^{-1}, which may be because thioridazine hydrochloride was oxidized quickly into fluorescence compound and the fluorescence compound could be further oxidized into less fluorescence product at lower flow rate. However, higher flow rate not only led to higher pressure of the oxidant column but also caused irreproducibility. As a compromise, a flow rate of 0.6 mL min^{-1} was chosen.

3.4. Comparison of sample pretreatment

In order to apply the proposed flow-injection fluorimetry to determination of thioridazine hydrochloride in human plasma, a comparison of sample pretreatment between SPE procedure and precipitation method was made, and the results were listed in Table 1. It can be clearly found that the recoveries obtained by the precipitation method were very high, whereas recoveries obtained by SPE procedure were acceptable. Statistical analysis showed that there was a serious systematic error present in the precipitation method because it could not make the albumen totally precipitate and the remaining albumen seriously interfered with the fluorescence determination. The comparison of experiment results showed that the SPE procedure was better than the precipitation method for preparing a human plasma sample in order to determine thioridazine hydrochloride with flow-injection fluorimetry proposed.

3.5. Working curve

In order to apply the proposed method to determination plasma samples, a working curve was obtained. The plot of fluorescence intensity to thioridazine hydrochloride concentration was rectilinear over the range of 0.015–2.0 µg mL^{-1}. Linear regression analysis of the data gave the following equation

$$F = (152.3 \pm 3.1)C + (4.5 \pm 0.2)$$

Table 1
Comparison of sample pretreatment between SPE procedure and precipitation method for flow-injection fluorimetry to determination of thioridazine hydrochloride in human plasma samples

Added (µg mL^{-1})	Found amount[a] with precipitation method			Found amount[a] with SPE procedure		
	Sample A	Sample B	Sample C	Sample A	Sample B	Sample C
0.10	0.11 ± 0.02	0.12 ± 0.01	0.11 ± 0.01	0.10 ± 0.02	0.11 ± 0.01	0.09 ± 0.01
0.50	0.55 ± 0.02	0.57 ± 0.03	0.54 ± 0.02	0.47 ± 0.03	0.48 ± 0.03	0.51 ± 0.02
1.00	1.13 ± 0.03	1.15 ± 0.04	1.11 ± 0.02	0.96 ± 0.02	0.97 ± 0.02	0.95 ± 0.03

[a] Mean ± S.D., $n = 3$.

Table 2
Results of determination of thioridazine hydrochloride in real patient plasma samples

Sample	Found amount[a] ($\mu g\,mL^{-1}$)	
	Proposed method	Reference (HPLC)
Patient 1	1.12 ± 0.01	1.09 ± 0.02
Patient 2	1.58 ± 0.03	1.61 ± 0.02
Patient 3	0.99 ± 0.01	0.97 ± 0.01
Patient 4	0.91 ± 0.01	0.89 ± 0.01
Patient 5	1.12 ± 0.02	1.15 ± 0.02

[a] Mean $\pm$ S.D., $n = 3$.

with a regression coefficient of 0.9991. Where F is the relative fluorescence intensity and C is the thioridazine hydrochloride concentration in $\mu g\,mL^{-1}$. The detection limit was $5.5\,ng\,mL^{-1}$ of thioridazine hydrochloride ($S/N = 3$). The relative standard deviation (R.S.D.) was estimated as 1.06% for 11 replicate determinations of $0.1\,\mu g\,mL^{-1}$ thioridazine hydrochloride.

3.6. Interference studies

Common tablet excipients, such as talc powder, starch, dextrine, magnesium stearate and gelatin, were investigated and did not interfere with the determination of $0.1\,\mu g\,mL^{-1}$ thioridazine hydrochloride assay. The coexistent times for other common substances investigated was glucose (3000), ascorbic acid (500), uric acid (400), urea (400), Ca^{2+} (400), Zn^{2+} (200), Fe^{3+} (100), SO_4^{2-} (1000), HCO_3^{-} (500) and $C_2O_4^{2-}$ (100).

3.7. Application to real patient plasma samples

Combined with SPE pretreatment procedure, the proposed method has been applied to determination of thioridazine hydrochloride in real patient plasma samples and the results are showed in Table 2. It can be found that the results obtained by proposed method are comparable with those obtained by HPLC method.

4. Conclusion

In this work, an overall condition optimization was carried out with three oxidants, lead dioxide, sodium bismuthate and manganese dioxide, filled as solid-phase reactor, for on-line oxidization and fluorimetric determination of thioridazine hydrochloride. As to the pretreatment of the plasma sample, a SPE procedure was recommended.

The results presented in this paper clearly show that a lead dioxide solid-phase reactor flow-injection on-line oxidization fluorimetric method for determination of thioridazine hydrochloride possesses several advantages over reported method such as simpler and inexpensive instrument, low detection limit, high rate of analysis, and good selectivity and accuracy. Combined with proposed SPE procedure, it can be adopted to pharmacokinetic studies and routine

clinical estimation of thioridazine hydrochloride in human plasma.

References

[1] C.M. Gaitania, A.S. Martinezb, P.S. Bonato, J. Pharm. Biomed. Anal. 36 (2004) 601.
[2] E.Z. Abdel-Moety, K.A. Al-Rashood, K. Florey (Eds.), Analytical Profiles of Drug Substances, vol. 18, Academic Press, New York, 1988.
[3] K. Farhadi, G. Teimouri, Talanta 65 (2005) 925.
[4] J. Palacios, M.R. Sepu'lveda, A.G. Lee, A.M. Mata, Biochemistry 43 (2004) 2353.
[5] G.A. Rivas, A.M. Romerob, J.M. Calatayud, Anal. Chim. Acta 326 (1996) 23.
[6] L. de la Peña, A. Gómez-Hens, D. Pérez-Bendito, Talanta 41 (1994) 1895.
[7] M.E. El-Kommos, K.M. Emara, Analyst 113 (1988) 1267.
[8] C.S. Torre, M.A. Martý'nez, E. Almarza, Forensic Sci. Int. 155 (2005) 193.
[9] C.E. Lin, K.H. Chen, Y.Y. Hsiao, W.S. Liao, C.C. Chen, J. Chromatogr. A 971 (2002) 261.
[10] J. Karpinska, B. Starczewska, J. Pharm. Biomed. Anal. 29 (2002) 519.
[11] C.B. Eap, L. Koeb, K. Powell, et al., J. Chromatogr. B 669 (1995) 271.
[12] The Pharmacopoeia of The People's Republic of China, 2, Chem Ind Press, 2000, 673.
[13] S.S. Razola, E. Aktas, J.C. Viré, J.M. Kauffmann, Analyst 125 (2000) 79.
[14] S.M. Golabi, M. Showkati-Shishevan, Talanta 38 (1991) 1253.
[15] R.Y. Wang, X.N. Lu, M.J. Wu, E. Wang, J. Chromatogr. B 721 (1999) 327.
[16] Y. Li, W. Niu, J. Lu, Talanta, in press, Available online July 17, 2006.
[17] A. Kojlo, J. Michalowski, E.B. Wolyniec, J. Pharm. Biomed. Anal. 22 (2000) 85.
[18] L.L. Zamora, Y.F. Mestre, M.J. Duart, G.M. Anton Fos, R.G. Domenech, J.G. Alvarez, J.M. Calatayud, Anal. Chem. 73 (2001) 4301.
[19] F. Geiser, M. Schultz, L. Betz, M. Shaimi, J. Lee, W. Champion, J. Chromatogr. A 865 (1999) 227.
[20] A. Pelander, I. Ojanperal, S. Laks, I. Rasanen, E. Vuori, Anal. Chem. 75 (2003) 5710.
[21] T.N. Decaestecker, S.R.V. Casteele, P.E. Wallemacq, C.H. Van Peteghem, D.L. Defore, J.F. Van Bocxlaer, Anal. Chem. 76 (2004) 6365.
[22] H. Hayen, U. Karst, Anal. Chem. 75 (2003) 4833.
[23] H.N. Choi, S.H. Cho, Y.J. Park, D.W. Lee, W.Y. Lee, Anal. Chim. Acta 541 (2005) 49.
[24] I.D. Merás, T.G. Díaz, M.A. Franco, Talanta 65 (2005) 7.
[25] F.A. Mohamed, H.A. Mohamed, S.A. Hussein, S.A. Ahmed, J. Pharm. Biomed. Anal. 39 (2005) 139.
[26] Z.-Q. Zhang, Y. Tang, Anal. Bioanal. Chem. 381 (2005) 932.
[27] A.M. Powe, K.A. Fletcher, N.N. St Luce, M. Lowry, S. Neal, M.E. McCarroll, P.B. Oldham, Anal. Chem. 76 (2004) 4614.
[28] P.R. Tomás, M.L. Carmen, T. Virginia, Anal. Bioanal. Chem. 372 (2002) 387.
[29] X. Chen, J. Wang, Talanta 69 (2006) 681.
[30] Y. Wei, J. Li, C. Dong, S. Shuang, D. Liu, C.W. Huie, Talanta 70 (2006) 377.
[31] Z.-Q. Zhang, G.X. Liang, Anal. Chim. Acta 536 (2005) 145.
[32] F.A. Mohamed, H.A. Mohamed, S.A. Hussein, S.A. Ahmed, J. Pharm. Biomed. Anal. 39 (2005) 139.
[33] S.A. Chan, S.W. Lin, K.J. Yu, T.Y. Liu, M.R. Fu, Talanta 69 (2006) 952.
[34] L. Vlase, S. Imreb, S. Leucuta, Talanta 66 (2005) 659.

[35] J. Sun, G. Wang, H. Xie, H. Li, G. Pan, I. Tucher, J. Pharm. Biomed. Anal. 38 (2005) 126.

[36] T.X. Maotian, F.S. Junfeng, L. Ning, Anal. Bioanal. Chem. 377 (2003) 1184.

[37] F. Belal, A. Al-Majed, S. Julkhuf, J. Pharm. Biomed. Anal. 31 (2003) 989.

[38] G. Lin, K.W. Chu, L.A. Damani, J. Pharm. Biomed. Anal. 14 (1996) 727.

[39] C.B. Eap, L. Koeb, K. Powell, P. Baumann, J. Chromatogr. B 669 (1995) 271.

[40] G.Z. Chen, J.G. Xu, Fluorescence Analytical Method, 2nd ed., Science Press, Beijing, China, 1990.